**UNIVERSITY OF SOUTHAMPTON**

FACULTY OF SOCIAL AND HUMAN SCIENCES

Geography and Environment

# Combining Multi-Source Satellite Sensor Imagery to Monitor and Forecast Land Use Change in Malaysia

by

**Mohd Rizal Bin Osman**

Thesis for the degree of Doctor of Philosophy

November 2014

UNIVERSITY OF SOUTHAMPTON

# ABSTRACT

FACULTY OF SOCIAL AND HUMAN SCIENCES

Geography and Environment

Thesis for the degree of Doctor of Philosophy

## COMBINING MULTI-SOURCE SATELLITE SENSOR IMAGERY TO MONITOR AND FORECAST LAND USE CHANGE IN MALAYSIA

by Mohd Rizal Bin Osman

The urban environment encompasses many interactive phenomena. In Malaysia, land use development is spatially complex, especially in built-up areas which comprise residential, commercial and industrial (RCI) land use areas which are part of the urban land use fabric. The planning solution is to prepare a comprehensive development plan to control the uses of land and to provide the basic framework for development of new areas. The land use plan can serve as a tool to guide development.

Based on remote sensing methods, the overall aim of the research in this thesis was to investigate how remotely sensed imagery can be used to monitor and forecast land use land cover (LULC) change in an urban environment in Malaysia. The specific focus in each of three separate "analysis" chapters was on (objective 1) the use of object-based image analysis (OBIA) to produce a very high accuracy LULC classification at fine spatial resolution for two time points (2005 and 2009) in order to analyse change in LULC, (objective 2) to combine these imagery with coarser spatial resolution, but more frequent Landsat Thematic Mapper imagery which have been calibrated to a high standard in order to analyse the *date* of the changes, and (objective 3) to use a cellular automata (CA) type model to forecast future change in LULC (in 2013, 2017 and 2021) and compare the forecast (in 2021) to existing formal planning documents for a similar year (2020). The remotely sensed data used to fulfil these objectives were a frequently acquired Landsat TM image time-series at a spatial resolution of 30 m and infrequent (two dates) IKONOS imagery with a spatial resolution of 1m (pan-sharpened).

Several research questions needed to be addressed to support the overall research objectives. Of importance in objective 1 was the need to classify LULC to a fine level by splitting built land into the residential, commercial and industrial (RCI) LULC classes. Thus, it was of interest to explore the ability of the OBIA approach to achieve this is the Malaysian context. To achieve objective 2 it was necessary to undertake rigorous calibration of the multi-date imagery. This involved image data standardisation for each year of Landsat ETM+ imagery from 2005 to 2009. A script in the IDL programming language was developed which took into account the pixel-level changes in Landsat reflectance and stored automatically the date of change based on the multi-date Landsat ETM+ satellite sensor imagery. Under objective 3, the result of land-use changes in pixels or cells from the change analysis (objective 1) (i.e., the set of transition probabilities) enabled a simulated forecast to be generated using a CA model. While several parameters of the CA model were explored, of

greatest interest was the comparison of the forecast with a formal Plan for LULC in 2020.

The significance of the findings and contributions of this research are in the process of preparing a complex land use classification (RCI) and analysis of change therein, the novel use of Landsat data to infer the date of LULC change and the comparison of the CA forecast with Planning Department data for the same period. All these methods are potentially useful in the practice of town planning in Malaysia.

# Contents

# List of tables

# List of figures

# DECLARATION OF AUTHORSHIP

I, Mohd Rizal Bin Osman

declare that the thesis entitled

Combining Multi-Source Satellite Sensor Imagery to Monitor and Forecast Land Use Change in Malaysia

and the work presented in the thesis are both my own, and have been generated by me as the result of my own original research. I confirm that:

- this work was done wholly or mainly while in candidature for a research degree at this University;
- where any part of this thesis has previously been submitted for a degree or any other qualification at this University or any other institution, this has been clearly stated;
- where I have consulted the published work of others, this is always clearly attributed;
- where I have quoted from the work of others, the source is always given. With the exception of such quotations, this thesis is entirely my own work;
- I have acknowledged all main sources of help;
- where the thesis is based on work done by myself jointly with others, I have made clear exactly what was done by others and what I have contributed myself;
- none of this work has been published before submission,

- Signed: ……..
- Date:……

# Acknowledgements

My greatest thanks go to Almighty Allah for his mercy and grace. First and foremost, my gratitude goes to '*Hadiah Latihan Persekutuan* (HLP 2010)' scholarship from Malaysian Government through the Public Service Department (JPA) for providing me with this great opportunity to pursue my Ph.D in the United Kingdom.

I would like to thank my main supervisors, Prof. Peter M. Atkinson and Dr. Jadu Dash for his supervision, understanding and moral support. His continuous encouragement, guidance and support has enabled me to achieve this uphill task. I gained a lot of experience as a 'research student' to improve the way of thinking about the complex landscapes of urban remote sensing studies. I also thank co-supervisor Prof. Ted Milton, for his direction and instruction in the context of scientific reasoning especially when dealing with calibration of multi date and multispectral remote sensing data. It has been my great honour to work with such renowned professors in the field of remote sensing. I appreciate their critical comments during their review of my work. The completion of this thesis has been achieved through the overwhelming support and help from many people and mentioning each may not be possible. I would like to express my sincere thanks to Dr. Debbie Milton who proof-read every single word of my Ph.D thesis. My sincere thanks go to Prof. David Martin who became my internal examiner during the upgrade meeting from M.Phil to Ph.D status and who reviewed my work and gave good comments. My special thanks go to Mr Chris Cullen, Coordinator of the EAP Support Programme, Centre for Language Study, University of Southampton who became my personal English teacher and helped improve my writing style.

Sincere thanks to my Ph.D colleagues in the Research Hub Building 44 room and Malaysian Southampton friends especially house 'Two Honeysuckle Boys' for providing a homely environment. Finally, it would have been impossible without the support of my entire family in Malaysia, my beloved mothers and fathers and my brothers and sisters. To my beloved wife Nora, daughter Zara Naura and son Zill Nouman, they are make my life everyday full of love and enthusiasm and are always there to cheer me up when I felt sad. Their continuous love, patience, and prayers made everything much easier for me. Indeed, 'it is the autumn that defines me and my life' – autumn, 2014.

# Definitions and Abbreviations

| | |
|---|---|
| ATCOR | Atmospheric and Topographic Correction |
| CA | Cellular Automata |
| CVA | Change Vector Analysis |
| DN | Digital Number |
| DOS | Dark Object Subtraction |
| FDTCP | Federal Department Town and Country Planning, Peninsular Malaysia |
| FLAASH | Fast Line-of-sight Atmospheric Analysis of Spectral Hypercubes |
| FS | Feature Space |
| H-res | High Resolution |
| IDL | Iterative Data Language |
| IR-MAD | Iteratively Reweighted Multivariate Alteration Detection |
| LULC | Land Use and Land Cover |
| L-res | Low Resolution |
| MAD | Multivariate Alteration Detection |
| MODTRAN | Moderate Resolution Atmospheric Transmission |
| NIR | Near-Infrared |
| NN | Nearest Neighbour |
| OB | Object-Based |
| OBIA | Object-Based Image Analysis |
| RCI | Residential-Commercial-Industrial of land use classes |
| RS | Remote Sensing |
| RTM | Radiative Transfer Model |
| SLC | Scan Line Corrector |
| SMMA | Standard Mixture Modelling Analysis |
| TC | Tasselled Cap |

*To Lovely Nora & ZNER*

His command is only when He intends a thing that He says to it, “Be”, and it is.  36:82

# 1. Thesis Aim and Objectives

## 1.1 Research Background

In this research, combining multi-source satellite sensor imagery to forecast and monitor land use change is presented.

The conversion of land, for example, from forest into agriculture and into urban land modifies the surface landscape affecting the local climate, biodiversity and causing potential environmental degradation (e.g., soil nutrients and underground water resources). The importance of the monitoring process is to avoid the negative effects of land use and land cover changes to sustain the production of basic resources, encouraging researchers and policymakers (town planners) to take action to protect the environment. According to this perspective, it was decided to focus on urban land use monitoring to help and sustain regional development and environmental quality. Healey (1996) suggested that information on spatial change in urban regions is needed to understand the complex dynamics of urban regions and the underlying strategies and actions, and this may be translated to influence planning.

Planning is the solution by environmental monitoring and management for tackling unbalanced and uncontrolled urbanisation which can cause fragmentation of the landscape and ecosystems and a consequent loss of natural capital and related changes to the functions of an area. The process involves the integration of a wide and diverse range of qualitative and quantitative data. Planning also regulates the use and development of land (in the public interest) and is, thus, an important influence on land values. It is a powerful tool to generate economic opportunities and facilitate economic development by, for example, reducing congestion costs and negative externalities. These initiatives require local authorities to respond to environmental and land use problems in new ways (Evans 1993). Through appropriate methods, urban planning can be carried out in a useful manner within developing countries' or cities' contexts. Planning is able to tackle issues from the complicated local neighbourhood context to national planning policy.

Dealing with time-series satellite sensor imagery in a tropical country (i.e. Malaysia) is challenging; clouds, cloud shadows and haze are problems that affect the use of satellite sensors such that consistent and cloud-free datasets over large areas are not always possible to achieve. It is, thus, important that planners explore the potential impact of a wide range of imaging spatial resolutions for research in town planning especially in a tropical country like Malaysia. Although land use maps for Peninsular Malaysia (West Malaysia) are available in digital format to the related government agencies, environmental public researchers and scientists have not been able to acquire these data because of the high cost (Razali et al. 2014). Therefore, the basic available framework of land use information can provide the set of land use classes to predict from a satellite sensor within the perspective of rapid urban growth and change, for which the methods of remote sensing are well suited. Nevertheless, updating or replacing these maps with a large amount of remotely sensed data remains a very challenging task (Franklin & Wulder 2002).

Making effective plans involves the integration of knowledge from science (remote sensing methods and application) and knowledge from the planning process such as to derive preferred strategies and an acceptable interpretation to be recommended to the relevant parties. The use of such research and technology can allow policy makers as well as the public (people affected) to visualise and understand the spatial implications of decisions made on urban development projects or growth.

## 1.2 Aspects of Urban Remote Sensing Studies

### 1.2.1 Urban Growth Issues

Rapid urban growth and sprawling development are seen as major problems because they lead to loss of production in agricultural and forest lands to urban uses; i.e., permanent impact of increased urban-space consumption (residential, commercial and industrial), infrastructures and open spaces for sustaining land developments.

The World Health Organization (WHO 2014) reported that the urban population in 2014 accounted for 54% of the total global population, up from 34% in 1960, and it continues to grow. The urban population growth, in absolute numbers, is concentrated in the less developed regions of the world. It is estimated that by 2017, even in less developed countries, a majority of people will be living in urban areas. The global urban population is expected to grow approximately 1.84% per year between 2015 and 2020, 1.63% per year between 2020 and 2025, and 1.44% per year between 2025 and 2030.

In 2012, 73% people stay in urban areas from the 29.2 million people in Malaysia with the population density at 89 people $km^{-2}$, and the surface area is covered by 330.8 thousand people $km^{-2}$ across the country (World Development Indicators 2014). There is a conflict between creating the optimum use of land with a good quality of urban living and at the same time promoting the existence of, and opening new areas to accommodate, the urban population.

Urban growth generates many other land transitions, with several varied land use types eventually converting to urban use (Clarke & Gaydos 2010). These spatial consequences of the urban transition deserve serious study by scientists and policy makers concerned with global change because they will impact humankind directly and profoundly. Urban transitions, including land use/land cover (LULC) changes, represent one of the few certainties of global change, because it is 'certain that they are going on, and certain that they are human-caused' (Vitousek 1994).

### 1.2.2 Periodic Monitoring Land Use

In this research, monitoring was undertaken using two types of data: continuous annual series data (frequent, coarse spatial resolution) and two different years with fine spatial resolution, but imaged infrequently. Both types of data are a series of images designed to fit the purpose of monitoring. This will affect the quality, quantity and timeliness of acquired imagery (Rogan & Chen 2004).

Monitoring of land uses change, and proposed new land uses, present significant challenges for decision makers and town planners. Rapid growth

due to urbanisation and industrialisation has increased the pressure on land and the environment (including Malaysia). Also involved is the conversion of forest and agricultural land into residential, commercial and industrial land use. Many cities are expanding in all directions and this has resulted in large-scale change in the types of urban land use. It has been demonstrated that remote sensing is cost effective for urban planning (Yu & Ng 2007). In meeting the demands of ever changing urban land uses, planners have adopted new programmes and strategies. These also require refined approaches and reliable tools to monitor and forecast complex landscapes (Hay 2003; Rashed 2008; Zhang & Atkinson 2008; Zurita-Milla 2008).

Aplin (2006) stated that urban remote sensing is a powerful tool. Mapping and change detection in urban areas are difficult because anthropogenic processes operate at widely varying spatial and temporal scales. These scales, together with logistical issues, require careful planning to update land use and land cover information. Monitoring may occur over a range of temporal scales and the scale used is generally related to the purpose of investigation.

According to Jensen (2000), three types of information should be considered when monitoring the urban environment using remote sensing data;

- Firstly, a baseline classification is required to identify the presence or absence of particular land uses and land covers. This is very difficult when these are experiencing a cycle of change themselves, such as vegetation-to-clear land-to-development.
- Secondly, one needs to know the exact time when the sensor collected the data. Updated information is needed for most urban applications such as SPOT HRV pointed off-nadir and Landsat Thematic Mapper. However, monitoring urban development and change is not so time-sensitive that it requires inter-annual frequency of monitoring, and generally requires imagery to be collected only once a year.
- Thirdly, decision makers, especially political masters or land managers like town planners, require information on change. For example, local planning agencies may need precise population or disaster area estimates. Most likely for urban applications, a temporal resolution between 1-5 years is ideal for monitoring land cover or land use (LULC)

change. Preferably, subsequent datasets will be obtained at the same time of year (Mather 2004).

Temporal resolution is significant where imagery is used to monitor changing environmental conditions over time (Aplin 2006). This involves multi-temporal analysis and multiple images acquired at different times, combined for analysis for the purpose of the investigation.

### 1.2.3 Defining Spatial Resolution for Land Use Classes

Spatial resolution of remote sensing images is determined by the altitude of the platform relative to the Earth's surface and the Instantaneous Field of View (IFOV) of the sensor. There has been a historical trend of increasing spatial resolution of imaging instruments used in urban remote sensing applications which have produced substantial benefits (Fugate et al. 2010).

Spatial resolution can be either fine (*H*-resolution – finer resolution than the size of objects) or coarse (*L*-resolution coarser resolution than the size of objects) (Strahler et al. 1986). Hard classification is nearly always based on an *H*-resolution model in which measurements are assumed to be samples of energy existing from objects that are larger than the resolution cell. However, in the *L*-resolution model the objective is often to estimate the total area within a pixel devoted to particular class elements, it is possible to formulate models explicitly for proportion.

Imagery at fine spatial resolution provides greater detail and, therefore, enables the delineation of smaller features than coarser spatial resolution imagery (Aplin 2006). For further analysis, especially of land cover and land use, fine spatial resolution in remote sensing applications has made an important contribution to levels of accuracy. Image-objects can be classified corresponding to real-world entities within the geographic extent of the scene (Hay 2003) and also in choosing the relevant method.

A considerable amount of literature has been published regarding the use of spatial resolution in classification. The results show that fine spatial resolution multispectral data with approximately less than 4 m spatial resolution

performs well to achieve a separation of urban areas (land use context) through object-based classification and less so in a pixel-based classification method. Lu et al. (2011) indicated that a fusion image with 10 m spatial resolution was suitable for mapping impervious surfaces, but a TM multispectral image with 30 m was too coarse in a complex urban-rural landscape. However, coarse spatial resolution data with approximately 30 m spatial resolution are still used by researchers to contribute to urban area classification by integration with other spatial data in order to increase the accuracy of results either in estimating the proportion of classes, or the separation into hard classes.

### 1.2.4 A Spectral Framework for Land Cover and Land Use Change

Dealing with multispectral images, whether there is coarse or fine spatial resolution, there must be a sufficient spectral contrast between the objects of interest to distinguish between buildings and the surrounding landscape. Land cover is best acquired using the visible (0.4-0.7μm), near-infrared (0.7-1.1μm), middle-infrared (1.5-2.5μm), and panchromatic (0.5-0.7μm) portion of the spectrum (Jensen 2000). In urban surfaces, there are mixed materials with great diversity such as human-made features (e.g., residential, commercial and industrial area), vegetation, bright surfaces and others. Herold & Roberts (2010) stated that the spectral resolution of a sensor is determined by the number of spectral bands, their bandwidths and locations along the electromagnetic spectrum. Increasing understanding of the spectral characteristics of urban surfaces needs characterisation of the distributions and most suitable spectral bands for discriminating urban land cover type, whether through empirical reflectance or other remote sensing methods. Spectral heterogeneity at scales comparable to sensor resolution limits the utility of conventional hard classification methods with multispectral reflectance data in urban areas. Small (2001) suggested that spectral mixture models may provide a physically-based solution to the problem of spectral heterogeneity. Zurita-Milla et al. (2008) introduced multi-temporal data fusion for land cover mapping and for monitoring vegetation dynamics at fine spatial, spectral and temporal resolutions. The increased spectral variance of land cover types associated with finer spatial resolution is one of the factors identified as influencing classification accuracy (Woodcock & Strahler 1987).

## 1.3 The Aim and Research Objective

Based on remote sensing methods, the overall aim of the research in this thesis was to investigate how remotely sensed imagery can be used to monitor and forecast land use land cover (LULC) change in an urban environment in Malaysia. The specific focus in each of four separate "analysis" chapters was (objective 1) the use of object-based image analysis (OBIA) to produce a very high accuracy LULC classification at fine spatial resolution for two time points (2005 and 2009) in order to analyse change in LULC, (objective 2) to combine these imagery with coarser spatial resolution, but more frequent Landsat Thematic Mapper imagery which have been calibrated to a high standard in order to analyse the *date* of the changes, and (objective 3) to use a cellular automata (CA) type model to forecast future change in LULC (in 2013, 2017 and 2021) and compare the forecast (in 2021) to existing formal planning documents for a similar year (2020). The remotely sensed data used to fulfil these objectives were a frequently acquired Landsat TM image time-series at a spatial resolution of 30 m and infrequent (two dates) IKONOS imagery with a spatial resolution of 1m (pan-sharpened).

Eight research questions were identified, based on the overall research theme as follows:

1a. What is the accuracy with which Residential, Commercial and Industrial (RCI) land uses can be classified?

1b. Can changes in land use be identified from remotely sensed imagery, including changes in and between the RCI land use classes?

2a. Can Landsat ETM+ be used to identify the *date* of change where change is known to have occurred?

2b. Can Landsat ETM+ be used to detect multiple changes of land use where change is known to have occurred?

2c. Can Landsat ETM+ provide an 'alarm' function where change is not known to have occurred?

2d. Do the changes fall into a small number of typical classes and does this help diagnose change?

3a. Can a Cellular Automata (CA) be used to forecast future land use distributions based on observed changes in RCI land use?

3b. What does a comparison of the forecasted LULC distribution with a formal Plan of LULC in 2020 reveal about the ability to forecast, and the planning process.

## 1.4 The Research Contribution

Eight research questions needed to be addressed to support the overall research objectives. Of importance in objective 1 was the need to classify LULC to a fine level by splitting built land into the residential, commercial and industrial (RCI) LULC classes. Thus, it was of interest to explore the ability of the OBIA approach to achieve this is the Malaysian context. To achieve objective 2 it was necessary to undertake rigorous calibration of the multi-date imagery. This involved image data standardisation for each year of Landsat ETM+ imagery from 2005 to 2009. A script in the IDL programming language was developed which took into account the pixel-level changes in Landsat reflectance and stored automatically the date of change based on the multi-date Landsat ETM+ satellite sensor imagery. Under objective 3, the result of land-use changes in pixels or cells from the change analysis (objective 1) (i.e., the set of transition probabilities) enabled a simulated forecast to be generated using a CA model. While several parameters of the CA model were explored, of greatest interest was the comparison of the forecast with a formal Plan for LULC in 2020.

The significance of the findings and contributions of this research are in the process of preparing a complex land use classification (RCI) and analysis of change therein, the novel use of Landsat data to infer the *date* of LULC change and the comparison of the CA forecast with Planning Department data for the same period. All these methods are potentially useful in the practice of town planning in Malaysia.

The specific research outputs as presented in Figure 1.1 are:

a. Object Based (OB) classification of land use classes of Residential, Commercial and Industrial (RCI) from multi-date infrequent fine spatial resolution IKONOS data.
b. Change detection (CD) analysis from the multi-date OB classification results.

c. Multiple-date image calibration and standardisation.
d. Time-series of unmixed classification, brightness and greenness for monitoring using Landsat ETM+.
e. The automated monitoring of land use change by developing a programming script.
f. The automated monitoring provides an 'alarm' for when change occurs.

g. Change vector analysis in feature space (FS) to highlight the real distribution of land use classes in 2D space.
h. Combination of fine and coarse spatial resolution remote sensing data to explain the date of changes and the type of land use changes in urban landscapes.
i. The empirical result from the FS distributions explains the magnitude and direction of land use change.

j. Cellular automata (CA) model created from the OB change detection result by transition probability value.
k. Design of the CA simulation based on central cell state neighbourhood.
l. Comparison of the CA forecast with the formal Plan for LULC in 2020.

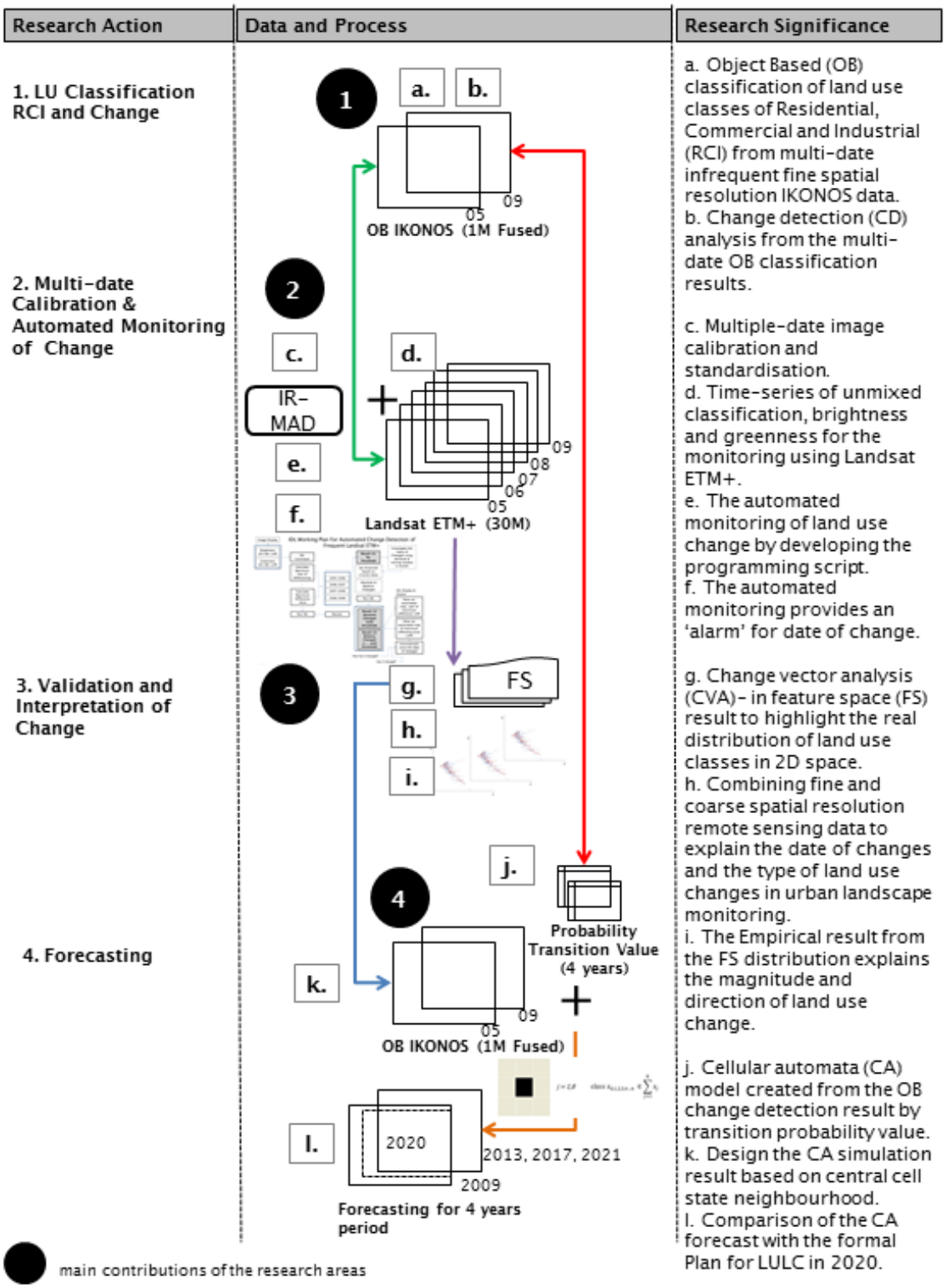


Figure 1.1 The research methodology defined at thesis level and research outputs.

## 1.5 The Thesis Structure

The thesis is organised into four major pieces of analysis and has, therefore, been presented as four individual chapters regarding classification, calibration and monitoring of change, analysis of land use change, and forecasting. The thesis is presented in ten chapters in total: introduction, town planning context, literature review, study area, four chapters of analysis, discussion and conclusion.

Chapter 1 concisely sets the context for the entire thesis by laying out the thesis theme, the aim and objectives. The town planning context in Malaysia is highlighted in Chapter 2, which is important because the final outcomes of the research will be applied by town planners.

Chapter 3 is a review that justifies the selection of methods used for classification, monitoring and forecasting. The first review is of mapping urban areas to produce a classification. The classification refers to satellite sensor imagery using pixel-based, contextual and object-based approaches for the purpose of classifying urban land use and land cover. The second review in this chapter focuses on monitoring methods, including the monitoring of land use and spectral change for urban research at large and small scales. The third review is of the use of Cellular Automata (CA) in urban simulation and forecasting. The CA method is described in the context of simulating the dynamics of change of land use and land cover so as to support planning and decision-making.

The study area is described in detail in Chapter 4. To accomplish the objectives of the thesis, the ideas needed to be grounded and tested in a real-word example. The analysis was undertaken within a study area covering Gombak District, state of Selangor, Peninsular Malaysia. Two types of remote sensing data, Landsat ETM+ between 2005 to 2009 with 30 m spatial resolution and IKONOS data for 2005 and 2009 with 1 m spatial resolution were used. The preparation of remote sensing imagery is described, including how to deal with the effects of the atmosphere on the reflectance values of the images, radiometric correction, geometric correction and normalisation.

The first analysis is in Chapter 5 entitled: 'RCI Object-Based Classification for Land Use Change Detection with Infrequent Data at Fine Spatial Resolution'. In the first part of the analysis it was considered very important to answer the two research questions; (i) what is the accuracy with which these Residential, Commercial and Industrial (RCI) land uses can be classified? and (ii) can changes in land use be identified from remotely sensed imagery, including changes in and between the RCI land use classes? Data were used from the IKONOS satellite for two different years, namely 2005 and 2009, with a 1 m spatial resolution (pan-sharpened PS data) for multiple-date classification. The research continued with change detection analysis between RCI classes for the four-year period, using a post-classification comparison: map-to-map comparison and simultaneous analysis of multi-temporal data (multi-date classification and image-to-image comparison). Both the results of RCI OB classification and monitoring of RCI change detection from the IKONOS data between 2005 and 2009 were used in the next chapter of analysis.

The second analysis in Chapter 6 involved an image calibration method that aimed to support the monitoring of changes in pixels that represented changes in land use. This second analysis is entitled 'Calibration for Automated Monitoring of Land Use Change from Frequent Data with Coarse Spatial Resolution'. The main process was to determine the success of the monitoring method using frequent satellite sensor imagery with coarse spatial resolution. Selection of Landsat ETM+ data (gap-filled) taken in series from 2005 to 2009 (annually) in the four-year period is in line with the IKONOS data that represented only two years, 2005 and 2009. Therefore, the selection of data over a four-year period was done to answer the following four research questions; (i) Can Landsat ETM+ be used to identify the *date* of change where change is known to have occurred?, (ii) Can Landsat ETM+ be used to detect multiple changes of land use where change is known to have occurred?, and (iii) Can Landsat ETM+ provide an 'alarm' function where change is not known to have occurred?, and another one research question is answered in Chapter 7. In this chapter, a number of analyses were conducted at an early stage to support a positive outcome in terms of automated monitoring of land use. Some of these analyses started with atmospheric correction to remove the effects of the atmosphere on the reflectance values of images. This is key to the calibration model and image normalisation. After that, the study was

extended through the calibration process for land use change monitoring, by estimation of proportional change and greenness and brightness that allows automated monitoring of land use and land cover.

The third analysis in Chapter 7 with the title "Validation and Interpretation of Change" aims to diagnose or identify land use change by interpreting (qualitatively) the vector direction distribution in feature space (FS). This is to answer the research question; do the changes fall into a small number of typical classes and does this help diagnose change? The feature space is defined by two related datasets (brightness and greenness) estimated by a feature extraction procedure that transforms raw data into sample vectors of some fixed length. The diagnosis is to identify the actual vector distribution of land use when it changes its position in the FS. The image space is the 2D plane of the image where pixels are located. It represents the spatial and feature space of the image. In other words, the difference of each pixel in an image can affect the differences in image space pixel distribution. On the other hand, feature space is about the reflectance values assigned to each pixel. Feature space is the space of these reflectance values; the brightness and greenness values of each pixel can be plotted in that 2D image space to analyse the direction of change from each category of land use. This section is a continuation of the monitoring of the results that were discussed to demonstrate that the results obtained from the changes are correct; the result of the object-based classification is used as the thematic monitoring change to support overall results of the occurrence of land use changes.

The Cellular Automata (CA) model was implemented in the fourth analysis in Chapter 8 with the title: 'Forecasting of Land Use Change through Cellular Automata Simulation', a final analysis to complete the whole process of this research. The CA-Markov model required as input the change that occurred between 2005 and 2009 from the raster image OB classification of two-date IKONOS satellite sensor imagery. This chapter used the OB classification in 2009 as a land use baseline and the transition probabilities for RCI to make a forecast. The objective of this chapter was to apply and explore the CA model that will be used to forecast future LULC distributions based on observed changes in RCI land use from the OB classification, as described in Chapter 5. The chapter described on a comparison of the forecasted result with a formal

Plan of LULC in 2020, an unusual opportunity afforded by access to the planning documents provided by the author.

The thesis concludes with the main findings discussed in Chapters 9 and 10. It draws conclusions and recommendations, particularly how the research may be developed further, and how the ideas of this thesis could be achieved within areas of planning practice. The limitations of this research and the future for classification of RCI, monitoring of urban land use and forecasting will be discussed, especially through the enhancement of analysis techniques in remote sensing.

# 2. Malaysia Town Planning Context

## 2.1 Introduction

According to the World Health Organization (WHO 1990), an urban area is a 'human-made' environment encroaching on and replacing a natural setting, having a relatively high concentration of people whose economic activity is largely non-agricultural. The US Census Bureau definition is more specific, defining 'urban' as areas with more than 4 people per hectare. In line with this, in Malaysia the National Urban Policy (NUP) (Federal Department of Town and Country Planning Peninsular Malaysia (FDTCP) 2006) definition of urban is when the minimum population for an area is more than 10,000 people with a density of 50 to 60 people per hectare. However, to achieve higher levels of land use efficiency, optimum use of infrastructure, public transport and to create a better quality urban environment with more parks and recreational areas, the National Physical Plan in Malaysia (NPP) (Federal Department of Town and Country Planning Peninsular Malaysia (FDTCP) 2005) presents an overall gross urban density of approximately 25 persons per hectare.

Monitoring land use change and evaluating proposed new land uses are a challenge for decision-makers and town planners. Rapid growth due to urbanisation and industrialisation processes has increased pressure on land and the environment in Malaysia. Of particular importance is the conversion of forest and agricultural land into urban land for residential, commercial and industrial use. To meet these demands and the ever-changing urban land uses, planning has adopted new programmes and strategies, which also require better approaches and more reliable tools.

In Malaysia, development is complicated, especially in the urban areas (built-up areas) that comprise residential (planned and unplanned (village areas, squatters)), commercial and industrial areas. The remedy to control the situation is to prepare a comprehensive development plan to control the uses of land and to provide the basic framework for development of new areas. In other words, a land-use plan can serve as a tool to guide development accordingly. A system for monitoring land-use change will help a lot of decision-makers to formulate future land use planning.

Urban remote sensing for land use change detection for town planning provides a fundamental tool for monitoring purposes. This provides an excellent historical framework for estimating the spatial development for certain areas. According to Singh (1989), there are two basic approaches to change detection; (a) comparative analysis of independently produced classification from different dates (post-classification comparison: map-to-map comparison) and (b) simultaneous analysis of multi-temporal data (multi-date classification and others: image-to-image comparison).

According to Somers et al. (2011), the potential of remotely sensed data analysis for monitoring processes on the Earth's surface has still not been maximised, mainly because of the problem of the composite nature of pixels. Therefore, methods of land-use change detection address the complexity of monitoring land use systems or land use management or land-use planning. These monitoring plans regulate the use of land in an attempt to avoid land use conflicts through implemented land division and use ordinances and regulations, such as zoning regulations and planning permission. The key to the monitoring of land use changes in land use planning is to ensure sustainable urban land use patterns and the preservation and conservation of environmentally sensitive areas and the green belt, including the status of forest areas (NPP 2005).

## 2.2 Land Use and Land Cover of Study Area

### 2.2.1 Town Planning and Land Use Planning in Malaysia

The history of town planning in Malaysia starting in 1912, based on the British system. In 1976, a new system of town and country planning was made available to states by the Federal Government based on the system then operating in England and Wales, involving a Structure Plan and Local Plan for development control. Nowadays, the Federal Department of Town and Country Planning (FDTCP) forms part of the Ministry of Urban Wellbeing, Housing and Local Government in Malaysia. The main objectives of the department are to strengthen the physical, social and economic development system in urban and rural areas in an effort to upgrade the standard of living in line with national policies (Bruton 2007).

Physical planning encompasses the development plan system, which consists of three major levels of planning: the National Physical Plan, the Structure Plan and the Local Plan including Special Area Plan. The other important aspect of physical planning is the fulfilment of a planning system in Malaysia. The planning system in Malaysia is provided under the Town and Country Planning Act, 1976 (Act 172) relating to the form and content of a National Physical Plan (NPP). The NPP has been produced under the authority of the National Physical Planning Council (NPPC), whereas the state-wide Structure Plans are produced by the states, and local authority-wide Local Plans are produced by the local planning Authority (Bruton 2007). The main output of development plans is the Land Use Plan, and it is used as a tool to control land use and manage and monitor development either on existing land or for future developments. In the National Physical Plan (NPP) 2005, mentioned that there are only two forms of monitoring; monitoring the policies and determining the conformity in land use between the NPP and the Structure Plan (SP). No strong methodology has been developed in the NPP for using remote sensing for monitoring rather than GIS. The urban environment encompasses all the planning processes for development plans as they take place within the spatial confinement of urban areas.

Figure 2.1 describes the four levels hierarchy of development plans in Malaysia. At the top of this planning hierarchy is the National Physical Plan (NPP). The preparation of the plan is under the Advisory Council at federal level chaired by the Prime Minister of Malaysia.

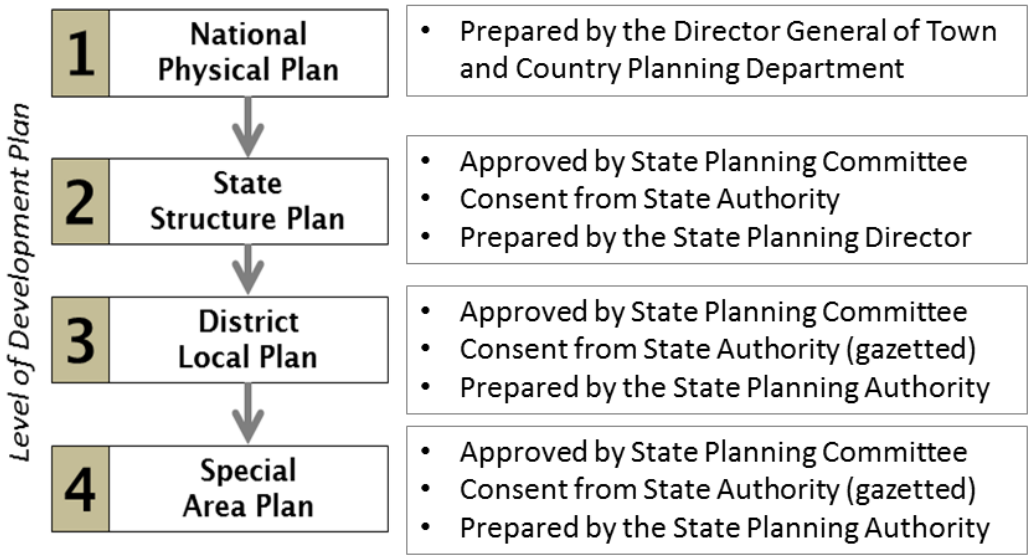


Figure 2.1 The hierarchy of development plans in Malaysia under Act 172 by FDTCP.

The NPP is a legal document containing planning strategies and policies at the national level to guide the planning activities in Malaysia between the state and local levels. NPP is prepared for a period until 2020 and has to be reviewed every 5 years in parallel with the Five Year Malaysia Plan. The NPP goals are

(i) to create an integrated strategic framework for national land use, working towards achieving developed nation status by the year 2020 through formulating planning and management policies and strategies on sustainable land use;

(ii) to ensure balanced, qualitative and effective land utilisation and development in meeting the demands of national social and economic aspects.

Figure 2.2 is the National Spatial Framework under the NPP. The land use pattern of the country is affected by historical and economic factors, where the more productive urban economic activities and concentration of population are found in the west coast areas. The Kuala Lumpur, George Town and Johor Bahru conurbations along the west coast are the most developed compared to the other urban areas of the Peninsula. In 2010, the National Physical Plan 2 (NPP-2) was launched to provide a spatial planning strategy for enhancing international competitiveness and a framework for strengthening national developmental cohesion and discipline. It added a spatial or geographic dimension to the more purely economic and social-based aspects of the

development plans. The spatial aspect of the NPP-2 will guide more effective national development planning to ensure that the national resources are used efficiently and sustainably, in particular making optimum use of existing capital and human resources.

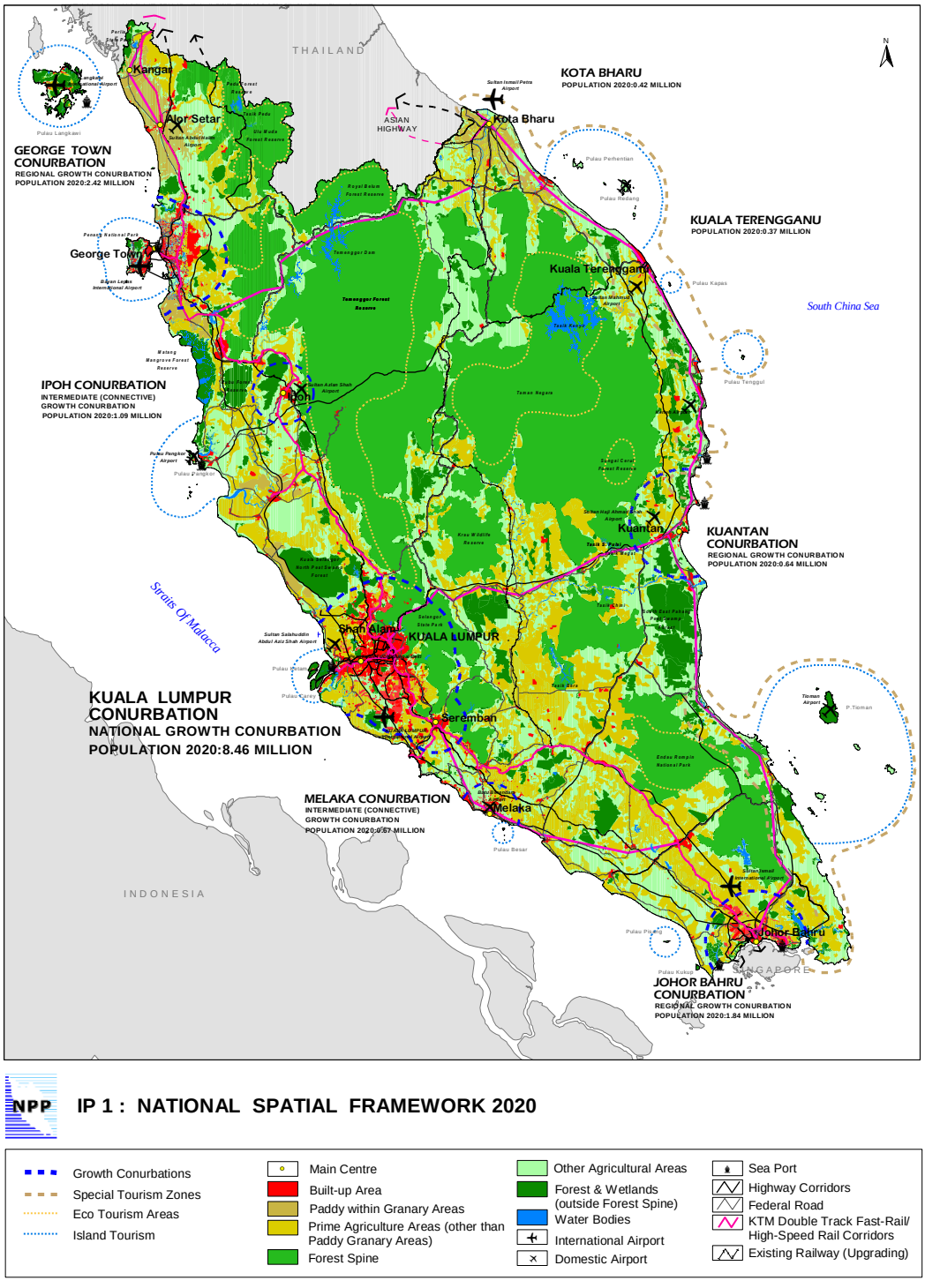


Figure 2.2 NPP; National Spatial Framework 2020 (NPP 2005).

These planning strategies and policies have been subsequently incorporated in the State Structure Plan (SSP) that covers the entire area of the states in Peninsular Malaysia. The State Structure Plan (SSP) is a written statement formulating the policy and general proposals in respect of the development and use of land, including measures for the improvement of physical environment, improvement of communications and the management of traffic of the state for a period of 15 to 20 years.

The third level is the Local Plan (LP), prepared to translate the policies and strategies from the SSP with more specific development proposals and control the land use plan for future development within the district in Peninsular Malaysia. The fourth level of the development plan is the Special Area Plan (SAP), a short term development plan for implementation purposes. The SAP is a development action plan comprising both the detailed layout within the master plan and a management plan for the implementation approaches between the implementer agencies in Malaysia. All the development plans are prepared under the Town and Country Planning Act 1976 (Act 172) including the National Physical Plan (NPP), Structure Plan (SP) and Local Plan (LP).

Town planning in Malaysia runs concurrently with the Federal Constitution and is structured parallel to the system of government. The administration system is divided into three levels: federal, state, and local levels as shown in Figure 2.3. Each level possesses its own town planning authorities. The FDTCP of the Ministry of Urban Wellbeing, Housing and Local Government formulates and administers policies pertaining to town and country planning nationally at federal level. The state level has their own state town and country planning departments, which serve as an advisory body of the all-state government in peninsular Malaysia. At the local level, the local planning authorities execute town planning functions. The Town and Country Planning Act 1976 defines a local authority as the local planning authority of a particular district or area (Mohd et al. 2009).

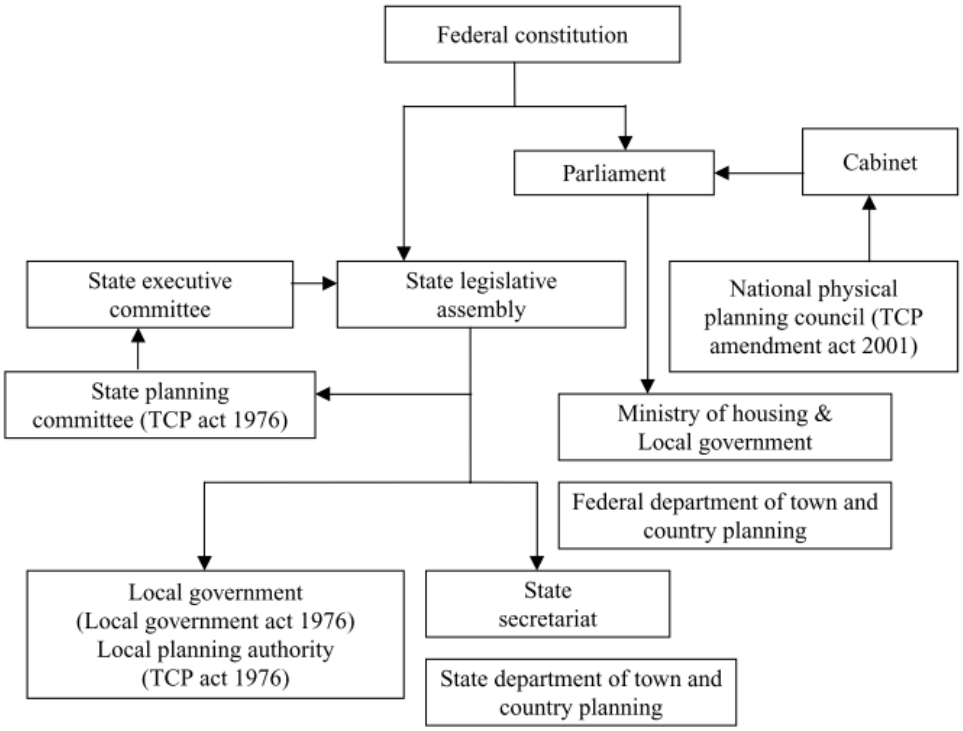


Figure 2.3 Institutional framework of the land use plan system in Malaysia (Mohd et al. 2009)

### 2.2.2 GIS and Land Use Practice by Federal Department Town and Country Planning, Peninsular Malaysia (FDTCP)

FDTCP Peninsular Malaysia has started to use Geographical Information System (GIS) software as a tool for storing and analysing the geospatial data collected in the Development Plan Studies (National Physical Plan (NPP), Structure Plan (SP), Local Plan (LP) and Special Area Plan (SAP)). Generally, the GIS database model of FDTCP is the National Land Use formed by layers of maps with the appropriate Malaysia Projection System. Database design addresses the contents, specifications, relationships and sources of data to be incorporated into the GIS database. A GIS database model defines the nature and usage of spatial (geographic) data with a database.

The FDTCP currently developed the land use portal namely JPBD Land Use Portal. The JPBD Land Use Portal has been developed to satisfy the public needs in accessing the existing and proposed land use information for planning purposes, development, property management, research, education,

monitoring and improving the public delivery system to the people. Land use portal is meant to be accessed by everyone. The JPBD Land Use Portal provides existing and proposed land use information (Zoning) in all the development plans prepared under the Town and Country Planning Act 1976 (Act 172) including the National Physical Plan (NPP), Structure Plan (SP) and Local Plan (LP). Data sources are always the most challenging task in building up a GIS. All the land use information in the Land Use portal is extracted from development studies conducted during the 8th Malaysia Plan programmes, including NPP, SP and LP. Other data are obtained from other government agencies in Malaysia involved with physical development.

In 2009, Quantum GIS (QGIS) was promoted by FDTCP as a suitable desktop GIS for adoption by this of geospatial mapping and analysis software as its user-friendliness makes it easy to use in a subject as complex as GIS (Wahab 2011). It will be an enormous saving for the government in terms of millions of ringgits since proprietary GIS are expensive. FDTCP found that to optimise the QGIS-GRASS (Geographic Resources Analysis Support System) it is best to use QGIS software for the mapping tool and GRASS as the analytical tool. Until today, this open-source software has been used for the land use plan preparation as the GIS medium in FDTCP. Besides the land use plan preparation, the software is also used for monitoring. With respect to physical planning, there is a professional need to constantly monitor land use development so that existing and proposed land use are in line with mandatory development plans and that relevant authorities at the micro lot-base level, the local planning authority (LPA), is responsible for ensuring that happens (Wahab 2011). The exercise concluded there are still limitations in current GIS to effectively monitor the land use development from past periods. Beyond this, site surveys must be carried out to confirm the actual situation on the ground, in order to confirm any changes in land uses classes. Selamat et al. (2012) state that the use of GIS in town planning can develop databases for spatial analysis. From the database development system, it can analyse planning needs according to the FDTCP. Its findings showed that the implementation of GIS in town planning can improve the resulting plans based on the quality of the method, saving time, and costs, and data can be obtained faster.

The current practice of the FDTCP in using satellite sensor images for planning depends on manual interpretation and is very subjective. Without elevation

information, some buildings were difficult to differentiate from other similar objects, and some non-buildings and buildings were incorrectly classified. In 2008, one of the core businesses of FDTCP was to become a National Land Use Information Centre. FDTCP is leading the way in land use preparation through development of the plan for Peninsular Malaysia. The conceptual framework of the National Land Use Information Centre is a compilation of the spatial data on land use in Peninsular Malaysia in a GIS-based format, involving standardised classifications of land use from the general and strategic to the most detailed, involving lots of information on the use of land for the State level. Information sharing among the four systems (Figure 2.1) will be crucial. Standardisation in terms of land use classes, scale, naming and colour schemes, using complementary GIS platforms has been developed by FDTCP so that the three components can be fully integrated and that data flows seamlessly from one subsystem to another.

Coordination requirements for the preparation of the GIS database for the Structure Plan and Local Plan are important. This coordination needs to ensure that there are no problems of integration between all prepared development plans. The coordination is also necessary to ensure that the data produced are accurate and correct. Effective urban planning requires different up-to-date information for development plan preparation. Currently, this information is mostly acquired by field surveys or from digitised aerial imagery. Many urban objects that are characteristic of urban structures can be recognised in the identified surface material map.

### 2.2.3 Land Use Classification Prepared by the FDTCP

Current land use information of urban areas is essential for urban planning and for other purposes. Urban land use patterns change rapidly in response to economic, social and environmental forces. Timely information on land use change is the basis for the formulation of policy in anticipation of the problems that accompany growth. In addition, there is also a need to project future land use patterns as they support the analysis of urban development pressures. The existing land use classification is under 'Manual of Geospatial Data Management December 2013, (FDTCP 2013)' that is used by FDTCP in the development plan. 13 categories of land use and land cover have been

developed as part of the National Land Use Information System project. The classification has been published by State Government and Local Government to provide a framework for harmonising existing classifications, to facilitate consistent collection and reporting of land use information and to provide a basis for creation of national data sets. In preparing the data layer of land use, land use classification (amendments) December 2013 should be consulted (FDTCP 2013). This is to ensure that the details or attributes are included in the database by the classification specified. Preparation of a land use plan without the complying classification set will complicate the coordination of information on land use for the rest of Peninsular Malaysia. The database will create diversity and store metadata of land use classification attributes. The practice of land use classification by the department is the same as that proposed by Anderson et al. (1976), using appropriate terms and it follows the correct LULC types in a local context.

In preparation of the land use plan, satellite sensor image data are used to update the relevant information to determine the location of land uses such as agriculture, forests, rivers, streams and roads. The satellite sensor data also need to be georeferenced to coordinate and project the overlay layer onto the basic plan. Satellite image data are used to assist easier and faster preparation of the land use data layer. However, data or information from satellite images still needs to be checked through field work to ensure data accuracy of land use.

Table 2.1 FDTCP Peninsular Malaysia practice with 13 Main Categories of Land Use Classifications (FDTCP 2013).

| Land Use Categories | |
|---|---|
| **Level 1** | **Level 2** |
| 1. Residential | Planned<br>Unplanned |
| 2. Industrial | Planned<br>Unplanned |
| 3. Commercial and Services | Planned<br>Unplanned |
| 4. Institutions and Public Amenities | |
| 5. Open Space and Recreation | Open Space<br>Sport and Public Amenities<br>Green Area |
| 6. Vacant Land | Natural<br>Man-made |
| 7. Transportation | |
| 8. Infrastructure and Utility | |
| 9. Agriculture | Oil Palm plantation<br>Rubber plantation<br>Paddy plantation |
| 10. Breeding and Aquaculture | |
| 11. Forest | |
| 12. Water Bodies | |
| 13. Beach | |

- **Residential**

Two categories of residential land use are defined as planned and unplanned. Planned residential includes all categories of residential areas such as land housing including detached house or bungalow, terraced houses, semi-detached and cluster homes. Each title is in lots or units of individual homes.

The strata of residential building types except detached dwellings, detached and terraces, provide many residential units in multi-storeys and has a separate title for each unit (Strata Title). Buyers only have part of the housing units, and buildings, parks and other facilities are owned and managed by the 'resident's corporation (buyer)'. Any structured village is part of planned residential land use. Normally, a village using less than 0.40469 hectares of land is classified as a residential village.

Unplanned residential land use includes the urban traditional village that normally accommodates a large number of people living with irregular physical conditions (slum area). Another unplanned residential land use is a traditional village catering for the rural population, and the density level is low. The settlement distribution is influenced by local economic activities such as agriculture, mining or fishing.

Residents in urban or suburban squatter settlements do not have real rights over land ownership. Squatters' villages have temporary status and only appear in the current land-use plan. It is assumed that squatters will be moved to another development in the future.

- **Industrial**

Planned industrial land use is defined based on proper planned building at industrial parks which have categories of medium, heavy, special, service and cottage industry in Malaysia. Medium industry is that which produces daily waste, noise, odour and gas in the manufacturing process. The activities using the most dangerous raw materials need to be located quite far from the residential areas creating a buffer such as "Physical Buffer" and "Green Buffer" of 200 m.

Heavy industry involves working with raw materials and waste products as well as contaminants in solid, liquid or gas. They have a high risk in terms of fire, explosion, pollution and environmental biology, for example. Heavy industry is placed in areas far away from residential areas and requires a buffer zone such as the "Physical Buffer" and "Green Buffer" of 500 m.

Special Industry involves heavy industry, using high and sophisticated technology and it uses raw materials in the process of manufacturing. The

services industry is an industry such as a vehicle repair workshop, painting workshop and so on. This industrial activity is based on human skills and less technology and machinery. Another planned industrial land use is cottage industry, a small-scale enterprise undertaken within the area provided and usually at the village level for activities such as shrimp paste, crackers and so on.

Unplanned industrial areas refer to the same activities as normal industry, but the difference is in using temporary buildings or the area is not suitable for industrial activities.

Overall, the industrial land use category is that which deals with the processing and storage of raw materials and the production, storage, and distribution of manufactured goods.

- **Commercial and Services**

Planned and unplanned commercial and services urbanised areas encompass retail activities, professional business activity and institutional services. The historic commercial and business centre of an incorporated city usually consists of a high-density mixture of commercial, business and institutional uses. Single purpose land uses within the district, such as exhibition halls, stadiums, parks, etc. that are larger than the minimum mapping size, are assigned to separate categories. The retail shops include shopping centres of all sizes and regional shopping malls.

The other retail and services class is individual establishments involved with the sale of consumer goods and services. These activities most commonly occur in strip commercial development along major roads, although not limited to that setting. It includes historic “neighbourhood” business districts as well as banks, restaurants, motels, hotels, household storage facilities and junkyards. It also includes entertainment and indoor recreational facilities that are frequently associated with commercial developments, such as indoor or drive-in movie theatres, miniature golf, driving ranges, go-cart racing, tennis clubs, bowling alleys, and recreation halls.

The dominant land use consists of offices for professional business activity including office complexes, office parks, research parks and high-rise office towers outside of the central business district. Commercial buildings within an office park, such as motels and restaurants, are assigned to the retail category.

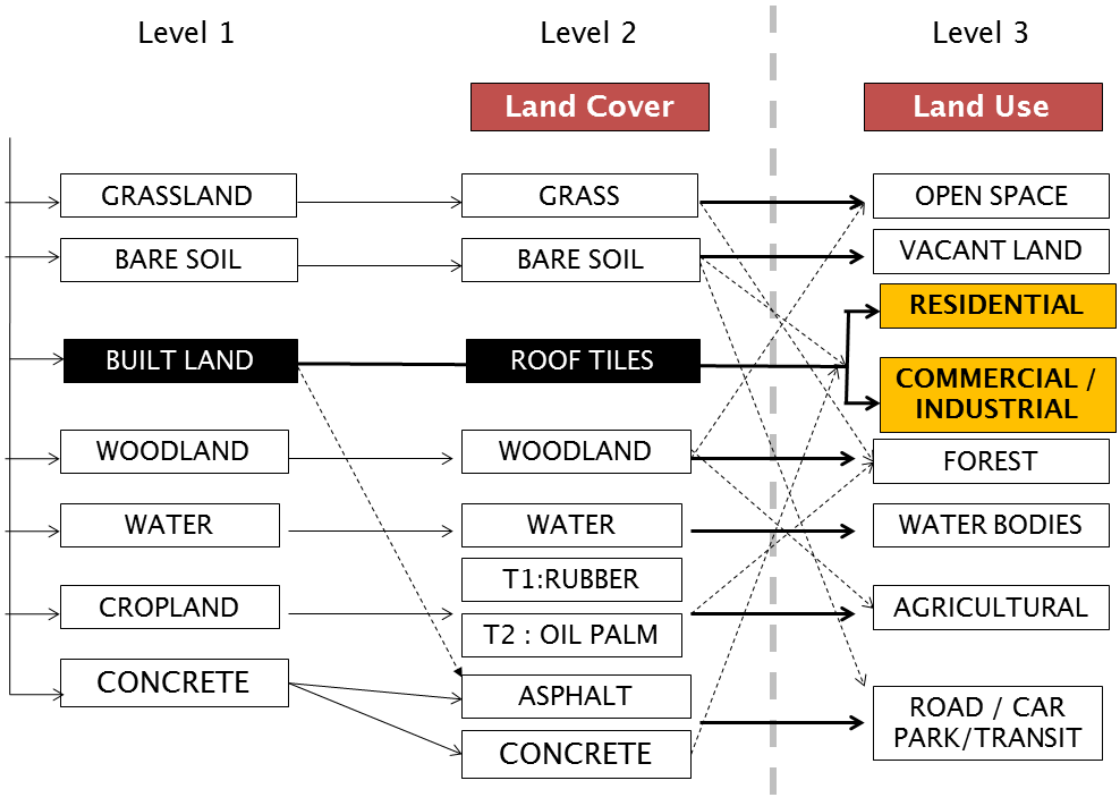


Figure 2.4 Aggregated land use and land cover (LULC) categories based on the objective of the classification (Anderson 1976 & FDTCP 2013).

Figure 2.4 shows the land use and land cover (LULC) categories. The land cover categories in Levels 1 and 2 are the basis of the land use classification categories in Level 3) which are adopted in this research. These aggregated LULC categories are based on remotely sensed data using the first phase of the classification procedure in chapter 5. Regarding a suggestion by Anderson et al. (1976), the classification system was developed to meet the needs of Federal and State agencies for an up-to-date overview of land use and land cover throughout the country. This is on a basis that is uniform in categorization at the more generalised first and second levels and that will be receptive to data from satellite and aircraft remote sensors.

- **Aggregate Classifications: Built-up land (Building), Bright Surface, Vegetation and Water Bodies**

Built-up land is comprised of areas of intensive use with much of the land covered by structures. Included in this category are cities, towns, villages, strip developments along highways, transportation and communications facilities, and areas such as those occupied by residential, commercial and industrial uses. Another aggregated classification finding in Figure 2.4 is the three categories of bright surface, vegetation and water bodies. Bright surfaces are defined as including vacant land areas, bare land areas and concrete covered areas such as roads and car parks. The second classification is vegetation, including open space and recreational areas, forestry, and agricultural areas including land used for raising livestock or under cultivation for food production purposes. Also included is land devoted to the cultivation of ornamental plant material. The third classification is water bodies Identified as either natural or human-made basins that usually contain water on a permanent basis.

## 2.3 Conclusion

The advent of satellite remote sensing has now made it possible to obtain in context of land cover, which is land use classification to produce a map. By detecting land use through remote sensing images with homogeneous features will be interesting after long time has been explored to identify them as objects are interested in the scene and interpreting. Urbanisation become is challenges for planners and urban managers. They must be able to predict the growth area as well as its magnitude to formulating spatial policies for the development. Land use information is an important component in the spatial context of town planning. The expansion of urban areas to accommodate housing demand and in a way contributed to the conversion of agricultural land and sensitive areas for urban use. This shows land use reflected the activities on the ground to reflect the amount of space may be situated and shaped for development of areas.

# 3. Methods

## 3.1 Introduction

This chapter will discuss methods that are relevant in land use and land cover classification, monitoring and forecasting of RCI for town planning purposes, using multispectral remote sensing data. This is achieved by assigning pixels (containing digital numbers) to land cover types (LULC classes) (Campbell 2006). Remotely sensed imagery is classified (using infrequent and multi-date series data) to allow monitoring and forecasting. The level of accuracy of RCI can be assessed during the classification analysis.

In this study context, the classification refers to satellite sensor imagery using pixel-based, contextual and object-based approaches for the purpose of classifying urban land use and land cover. The second review of this chapter focuses on monitoring methods, including the monitoring of land use and spectral change for urban research at large and small scales. The third review is of the use of Cellular Automata (CA) in urban simulation and forecasting. The CA method is described in the context of simulating the dynamics of change of land use and land cover so as to support planning and decision-making.

## 3.2 Classification Methods

This section explores the role of classification methods for improving urban land use classification, using satellite sensor imagery to discriminate residential (R), commercial (C) and industrial (I) land use for generating thematic interpretation. Many methods of land cover classification have been established by many researchers and pioneers. In this chapter some of these methods using parametric or non-parametric classifiers will be explored to rest their relevance to the urban classification approach.

The major steps of image classification in this research include exploration of previous pixel-based, contextual and object-based classification methods. Mather & Brandt (2004) highlight the requirement of the user to perform the

following: (i) to determine a priori the number and nature of categories in which the land cover is to be described and (ii) assign numerical labels to pixels based on their properties using a decision-making procedure, usually termed a classification rule or decision rule. Aplin et al. (1999) used pre-defined boundaries through 'per-parcel classification' or 'per-field classification' related to context and texture considerations in land use classification.

Foody & Mathur (2004) identify many of the problems in mapping land cover noted in the literature relating to methods used to accurately extract land cover information from discrete imagery, whether from the early work based on basic classifiers such as the minimum distance to means algorithm (MDM), sophisticated statistical classifiers such as the maximum-likelihood classification (ML), non-parametric classifier neural network (ANN) and support vector machines (SVMs).

Figure 3.1 below shows the conceptual model of urban land use classification from land cover determinations. The strategy derived to identify land cover (form) from multispectral remote sensing images uses the pixels' (spectral) value to infer land use (function), represented as objects (spatial) in the second order of the classification. However, the methods of land use classification are not straightforward when spatial and spectral information contribute to context, statistical or geo-statistical methods. Researchers in urban land use classification use it as guidance to choose the best method for urban land use classification. Section 3.2.1 describes a pixel-based image analysis method relevant to urban remote-sensing and Section 3.2.3 is an object-based image analysis commonly described from the segmentation of the image into individual objects to form an object-based classification.

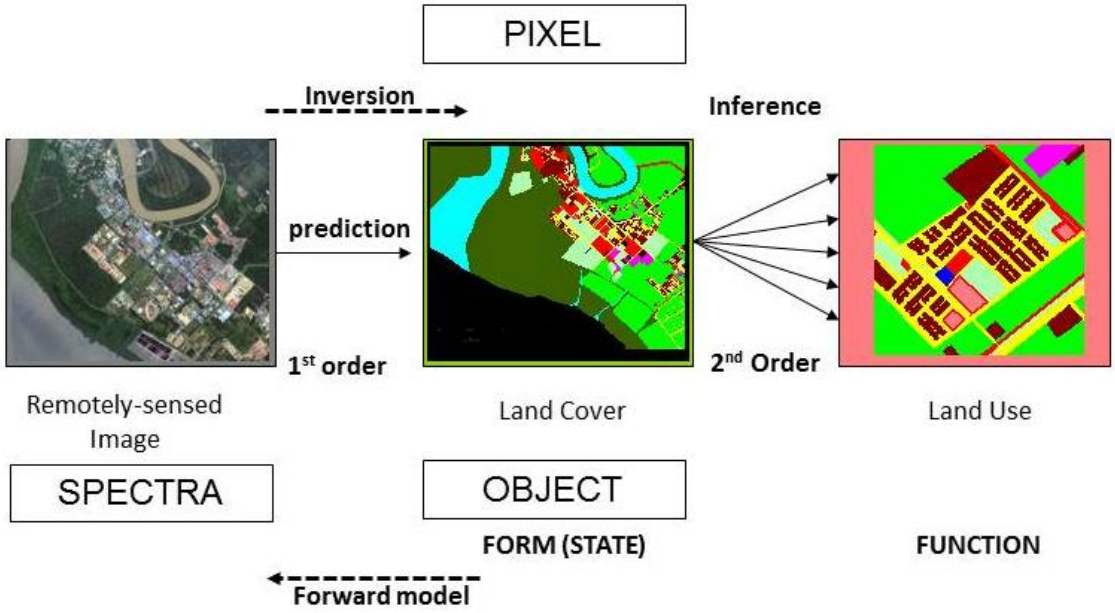


Figure 3.1 Model of urban land use classification.

Figure 3.1 shows the overall methods that were developed in various scientific disciplines to handle and quantify remote sensing data, used to capture information about urban land use from pixels or objects based on inversion and forward model. At the first level, it shows that remotely sensed images can produce LULC through inversion, for example, through direct interpretation or through image classification analyses to organise data into land use categories. Then, this model can predict or infer *land use* based on spatial context, for example, by an analyst (supervised classification) or automatic clustering (unsupervised classification) in a desired number of categories (e.g., the residential (R), commercial (C) and industrial (I) land uses).

A summary of published literature is shown in Table 3.1. The maximum likelihood (ML) is the most popular method for land cover or land use classification, using a pixel-by-pixel classification algorithm or integration with two dimensions with spectral and spatially mixed pixels to producing better results in pixel and context.

Table 3.1 A summary of major contributions to the study of urban classification from multispectral remote sensing images using per-pixel and object-based classification methods.

| **Category** | **Methods** | **Author** |
|---|---|---|
| Urban area discriminate : **per pixel classification** | Artificial Neural Network | (Lloyd et al. 2004), |
| | Artificial Neural Network & Maximum Likelihood | (Berberoglu 2000), |
| | Decision Tree, | (Huang et al. 2010), |
| | Linear Spectral Mixture Analysis & Expert Rule Based Approach | (Lu & Weng 2006) , |
| | Maximum Likelihood & Back Propagation (BP) Neural Network | (Ji 2000) |
| | Principal Component Analysis (PCA) | (Owen et al. 2006), |
| | Multilayer Perception (MLP) Neural Network | (Bellens et al. 2008), |
| | Maximum Likelihood & Hierarchical Fuzzy Classification | (Shackelford & Davis 2003) |
| Urban area discriminate : **object-based classification** | Maximum Likelihood & Object-Based | (Bhaskaran et al. 2010a), (Geneletti & Gorte 2003), (Wang,L. et al. 2004), (Walter 2004), (Bouziani et al. 2010), |
| | Object-Based (Knowledge Based) | (Taubenböck et al. 2006), (Herold et al. 2003), (Zhou & Troy 2008), (Bauer & Steinnocher 2001), (Sims & Mesev 2007), (Rizvi et al. 2010), |
| | Object-Based & Support Vector Machines (SVMs) | (Li et al. 2010), |
| | Nearest Neighbour / Fuzzy Membership Function | (Jacquin et al. 2008) |

*Contd….*

| Category | Methods | Author |
|---|---|---|
| Residential & Commercial/Industrial **(RC/I) classified : per pixel classification** | Maximum Likelihood & Expert System Approach | (Kahya et al. 2010), |
| | Support Vector Machines (SVMs) Classifier | (Tuia et al. 2009) |
| Residential & Commercial/Industrial **(RC/I) classified : object-based classification** | Object-Based Classification & Rule Based | (Ban et al. 2010), |
| | Object-Based & Vegetation Proportion (V-I-S) | (Stow et al. 2007) |

### 3.2.1 Pixel-Based

Pixel-based classifications produce the best results for single class classification through the traditional per-pixel classifiers, although they may lead to 'salt and pepper' effects in classification maps. The major methods related to pixel classification are the methods of minimum distance to means, maximum likelihood, artificial neural network, random forests, spectral angle mapper, decision trees and support vector machine.

In other words, pixel-based classification as a traditional classifier typically develops a signature by combining the spectral value of all pixel sets from remote sensing imagery (Lu & Weng 2007). Commonly, results of pixel-based classification ignore the mixed pixel problem. Land use classification needs to produce a unique reflectance value for a specific land cover based solely on spectral properties in order to identify the class.

One major drawback of this approach is contextual information. In context with other measurements, further information might be derived. Context can be defined along three different dimensions: i) the spectral; ii) the spatial; and iii) the temporal dimension (Fung et al. 1990).

**Minimum Distance to Means (MDTM)**

The method classifies data into the class whose known or estimated distribution most closely resembles the estimated distribution of the sample to be classified (Wacker & Landgrebe 1972). The method is adapted from a mean clustering algorithm that determines a pixel's label as the minimum distance between the pixel and the class centres, measured either by Euclidean distance or the Mahalanobis generalised distance.

Training samples are used in supervised classification to classify the spectral data in a thematic map with several possible explanations about land cover class that each pixel is allocated to single class. The area estimation by hard classification may produce large errors, especially for coarse spatial resolution data due to the mixed pixel problem (Lu & Weng 2007).

In practice, the minimum (mean) distance classifier works well when the distance between means is large compared to the spread (or randomness) of each class with respect to its mean. It is simple to implement and is guaranteed to give an error rate within a factor of two of the ideal error rate, obtainable with the statistical, supervised Bayes's Classifier. However, the method is used to assign each pixel to thematic classes and as a result the classification of this homogeneous image is still based on spectral information.

**Maximum Likelihood (ML)**

Characteristics of the Maximum Likelihood (ML) classification are defined through supervised classification as a classification technique (also MTDM etc.). Sufficient reference data must be available and used as training samples with the parameters (e.g. mean vector and covariance matrix). The signatures generated from the training samples are used to classify the spectral data into a thematic map. This method uses parametric classifiers and one of its characteristics is that the Gaussian distribution is assumed. Classifiers often produce 'noisy' results with a complex landscape (Lu & Weng 2007).

Another possible difficulty with this method is that the per-pixel classifier typically develops a signature by combining the spectral information of all training-set pixels from a given feature. The resulting signature contains the contributions of all materials present in the training-set pixels, ignoring mixed pixel problems. In another major study, Aplin et al. (1999) and Aplin &

Atkinson (2001) used the ML method with classification per-pixel to per-field (spatial data) of delineation of urban area as the methods to solve the mixed pixels. The results showed an urban area successfully classified with an accuracy of more than 85 per cent. Another contribution, Berberoglu (2000) and Ji (2000), used ML methods alongside other methods (e.g. artificial neural network) to discriminate urban areas through a pixel based approach.

Besides the pixel wise approach, ML methods have been combined with object-based classifications (Bhaskaran et al. 2010; Geneletti & Gorte 2003; Wang et al.2004; Walter 2004; Bouziani et al. 2010). For urban land use classification, ML can be strongly justified for use in discriminating multiple classes of pixel. However, the method by itself does not give the most accurate results for urban classification and other procedures need to be incorporated. Kahya et al. (2010), studied urban land use classification using a combined per-pixel Maximum Likelihood method and expert system. The results showed the residential area remarkably well classified with an overall accuracy up to 90 per cent.

**Artificial Neural Network (ANN)**

Artificial Neural Network (ANN) usually called Neural Network (NN) is one of several artificial intelligence techniques that have been used for automated image classification as an alternative to conventional statistical approaches. The method is a per-pixel approach with a non-parametric classifier that does not involve parameters such as the mean vector and covariance matrix in calculating class separation. The method is suitable for incorporation of non-remote sensing data into classification procedure (Lu & Weng 2007). There were no significant differences between other pixel-based classification methods with disadvantages related to influence on misidentification of an individual training sample pixel.

**Support Vector Machines (SVMs)**

Support Vector Machines (SVMs) perform very well with multi-dimensional data or other remote sensing data such as DEM or raster data, forming the input to a classifier (Watanachaturaporn et al. 2008). The classification from a non-parametric classifier is likely to be better than that obtained from a parametric

classifier. Foody & Mathur (2004) provided in-depth analysis of SVM classifications, showing them to be more accurate than comparable classifications derived from other classification techniques. However, the classification accuracy is only based on general data and is not specific to classification of urban areas. Tuia et al. (2009) explored SVMs to classify residential and commercial areas separately and the overall accuracy was less than 50 per cent. However, through integration with spatial data such as the cadastral map, aerial imagery and ground survey, the overall accuracy assessment increased to above 80 per cent. From this observation, based on the per-pixel classification of SVMs, it was distinctly classified when the spectral data was integrated with the spatial data.

**Spectral Mixture Analysis (SMA)**

Some researchers (Zurita-Milla et al. 2008 & Lu & Weng 2006) adopted the term Linear Unmixing Spectra and some refer to Spectra Mixture Analysis (SMA), both aiming to unmix the multispectral or hyperspectral variability in the heterogeneous landscape. The goal of SMA is to 'unmix' the relative proportion of end members assumed to be correlated with the area covered by each material present. The concept of an unmixing processor in the majority of pixels in remotely sensed imagery is assumed to be a spatial average of spectral signatures from two or more surface categories or end members. Boucher & Kyriakidis (2006) stated that the spectral unmixing procedures only determine the fractions of such classes within a coarse pixel without locating them in space. Super-resolution or sub-pixel mapping aims to provide a fine resolution map of classes, one that displays realistic spatial structure and reproduces the coarse resolution fractions. Atkinson et al. (1997) compared three techniques for mapping the sub-pixel proportions of land cover classes in the New Forest, U.K.: (i) artificial neural networks (ANN); (ii) mixture modelling; and (iii) fuzzy c-means classification.

The original design of unmixing or using a sub-pixel classifier is not appropriate for urban mapping, since it was originally designed to identify the percentage distribution of different land cover at a coarse resolution (Asner & Heidebrecht 2002). However, since 1989, linear unmixing has been used to discriminate urban classes, especially human features and it is one of the most appropriate methods to use. Rashed et al. (2003) mapped the resultant end

member fractions into four main components of urban land cover: Vegetation, Impervious surfaces, Soil, and Water/Shade. The mapped fractions were validated using aerial photos. Dealing with land use is different from land cover and characterisation of urban land cover remains a challenge in remote sensing applications because of the complex landscape. Ridd (1995) and Gluch & Ridd (2010) introduced the fundamental V-I-S (Vegetation-Impervious-Soil) model to characterise, map and quantify the composition of urban environments. The urban landscape can be characterised as a continuous surface of V-I-S components and can be resolved at the sub-pixel level using the SMA technique to derive the sub-pixel abundance of each land cover component (Rashed et al. 2003). The success of this method is dependent on a priori knowledge of the required components.

According to Zurita-Milla et al. (2009), this method depends heavily on a proper identification of the main components present in the scene and their pure spectra. The key to successful SMA is appropriate end member selection of the model inputs and results reveal that this modified approach to end member selection provides physically realistic spectral end members that in many cases represent purer components than could be found in any pixel in the image scene (Elmore et al. 2000; Tompkins et al. 1997).

### 3.2.2 Contextual Classification

Many methods related to context classification have been developed and the essential application is associated with spectral information (pixel) and spatial information (shape, texture, etc.) to perform the analysis and produce the best result with the statistical algorithm. Once spatial features are extracted, any per-pixel classification algorithm can be used.

Contextual classification in urban remote sensing is an important component of the characterisation of spatial form (Gong & Xu 2006). However, there are no clear specific direction classifiers used to discriminate urban features such as residential from commercial areas. Any method regarding per-pixel such as maximum likelihood, minimum distance to means or artificial neural network classification will perform well through a combination of the contextual

algorithm in the processing classification, which is pre-processing or post classification using the statistical method.

Section 3.2.1 emphasised the major problem of pixel isolation in discriminating spectral classes and making labelling without contextual information. Three dimensions – spectral, spatial and temporal – were highlighted as contributing to contextual information (Fung et al. 1990). However, for the purpose of the classification, two dimensions – spectral and spatial – were used. The spectral dimension refers to different bands of the electromagnetic spectrum to improve the separation between various ground cover classes compared to image data. However, the spatial context is defined as correlations between spatially adjacent pixels in spatial neighbourhood pixels through class labels.

### 3.2.3 Object Based Classification

This section explains in detail the method of object based classification of urban land use. Bauer & Steinnocher (2001) stated that the conventional supervised classification techniques were poor at discriminating between urban land use categories but they still supplied reliable results for mapping the required land cover objects within the scene. The vital concept of an object based classification is that the important information essential to interpret an image is not represented in single pixels, but in meaningful image objects and their mutual relationship. Image-objects are defined by Hay et al. (2001) as basic entities, located within an image that is perceptually generated from high resolution pixel groups, where each geographical relationship models the real-world scene component.

The benefit of choosing an object-based classification with the capability of analysing shape and context is that this is neglected in pixel based classifications (Blaschke et al. 2006). In short, the method is one of the appropriate approach to identifying human-made features such as urban land use (e.g. residential, commercial/industrial).

Several researchers have demonstrated that object-based approaches are superior to per-pixel analysis in discriminating urban land cover (e.g.

Bhaskaran et al. (2010a); Wang,L. et al. (2004); Walter (2004); Bouziani et al. (2010); Taubenböck et al. (2006); (Herold et al. 2003) ; Zhou & Troy (2008) ; Bauer & Steinnocher (2001) ; Sims & Mesev (2007) ; Rizvi et al. (2010) ; Li et al. (2010) ; Jacquin et al. (2008)). According to Ban et al. (2010) and Stow et al. (2007) object-based analysis successfully discriminated residential and commercial classes within urban land cover.

The object-based approach to remote sensing aims to overcome the inaccuracies of pixel-based approaches by incorporating the spatial domain (Corcoran et al. 2010). In addition, through the use of fine spatial resolution data, identification of the object to be classified. The introduction of fine resolution data from satellites has opened up the possibility of capturing highly detailed land-use classifications of the Earth's surface (Aplin et al. 1999).

Stow et al. (2007) has demonstrated a segmentation and hierarchical classification approach applied to high spatial resolution multispectral satellite data, with the goal of delineating residential land use polygons and identifying low and high socio-economic status of neighbourhoods. Two types of object-based classification strategies were tested, one based on spatial frequency characteristics of multispectral data, and the other based on proportions of Vegetation- Impervious-Soil sub-objects. However, far too little attention has been paid to identifying, mapping and monitoring RCI from high spatial resolution satellite data.

Blaschke (2010) states that object-based classifications are able to aggregate pixels to segments to objects and to address objects characteristics through sub-objects, allowing one to explicitly treat various kinds of 'within-patch heterogeneity', which enables applications in studying forest gaps, vegetation patchiness or landscape complexity. Rizvi et al. (2010), In order to avoid the time-consuming 'trial-and-error' practice while seeking for significant class separating object features approaches towards an automatic feature extraction were used.

**Principle and Method of Object-Based Classification**

In object-based classification methods, a crucial step is image segmentation, known as multi resolution image segmentation. Image segmentation is the partitioning of an array of measurements assuming homogeneity, and it involves the division of an image into spatially continuous, disjoint and homogeneous regions (refer to Figure 3.2).

Baatz & Schäpe (2000) used a novel algorithm which not only has spectral properties but also has region-based metrics of shape, texture, structure, size and context. These automatically extract all objects of interest into group segments. One of the most significant features regarding image segmentation is that algorithms need to address a certain scale and use thresholds which usually embrace the summed variation of all bands used.

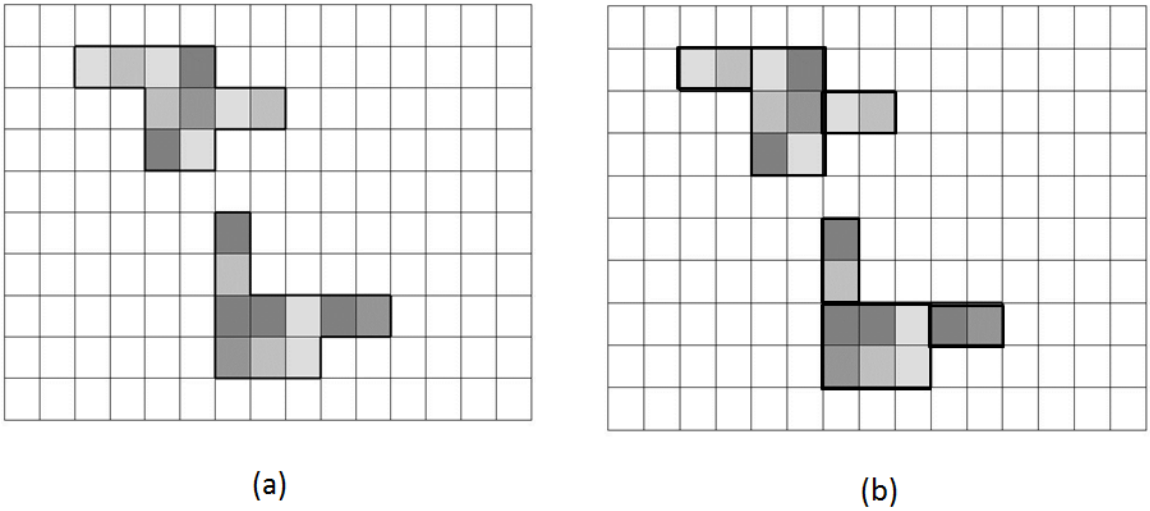


Figure 3.2 Criteria of homogeneity through a combination of parameters; (a) Spectral homogeneity by colour (mean spectral value); (b) Similarity in form or shape (geometric form of the object) adapted from (Schöpfer et al. 2010).

According to Thomas et al. (2003), the most important parameter in image segmentation is the scale representing the relative size of output polygons. Image segmentation involves colour, smoothness and compactness are all variable as one parameter defined as within-segments heterogeneity (flexible and a trade-off between homogeneity in spectral domain and spatial domain), which applied depends on the desired output.

$$f = w \cdot h_{color} + (1 - w).h_{shape} \quad (3.1)$$

Where $f$ is the heterogeneity criterion, also called scale factor, $w$ is the user defined weight for colour with $0 = w = 1, h_{color}$ is the colour criterion, and $h_{shape}$ is the shape criterion.

$$h_{shape} = w_{cmpt}.h_{cmpt} + (1 - w_{cmpt}).h_{smooth} \quad (3.2)$$

The shape criterion consists in two parameters: the smoothness and the compactness criterion. They have to be mixed using the user defined weights with $0 = w_{cmpt} = 1$ being the user defined weight for the compactness criterion (Definiens Imaging 2003).

$$h_{Smooth} = n_{Merge} \cdot \frac{I_{Merge}}{b_{Merge}} - (n_{Obj1} \cdot \frac{I_{Obj1}}{b_{Obj1}} + n_{Obj2} \cdot \frac{I_{Obj2}}{b_{Obj2}}) \quad (3.3)$$

$$h_{Smooth} = n_{Merge} \cdot \frac{I_{Merge}}{\sqrt{n}_{Merge}} - (n_{Obj1} \cdot \frac{I_{Obj1}}{\sqrt{n}_{Obj1}} + n_{Obj2} \cdot \frac{I_{Obj2}}{\sqrt{n}_{Obj2}}) \quad (3.4)$$

Where $n$ is the object size, $I$ object perimeter and $b$ the perimeter of the bounding box. Where $Merge$ is referring the action to combine to form a single entity and $Obj$ is the object (feature) to selected. However, in new version of Definiens software is eCognition Developer 8 they have 2 parameters needing to be defined by the user regarding the segmentation process which is colour, $0 = w = 1, h_{color}$ to produce greater emphasis results of image objects and scale, $5 = w = 250, h_{scale}$ which is the higher value, will tend to create larger objects as the segmentation result. Frauman & Wolff (2005) examined the relationship between the size of objects contained in the image and the heterogeneity criterion defined by the user as the best segmentation threshold before any other image analysis. As the result, is not indicating the 'ideal' or best scale factor to a user define for the best segmentation result between the two parameters.

In order to identify objects using segmentation object-based classification, there are two different classification methods; (1) classification based on samples and (2) classification based on the integration of prior external knowledge stored in rule bases. According to Ban et al. (2010), the object-based classification classified land use classes of residential and commercial through integration with the rule based approach. Overall accuracy was more than 87 per cent and showed that integrating knowledge is adequate to overcome spectral similarities when differentiating between urban and rural geographical features.

**Combination of OB Classification**

The core objectives of this research were to classify RCI through object-based classification methods. Using previous research, it is intended to evaluate the methods used in urban remote sensing to classify the detailed land use, especially RCI.

Ban et al. (2010) and Stow et al. (2007) used object-based analysis to successfully discriminate residential and commercial classes from urban land cover using the combination approach. The object-based classification involved a nearest neighbour (NN) classifier especially to discriminate vegetation areas produced from the sample. However, the result was not good based on spectral information alone and based on limitations of NN, a rule-based approach was used to reduce misclassification with similar spectral properties.

Besides rule-based approaches, other combination object based classifications have been used, with the V-I-S model (Vegetation-Impervious surface -Soil) to characterise, map and quantify the ecological composition of urban areas (Stow et al. (2007); Gluch & Ridd 2010). As the results from Stow et al. (2007) have shown, the proportion of V-I-S land-cover sub-objects within objects produced a map with an accuracy that was essentially identical to the distribution and patterns of general land-use types.

Johnson et al. (2013) proposed a method involving hybrid intensity-hue-saturation smoothing filter-based intensity modulation (IHS-SFIM) pan

sharpening approach to obtain more spatially and spectrally accurate image segments.

Amarsaikhan et al. (2009) included apartments, residential houses, industrial buildings and all other building areas in the building area class, because on the remotely sensed images it was not possible to distinguish among these classes because of their very similar spectral characteristics in pixel classification. However, using ground truth data and knowledge about some local areas they can be observed. Alberti et al. (2004) used a supervised classification approach with a spectral unmixing (pixel classification) approach to discriminate among urban land cover classes and to perform a land cover change analysis at the regional and watershed scales. Remote sensing imagery needs to be converted into tangible information which can be utilised in conjunction with other data sets, often within widely used Geographic Information Systems (GIS) (Blaschke 2010). Objects and classification results can be stored in either raster or vector formats, which is integration which other software GIS as post processing approach (Schöpfer et al. 2010; Blaschke et al. 1995).

### 3.2.4 RCI Classification

In order to identify the objects through segmentation and object-based classification, two different classification methods can be used: (1) classification based on training samples and (2) classification based on the integration of prior external knowledge stored in rule bases.

Object-based classification based on training samples is exemplified by nearest neighbour (NN) classification. The NN classifier returns a membership value of between zero (not true) and one (true), based on the image object's feature space distance to its NN (Definiens AG 2009). NN Classification is used to declare image objects to be significant members of a certain class. The NN algorithm then finds image objects that resemble the samples. The concept of a NN sample classifier is similar to a partitioning concept (Figure 3.3). For a given query sample image object, the algorithm works by first descending the tree to find the data samples lying in the segment that contains the query sample object as the class label for the unknown $x_1$. An example is $x_1 \geq t_1$,

where the class is positive and identifies the class label $\delta$ and where, $x_1 < t_1$, the class is negative and it falls under a different class label $\varepsilon$. The classifier returns a membership value of between zero and one. Based on the image object feature space distance to its nearest neighbour, the membership value has a value of one when the image object is identical to a sample (1=positive sample). If it is not identical, this means there is no membership and has a value of zero (0=negative sample). If the image object differs from the sample, the feature space distance has a fuzzy dependency on the feature space distance to the nearest sample of a class. The user can select the features considered for the feature space.

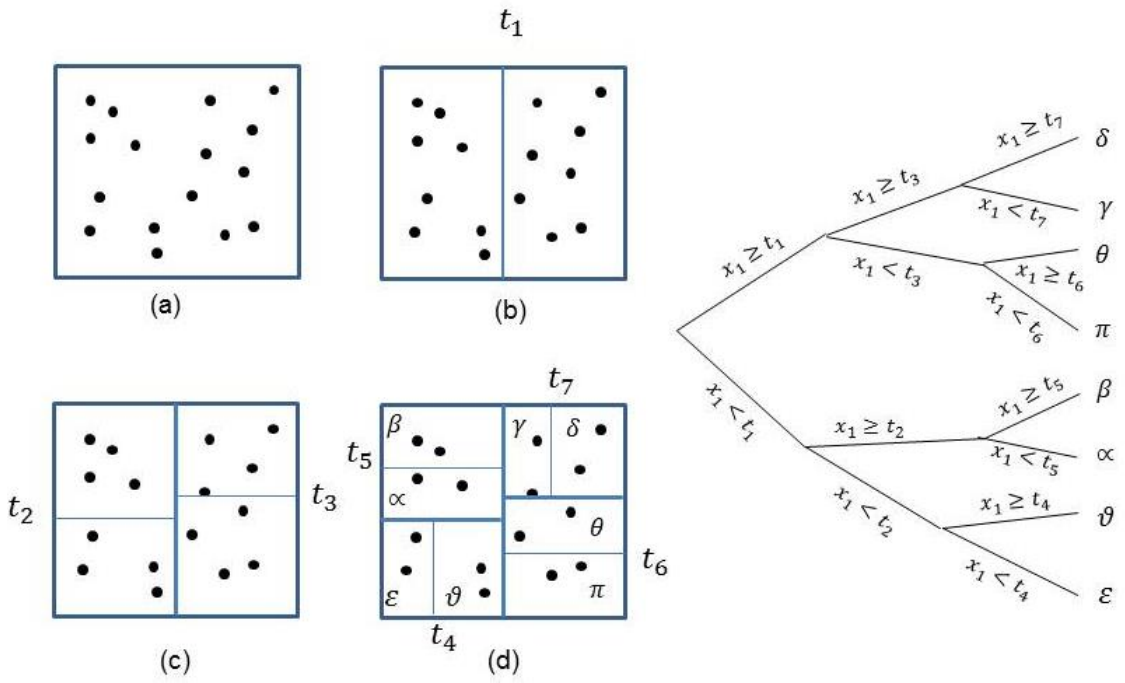


Figure 3.3 Nearest neighbour (NN) sample partitioning.

### 3.2.5 Change Detection Analysis of RCI Classification

In urban remote sensing, post-classification change detection using the most popular methods produces a land use change map based on a simple classification overlay. Change detection is the process of identifying differences in the state of an object or phenomenon by observing it at different

times. Essentially, it involves the ability to quantify temporal effects using multi-temporal data sets. One of the major applications of remotely-sensed data obtained from Earth-orbiting satellites is change detection because of repetitive coverage at short intervals and consistent image quality (Anderson 1977, Singh 1989).

According to Aspinall and Hill (1997) there are two major sources of uncertainty in the change detection process regarding (a) slivers resulting from misalignment of boundaries of land cover polygons and (b) false positive change associated with classification errors in the production of the land cover map. This means that the accuracy of change detection is dependent on the accuracy of individual classification. Singh (1989) showed that the comparative performance of various techniques in different environments must be evaluated quantitatively; otherwise those interested in monitoring changes in a specific environment may not achieve optimal results because of lack of knowledge about tried and tested procedures of change detection.

The overall process of change detection methodology is explained in Figure 3.4 and Figure 3.5. It consists of overlaying the classified images for comparison. The cross-classifier using two images from different times allows the analyst to know the extent and nature of changes in land use - the transition between different land use classes and corresponding areas of change.

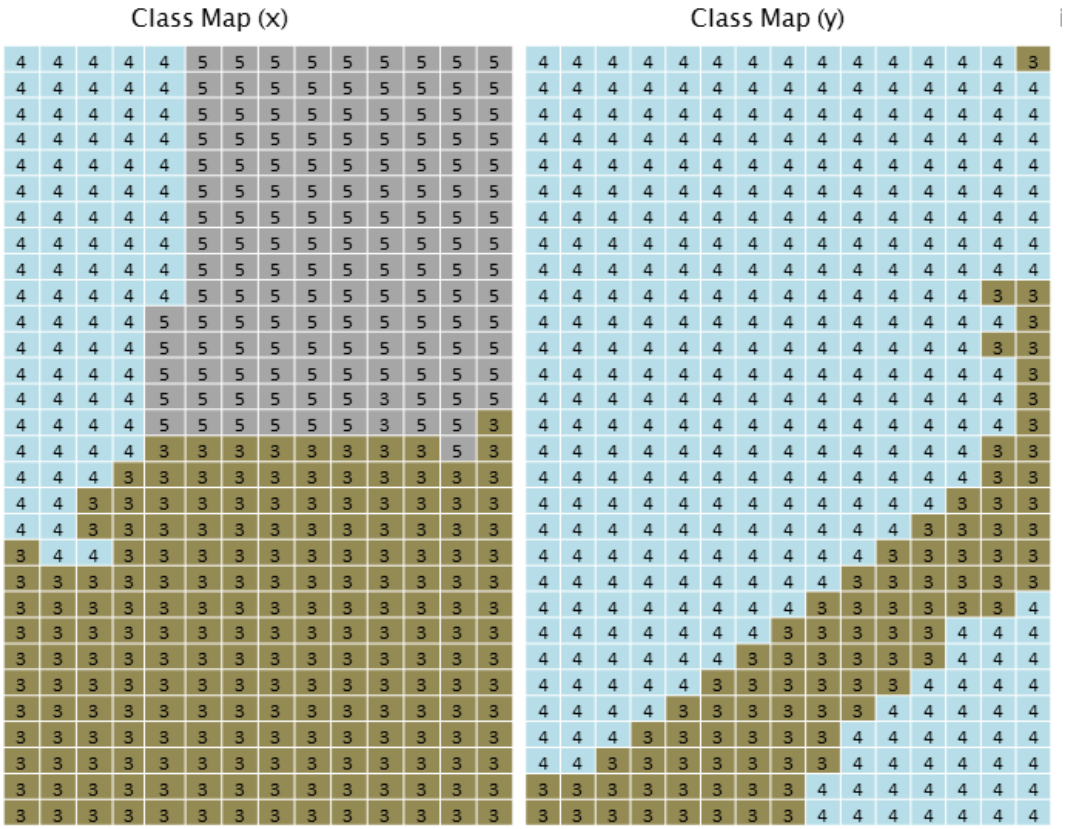


Figure 3.4 Illustration of method of land use change detection based on post-classification analysis with independent classification maps.

i. Count the cross value between map x,y

| x \ y | 1 | 2 | 3 | 4 | 5 | 6 |
|---|---|---|---|---|---|---|
| 1 | 0 | 0 | 0 | 0 | 0 | 0 |
| 2 | 0 | 0 | 0 | 0 | 0 | 0 |
| 3 | 0 | 0 | 81 | 112 | 0 | 0 |
| 4 | 0 | 0 | 0 | 79 | 0 | 0 |
| 5 | 0 | 0 | 8 | 140 | 0 | 0 |
| 6 | 0 | 0 | 0 | 0 | 0 | 0 |

ii. Transition Probability Matrix p(t)

| x \ y | 1 | 2 | 3 | 4 | 5 | 6 |
|---|---|---|---|---|---|---|
| 1 | 0 | 0 | 0 | 0 | 0 | 0 |
| 2 | 0 | 0 | 0 | 0 | 0 | 0 |
| 3 | 0 | 0 | 0.419 | 0.581 | 0 | 0 |
| 4 | 0 | 0 | 0 | 1.00 | 0 | 0 |
| 5 | 0 | 0 | 0.05 | 0.95 | 0 | 0 |
| 6 | 0 | 0 | 0 | 0 | 0 | 0 |

$$p(t)=\frac{m}{n}$$ $m$ is number of class transition (map x,y), where $n$ is the number of counts across the relevant row

(3.5)

Figure 3.5 Transition matrix table of change $p(t)$ (shown in ii) based on normalising the count of cross values between independent pixels (i).

## 3.3 Monitoring: Change Detection and Image Differencing

Urban remote sensing–land use change detection for town planning especially involving human activities–provides a fundamental monitoring function through temporal resolution and offers an excellent historical framework for estimating the spatial development and growth for certain areas. As Guttenberg (1959) wrote many years ago, 'Land use' is a key term in the language of city planning. According to Singh (1989), there are two basic approaches for change detection;

a) Comparative analysis of independently produced classification from different dates (post-classification comparison: map-to-map comparison).
b) Simultaneous analysis of multi-temporal data (multi-date classification and others: image-to-image comparison). In urban remote sensing, post classification change detection is the most popular method to produce a land use map with a simple overlay of the classified map.

Somers et al.(2011) observe that the full potential of remotely sensed data analysis for monitoring processes on the earth surface is still not fully employed because the main reason is the composite nature of pixels. Therefore, land use change methods can only represent part of the complexity of the land use system, management or planning. The latter regulate the use of land in an attempt to avoid land use conflicts through implementing land division and use ordinances and regulations, such as zoning regulations and planning permission.

In order for change detection methods to be successful, the time-series data must be standardised for condition of real surface change. In addition, differences in the sensor, solar illumination or atmospheric conditions make it difficult, if not impossible, to accurately compare satellite images acquired on different dates and/or different platforms. To ensure the appropriate use of time-series data for change detection, radiometric normalisation is required. Normalisation can be addressed by performing an atmospheric correction of each image in the time series. Modifying imagery for atmospheric attenuation reduces the variation between temporally separate images, so they appear to

have been acquired under the same solar and atmospheric conditions, allowing for more accurate detection of landscape change. As a result, it is widely recognised that a set of remotely sensed images must be radiometrically normalised before being used in change detection analysis. Hence atmospheric correction for a single date image is often equivalent to subtracting a constant from all pixels in a spectral band (Song et al. 2001) & (Bakr et al. 2010).

However, in a two-image change detection analysis, the effect of atmospheric correction is on the same relative scale (corrected or uncorrected).
When comparing multispectral images of a given scene taken at different times, it is desirable to correct the pixel intensities as much as possible for uninteresting differences such as those due to illumination, atmospheric condition or sensor calibration. If comparison is on a pixel by-pixel basis, then the images must also be co-registered to a high accuracy (close to the true value) in order to avoid spurious signals resulting from misaligned pixels (Canty 2010).

Canty & Nielsen (2008) developed the Multivariate Alteration Detection (MAD) procedure which uses two band multispectral images of the same scene acquired at different times. The method assumes both images generally to have pixel intensities with a zero mean. The iteratively reweighted MAD (IR-MAD) algorithm introduced by Canty (2010) to evaluate the normalisation procedure, holds back one-third of the no change pixels for testing purposes. These are used to calculate means and variances before and after normalisation and also to perform statistical hypothesis testing of equal means and variances of the invariant pixels in the reference and normalised target images. Results are given in the Landsat ETM+ 2005 image with the target images showing no change in the test pixels. The significant values (*P*-values) for the *t*-test for equal means and for the *F*-test for equal variances indicate that the hypotheses of equality cannot be rejected for any of the spectral bands. Using this method, the only differences between reference and target images will be due to random effects like instrument noise and atmospheric fluctuation. However, in this case the atmospheric correction was done for the reference image, and some of the differences were taken into consideration. The multivariate alteration detection (MAD) is an algorithm from Nielsen et al. (1998) and this was extended to include an iteratively reweighted multivariate

alteration detection (IR-MAD) by Nielsen (2007). This is the inverse application of change detection, in which unchanged pixels are used for automatic relative radiometric normalisation of multi-temporal imagery. The IR-MAD can be done in an iteration scheme in which, when calculating the means and covariance matrices for the next iteration of the MAD transformation, observations are weighted by the probability of no change determined at the preceding iteration (Canty 2010).

### 3.3.1 Post Classification Change Detection

In urban remote sensing, post classification change detection methods produces a land use map with a simple overlay of the classified map. Aspinall and Hill (1997) highlighted two major sources of uncertainty in the change detection process: (a) slivers resulting from the misalignment of boundaries of land cover polygons and (b) false positive change associated with misclassification errors in the production of land cover maps. However, the accuracy of change map is highly dependent upon the accuracy of classificationand all the errors within the independently classified maps will be transferred to change map and for example, if two land-cover maps each have a producer's accuracy of 90%, the accuracy of the post-classification change map accuracy will be about 81% (Stow et al. 1980).

Change detection can be performed by supervised or unsupervised approaches (Singh 1989). Both classification techniques, including the object based classification require very good accuracy and information about the spatial and spectral signatures of the changes that occur in the considered area between two dates to perform post-classification change detection. To control the quality of post-classification image to image differences, researchers suggest the data need registration, calibration and atmospheric correction (Alberti et al. 2004) & ( Amarsaikhan et al. 2009) and some researcher skip these step if the data remote sensing as long as the training data and the image to classified are on the same relative scale (Song et al. 2001) & (Bakr et al. 2010).

Tehrany et al. (2013) presented a space-borne satellite-based approach to demonstrate urban change and its relation to land surface temperature (LST) variation in urban areas of the Klang valley, Malaysia. For this purpose an object-based nearest neighbour classifier (S-NN) approach was first applied on the classified maps which were then used as inputs to perform the post classification change detection.

### 3.3.2 Vegetation Index Comparison

Another combination method for the purpose of monitoring change is the Normalised Difference Vegetation Index (NDVI). According to Small & Lu (2006), SMA offers the advantage of providing estimates of real vegetation abundance that can be compared directly to other measures of vegetation cover per unit area. However, Zurita-Milla et al. (2003) used the time series data to compute land cover specifically using NDVI and other methods, to show consistent patterns for each of the land cover types under investigation. This creates new opportunities to monitor vegetation dynamics (phenology) at high spatial and temporal resolution. The specific function of NDVI was used for monitoring change and indicated when change occurred. Vegetation indices (Vis) take advantage of vegetation's reflective contrast between the near infrared (NIR) and visible red (VIS) wavelength. Nutini et al. (2013) used a supervised classification approaches to test differences between a spectral classification of single Landsat data, a temporal classification of normalised difference vegetation index time series from Landsat images, and a two-step classification integrating both these approaches for analysis of vegetation cover.

### 3.3.3 Change Vector Analysis and Tasselled Cap

Change vector analysis is a technique to analyse changes in vector position between magnitude (type of change) and direction (time or period) (Malila 1980). The method is not a stand-alone one, but works in combination with multi-date pairs of spectral measurements of red and NIR bands in NDVI, or 'greenness' and 'brightness' spectral in the Tasselled Cap (TC) transformation method. All the analysis performed well in change vector with the spatial

registration of multi-date data, spectral transformation and normalisation, spatial entity selection (individual vs. clusters of pixels), logic interpretation and level of application (stratification, classification, measurement). In this study, the TC transformed method has input to change vector analysis. Baisantry et al. (2012) developed a systematic approach to detect and describe different types of changes in brightness and greenness presented in feature space. Figure 3.6 illustrates the change vector describing the change of land use and stores the date of change. Smits & Annoni (2000) stated that the performance of the change detection is completely defined by the end user's requirements and depends mainly on the choice of the reference texture transitions (features). The user's knowledge about the change detection problem is contained in a database for both change and no-change cases of the area.

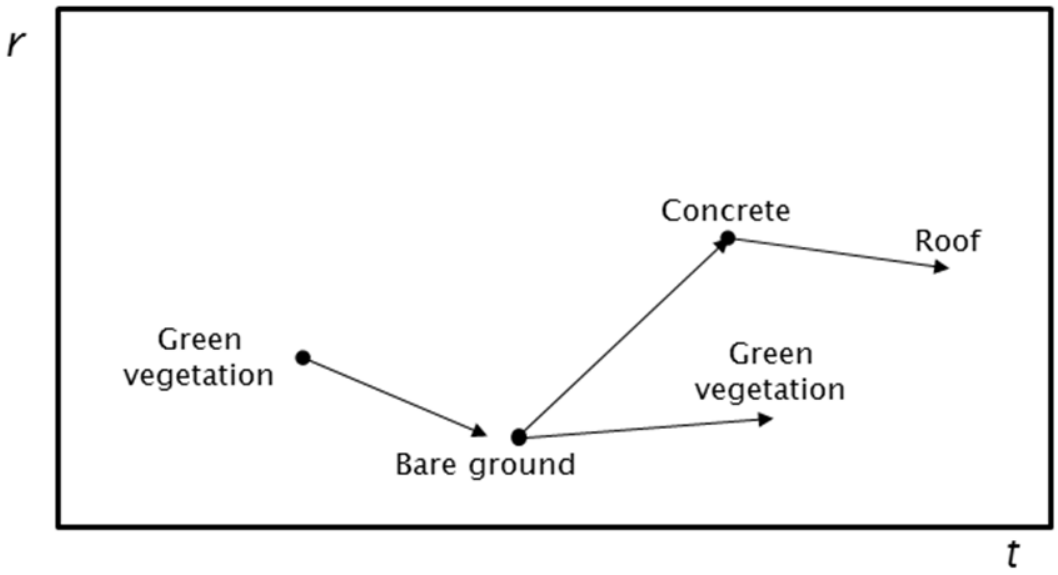


Figure 3.6 Illustration of data to tell the situation of monitoring prediction between *r* (reflectance) and *t* (period or year).

The Scientific Investigation Report 2012-5057 by Yamamoto & Finn (2012) from US Department of the Interior and U.S Geological Survey, used the Tasselled Cap transformation as a method of image band conversion to enhance spectral information. It is primarily used to detect vegetation using the derived brightness, greenness, and wetness bands for the Advanced Land Imager and was compared with the Landsat Thematic Mapper Tasselled Cap

values. Silva & Tagliani (2012) described the land change prediction model for planning and composite satellite images were obtained using a Tasselled Cap transformation in Brightness, Greenness and Moisture bands.

Gómez et al. (2011), calibrated radiometrically normalised imagery from Landsat sensors and used two metrics derived from the Tasselled Cap Transformation components, greenness and brightness, to generate the Tasselled Cap Angle (TCA). The TCA is a measure of the proportion of vegetation to non-vegetation (the occupation state), and its derivative, the Process Indicator (PI), a measure of change in this proportion through time. Baisantry et al. (2012) present a systematic approach to detect and describe different types of changes in satellite imagery using change vector analysis (CVA) and a unified change or no-change threshold method using principal component difference (PCD) and inverse triangular function. The Kauth-Thomas Tasselled Cap transformation rotates the MSS data plane such that the vast majority of data variability is concentrated in two features which are directly related to physical scene characteristics. Brightness is a weighted sum of all the bands, and can be defined in the direction of principal variation in reflectance. It thus measures total reflectance. The second feature, greenness, is a contrast between the near-infrared bands and the visible bands. High Greenness values represent targets with high densities of green vegetation, while the flatter reflectance curves of soils are expressed in low Greenness values. Further, it is a linear transformation maintaining the affine relationship between the raw data. The transformation is invariant and consistent over different data sets. Fraser et al. (2011) described a change detection method suitable for long term analysis of northern vegetation at local to regional scales. It employs a temporally dense stack of Landsat TM/ETM+ imagery time series to reveal trends in reflectance indices associated with vegetation and other physical changes to the landscape. The Tasselled Cap brightness, greenness, and wetness indices, representing linear transformations of the optical channels, are analysed for per-pixel trends using robust linear regression.

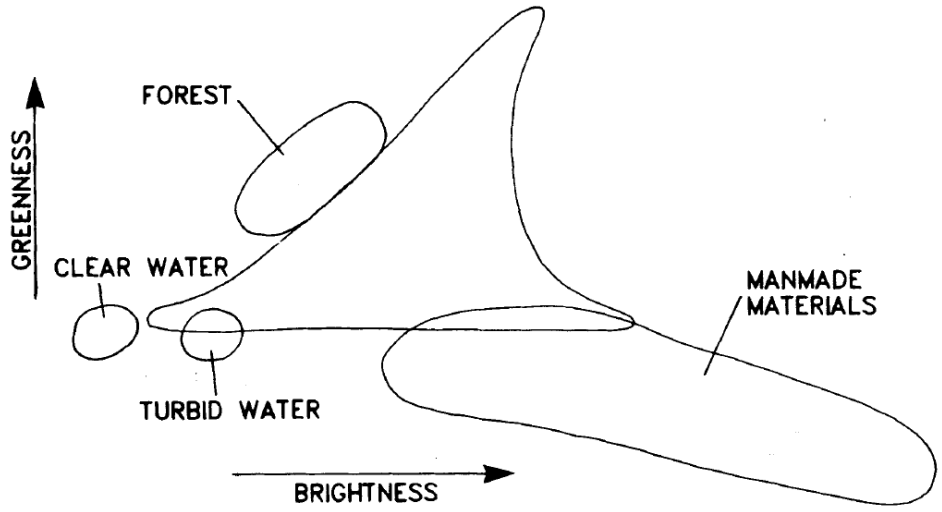


Figure 3.7 The Plane between human made (manmade materials) in brightness (TC1) and vegetation (forest) in greenness (TC2) views (Crist & Cicone 1984).

Regarding Crist & Cicone's (1984) investigation in Figure 3.7, when chlorophyll-containing leaves are exposed to sun, they absorb most of the blue and red light in the visible spectrum thus appear green to the human eye, but reflect a high amount of near infra-red (NIR) wavelengths. Annual range of reflectance in the visible spectrum is 4.0 - 6.9% for urban vegetation and 8.1 - 9.6% for built-up areas.

The result of the Tasselled Cap transformation is that, tasselled cap band 1 (TC1) matches the overall brightness of the image. The second tasselled cap band (TC2) matches "greenness" which is commonly used as a photosynthetically active vegetation index. The third tasselled cap band (TC3) is often interpreted as an index of "moisture" (eg, soil or surface moisture) or "yellow" (i.e., the number of dead or dry plants).

Table 3.2 The Landsat 7 multispectral Tasselled Cap coefficients transformation.

| | TM Band | | | | | |
|---|---|---|---|---|---|---|
| | 1 | 2 | 3 | 4 | 5 | 7 |
| Brightness | 0.3561 | 0.3972 | 0.3904 | 0.6966 | 0.2286 | 0.1596 |
| Greenness | -0.3344 | -0.3544 | -0.4556 | 0.6966 | -0.0242 | -0.263 |
| Third (wetness) | 0.2626 | 0.2141 | 0.0926 | 0.0656 | -0.7629 | -0.5388 |
| Fourth | 0.0805 | -0.0498 | 0.195 | -0.1327 | 0.5752 | -0.7775 |
| Fifth | -0.7252 | -0.0202 | 0.6683 | 0.0631 | -0.1494 | -0.0274 |
| Sixth | 0.4 | -0.8172 | 0.3832 | 0.0602 | -0.1095 | 0.0985 |

"Greenness" or "brightness" bands can be used to determine threshold values above which a given surface could be considered vegetation or built-up. Kauth & Thomas (1976) called this transformation process the "tasselled cap transformation" (TCT) of Landsat data for the quantification of greenery, as shown in Table 3.2. The validity of the procedure to quantify greenness was shown by Crist & Cicone (1984) using actual and simulated TM data. Extensive use of TCT has been made in recent years to quantify agricultural as well as urban greenery. Crist and Cicone calculated that the six bands of reflected TM data effectively occupy three dimensions, defining planes of soils, vegetation and a transition zone between them. The third feature called wetness relates to canopy and soil moisture.

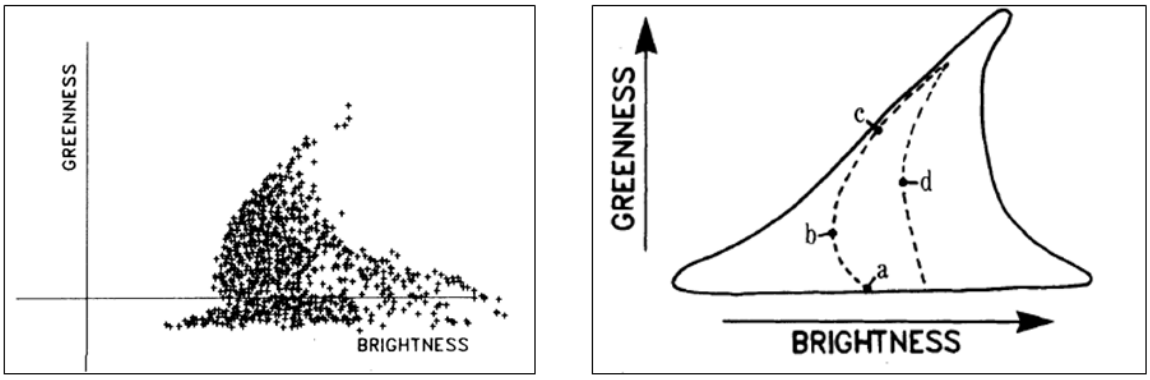


Figure 3.8 Real data of TM Tasselled Cap transformed data between TC1 (brightness) and TC2 (greenness) in the plane simulation view. Point descriptions: (a) bare soil, (b) greening up, (c) full canopy closure, (d) senescence (Crist & Cicone 1984).

Figure 3.8 and Figure 3.9 described the result of TC1, TC2 and TC3 bands are directly associated with physical scene attributes and are easily examined. The TC1 band is weighted as the sum of all six bands and can be interpreted as the overall brightness or albedo. The TC2 band primarily measures the contrast between visible bands and near-infrared bands and is similar to a vegetation index. The TC3 band measures the difference between the weighted sum of the visible band and near-infrared bands and the mid-infrared bands as band 5 and band 7 in Landsat ETM+, it is sensitive to moisture and water absorption. The TC3 band also can be diagnosed as a measure of soil and plant moisture.

i. Brightness (TC1)

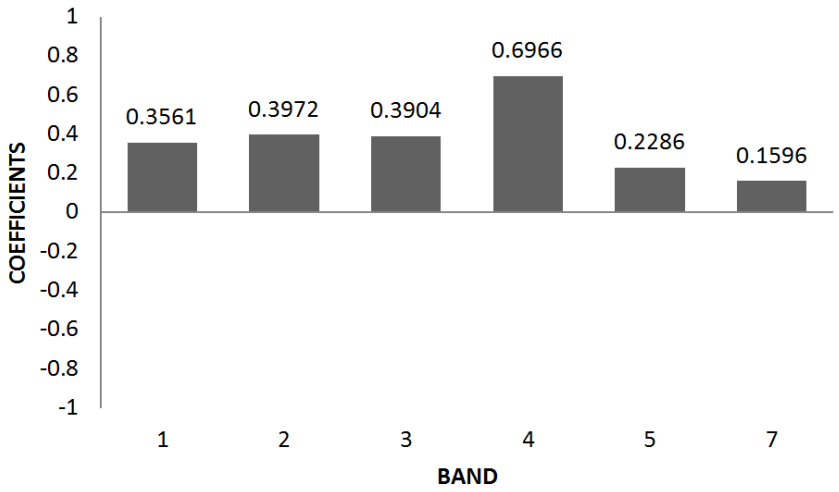


ii. Greenness (TC2)

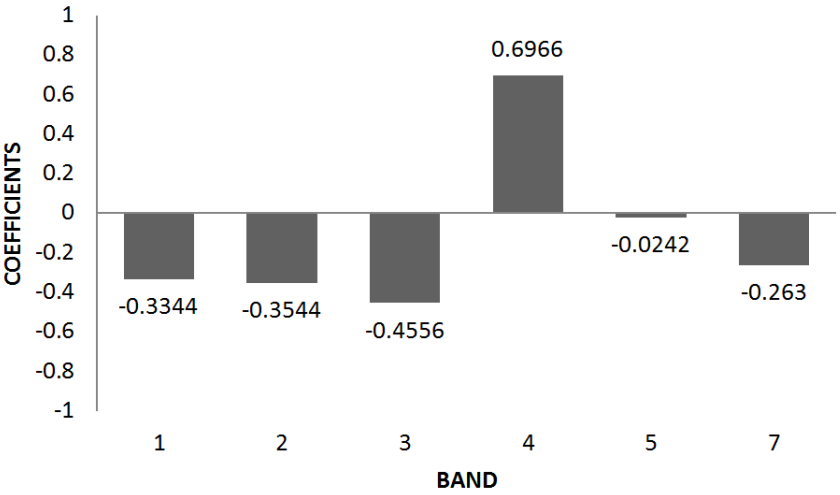


Figure 3.9 The Landsat ETM+ Tasselled Cap (i) brightness and (ii) greenness coefficients used to identify the human made activities in the urban study (Crist & Cicone 1984).

### 3.3.4 Image Differencing (Comparing) as Automated Approach

The difference between two or more images is calculated by finding the difference between each pixel in each image, and generating an image using either a supervised or unsupervised classification. The images must be aligned so that corresponding points coincide and their values must be compatible through the calibration to locate objects that fluctuate in certain periods. Hall (2003) showed that this approach has the ability to automatically detect changes at multiple scales. First, a multi-scale dataset must be generated. Second, a change detection framework must be applied to the multi-scale dataset. Third, a procedure must be developed to delineate individual image-objects and identify them as they change through scale. Bruzzone (2000) stated that problems in unsupervised change detection methods based on the "difference image" lie in the lack of efficient automatic techniques for discriminating between changed and unchanged pixels in the difference image. To overcome this issue, one can allow an automatic selection of the decision threshold that minimises the overall change detection error probability under the assumption that pixels in the difference image are independent of one another. The other analyses the difference image by considering the spatial-contextual information included in the neighbourhood of each pixel.

Image differencing is found to be a superior technique than that of classical change detection methods with combinations of change vector analysis and principal component analysis (Raja et al. 2012). A crucial component of this image differencing change detection method is the selection of a threshold value between 'change' and 'no change'. Weeks et al. (2013) applied standard deviation threshold levels to the lower and higher tail of each distribution to find the threshold value that produced the highest accuracy for detecting change.

The ability to manually toggle the display threshold allows for complete control over the land change mapping process, giving the expert operator the ability to focus on locations known to have experienced true land-cover change. Schwert et al. (2013) stated that locating true land change and recording the varying thresholds at which it occurs is an arduous, time consuming and resource-intensive task. Large-area mapping projects may not have adequate resources necessary to employ such methods. The automated method is one

solution to detect the change in the larger area (Gray & Song 2013; Goodwin et al. 2013).

Table 3.3 summarises the major change detection techniques related to land use change. Selection of an appropriate method for detecting change in an object or a phenomenon on the landscape depends on the number of classes, including the characteristics of the study area and the spatial resolution of the sensor which should be taken into account before applying a suitable technique for the identification of change pixels or objects.

Table 3.3 A summary of major contribution in urban change detection.

| Type of Method Change Detection | Author | Methods | | | | | | Change Detection Results | | |
|---|---|---|---|---|---|---|---|---|---|---|
| | | Post Classification | Change Vector | Pixel | Feature | Object | RS Image | Rural | Urban | R, C/I |
| Neighbourhood Correlation Image (NCI) and Decision tree classification | (Im & Jensen 2005) | √ | | √ | | √ | ADAR5500 | √ | √ | |
| Maximum Likelihood Classification Algorithm | (Elhadi & Zomrawi 2010) | √ | | √ | | √ | IKONOS, Quick Bird | √ | √ | |
| Combining Principal Component Analysis (PCA) | (Deng et al. 2009) | √ | | | √ | | SPOT 5, Landsat 7 ETM | √ | √ | |
| PCA & Hybrid Classification (supervised & unsupervised) | (Deng et al. 2008) | √ | | | √ | | PCA & Hybrid Classification (supervised & unsupervised) | √ | √ | |

*Contd….*

| Type of Method Change Detection | Author | Methods | | | | | | Change Detection Results | | |
|---|---|---|---|---|---|---|---|---|---|---|
| | | Post Classification | Change Vector | Pixel | Feature | Object | RS Image | Rural | Urban | R, C/I |
| Contextual Knowledge, Mahalanobis Distance Classifier (MDC) | (Amarsaikhan et al. 2009) | √ | | √ | | | Landsat TM, SPOT PAN & Landsat ETM+ | √ | √ | |
| Decision rule- based, MLC, Grey Level Co-occurrence Matrix | (Chen & Wang 2010) | √ | | √ | | | Landsat 5TM, Landsat 7 ETM+, ASTER, & Chris-Proba | √ | √ | |
| Integrates Fuzzy logic & change reasoning | (Hester et al. 2010) | √ | | √ | | | Quick Bird | √ | √ | |
| Maximum likelihood Classification (MLC) | (Bayarsaikhan et al. 2009) | √ | | √ | | | Landsat 5 TM & Landsat 7 ETM+ | √ | | |

*Contd….*

| Type of Method Change Detection | Author | Methods | | | | | | Change Detection Results | | |
|---|---|---|---|---|---|---|---|---|---|---|
| | | Post Classification | Change Vector | Pixel | Feature | Object | RS Image | Rural | Urban | R, C/I |
| Change Vector Analysis – Image Differencing | (Lunetta 2004) | | √ | √ | | | Landsat 5 TM | √ | | |
| Image Differencing –Object Analysis & segmentation | (Hall 2003) | | | | √ | √ | SPOT Panchromatic | | | |
| Pattern Analysis | (Alberti et al. 2004) | | | √ | | | Landsat TM | √ | √ | |
| Post Classification – OB Classification and Standard Image Comparison | (Willhauck 2000) | √ | | √ | | √ | SPOT | √ | | |

*Contd….*

| Type of Method Change Detection | Author | Methods | | | | | | Change Detection Results | | |
|---|---|---|---|---|---|---|---|---|---|---|
| | | Post Classification | Change Vector | Pixel | Feature | Object | RS Image | Rural | Urban | R, C/I |
| Thematic generalization & Classification | (Petit & Lambin 2001) | √ | | √ | | | SPOT XS | √ | | |
| Object Oriented | (Gamanya et al. 2009) | √ | | √ | | √ | Landsat TM & ETM+ | √ | √ | |
| CVA & Tasselled Cap | (Johnson & Kasischke 1998) | | √ | | | | Landsat TM | √ | √ | |
| CBR-based quantitative prediction for land use change | (Du et al. 2010) | | | √ | | | Landsat TM | | √ | |

*Contd….*

| Type of Method Change Detection | Author | Method | | | | | | Change Detection Result | | |
|---|---|---|---|---|---|---|---|---|---|---|
| | | Post Classification | Change Vector | Pixel | Feature | Object | RS Image | Rural | Urban | R, C/I |
| Artificial Neural Network & Principal Component Analysis | (Liu & Jr 2002) | | | √ | √ | √ | Landsat TM | | √ | |
| Image Differencing ; Visual Analysis & Supervised Classification | (Martin & Howarth 1989) | | | √ | | √ | SPOT XS | √ | √ | |
| Land Transformation Model (LTM) & Artificial Neural Networks (ANN) | (Pijanowski et al. 2002) | | | √ | | √ | *Land Use Data | √ | √ | |
| Sub-pixel Impervious Change Detection | (Yang et al. 2003) | | | √ | | | Landsat TM & ETM+ | √ | √ | √ |

### 3.3.5 Standard Mixture Modelling Analysis (SMMA) for pixel proportion classification

Standard Mixture Modelling Analysis (SMMA) was used for pixel-based classification for dealing with Landsat ETM+ data with 30 m spatial resolution.

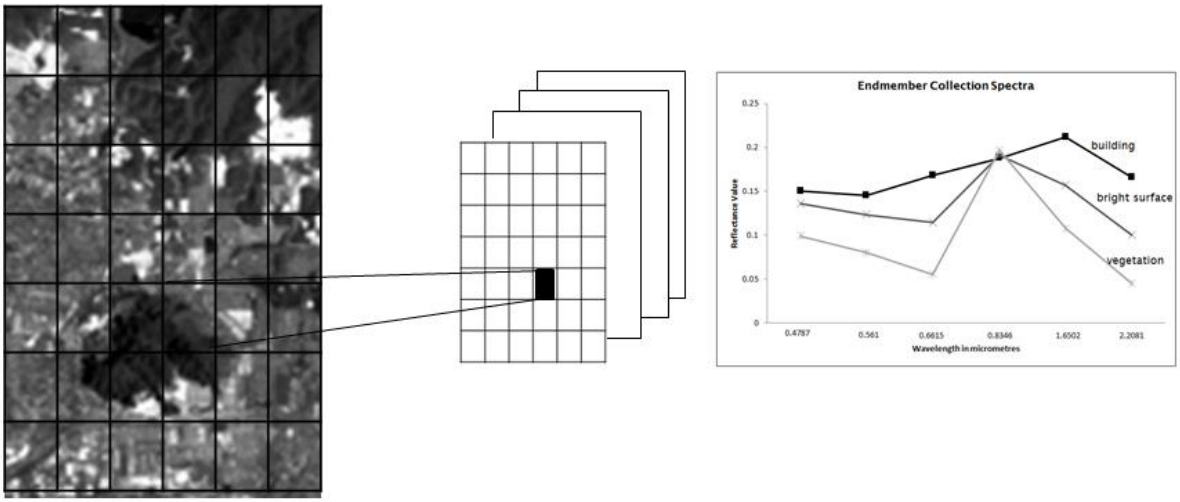


Figure 3.10 Spectra of pure pixels (end-members) found in the image scene.

To fit the SMMA, simultaneous equations were used regarding end-member selection and calibration between the images as shown in Figure 3.10. To produce end-members (M) the equations described by Settle and Drake (1993) were used below:

**End-member equation (M)**

$$M=(F^{T}F)^{-1} \times F^{T}X \qquad (3.6)$$

Where, F is the proportional value and $F^{T}$ is the predicted proportional value and X is the reflectance values from observed vector ($x_1$, $x_2$, $x_3$…….$x_n$) for each band to generate the pure end-member pixel.

In the calibration equation introduced by Nguyen et al. ( 2006), the local end-member can be defined based on proportions and the reflectance value of the corresponding pixel *(x, y). A*n equation exists as follows:

**Calibration equation (forward model)**

$$X_{Bi}^{xy} = M_{BiC1} F_{C1}^{xy} + M_{BiC2} F_{C2}^{xy} + \ldots + M_{BiCn} F_{Cn}^{xy} \quad (3.7)$$

Where $X_{Bi}^{xy}$ is the digital number of pixel $(x, y)$ in the spectral band $B_i$, $F_{C1}^{xy}, F_{C2}^{xy}, \ldots F_{Cn}^{xy}$ are the class proportions and $M_{BiC1}$, $M_{BiC2}$, …, $M_{BiCn}$ are the local end-member spectra of the pixel $(x,y)$ in spectral band $B_i$.

To fit this model, the following equations are solved for each pixel over each band in all Landsat ETM+ datasets from 2005 to 2009.

$$X_{Bi}^{xy} = \sum Fi * X_{BiC1}^{xy} + E_{BiC1} \quad (3.8)$$

$$\sum Fi = 1 \quad (3.9)$$

$$RMSE = \sqrt{\sum} E_{BiCi}^2 \quad (3.10)$$

*Fi* is the proportional abundance of a particular end-member. $X_{BiC1}^{xy}$ is the intensity of the image end-member for each particular land use class. $E_{BiC1}$ is the error of the fit for each particular land use class. SMMA is assessed using the root mean square error (RMSE) for all bands used in the analysis. The residuals are the differences between the original DN pixels and the predicted DN. The overall result of the model was judged to be accurate if the band residual or RMSE has a low value and if the fraction was between 0 and 1.

### 3.3.6 Multiple image differencing

The method of differencing images acquired in the same geographical area at two different times aims to identify land use and land cover changes that have occurred. The difference between two images (or more) is calculated by finding the difference between each pixel in each image, and generating an image based on the result. The images must be aligned so that corresponding points coincide and their values must be compatible through calibration (as described

above) to be confident that the changes identified in the images represent real changes on the ground.

In this research, the date of greatest change was identified by calculating the maximum difference, absolute difference and relative difference along the time-series.

### i) Maximum Difference Value and Year of Difference

The maximum difference was calculated as:

$$\text{diff} = \text{image}_{all}(\mathbf{i,j,k}) - \text{image}_{all}(\mathbf{i,j,k-1}), \quad \text{if } (\text{diff} > \text{max\_diff}) \qquad (3.11)$$

where, **i, j** is image array, size of image, referring to the number of maximum pixels in columns and rows acquired in the same geographical area at two different times, **k** refers to the first corresponding image, **k-1** refers to the second corresponding image. The largest value (maximum difference) in each changed pixel determines that the change has occurred.

### ii) Absolute Difference of Maximum Difference Value and Year of Difference

The absolute difference was calculated so as to eliminate pixels that have not changed and the formula was set by deciding a threshold value. The absolute difference is calculated before identifying the maximum absolute difference.

It is required to know if the change detected in each pixel is worthy of attention. Thus, a threshold value was applied to the result generated in equation 3.12.

$$\text{diff} = \sqrt{\left(\left(\text{image}_{all}(\mathbf{i,j,k}) - \text{image}_{all}(\mathbf{i,j,k-1})\right)\right)^2}, \quad \text{if } (\text{diff} > \text{max\_diff}) > \mathbf{K}t, \qquad (3.12)$$

if differences (**i, j**) of maximum value are greater than **Kt** (threshold) in each changed pixel determines the change has occurred based on absolute value of maximum differences.

## 3.4 Forecasting – Simulation by Cellular Automata (CA) Model

The last method of analysis described in this chapter supports the analysis on cellular automata (CA) for the land use change prediction model. Many researchers have used models ranging from the original CA to the simulation of an impressive range of urban phenomena to land use dynamics (Alkheder & Shan 1997; Almeida et al. 2003; Batty 1997; Bhatta et al. 2010; Guan et al. 2011; Jantz et al. 2010; Morandé et al. 2008; Samat 2007; White et al. 2012; Wu et al. 2009). The entire CA model for urban simulation consists of five basic elements; The Cell, The State, The Neighbourhood, The Transition Rule and The Time (Liu 2009). The basis of the Markov-CA model for urban simulation, also used by Liu (2009), consists of five basic elements; The Cell, The State, The Neighbourhood, The Transition Rule and The Time (Liu 2009) are:

i. The Cell is the basic spatial unit in a cellular space, arranged in a spatial tessellation. The most common form of CA used in land use change modelling is a two-dimensional grid.
ii. The State defines the attributes of the system and can be a number that represents a property. In this case, the states of the cells may represent the types of land cover and land use.
iii. The Neighbourhood is a set of cells with which the cell in question interacts. By default (i.e., in a strict CA) the Neighbourhood is the closest set of adjoining cells, of which there are eight (i.e., the "queen's case").
iv. The Transition Rule defines how the state of one cell changes in response to its current state and the states of its neighbours.
v. The Time specifies the temporal dimension in which a CA exists; all cells are updated simultaneously at all iterations over time.

There are two basic types of neighbourhoods: the von Neumann Neighbourhood (four cells) and the Moore Neighbourhood (nine cells) and refer to Figure 3.11. Other kinds of neighbourhoods within a circle of a certain distance have also been used in urban modelling ( White & Engelen 1997 ) and (White et al. 2012).

The CA model usually consists of a set of 'IF-THEN' statements that imply specific transition rules;

IF something happens in the neighbourhood of a cell

THEN something else will happen to the cell at the following time step

White & Engelen 1993 used the CA to develop a model of urban land use dynamics with high spatial resolution. The method suggested, through a combination with the detailed spatial data such as land use data in GIS more sensible to complete understanding of phenomena being modelled.

Liu & Phinn 2003 and Liu 2009 introduced the incorporation of fuzzy set approaches in CA. The model was based on an understanding of the logistic trend of urban development processes. The model assigns membership of urban areas to multiple states of urban development using a fuzzy membership function and applies the transition rules based on linguistic variables or uses principles from fuzzy set theory to allow human behaviour, specifically the planning and decision making process (Al-Ahmadi et al. 2009; Al-Ahmadi et al. 2009a; Al-Ahmadi et al. 2009b).

Wu & Martin (2002) used CA to model urban growth, characterising the distribution of land development with two different approaches of computing the strength of local growth. The first model simply counts the number of developed sites in a 3 by 3 neighbourhood. The second model incorporates a spatial interaction equation to calculate the local attractiveness.

### 3.4.1 Strict CA- Central Cell and Neighbours

Estimating transition probabilities for the central cell conditional upon its neighbours needed by calculating the probability of the central pixel changing conditional upon all 8 neighbours. This requires calculating the relative frequency (across the whole image) for each change vector given each possible combination of classes of neighbours at the previous time.

There are alternatives to this which might be simpler: e.g., to calculate the probability of change for a single change class e.g., the probability of vegetation changing to bare ground when 1 (or 2 or >2) of the neighbours are bare ground, or the probability of bare ground changing to built land when 1 (or 2 or >2) of the neighbours are built land.

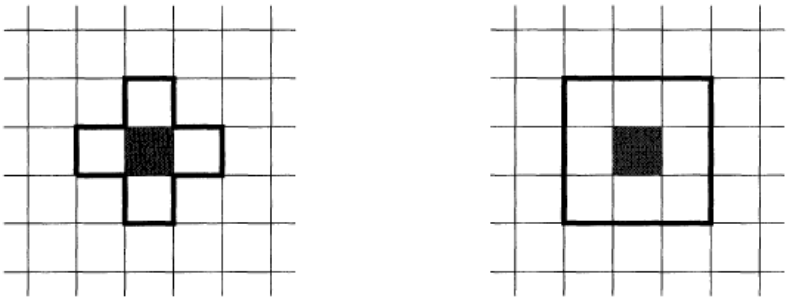


Figure 3.11 (a) Von Neumann and (b) Moore neighbourhoods (strict CA 3x3). The shaded region indicates the central cell which is update according to the state of the cells located within the domain marked with the bold line (Chopard & Droz 1998).

### 3.4.2 Markov Chain Cellular Automata

The Markov chain model (Lopez et al. 2001) is a simple method to describe the complex and long-term process of land use conversion using transition probabilities. The Markov chain model states that land use at some point in the future *(t + 1)* can be determined as a function of current land use *(t)*. This existing method also combines with another technique to highlight the

potential of the Markov chain analysis. Chen et al. (2013) simulated the future land use and land cover in China by using NDVI time-series data sets, and the PCA-Markov constructed transition probability matrixes and transition rules. Jokar Arsanjani et al. (2013) used a hybrid model consisting of a logistic regression model, Markov chain (MC), and cellular automata (CA), designed to improve the performance of the standard logistic regression model. The approach is capable of predicting the most probable sites for development, estimating the likely amount of change as well as allocating the estimated quantity within the study area.

Guan et al. (2011) demonstrates a combined Markov-Cellular Automata model to analyse temporal change and spatial distribution of land use. The forecasting outcome is anticipated to help local authorities better understand and address a complex land use system, and develop improved land use management strategies that can better balance urban expansion and ecological conservation. Yang et al. (2012) highlighted the limitations of the model, including the restriction of local transition rules affecting the quantity of land use whilst ignoring the effect of the spatial distribution. The Markov model can also be validated with the actual data of the land use to show satisfactory reliability.

## 3.5 Conclusion

Frequent monitoring using remote sensing data provides an opportunity to monitor the Earth's surface using fine spatial resolution data. To take advantage of this opportunity it is necessary to move beyond the traditional image-by-image approach to analyses. A new automated approach to monitoring large areas is to extend the application of a trained image classifier to data beyond its original temporal, spatial, and sensor domains. The accuracy of the classification method is also important in understanding the relationships and interactions between human and natural phenomena from captured data.

A proportion prediction algorithm has potential to estimate the proportions of urban classes including building (residential, commercial and industrial) using coarse spatial resolution trained with highly accurate object-based

classification based on fine spatial imagery. The land use classification at multiple time-points is also potentially useful in monitoring land-use change between transition object change and change reflectance. The derived information can be fitted to a cellular automata (CA) model with which to characterise and simulate the change under different scenarios.

# 4. Study Area and RS Data Pre-Processing

## 4.1 Study Area Background

The study area is located in the Gombak District, Selangor, Peninsular Malaysia. Geographically, it lies between latitudes $3^0 14' 32''$ N and $101^0 66' 29''$ W and longitude $3^0 33' 05''$ N and $101^0 77' 05''$ W (Figure 4.1). Rapid development in Kuala Lumpur has spread out into the study area, especially the growth of residential, commercial and industrial development based on demands and for a better living environment. Rapid urban development in Selangor has caused clear changes in land use. From the State Structure Plan of Selangor, between 1991-2002 the urban area in Selangor increased from 33,680 hectares to about 127,591 hectares (see Table 4.1). Even though urban development should be regarded as something positive, it is important that the urbanisation process does not affect the quality of life of the society, nor the quality of the environment (Figure 4.2). Providing affordable housing and a high quality environment is the utmost challenge for the development of Selangor State. An increase in population not only brings about greater economic challenges in providing jobs but also in providing high quality social amenities. The most basic social amenity is housing. With population growth, housing requirements have also increased 32.51% from 2005 to 2010. Table 4.2 shows the number of housing units in Gombak district. The challenge faced in providing housing units is to ensure that the housing units are distributed according to the actual requirements of an area (Table 4.2). At the same time, the quality of housing and environment must be able to improve the quality of life of the community. Industry is an important sector in the Selangor economy. Thus, industrial development should be emphasized in Selangor state for future economic development. Table 4.3 shows the projections of land area required to cater for industrial development in Selangor. The challenge for Selangor is to ensure that industrial land and floor area provision follows the distribution that has been made. Enough floor area should be provided for industrial development activities, especially in other districts in Selangor state. Similar to providing floor areas for industries, providing floor areas for businesses must also follow requirements to avoid aerial and financial wastage. Table 4.4 shows the projections of commercial floor area requirements until 2020. The challenge faced by the Gombak district is to ensure the floor areas' provision does not

exceed the projected requirement stated in the Selangor SP gazzetted document. Two types of remote-sensing data were used for this research: Landsat ETM+ and IKONOS multispectral data.

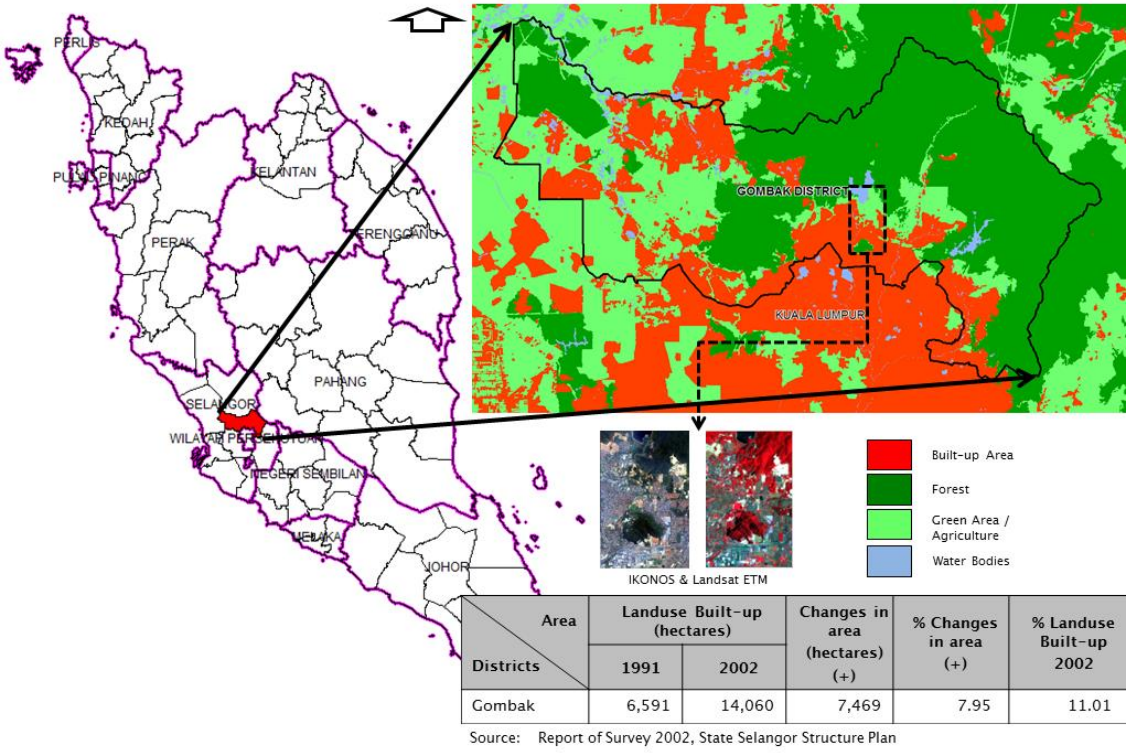


| Area / Districts | Landuse Built-up (hectares) 1991 | Landuse Built-up (hectares) 2002 | Changes in area (hectares) (+) | % Changes in area (+) | % Landuse Built-up 2002 |
|---|---|---|---|---|---|
| Gombak | 6,591 | 14,060 | 7,469 | 7.95 | 11.01 |

Source: Report of Survey 2002, State Selangor Structure Plan

Figure 4.1 Study Area in Gombak District, Selangor, Peninsular Malaysia (FDTCP 2002).

Figure 4.2 A part of land use and land cover in the study area (source from google earth).

Table 4.1 Recorded changes in land use (built-up) for the study area and other districts in the state of Selangor, 1991-2002.

| Districts | Land use Built-up (hectares) | | Changes in area (hectares) (+) | % Changes in area (+) | % Land use Built-up 2002 |
|---|---|---|---|---|---|
| | 1991 | 2002 | | | |
| **Gombak** | **6,591** | **14,060** | **7,469** | **7.95** | **11.01** |
| Klang | 7,901 | 18,329 | 10,428 | 11.10 | 14.40 |
| Kuala Langat | 893 | 7,418 | 6,525 | 6.94 | 5.81 |
| Kuala Selangor | 598 | 4,647 | 4,049 | 4.31 | 3.64 |
| Petaling | 14,304 | 33,861 | 19,557 | 20.82 | 26.53 |
| Sabak Bernam | 475 | 1,703 | 1,228 | 1.31 | 1.33 |
| Sepang | 744 | 22,885 | 22,141 | 23.60 | 17.93 |
| Hulu Langat | 893 | 7,418 | 6,525 | 6.94 | 5.81 |
| Hulu Selangor | 1,281 | 17,270 | 15,989 | 17.03 | 13.53 |
| *Selangor* | *33,680* | *127,591* | *93,911* | *100.00* | *100.0* |

Source: State Structure Plan (RSN) of Selangor 2002 Report of Survey

Table 4.1 also describes the percentage change between built-up land uses over approximately 11 years (1991-2002) within the districts in Selangor state. For the study area, namely Gombak district, the percentage change in built-up land use between 1991-2002 was 7.95%, which is among the fastest- growing areas due to spillover development of the surrounding areas of Petaling, Kuala Selangor and Kuala Lumpur.

Table 4.2 Projections of Residential requirements in Gombak District, 2005 – 2020.

| | Residential Units | | | |
|---|---|---|---|---|
| | 2005 | 2010 | 2015 | 2020 |
| Gombak District | 128,512 | 170,298 | 192,787 | 216,317 |

Source: State Structure Plan (RSN) of Selangor 2002 Report of Survey

Table 4.3 Projections of Industrial land requirements in Gombak District, 2005 – 2020.

| | Area (hectares) | | | |
|---|---|---|---|---|
| | 2005 | 2010 | 2015 | 2020 |
| Gombak District | 1,397 | 1,770 | 1,962 | 2,070 |

Source: State Structure Plan (RSN) of Selangor 2002 Report of Survey

Table 4.4 Projections of Commercial floor area requirements in Gombak District, 2005 – 2020.

| | Area (square meter) | | | |
|---|---|---|---|---|
| | 2005 | 2010 | 2015 | 2020 |
| Gombak District | 1,621,390 | 1,907,269 | 2,269,072 | 2,724,810 |

Source: State Structure Plan (RSN) of Selangor 2002 Report of Survey

Figure 4.3 Planned residential area (fieldwork photo).

Figure 4.4 High rise, multi-storey residential unit and traditional squatter village (landed-unplanned) (fieldwork photo).


Figure 4.5 Industrial building (fieldwork photo).

Figure 4.6 Terraced retail building (Commercial) (fieldwork photo).

Figure 4.7 Vacant land with bushes (green area) (fieldwork photo).

Figure 4.8 Stream (water feature) (fieldwork photo).

## 4.2 Remote Sensing Data

### 4.2.1 Frequent Coarse Spatial Resolution Remote Sensing Imagery: Landsat ETM+ 2005 to 2009

Urban remote sensing analysts in urban planning consider the spatial resolution to be more important than spectral resolution. This is because it increases the identification of urban objects, especially terrestrial features.

Landsat Thematic Mapper (Landsat TM) or Landsat Enhanced Thematic Mapper Plus (ETM+) is an outstanding sensor for this type of monitoring, especially on multiple time series or multiple time monitoring. The reason is that the images are free and available for everyone at the Earth Resources Observation and Science Center (EROS) website. From this opportunity, they allow researchers to explore many research objectives from past to present.

Landsat Enhanced Thematic Mapper Plus (ETM+) images consist of eight spectral bands with a spatial resolution of 30m for Bands 1 to 7 (Table 4.5). The resolution for Band 8 (panchromatic) is 15m. All bands can be acquired in one of two gain settings (high or low) for increased radiometric sensitivity and dynamic range, while Band 6 can be acquired in both high and low gain for all scenes. The approximate scene size is 170km north-south by 183km east-west (106mi by 114mi).
http://landsat.usgs.gov/band_designations_landsat_satellites.php

Table 4.5 Landsat 7 (ETM+) bands.

| **Enhanced Thematic Mapper Plus (ETM+)** | **Landsat 7** | **Wavelength (micrometers)** | **Resolution (meters)** |
|---|---|---|---|
| | Band 1 | 0.45–0.52 µm | 30 |
| | Band 2 | 0.52–0.60 µm | 30 |
| | Band 3 | 0.63–0.69 µm | 30 |
| | Band 4 | 0.77–0.90 µm | 30 |
| | Band 5 | 1.55–1.75 µm | 30 |
| | Band 6 | 10.40–12.50 µm | 60 * (30) |
| | Band 7 | 2.09–2.35 µm | 30 |
| | Band 8 | 0.52–0.90 µm | 15 |

* ETM+ Band 6 is acquired at 60m resolution. Products processed after February 25, 2010 are resampled to 30m pixels.

The research used five available images of Landsat ETM+ or Landsat 7 from 07 March 2005, 06 February 2006, 09 February 2007, 27 January 2008, and 03 April 2009 of a study area in Gombak District, Selangor, Malaysia with the path 127, rows 58 supplied by U.S. Geological Survey (USGS), Earth Resources Observation and Science Center (EROS). All the images are SLC-off (Scan Line Corrector), which compensates for the forward motion of Landsat 7 that failed to start from 2003 onwards, but the data still can be used to fill in the gaps. 2005 was chosen as the starting year because it could be linked to the fine spatial resolution of an existing 2005 IKONOS image.

### 4.2.2 Infrequent Fine Spatial Resolution Remote Sensing Imagery: IKONOS 2005 and 2009

IKONOS is a commercial Earth observation satellite, and was the first to collect publicly available high-resolution imagery at 1 and 4 m resolution (Table 4.6). It offers multispectral (MS) and panchromatic (PAN) imagery. IKONOS imagery began being sold on 1 January 2000. The sensor collects data with an 11-bit (0-2047) sensitivity which are delivered in an unsigned 16-bit (0-65535) data format. From time-to-time the data are rescaled down to 8-bit (0-255) to decrease file size. The revisit rate for IKONOS is three to five days off-nadir and 144 days for true-nadir.

Spatial resolution for IKONOS images:

- 1 m pan-sharpened (1 m PS)
- 4 m multispectral (4 m MS)

Table 4.6 Spectral Resolution (bands) of IKONOS

| IKONOS | Band | 1 m PAN (micrometers) | 4 m MS (micrometers) |
|---|---|---|---|
| | Band 1 (Blue) | 0.445–0.516 µm | 0.445–0.516 µm |
| | Band 2 (Green) | – | 0.506–0.595 µm |
| | Band 3 (Red) | – | 0.632–0.698 µm |
| | Band 4 (Near IR) | – | 0.757–0.853 µm |

The first image used is IKONOS 2005 multispectral imagery with a spatial resolution of 1 m (pan-sharpened) with 11 bits per pixel; Sun Angle Azimuth is 46.9962°, and Sun Angle Elevation is 60.90609° acquired on 9th July 2005, 03:48 GMT supplied by the Federal Department Town and Country Planning, Peninsular Malaysia. The second image is IKONOS data is in 2009; Sun Angle Azimuth is 109.9884°, and Sun Angle Elevation is 62.33025° acquired on 4th March 2009, 03.41 GMT with 11 bits in collaboration with the School of Geography (Geography and Environment), University of Southampton and the Federal Department Town and Country Planning, Peninsular Malaysia. Figure 4.9 shows the two types of data have been combined – frequent coarse spatial resolution images and infrequent fine spatial resolution images, in 2005 and 2009.

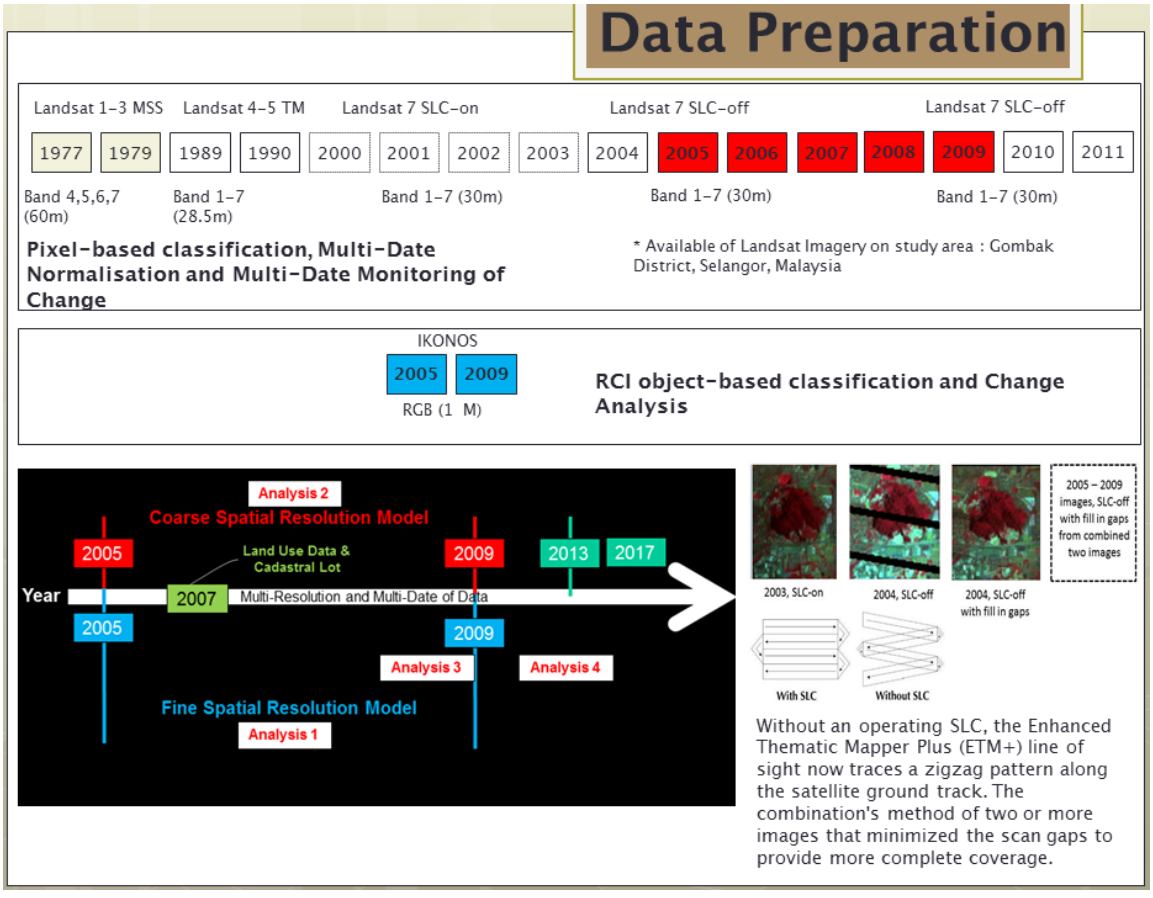


Figure 4.9 Historical data of Landsat available in study area where two types of data have been combined – frequent coarse spatial resolution images and infrequent fine spatial resolution images, in 2005 and 2009.

## 4.3 Remote Sensing data pre-processing

Remotely sensed data pre-processing was necessary for three reasons. First, to convert the remotely sensed data to physical units, so as to allow comparison and merging of data from different sensors. Second, to correct for geometric distortions in the data, and third, in order to correct for the effect of the atmosphere. The extent to which such pre-processing is necessary for change detection studies is a debatable point. If change detection is to be based only on the comparison of independent classified images it could be argued that radiometric and atmospheric correction are unnecessary (Song et al. 2001). However, in the present research, the need to combine data from different sensors and the requirement to produce a method that would be transferrable to other sensors and platforms in the future meant that there was advantage in standardising the input data as far as possible. Furthermore, the pre-processing steps involved are now readily available in common image processing packages and so are easy and quick to apply.

### 4.3.1 Radiometric correction

The data from Landsat ETM+ and IKONOS were delivered as digital number (DN) values, so one of the first tasks was to convert these to radiance units using the calibration data provided by the supplier. Historically, NASA have used two different methods of radiometric calibration, the first based on '*Lmax*' and '*Lmin*' values, the second based on gain ($C_1$) and bias ($C_0$) values:

$$L = \left(\frac{Lmax-Lmin}{255}\right) \mathrm{DN} + Lmin \qquad (4.1)$$

Where,
$L$ = spectral radiance
*Lmax* = radiance at which channel saturates
*Lmin* = minimum recordable radiance

$$L=C_0+C_1\ DN \quad (4.2)$$

where the $C_0$ is bias and $C_1$ is gain radiometric calibration coefficients.

Table 4.7 Table showing the *L*min, *L*max, gain ($C_1$) and bias ($C_0$) values for Landsat ETM+ 2005 to 2009.

| **Bands** | **Wavelengths** (µm) | **FWHM** (µm) | ***L*min** mW cm$^{-2}$ sr$^{-1}$ µm$^{-1}$ | ***L*max** mW cm$^{-2}$ sr$^{-1}$ µm$^{-1}$ | **Bias ($C_1$)** mW cm$^{-2}$ sr$^{-1}$ µm$^{-1}$ | **Gain ($C_0$)** mW cm$^{-2}$ sr$^{-1}$ µm$^{-1}$ |
|---|---|---|---|---|---|---|
| 1 | 0.4787 | 0.0710 | -6.200 | 191.600 | -0.69787 | 0.077874 |
| 2 | 0.5610 | 0.0800 | -6.400 | 196.500 | -0.71988 | 0.079882 |
| 3 | 0.6615 | 0.0610 | -5.000 | 152.900 | -0.07199 | 0.007988 |
| 4 | 0.8346 | 0.1260 | -5.100 | 241.100 | -0.0072 | 0.000799 |
| 5 | 1.6502 | 0.2000 | -1.000 | 31.060 | -0.00072 | 0.0000799 |
| 7 | 2.2081 | 0.2800 | -0.350 | 10.800 | -0.03939 | 0.00439 |

Table 4.7 showing the absolute radiometric correction converts the at-sensor radiance (*L*) value into accurate and reliable surface reflectance, requiring both the atmospheric properties and sensor calibration parameters. The gain and offset in values mW cm$^{-2}$ sr$^{-1}$ µm$^{-1}$ unit will be applied to the sensor data band by band to remove the path radiance and illumination effects.

### 4.3.2 Geometric correction

Kardoulas et al. (1996), stated that geometrically corrected images are needed for the following purposes:

- to bring an image into a standard projection,
- to locate points of interest,
- to bring adjacent images into registration,
- to overlay images of the same area from different dates and sensors, and
- to overlay an image on a map or merge it into a geographic database.

Accurate co-registration is critical in change detection studies involving the comparison of small areas, so a lot of effort was put into making sure that the geometric correction of the images was as good as possible. The Landsat ETM+ images were provided as orthorectified products with a specified accuracy of better than 250 metres (1 s.d.) in low relief areas at sea level (USGS 2014, http://landsat.usgs.gov/geometric_accuracy.php).

The images were geometrically corrected by the ENVI software using a polynomial method. The degree of polynomial method includes an X (base) and Y (warp) interaction term to account for image shear: $x = a_1 + a_2X + a_3Y + a_4XY$ *and* $y = b_1 + b_2X + b_3Y + b_4XY$ to resampling by nearest neighbour (NN). This resampling performed as the nearest pixel without any interpolation to create the warped image. The output pixel size XY fields are the pixel sizes of the output warped image. Warp is useful when the raster requires a systematic geometric correction that can be modelled with a polynomial. This tool will determine the extent of the target raster and will set the number of rows and columns to be about the same as in the base raster. In this study, base raster is images 2005 (IKONOS and Landsat ETM+). Some minor differences may be due to the changed proportion between the output raster's sizes in the x and y directions.

The results shown in Table 4.8 as area-based matching for automatic image co-registration to obtain the tie points (GCPs). The results of area-based matching largely depend upon the quality of the approximate relationship between the base image and warp image. The IKONOS images were slightly different viewing geometry. The process includes locating and matching a number of features points or tie points as become ground control points (GCPs) into the same coordinate system so that corresponding pixels represent the same objects. The geometric transformation equation was computed using 20 ground control points. The root mean square error (RMSE) which measured the accuracy of geometric correction result was less than 0.2 pixels (0.204391) as GCPs selected from accurate topographic maps were used to improve the system corrected products further. IKONOS image 2009 and cadastral land use map of proposed 2020 (P2020) follow the same method of geometric correction through the first-order polynomial method then resample to a 1 m

pixel size using the nearest neighbour algorithm with the RMS error 0.864 pixels.

Assessing geometric accuracy is normally expressed for each control point and overall root mean square error (RMS). High RMS values (>1) can indicate how inaccurate the transformation is and whether the chosen GCPs were adequate. All Landsat ETM+ images (2005 to 2009) follow the same method of geometric correction. The georeferencing through the first-order polynomial method then resample to a 30 m pixel size using the nearest neighbour algorithm with the RMS error average between 0.78 pixels to 0.901 pixels (2006, 2007, 2008, and 2009) from the corrected image base in 2005 by using 20 GCPs. The process of geometric correction faced some challenges with the coarse data (Landsat ETM+ images), and between raster and image (IKONOS and cadastral-raster). This is due to the identification of objects blurred and there are some features that are not obvious target points to get quality of georeferencing.

Table 4.8 Table showing number of GCPs used (image to image registration) for IKONOS, Cadastral and Landsat ETM+, based on degree of polynomial method and RMS error.

| Data | | No. of GCPs | Average RMS error (pixels) | Resampling Order |
|---|---|---|---|---|
| IKONOS | 2005 & 2009 | 20 | 0.204 | NN |
| | 2009 & Cadastral P2020 | 20 | 0.864 | NN |
| LANDSAT ETM+ | 2005 & 2006 | 20 | 0.836 | NN |
| | 2005 & 2007 | 20 | 0.789 | NN |
| | 2005 & 2008 | 20 | 0.901 | NN |
| | 2005 & 2009 | 20 | 0.891 | NN |

### 4.3.3 Atmospheric correction

The atmosphere has a very significant effect on the radiance measured from space in the optical region. Over 35% of the radiance measured by a satellite

sensor in the blue region (450nm) results from light scattered by the atmosphere that carries no information on the properties of the surface. In the near infra-red region (850nm), the proportion is much less, but still the atmosphere has a small effect. Clouds and cloud shadows are additional problems that affect the use of satellite sensors, especially in the tropics. In most cases, clouds have to be masked out, although a geostatistical method has been proposed to 'fill in' clouds (Rossi et al. 1994). Data from within cloud shadows can sometimes be retrieved using advanced methods of atmospheric correction (Choi & Milton 1999) or their influence can be minimised by using multispectral ratios (Crippen 1990). Although the use of ratios is a simple procedure, it is important to note that this assumes that the effect of the atmospheric path radiance has already been removed from the image, for example by the 'dark object subtraction' (DOS) method (Chavez 1996). Commonly, there are several methods for atmospheric correction, including Image-Based Methods (including DOS and regression methods), the Empirical Line Method (Smith & Milton 1999) and use of a Radiative Transfer Model (RTM);

i. The DOS method describes pixel values in all bands from the pixel values of low reflectance areas near zero. Some of the pixels will recognize exposures of dark-coloured rocks, deep shadow and clear water. Lowest pixel values in visible and near-infrared wavelengths are approximations of the atmospheric path radiance and minimum values subtracted from the image.

ii. The regression method is applicable to dark pixel areas. Near-Infrared pixel values are plotted against values in other bands. The least square line fit using standard regression methods to know the offset is an approximation for atmospheric path radiance and the offset can be subtracted from the image.

iii. The Empirical Line Method is the method of selecting multiple dark and bright targets from ground reflectance measurements using a field radiometer. Sensor radiance is computed from the slope s = cos (α) and intercept of the best-fit line.

iv. The RTM method supplies data about atmospheric conditions at the time of acquisition and is mostly used with 'standard atmospheres'. The numerical models currently available include MODTRAN (Moderate Resolution Atmospheric Transmission) and 6S (Second Simulation of the Satellite Signal in the Solar Spectrum), and the packages available to implement these RTMs include ATCOR (Richter & Schläpfer 2011), FLAASH (Kaufman et al. 1997) and Py6S (A Python interface to the 6S) (Wilson 2013).

The ATCOR software has been developed by the German Aerospace Centre-ReSe Applications (Richter & Schläpfer 2011). ATCOR consists of two separate codes optimised for narrow or medium FOV satellite sensors; specifically ATCOR 2 for flat terrain and ATCOR 3 for rugged terrain. All the objects have characteristic reflectance values measured by the sensor. Vegetation has a reflectance value between 0.5-14% with the largest values in the NIR band. Building objects, including RCI, reflected between 20% to 28% in the visible but decreased in the NIR, gradually increasing in the MIR band up to a 30% reflectance value. However, the bright surface, including road, asphalt, concrete and bare land had the highest reflectance value in the visible bands for all classes, and increased further in the MIR band. From these results, it is reasonable to trust the end-member (pure pixel) generated from the image atmospheric correction for the purpose of image calibration and standardisation of the target images.

### 4.3.4 Normalisation

As an alternative to full atmospheric correction, or in addition to an imperfect correction, an empirical normalisation process can be used to bring two or more images into a common frame of reference. Most methods of image normalisation assume that in any image there are at least a few pixels that are stable over time and that do not vary in reflectance. Because such areas will inevitably be imaged from different locations in space at different times, the most useful normalisation targets are diffuse (Lambertian) surfaces, such as areas of concrete and flat sand.

The Ridge Method is a simple empirical method of normalisation based on the assumption of a simple linear relationship among images across time and dominance of stable features in the scene.

Figure 4.10 below is the example use of a density plot for all the pixels in a scene with one axis being the DN value of date 1 and the other being the DN value of date 2 (Song et al. 2001). In such a plot, DN values of all stable features form a “ridge” with a straight line passing along the ridge defining the relationship between dates of imagery.

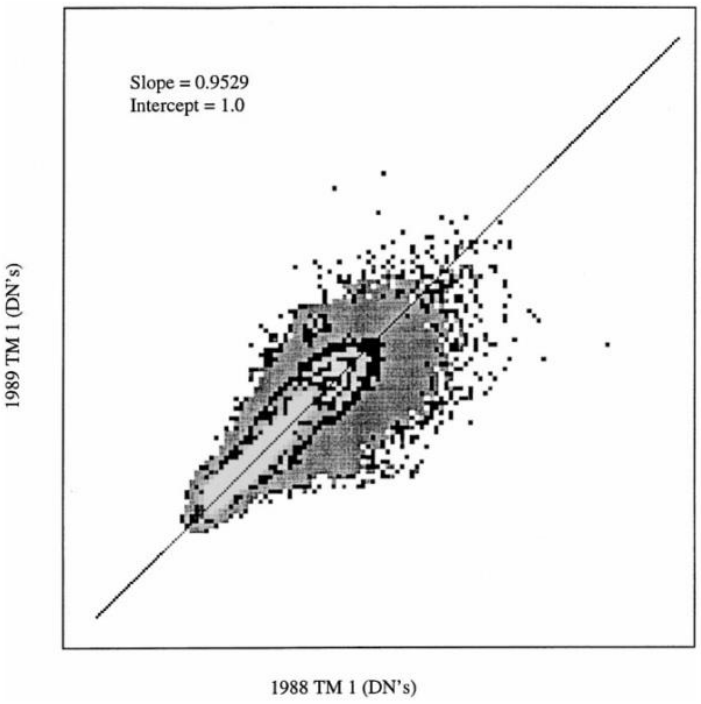


Figure 4.10 Example of a density plot for Landsat TM data images with grey levels illustrating differences in density. The line that passes the ridge in the centre defines the relationship used to match the two images (Song et al. 2001).

According to Caselles & Garcia (1989), relative atmospheric correction does not require estimation of any atmospheric optical properties, and it corrects not only the relative difference in atmospheric conditions, but also all other perturbative factors such as sensor response and noise. Accurate normalisation is important for image processing procedures using multi-date images, such as change detection. Heo & Thomas (2000) proposed a

standardised computation procedure for image normalisation which used band-by-band linear regression, single pixel targets, and a very conservative 99% confidence interval for determining outliers. A more robust method has been developed by Canty (2010), based on the Multivariate Alteration Detection (MAD) procedure first described by Nielsen (2007). The iteratively reweighted MAD (IR-MAD) algorithm introduced by Canty (2010) holds back one-third of the no change pixels for testing purposes. These are used to calculate means and variances before and after normalisation and also to perform statistical hypothesis testing of equal means and variances of the invariant pixels in the reference and normalised target images.

Atmospheric correction was applied to one ETM+2005 image using the ATCOR 2 (Atmospheric and Topographic Correction) software as an absolute radiometric correction of atmospheric conditions. Justification of the selection of a single 2005 image for the atmospheric correction process is that it enabled the next series of images to have characteristics very similar and relative to the reference image. This process is known as image standardisation or relative normalisation. This is done because the data will be used for monitoring the changes in a pixel such that relative changes are most important. The software usually makes the assumption that the relationship can be approximated by a linear function.

## 4.4 Conclusion

Remote sensing is a very useful tool to extract information from images on urban features. With the right approach, pre-processing and analysis procedures, variation within land use features can be discriminated and classified accordingly.

Remote sensing provides several significant major benefits for urban studies. First, the capability of acquiring photos or images which cover a large area, synoptically allows identification of objects, patterns and human-land interaction. Second, remote sensing provides additional measures for urban studies. Urban researchers frequently use data collected from field surveys but

it can become prohibitively expensive over a large area. Remote sensing can collect unbiased data effectively and can measure beyond the range of human vision in the electromagnetic spectrum (uv, near-infrared, etc.) to help obtain knowledge beyond our human visual perception from different sensors to improve urban mapping and analysis. Third, time-series data can be used to develop a historical perspective to examine significant natural processes or human activities. Fourth, remote sensing can help make connections across levels of analysis for urban studies. In this case, data can be combined to allow work at any scale or level of analysis including dynamic modelling, offering an indispensable framework of monitoring, synthesis and modelling of the urban environment. Last, they can also be used to relate different human and natural variables for developing an understanding of indirect and direct drivers of urban changes and the potential feedback of such changes on the drivers in the urban environment.

Regarding the availability of remote sensing data, medium-resolution remote sensing data have been used to examine urban phenomena and processes since the early 1970s when Landsat-1 was successfully launched. Free access to the Landsat archive from mid-2008 has enabled the town planner or urban researcher to view the Earth's surface retrospectively. Time-series of remotely-sensed data can be used to develop a historical perspective of urban attributes or changing processes. The launch of IKONOS, a very fine spatial resolution imaging satellite, signified the start of a new era of high spatial resolution sensing of the urban environment. The challenge now is to make optimal use of these exciting new tools and approaches, within the context of operational urban planning in Malaysia.

# 5. Analysis 1: RCI Object-Based Classification for Land Use Change Detection with Infrequent Data at Fine Spatial Resolution

## 5.1 Introduction

This chapter is considered very important to answer the two research questions; (i) “what is the accuracy with which the Residential, Commercial and Industrial (RCI) land uses can be classified?” and (ii) “can changes in land use be identified from remotely sensed imagery, including changes in and between the RCI land use classes?”. The research to date has tended to focus on classifying urban features from satellite sensor imagery (e.g. building, roads and pavements). This is a single class of built-up area rather than distinct component land use classes (RCI) for the purpose of urban management plans, sustainable mapping, planning control, monitoring and future planning forecasting.

In the first stage of analysis, the data were used from the IKONOS satellite for two different years, namely 2005 and 2009 with a 1 m spatial resolution pan-sharpened (1 m PS) for multiple-date classification. The IKONOS dataset is an example of fine spatial resolution satellite sensor data suitable for the identification of human-made features. Analysis of both IKONOS 2005 and 2009 datasets started with an Object-Based (OB) classification to classify the RCI land use classes and also to detect changes of land use and land cover (LULC) between the two sets of data in the four year period. The OB classification is a semantic classification based on spatial characteristics and context. The RCI objects were accurately delineated and classified from this OB classification. This first analysis involves a deceptively simple approach, but provides an important input to further analysis on monitoring changes in RCI land use classes.

To demonstrate that the RCI was classified with acceptable accuracy and validity, the analysis procedure involved the segmentation of the large-scale

conceptual objects such as trees, building, roads, bare land and bright surfaces into a single classification of land use classes. OB classification technique was carried out using a sampled selection of the objects (not pixels) derived from the segmentation of RCI properties that can utilise spatial and geometrical properties as well as the relationships among objects. The segmentation generated object features which were automatically classified by multi-resolution segmentation and supervised classification with additional characteristics such as the size or shape of the objects. The OB classification was used to identify the RCI classification with an acceptable accuracy.

Classification results of the RCI classes will be the basis of further analysis demonstrating that the monitoring of IKONOS data can contribute significantly to research in change detection remote sensing analysis. The research will continue with transition change detection analysis between RCI classes for the four year base period, using two basic approaches highlighted by Singh (1989); that is, comparative analysis of independently-produced classification from different dates (post-classification comparison: map-to-map comparison) and simultaneous analysis of multi-temporal data (multi-date classification and image-to-image comparison).

Both the results of RCI OB classification and monitoring of RCI change detection from the IKONOS data between 2005 and 2009 will be used in the next analysis chapter.

## 5.2 Research Methodology

### 5.2.1 A General Workflow for RCI Classification and Change Detection

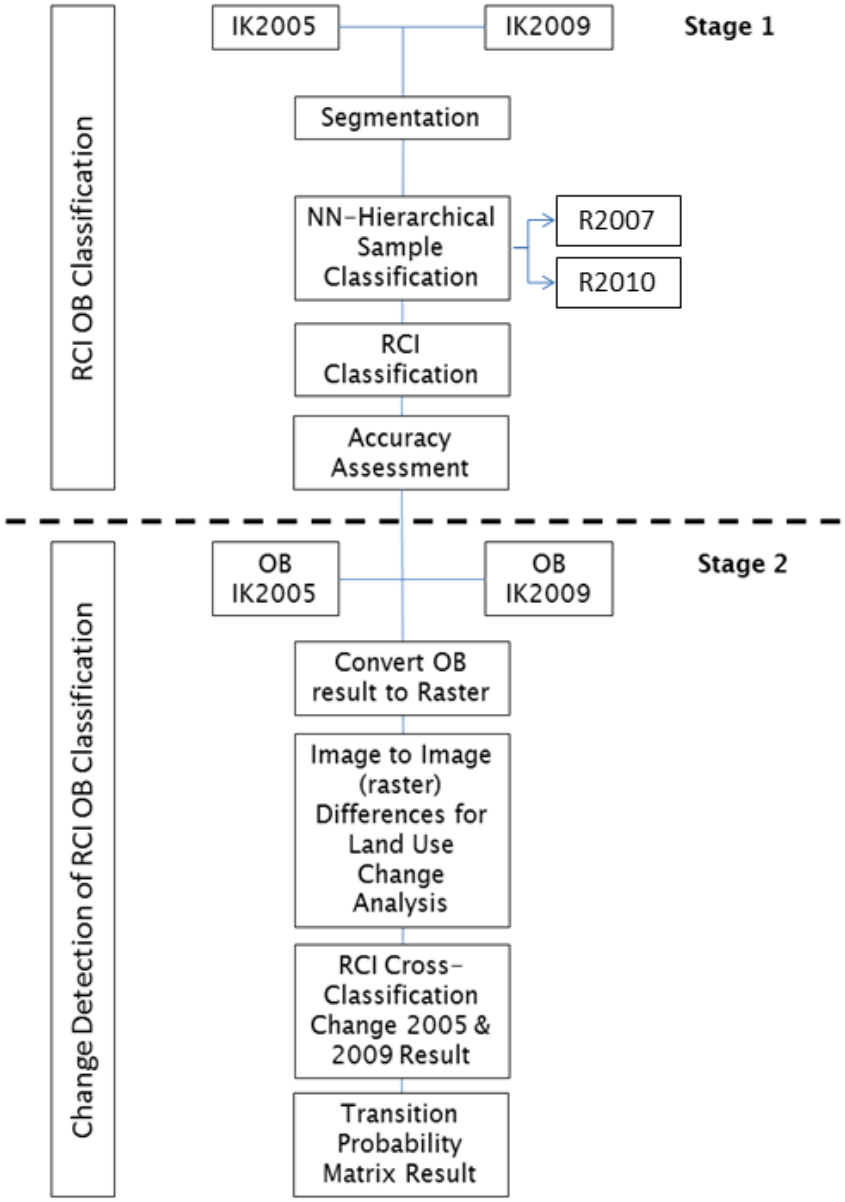


Figure 5.1 A general workflow for RCI classification and change detection.

**Stage 1- RCI OB Classification**

Figure 5.1 shows a general workflow for RCI classification and change detection analysis. The RCI object-based classification process can be understood as four distinct and interrelated stages; (i) Image Segmentation

aims to partition the image into a set of regions which are distinct and uniform with respect to some properties in the image, such as grey level, texture and colour, (ii) nearest neighbour classification (supervised classification) usually requires several rounds of sample selection and classification. This is also a sample-based classification algorithm. Based on user-defined samples (i.e., training data), a nearest neighbour algorithm combined with predefined feature sets is used to assign objects to classes. In this case, the reference data come from the cadastral map 2007 (R2007) and Google Earth image 2010 (R2010) to guide the selection of the 2005 and 2009 sample data. The procedure consists of two major steps; teaching the system by giving it certain image objects as samples and classifying image objects in the image object domain based on their nearest sample neighbours (Definiens AG 2009). (iii) RCI classification is generated, and (iv) accuracy assessment in undertaken to test the image object-based classification. Figure 5.2 shown the principles and methods of RCI object-based classification in this research.

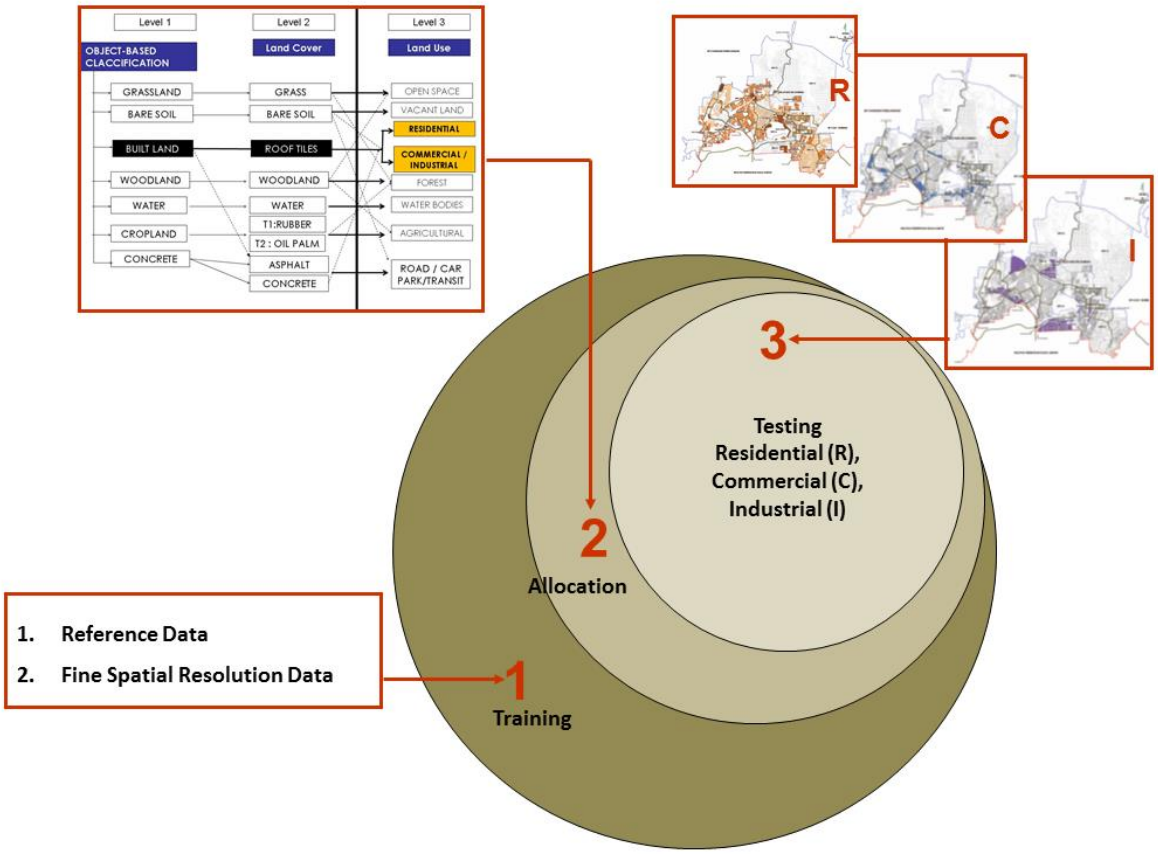


Figure 5.2 A representation of the principles and methods of RCI object-based classification.

**Segmentation (Multi-resolution) in eCognition**

The eCognition software uses the multi-resolution segmentation algorithm to create image objects, which merges consecutive pixels or existing image objects. It is a bottom-up segmentation based on a pairwise region merging technique (Definiens AG 2009). Multi-resolution segmentation is an optimization procedure which, for a given number of image objects, minimizes the average heterogeneity and maximizes their respective homogeneity.
The following are examples of typical uses:

- Extracting features that are characterised not purely by colour but also by shape homogeneity.
- Extracting land cover or human-made features from remote sensing imagery.

In this process parameters are set through an iterative process of 'trial and error' until the best parameter set is found to apply the segmentation of objects to the RCI classification. A higher larger parameter will tend to create larger objects. Larger values will often produce results with greater emphasis on the colour of image objects. The most important parameter is based on the objective of the segmentation result. In this research, the objective of the segmentation is to detect the outlined buildings or any appropriate objects that can be mapped in this way. As a result, the best parameter set for the objective of RCI classification segmentation was selected as 180 for scale and 0.75 for colour. The key to high accuracy in the segmentation depends on the outline created to identify the objects.

**Classification (Nearest Neighbour) in eCognition**

The Classification using the nearest neighbour algorithm classifies image objects by using training samples. In the eCognition software, objects generated through segmentation can be classified using two different classification methods: (i) samples or (ii) integration of prior external knowledge stored in rule bases. In this research, the OB classification was based on samples through supervised training based on reference data (R2007) from raster-to-raster comparison. The result of samples generated from the object-based segmentation includes the image objects needing to be classified based on supervised classification. The members of the input class

will be assigned or reassigned to the classes in the output fields. The colour feature space classifies image objects based on the image pixel values. It allows the separation of areas by context, which cannot be distinguished based on colour alone. These sample objects should be well separated using the most representative and clearly distinguished class features. To finalise, accuracy assessment results can be evaluate and the OB classification stored in raster format for the next analysis.

**Stage 2 – Change Detection of RCI OB Classification**

The second phase of analysis in this chapter deals with the use of two-date IKONOS fine spatial resolution data for Object-based Change Detection Analysis. This method is an extension to the classification analysis, to investigate the changes that may exist between RCI 2005 and 2009.

The results of RCI OB classification between 2005 and 2009 were converted into a raster file from the eCognition software. However, it is not sufficient to run both datasets for image differences analysis in the IDRISI selva software. Both datasets in raster format needed to be converted into ASCII files in ArcGIS to make sure that the OB classification transformed into size of pixel image in raster data to ensure the characterised the pixel value is perfectly through the change detection analysis (in pixel-based). The eConition software allows the automated extraction of polygons based (vector) on image objects generated.

Land use change analysis in IDRISI can be a convenient tool for modelling land use changes when change and processes in the landscape are difficult to describe (Ronald 2003). In the IDRISI software, the Markov Chain Analysis tool describes land use change from one period to another period and uses this as the basis to project future changes. This is accomplished by developing a transition probability matrix of land use change from time one to time two, which will be the basis for projecting to a later time period.

The transition probabilities matrix records the probability that each land cover category might change to every other category. In this case, the results vary depending on the class category from the OB classification between 2005 and 2009. This matrix is the result of cross tabulation of the two images adjusted

by the proportional error. As a result, the transition matrix records the number of pixels that are expected to change from each land cover type to all other land cover types over the next four years. This matrix is produced by multiplication of each column in the transition probability matrix by the number of cells of corresponding land use in the later image. In both of these matrix results, the rows represent the older land cover categories and the columns represent the newer categories.

### 5.2.2 Data Preparation

The first image used is the IKONOS 2005 multispectral imagery with a spatial resolution of 1 m pan-sharpened with the original 11 bits per pixel, acquired on 9th July 2005, 03:48 GMT and supplied by the Federal Department of Town and Country Planning, Peninsular Malaysia. The second image is the IKONOS data acquired on 4th March 2009, 03.41 GMT with 11 bits, funded in collaboration with Geography and Environment, University of Southampton and the Federal Department of Town and Country Planning, Peninsular Malaysia. Both datasets were supplied already pan-sharpened to increase the resolution with the same map projection of the Universal Transverse Mercator (Hemisphere: N, Zone Number: 47 with datum WGS 84).

There are differences in the radiometric resolution (8 bits and 11 bits) of the data supplied. The IKONOS data of 2005 were rescaled down to 8 bits. Also it lacks the near infrared (NIR) band. Regarding these issues, the three remaining bands red, green and blue (RGB) were used for object-based classification for both the IKONOS 2005 and 2009 datasets.

Ideally, one would have compared data from similar months in different years. However, due to thick and persistent cloud coverage in Malaysia such data were not available. So the IKONOS data in March 2009 were considered the best to compare with July 2005.

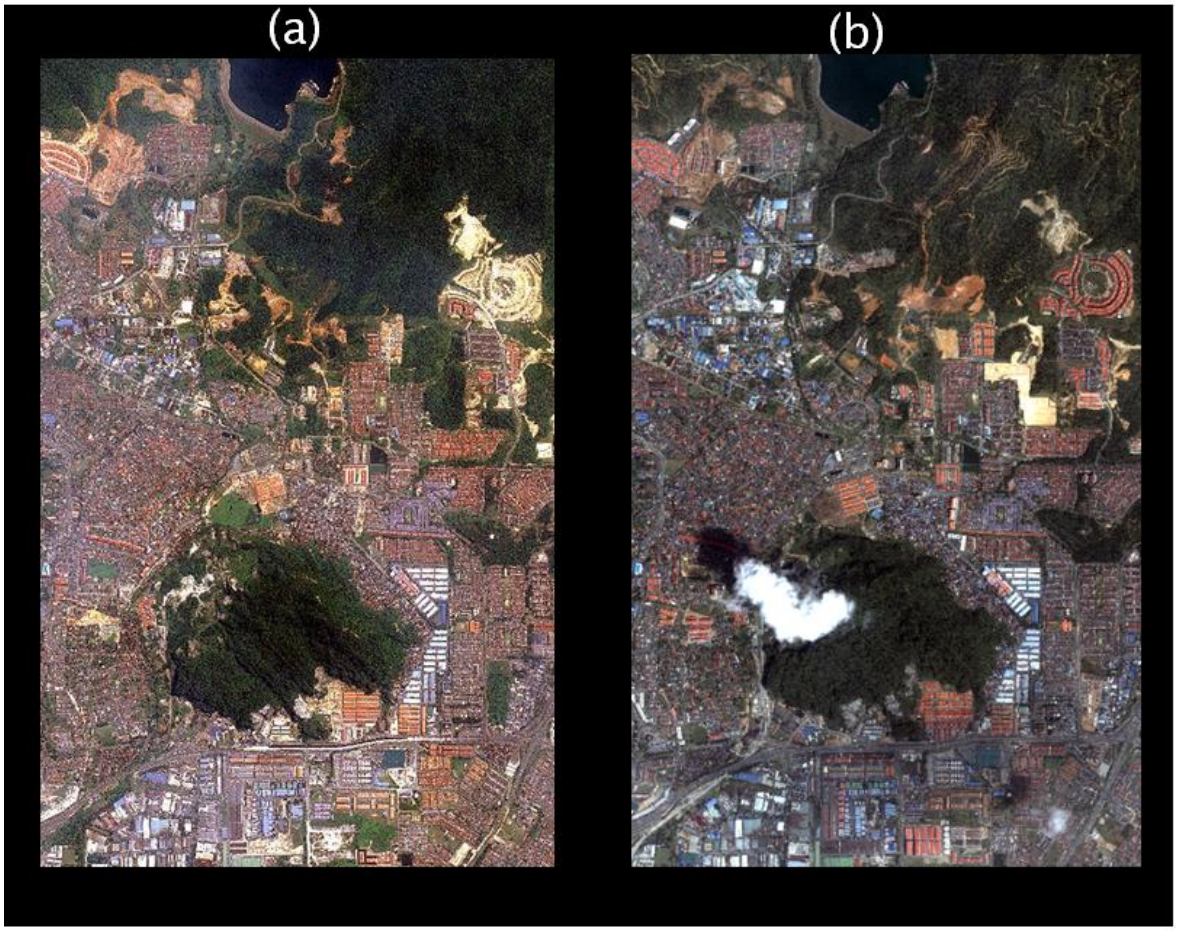


Figure 5.3 IKONOS-2 multispectral imagery RGB with 1 m pan-sharpened resolution: (a) 09 July 2005, (b) 04 March 2009.

The two IKONOS images in 2005 and 2009 in Figure 5.4 follow the same subset image as the training site for the Gombak District with the three wavebands. The subsequent analysis used wavebands 0.45-0.90$\mu m$ (Blue-PAN), 0.506-0.595$\mu m$ (Green) and 0.632-0.698$\mu m$ (Red). These wavebands are linked with the six classes of land use and land cover type within the Gombak District: (a) Residential, (b) Commercial, (c) Industrial, (d) Bright Surface, (e) Vegetation and (f) Water. Typical examples are shown in Figure 5.5.

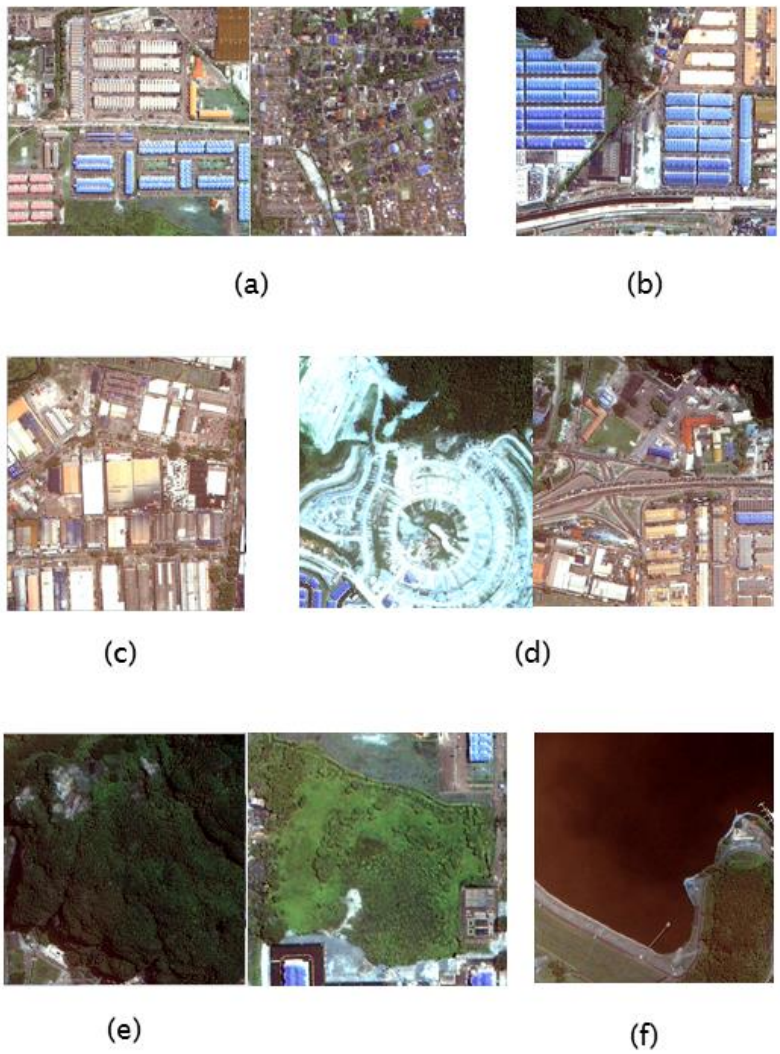


Figure 5.4 Examples of land cover and land use types in the Gombak District shown on the IKONOS images; (a) residential, (b) commercial, (c) industrial (d) bright surface, (e) vegetation, (f) water.

### 5.2.3 Reference data and Site Familiarisation

The study area has the legal status of the "Local Plan" including the land use plan for planning control and future development. For reference purposes, the cadastral data (vector) of the land use plan is a solid foundation that helps the OB RCI classification to be accurate and a training data for validation. The

cadastral data were obtained from a joint land-use plan prepared in 2007 (Figure 5.5). Land use data have been obtained from field studies involving on-site "validation" by the custodian of the plan at the Department of Town and Country Planning, Peninsular Malaysia, together with representatives from the Selayang Municipal Council. Verification was conducted by two methods of applying GPS (i) by the determination of lots on land use and (ii) through a series of meetings to ensure the accuracy of the land use. Thus, these data are very reliable in describing land use because it has been approved by the relevant authorities in the management of the plan and planning control. This process included:

- The reference data for land use in 2007 (R2007) were certified by ground verification, carried out by the Federal Department of Town and Country Planning, Peninsular Malaysia (FDTCP) and Selayang City Council (FDTCP 2010).
- The background research identified issues and current conditions of the study area, and referred to the report of Selayang City Council's Local Plan 2007-2020, produced by the Federal Department of Town and Country Planning, Peninsular Malaysia (FDTCP).
- Land Use Map 2007 with Selangor Cassini State Projection (MapInfo file - .TAB) was used as reference data to guide the RCI classification.
- All relevant data and information (e.g. on planning and other legislation, maps, existing development plans) were reviewed.

To avoid bias, Google Earth archive data for 2010 (23 January 2010), referred to as R2010, were included using a subset (Figure 5.4) of the generated sample points identified during visits to the study area. The R2010 image is shown in Figure 5.8. The existence of reference data from Google Earth (R2010) were used, including the street view function, to help identify the authenticity of object-based LULC classification. This approach can be used to produce a valid main reference dataset in place of field studies or ground survey, and the approach is used commonly.

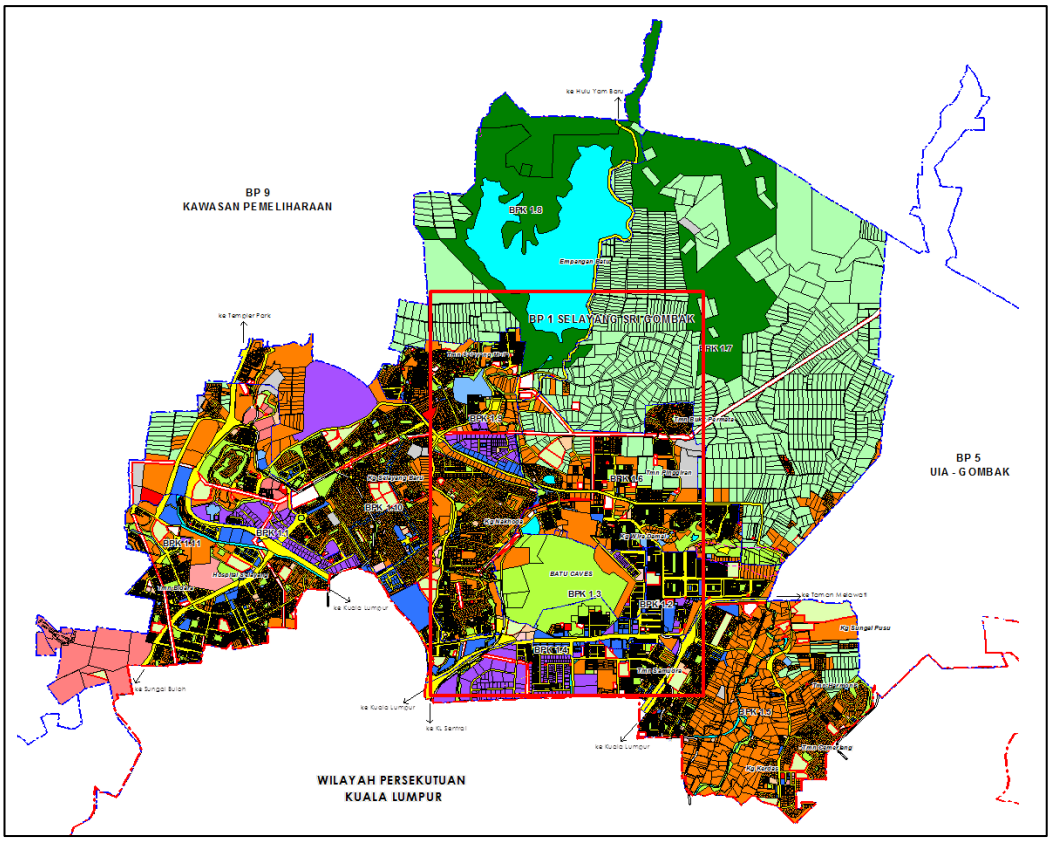


Figure 5.5 The Reference Data; Existing Land Use Cadastral Map 2007 in the study area (overall area 5,925.96 ha). The red box indicates the training site of IKONOS data for 2005 and 2009 (3.4 km x 5.3 km).

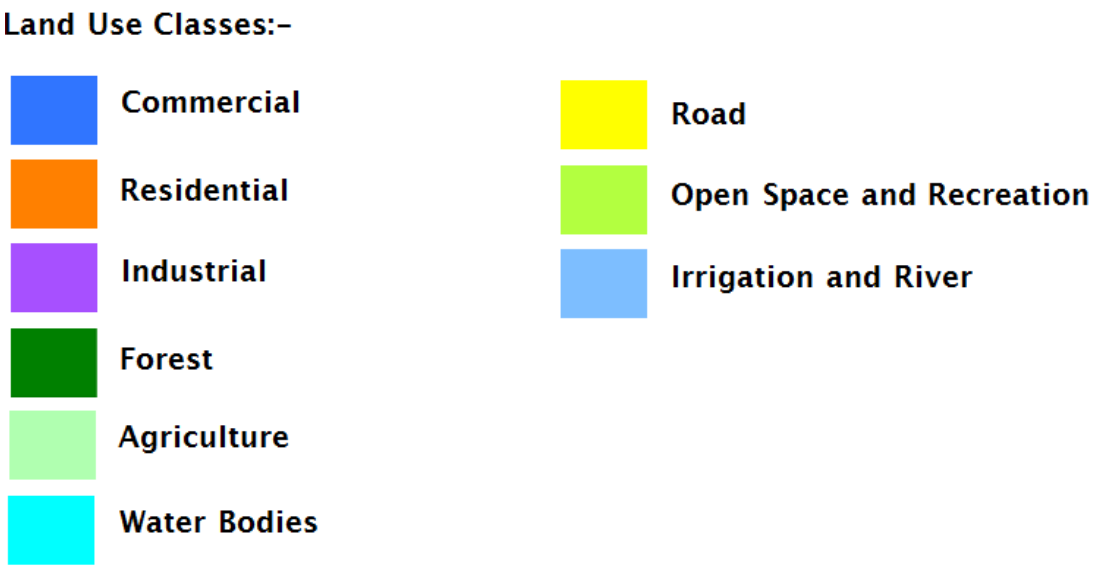


Figure 5.6 Cadastral land use classes and colour codes by FDTCP.

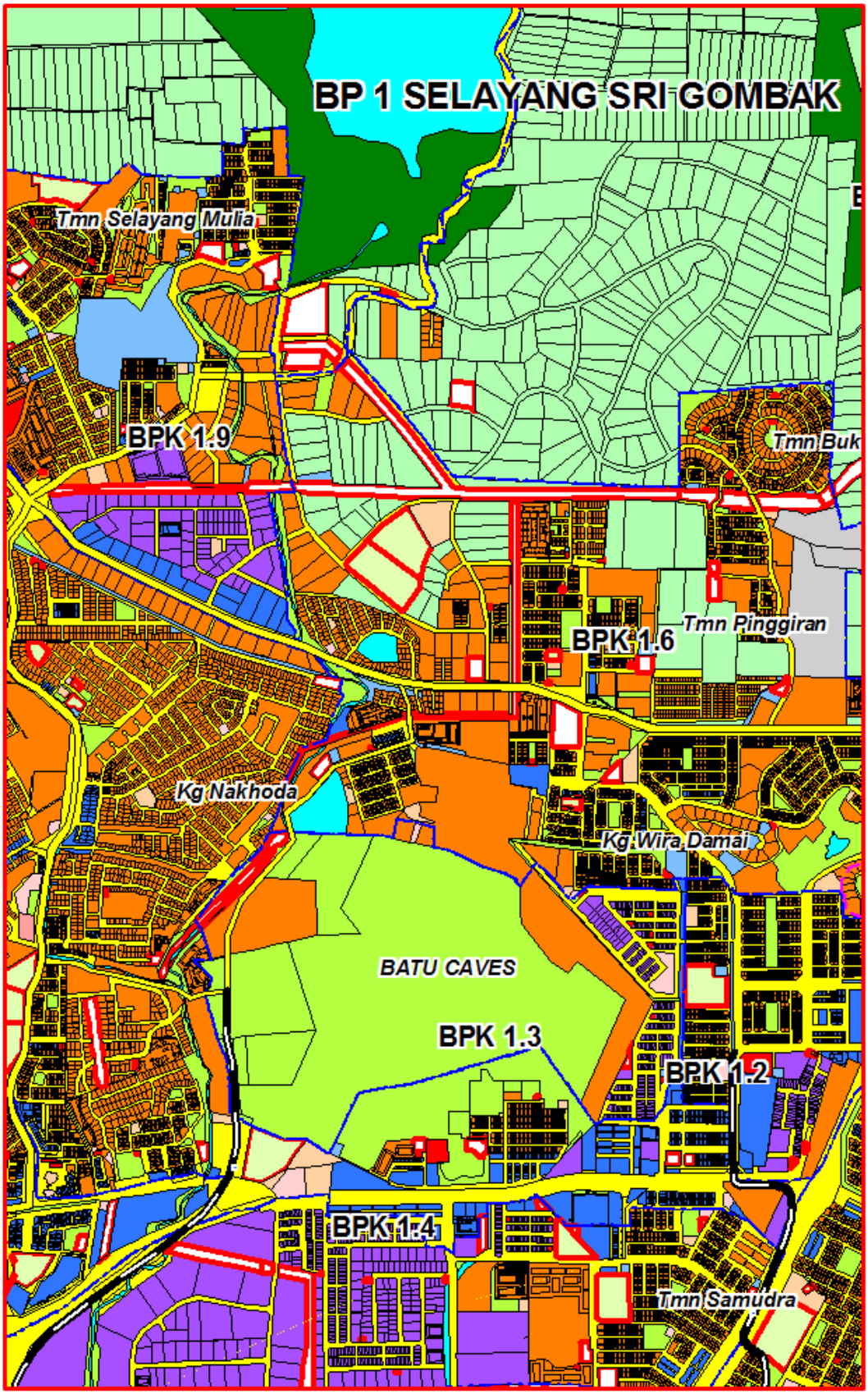


Figure 5.7 The reference data; land use cadastral map in GIS-vector (R2007) for the training site (3.4 km x 5.3 km).

Figure 5.8 The reference data from Google Earth imagery captured on 23 January 2010 (R2010).

Table 5.1 Land use 2007 (R2007) proportion of the study area.

| Land Uses | Acreage (Ha) | Percentage (%) |
|---|---|---|
| Residential | 380.40 | 21.11 |
| Commercial | 33.37 | 1.85 |
| Industrial | 100.1 | 5.55 |
| Road | 532.02 | 29.52 |
| Infrastructure and Utilities | 47.03 | 2.61 |
| Agriculture | 333.12 | 18.49 |
| Open Spaces and Recreation | 51.81 | 2.88 |
| Forest | 185.07 | 10.27 |
| Institution and Public Amenities | 84.88 | 4.71 |
| Water Bodies | 36.31 | 2.01 |
| **Total** | **1,802.00** | **100.00** |

Source: Report of Selayang City Council Local Plan 2007-2020.

Table 5.2 Aggregated land use and land cover of Residential, Commercial, Industrial, Vegetation, Bright Surface and Water (R2007).

| Land Uses | Acreage (Ha) | Percentage (%) |
|---|---|---|
| Residential | 380.40 | 21.11 |
| Commercial | 33.37 | 1.85 |
| Industrial | 100.1 | 5.55 |
| Bright Surface* | 663.93 | 36.84 |
| Vegetation* | 570.00 | 31.63 |
| Water | 54.2 | 3.01 |
| ** (bright surface = road, infrastructure & utilities, Institution and Public Amenities)* **(vegetation = agriculture, open spaces & recreation, forest)* | | |
| **Total** | **1,802.00** | **100.00** |

Source: Report of Selayang City Council Local Plan 2007-2020.

Table 5.1 is the total area of land use in the study area based on the Local Plan document, while Table 5.2 classifies land use according to six categories that are consistent across the training site and reference data R2007.

Bright Surface refers to sub-objects of land use and land cover including road, pavements, bare land or cleared land (earth works), and utilities and infrastructure. Meanwhile, the vegetation class includes the greenery areas including 'trees', 'crops' and 'grass' coverage as well as agricultural land, forest reserves, recreational green area and areas of open spaces.

### 5.2.4 Software used

To run the object-based classification, eCognition 8 was used for the segmentation and RCI classification. For IKONOS 2005 and 2009 the change detection analysis used two types of software; (i) ArcGIS 9.3 to convert the result of object-based classification of raster data to ASCII data and (ii) IDRISI Selva software for the change detection analysis (object-to-pixel change).

## 5.3 Analysis of RCI Classification and Change Detection between 2005 and 2009

### 5.3.1 RCI Classification Analysis for 2005 and 2009

In the first step, the image pixels from the IKONOS 2005 image were grouped to form objects with the aid of multi-scale segmentation. The segmentation process involved generating regions from the spectral values of the pixels to be represented in the object-base. From the user-defined segmentation threshold of scale=180 and colour=0.75, execution generated 2223 objects for image 2005 and 3864 objects for image 2009. Although both segmentations used the same parameters, due to the differences in terms of spectral reflectance, the area of the identified objects differed slightly. The selected parameters through trial and error were the best for segmentation for both images (see Figure 5.9). This segmentation evidence shows a larger scale value will tend to create larger objects, and also larger values will tend to produce results with greater emphasis on the colour or spectral value of image objects (Definiens AG 2009).

The NN classifier has advantages because the method is very fast and allows easy handling of class hierarchies for the classification. The combination of membership function also demands precise class definition, which needs knowledge of the best parameters for object separation of the classes, and this classification process is based upon nearest neighbour and membership.

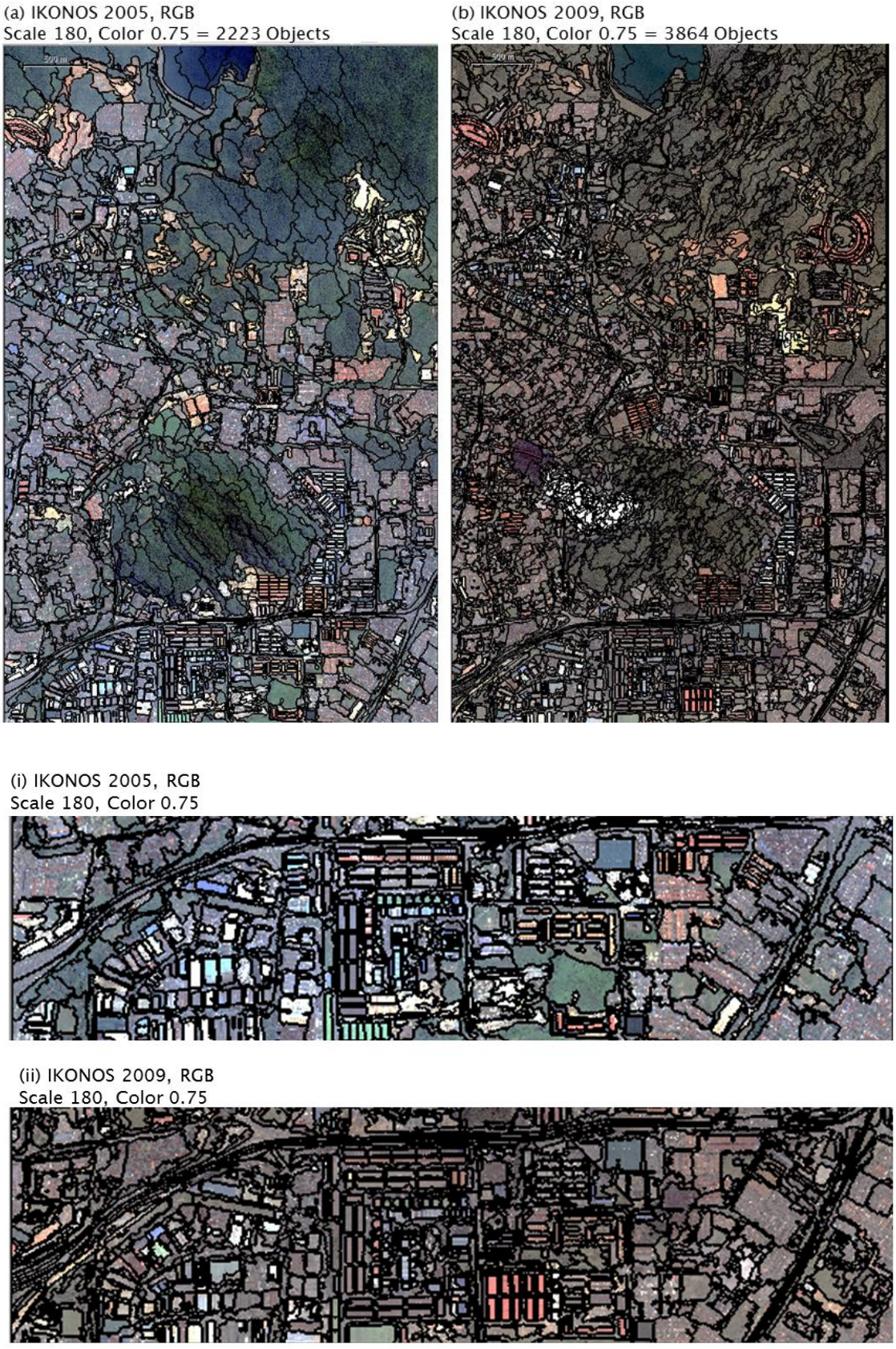


Figure 5.9 The result of IKONOS segmentation based on scale (shape and compactness) and colour. (a), (i) IKONOS 2005 and (b), (ii) IKONOS 2009.

The objective at the beginning was to use the eCognition software with the IKONOS multispectral 1 m PS spatial resolution with RGB bands, to identify the prominent land uses in residential, commercial and industrial (RCI) areas and perform accurate mapping.

The NN classifier illustrated in Figure 5.10 is like a partitioning tree diagram. As a result, six classes of land use were identified through the NN classifier based on segmentation, with the selected scale and colour parameters. The process involved a step-by-step approach drawing samples chosen from the object segmentation, resulting in the object-based classification.

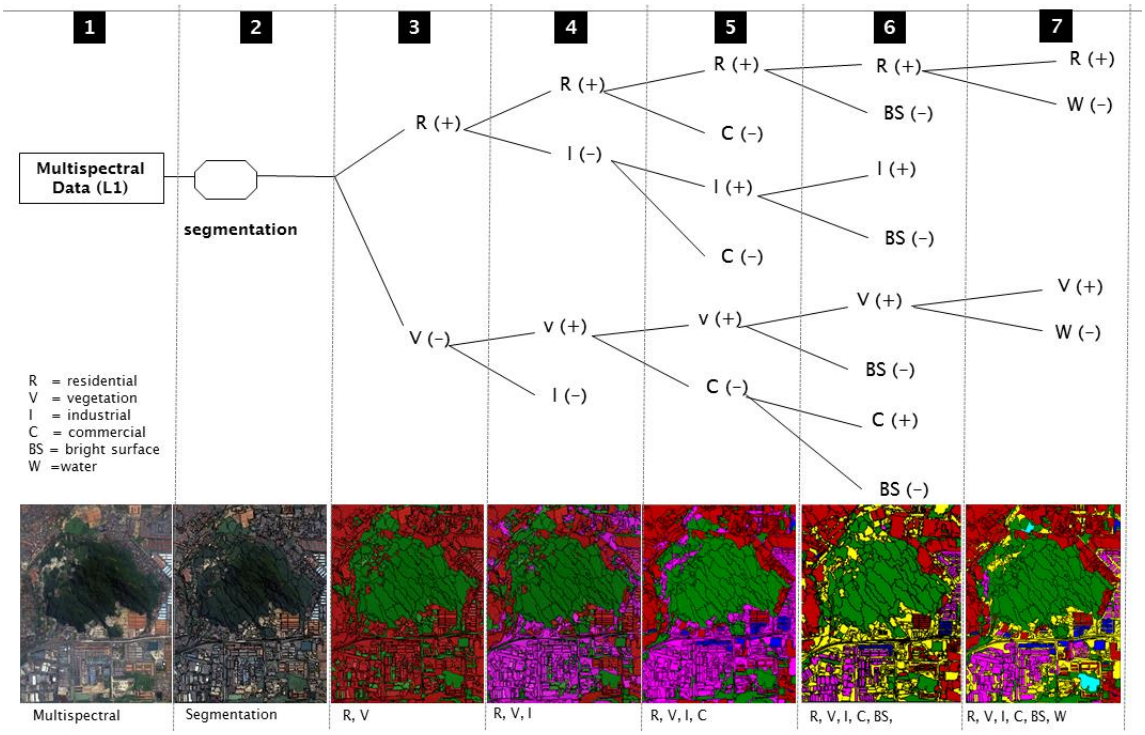


Figure 5.10 The steps through the sample selection process using the NN classifier tool.

In the class hierarchy in Figure 5.10, for example, all residential types were registered as a single residential land use class. This method is significantly faster, but only works if the sample selected is correct and similar to the supervised classification technique.

To run the NN classification, the training sample created is important to achieving a high accuracy of classification. The NN classification segmentation result varies depending on the numbers of samples created to assign the class of land use and land cover (LULC) to classes. With more samples of classes the classification result may be more accurate. If the selected object has segmentation-sized building blocks, detailed sampling is needed to ensure accuracy in its classes such as commercial and industrial. The NN classifier returns a membership value between 0 and 1 on the image object's feature space distance to its NN. The membership value is 1 if the image object is identical to a sample of the class and 0 values for other classes if not identified. The NN classification sample performed refers to the land use data, point data through ground validation and image interpretation. As a result of the classification, six classes were identified, which are residential (R), commercial (C), industrial (I), vegetation, water, and bright surface (a combination of road/asphalt/concrete/bare land) as in the training data. Both classification results are shown in Figure 5.11 dan Figure 5.12.

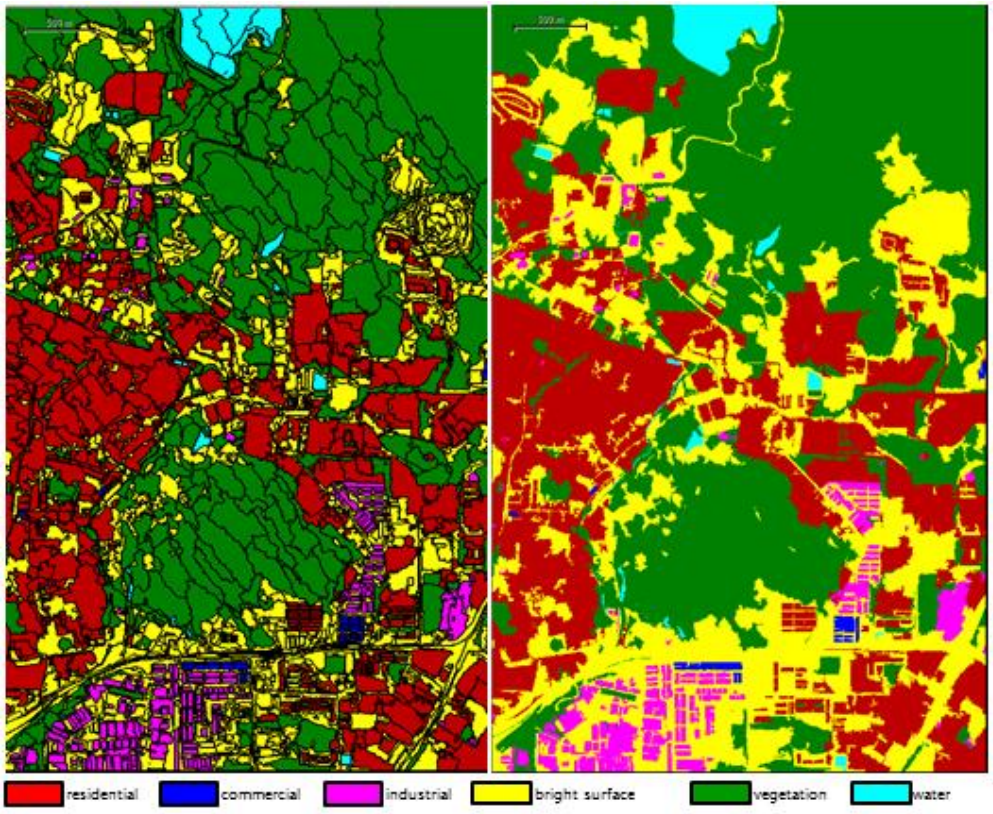


a. IKONOS 2005- segmentation line on and off

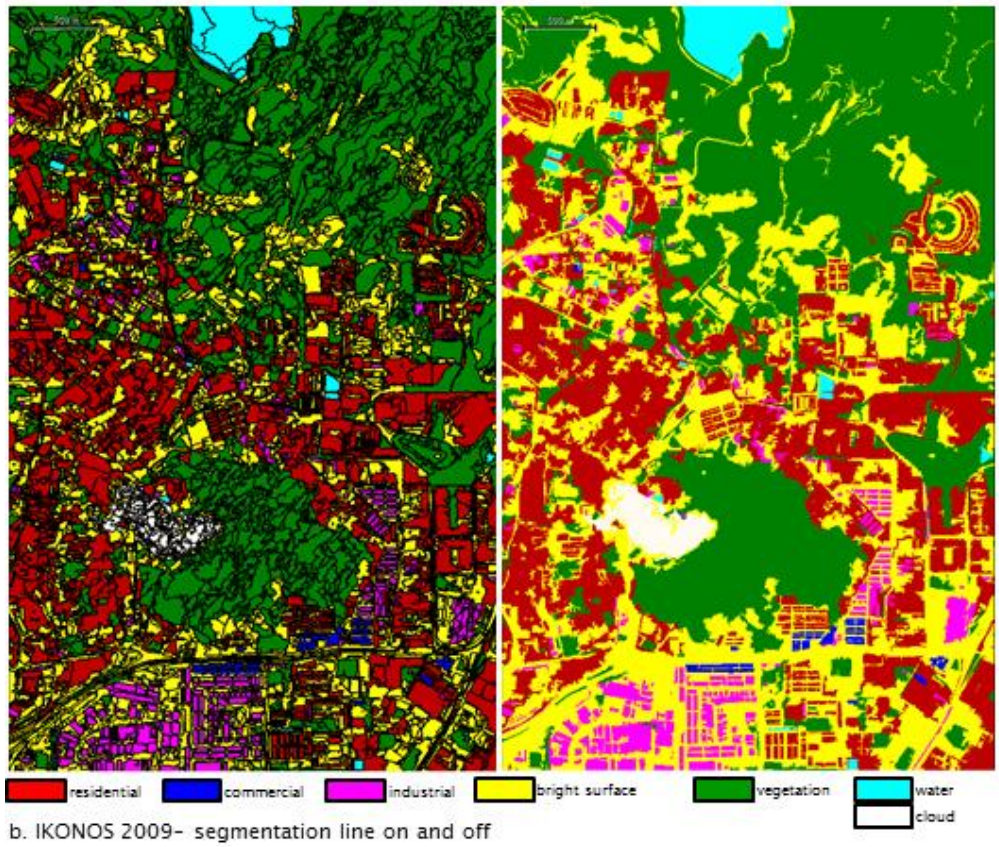


b. IKONOS 2009- segmentation line on and off

Figure 5.11 The NN object-based classification of (a) IKONOS 2005 and (b) IKONOS 2009.

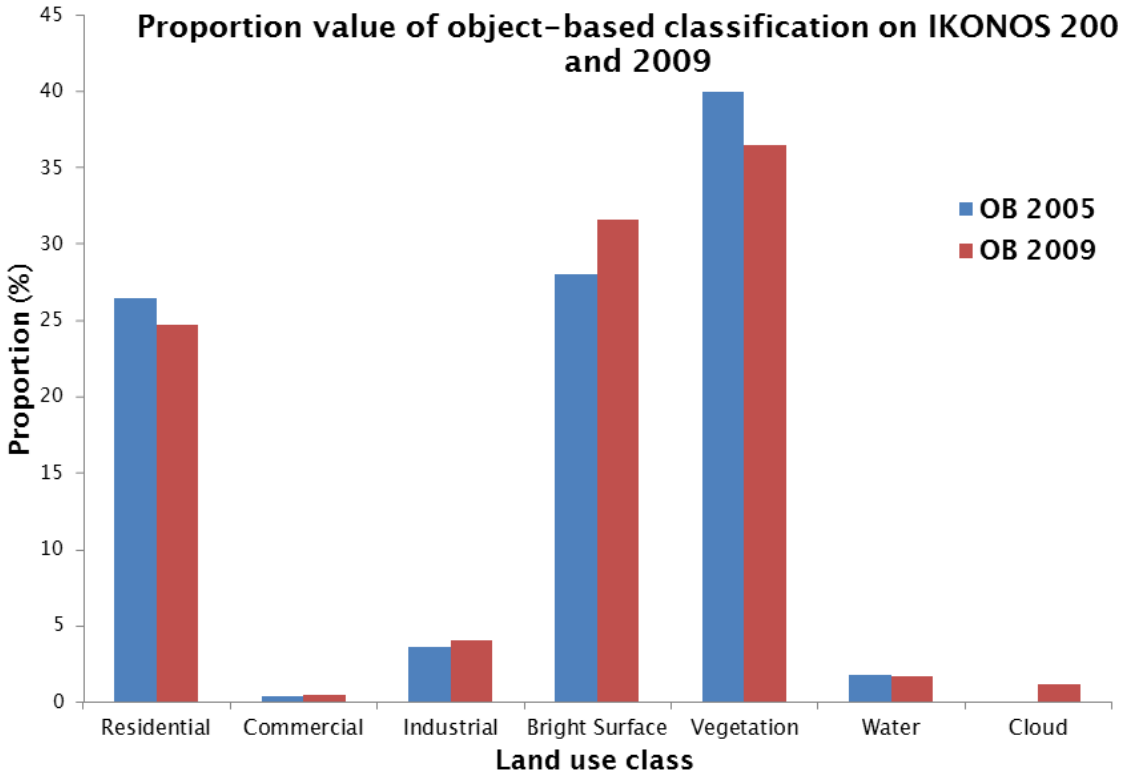


Figure 5.12 Proportion of each land use class in the object-based classification, IKONOS 2005 (OB 2005) and IKONOS 2009 (OB 2009).

### 5.3.2 RCI Classification Accuracy Test and Validation

To test the results of object classification, three assessment methods were used:

- Accuracy Assessment
- Screen Interpretation Validation
- Proportional Comparison

**Accuracy Assessment**

To assess classification accuracy, the reference land use (R2007) and Google Earth (reference image (R2010)) were compared to each of the six classified images. Google Earth imagery (R2010) was used to ensure that the training of the OB classification 2009 was sufficiently independent of the 2005 OB classification, which was done using cadastral data (R2007). These data were used to avoid the potential for bias when using the same dataset to train two separate image classifications. The method of accuracy assessment was based on the training sample data for object-based classification of randomly-supervised selected objects from the moving window from both reference datasets (R2007 and R2010). The resulting accuracy is high, representing the number of samples generated; more than 10% of the image objects were assigned iteratively to the appropriate LULC classes in the training process. In both results, at least 50 point objects per class sample were used to segment the LULC classes from the class types determined from reference source R2007 and R2010 to the OB land use classification for 2005 and 2009, respectively. In total, 300 samples were selected from the six land use classes.

To represent the results, a series of tables were produced presenting the overall classification accuracies; the confusion (error) matrices, the producer's and user's accuracy. Results of accuracy assessment are presented in Table 5.3 (2005) and Table 5.4 (2009). Overall map accuracies were similar at 79.3% for 2005 and 78.0% for 2009.

Table 5.3 Confusion matrix of the object-based classification for 2005, User's and Producer's accuracy.

| Class Types determined from Classified Map 2005 | Class types determined from reference source (R2007) | | | | | | | | User's Accuracy |
|---|---|---|---|---|---|---|---|---|---|
| | No. of Sample | R | C | I | BS | V | W | Totals | |
| | R | 38 | 2 | 2 | 4 | 3 | 1 | 50 | 76.0 |
| | C | 2 | 45 | 0 | 2 | 1 | 0 | 50 | 90.0 |
| | I | 2 | 1 | 40 | 5 | 2 | 0 | 50 | 80.0 |
| | BS | 3 | 1 | 3 | 38 | 4 | 1 | 50 | 76.0 |
| | V | 1 | 1 | 2 | 3 | 41 | 2 | 50 | 82.0 |
| | W | 4 | 0 | 0 | 5 | 5 | 36 | 50 | 72.0 |
| | **Totals** | 50 | 50 | 47 | 57 | 56 | 40 | 300 | |
| Producer's Accuracy | | 76.0 | 90.0 | 85.1 | 66.7 | 73.2 | 90.0 | | |
| Overall Accuracy | | **79.3** | | | | | | | |

Table 5.4 Confusion matrix of the object-based classification for 2009, User's and Producer's accuracy.

| Class Types determined from Classified Map 2009 | Class types determined from reference source (R2010) | | | | | | | | User's Accuracy |
|---|---|---|---|---|---|---|---|---|---|
| | No. of Sample | R | C | I | BS | V | W | Totals | |
| | R | 36 | 2 | 1 | 10 | 1 | 0 | 50 | 72.00 |
| | C | 2 | 41 | 2 | 4 | 0 | 1 | 50 | 82.00 |
| | I | 2 | 3 | 38 | 6 | 1 | 0 | 50 | 76.00 |
| | BS | 5 | 3 | 2 | 37 | 2 | 1 | 50 | 74.00 |
| | V | 1 | 1 | 2 | 0 | 42 | 4 | 50 | 84.00 |
| | W | 1 | 0 | 0 | 5 | 4 | 40 | 50 | 80.00 |
| | **Totals** | 47 | 50 | 45 | 62 | 50 | 46 | 300 | |
| Producer's Accuracy | | 76.6 | 82 | 84.4 | 59.6 | 84 | 86.9 | | |
| Overall Accuracy | | **78.0** | | | | | | | |

**Screen Interpretation Validation**

Figure 5.13 and Table 5.5 show the results of screen-to-screen (visual) validation of the classification of IKONOS data. The cadastral land use map in 2007 was used as a reference and guide in the analysis process. As the alternative result stated in Table 5.5 shows, if the segmentation result is based on the building outline, this means that the land use classes are properly defined. However, if the segmentation defines coarser or larger outlines, the classification will produce potentially mixed classes of vegetation, building (RCI) and bright surface.

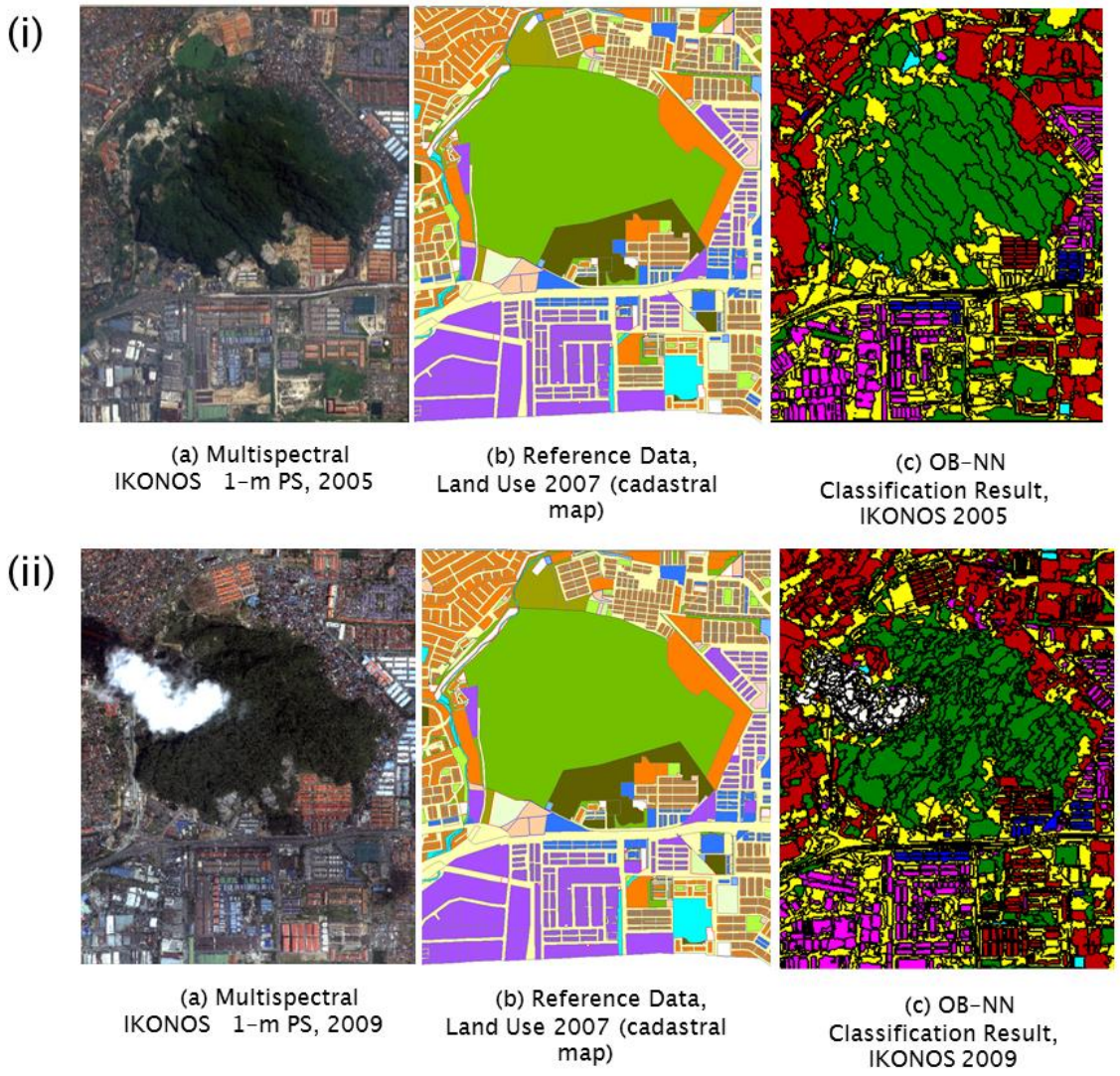


Figure 5.13 The validation result based on three dimensions of (a) IKONOS data, (b) Reference data, and (c) Prediction-Result of RCI classification.

Table 5.5 Manual Interpretation (Validation Comparison) - between the (a) original multispectral IKONOS 1 m data, (b) Reference Data, Land Use 2007, and (c) OB-NN Classification Result.

| Classes | Prediction (Imagery) | Reference Data | Prediction (result) |
|---|---|---|---|
| Residential | Too Coarse | OK | Too Coarse |
| Commercial | Too Fine | OK | OK |
| Industrial | Too Fine | Too Coarse | OK |
| Bright Surface | Too Fine | OK | OK |
| Vegetation | Too Fine | OK (Slightly too coarse) | Too fine |
| Water | Too Fine | OK | OK |

**Proportional Comparison of OB Classification vs. Reference Data R2007**

Figure 5.14 shows the result of a validation assessment test between the real reference data and the two results of RCI land use classification between 2005 and 2009. This validation tests the predicted proportional value for each land use component (residential, commercial, industrial, bright surface, vegetation and water) from the RCI classification result.

The reference dataset of R2007 provide a valid dataset as it lies between the years 2005 and 2009 of the classification analysis. Nevertheless, it is impossible to get 100% accurate results based on this comparison. However, it does provide a reasonable way to test, in a broad sense, the results obtained.

The bright surface has a slightly different result between the proportional reference data and object-based classification. In object-based classification, IKONOS imagery in 2005 and 2009 shows village buildings and the small items segmented together, falling into the same category and classified as bright surface.

Vegetation areas show a decrease due to anticipated development while clear land (bright surface) is used frequently as preparation for new development projects including RCI areas.

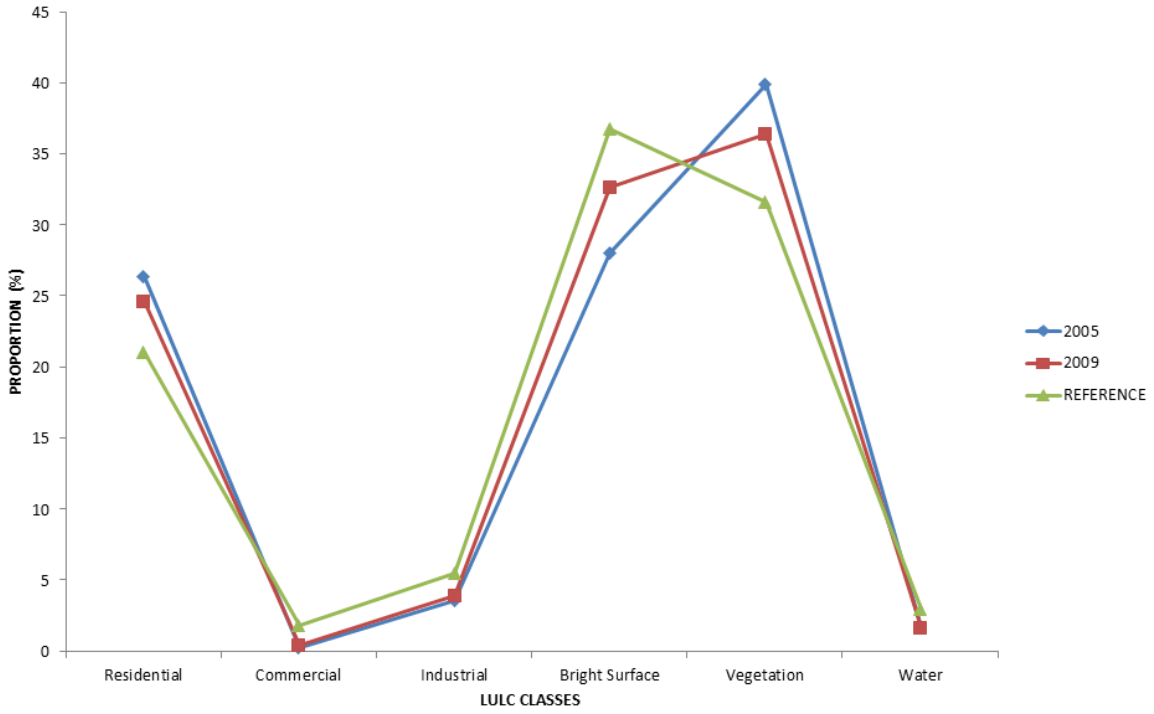


Figure 5.14 Validation result of Object-based Classification 2005 and 2009 with reference land use data 2007.

### 5.3.3 RCI Change Detection Analysis between 2005 and 2009

The next stage in the analysis involved the monitoring of land use, starting with the IKONOS data of 2005 and 2009. Object-Based Change Detection, based on post-classification methods involves the analysis of two multi-temporal images that are classified separately and labelled with proper class attributes from the result of object-based classification. In this case, two IKONOS images with 1 m pan-sharpened spatial resolution in years 2005 and 2009 and with six classes (residential, commercial, industrial, brightness surface, vegetation and water) were used. The results were classified and converted to raster data with 1 meter cell size to analyse the change of LULC class between the object-based classifications. A total of 18020000 pixels were analysed for each image. The detailed results are displayed in Figure 5.15.

The method of post-classification change detection consists of overlaying the classified images, assuming pixels are independent and perfectly co-registered

(RMS Error = 0.20). Three main steps are involved (i) transition probability matrix-post classification change detection, (ii) analysis of change in the annual period of four years for each class and (iii) generation of lookup tables (frequencies for each pixel representing transition/change over six classes) to populate the $p(t)$ matrix.

Figure 5.16 shows the result of the cross-classification of images between 2005 to 2009. The result is significant and useful because it represents land-use changes that occurred in the last four years. This analysis produced from the total set of classifications provides a clear picture of the changes in land use; 'change to' another land use and the accuracy of this decision are the result of the OB classification analysis. The results are also shown in Table 5.6 and Table 5.7. The lookup table transition over six classes is based on the transition probability matrix

$$\boldsymbol{p(t) = \frac{m}{n}}$$

where, $\boldsymbol{m}$ is the number of class transitions mapped between 2005 and 2009, and $\boldsymbol{n}$ is the number of counts across the relevant row.

These images are calculated as projections from the later of the two input land use and land cover images. The proportional error expresses the probability that the classifications in the input maps are incorrect around 0.15 (15%). The output conditional probabilities are multiplied by (1-proportional error) to produce the final output conditional probability values.

The transition probability matrix is the result of cross-tabulation of the two images adjusted by the proportional error. The transition area matrix is produced by a multiplication of each column in the transition probability matrix by the number of cells of the corresponding land use in the later image.

The data being projected forward is an even multiple of the training period, and then the new transition probability matrix is calculated through a simple powering of the base matrix. The training period is from 2005 to 2009 (4 years) and provides the transition probability (change value) for four years forward. This result will be further discussed in Chapter 8 in the context of projection analysis $\boldsymbol{t^1}$ 2009 to 2013 (4 years forward).

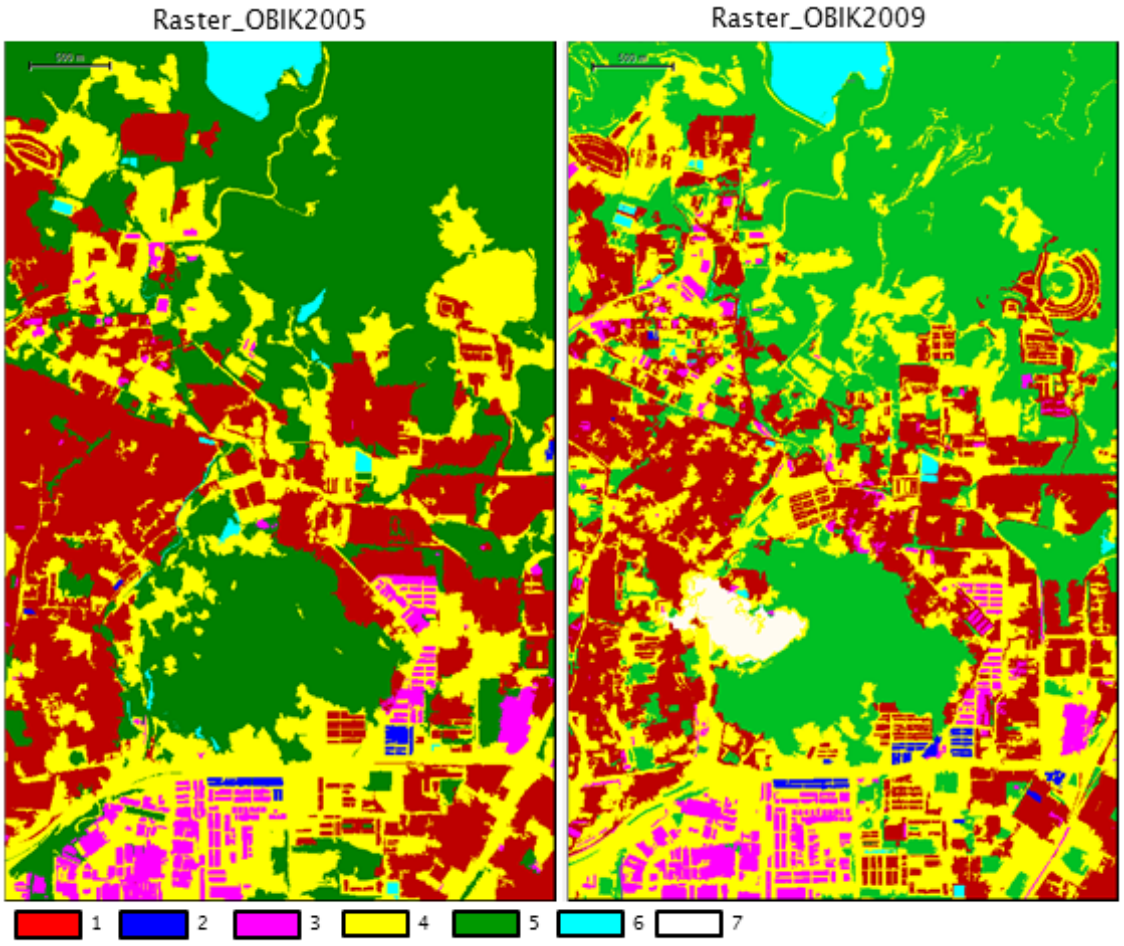


| Classes | | No. of Pixel OB_IKONOS 2005 | % | No. of Pixel OB_IKONOS 2009 | % |
|---|---|---|---|---|---|
| 1 | R | 4,759,995 | 26.42 | 4,447,033 | 24.68 |
| 2 | C | 61,533 | 0.34 | 80,269 | 0.45 |
| 3 | I | 644,995 | 3.58 | 716,817 | 3.98 |
| 4 | BS | 5,052,880 | 28.04 | 5,690,074 | 31.58 |
| 5 | V | 7,193,448 | 39.92 | 6,573,068 | 36.48 |
| 6 | Water | 307,149 | 1.70 | 305,235 | 1.69 |
| 7 | *Cloud | – | | 207,504 | 1.15 |
| Totals | | 18,020,000 | 100.00 | 18,020,000 | 100 |

*cloud = confident that the land use class under the cloud layer consist of bright surface (BS) and vegetation (V)

Figure 5.15 Raster Object-based Classification of six classes (R) residential, (C) commercial, (I) industrial, (BS) bright surface, (V) vegetation, (W) water, (C) cloud.

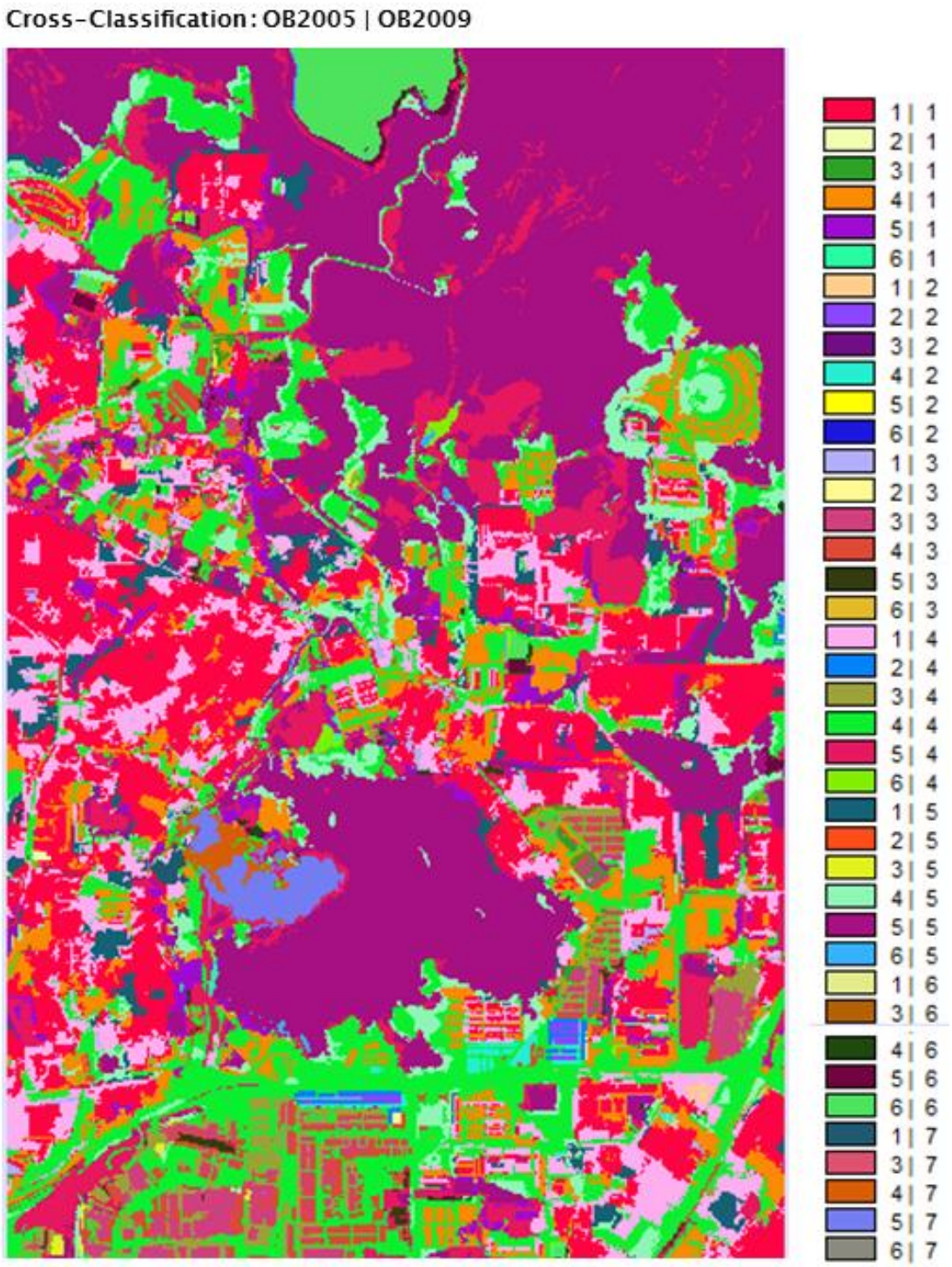


**(1) Residential (2) Commercial (3) Industrial (4) Bright Surface**
**(5) Vegetation (6) Water (7) Cloud**

Figure 5.16 Transition Matrix Map (Cross-Classification on raster OB 2005 and 2009).

Table 5.6 The lookup table of transition post-classification change detection analysis-transition areas

| | | Land Use-Land Cover at time *t2009* | | | | | | | |
|---|---|---|---|---|---|---|---|---|---|
| | | **(1)** | **(2)** | **(3)** | **(4)** | **(5)** | **(6)** | **(7)** | |
| | | **Residential** | **Commercial** | **Industrial** | **Bright Surface (BS)** | **Vegetation** | **Water** | **Cloud** | ***t2005* Total** |
| Land Use-Land Cover at time *t2005* | **(1)Residential** | **2752901** | 12163 | 72506 | 1451054 | 451584 | 2287 | 17500 | 4759995 |
| | **(2)Commercial** | 4098 | **24381** | 1403 | 31650 | 1 | 0 | 0 | 61533 |
| | **(3)Industrial** | 41573 | 429 | **286316** | 299862 | 16573 | 43 | 199 | 644995 |
| | **(4)BS** | 1266455 | 42952 | 309686 | **2569588** | 793923 | 16521 | 53755 | 5052880 |
| | **(5)Vegetation** | 367517 | 266 | 46902 | 1306586 | **5295517** | 41038 | 135622 | 7193448 |
| | **(6)Water** | 14489 | 78 | 4 | 31334 | 15470 | **245346** | 428 | 307149 |
| | ***t2009* Total** | 4447033 | 80269 | 716817 | 5690074 | 6573068 | 305235 | 207504 | 18020000 |

Table 5.7 The lookup table of transition post-classification change detection analysis-probability values

| | | Land Use-Land Cover at time *t2009* | | | | | | | |
|---|---|---|---|---|---|---|---|---|---|
| | | **(1)** | **(2)** | **(3)** | **(4)** | **(5)** | **(6)** | **(7)** | |
| | | **Residential** | **Commercial** | **Industrial** | **Bright Surface (BS)** | **Vegetation** | **Water** | **Cloud** | ***t2005* Total** |
| Land Use-Land Cover at time *t2005* | **(1)Residential** | **0.5783** | 0.0026 | 0.0152 | 0.3048 | 0.0949 | 0.0005 | 0.0037 | 1.0000 |
| | **(2)Commercial** | 0.0666 | **0.3962** | 0.0228 | 0.5144 | 0.00002 | 0.0000 | 0.0000 | 1.0000 |
| | **(3)Industrial** | 0.0645 | 0.0007 | **0.4439** | 0.4649 | 0.0257 | 0.0001 | 0.0003 | 1.0000 |
| | **(4)BS** | 0.2506 | 0.0085 | 0.0613 | **0.5085** | 0.1571 | 0.0033 | 0.0106 | 1.0000 |
| | **(5)Vegetation** | 0.0511 | 0.0000 | 0.0065 | 0.1816 | **0.7362** | 0.0057 | 0.0189 | 1.0000 |
| | **(6)Water** | 0.0472 | 0.0003 | 0.0000 | 0.1020 | 0.0504 | **0.7988** | 0.0014 | 1.0000 |
| | ***t2009* Total** | **0.5783** | 0.0026 | 0.0152 | 0.3048 | 0.0949 | 0.0005 | 0.0037 | 1.0000 |

## 5.4 Result of RCI Classification and Change Detection between 2005 and 2009

### 5.4.1 RCI Classification for 2005 and 2009

The RCI object-based classification accuracy was evaluated for two IKONOS datasets for 2005 and 2009; an error matrix and accuracy assessment was generated for the six classes of residential, commercial, industrial (same as building class in per-pixel classification), vegetation, bright surface and water. Based on the sample defined, fine spatial resolution data were sufficient to identify the land use of "building" as representative of the residential, commercial and industrial (RCI) land uses. The accuracies for 2005 and 2009 OB classification are 79.3% and 78.0%, respectively. The accuracy assessment method used is simple and straightforward given the sample data of LULC collection. The error matrix is expressed the sample and object (segmented) classification result. In every case of an object-based classification using eCognition, the use relies on the accuracy assessment in this way. However, since the accuracy assessment here is based on a known given sample (which is considered as accurate as taken from reference data), this obtain to the knowledge of an analyst who has taken the samples. Nevertheless, although the overall result appears acceptable, misclassification remains an issue especially between residential classes, including the planned and unplanned housing area and bright surfaces. These both produced misclassification even though a large supervised sample was developed for each type of land use class. This problem occurred because both categories occur in the same area, especially when the residential areas are mixed with bright surfaces and roofs which are not clearly identified and the generalised result is based on neighbouring pixels or surrounding land use.

### 5.4.2 RCI Change Detection between 2005 and 2009

To evaluate the effectiveness of the proposed method of change detection when dealing with object-based classification, results are shown in Figure 5.15

and the lookup tables of transition probabilities in Table 5.6 and Table 5.7, which show that the probability of change has a proportional error of around 0.15 (15%), using the default software. It is typical that land use maps produced by remote sensing are 85% accurate (Foody 2002) . The overall result of change detection varies depending on the quality of the classification. In this case, distinctions between bright surface, vegetation and building classes need to be more accurate in order to identify and evaluate real changes on the ground during the period of change. It could be hypothesised that an ideal result is when LULC changes from vegetation to bright surface to building (RCI), in that order, in which case these changes are expected (E). Otherwise the change could be classified as an error or pseudo-expected (PE).

From the result, the change of value from building (residential, commercial, and industrial) to the bright surface (class4) has slight errors and this problem contributes to the misclassification in the object-based classification results. This change from building to bright surface can happen in the study area, because some areas of the residential class are old villages, and some areas have squatters' residences. Through land acquisition and redevelopment, such areas will become a bright surface before a new housing scheme or business area is developed.

### 5.4.3 Between RCI OB Classification and OB Change Detection

The main objectives of this chapter were to classify RCI with multi-date fine spatial resolution data and to use the result for change detection. Both objectives seek to answer the two research questions:

1. What is the accuracy with which these classes of Residential, Commercial and Industrial (RCI) land use can be classified?

2. Can changes in land use be identified from remotely sensed imagery, including changes in and between the RCI land use classes?

To address the accuracy question, the IKONOS 2005 and 2009 RCI land use classification result was compared with the reference data as accuracy results. The accuracy of RCI was assessed through the three types of accuracy test

(*error matrix sample result*, *manual interpretation validation* and *proportional comparison* ) comparing the two classification results with the reference data land use classification (R2007 and R2010).

From the sample collection (testing data) an error matrix for the RCI classification generated a 79.3% and 78.0% level of accuracy overall across the six LULC classes. The second accuracy test using manual interpretation produced some further reassurance, but site familiarisation was required as the main input.

When analysing an object-based classification from the IKONOS data, the most important information is knowledge-based and there needs to be reference data for the particular area. In this case, at the first stage site familiarisation is used as an important tool to understand the remote-sensing data. The other option is that information will be attained through reference data such as, here, through a cadastral plan of land use. This reference information provides a suitable input to the object-based classification before the analysis run to produce the classification results.

The accuracy of the RCI classification is dependent on the object-based segmentation. To achieve an accurate segmentation depends on the scale and parameters used and the type of remote sensing data. The most accurate result of segmentation is from the fine spatial resolution remote sensing data. It clearly distinguishes between human-made and other landscapes. Another important finding was that the larger objects like ponds, lakes, stand-alone buildings or detached buildings with a clear building outline could be generated with a segmentation outline. However, small buildings like a village house or a small patch of land like a small garden or small green area normally will be joined together if the types of class are neighbours. It is somewhat surprising that that bright surface class includes misclassification of small areas like village areas in both IKONOS datasets for 2005 and 2009. To solve this problem involves manually assigning the class.

In object-based classification, it is interesting to note that two important procedures were necessary to make the RCI classification sufficiently accurate. The accurate result of segmentation between the objects also taking into from value added of knowledge-based between the study area and the data familiarisation were analysing.

The third approach to test the classification result was through comparison of the proportional area for each class between the predicted maps and the reference data (Figure 5.14).

To answer the second research question, (Can changes in land use be identified from remotely sensed imagery, including changes in and between the RCI land use classes?) the changes in land use were identified from remotely sensed imagery, including changes in and between the RCI land use classes. This requires the comparison of independently produced classified images from the RCI classification results. Six classes of land use were coded in the classification results for times $t_{2005}$ and $t_{2009}$. *T*he analysis produced change maps which were used to produce a complete transition matrix of changes between the classes. This change detection method makes comparison of the two images. Their separate classification minimised the normalising for atmospheric and sensor differences between two dates. The method also does not require an accurate registration of multi-date images for the same reason.

It seems possible that the obtained result of OB classification is due to the bright surface class (bare land/clear land/road and infrastructure) influencing the overall transition matrix of changes between the RCI transition values as presenting in Table 5.7. This misclassification or discrepancy may be due to the level of transition value of change between RCI and bright surface. However, the assumption is that the bright surface is a part of a development area and becoming an RCI transition area in the clear land area before the development of RCI was completed.

Table 5.8 Assumption of bright surface change to other classes (2005 to 2009).

| LULC Classes | *t*= 4<br>Probability of Change Values *(p)* |
|---|---|
| Residential | 0.2508 |
| Commercial | 0.0085 |
| Industrial | 0.0613 |
| Vegetation | 0.1571 |
| Water | 0.0057 |

During the four year period 2005-2009, the transitions from bright surfaces shown in Table 5.10 is ±25% change to residential, ±0.85% change to commercial, ±6% change to industrial, ±15% change to vegetation and ±0.57% change to water. Another important finding was that transition change from vegetation to bright surface was ±18% and from water to bright surface (filled the water features area to development) was ±1%. This result was generated from Table 5.9 when read horizontally class changes. The result shown is an early finding and needs further to investigate for the amount of land-use changes as further discussed in Chapter 6 and Chapter 7.

The results of this study show that a significant change between the bright surface class and RCI classes occurred in the four year period. This finding has important implications for developing the forecasting value of 4-year periods to generate the simulation of urban growth in the study area. However, this combination of findings still needs various techniques and input to improve monitoring land use change using different scales of remote sensing data, before producing the forecasting simulation based on four years changes period.

## 5.5 Discussion

Results from the OB classification were regarded as sufficiently accurate to be used in subsequent analysis in this thesis. It is particularly useful for extracting

and mapping features from fine spatial resolution data when two images are combined in the entire specified period with high-quality results of spatial data (Bhaskaran et al. 2010). Two main cases are considered to be important in discussing the OB classification process; accuracy, and 'time (*t*)'. Urban land use change and the fine resolution scene model of IKONOS image allow H-resolution analysis with the certain accurate level, but the problem is needed for very accurate co-registration. Some finding from the OB classification result to change detection analysis, the data is good for single date classification but not for image differencing. However, the post-classification comparison can perform well within the analysis.

The accuracy result in this analysis is considered acceptable for the purpose of change detection. OB classification is demonstrated to have a high level of accuracy (Bhaskaran et al. (2010); Stow et al. (2007); Drăguţ and Blaschke (2006)).

The results for 2005 and 2009 OB classification based on image segmentation have accuracies of 79.3% and 78.0%, respectively (refer to Tables 5.3 and 5.4).

The segmentation is the result of an iterative process of 'trial and error' to find the best parameters for RCI classification. The segmentation process involved regions generated from the spectral values of their pixels to represent categories in the object-based classification for the spatial context. User-defined segmentation threshold with scale 180 and colour 0.75 was acceptable to apply to fine spatial resolution data, especially for IKONOS imagery. A large scale parameter will tend to create larger objects and larger values will tend to produce results with greater emphasis on the colour or spectral value of image objects.

Time (*t*) in the context of these results of OB classification is very useful when multi-date data from fine spatial resolution is used to monitor changes in land use that occurred in the past four years. The post-classification method has been used commonly as identified by Singh (1989). The image objects generated allows the automated extraction of polygons as vector and not in raster (pixel-based). The results of both raster datasets from OB classification have to be converted .This means that, although the results are found in the

spatial or OB classification, when looking for the changes in land use these are still closely connected to the pixel or cell. It is intended that results of this change detection will be used to make forecasts in the next four years through cellular automata. This matter will be discussed further in Chapter 8.

The limitations which exist with this method vary depending on the best classification result in OB classification as single classification. Land use classes should be accurately represented on land use maps. It is quite impossible to achieve the detailed level of classification on the vector cadastral map. Therefore, the results of classification based on a predetermined objective are adequate for looking at changes in the RCI classes. In this case, a change in four-year period of the RCI is a major decision and requires further investigation.

## 5.6 Conclusion

This chapter has described OB classification and multi-date change detection based on image differences and with fine spatial resolution. Although the methods are simple, importantly high accuracy was achieved through careful and rigorous analysis such that the results can be considered acceptable for the purposes of further research on LULC dynamics in the next analysis chapters. RCI and others classes (vegetation, bright surface and water) are a combination of further LULC classes and were properly classified through OB analysis achieving highly accurate urban mapping. The chapter provided a detailed description of how each class changes within the five-year period through a transition matrix. This transition provides an overview of descriptive values of change in land use during the period for monitoring to show the extent of the change that has occurred. The result of land-use changes in pixels or cells enables a simulated forecast to be generated according to the value of changes that have been obtained, and this will be investigated in Chapter 8.

# 6. Analysis 2: Calibration for Automated Monitoring of Land Use Change from Frequent Coarse Spatial Resolution Satellite Sensor Imagery

## 6.1 Introduction

The second part of the analysis for this thesis is described in this chapter. It involves an image calibration method that aimed to monitor changes in the pixels that represented changes in land use. The main aim was to determine the accuracy of methods for monitoring land use change with frequent satellite sensor imagery with coarse spatial resolution. Selection of Landsat ETM+ data taken in series annually from 2005 to 2009 is in line with the IKONOS data that were available for only two years, 2005 and 2009. Three research questions were posed based on these data: (1) Can Landsat ETM+ be used to identify the date of change where change is known to have occurred?, (2) Can Landsat ETM+ be used to detect multiple changes of land use where change is known to have occurred?, and (3) Can Landsat ETM+ provide an 'alarm' function where change is not known to have occurred?

The calibration procedure, in turn, led to a method of monitoring changes in land use in an automated process that became one of the major foci of this research. There are many studies that discuss land-use monitoring tools. However, a more systematic and automated method is less well developed. Monitoring rules commonly used in land use such as image overlay and image differencing are fundamental to the formation and development of the programming scripts needed to create an automated and uniform method of monitoring land use. Once developed, such a method can be applied to any area with available image satellite sensor data.

In this chapter, a variety of analysis was conducted at an early stage to ensure the eventual development of an automated method suitable for monitoring land use. Some of these analyses started with atmospheric correction to remove the effects of the atmosphere on the reflectance values of images. This was key to the development of the calibration model and image normalisation.

After that, the research was extended by proportional classification of change and greenness and brightness. Both are applied here to support the goal of automated monitoring of land use and land cover.

## 6.2 Research Methodology

### 6.2.1 A General Workflow

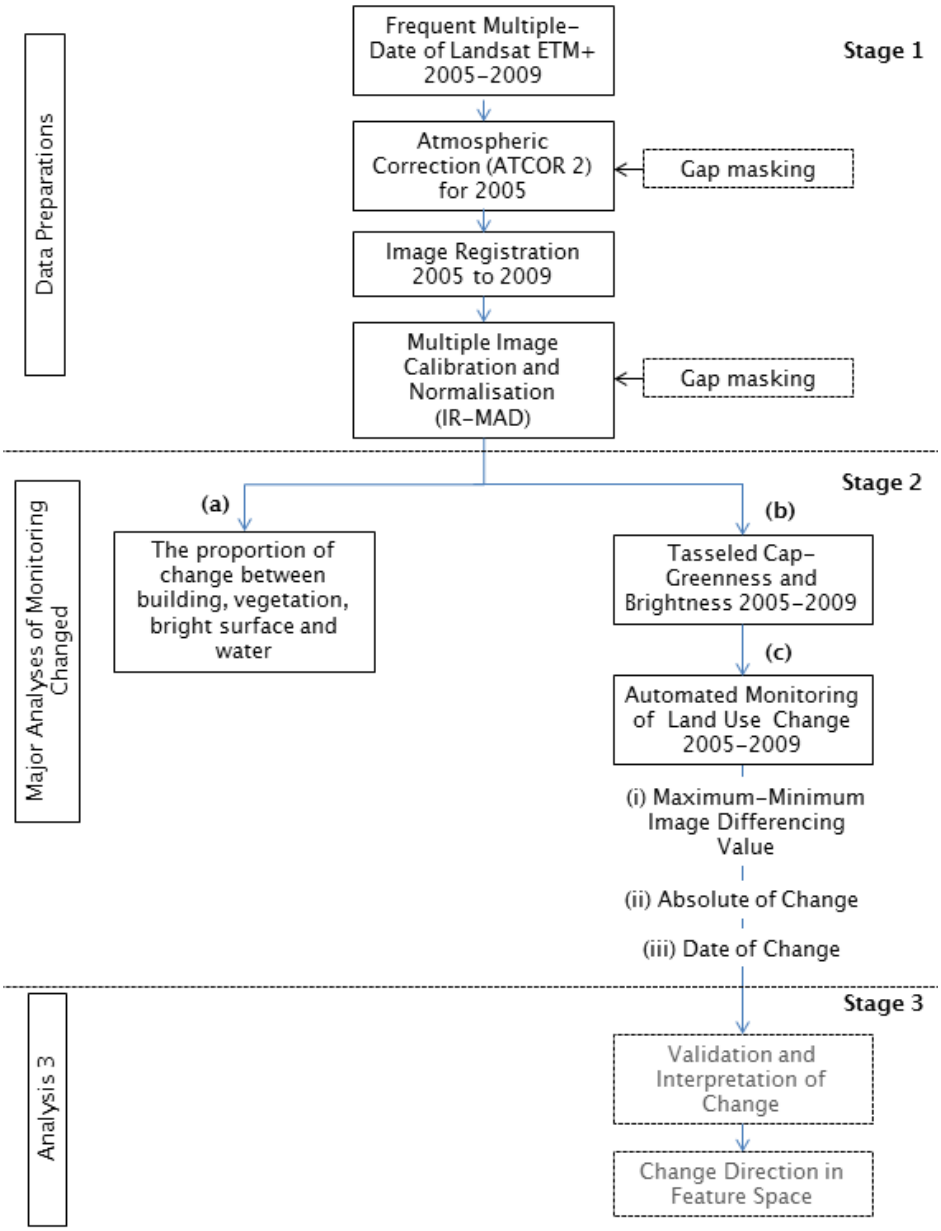


Figure 6.1 A general workflow describing the calibration process for automated monitoring of land use change.

As illustrated in Figure 6.1, this part of the research was important because it involved the complex and detailed calibration of the time-series of images before further analysis was carried out. In the first stage, the preparation of data involved a subset of data in line with the training needs within the study area.

In addition, the atmospheric correction was carried out in advance of the 2005 image before applying gap-filling analysis. The data were geo-referenced, essential for the success of the calibration process and image normalisation.

This chapter describes the major monitoring analyses using the time-series Landsat ETM+ data, described in this chapter as the second analysis (i.e., Part 2):

(i) Part 2a is an analysis of the mixed pixel classification using coarse data. The results of proportional land cover and land use serve as a guide to the monitoring process.

(ii) Part 2b is an analysis based on Tasselled Cap Transformation, greenness and brightness. It contributes to calibration by the relative radiometric normalisation of multi-temporal imagery.

(iii) Part 2c involves automatic monitoring. The results from the calibration and normalisation images were used to identify changes in land use within the stipulated period of four years. Greenness and brightness classes were used in automatic monitoring by developing programming scripts that allowed monitoring to be conducted based on Landsat ETM+ time-series data.

The third analysis part (Part 3 - validation and interpretation) is an extension of the monitoring described here, and the result will be explained in detail in Chapter 7.

### 6.2.2 Data Preparation

This research used five images of Landsat ETM+ with the path 127 and row 58, from 2005, 2006, 2007, 2008, and 2009 of a study area in Gombak District, Selangor, Malaysia, supplied by the U.S.Geological Survey, Earth Resources Observation and Science Center (EROS). All the images are SLC-off (Scan Line Corrector), which compensates for the forward motion of Landsat 7 that failed to start from 2003 onwards, but the data can still be used by filling in the

gaps. Individual bands for each image need to have gaps filled before creating the whole scene. In this case, the 2003 image with SLC-on was used as a reference image to fill the gaps from 2004 onwards. These steps were repeated for every single image until 2009. The challenge of this research is work on a time series of SLC-off images to study change detection.

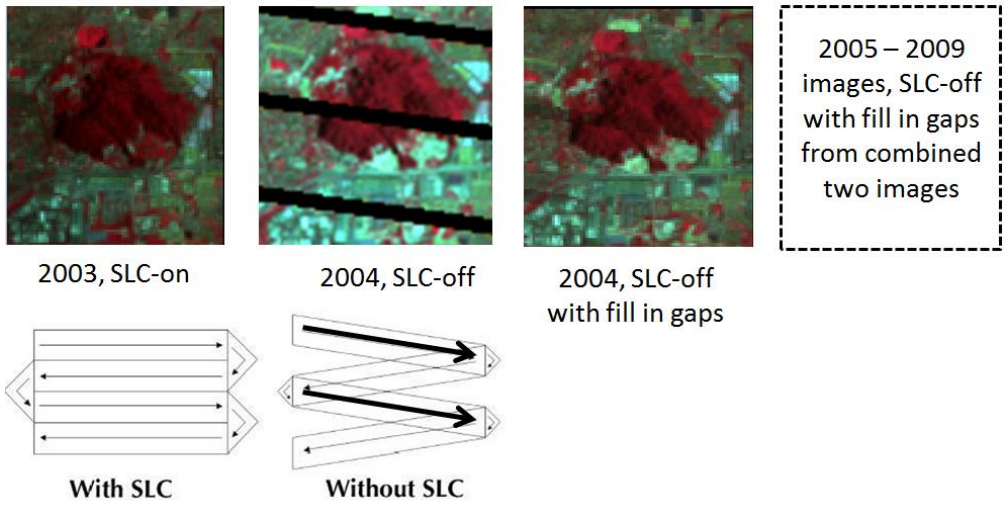


Figure 6.2 Without an operating SLC, the Landsat ETM+ line of sight traces a zigzag pattern along the satellite ground track (adapted from U.S.Geological Survey, Earth Resources Observation and Science Center (EROS).

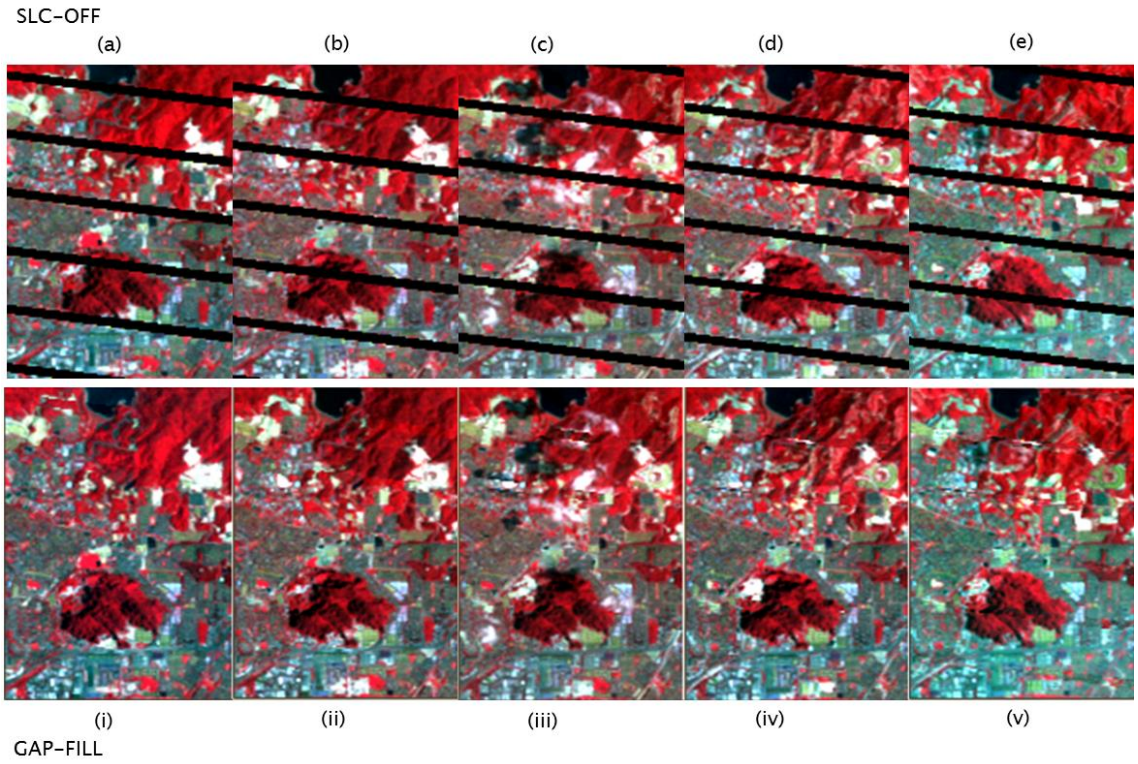


Figure 6.3 Frequent Landsat ETM+ subsets with 115 rows x 179 columns (20,585 pixels) at 30 m spatial resolution with (a-e) SLC-off and (i-v) gap-filled: (a)(i) 07 March 2005, (b)(ii) 06 February 2006, (c)(iii) 09 February 2007, (d)(iv) 27 January 2008, and (e)(v) 03 April 2009.

To fill the scan gap requires knowledge of which pixels are valid in an image and which are to be filled. The simple method applied in this study was through image mosaicking, using the mask to match areas of the unfilled 2005 image from previous images. This used a full Landsat 7 image obtained in 2003 to fill the gaps of the SLC-off scene. A scan gap mask was created for individual bands 1, 2, 3, 4, 5 and 7 that marks existing data as 1 and missing data regions as 0. These scan gap masks are created through the ENVI software and overlays the mask layer with the corresponding image band files.

A SLC-On fill scene X and a SLC-Off primary scene Y, assumes that:

$$\mathbf{Y} \approx \mathbf{X} + \mathbf{B} \qquad (6.1)$$

where

**B** = the gap masks which match the fill image to the primary image.

**X** = the existing (SLC-On) scene array.

**Y** = the 2005 image (SLC-Off) scene array.

Visually, most land types are restored adequately in the gap-filled images. Some striping appears around land cover changes such as vegetation and human activity, and also around temporary objects such as clouds and shadows. However, the gap-fill results were satisfactory for the purposes of the subsequent analysis of atmospheric correction, calibration, image standardisation and monitoring.

### 6.2.3 Software used

For the purpose of the analysis in this chapter four types of software were used; (i) ATCOR 2 software for atmospheric correction, (ii) ENVI 4.8 Software for image preparation classification and calibration, (iii) IDL (Interactive Data Language) version 8 programming and (iv) ArcGIS 9.3 for automated monitoring of change.

## 6.3 Calibration and Standardisation

Using the regression, the data needed to have the atmospheric modulation effects removed in order to estimate the surface reflectance, assuming that the spectral reflectance of the reference image is known accurately. This approach relies upon the assumption that there are some pixels in a scene with quite stable reflectance through time as invariant-objects. The linear relationship between the at-sensor radiance of the invariant-pixels and surface reflectance can be used to normalise imagery acquired at different times. Table 6.1 shows the regression values (correlation coefficient and error) before calibration of the two sample images - reference image 2005 and target image 2006 (Figure 6.4). The result shown in Figure 6.5 as linear regression (1-to-1 ortho-normal regression) before calibration between Landsat ETM+ images for 2005 and 2006.

Table 6.1 Sample result of regression and mean error before calibration between two images, Landsat ETM+ 2005 and 2006.

| | **Band 1** | **Band 2** | **Band 3** | **Band 4** | **Band 5** | **Band 7** |
|---|---|---|---|---|---|---|
| $R^2$ | 0.753 | 0.7444 | 0.7677 | 0.6627 | 0.8048 | 0.8256 |
| Mean Error | 0.1222 | 0.1072 | 0.1044 | 0.1097 | 0.10309 | 0.0581 |

*N*= 20858 pixels

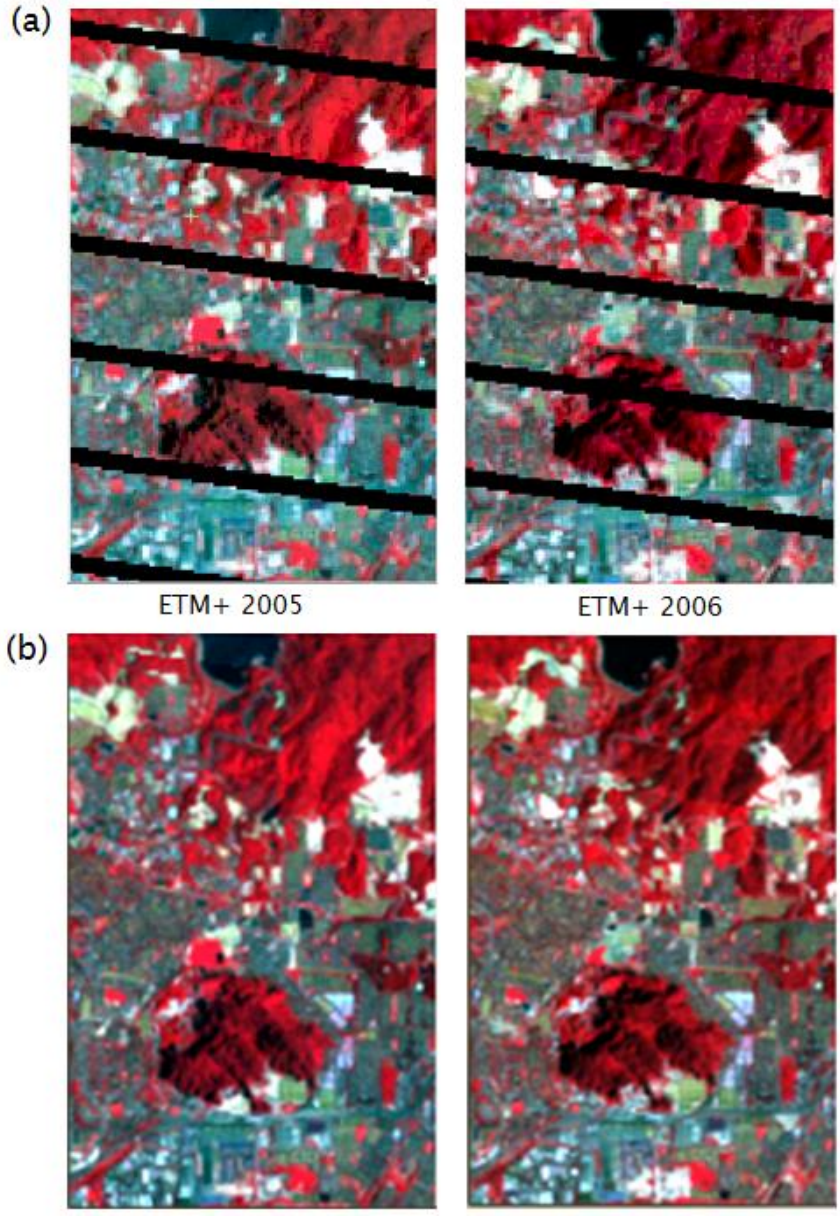


Figure 6.4 (a) the original Landsat ETM+2005 and ETM+2006 with the striping problem (SLC-off) and (b) result of atmospheric correction of Landsat ETM+2005 and radiometric normalisation of Landsat ETM+2006.

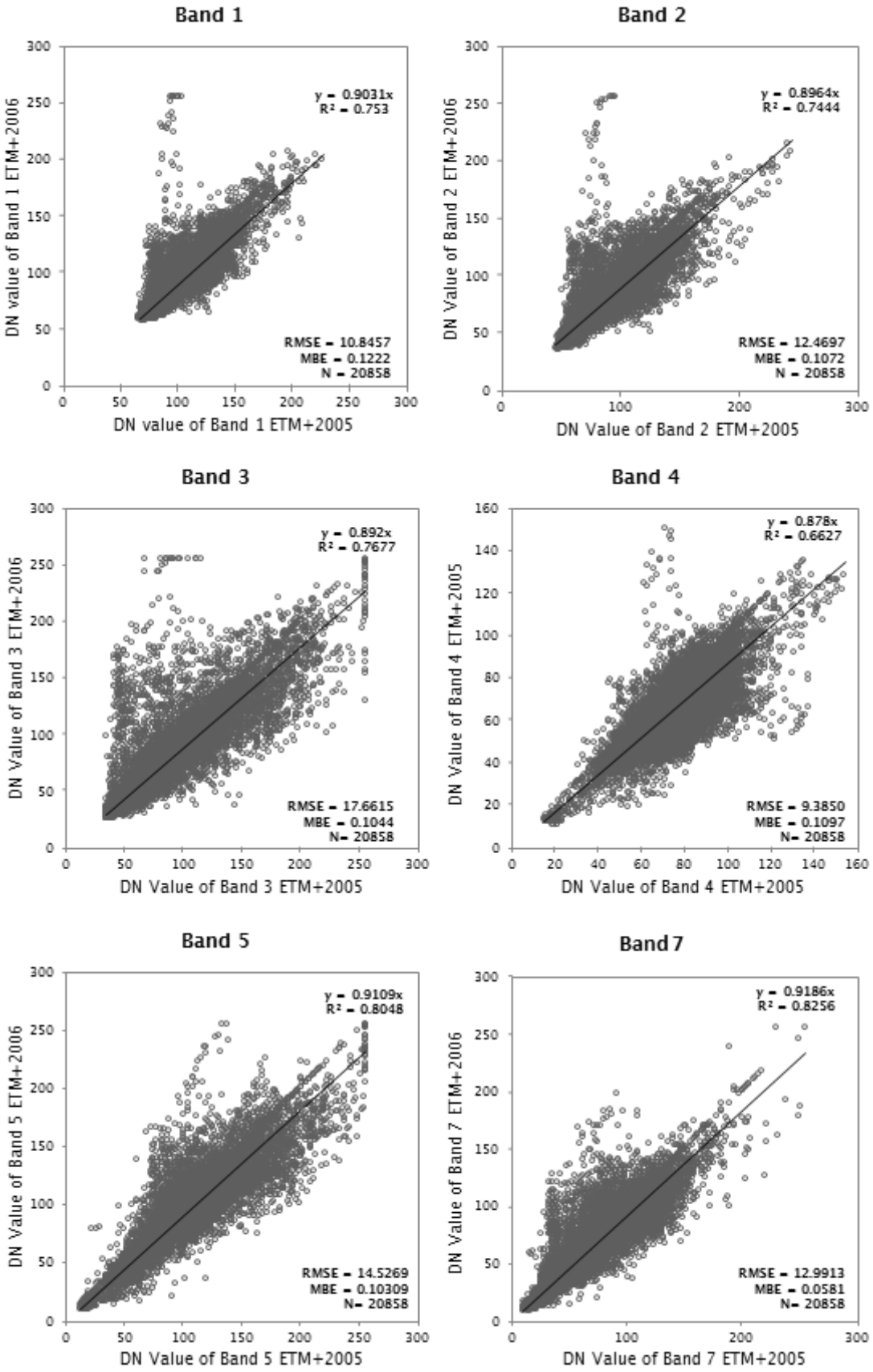


Figure 6.5 The linear regression (1-to-1 ortho-normal regression) before calibration between Landsat ETM+ images for 2005 and 2006.

### 6.3.1 Multiple image calibration and normalisation

The IR-MAD can be applied in an iteration scheme in which, when calculating the means and covariance matrices for the next iteration of the MAD transformation, observations are weighted by the probability of no change determined at the preceding iteration (Canty 2010).

For a radiometric normalisation result, the statistical test on the one-third of the time-invariant pixels between reference and target indicates an acceptable result of 95% probability of no-change pixels are significant. A fraction of the invariant pixels from the regression fit were used to test the normalised and reference images for equal radiometric characteristics. The steps involved, as described by Canty & Nielsen (2008), are as follows:

- Set weights equal to one for all pixels in the bi-temporal scene.
- Repeat until canonical correlations cease to change significantly to determine its mean and covariance matrix, perform CCA and construct the MAD variates and recalculate the weights accordingly.
- Select pixels with no change probability; that is exceeding a threshold.
- Perform an orthogonal regression on the selected pixels to determine the relative radiometric normalisation coefficients (slope and intercept).

The MAD script only uses the pixels under the mask in order to calculate the transformation coefficients. But in generating the MAD variates and the chi-squared band it applies the coefficients to all of the pixels. So anything appearing where the mask is 0 is just spurious and can be ignored. In this case the scan a line apparently is not coincide exactly and need get structure in the scan line gaps. (In RADCAL should use the same mask when choosing the chi-squared band.)

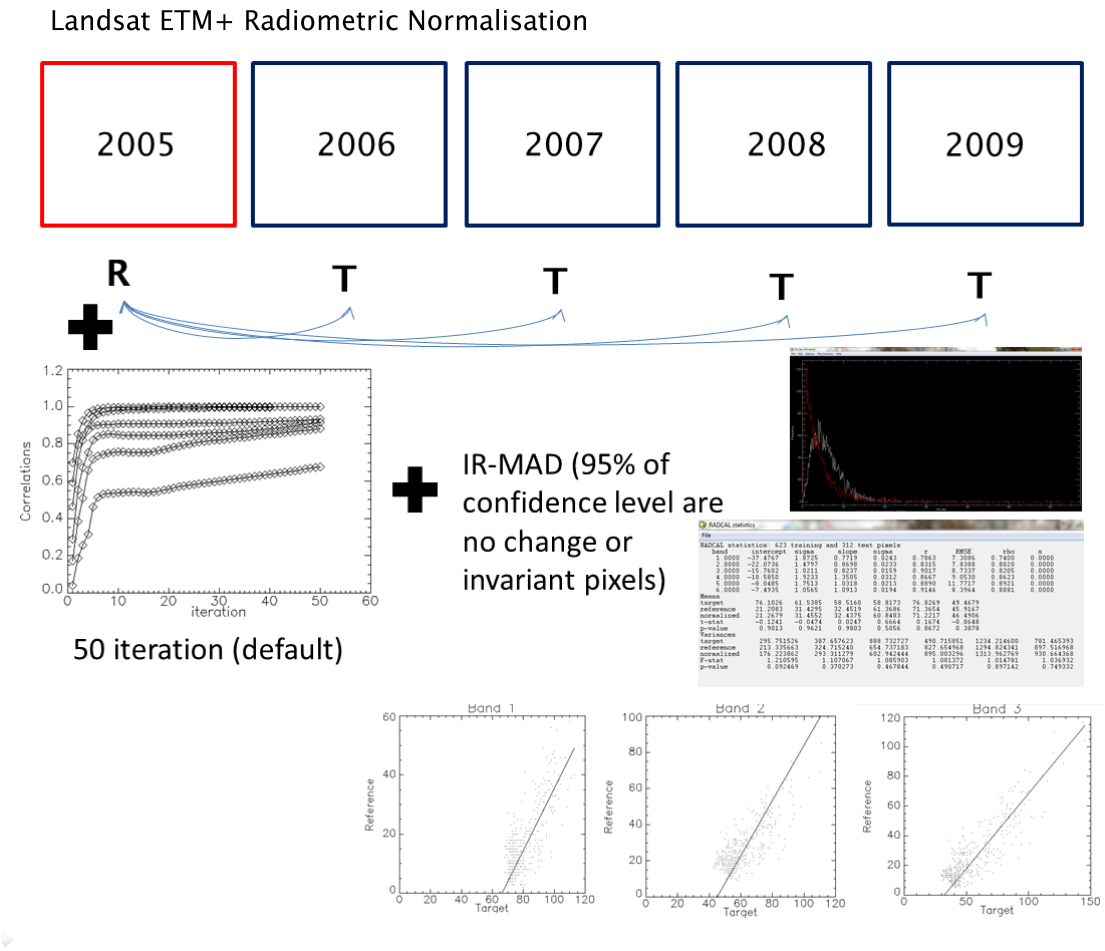


Figure 6.6 Illustration of the process of radiometric normalisation using IR-MAD between reference image (R) and target (T) images.

From Figure 6.6, the data from the Landsat ETM+2005 reference image (R) were applied for absolute radiometric correction and the rest of the images (Landsat ETM+ 2006 to 2009) were target images (T) to be normalised to the reference image (R) using linear regression based upon iteratively reweighted MAD (IR-MAD) to determine time invariant pixels. To take advantage of invariance, one can apply the MAD transformation to select the no-change pixels in un-normalised bi-temporal images, and then use them for relative radiometric normalisation. An ENVI/IDL extension RADCAL_RUN for radiometric normalisation with the MAD transformation is given. Two multispectral images (reference and target) are chosen at the prompts, then the output destination is entered. If the images are not of the same spectral or spatial dimension, the program will abort. The program reads the output from a previous IR-MAD transformation that has been performed on overlapping

portions of the images to be normalised. The programme is used to select pixels with a high no-change probability, by default 0.95 or above.

The Chi-square image generated previously by MAD_RUN on the same spatial or spectral subsets is needed. The histograms of the Chi-square images are displayed to compare with the theoretical histogram for purely no-change observations, that is, the Chi-square distribution for uncorrelated, normally distributed MAD variates (lower curve). Using the 95% probability to identify no change pixels must then be chosen as well as the output destination for the normalised target images (Landsat ETM+ 2006, 2007, 2008 and 2009). During the calculation, orthogonal regressions are plotted in separate plot windows, once for each spectral band in Figure 6.7. Regression statistics and results of statistical tests calculated with the invariant pixels can be found in Table 6.2 and Appendix 4.

The orthogonal regression coefficient and lines obtained for other images Landsat ETM+ 2007, 2008 and 2009 show the association of radiometric normalisation with the reference Landsat ETM+2005 image in Appendix 4.

## a) Calibration and standardisation of the 2005 and 2006 images

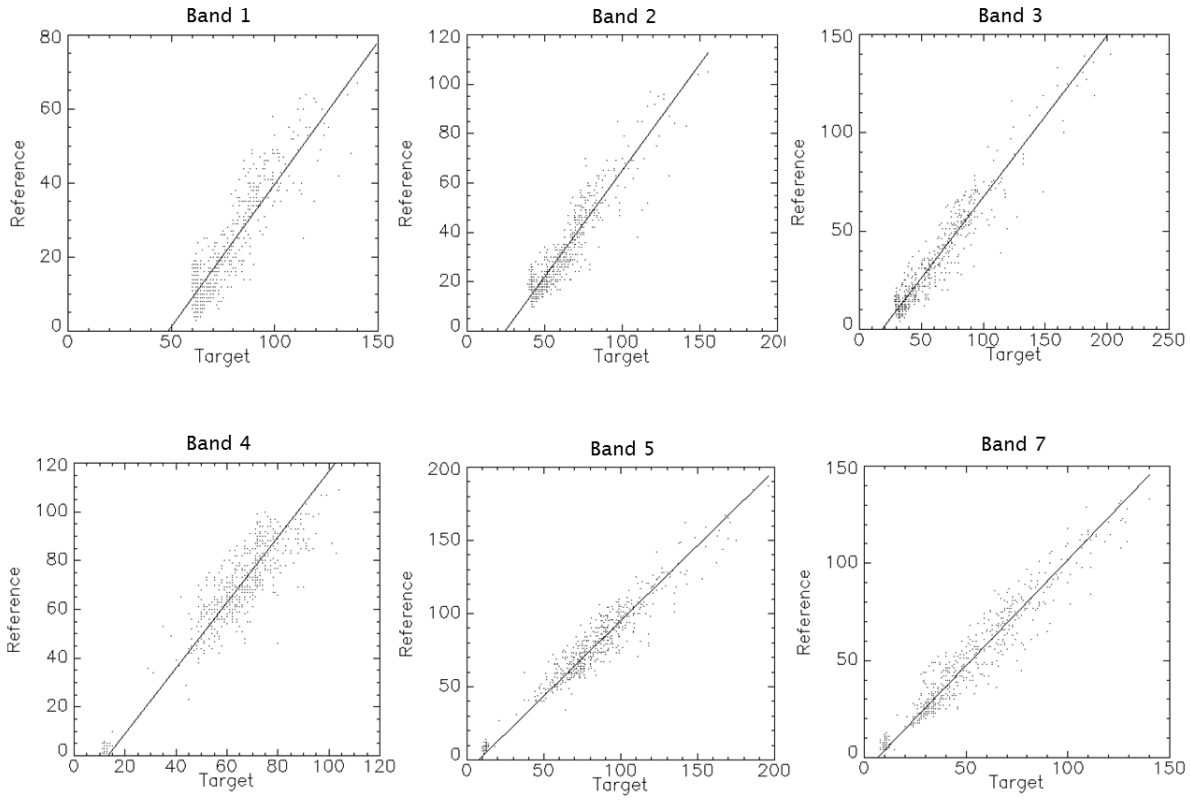


Figure 6.7 Regressions of the Landsat ETM+ 2005 reference scene on the Landsat ETM+2006 target (uncalibrated) scene.

Table 6.2 Orthogonal regression coefficients and statistics for radiometric normalisation of the images of Landsat ETM+2005 and Landsat ETM+2006.

| Band | Intercept | Sigma | Slope | Sigma | Correlation (r) | RMSE |
|---|---|---|---|---|---|---|
| 1 (0.4787) | -37.4767 | 1.8725 | 0.7719 | 0.0243 | 0.7863 | 7.3086 |
| 2 (0.5610) | -22.0736 | 1.4797 | 0.8698 | 0.0233 | 0.8315 | 7.8388 |
| 3 (0.6615) | -15.7602 | 1.0211 | 0.8237 | 0.0159 | 0.9017 | 8.7337 |
| 4 (0.8346) | -18.5850 | 1.9233 | 1.3505 | 0.0312 | 0.8667 | 9.0530 |
| 5 (1.6502) | -8.0485 | 1.7513 | 1.0318 | 0.0213 | 0.8890 | 11.7717 |
| 7 (2.2081) | -7.4935 | 1.0565 | 1.0913 | 0.0194 | 0.9146 | 8.3964 |

Table 6.3 Comparison of means and variances for Landsat ETM+2005 and Landsat ETM+2006, with *t*-test and *F*-test for 623 training and 312 test pixels.

| | Band 1 | Band 2 | Band 3 | Band 4 | Band 5 | Band 7 |
|---|---|---|---|---|---|---|
| Target mean | 76.1026 | 61.5385 | 58.5160 | 58.8173 | 76.8269 | 49.4679 |
| Reference mean | 21.2083 | 31.4295 | 32.4519 | 61.3686 | 71.3654 | 45.9167 |
| Normalised mean | 21.2679 | 31.4552 | 32.4375 | 60.8483 | 71.2217 | 46.4906 |
| t-Statistic | -0.1241 | -0.0474 | 0.0247 | 0.6664 | 0.1674 | -0.8648 |
| *P*-value | 0.9013 | 0.9621 | 0.9803 | 0.5056 | 0.8672 | 0.3878 |
| Target variance | 295.751526 | 387.657623 | 888.732727 | 490.715851 | 1234.214600 | 781.465393 |
| Reference mean | 213.335663 | 324.715240 | 654.737183 | 827.654968 | 1294.824341 | 897.516968 |
| Normalised mean | 176.223862 | 293.311279 | 602.942444 | 985.003296 | 1313.962769 | 930.664368 |
| *F*-Statistic | 1.210595 | 1.107067 | 1.085903 | 1.081372 | 1.014781 | 1.036932 |
| *P*-value | 0.092469 | 0.370273 | 0.467844 | 0.490717 | 0.897142 | 0.749332 |

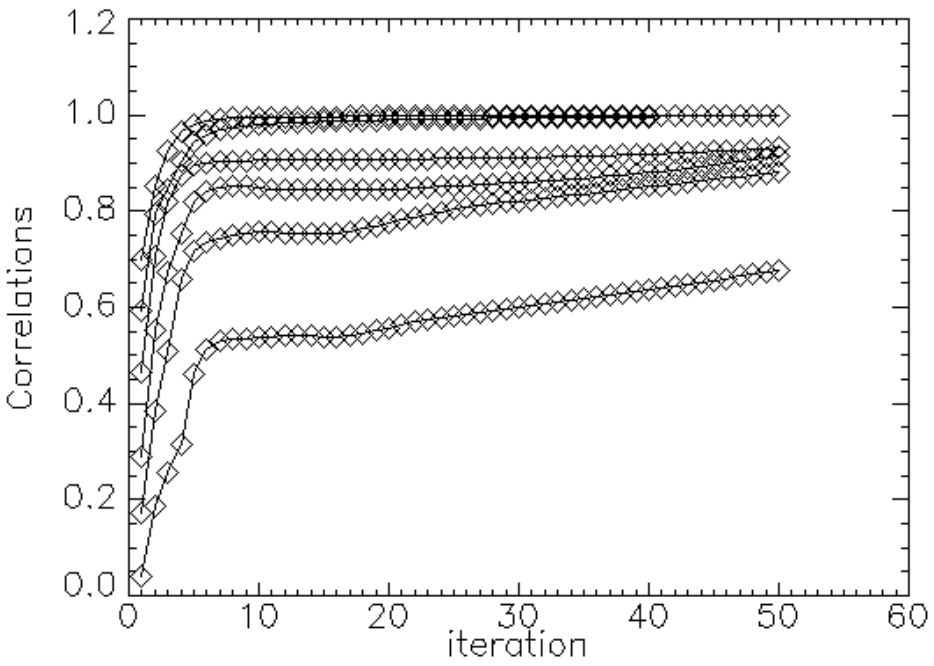


Figure 6.8 The canonical correlations pi, i=1...6, under 50 iterations of the MAD transformation of the bi-temporal images Landsat ETM+2005 and Landsat ETM+2006.

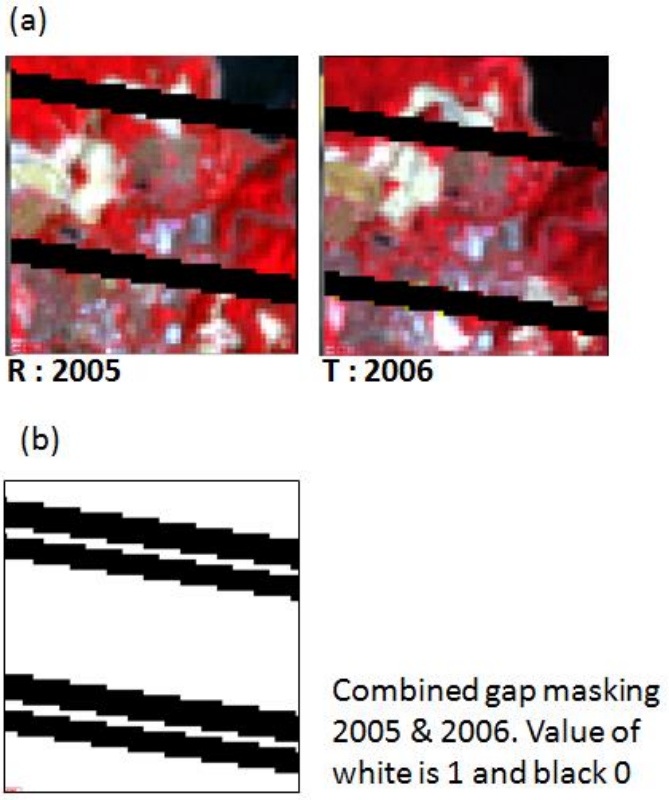


Figure 6.9 (a) Shows images 2005 and 2006 of the targets picked out as invariant, (b) combined gap masking.

Results of hypothesis testing for equal means and variance are included in terms of *P*-value as shown in Table 6.3. The *P*-value for tests for equal means and variances of the reference and normalised images are in both cases satisfactory, indicating that in this case a single iteration suffices for adequate identification of invariant pixels.

Detailed explanations of the comparison of means and variances for the normalised images for 2006 to 2009 as are follows:

- *P*-value is the lowest level of significance at which the null hypothesis could have been rejected. In this case, values close to one strongly support the null hypothesis of equal means and variances.
- Both the paired *t*-test and the *F*-test (which test the hypotheses of equal means and variances after normalisation) are two-sided tests. This means that values of the *t*-test close to zero and *F*-test close to one indicate better results. In both cases the best *P*-values are close to one (the closer the better). One can accept the hypotheses of equal means or equal variances for *P*-value above some pre-set value that is traditionally often set to 5%.

The statistical test on the one-third of the time-invariant pixels between the reference (i.e., 2005) and all target images indicate a significant result of 95% probability of no-change pixels. The IR-MAD method for performing radiometric normalisation can, therefore, be accepted for the creation of multispectral normalised images. All the results presented in Table 6.3 of the *P*-value test were accepted and produced similar multi-date calibration images (2006 to 2009). The linear regression was acceptable and corresponded to results of the *P*-value test. Thus, the IR-MAD calibration method succeeded in identifying suitable invariant pixels for the purpose of radiometric normalisation. The target image can be normalised to a reference image using linear regression using iteratively reweighted MAD (IR-MAD) to determine time invariant pixels by ENVI/IDL. Analysis was done through MAD transformation to select the no-change pixels in the un-normalised bi-temporal Landsat ETM+ 2005 image and then used for relative radiometric normalisation for Landsat ETM+ 2009. An ENVI/IDL extension RADCAL_RUN for radiometric normalisation with the MAD transformation is given with a high no-change probability, by default 0.95 or above. The result was automatically generated from the output of the reference and target images. This was carried out on

overlapping portions of the images to be normalised, to show the changed pixels.

The procedure of the automated change detection started from an invariant pixel – Multivariate Alteration Detection (MAD) for 2005 and 2009 data performed in a simple IDL GUI (Graphics User Interface), called MAD_VIEW that determined change thresholds and displayed the threshold MAD variates in various colour combinations and histogram stretches as an unsupervised classification. A threshold (parameter ±32) standard deviations of the no-change observations was set. This very large dynamic range typifies the sensitivity of the IR-MAD method. The result is displayed in Figure 6.10 (surely some of these are in the gap-filled areas).

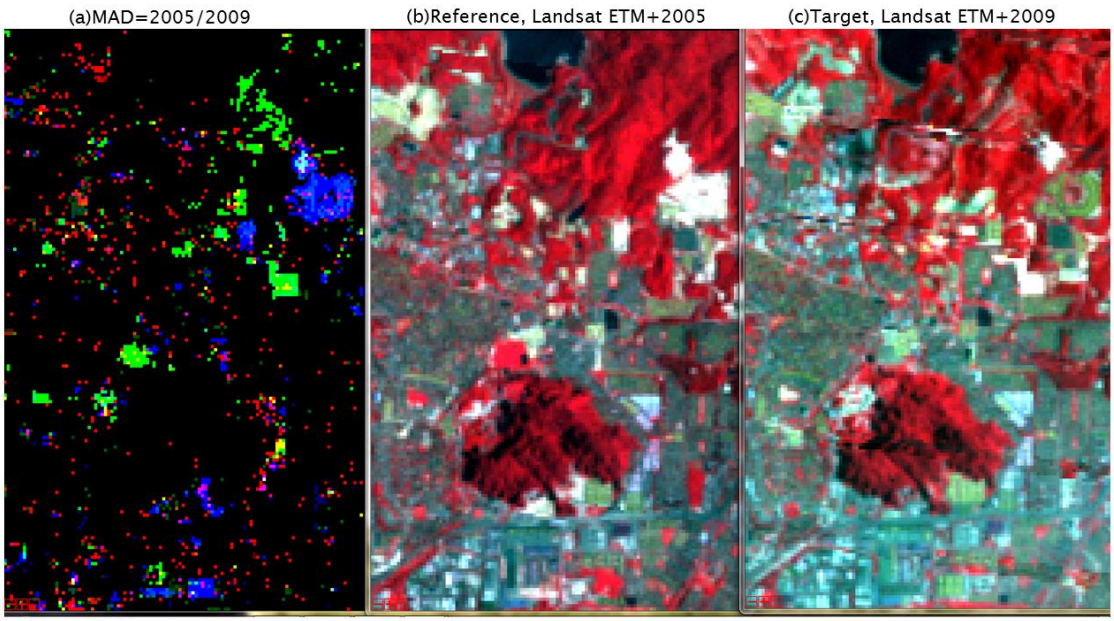


Figure 6.10 (a) MAD for Landsat ETM+2005 and 2009 showing changes with the invariant pixels between positive (2009) and negative (2005) with red, green and blue changes: green-yellow (bright surface), blue-purple (building) and red (vegetation) within the 4-year period from (b) Landsat ETM+2005 and (c) Landsat ETM+2009.

To accomplish automated monitoring, prior calibration of multi-date imagery is important. This involves image data standardisation. Normalisation used 2005 data as a reference, whilst the following year was the target. The overall

result of calibration is acceptable when the *P*-value test value is close to one (the closer the better). This allows rejection of the null hypothesis and hence adequate identification of invariant pixels. As a result, the hypothesis of equal means and equal variances for the *P*-value can be accepted. The *t*-test value must be close to zero and *F*-test values close to one in order to obtain a confident result. The software automatically detects the change pixels between the reference and target images. The statistical design for one-third sample of time-invariant pixels has a 95% significance level of accepting no-change pixels.

Table 6.4 Year 2005 vs. 2009, comparison of means and variances

| | **Band 1** | **Band 2** | **Band 3** | **Band 4** | **Band 5** | **Band 7** |
|---|---|---|---|---|---|---|
| *t*-test | 1.2062 | 0.8518 | 1.0842 | 0.3777 | 0.2989 | 0.6497 |
| *P*-value | 0.2817 | 0.4332 | 0.3278 | 0.7212 | 0.7770 | 0.5445 |
| *F*-test | 1.412069 | 1.947580 | 1.249838 | 2.097006 | 1.796540 | 1.097452 |
| *P*-value | 0.714193 | 0.482002 | 0.812641 | 0.435669 | 0.535830 | 0.921209 |

Table 6.4 highlights the calibration of reference image 2005 with target image 2009 to illustrate the overall result of calibration between the period of investigation of changed pixels. The calibration is accepted from identifying invariant pixels for the purpose of normalisation of frequent Landsat ETM+ imagery.

The result of MAD highlighted initial changes of the invariant pixels between positive (2009) and negative (2005). Red, green and blue show change: green-yellow (bright surface), blue-purple (building) and red (vegetation) within the 4-year period. The result is displayed in Figure 6.10, showing the automated changes that occurred between pixels, representing the LULC changes for a single normalisation image result. However the result is not sufficient to define a single 3D array for the five images (i.e., x, y and t), which refers to the pixel (x, y) and the time period (t) between images 2005 to 2006, 2006 to 2007, 2007 to 2008 and 2008 to 2009. There is a need to run concurrent simultaneous analysis of changes. The result is only sufficient to calibrate the multi-date imagery between two dates, which are the reference and target data for image normalisation.

## 6.4 Analysis and result of the monitoring of land use change

### 6.4.1 The proportion of change between building, vegetation, bright surface and water

In order to assess the land use and land cover (LULC) change in the study area from coarse spatial resolution, the method of SMMA was adopted for five multispectral Landsat ETM+ images with 30 m spatial resolution from 2005 to 2009 (all including gap-filled images). Conducting classifications of coarse spatial resolution images helps to identify LULC types and aids interpretation of LULC change for multi-date data.

The basic principle of mixture modelling within a given scene is that the surface is dominated by a small number of common materials that have characteristic spectral properties. In this case, the spectral properties refer to end-members or pure pixels and it is assumed that spectral variability can be modelled by a mixture of end-members.

The standard method of SMMA involves image pre-processing, image end-members selection, image classification proportion and interpretation. Throughout the analysis, the objective was to estimate the proportion of each ground pixel divided up among different LULC types. From the analysis, the result produced is a series of images based on the selection of end-members for building, bright surface, vegetation and water. The study used image end-members because they could be obtained easily, and they represented reflectance measured at the same scale as the five Landsat ETM+ images.

Regarding Landsat ETM+, six bands were chosen for the purpose of the research. The six wavebands used in the subset of 20,858 pixels (NS115xNL179) included Band 1 (0.45-0.52*μm,* blue green), Band 2 (0.52-0.60*μm,* green), Band 3 (0.63-0.69*μm,* red), Band 4 (0.76-0.90*μm,* near infrared), Band 5 (1.55-1.75*μm,* mid infrared) and Band 7 (2.08-2.35*μm,* mid-infrared). A total of four specific end-members were selected from the first image in 2005, where each class represented a common land cover type of

Gombak District; (a) bright surface (b) building (c) vegetation (d) clear water. Typical examples are shown in Figure 6.11.

The Landsat ETM + image was classified using the categories of the object-based (OB) classification in Chapter 5. After a thorough analysis, it was found to be rather difficult to isolate the spectral values (end-members) that describe the differences within the RCI (residential, commercial, industrial) classification. A single building may have a wide range of reflectance values because of the effects of materials and shading. The coarse spatial resolution data were adequate for classifying RCI as one group labelled 'building'. The other classes of land use were the same as for the OB classification.

Based on the calibration principle, end-member values from the 2005 data were applied to the rest of the images, given that all images were adequately calibrated with radiometric normalisation. Figures 6.11 and 6.12 show the spatial distribution and abundance of the end-member components in the scene. The end-member pixels identified in the first phase represented only a small percentage of all image pixels. The second stage aimed to make an optimal separation between these two groups, including the identification of the respective surface material for the really pure end members. For this purpose an algorithm was chosen based on a linear unmixing classification from the end-member selection of the appropriate land use and land cover.

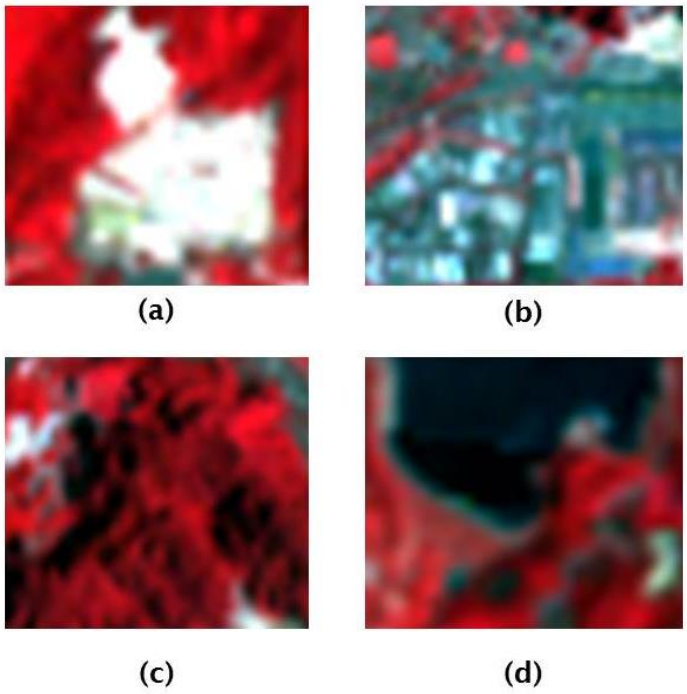


Figure 6.11 Example of Landsat ETM+ sub-images representing the different LULC classes (band 4, band 3, band 2) with (a) bright surface, (b) building, (c) vegetation (d) clear water.

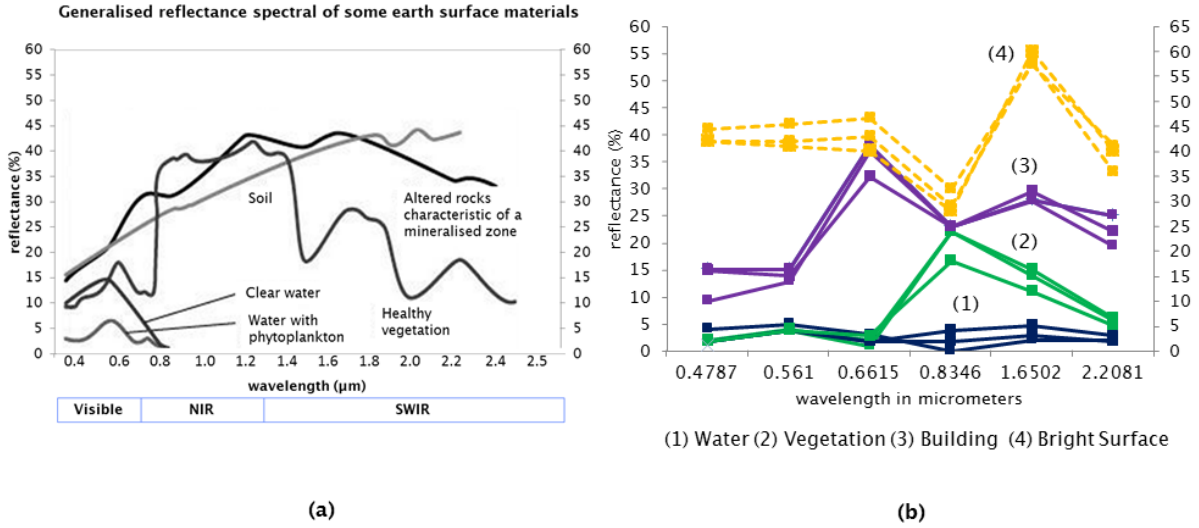


Figure 6.12 Spectral reflectance (a) general reflectance spectra, (b) pure pixels (end-members) for four classes from the Landsat ETM+ 2005 image.

Table 6.5 The proportion of change between building, vegetation, bright surface and water from 2005 to 2009 *(N=20858).*

| **Classes** | **OB range 2005 to 2009** | **Proportion (%) rate F (SMMA)** | **Number of pixels fraction counts from the value 0.0-1.0** | **Number of error fraction counts from value <- 0.0 - > 1.0** | **RMSE** |
|---|---|---|---|---|---|
| **ETM+2005** | | | | | |
| Building | 30-31% | 24.85% | 10911 | 9947 | 0.001488558 |
| Vegetation | 37-40% | 36.5% | 16030 | 4828 | 0.0050742 |
| Bright Surface | 28-32% | 25.19% | 11061 | 9797 | 0.0020535 |
| Water | 1.7% | 13.43% | 5897 | 14961 | 0.005206 |
| **ETM+2006** | | | | | |
| Building | 30-31% | 26.56% | 10964 | 9894 | 0.001568826 |
| Vegetation | 37-40% | 32.47% | 13401 | 7457 | 0.003696296 |
| Bright Surface | 28-32% | 27.58% | 11384 | 9474 | 0.002889987 |
| Water | 1.7% | 13.43% | 5520 | 15338 | 0.005926613 |
| **ETM+2007** | | | | | |
| Building | 30-31% | 27.93% | 10895 | 9963 | 0.211383763 |
| Vegetation | 37-40% | 33.14% | 12924 | 7934 | 0.003386707 |
| Bright Surface | 28-32% | 25.05% | 9772 | 11086 | 0.002534697 |
| Water | 1.7% | 13.87% | 5413 | 15445 | 0.006100409 |
| **ETM+2008** | | | | | |
| Building | 30-31% | 30.24% | 10388 | 10470 | 0.062700441 |
| Vegetation | 37-40% | 33.81% | 11612 | 9246 | 0.002332033 |
| Bright Surface | 28-32% | 20.70% | 7111 | 13747 | 0.002487781 |
| Water | 1.7% | 15.22% | 5413 | 15445 | 0.006100409 |
| **ETM+2009** | | | | | |
| Building | 30-31% | 28.54% | 10364 | 10494 | 0.078946948 |
| Vegetation | 37-40% | 33.44% | 12144 | 8714 | 0.002807853 |
| Bright Surface | 28-32% | 23.73% | 8618 | 12240 | 0.002490659 |
| Water | 1.7% | 14.28% | 5189 | 15669 | 0.006432258 |

Each pixel was extracted based on a spectral mixture of end-members in order to determine the proportion (F) of land use and land cover from 2005 to 2009 as result shown in Table 6.5. Overall, the area of building increased from 24.85% to 28.54%, whilst the proportions of the vegetation and bright surface classes decreased. The increased area of water can be explained by new dark surfaces in the new building class which were misclassified.

The area of building increased slightly between 2006 and 2008. This can be explained by the growth of human activities including RCI development. However, comparing the building and bright surface classes, there was variation between them over the years. This was due to removal of vegetation and squatter settlements that affected the bright surface value. When the vegetation and bright surface classes were compared, results showed changes that could be explained by human activities.

The number of pixels fraction counts (0.0-1.00) refers to the value for each class and a negative value counts (<- 0.0 -> 1.0) refers to the error fraction in other classes. All the results were generated from the calibration equation to ensure that the rules of the end-members were functioning to predict proportional values and X are reflectance values from observed vector $(x_1, x_2, x_3 \ldots\ldots x_n)$ for each band to land cover.

The error fraction is the error of the fit for each particular land use class. To assess the accuracy of SMMA, the RMSE was used for all bands. The residuals are the differences between the original DN pixels and the predicted DN. The overall result of the model is judged to be accurate if the band residual or RMSE has a low value and if the fraction is not lower than 0 or larger than 1 as in Table 6.5. Whereas, if the class pixels have a large RMSE value and / or fractions lower than 0 or larger than 1, this indicates an error fraction reflecting the compositional variability in the data.

The result of proportional (F) separation images is displayed in Figures 6.13 to Figure 6.15.

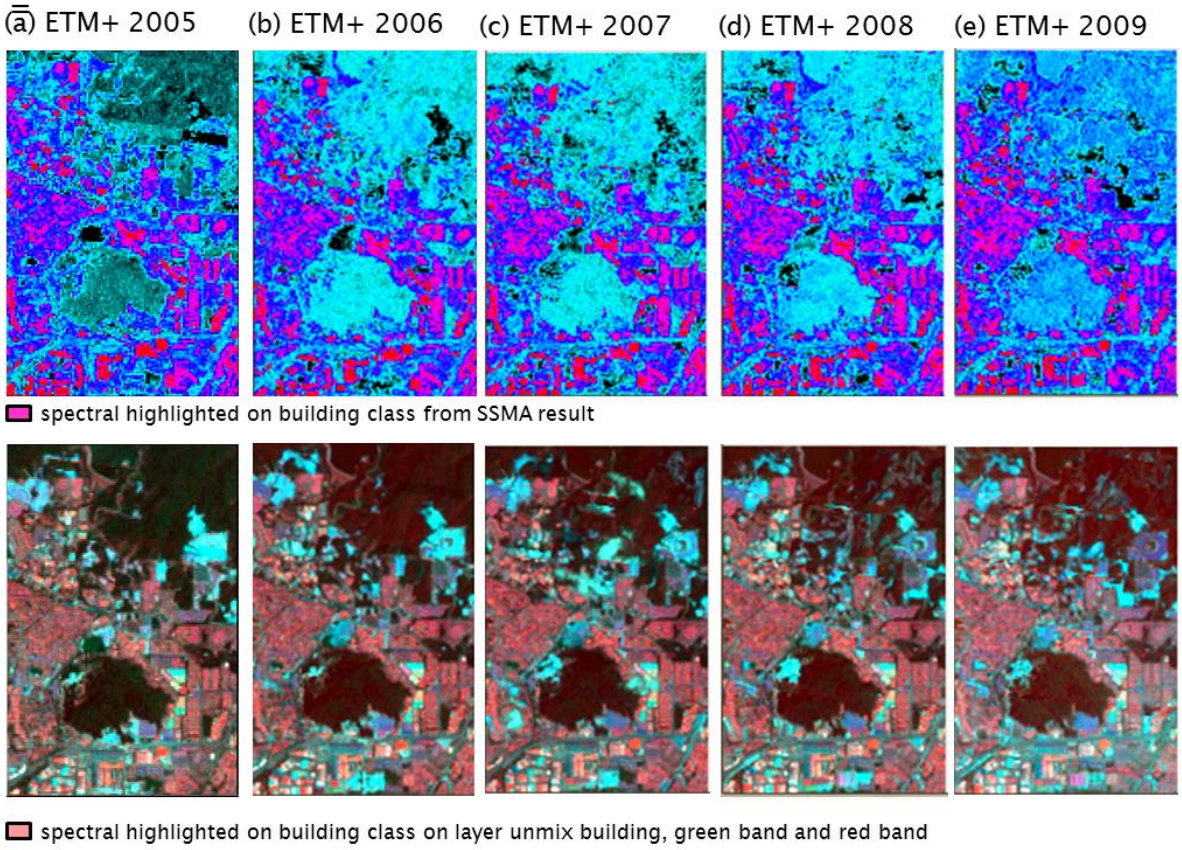


Figure 6.13 A set of Landsat ETM+ (gap-filled) time-series results of SMMA for building proportion (F) is 24.8% in 2005 to 28.54% in 2009.

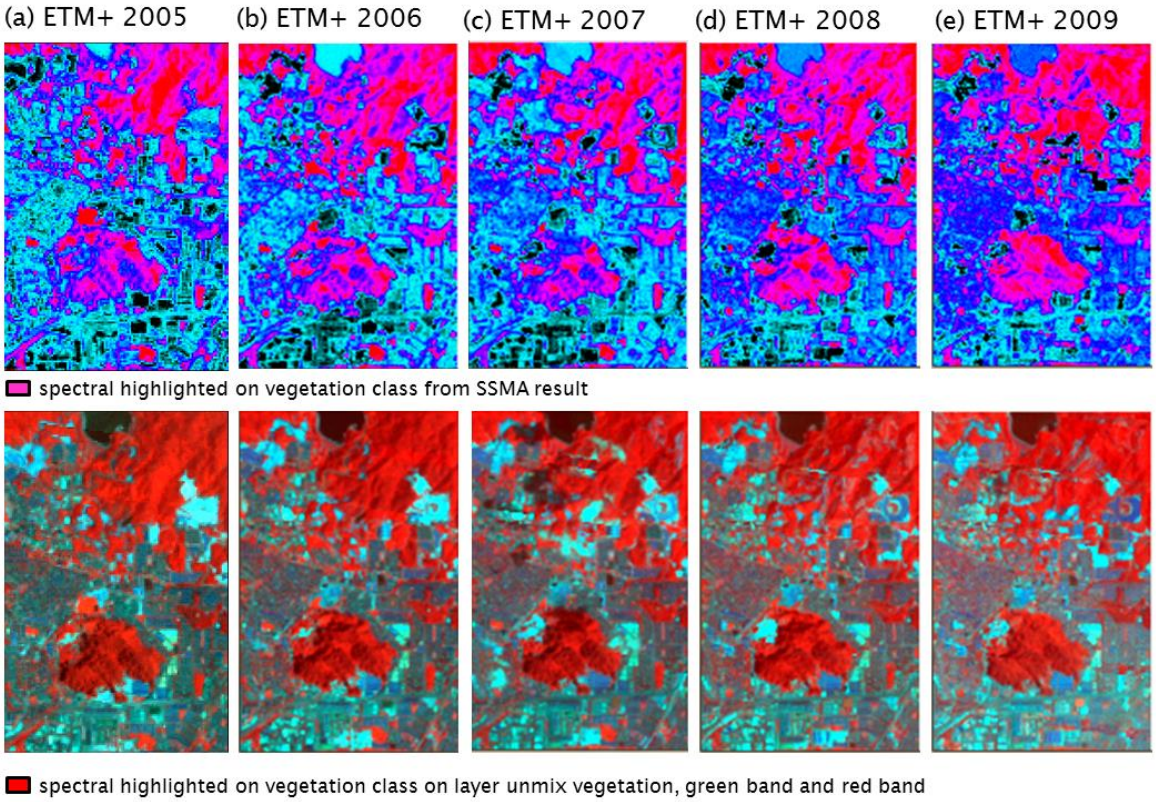


Figure 6.14 A set of Landsat ETM+ (gap-filled) time series results of SMMA for vegetation proportion (F) is 36.5% in 2005 to 33.44% in 2009.

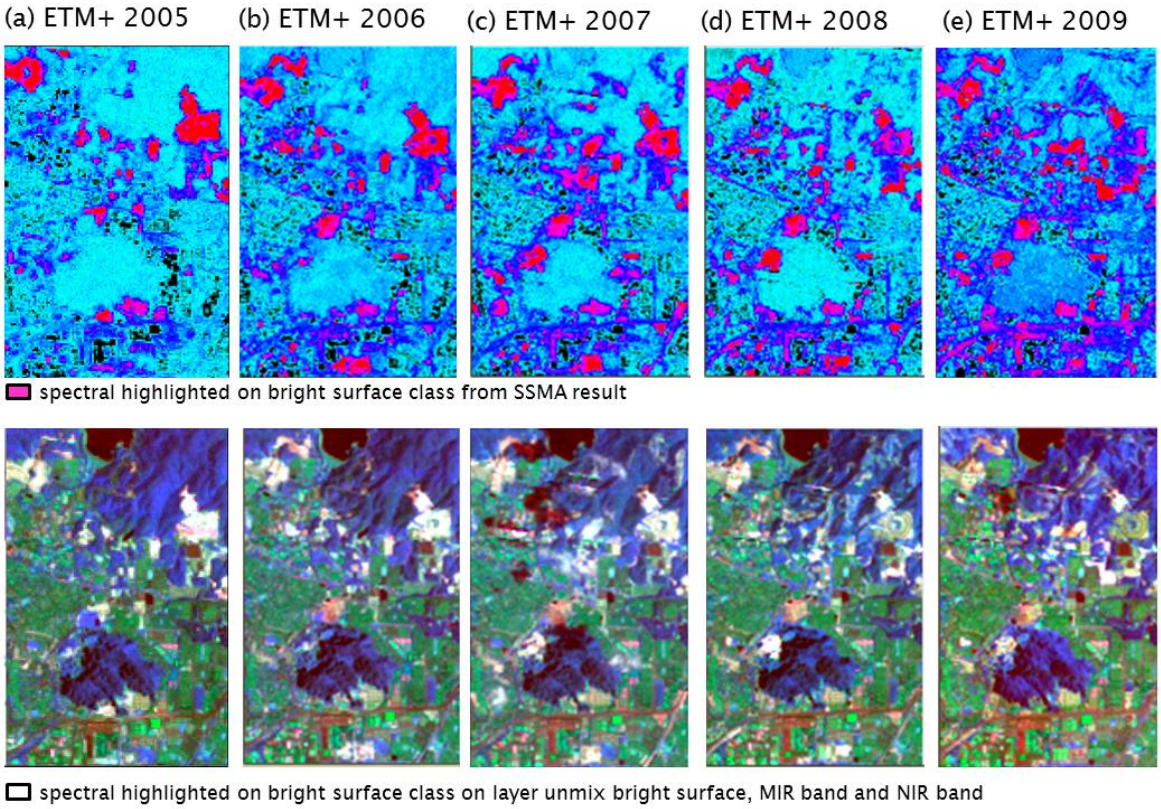


Figure 6.15 A set of Landsat ETM+ (gap-filled) time series results of SMMA for bright surface proportion (F) is 25.19% in 2005 to 23.73% in 2009.

The proportional method for the classification of SMMA from five images showed that there was fluctuation of spectral reflectance end-members each year within the four categories (building, vegetation, bright surface and water).

Figure 6.16 is a bar chart that illustrates the proportion value (%) for each category of LULC class using a frequent classification of Landsat ETM+ satellite sensor imagery from 2005 to 2009. Almost 33% is vegetation in the study area of Landsat ETM+. The vegetation proportion value was reduced after 2005 and it can be assumed that deforestation or devastation of green areas occurred or error. The building class proportion gradually increased and it was known that development occurred in the study area accounting for 24% to 30%. In 2009, the building proportion value decreased in the study area, it due to redevelopment with removal of the buildings and the land had been cleared for new development. This result is also related to the proportion value of bright surface in 2009. There is a remarkable increase due to cleared land and the

removal of trees or physical objects like buildings (with assuming squatters building).

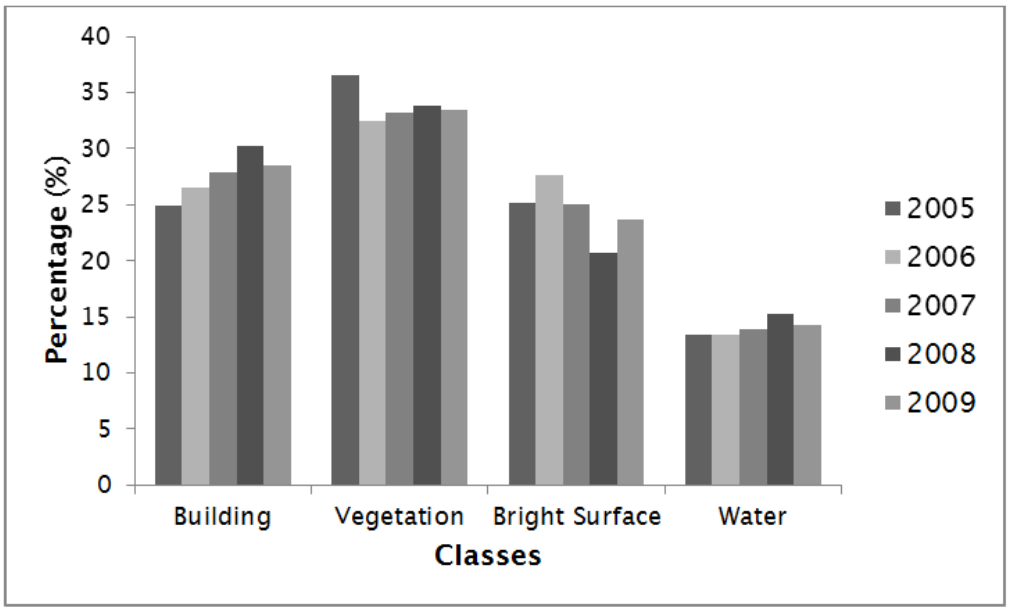


Figure 6.16 Percentage (%) of SMMA Classification, Landsat ETM+ 2005 to 2009.

### 6.4.2 Multi-Date Change Detection through Brightness and Greenness between 2005 and 2009

Multi-date change detection through TC-brightness and greenness from 2005 to 2009 is comparing images and is shown in Figure 6.17. The original result is a TC transformation with rotated TM data and it created three planes: TC1-brightness, TC2-greenness and TC3-wetness. The image from the original bands of Landsat ETM+ was converted to a new set of bands, where the interpretation is useful for crop monitoring and urban mapping. The TC result for the first band TC1 corresponds to the overall brightness of the image and normally the value is positive near to zero value. In the case of urban areas, the 'brightness' shows the most pixels of built-up surface.

The second band TC2 corresponds to the 'greenness' and is typically used as an index of photosynthetically-active vegetation to indicate variation in vegetation cover. The value lies between positive and negative values, but real pixels corresponding to greenness are mostly positive.

The output of a Tasselled Cap transformation is a new set of image bands that have specific interpretations. Using the analysis, the TCT can be displayed as follows: layer 1 (red band) is the brightness component (indicating areas of low vegetation and high reflectors). Layer 2 (green band) is the greenness component (indicating vegetation) and Layer 3 (blue band) is the wetness component (indicating water or moisture).

Brightness and greenness results are very dynamic and useful to examine in more detail, through a combination with other methods. In this study, the results of the brightness and greenness can be further used in the study of vectors through Feature Space (FS) correlation and analysis of image differences.

The overall results of TC-brightness and greenness analysis deal with multispectral images with six bands, mainly converting the original band to a new set of bands as independent multi-date for the change detection method.

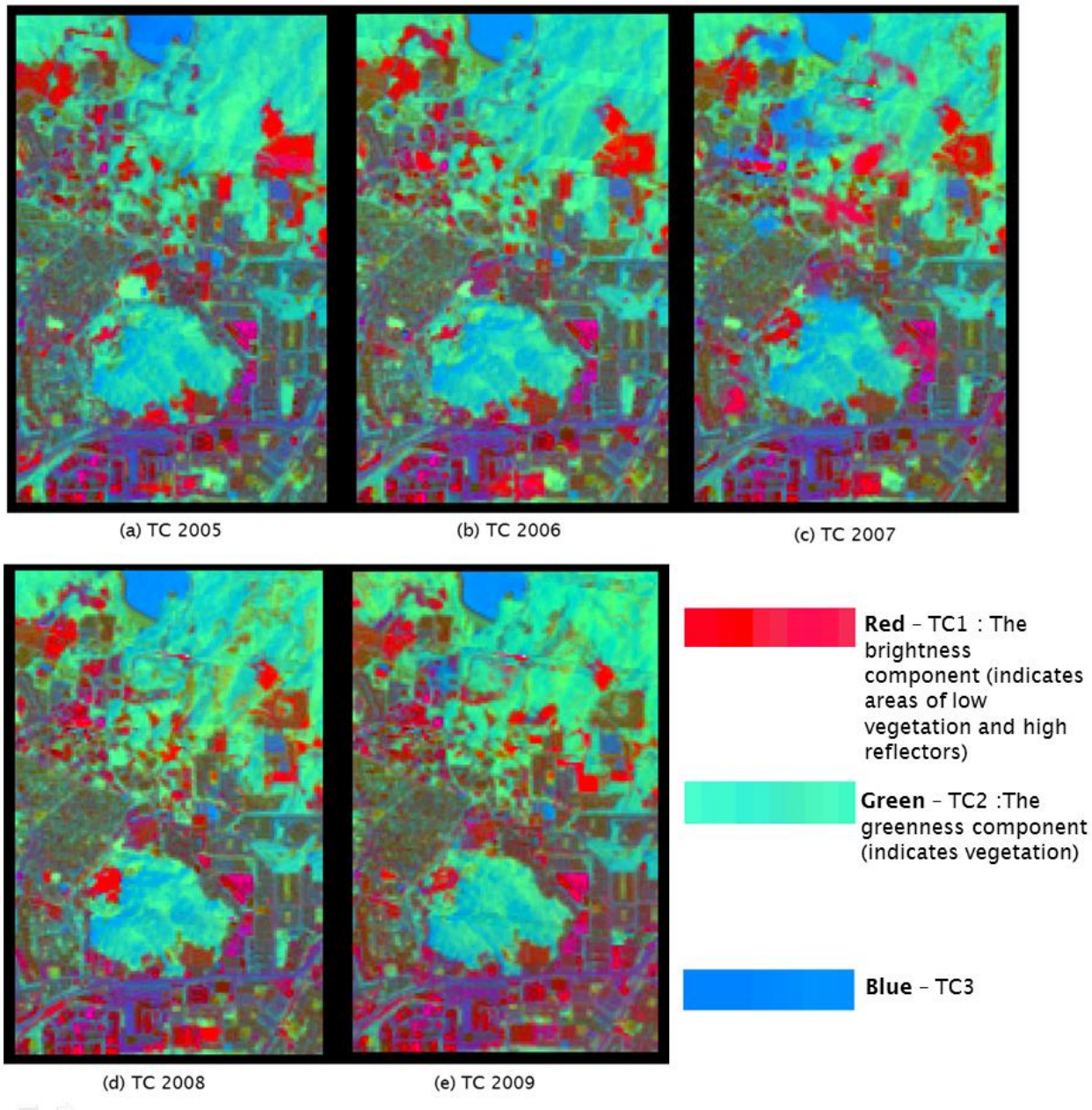


Figure 6.17 Results of a Tasselled Cap Transformation with Layer 1 (Red), Layer 2 (Green) and Layer 3 (Blue) for atmospheric correction data and radiometric normalisation of Landsat ETM+ 2005 to 2009 (gap-filled).

Table 6.6 Statistics of Tasselled Cap comparing brightness (TC1) and greenness (T2), Landsat ETM+ 2005 – 2009.

| | 2005 | | 2006 | | 2007 | |
|---|---|---|---|---|---|---|
| **TCA** | **TC1** | **TC2** | **TC1** | **TC2** | **TC1** | **TC2** |
| Mean | 29.37984 | -3.42073 | 29.14729 | -3.189 | 30.40395 | -4.16277 |
| Standard deviation | 11.82949 | 9.949843 | 12.2387 | 9.264425 | 13.48854 | 9.49656 |
| Min. | 0.3882 | -43.6434 | 0.284671 | -44.9097 | -1.23998 | -54.3987 |
| Max. | 108.5709 | 19.7516 | 115.0349 | 19.59333 | 124.7129 | 22.90816 |
| Correlation | -0.75868 | | -0.76516 | | -0.74033 | |
| N = 20585 | | | | | | |

| | 2008 | | 2009 | |
|---|---|---|---|---|
| **TCA** | **TC1** | **TC2** | **TC1** | **TC2** |
| Mean | 30.61418 | -4.52739 | 28.89776 | -4.17475 |
| Standard deviation | 11.19947 | 8.754057 | 9.424082 | 8.902595 |
| Min. | 2.187544 | -50.8703 | 0.961298 | -38.122 |
| Max. | 109.7629 | 19.00233 | 88.09615 | 15.92999 |
| Correlation | -0.71933 | | -0.76949 | |
| N = 20585 | | | | |

The standard deviation of the 'Tasselled Cap' (TC) is described in Table 6.6 and shows that the lowest standard deviation in the pixel values occurred between 2008 and 2009, as expected. However, due to the fact that the area is large some important information will be missing. The result of predicted changes is summarised by the standard deviation but is not enough to interpret pixel-based change. Summarising change by year is a useful approach, but sometimes a more detailed pixel-based examination is necessary for detecting trends.

Figures 6.18 and 6.19 are separate layers of brightness and greenness from 2005 to 2009 and will be used for further monitoring analysis.

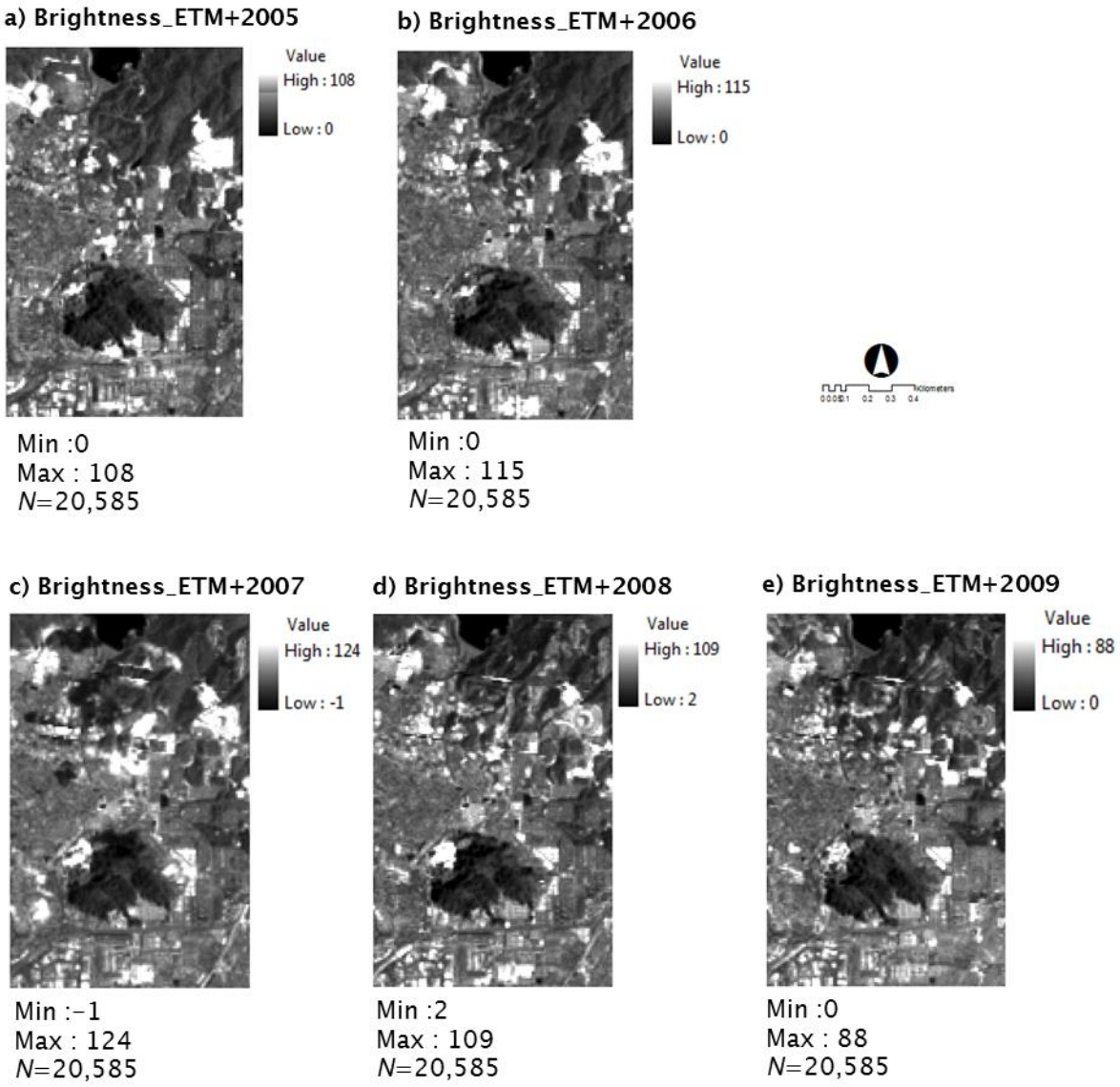


Figure 6.18 Results of TC 1- brightness from a single layer Landsat ETM+ 2005 to 2009.

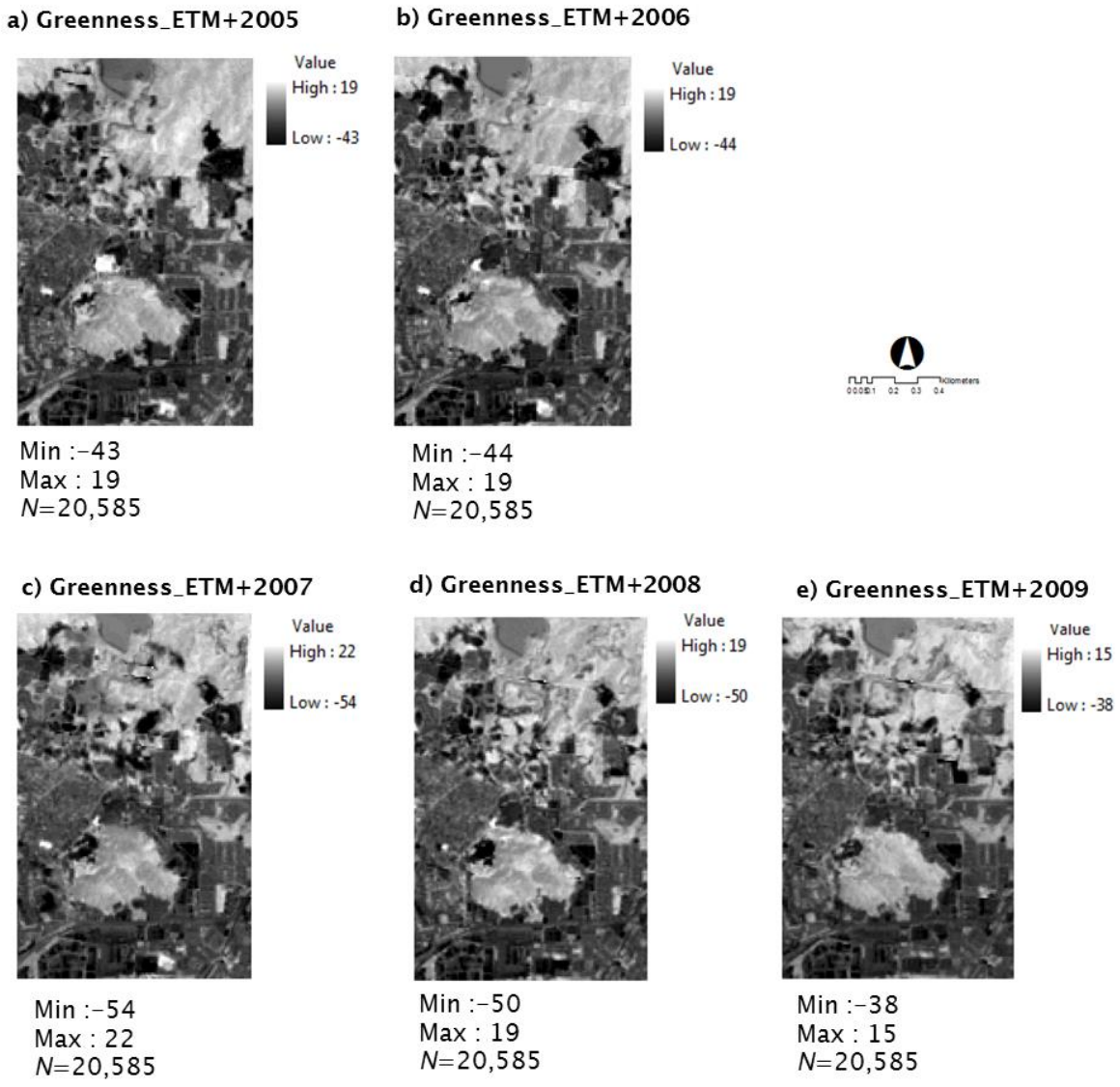


Figure 6.19 Results of TC 2- greenness from a single layer Landsat ETM+ 2005 to 2009.

Monitoring pixel changes began with an analysis of brightness and greenness. Although the results of the TC greenness and brightness analysis were presented in the form of a clear colour image, a more detailed interpretation needed to be done. This included a basic statistical approach to show that the lowest standard deviation in the pixel values occurred between 2008 and 2009. However, due to it being such a large area, not all the changes could be identified solely through brightness and greenness. Predicted changes were

derived from the standard deviation value and are not enough to interpret the change by pixel-based monitoring.

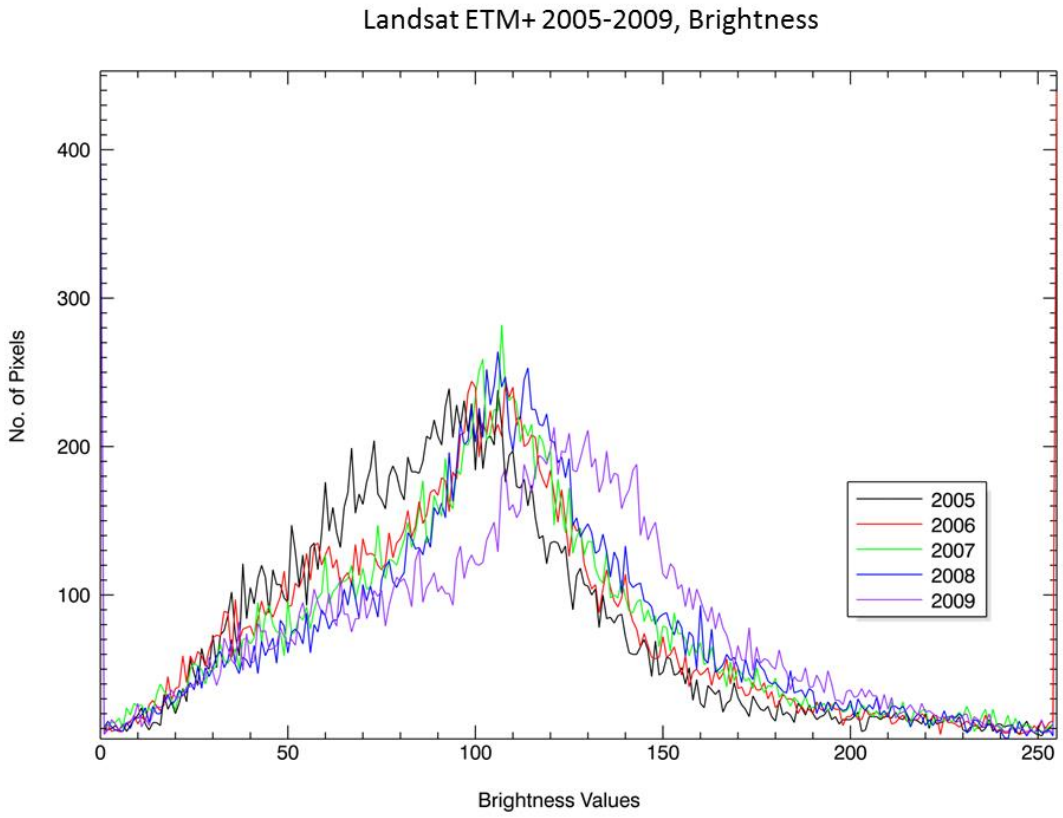


Figure 6.20 Trend of TC1 – brightness

The overlay result shown in Figure 6.20 is based on the total number of pixels for the brightness value. In principle, the largest brightness value provides a clue to the human made activities that exist throughout the area, either in development or land under construction following flattened buildings.

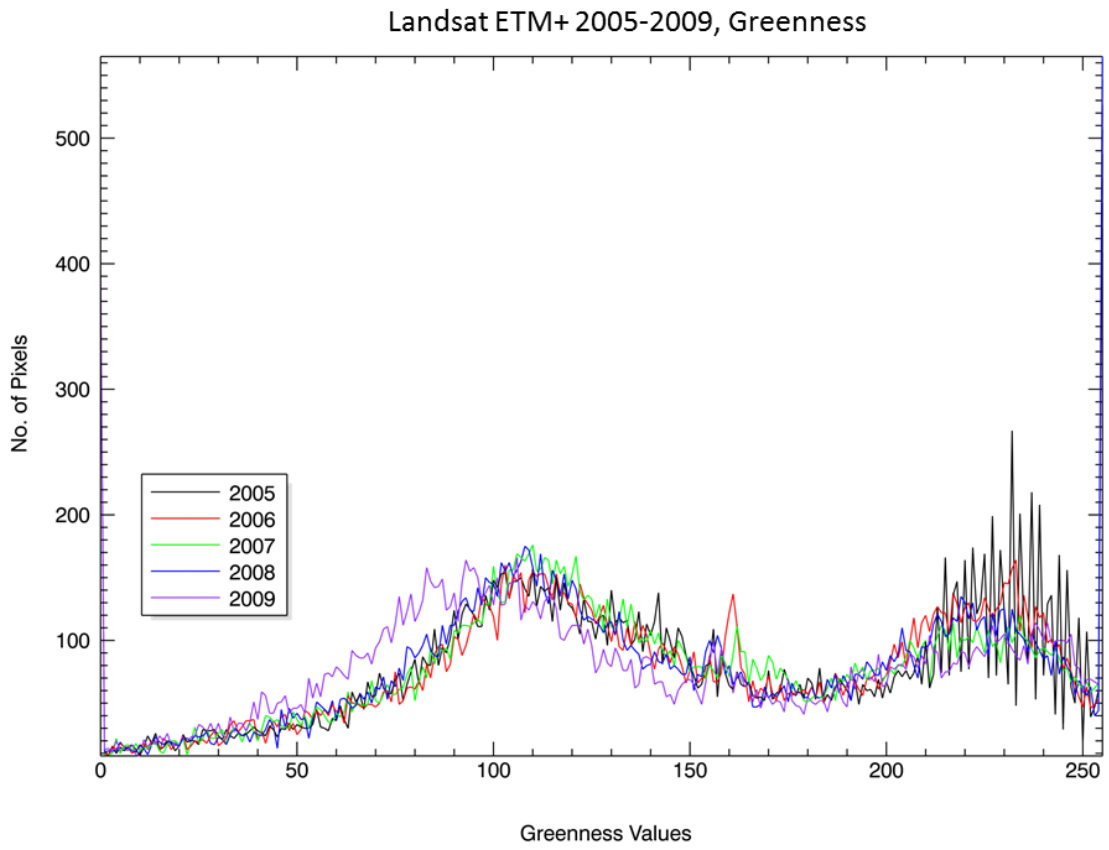


Figure 6.21 Trend of TC2 – greenness

The greenness layer is in the format of geoTIFF data extracted from the TC result and read as an 8-bit raster with display values from 0-255. Figure 6.21 shows the overlay trend of greenness for each year from 2005 to 2009. The green line shows the group of layers between 2005 and 2008 and the purple line is the greenness data for 2009. Initially, the values between 0 – 150 refer to human activities and values from 150 – 255 refer to the changes in greenness or vegetation.

These changes refer to human activity on the land. This systematic monitoring and automated change in brightness and greenness will discussed in Section 6.4.3 and the overall results of automated monitoring will now be further discussed.

### 6.4.3 Automated Monitoring of Land Use Change by Multiple Image Differencing between 2005 to 2009

This section describes the approach for automated monitoring of change in LULC using a time-series of coarse spatial resolution remote sensing imagery. The method involves the development of a programming script based on an image differencing method for automated monitoring of changes in multiple coarse spatial resolution satellite sensor imagery. The software IDL (Interactive Data Language) was used to achieve the objective of this analysis. All images from the TCT between brightness and greenness from 2005 to 2009 are shown in Figure 6.22.

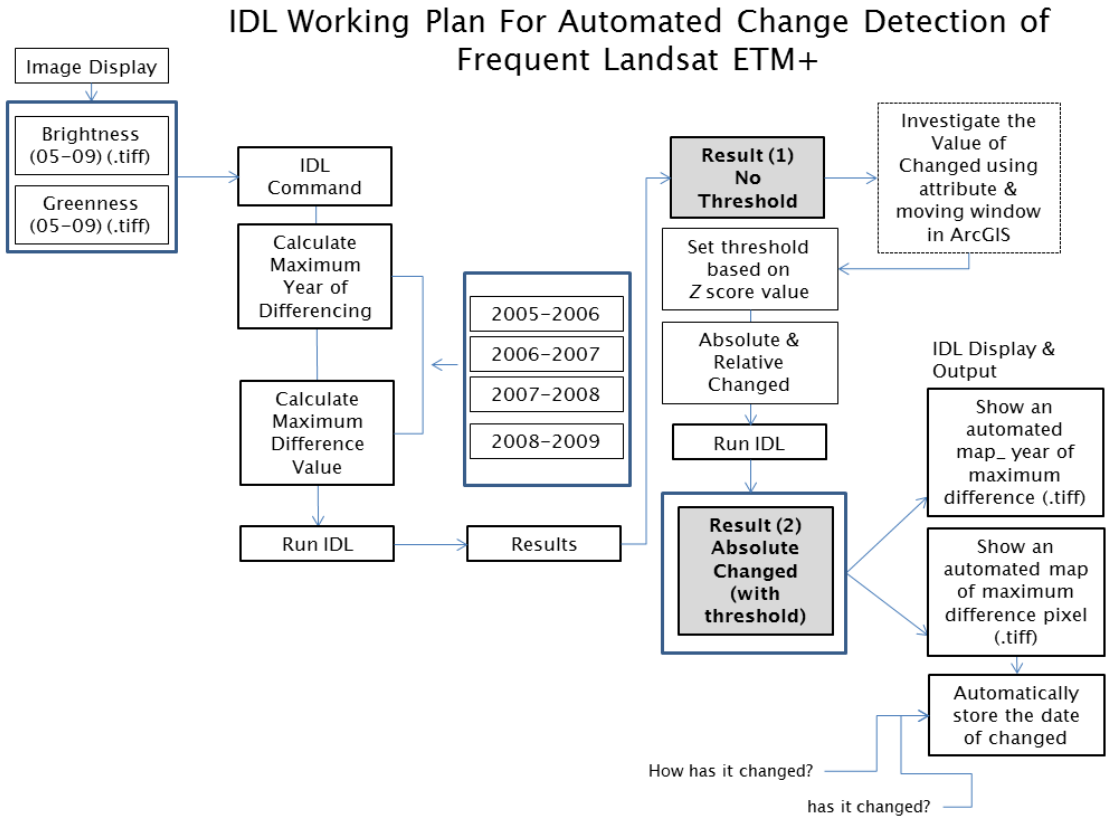


Figure 6.22 IDL working plan for multiple data monitoring of change.

In this analysis, the differences of multiple images were used to calculate the maximum difference (Test 1) and absolute difference (Test 2) to generate the resulting image date of change. Analysis started with an overlay to show the large amount of change by 2009 (purple) compared with earlier data (Figure 6.20 and Figure 6.21). However, to answer the research questions, a more precise analysis was undertaken. This involved analysing the position of changed pixels.

## Developing the Programming Scripts

### 1) Test 1: calculate maximum year of difference and maximum difference value (without threshold)

The largest value of maximum difference in each pixel changes determined the change that had occurred. The IDL commands to calculate the maximum difference and year of maximum difference based on equation 6.6 and the full script type are shown below.

```
diff=0.00

for i = 0,114 do begin
  for j = 0,178 do begin

    max_diff(i,j) = 0.00
    year_of_max_diff(i,j) = 0.00

    for k=1,4 do begin

      diff = image_all(i,j,k)-image_all(i,j,k-1)

      if (diff gt max_diff(i,j)) then begin
        year_of_max_diff(i,j) = k
        max_diff(i,j) = diff
      endif

    endfor
  endfor
endfor
```

All Landsat ETM + images from 2005 to 2009 underwent simultaneous analysis by categories of brightness and greenness, with a table of array 115 x 179 (size of image). All data were calibrated and radiometric normalisation was

carried out from the TC result by conversion of each category of data to TIFF (raster) and displayed as image 1 (2005), image 2 (2006), image 3 (2007), image 4 (2008) and image 5 (2009). As a result, the IDL image showed the resulting maximum difference value image and the year of maximum difference image.

```
image_all=intarr(115,179,5)
image_all(*,*,0)=image1(*,*)
image_all(*,*,1)=image2(*,*)
image_all(*,*,2)=image3(*,*)
image_all(*,*,3)=image4(*,*)
image_all(*,*,4)=image5(*,*)

max_diff=intarr(115,179)
year_of_max_diff=intarr(115,179)
```

As the result displayed in Figure 6.23 shows, obvious changes inherent in each pixel data according to the maximum value in the given year were generated automatically by the program.

**Maximum Difference Value (max_diff i,j)**

- **Change in brightness, 2005 to 2009**

From the analysis of IDL, the change in brightness image was classified into ten colours with a pixel value from 0 to 255, in order to check that the maximum value referred to a change in a pixel (i.e. this means changes to bright surface (cleared land, building, road)). During the 4-year period, the final pixel selection showed a change in land use due to human activities that led to development in the area.

- **Change in greenness, 2005 to 2009**

Changes in pixels for greenness, have a strong association with human activities that contribute to the green areas cleared for development purposes or areas that have been flattened and regenerated with trees planted for agriculture or plantations. The image was classified into ten colours with a pixel value from 0 to 255.

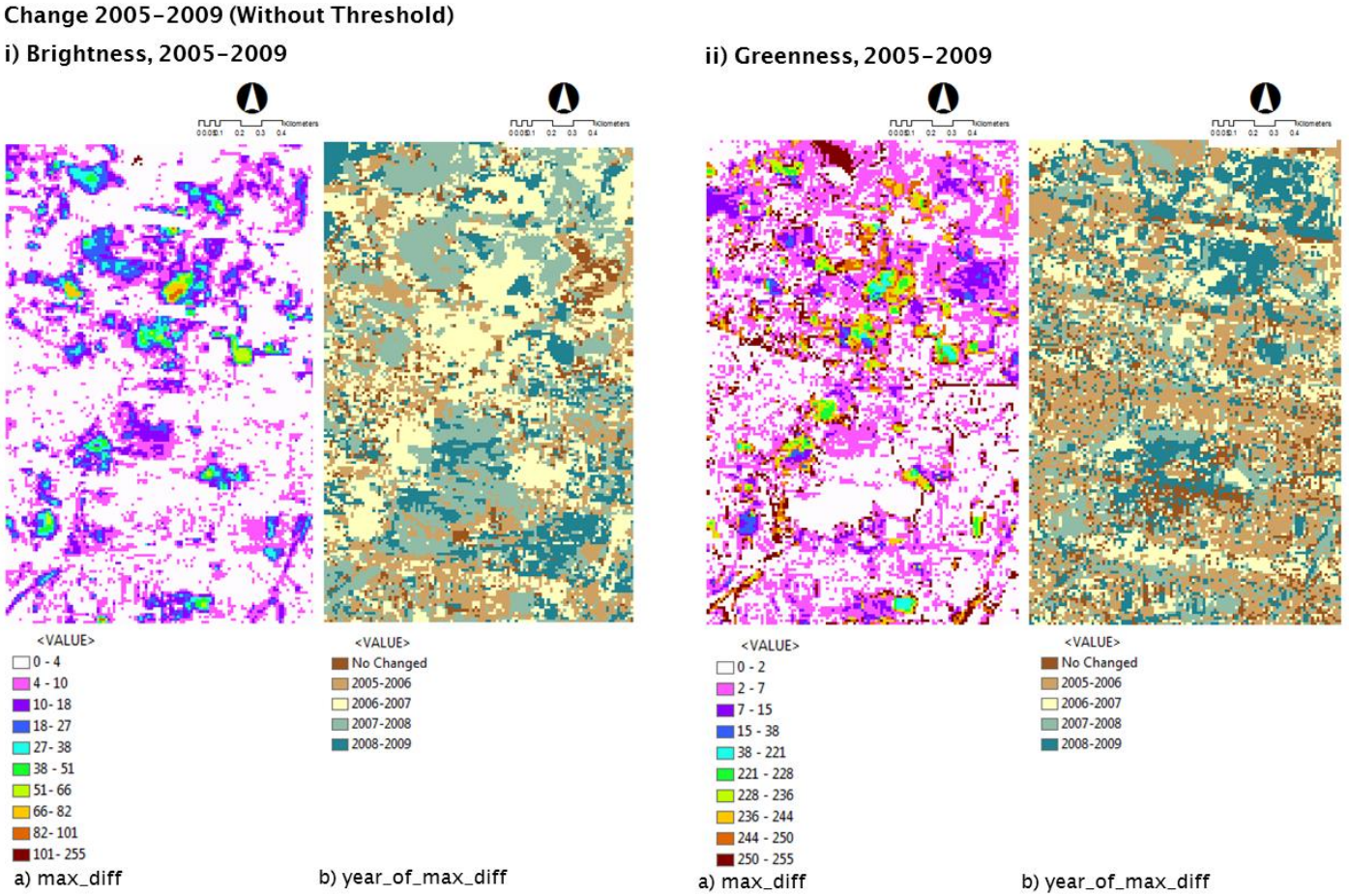


Figure 6.23 (a) Maximum difference value image and (b) Year of maximum difference image for brightness and greenness from 2005 to 2009 (without threshold).

## Calculate the threshold (Kt) by *Z* score

To ensure that all processes carry out monitoring automatically, the selection threshold (**Kt**) was determined by the *Z* score. The pixel value in brightness and greenness in Figure 6.33 was reviewed in advance before identifying a value threshold (**Kt**) to be used as a measure of the absolute and relative monitoring of the yearly images.

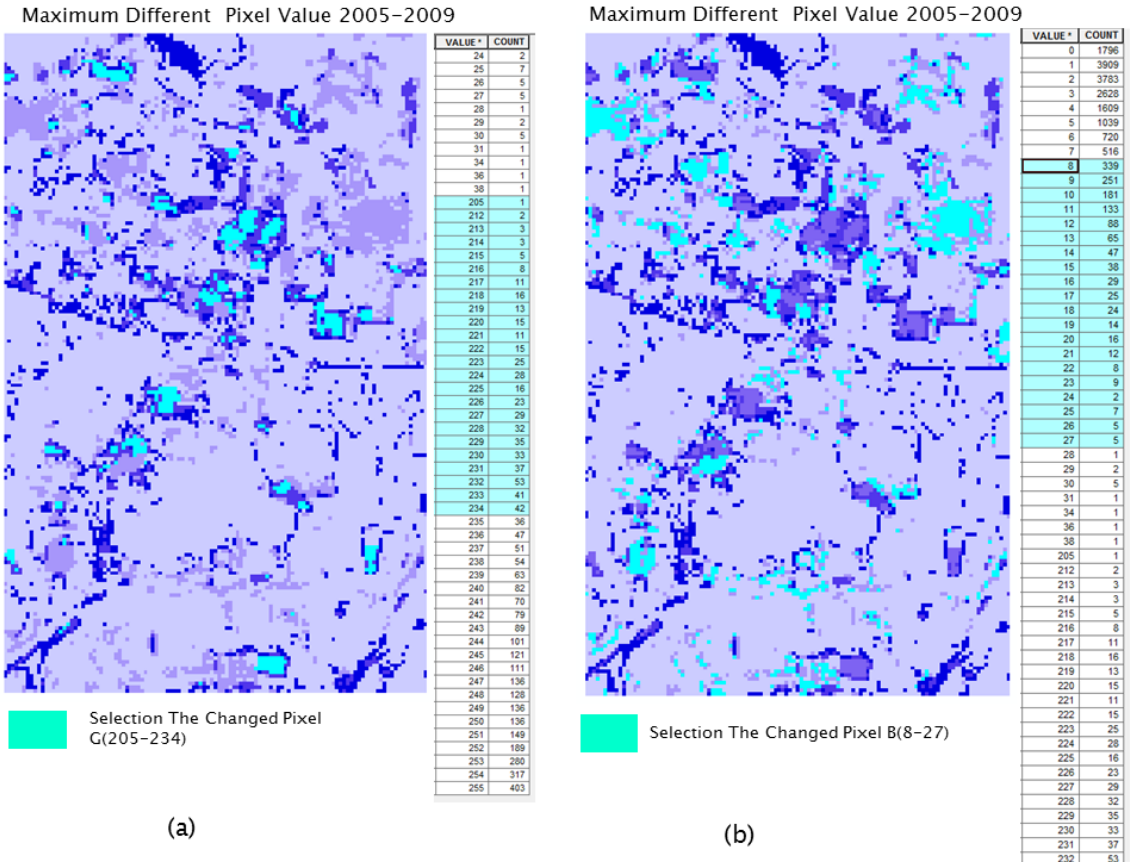


Figure 6.24 (a) Selection of correspondence values of greenness and (b) Selection of correspondence values of brightness.

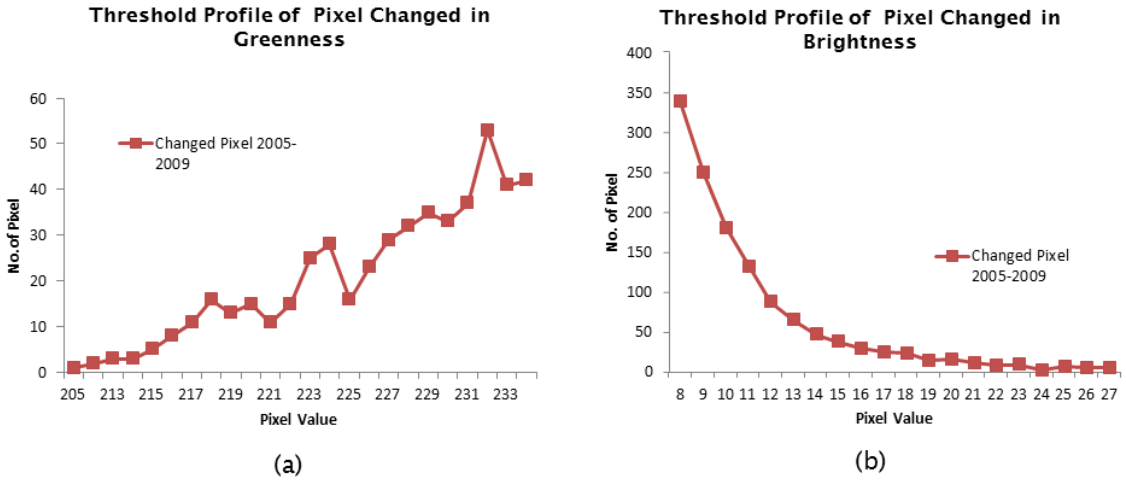


Figure 6.25 (a) Profile values of maximum difference in greenness and (b) Profile values of maximum difference in brightness.

Automated calculation of the threshold value by *Z* scores standardises the result, transforming it to a distribution with a mean value of zero and standard deviation of 1. A normally distributed experiment result max_diff (**i,j**) is thus standardised by subtracting the mean and dividing by the standard deviation of the highlighted value in Figure 6.24 and Figure 6.25.

$$Z = \frac{x-\mu}{\sigma} \qquad (6.1)$$

The threshold value (**Kt**) for both the data of brightness and greenness was decided with a value of 15 (maximum positive) and -15 (minimum negative) which is close to the value of *Z* score between 14 and -18 of *Z* score. The *Z* score results are shown in table below:

Table 6.7 The *Z* score result.

| | Brightness | Greenness |
|---|---|---|
| Mean ($x$-$\mu$) | 17.5 | 222.25 |
| Standard Deviation ($\sigma$) | 2.2360681 | 10.54158 |
| *Z* Score | 14.08392 (14) | -18 |

### 2) Test 2: Absolute difference (with threshold)

To answer the research question "Has land use changed?", the absolute difference value was calculated so as to eliminate the possibility of pixel change and the formula was set by deciding the threshold (**Kt**) which was a non-negative value.

It was required to know if each pixel had really changed. The threshold value was the pixel value generated in equation 6.1, and the IDL commands script is below.

```
diff=0.00
Kt=15.00


for i = 0,114 do begin
  for j = 0,178 do begin

    max_diff(i,j) = 0.00
    year_of_max_diff(i,j) = 0.00

    for k=1,4 do begin

      diff = sqrt(((image_all(i,j,k)-image_all(i,j,k-1)))^2)

      if (diff gt max_diff(i,j)) then begin
        if (diff gt Kt) then begin
          year_of_max_diff(i,j) = k
          max_diff(i,j) = diff

        endif
      endif

    endfor
  endfor
endfor
```

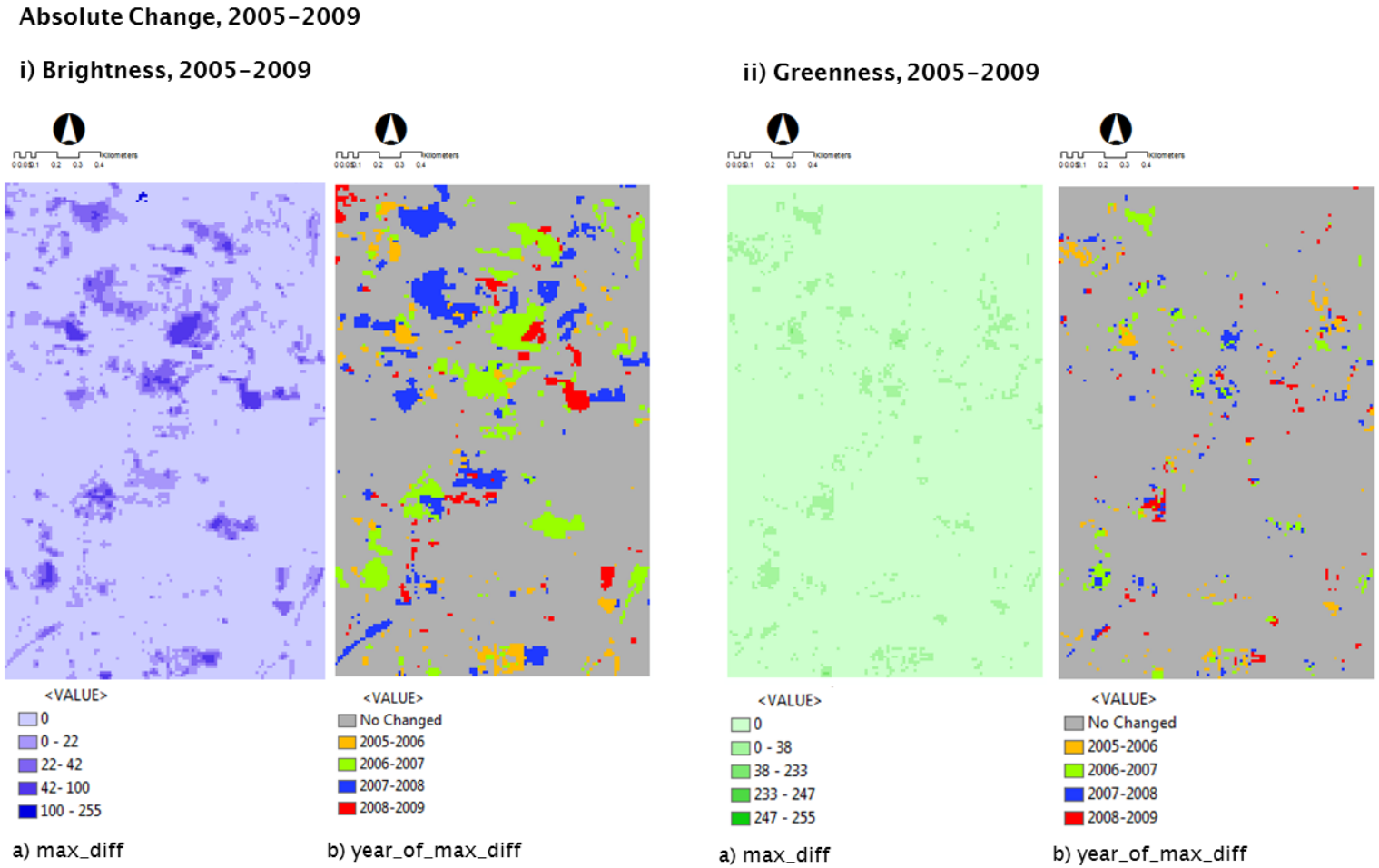


Figure 6.26 Absolute differences of greenness and brightness from 2005 to 2009, (a) maximum difference value (**i,j**) and (b) year of maximum difference (**k**).

If difference (**i, j** = brightness and greenness pixels (2005-2009), of maximum value are greater than **Kt** (threshold = 15), changes in each pixel are accounted for by determining the change that has occurred based on the absolute value of maximum differences. Using IDL the images were classified into five colours of pixel value from 0 to 255 between brightness and greenness as the value of maximum of difference (Figure 6.26). These refer to the changes in bright surface and greenness in monitoring of **k** (time of difference of brightness and greenness pixel between year 2005-2006, 2006-2007, 2007-2008, 2008-2009. As the result in Figure 6.26, the brightness image showed that the largest changes took place between 2006 to 2007 represented by green colour pixels. The greenness result also showed that observable changes took place from 2006 to 2007.

### 3) Date of Change (year_of_max_diff)

- **Brightness and greenness, 2005 to 2009**

The script defines a single 3D array for the five images (i.e., **x**, **y** and **t**), which refers to the pixel acquired in the same geographical area at two different times, (**x, y**) and the time period (**t**) between image 2005 to 2006, 2006 to 2007, 2007 to 2008 and 2008 to 2009 (**k**). The results showed that the maximum pixel values of the different years have changed. There are pixels in brightness and greenness that do not change, but the results shown represent only a small number of pixels. Therefore, the maximum differences within pixels showed large differences in every year. To overcome this problem, a threshold was necessary; so that the pixel (**x, y**) changes gave a clear meaning for the year of maximum difference (**t**).

The main objective of this section of the research was to test if Landsat TM imagery which are infrequent and of relatively coarse spatial resolution can be used to determine the date (specifically the year) of change previously identified using infrequent and fine spatial resolution IKONOS imagery. The problem with change detection using such IKONOS imagery is that the specific year of change is not identified. In the present case, change is identified as having occurred sometime between 2005 and 2009 for example. In order to identify the specific year of change, it is suggested here that time-series Landsat TM imagery provided on an annual basis (or more frequently in other

applications) can be used to pin-point the precise year of change. In order to identify the year of change the maximum difference was calculated from across all time-series differences between successive years. Note also, that the absolute difference was calculated such as to be able to identify the maximum, whether positive or negative in nature. Then, because every pixel will have associated with it a maximum difference, it was necessary to remove those differences that were less than some specific threshold. This left a small subset of the entire image for which the identified differences could be accepted as important or sufficiently large to merit attention. Finally, for those maximum differences previously identified as above, the year in which the maximum difference occurred was identified. In this way, it was possible to produce an image of dates on which change was identified to have occurred.

The IDL program, answered the three research questions:

*(1) Can Landsat ETM+ be used to identify the date of change where change is known to have occurred?*

Analysis of multi-date imagery is difficult using only customized software as an automated way of monitoring. The development of the script in the IDL program took into account the results at time (**t**) of the pixel change (**x, y**) in a table array. As a result, a change in each pixel represents the year, meaning it will automatically store the date of change between the multi-date data. Figure 6.20 and Figure 6.21 shows the significant contributions of frequent monitoring methods for Landsat ETM+ data through an automated approach. The largest change in pixel brightness occurred between 2006-2007 and 2007-2008. From this, it is possible to conclude that, these areas have seen quite drastic development.

Change in greenness is not as great compared with changes in brightness. Results of changes in pixels were in line with known changes on the ground. Large changes in greenness occurred in 2005-2006, but in subsequent years, the distribution of pixel change is even.

*(2) Can Landsat ETM+ be used to detect multiple changes of land use where change is known to have occurred?*

Landsat ETM+ can be used to detect a variety of land use changes in pixels for which changes are known to have occurred. Figure 6.27 represents changes in brightness and greenness between 2005-2009 using the maximum difference value. The method is a suitable and effective way to monitor land use using coarse spatial resolution data, particularly when used in a frequent series. The brightness value represented the built-up area that included land-use categories of residential, commercial, industrial, bare land, road and other bright surfaces. The change in greenness clearly indicated there was an increase in the area of tree crops, referring to replanting or reforestation.

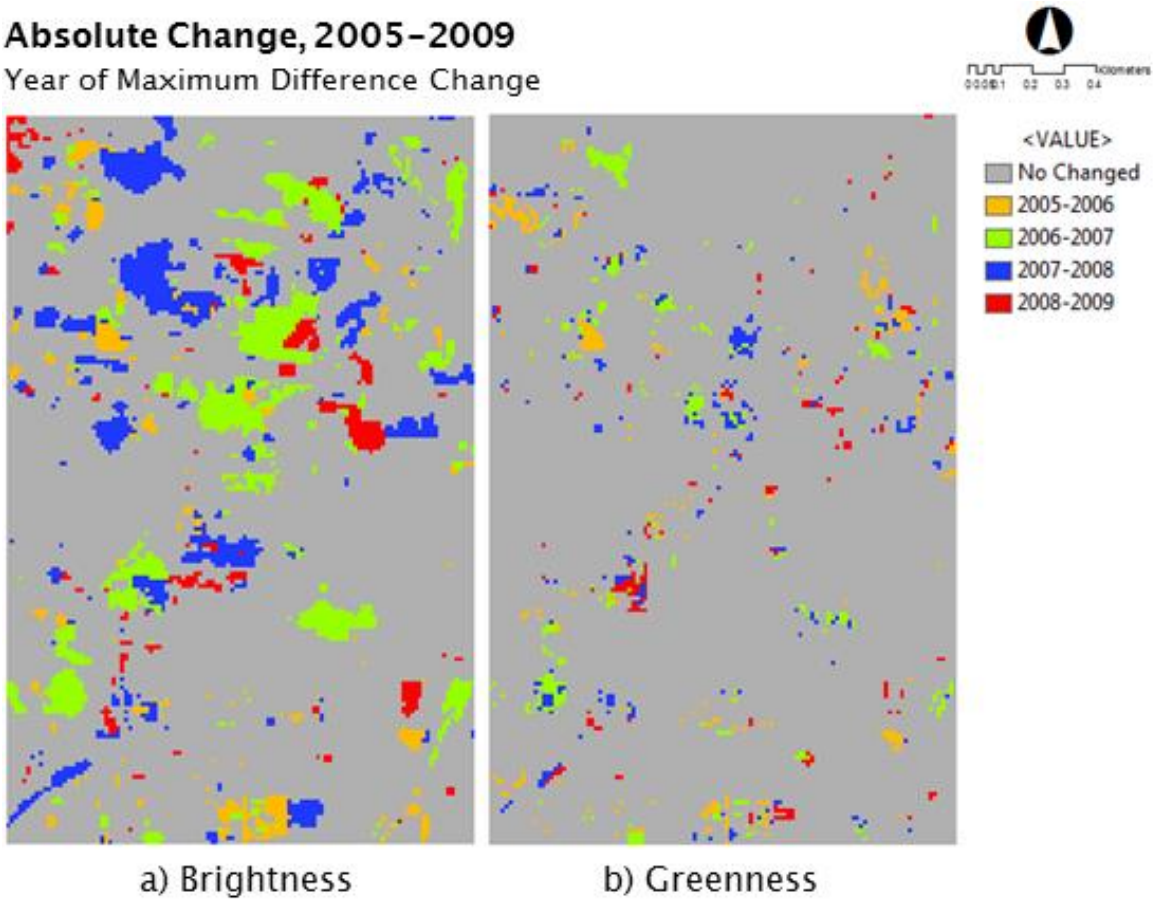


Figure 6.27 Date of change between brightness and greenness.

*(3) Can Landsat ETM+ provide an 'alarm' function where change is not known to have occurred?*

The infrequent Landsat ETM+ data were used in automated monitoring of change to answer the question about an 'alarm function' where change is not

known to have occurred. The five images were displayed simultaneously and automatically compared using the comparative difference between each image. However, the comparison through a screen or overlay did not achieve the results of the automated monitoring as shown in Figure 6.23.

As such, the results shown in Figure 6.28 showed clearly the areas that had undergone change. The result was aggregated into five categories of colour tone while the value of absolute zero meaning 'no change area' was indicated with very light colour. The darker colour indicates a high degree of change occurring between brightness and greenness area.

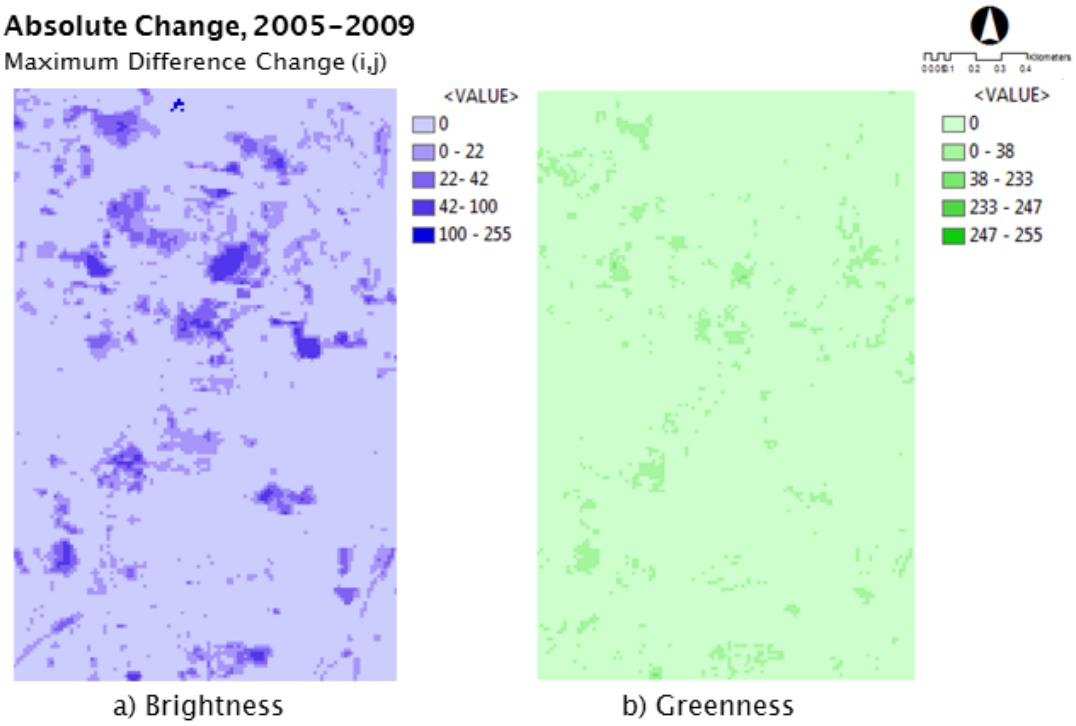


Figure 6.28 The difference images showing change that occurred between brightness and greenness between 2005 and 2009 from maximum difference values (**i,j**)

## 6.5 Discussion

This discussion section highlights the significance, advantages of automated monitoring techniques for further research contributions and also the limitation of the results, especially contribution of urban land use change through L-resolution scene model of ETM+ images in urban environment. Multiple images (ETM+) are referring to more frequent images but more episodic problems especially related with the scan line gaps and clouds in tropics. These need a method to analyses changed that is resistant to parts of an image being unusable.

Calibration is very important in making the overall result of monitoring acceptable, especially when dealing with multi-date frequent Landsat ETM+. Mas (1999) showed that it may be extremely difficult to obtain multi-date data at the same time of year, particularly in tropical regions where cloud cover is common. Data from the frequent spatial coarse spatial resolution of Landsat ETM+ between 2005 to 2009 were used to fill the missing information of infrequent fine spatial resolution imagery data. This was discussed in detail in Chapter 4. To normalise a series of five Landsat ETM+ images in Malaysia dataset need to apply a mask to remove the scan line gaps. In this stage, created a composite gap mask based on all five images is necessary. The data must accurately co-register to reduce the problem in multi-date error to ensure the data with similar information. In early assumption, the problem might be spurious values at the edges of the scan line gaps and need introduced by the resampling process. The resampling process involved the creating of the 'ComboMask' (combination of masking 2005 to 2009) by manual on-screen digitising, making sure is not include any of the pixels at the edges of the gaps on any of the dates.

A large amount of coarse spatial resolution data was used for monitoring land use. TC-brightness and greenness analysis using multispectral images of Landsat ETM+ with six bands was converted into geoTIFF data for the automated monitoring of change. Brightness and greenness results showed the amount of pixel change, and were evaluated using the value of maximum difference (**i, j**). This gives a prediction of land use change using frequent coarse spatial resolution data within four years (**k**).

The method involves the development of a programming script based on an image difference method for automatic monitoring of changes using the maximum difference value. This method is different from that used by Bruzzone (2000) in that it proposes two automatic techniques (based on the Bayes theory) for the analysis of the difference image (based on unsupervised change detection). This allows an automatic selection of the decision threshold to minimise the overall change detection error probability under the assumption that pixels in the difference image are independent of one another.

The software IDL (Interactive Data Language) was used to achieve the objective of this analysis. Multi-date coarse spatial resolution data of brightness and greenness between 2005 and 2009 were analysed in the IDL program with three different scripts. These included a test for change (i) without threshold, (ii) with threshold and absolute value, and (iii) with threshold and relative value (positive and negative). From test (i), the script did not consider a threshold, and it was based on the original maximum difference value. The output represents the mass distribution of changed pixels. From this result, the absolute change was tested providing test (ii). The absolute difference was calculated and a formula was set up by deciding the threshold (**Kt**) value with a non-negative value to eliminate unchanged pixels. The threshold value depended on the absolute value, either from the *Z* score calculation or when the user defines the value, and both approaches are valid in this technique. The generated images allowed clear identification of changed areas between brightness and greenness.

Figure 6.29 illustrates the monitoring of change between infrequent fine spatial resolution and frequent coarse spatial resolution. The result is represented by $\mathbf{M}ij^{05-09} = \mathbf{F}ij^{05} + (\mathbf{C}ij^{b1} + \mathbf{C}ij^{g1} + \mathbf{C}ij^{b2} + \mathbf{C}ij^{g2} + \mathbf{C}ij^{b3} + \mathbf{C}ij^{g3} + \mathbf{C}ij^{b4} + \mathbf{C}ij^{g4}) + \mathbf{F}ij^{09}$ . Monitoring began in 2005 ($\mathbf{M}ij^{05-09}$), with change detection from infrequent fine spatial resolution (**F**), frequent coarse spatial resolution (**C**), and monitoring of change between brightness (*b*) and greenness (*g*). The analysis demonstrated that Landsat ETM+ can be used to identify the date of change through detecting multiple changes of land use. It can be

shown also that it can provide an 'alarm' function to alert the monitoring process when change has occurred.

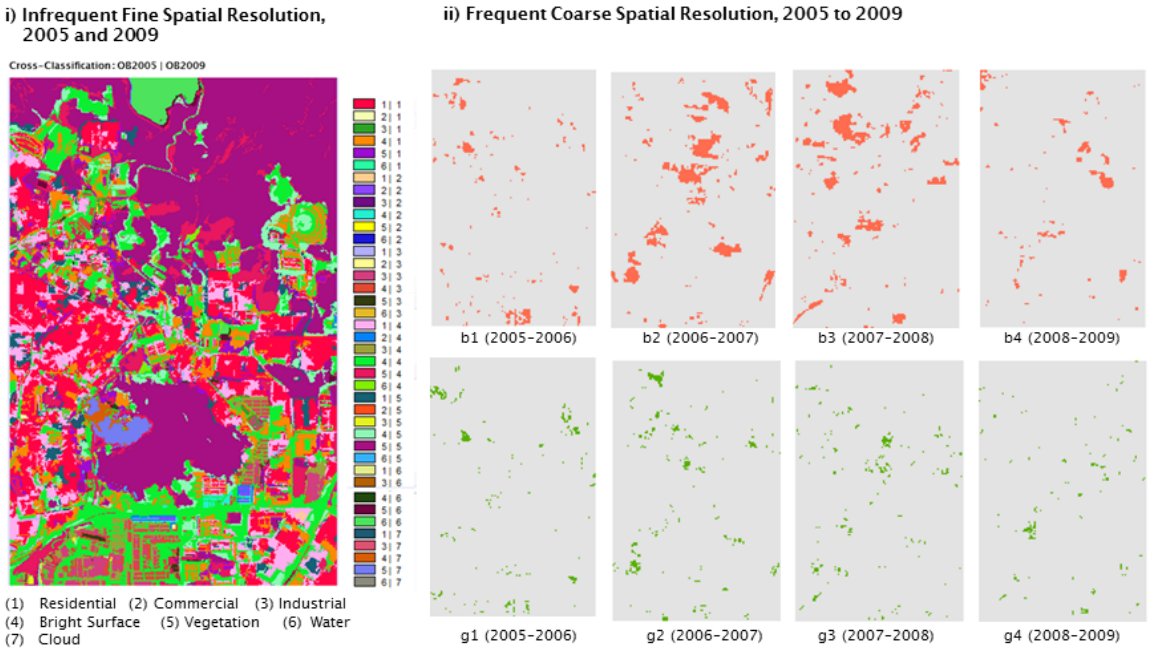


$$(\mathbf{F}ij^{05} + \mathbf{F}ij^{09})$$

$$(\mathbf{C}ij^{b1} + \mathbf{C}ij^{g1} + \mathbf{C}ij^{b2} + \mathbf{C}ij^{g2} + \mathbf{C}ij^{b3} + \mathbf{C}ij^{g3} + \mathbf{C}ij^{b4} + \mathbf{C}ij^{g4})$$

Figure 6.29 The animation of monitoring change detection results by illustrating the change between infrequent fine spatial (F) resolution and frequent coarse spatial resolution (C).

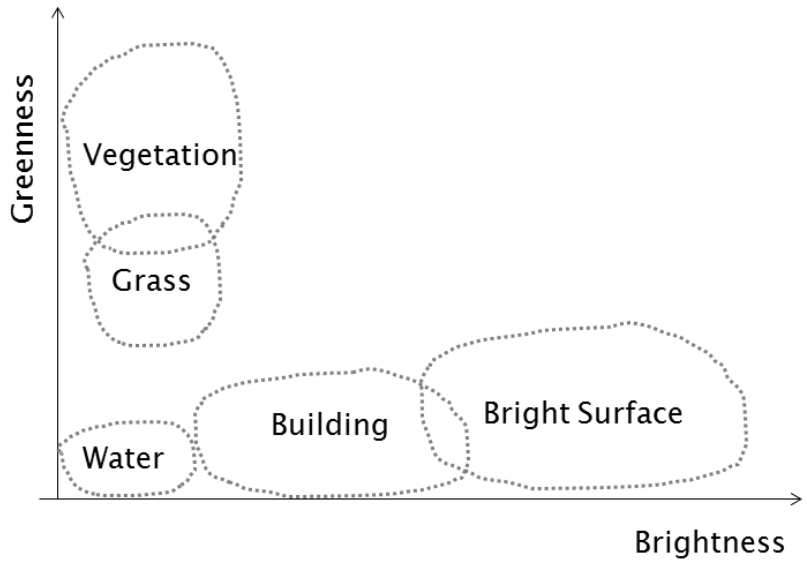


Figure 6.30 The distribution of LULC in a feature space between greenness and brightness.

Figure 6.30 illustrates a land use distribution between brightness and greenness. This relationship offers guidance to identify the direction of change in a pixel from one type of land use and land cover to another, and was presented in the feature space (FS) distribution. The direction of change in FS identified the type of land use change that occurred (**i,j**) from the date (**k**). This monitoring was expanded through the study of land use change of direction in the FS and will be refined in the subsequent analysis in Chapter 7.

## 6.6 Conclusion

Chapter 6 presents an analysis of a time series of ETM+ images. It is suggested that the method is innovative in some way. Scan line gaps is a feature of the data set, so the interest is how these were dealt with in order to focus the analysis on real change.

In addition, it has been demonstrated that coarse spatial resolution imagery can be used as a tool for monitoring urban change. This is the biggest contribution to this research in simultaneous automated monitoring to detect multiple changes of land use where change is known to have occurred. It can

store the date or time (t) of changes for the purpose of close monitoring on the ground, based on satellite sensor imagery information. The results of automated multi-date change can be used for further analysis in Chapter 7 that diagnoses land use change through validation and interpretation. Further investigation of pixel change direction-magnitude of change between greenness and brightness will be presented in feature space (FS).

# 7. Analysis 3: Validation and Interpretation of Change

## 7.1 Introduction

This chapter aims to diagnose or identify the land use change reflectance by interpreting the vector direction distribution in feature space (FS). The feature space refers to two related data (brightness and greenness) defined by a feature extraction procedure that transforms raw data into sample vectors of some fixed length. The analysis aimed to identify the actual vector distribution of land use when it changes from the form of space x and y axis. The image space is the 2D plane of the image where pixels are located. It represents the spatial space of the image. In other words, the difference of each pixel in an image can affect the differences in image space pixel distribution. On the other hand, feature space is about the reflectance values assigned to each pixel. Feature space is the space of these reflectance values; the brightness and greenness values of each pixel can be plotted in 2D image space to analyse the direction of change from each of the land use classes.

To prove that the results of recorded changes were correct, the object-based classification was used. The detailed thematic map shows the change that occurred by using 18 point target zones in the study area. To validate the results, 18 sample points were also tested where no changes occurred. The validation result assumed that within a five-year period, if the land use and land cover are still the same, at least 90% of the land use has not changed between 2005 and 2009. The threshold assumption is based on the percentile from the spatial transition result.

This analysis was an empirical experiment using the distribution of pixels (vector) in axis x, y between the magnitude of change direction either from brightness and greenness. This showed the equivalent and real data of reflectance value in the land use classes between 2005 to 2009 represented in 2D space.

## 7.2 Research Methodology

### 7.2.1 Data Preparation

The main data used was Landsat ETM+ 2005 to 2009 with a subset of 15 x 15 pixels (225pixels) from the result of a TC transformation between brightness and greenness. To support the analysis, the same subset (with 4m x 4m pixel size) from the OB classification was identified, using infrequent fine spatial resolution data of IKONOS 2005 and IKONOS 2009. This OB classification data was used to represent land use type to identify land use change in feature space between the correlation of greenness and brightness.

### 7.2.2 A General Workflow

Diagnosing land use change started with identifying 18 point zone samples between changed and no change areas using the results from the Multivariate Alteration Detection (MAD) of Landsat ETM + in 2005 and 2009. A general workflow of procedures is shown in Figure 7.1.

The identification of samples were based on 15 pixels x 15 pixels using brightness and greenness. This means that the subset images of 18 point zone samples were used for each year from 2005 until 2009.

The samples were converted into ASCII text that presented the value for each pixel between both brightness and greenness and showed in feature space correlation X and Y values. Results from FS showed the direction and magnitude of change from the differences of vector point distribution in 2D space.

The spatial threshold value was designed and applied to the manual interpretation by a direct recognition method to estimate the amount of land use change. The results from the infrequent data of both OB classifications in 2005 and 2009 were used to identify the type of land use change. In order to test the effectiveness of the approach, the 18 point zone samples of no change areas were presented in feature space to validate the vector point distribution from the actual unchanged area.

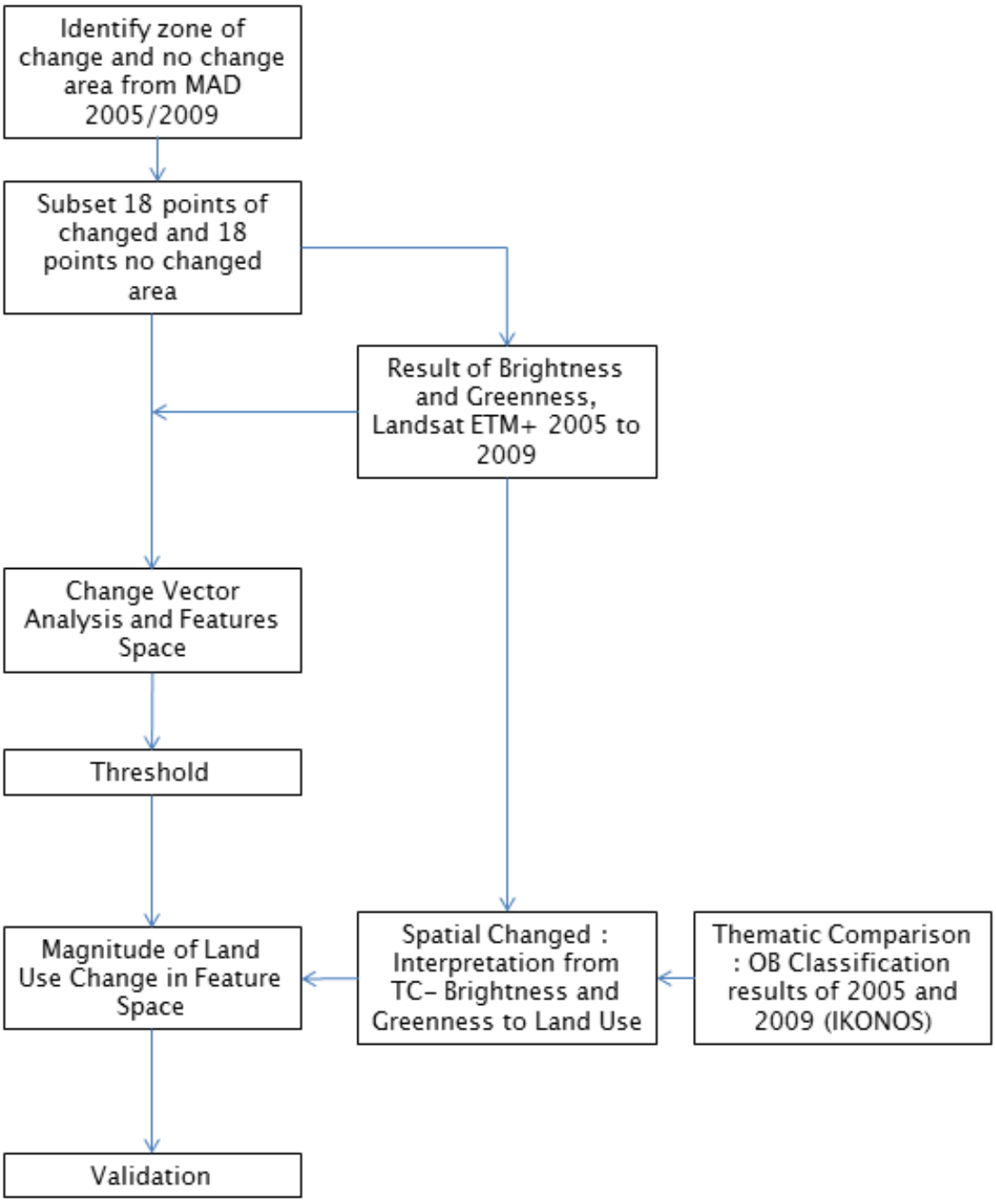


Figure 7.1 The general workflow of validation and interpretation land use change.

### 7.2.3 Change Vector Analysis (CVA) and Feature Space (FS)

Change vector analysis is a technique to analyse changes in vector position between magnitude (type of change) and direction (time or period) (Malila 1980). The method cannot be used in isolation to generate results. It was combined with multi-date pairs of spectral measurements between greenness and brightness in Tasselled Cap (TC) transformation. The result from the TC transformed method was used to change vector analysis in feature space (FS) correlation. Baisantry et al. (2012) also presents a systematic approach to detect and describe different types of changes in brightness and greenness represented in feature space.

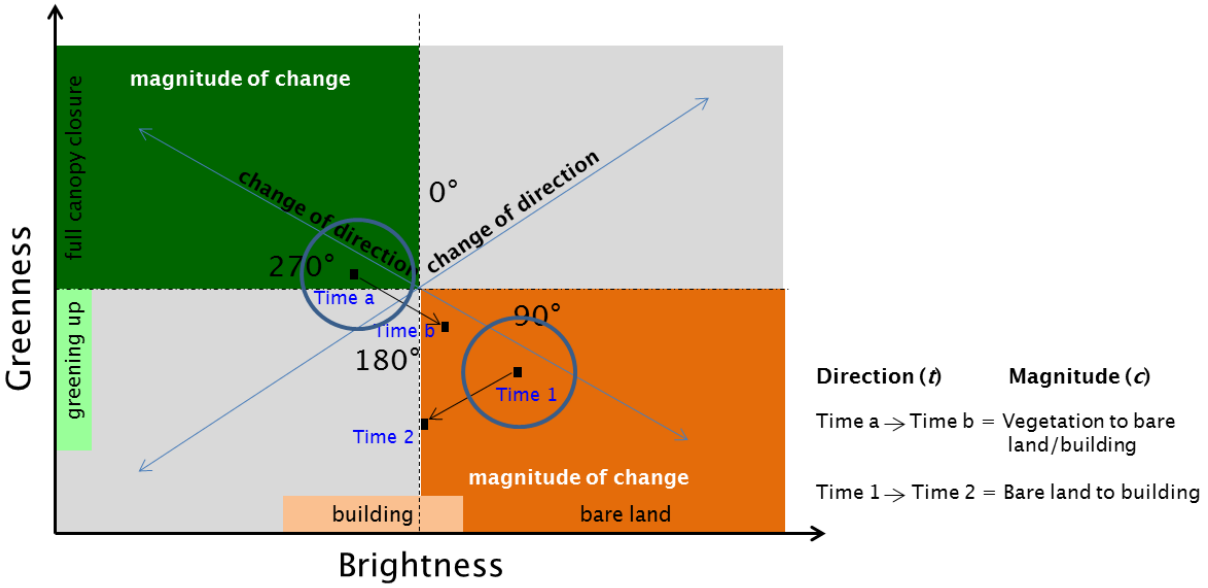


Figure 7.2 Model for detecting the direction and magnitude of change within the change vector analysis in feature space.

The TC rotates the Landsat data plane such that the majority of data variability is concentrated in two features that are directly related to physical scene characteristics as shown in Figure 7.2. The change vector of greenness and brightness is normally a negative linear convergence with both directions of change between 0° and 180° or 90° and 270°, with the magnitude of change between bare land to building and vegetation to bare land or bare land to vegetation.

### 7.2.4 Spatial Threshold

In order to define the threshold from the TC result, three categories were suggested. The threshold is determined based on the *P*–th percentile ($0 \leq P < 100$) of N (225 pixels) by calculating the values $\frac{P}{100} \times N$. The three categories of threshold are;

(i) Slightly changed if $0 \leq P < 100$ = 20% (45 pixels are changed)

(ii) Moderately changed if $0 \leq P < 100$ = 50% (113 pixels are changed) and

(iii) Extremely changed if $0 \leq P < 100$ =90% (203 pixels are changed) from the reference image 2005.

The spatial threshold is illustrated in Figure 7.3 showing the pixel pattern recognition and the correlation distribution of brightness and greenness.

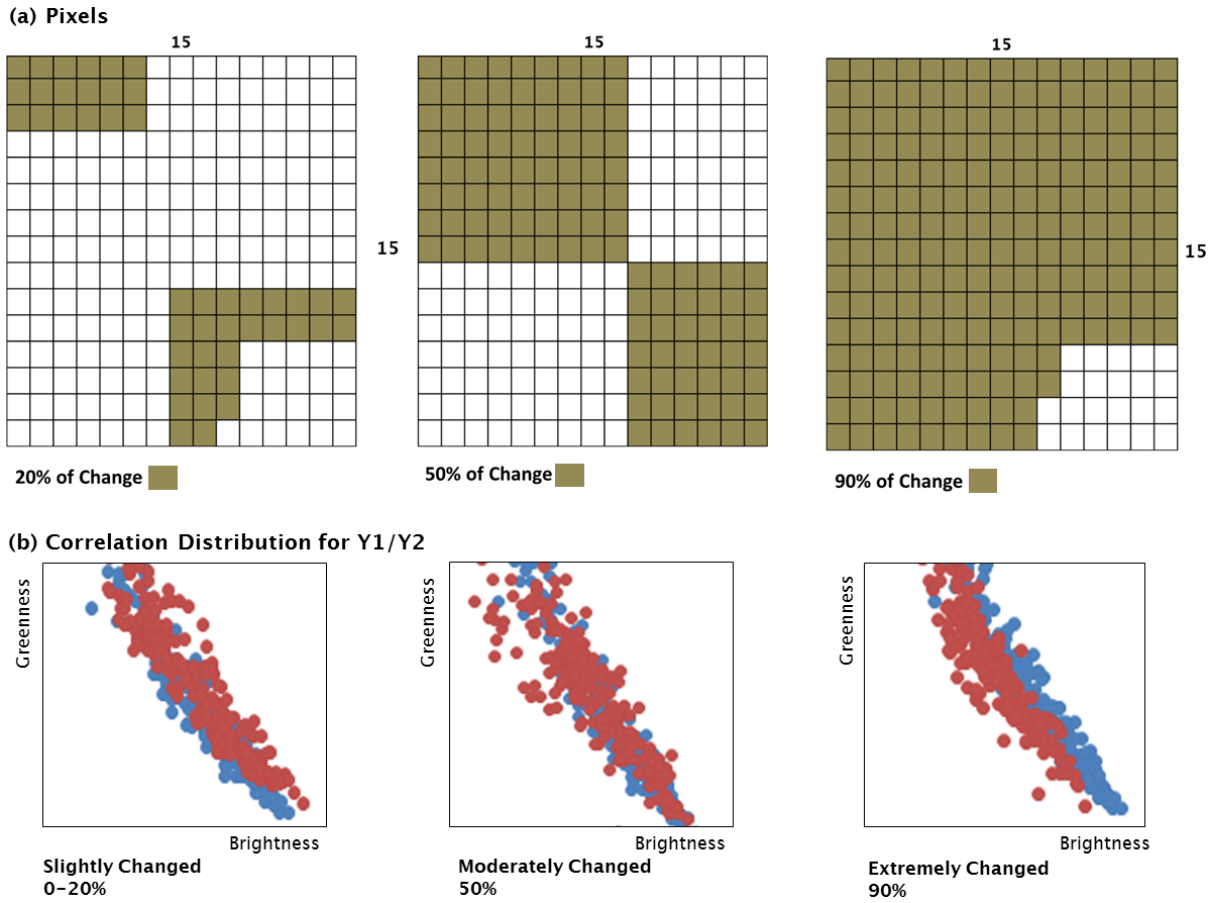


Figure 7.3 The threshold outline *P*–th percentile of unchanged and changed pixels.

### 7.2.5 Image Interpretation – Direct Recognition

Results from the classification and transformation of brightness and greenness need to be clearly visualised in order to interpret the target area if it is small in size. In this analysis, the size of image is small, allowing visual interpretation from the time series of image differences. The basic method of image interpretation is based on knowledge of the subject that motivates a researcher to interpret the image (Campbell 2006).

Direct recognition is the application of an interpreter's experience, skill and judgement to associate the image patterns with thematic classes. This process is essentially a qualitative subjective analysis of an image using the elements of image interpretation as visual and logical clues.

## 7.3 Analysis

This part involves a combination of the change vector analysis (CVA) and direct recognition of image interpretation to visualise the 18 points samples as the magnitude of 'change' and 'no change' in feature space. The target points are displayed in Figure 7.4.

The main questions to be asked are:

- What is the vector (land use) distribution in axis x and y (brightness and greenness) between the two observed data?
- What is the direction of vector when change occurs between land use classes?
- How will vector distribution present the type and amount of land use change?
- How can land use change be validated?

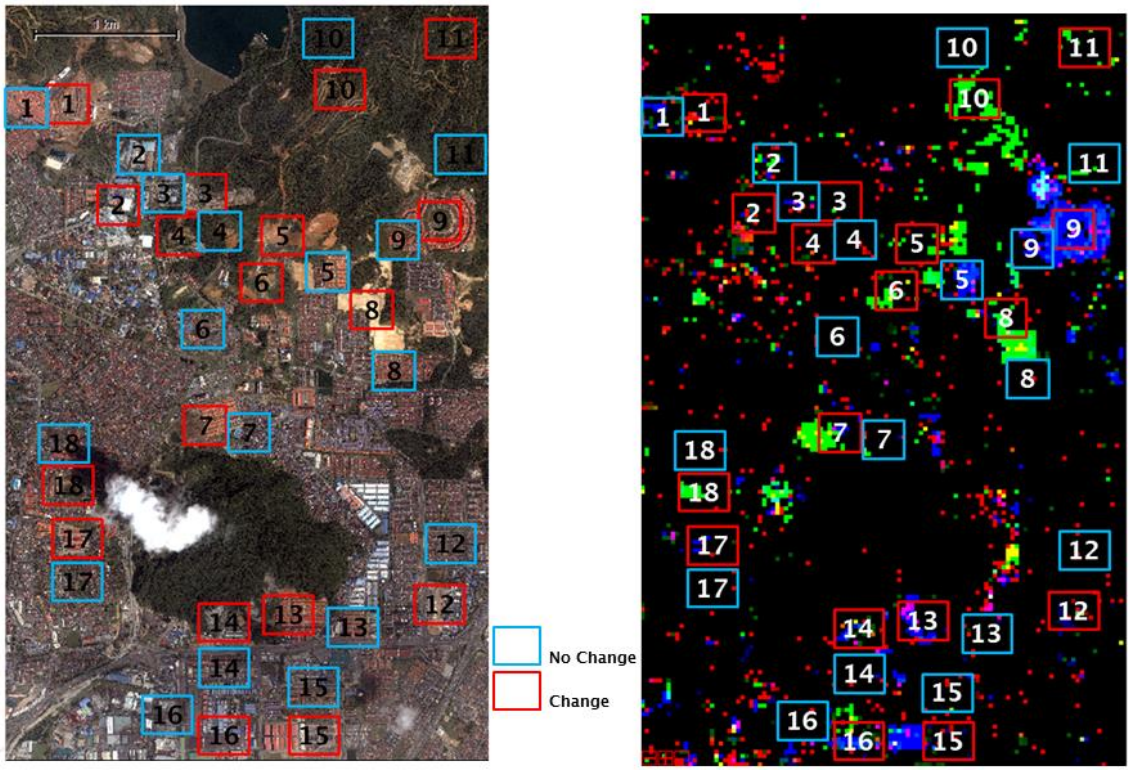


(a) Screen to screen comparison from IKONOS image 2009.

(b) Automated detection of changes by MAD from Landsat ETM+ 2009.

Figure 7.4 (a) 18 point samples of 'change' and 'no change' in IKONOS image and (b) Automated Change Detection from MAD.

The selection of the 18 target zone was very clear because the area had changed over four years and this evidence was further strengthened by the results of automated change detection analysis, Multivariate Alteration Detection (MAD) of Landsat ETM + in 2005 and 2009.

The number of 225 pixels (15 pixels x 15 pixels) for each point sample was represented in feature space. The value of X axis is brightness and Y axis is greenness with the vector data 2005 to 2009 comparing correlation. The comparison type starts with 2005 and tests the data from 2005/2006, 2005/2007, 2005/2008, and 2005/2009 to represent the changed land use. This analysis established the identification of different gaps of land use change distribution.

The brightness and greenness correlation visualised the shape of land use distribution in feature space (FS). The results from FS were identified using the Object -Based (OB) classification. This means that both the OB classification and the IKONOS data defined the type of changes. The CVA and image interpretation-direct recognition were used to make assumptions on the distribution of vectors on axis, brightness and greenness. The negative linear convergence of vector point in FS represented the direction of change between 0° and 180° magnitude of change between bare land (bright surface) to building including residential, commercial and industrial land use. The positive linear convergence with direction of change between 90° and 270° represented change between vegetation to bare land or bare land to vegetation. The detailed results are discussed in Section 7.4.

The spatial threshold was applied to the 18 point target area in order to represent the amount of change of brightness and greenness within the four-year monitoring period. The threshold parameters were described in Section 7.2.4. The main reason for using a spatial threshold was to estimate the year when pixels showed changing land use. It indicates the progress of development for the particular year and the amount of area involved.

Validation analysis was run using the comparison technique to identify the 18 point samples of ‘no change’ areas, allowing investigation of the FS trend distribution. The blue boxes indicate areas of no change in Figure 7.4 with each target representing 225 pixels. These targets were examined along the

starting year of 2005 with the data test of 2005/2006, 2005/2007, 2005/2008, and 2005/2009 to represent the 'no change' in land use.

Four main outputs were produced from the analysis; (i) feature space distribution result, (ii) magnitude direction of land use change, (iii) type of land use change, and (iv) validation of the 'no change area' in FS.

## 7.4 Results

### 7.4.1 Interpretation of Land Use Change Direction

The overall results of the 18 point target zones of change, as presented in Table 7.1, highlight the 'change to' land use from 2005 until 2009 with the amount of probability threshold change in the first grey box. The FS result in Figure 7.5 to Figure 7.7 represents the magnitude of change distribution for the 18 point of change samples.

The major change was from bright surface to building, involving change in ten zones (1,2,6,7,9,13,14,16 and 17). In particular, Zone 6 underwent prominent change, starting in 2007 when 90% of the area was converted to building.

The second obvious change was from vegetation to bright surface/building and this occurred in Zones 3,8,10,11,12,15 and 18. This change of land use was not confined to any particular year but Zone 15 experienced 90% change to bright surface/building in 2008.

Zone 4 was the only area to increase its vegetation cover over time, shown by the increase of 20% starting in 2006. This may be due to the clearance of building but a delay in development allowing grass cover to develop.

The loss of 90% water to bright surface was clearly shown to have occurred in 2007 and this was probably due to the filling of ponds for development.

Figures 7.5 to Figure 7.7 show the feature space (FS) for the vector distribution of land use change from 2005 to 2009. It was estimated that 90% (203 out of the total number of 225 pixels) of the land use changed between 2005 and

2009. The 18 point samples correlation clearly shows the different reflectance value between brightness and greenness. The blue dotted colour represents the land use vector in 2005 and the red dotted colour represents 2009. The detailed empirical results for the 18 point change zone are shown in Figure 7.8 to Figure 7.10 as example. The rest of the results and figures in Appendix 5. The change vector analysis and feature space (CVA-FS) represent the transition series over the five-year period as a vector point changed distribution.

Table 7.1 Summary table of the 18 point target zone of change reflectance and thematic change between 2005 and 2009.

| Target Zone | CVA (Period/Direction of Change) (15x15=225pixels) | | | | | TC Magnitude (Type of Change Land Use) |
|---|---|---|---|---|---|---|
| | **From** (March 2005) | 2006 Feb | 2007 Feb | 2008 Jan | 2009 April | **To** |
| #1 | Bright Surface | | | (20%) | | Building |
| #2 | Bright Surface | (50%) | | | | Building |
| #3 | Vegetation | (50%) | | | | Bright Surface / Building |
| #4 | Bright Surface | (20%) | | | | Vegetation |
| #5 | Water | | (90%) | | | Bright Surface |
| #6 | Bright Surface | | (90%) | | | Building |
| #7 | Bright Surface | (50%) | | | | Building |
| #8 | Vegetation | | | | (50%) | Bright Surface |
| #9 | Bright Surface | | (50%) | | | Building |
| #10 | Vegetation | | (20%) | | | Bright Surface |
| #11 | Vegetation | | (20%) | | | Bright Surface |
| #12 | Vegetation | | | | (50%) | Building |
| #13 | Bright Surface | | (50%) | | | Building |
| #14 | Bright Surface | | (50%) | | | Building |
| #15 | Vegetation | | | (90%) | | Bright Surface / Building |
| #16 | Bright Surface | | (50%) | | | Building |
| #17 | Bright Surface | | | (50%) | | Building |
| #18 | Vegetation | | | (20%) | | Bright Surface |
| | **2005** | **2006** | **2007** | **2008** | **2009** | **Magnitude of Change** |

*the first grey box refers to the starting year of change with:

(20%) slightly changed, (50%) moderately changed, (90%) extremely changed

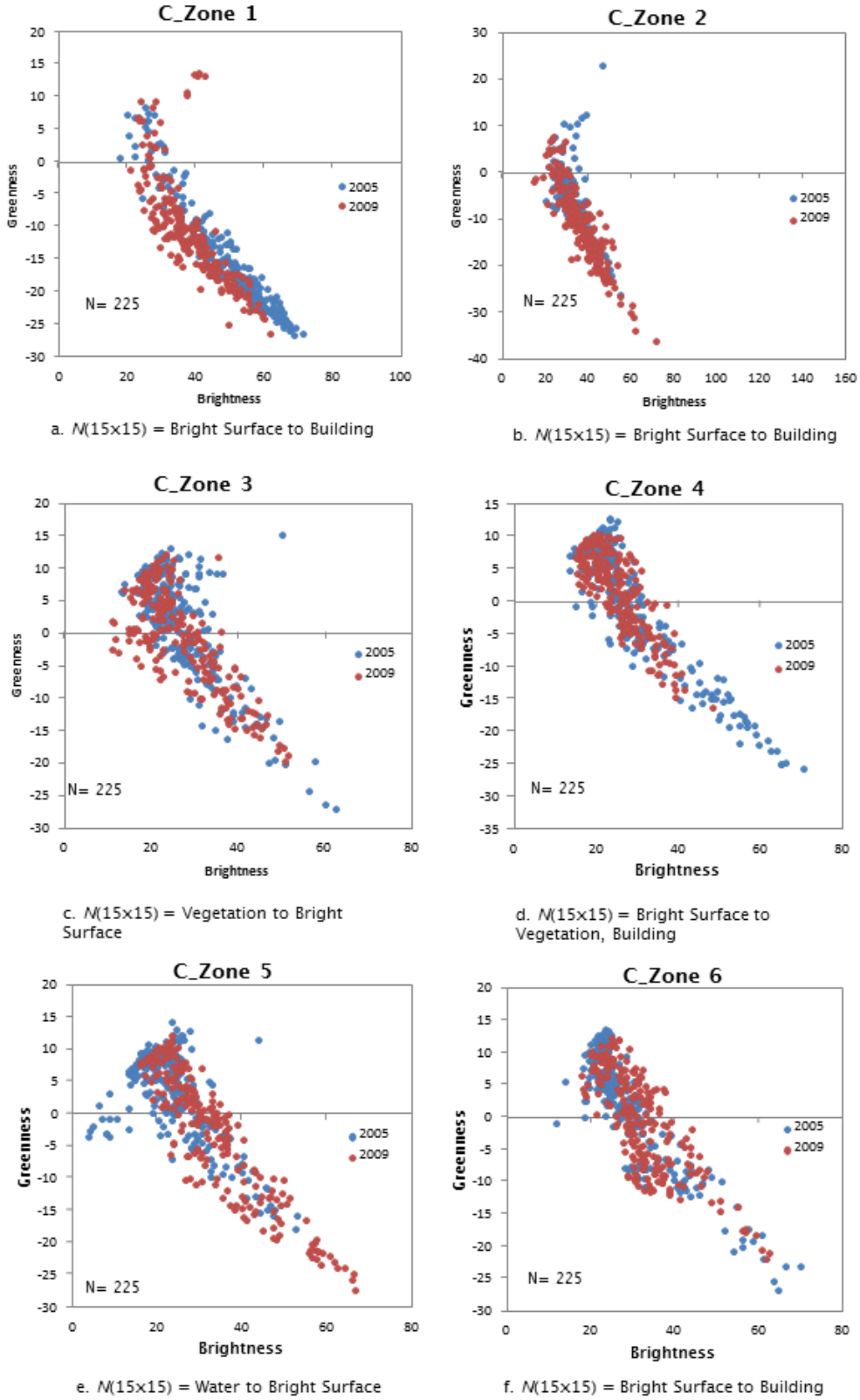


Figure 7.5 Change (C) between greenness and brightness for the 18 point target zone where change occurred between 2005–2009 for zone 1 to zone 6.

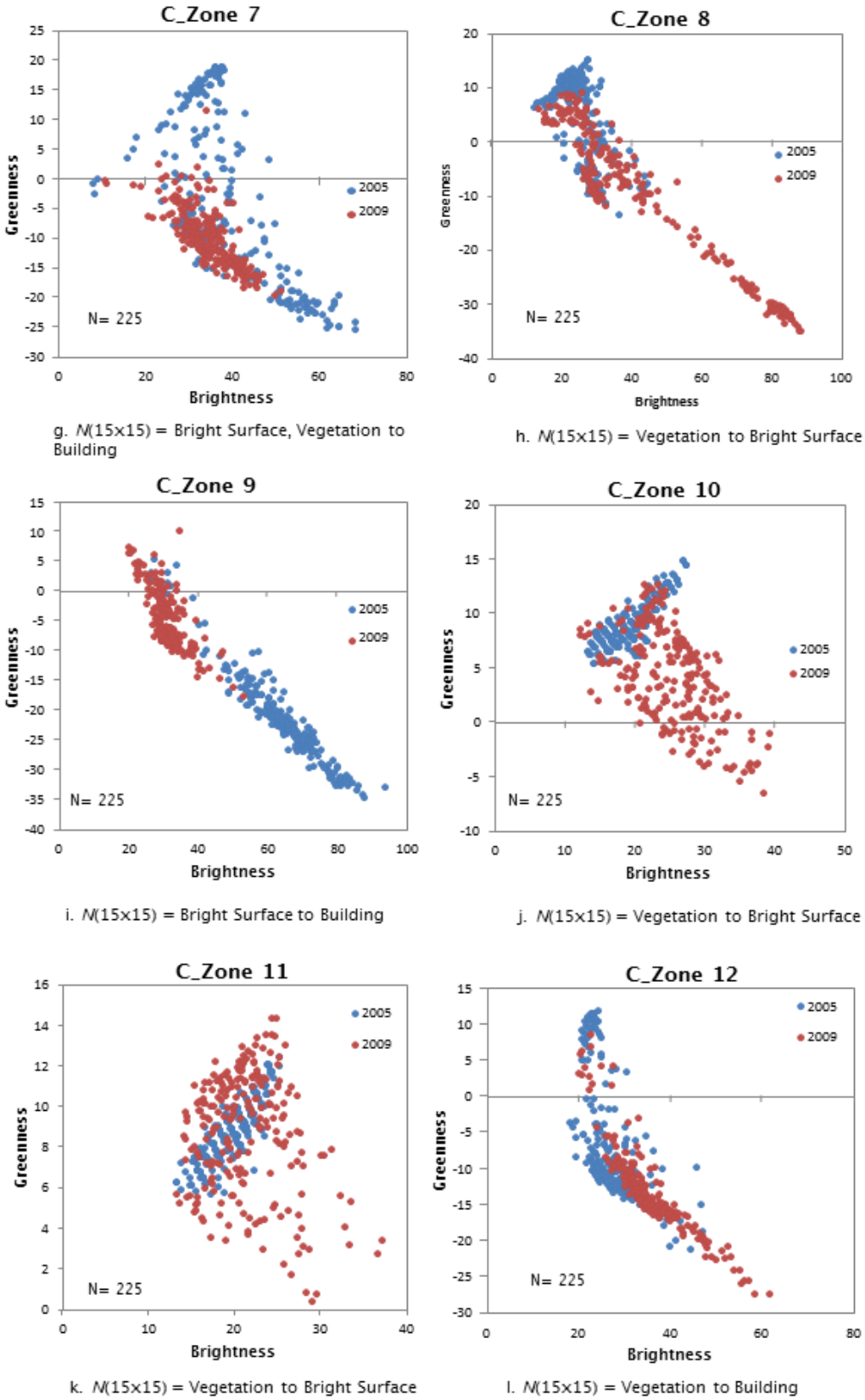


Figure 7.6 Change (C) between greenness and brightness for the 18 point target zone where change occurred between 2005-2009 for zone 7 to zone 12.

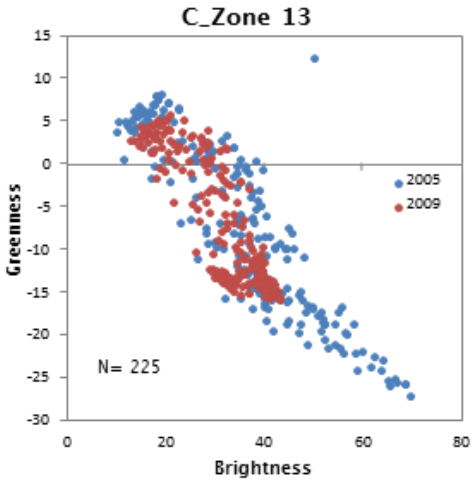


m. *N*(15x15) = Bright Surface to Building

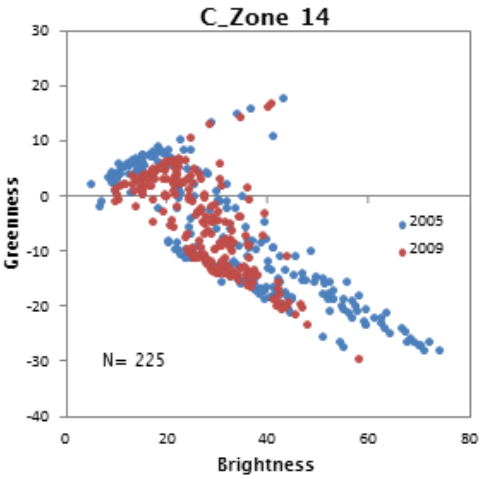


n. *N*(15x15) = Bright Surface to Building

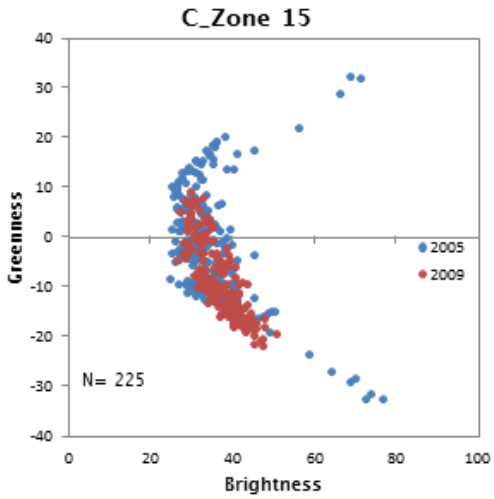


o. *N*(15x15) = Vegetation to Bright Surface, Building

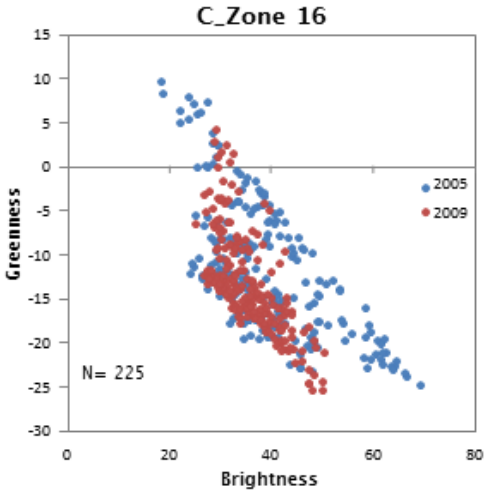


p. *N*(15x15) = Bright Surface to Building

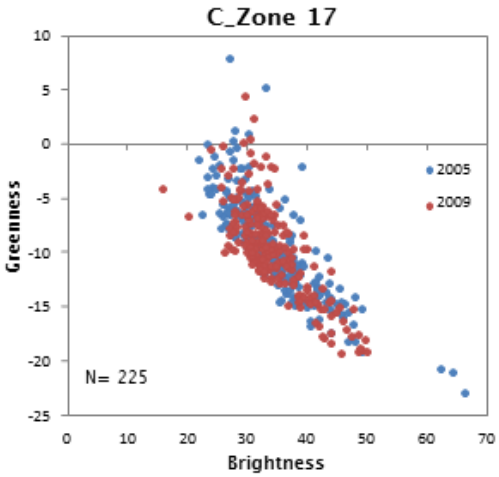


q. *N*(15x15) = Bright Surface to Building

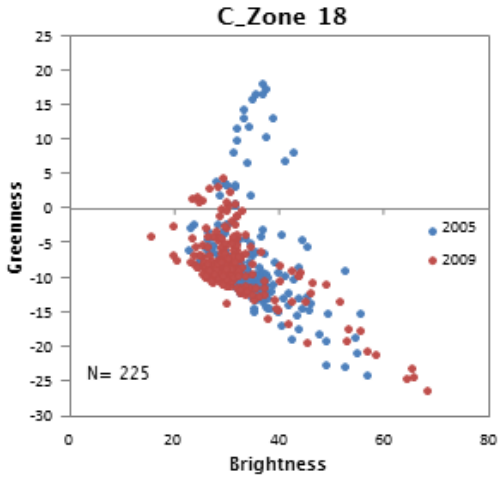


r. *N*(15x15) = Vegetation to Bright Surface

Figure 7.7 Change (C) between greenness and brightness for the 18 point target zone where change occurred between 2005-2009 for zone 13 to zone 18.

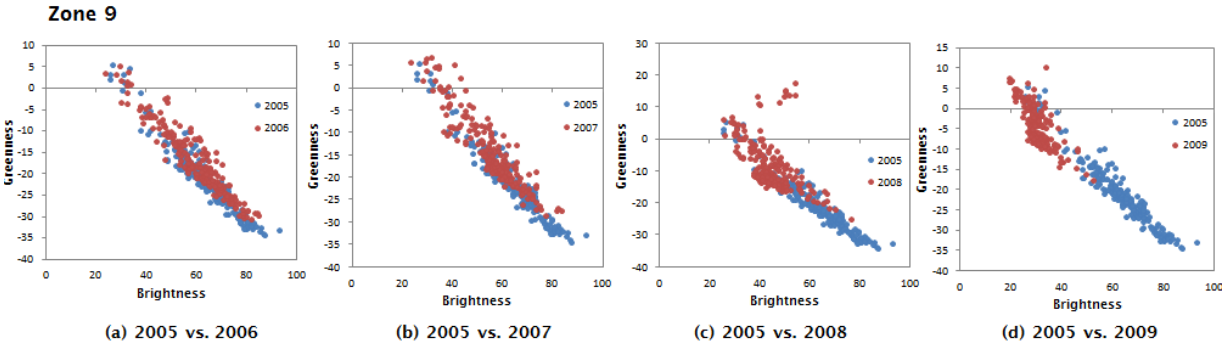


Figure 7.8 The direction and magnitude of change within yearly time series in feature space, example of zone 9.

From the correlation distribution result, the starting year of change for Zone 9 is 2007 with 50% change from bright surface to building.

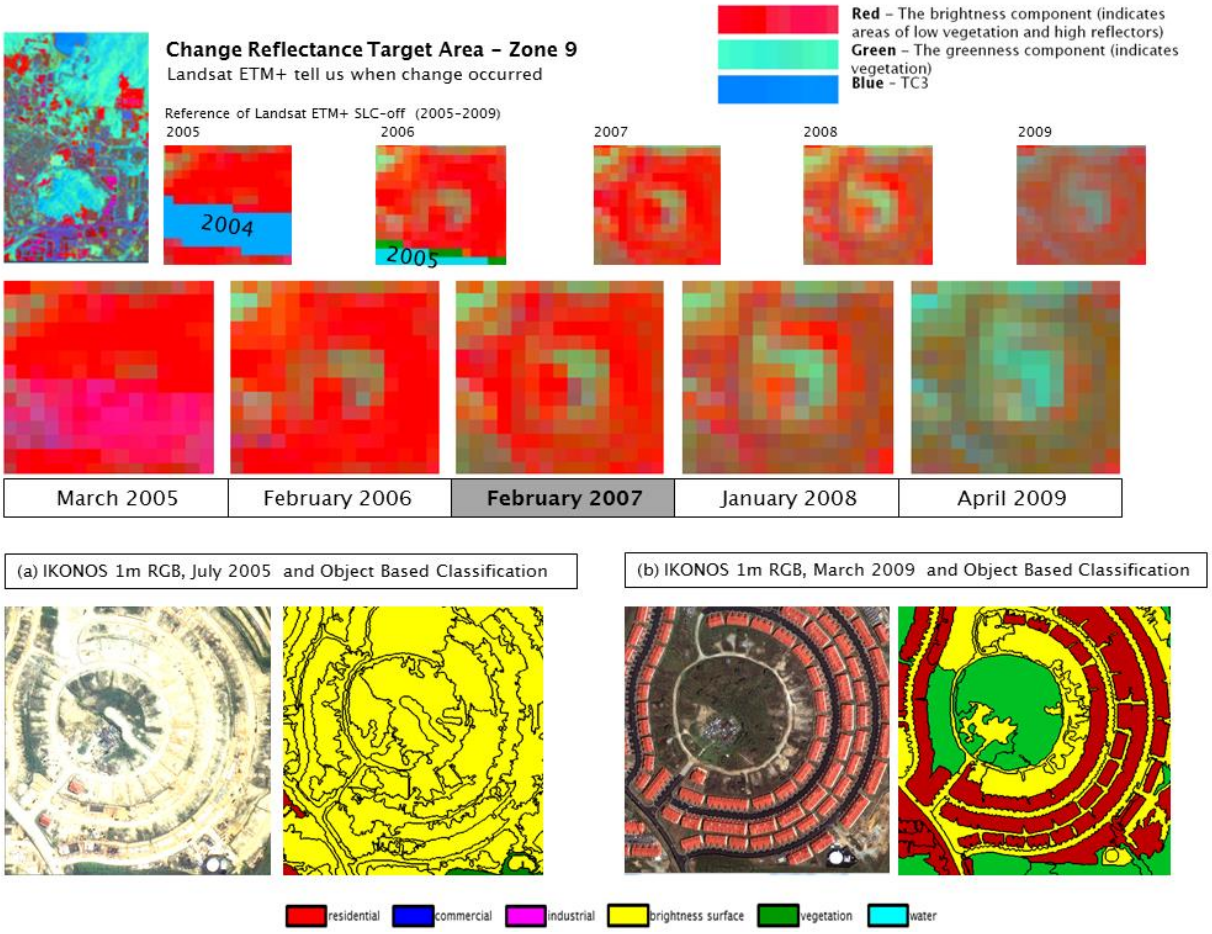


Figure 7.9 The transition of change between greenness and brightness from Landsat ETM+ 2005 to 2009 for zone 9 denotes when change occurred.The IKONOS data defined the type of change.

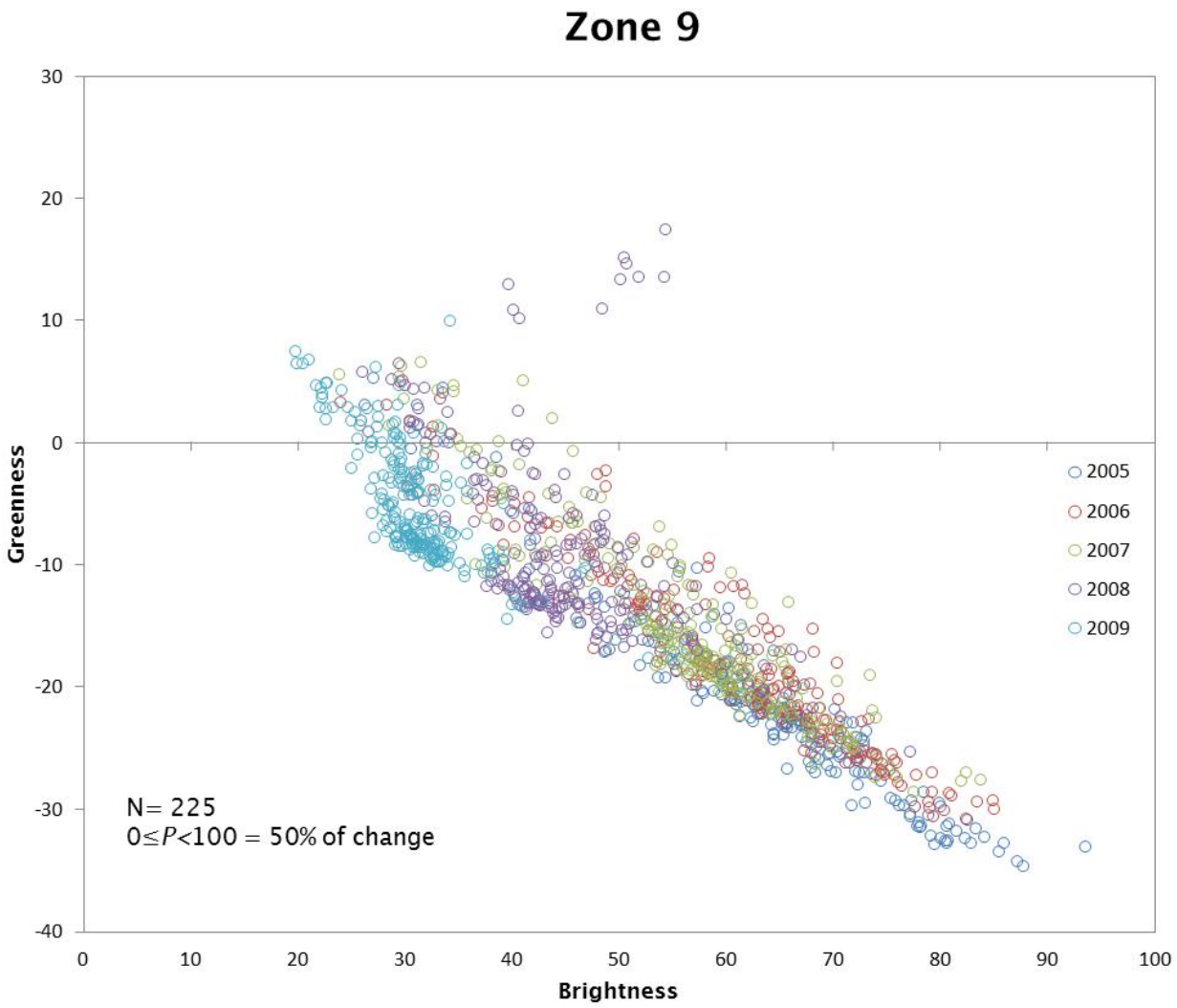


Figure 7.10 The feature space transition of change vector between greenness and brightness from Landsat ETM+ 2005 to 2009, zone 9.

### 7.4.2 Model of Vector Change in Feature Space (FS)

The overall result of change vector analysis in feature space can be highlighted as a model of transformation between greenness and brightness for the monitoring of urban land use change. A common practice is to organise the information provided by all these descriptors as the elements of one single vector, commonly referred to as a feature vector. The set of all possible feature vectors constitutes a feature space.

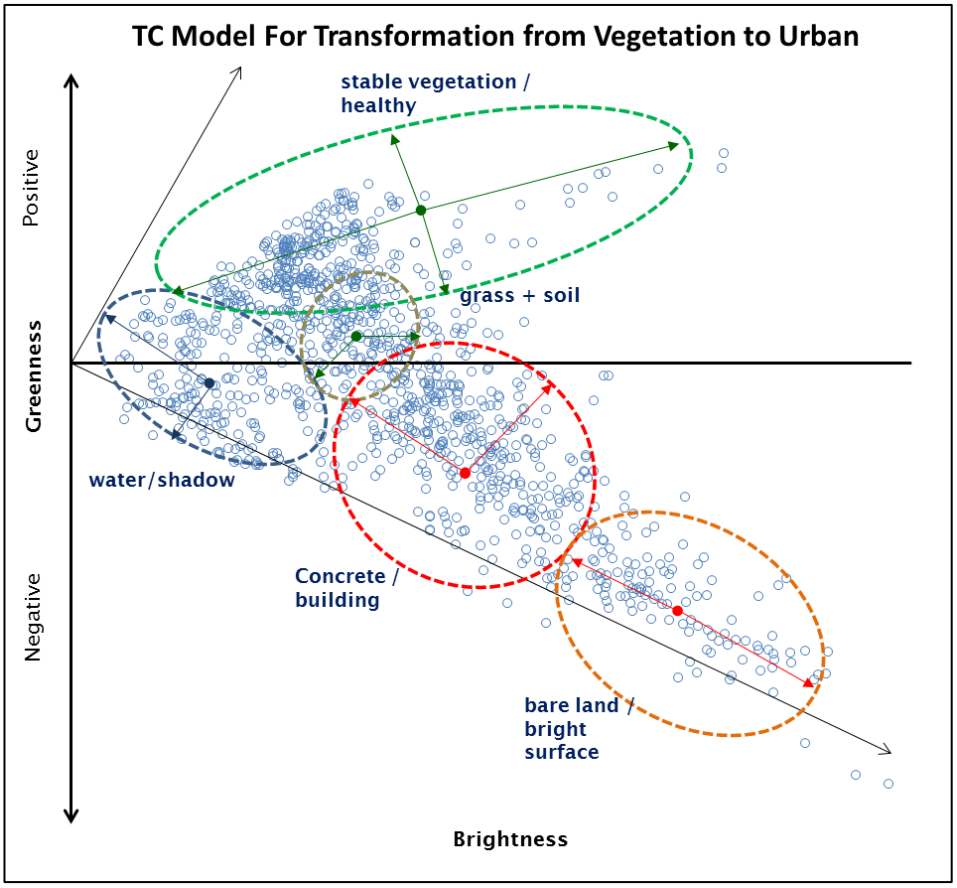


Figure 7.11 The model of feature space transition of change.

FS appears when each image point is classified as belonging to a specific class. The class images of brightness and greenness describe the vector point with positive and negative values. This is followed by vegetation, water, building and bright surface as classified by coarse resolution data using Landsat ETM+ 2005 to 2009. Assuming that each image point has a corresponding feature vector based on a suitable set of features, each class was well separated in the corresponding feature space. The classification of each image point was completed using Tasselled Cap (TC) transformation. This is shown in Figure

7.11 and it clearly describes the direction and magnitude of vector change from the land use type.

The model was generated from the result of TC transformation between brightness (X) and greenness (Y) axis data from Landsat ETM+. The result shows that the vegetation vector point is commonly distributed above other vector points with positive values. It represents healthier vegetation with the green canopy trees in positive values. The water class vector point is exactly below the vegetation vector point with a near to zero value in axis X and Y with positive and negative values. These values also included the shadow vector point or dark surface area. Building class or concrete features are commonly in the middle of the overall vector point with negative values. It shows the negative convergence magnitude from the zero value. The vector point is mixed between the bright surface points, but can still be clearly identified. The bright surface took place beside the building vector point with the higher positive value of brightness and lower negative value in greenness, meaning the point is an edge of the overall vector point distribution in negative convergence.

### 7.4.3 Validation of 'No Change' Land Use in Feature Space

Validation compares the vector point distribution in feature space to ensure that the land use classes are correctly identified and provide a comparison between 'changed' and 'no change' land use.

This analysis used the 'inverse change land use' to investigate and identify 18 point samples of "no change" land use between 2005 and 2009. Obviously, the comparison data is highlighted between 2005 and 2009 to identify the shape and vector point distribution for the different land use types as represented in the training site. The results are shown in Figure 7.12 to Figure 7.14 with the dark-blue colour for 2005 data and light-blue colour for 2009. The approach validated the data represented in 2D space. Most of the 18 point data (at least 90%) using 225 vector points show no change within the four-year period, with data showing a close overlay. As example (Zone 14) shown in Figure 7.15 of the feature space of no change (NC) that occurred in the TC result between greenness and brightness. Another results and figures as shown in Appendix 6 for Zones 1 to 18, using Landsat ETM+ 2005 to 2009.

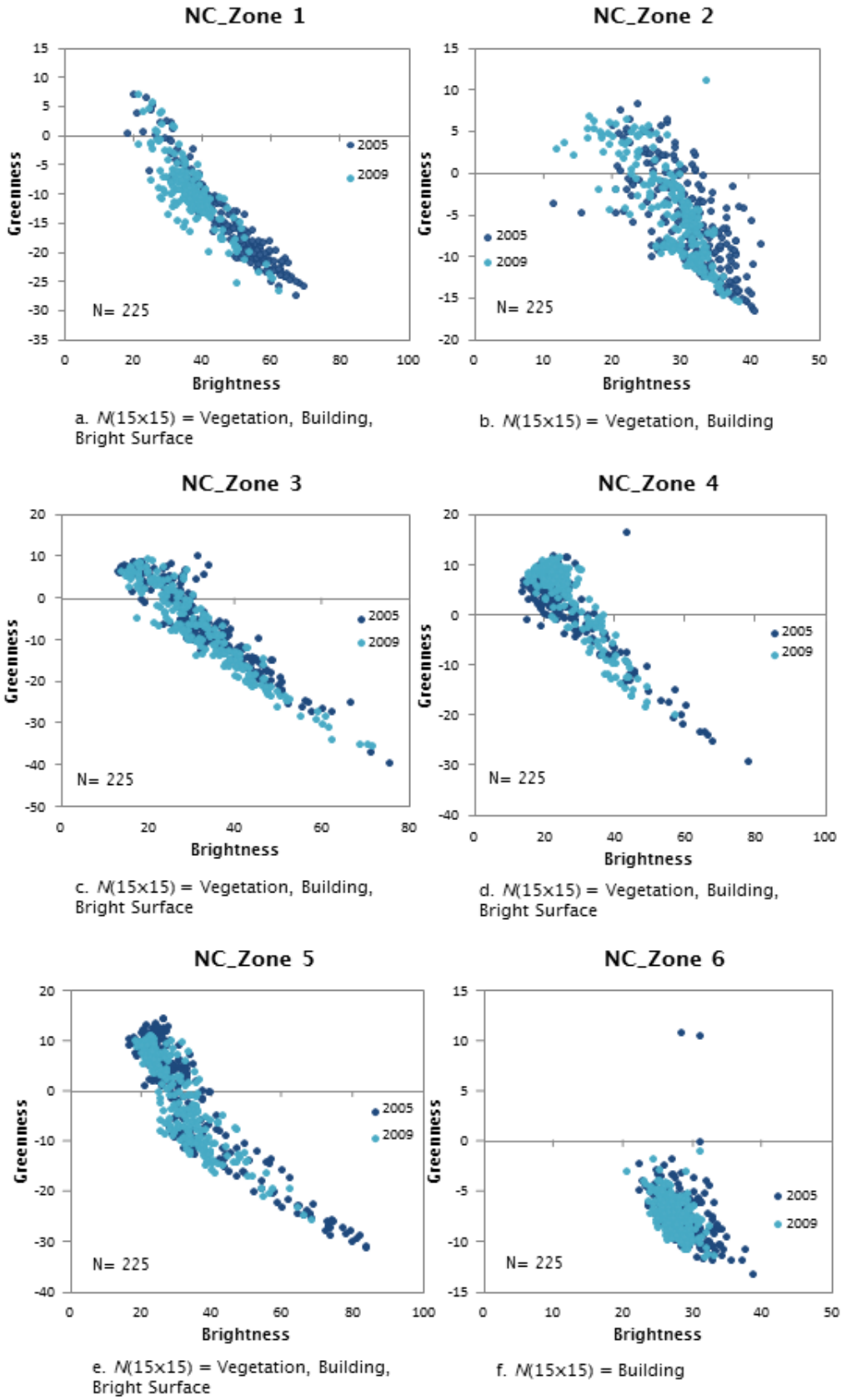


Figure 7.12 Validation result of no change (NC) between 2005-2009 for zone 1 to zone 6.

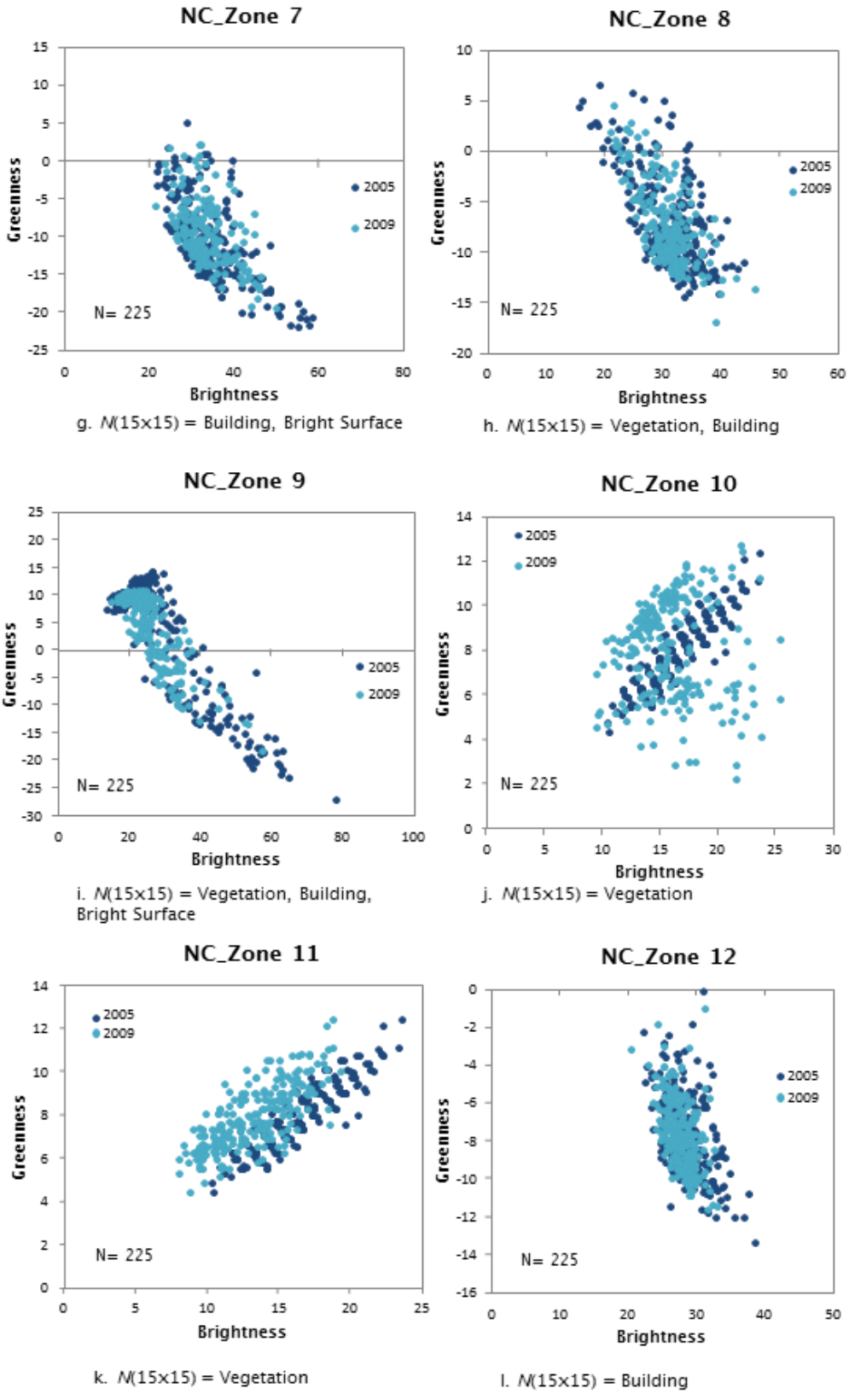


Figure 7.13 Validation result of no change (NC) between 2005-2009 for zone 7 to zone 12.

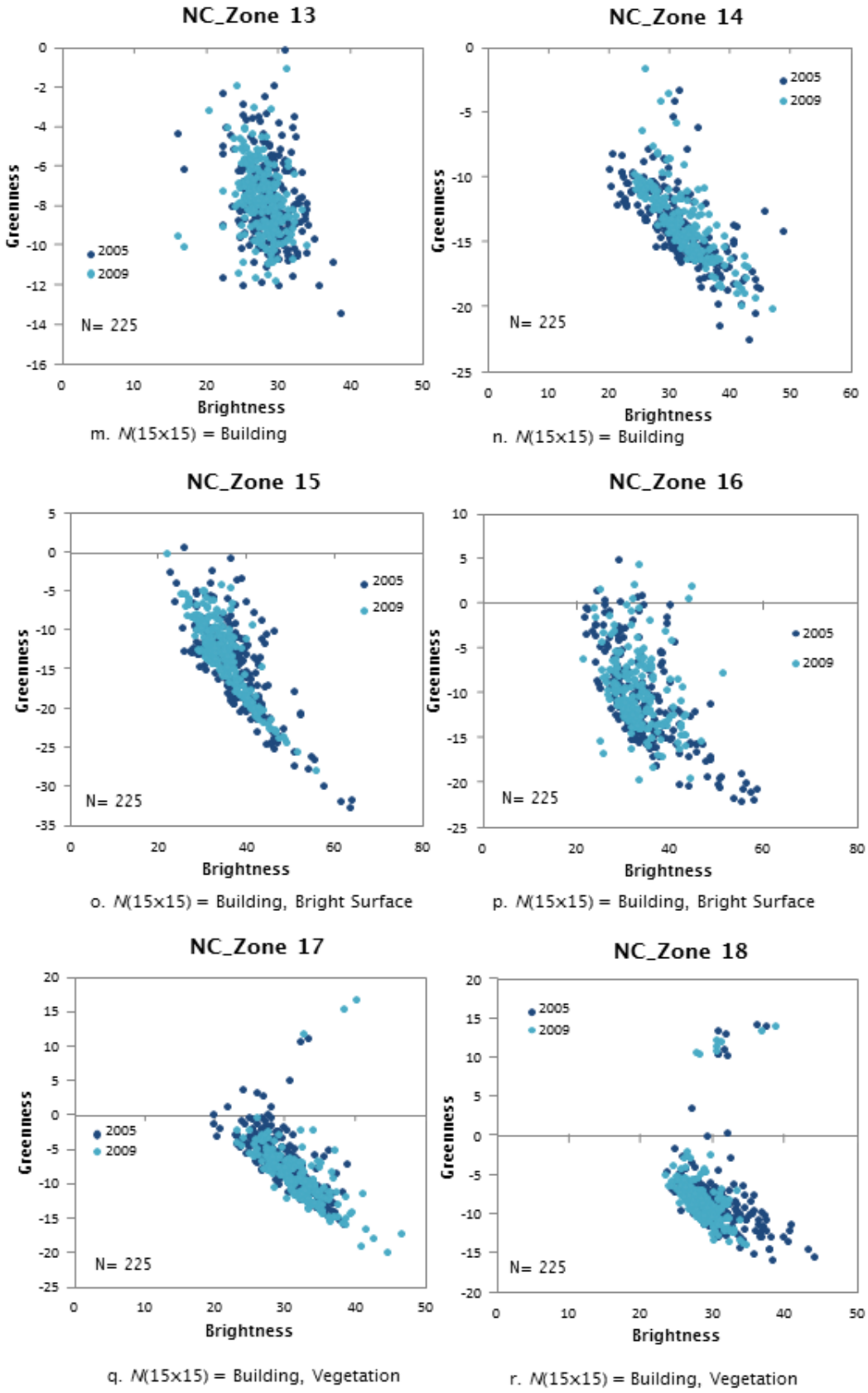


Figure 7.14 Validation result of no change (NC) between 2005-2009 for zone 13 to zone 18.

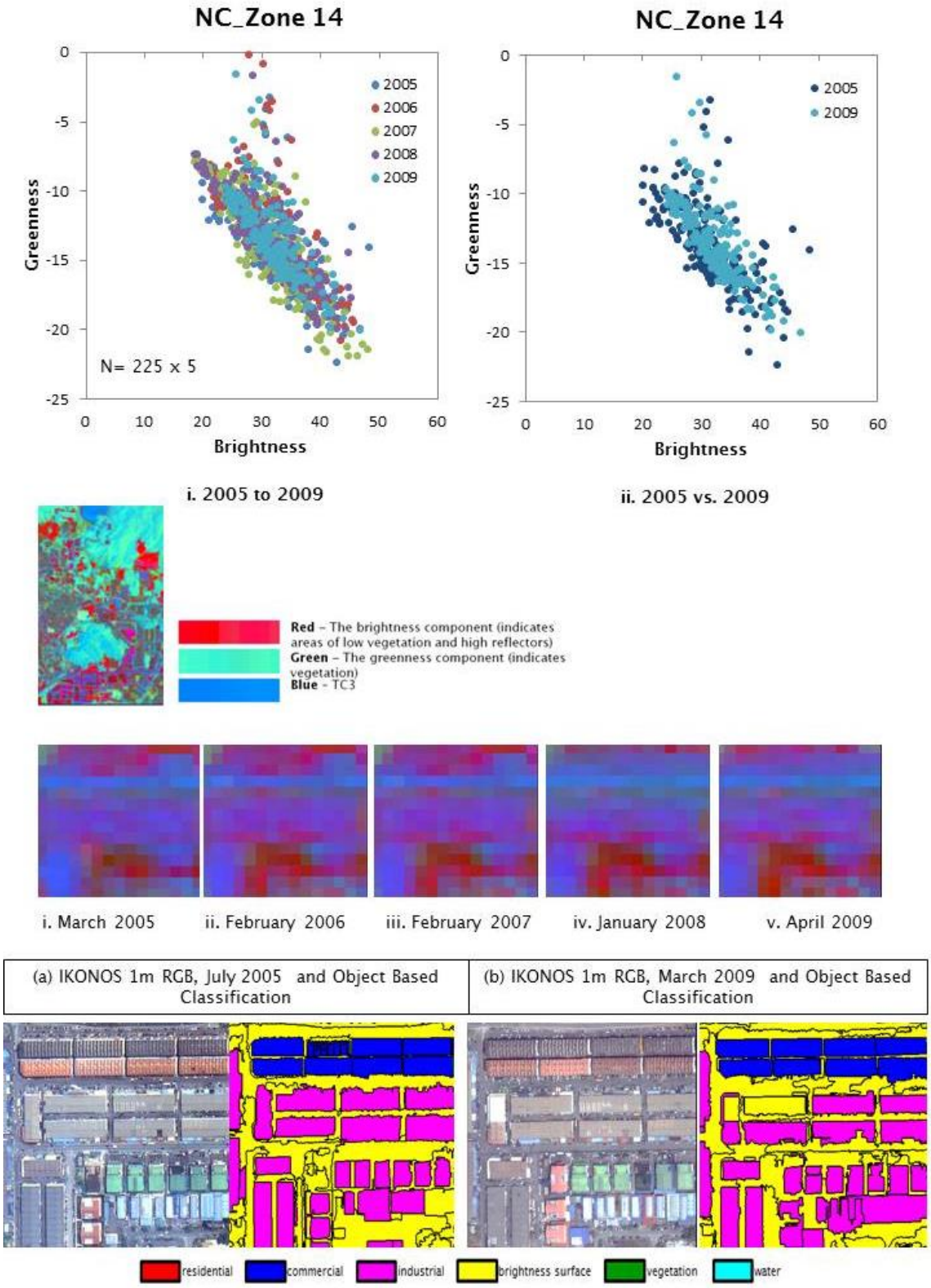


Figure 7.15 Validation from the feature space of no change (NC) shown by the TC result between greenness and brightness from example of Zone 14, Landsat ETM+ 2005 to 2009.

## 7.5 Discussion

The analysis of land use change can be applied for multiple date analysis in classifying data in 2D feature space. Figure 7.16 the feature space model for diagnosis of land use change – prove model for transformation from vegetation to urban. The model highlights the vector point distribution for each land use category using brightness and greenness. The advantages of the CVA, one of the most widely used methods for detecting land cover change, are that it gives clear information of direction and magnitude of land use change using the distribution of vector points for the axes of brightness and greenness. The analysis answers the final research question; *Do the changes fall into a small number of typical classes and does this help in diagnosing change?*

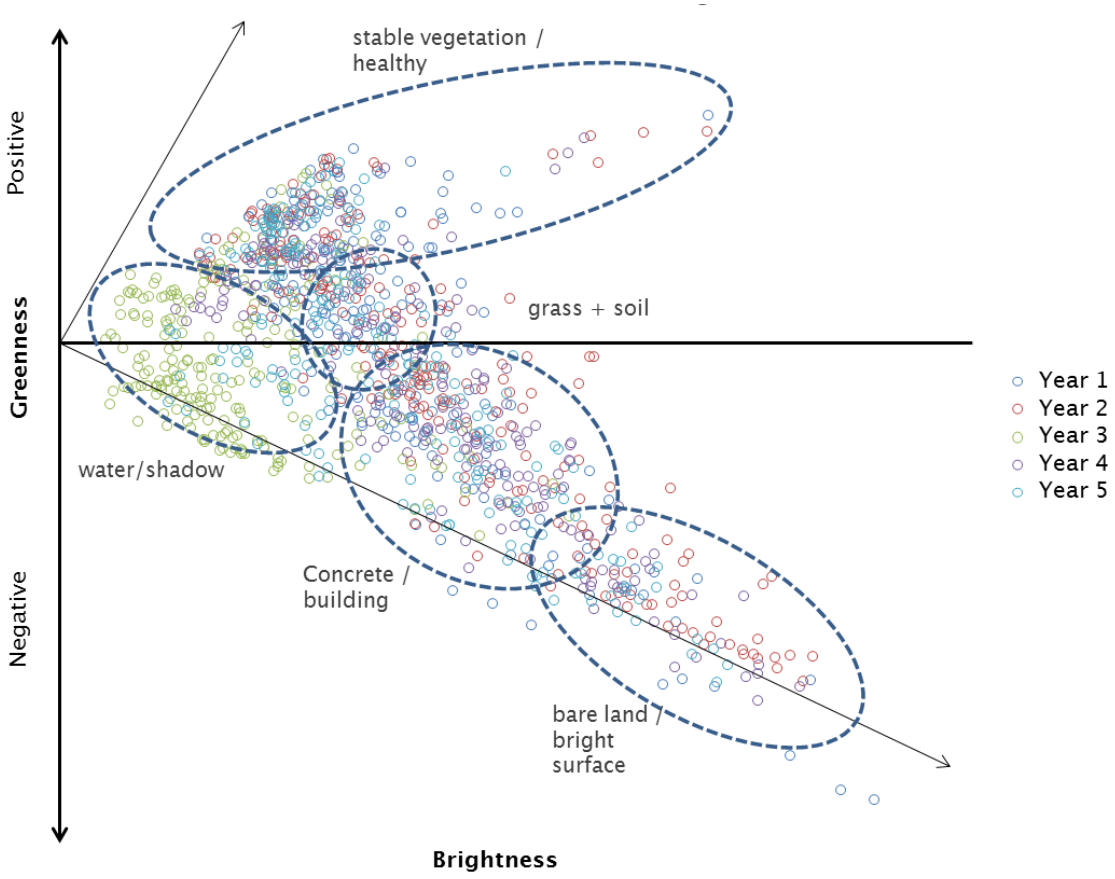


Figure 7.16 The feature space model for diagnosis of land use change – prove model for transformation from vegetation to urban.

The correlation investigates the direction and magnitude in FS, and thematic classification aids the interpretation of land use type represented by brightness and greenness. It is worth noting that the application of CVA-Feature Space has some limitations. The approach is best used in distinguishing land use and land cover monitoring of change from the vector point distribution. Three limitations will be discussed; (i) the scale chosen (image size), (ii) the role of manual interpretation and (iii) sampling issues.

The scale chosen in this analysis was a small pixel zone showing change, in order to evaluate the empirical result of vector point distribution in feature space. It may be easier to interpret the results if the selected area is small, because only one type of change occurs within a limited area. However, it is important to try to improve the method if the pixel zone is larger, because more complex changes may occur. This is because when a larger area involves change in its land use, it is no longer a 'one to one' land use change but a mixture of changes. This will be complicated when the monitoring data is more than a five-year span because many changes may occur over time.

This method also used a manual interpretation-direct recognition that depends on the interpreter's experience, skill and judgement to understand the image from the OB classification. This manual identification (comparing IKONOS and Landsat ETM+ images) is a new contribution to this research. However, this method needs to be developed as fully automatic in order to identify the pattern recognition for vector point distribution in feature space.

Another limitation issue is that validation samples were chosen only using the feature space to represent the exact vector point distribution for the amount of no change area (see Figure 7.12 to Figure 7.14). This method would be more dependable if the validation result could quantify within certain parameters using a statistical method. However, it also depends on the objective of the validation purpose. In this case, it provided a useful comparison and showed what the feature space point vector distribution for the 'no change area' looked like.

Despite the limitations, the methods used and the results that were generated offer a good analytical approach to achieving the objective of this chapter. The model design provided the basic approach to identifying the type of land use

change, whilst it described the vector point distribution based on direction and magnitude.

## 7.6 Conclusion

The purpose of this chapter is to diagnose change by interpreting changes in feature space vector point distribution, magnitude direction of land use change, type of land use change and validation of the changed zone area based on unchanged land between 2005 and 2009. The development of an actual spatial threshold using brightness and greenness data helped to estimate when and how much change occurred in each zone. Direct recognition based on thematic information from the infrequent OB classification between 2005 and 2009 was a very useful approach to identify the type of land use change. The multi-date brightness and greenness change detection method produced more effective results and required considerably less time and was an effective automated method. Another automated method of updating land use and land cover change used in this analysis was the CVA-FS (Change Vector Analysis-Feature Space), a tested model to diagnose the type of land use change by determination of vector point distribution.

# 8. Analysis 4: Forecasting Land Use Change through Cellular Automata Simulation

## 8.1 Introduction

In this chapter, a cellular automata (CA) model is applied to the data provided on land use through earlier chapters of this thesis in order to forecast future land use in the study area, thus, completing the set of goals of this thesis. Specifically, the Markov-CA model was used to forecast land use and land cover (LULC) changes into the medium-term future based on changes which occurred between 2005 and 2009 as detailed in the raster object-based (OB) LULC classification of IKONOS satellite sensor images. This chapter uses the OB LULC classification in 2005 as a base and the 2009 equivalent as the outcome such as to calculate transition probabilities for the residential, commercial and industrial LULC classes (RCI), which can then be used to forecast future changes, using the 2009 LULC image as a base.

In the Malaysian context, land use allocation is still being conducted in a rather *ad-hoc* manner, often assuming detailed knowledge of town planners. The objective of this chapter was to develop the CA model that will be used to forecast future LULC distributions based on observed changes in RCI LULC class from the OB classification as described in Chapter 5. This model will be used to project the observed historical land use change forward into the future, and this means effectively projecting recent land use planning *policy* into the future. This represents an interesting opportunity to consider the forecasted LULC patterns produced in this chapter using CA approaches against Malaysian planning documents for the same dates in the medium-term future. This would effectively amount to a test of whether medium-term planning in the study region is commensurate with the recent (2005-to-2009) pace of development.

The Markov-CA algorithm used in this chapter is available in IDRISI Selva to simulate and forecast LULC change. The forecast was achieved by analysing a pair of LULC maps using the Markov change detection model. It produces a transition probability matrix that shows the likelihood of change from each LULC type to the other six classes over the period of time observed. The Markov transition probability model is relatively simple and its intuitive logic is an attractive alternative to more complex formulations of the stochastic land use model for

planning forecasts. Thus, the approach may be readily adopted by other users in other situations. It also allowed a straightforward link between the work in previous chapters on defining probability matrices and the forecasting objective of this chapter. For these reasons, the approach was adopted here.

## 8.2 Research Methodology

### 8.2.1 Data Preparation

Firstly, data from the IKONOS OB LULC classification using the 2005 and 2009 images were used to perform the analysis. The OB LULC classification was converted into raster data format to perform a cell-based or pixel-based analysis. Secondly, data from the transition probability matrix were used to provide the required change probabilities within a four-year period. All these data were taken from the analysis in Chapter 5.

### 8.2.2 The General Workflow

The CA-Markov model uses a cellular automata procedure in combination with two land use maps that had previously been used to establish the quantity of expected LULC change from each existing category to each of the other categories in the four-year period. The IDRISI CA-MARKOV model is an efficient way of using these transition probabilities to forecast changes, meaning that it is not necessary to build all of the rules from the bottom up. It also means that the methodology used here would be readily replicated and generalizable to other regions around Malaysia and, indeed, in other countries. The main objective of the analysis was to forecast the land use in 2013, 2017 and 2021; the CA-MARKOV approach provides a reasonable and justifiable way of doing this. The 2005 LULC image was used as the starting point, while the 2009 LULC image was used as the end point for the estimation of the transition probabilities. The 2009 LULC map was then used as the starting point for the forecasting model. The process of CA modelling is shown in Figure 8.1:

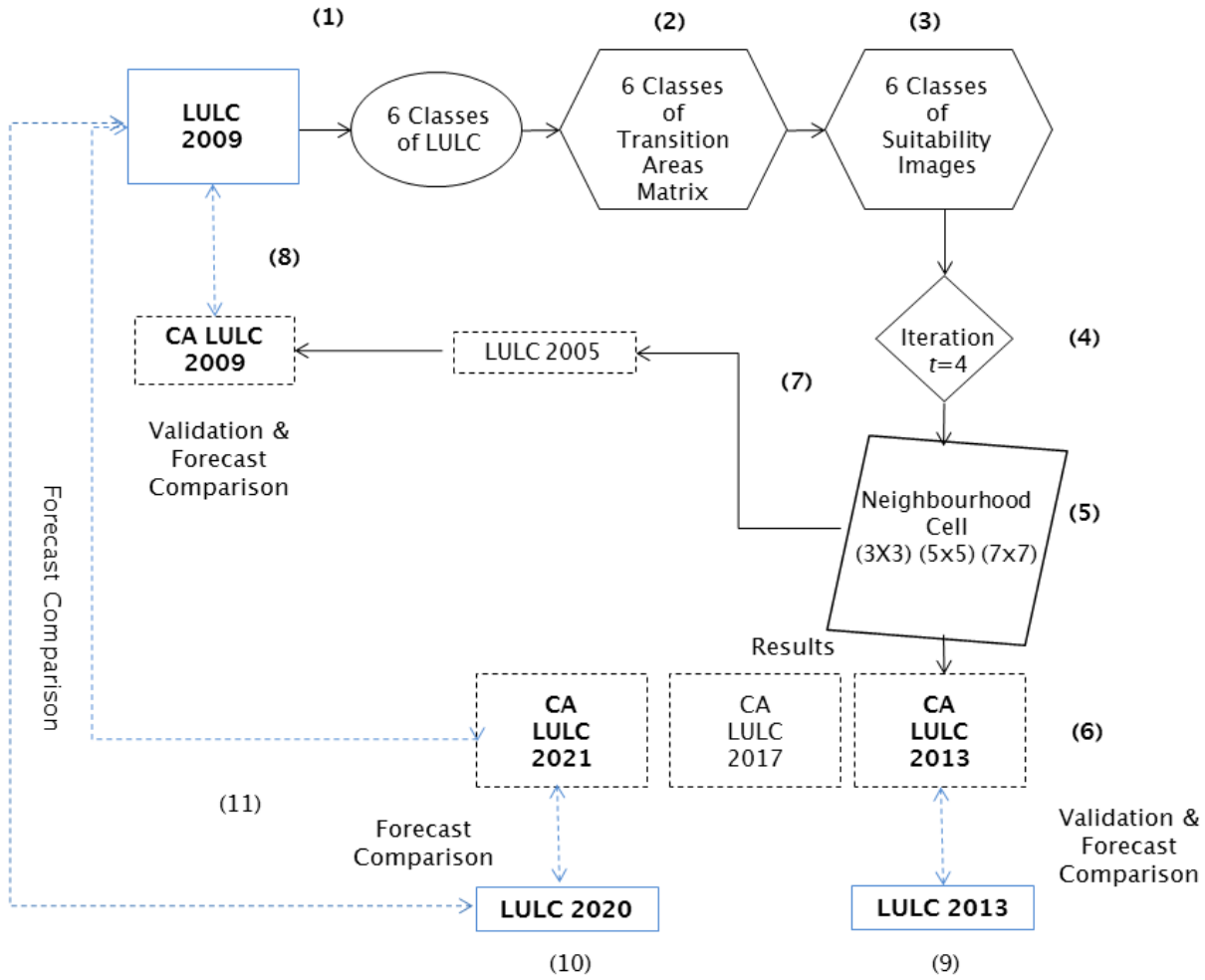


Figure 8.1 The general workflow of the CA model.

In Figure 8.1, the numbers have the following meanings:

(1) Land use base map in 2009,

(2) The transition probability matrix from 2005 to 2009 records the probability of LULC change. It records, as a proportion, the number of pixels that are expected to change from each LULC type to each other LULC type over the specified number of time units (four years in the present case). The probability values can equally be represented as percentage change (see Table 5.8 and 5.9). In both of these files, the rows represent the original, older land cover categories and the columns represent the newer categories.

(3) The conditional probability images show the probability of each land cover type that would be found at each pixel after the specified number of time units. These images are calculated as projections from the 2009 land cover image.

(4) The number of iterations is chosen to reflect the number of time steps used in the simulation. Cellular state represents the LULC types for each cell with a time step of four years.

(5) The transition probabilities can be determined based on the pixel in question only. However, the CA transition rules are set based on a (e.g., 3 by 3 cells, 5 by 5 cells and 7 by 7 cells) neighbourhood such as to forecast the LULC type in the future. The adjusted probability and future state of each cell is, thus, affected by the choice of filter. An objective here was to explore the effect of the choice of this parameter (i.e., window size) and select the most accurate from the three cases.

(6) The output of the CA process is a forecast of the LULC pattern in 2013, 2017 and 2021 (i.e., forecasts at a sequence of four-yearly intervals).

(7) The output of the CA process is a forecast of the LULC 2009 (CA 2009) from the LULC 2005.

(8) Validation and Forecast “comparison”, comparing the CA result for 2009 with the land use plan for 2009.

(9) Validation and Forecast “comparison”, comparing the CA result for 2013 with the land use plan for 2013.

(10) Forecast “comparison”; comparing the CA result for 2021 with the land use plan for 2020 of the Planning Department.

(11) Comparing the LULC 2009 with the CA result for 2021 and the land use plan for 2020 of the Planning Department. It is important to note that neither dataset is “correct” since they both represent forecasts, so this does not represent a “validation”. As suggested above, this offers an interesting opportunity to explore the differences between projecting forwards what is happening in recent times (2005-to-2009) with planning expectations, and to explore the reasons for these differences.

## 8.3 Strict CA: Central Cell Model

Applications of Markov chains to urban land use dynamics began to appear in the 1970s as an alternative to the use of large-scale urban simulation models for land use forecasting as introduced by Bourne (1971). The transition areas from a Markov Chain analysis of two previously classified land use maps established the quantity of expected LULC change from each existing category to each other category in the next time period.

The rules governing the CA can be summarised by the following generic equation.

$$S^{t+1}=f(S^t,S_N) \tag{8.1}$$

where,

$S^{t+1}$ = the state of the cell at time $t+1$

$f$ = a function representing a set of transition rules

$S^t$ = the state of the cell at time $t$

$S_N$ = the set of states of the neighbourhood.

The determination of the neighbourhood of cells is also an important aspect to consider when applying a CA-based model, as the choice may affect the accuracy of the data generated. In a basic CA model, the state of any cell depends on the configurations of other cells in the neighbourhood of that cell, where the neighbourhood is the immediate adjacent set of cells defined specifically next to the cell in question (Batty 2005). White et al., (2012) introduced a CA-based approach that models both activity levels and land use. In this approach, which makes use of a variable grid CA, activities attract or repel each other at all spatial scales within the modelled area.

The basic CA requires updating the state of the cell in question based on its current value and the values of its neighbourhood. To enhance the pattern effect of the simulated results, a moving window (e.g. 3 by 3 cells) was applied to identify the majority state of cells (the state that appears most frequently) within the extent of the window of the central cell. Subsequently, this majority state was assigned to the central cell in the neighbourhood window as its new membership value. If there was

more than one majority state for cells within the extent of the kernel, the one with the same state as the output cell was allocated to the neighbourhood.

This research used the probability of 'Cell-State' change approach as developed within the IDRISI software platform. It is a combination between the transition probability of change method for the central cell, and the CA-window approach described above. The model probability and central cell model is defined using the Transition Rule between at least two datasets derived from the probability of change. By application of a simple mathematical equation and some manual re-arrangement of the strict CA by central cell neighbourhood (i.e., CA window is 3 by 3 cells), a set of transition rules was designed as follows;

If $x_{o_{t-1}}$ = *BS* class and from $x_i$ $i$= 1,8 , $n \geq 1$ of $x_i$ is *Built Land* class then

$$p\left(x_{o_t} = Built\ Land \mid x_{o_{t-1}} = BS \text{ and } x_j = Built\ Land\right) = probability\ value_{class}.$$

(8.2)

For example,

If $x_{o_{t-1}}$ = *BS* class $c_4$ and from $x_i$ $i$= 1,8 , $n \geq 1$ of $x_i$ is *Built Land* class $c_3$ then

$$p\left(x_{o_t} = Built\ Land \text{ class } c_3 \mid x_{o_{t-1}} = BS \text{ class } c_4 \text{ and } x_j = Built\ Land \text{ class } c_3\right) = probability\ value_{class}$$

(8.3)

where *BS* is the bright surface land cover class in cell *x* and *i*=1,8 is the neighbourhood. Then, the probability (*p*) is calculated using the nearest magnitude from the centre of cell *j* to the outer neighbourhood limit and so it is possible to identify change to the built land class ($c_3$).

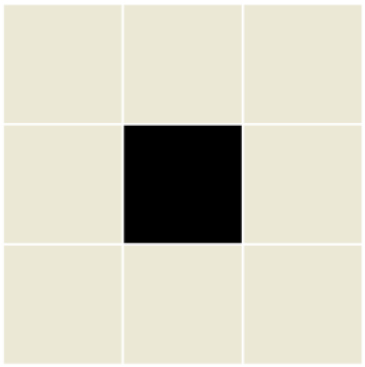

$$j = 1,8 \qquad class\ x_{0,1,2,3,4\ldots n} \in \sum_{j=1}^{8} x_j$$

Figure 8.2 Example by illustration of cell *x* (land use) and nearest magnitude of *j* (centre of cell).

Figure 8.2 shows, where *j* is the neighbourhood (centre of cell) of a strict CA of 3 by 3 (neighbourhood is 1, 8) cells, and $c_{o_{t-1}}$ is the initial class (state) of the central cell. From the expression of the transition rule, one obtains the potential of cell $x_i$ to change to state $c_j$ at time *t*, where $c_j$ refers to a certain land-use type (built land; residential, commercial, industrial).

In the above case, if the bright surface (BS) land use cell is surrounded by one or more built land cells, it may become built land as well (based on the probability value). The forecast is based on strict CA neighbourhoods. The result of the transition (i.e., whether the simulation results in a change or not) is based on the probability of change within the transition period. Specifically, a random value is drawn from between 0 and 1 and if the draw is greater than the probability value then a change is made. The simulation's purpose is to rearrange those pixels that are proximate to the existing land cover types under consideration. The net effect is that, to be a likely choice for land cover conversion, the pixel must be both inherently suitable and near to existing areas of that class. For the central cell filter, the following three kernel window sizes were used: 3 by 3 cells, 5 by 5 cells and 7 by 7 cells (Figure 8.3)

(a) 3 x 3

| | | |
|---|---|---|
| 0 | 1 | 0 |
| 1 | 1 | 1 |
| 0 | 1 | 0 |

(b) 5 x 5

| | | | | |
|---|---|---|---|---|
| 0 | 0 | 1 | 0 | 0 |
| 0 | 1 | 1 | 1 | 0 |
| 1 | 1 | 1 | 1 | 1 |
| 0 | 1 | 1 | 1 | 0 |
| 0 | 0 | 1 | 0 | 0 |

(c) 7 x 7

| | | | | | | |
|---|---|---|---|---|---|---|
| 0 | 0 | 1 | 1 | 1 | 0 | 0 |
| 0 | 1 | 1 | 1 | 1 | 1 | 0 |
| 1 | 1 | 1 | 1 | 1 | 1 | 1 |
| 1 | 1 | 1 | 1 | 1 | 1 | 1 |
| 1 | 1 | 1 | 1 | 1 | 1 | 1 |
| 0 | 1 | 1 | 1 | 1 | 1 | 0 |
| 0 | 0 | 1 | 1 | 1 | 0 | 0 |

Figure 8.3 The three windows of central cell tested for CA model.

Figure 8.3 shows that the filter is integral to the action of the CA component. Its purpose is to down-weight the suitability of pixels that are distant from existing instances of the land cover type under consideration.

The Markov-CA model automatically normalises the filter kernel to force the values to sum to 1. This filter was passed over a Boolean image for each class from the current land cover image within each iteration, and a set of weighted images was produced. The pixel values of these images were multiplied by the original values of the suitability maps to down-weight suitability by distance from existing areas of each class. The results were then stretched back to a byte (0-255) range. The net effect is that down-weighted suitability never exceeds a down-weighting in excess of 90% of the original value. This ensures that suitable areas can be found if none are available in proximate areas.

## 8.4 Analysis and Results

### 8.4.1 Standard Model CA-Markov

The standard model CA-Markov in the IDRISI software uses a 5 by 5 contiguity filter by default. This analysis involves two techniques; specifically, Markov transition and cellular automata (Araya & Cabral 2010). The forecasting was achieved by running the Markov model using the 2005 and 2009 land use maps. The CA-Markov algorithm was run to simulate the land use forecast for 2013 based on changes that had occurred between 2005 and 2009. In every run, the model gave a transition probability matrix which showed the likelihood of change from each LULC type to each of the other ones over the following four years. In the probability matrix, rows indicate older LULC classes and columns refer to newer LULC classes using a proportional error of 0.15 (based on assumption).

The analysis used LULC maps of 2005 and 2009 from the OB classification of IKONOS data to forecast LULC changes by 2013. The basic LULC image (the later IKONOS image, i.e., for 2009, used in the Markov transition probability analysis was used as the starting point for the change simulation.

Table 8.1 Land cover change count matrices for each transition period of four years obtained using OB LULC data for 2009 and simulated using the CA for 2013, 2017 and 2021.

| 2005/2009 | Cl. 1 | Cl. 2 | Cl. 3 | Cl. 4 | Cl. 5 | Cl. 6 |
|---|---|---|---|---|---|---|
| CLASS 1 | **2571902** | 11363 | 67739 | 1371999 | 421893 | 2137 |
| CLASS 2 | 5346 | **31805** | 1830 | 41287 | 0 | 0 |
| CLASS 3 | 46202 | 477 | **318198** | 333474 | 18418 | 48 |
| CLASS 4 | 1478170 | 50132 | 361457 | **3061892** | 926644 | 19283 |
| CLASS 5 | 335821 | 243 | 42857 | 1317829 | **4838819** | 37499 |
| CLASS 6 | 14399 | 78 | 4 | 31564 | 15374 | **243817** |
| **2009/2013** | | | | | | |
| CLASS 1 | **4373565** | 129 | 1933 | 6424 | 75834 | 0 |
| CLASS 2 | 413 | **84366** | 832 | 1530 | 0 | 0 |
| CLASS 3 | 0 | 0 | **785935** | 5604 | 0 | 0 |
| CLASS 4 | 86987 | 9688 | 74903 | **5985657** | 1693 | 26 |
| CLASS 5 | 723 | 19 | 4459 | 381965 | **5839144** | 7693 |
| CLASS 6 | 10019 | 0 | 644 | 11126 | 0 | **268689** |
| **2013/2017** | | | | | | |
| CLASS 1 | **4395159** | 0 | 314 | 0 | 75510 | 0 |
| CLASS 2 | 298 | **84077** | 845 | 375 | 0 | 0 |
| CLASS 3 | 0 | 0 | **864216** | 0 | 0 | 0 |
| CLASS 4 | 83775 | 0 | 73481 | **6242394** | 0 | 2 |
| CLASS 5 | 0 | 0 | 0 | 362045 | **5566552** | 0 |
| CLASS 6 | 7252 | 0 | 734 | 10225 | 0 | **252746** |
| **2017/2021** | | | | | | |
| CLASS 1 | **4410786** | 0 | 0 | 0 | 75775 | 0 |
| CLASS 2 | 291 | **82590** | 829 | 369 | 0 | 0 |
| CLASS 3 | 0 | 0 | **938774** | 0 | 0 | 0 |
| CLASS 4 | 86245 | 0 | 76195 | **6452600** | 0 | 0 |
| CLASS 5 | 0 | 0 | 0 | 344546 | **5297519** | 0 |
| CLASS 6 | 6882 | 0 | 0 | 9466 | 0 | **237133** |

Note: Class (1) Residential, (2) Commercial, (3) Industrial, (4) Bright Surface, (5) Vegetation, (6) Water.

Table 8.2 Land cover change probability matrices for each transition period of four years obtained using OB LULC data for 2009 and simulated using the CA for 2013, 2017 and 2021.

| 2005/2009 | Cl. 1 | Cl. 2 | Cl. 3 | Cl. 4 | Cl. 5 | Cl. 6 |
|---|---|---|---|---|---|---|
| CLASS 1 | **0.5783** | 0.0026 | 0.0152 | 0.3085 | 0.0949 | 0.0005 |
| CLASS 2 | 0.0666 | **0.3962** | 0.0228 | 0.5144 | 0 | 0 |
| CLASS 3 | 0.0645 | 0.0007 | **0.4439** | 0.4652 | 0.0257 | 0.0001 |
| CLASS 4 | 0.2506 | 0.0085 | 0.0613 | **0.5192** | 0.1571 | 0.0033 |
| CLASS 5 | 0.0511 | 0 | 0.0065 | 0.2005 | **0.7362** | 0.0057 |
| CLASS 6 | 0.0472 | 0.0003 | 0 | 0.1034 | 0.0504 | **0.7988** |
| **2009/2013** | | | | | | |
| CLASS 1 | **0.9811** | 0 | 0.0004 | 0.0014 | 0.017 | 0 |
| CLASS 2 | 0.0047 | **0.9682** | 0.0095 | 0.0176 | 0 | 0 |
| CLASS 3 | 0 | 0 | **0.9929** | 0.0071 | 0 | 0 |
| CLASS 4 | 0.0141 | 0.0016 | 0.0122 | **0.9719** | 0.0003 | 0 |
| CLASS 5 | 0.0001 | 0 | 0.0007 | 0.0613 | **0.9367** | 0.0012 |
| CLASS 6 | 0.0345 | 0 | 0.0022 | 0.0383 | 0 | **0.925** |
| **2013/2017** | | | | | | |
| CLASS 1 | **0.983** | 0 | 0.0001 | 0 | 0.0169 | 0 |
| CLASS 2 | 0.0035 | **0.9823** | 0.0099 | 0.0044 | 0 | 0 |
| CLASS 3 | 0 | 0 | **1** | 0 | 0 | 0 |
| CLASS 4 | 0.0131 | 0 | 0.0115 | **0.9754** | 0 | 0 |
| CLASS 5 | 0 | 0 | 0 | 0.0611 | **0.9389** | 0 |
| CLASS 6 | 0.0268 | 0 | 0.0027 | 0.0377 | 0 | **0.9328** |
| **2017/2021** | | | | | | |
| CLASS 1 | **0.9831** | 0 | 0 | 0 | 0.0169 | 0 |
| CLASS 2 | 0.0035 | **0.9823** | 0.0099 | 0.0044 | 0 | 0 |
| CLASS 3 | 0 | 0 | **1** | 0 | 0 | 0 |
| CLASS 4 | 0.013 | 0 | 0.0115 | **0.9754** | 0 | 0 |
| CLASS 5 | 0 | 0 | 0 | 0.0611 | **0.9389** | 0 |
| CLASS 6 | 0.0272 | 0 | 0 | 0.0373 | 0 | **0.9355** |

Note: Class (1) Residential, (2) Commercial, (3) Industrial, (4) Bright Surface, (5) Vegetation, (6) Water.

Tables 8.1 and 8.2 are the result of the transition area applied in order to calculate the projected land cover in 2013, 2017 and 2021 based on the OB LULC in 2005 and 2009. The transition area matrices express (Table 8.1) the total area in pixels (cells) and the probabilities (Table 8.2) expected to change in each four year time period. These resulting matrices are used to control the cellular automata model of

the growth of certain LULC classes, as expected, with the appropriate probability values and CA-window (contiguity filter).

Table 8.3 Results of conditional probability of change to other classes.

| **LULC Classes** | ***t*= 4**<br>**Probability of Change Values *(p)*** |
|---|---|
| Residential | 0.017 |
| Commercial | 0.018 |
| Industrial | 0.007 |
| Bright Surface | 0.0245 |
| Vegetation | 0.06 |
| Water | 0.065 |

From Table 8.3 the probability values show that, for any four-year period (starting from any point), the probability values. The least change is from Industrial with a probability of change of *0.0071 or not changed.* In the forecasting model, these probability values apply to the central cell of the neighbourhood.

New development of RCI cannot take place on restricted land like reserved forest and water bodies. The result shows that the spatial pattern of RCI remains within the neighbourhood area and is not isolated from the same type of land use. In general, the forecasts display large new areas of built land (including RCI), as well as new areas of vegetation and water bodies. It was necessary to take into account these constrained area (water bodies, forest and agriculture) and areas under existing urban use (RCI and cleared land). In order to include the constraint map, all the elements of the required layers were reclassified by giving the value zero (0) to all constraints. A constraint model was, thus, developed as shown in Figure 8.4 and used to conduct this exercise. The map shows all the constraints in combination and the developable areas in the case study area.

Suitability maps for each LULC class established the inherent suitability of each pixel for each LULC type (residential, commercial, industrial, bright surface, vegetation and water) as presented in Figure 8.5. These maps, therefore, show areas where there is most likely to be contiguous change in land use. The

probability of change *(p)* values within each class were highlighted from zero to the largest value by presenting the map in contrasting colours. The probabilities map of being each class for the four-year period for residential is 0.9811, commercial is 0.9682, industrial is 0.9929, bright surface is 0.9719, vegetation is 0.9367 and water is 0.925 using LULC data for 2005 and 2009. This analysis shows that probability of cells belonging to the same class in the next time period is very high, leading to a fairly stable spatial pattern in LULC. This stability is reassuring, since this reflects our expectations.


Figure 8.4 The constraint map.
(0 = constraint on development, 1 = developable area).

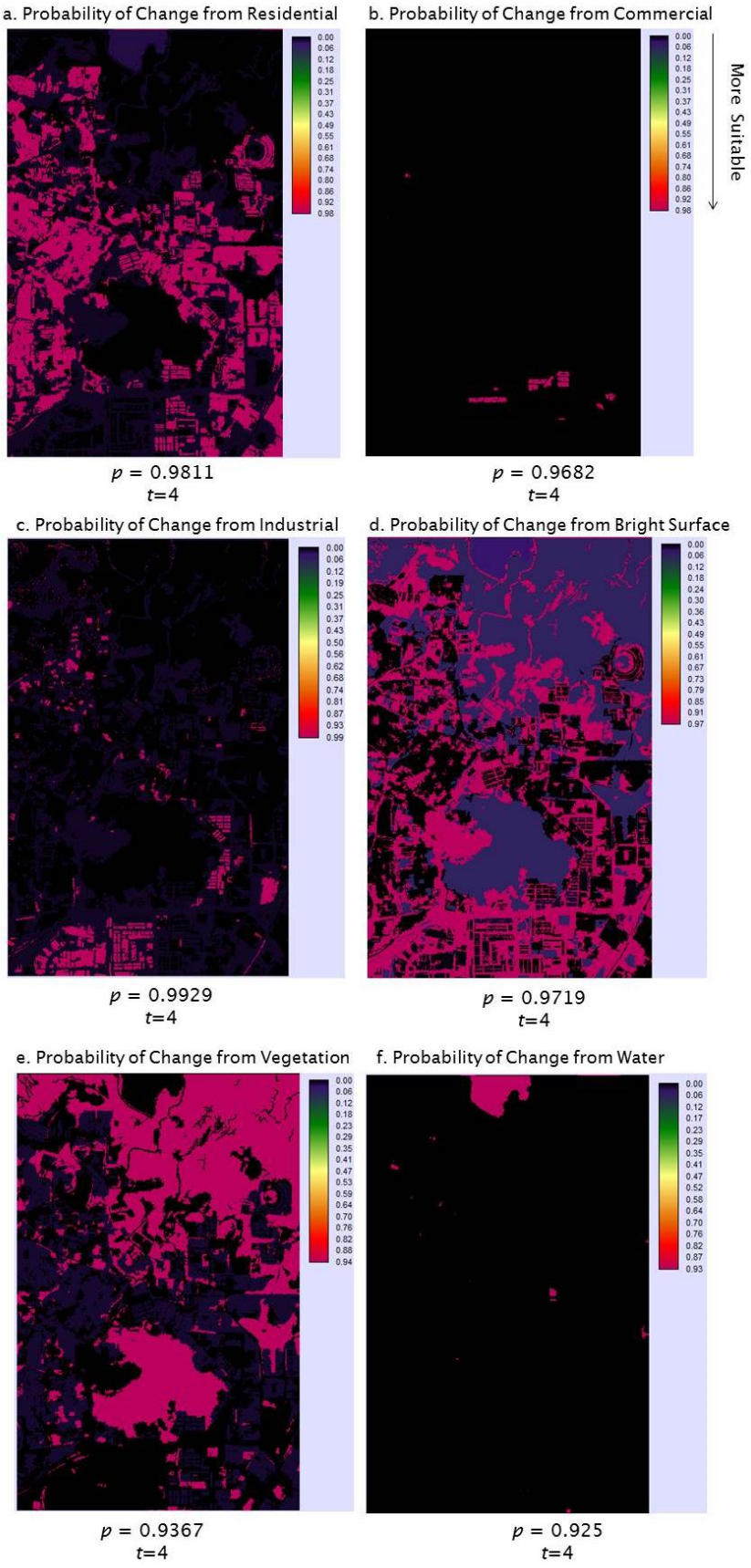


Figure 8.5 Suitability maps derived from the probability of changes in the six LULC classes.

### 8.4.2 Varying the probability matrix

In any LULC classification, one expects there to be some level of error in the predicted map. Although the LULC maps used here for 2005 and 2009 were produced using object-based image analysis for which the accuracies are known to be generally higher than for pixel-based approaches, and although the accuracies assessed in this thesis were high, some error will inevitably remain. Moreover, the prediction task taken on in earlier chapters was challenging in that it included separation of bright surfaces into residential, commercial and industrial, such that error will inevitably occur amongst these classes. When such LULC maps are used in change analysis this error can lead to false positives (i.e., changes) which are erroneous (and also to false negatives). This error in the change analysis will manifest itself in the confusion matrix or contingency table as a set of off-diagonal probabilities that are greater than zero. Thus, it was of interest to explore the effect of these off-diagonal elements on the CA result.

To explore the effect of the error in the transition probability matrix on the CA result, an adjusted probability matrix was produced by effectively cleaning up the matrix so that the off-diagonal elements were forced to zero in cases where the change was unexpected (i.e., where the change was most likely due to error) (Table 8.4). Note that this does not mean that the removed off-diagonal elements are actually error – the exercise is more about exploring the effect of these elements to determine whether the CA analysis is robust. Specifically, the changes made were; reducing the changes amongst RCI (class 1 to class 3) to zero within the first transition (to increase the accuracy of the result of the 2005-2009 transition). While possible, it is most likely (based on common sense) that a change from residential to industrial, for example, is an error. However, the probabilities for the other classes (bright surface, vegetation and water) were kept the same as for the previous result of the probability matrix, as shown in Table 8.2. This adjusted probability matrix amounts to fixing the model of change within the 4-year period for subsequent use in the forecast.

Table 8.4 Adjusted probability matrix within the 4-year change period

| | | | | | | |
|---|---|---|---|---|---|---|
| Residential | **1** | 0 | 0 | 0 | 0 | 0 |
| Commercial | 0 | **1** | 0 | 0 | 0 | 0 |
| Industrial | 0 | 0 | **1** | 0 | 0 | 0 |
| Bright Surface | 0.0131 | 0 | 0.0115 | **0.9754** | 0 | 0 |
| Vegetation | 0 | 0 | 0 | 0.0611 | **0.9389** | 0 |
| Water | 0.0268 | 0 | 0.0027 | 0.0377 | 0 | **0.9328** |

*By doing this, Edit (IDRISI menu) provides an ASCII text editor of the transition area text (area.txt) for creating new adjusted probability matrix.*

To explore its effect, this new adjusted probability matrix was used with the three CA-windows of 3 by 3 cells, 5 by 5 cells and 7 by 7 cells.

### 8.4.3 Varying the CA window

The nature of this operation is determined by the values stored in each 3 by 3, 5 by 5, 7 by 7 cells, or variable-sized kernel, that is centred over each pixel as it is processed. The pixel and its neighbours are multiplied by the values stored in the corresponding positions of the kernel, and the resulting values are summed to arrive at a new value for the pixel. Gaussian filters are used (default algorithm in IDRISI) to generalise an image for simulation modelling. When this occurs, only the values where the kernel overlaps the image cells are used in the calculation. The output cell values are adjusted for the proportion of the kernel used in Figure 8.5. These three alternatives CA-windows are shown in Figure 8.6. The objective is to explore the effect of these windows such as to choose the most suitable window for the simulation process to accommodate the amount of change within the period of interest.

**(a) 3 x 3**

| | | |
|---|---|---|
| 0.005 | 0.02 | 0.005 |
| 0.02 | **0.88** | 0.02 |
| 0.005 | 0.02 | 0.005 |

**(b) 5 x 5**

| | | | | |
|---|---|---|---|---|
| 0.008 | 0.017 | 0.02 | 0.017 | 0.008 |
| 0.017 | 0.06 | 0.09 | 0.06 | 0.017 |
| 0.02 | 0.09 | **0.14** | 0.09 | 0.02 |
| 0.017 | 0.06 | 0.09 | 0.06 | 0.017 |
| 0.008 | 0.017 | 0.02 | 0.017 | 0.008 |

**(c) 7 x 7**

| | | | | | | |
|---|---|---|---|---|---|---|
| 0 | 0.005 | 0.01 | 0.01 | 0.01 | 0.005 | 0 |
| 0.005 | 0.01 | 0.02 | 0.03 | 0.02 | 0.01 | 0.005 |
| 0.01 | 0.02 | 0.04 | 0.06 | 0.04 | 0.02 | 0.01 |
| 0.01 | 0.03 | 0.06 | **0.07** | 0.06 | 0.03 | 0.01 |
| 0.01 | 0.02 | 0.04 | 0.06 | 0.04 | 0.02 | 0.01 |
| 0.005 | 0.01 | 0.02 | 0.03 | 0.02 | 0.01 | 0.005 |
| 0 | 0.005 | 0.01 | 0.01 | 0.01 | 0.005 | 0 |

Figure 8.6 CA window by Gaussian Filter; 3 by 3, 5 by 5 and 7 by 7 cells.

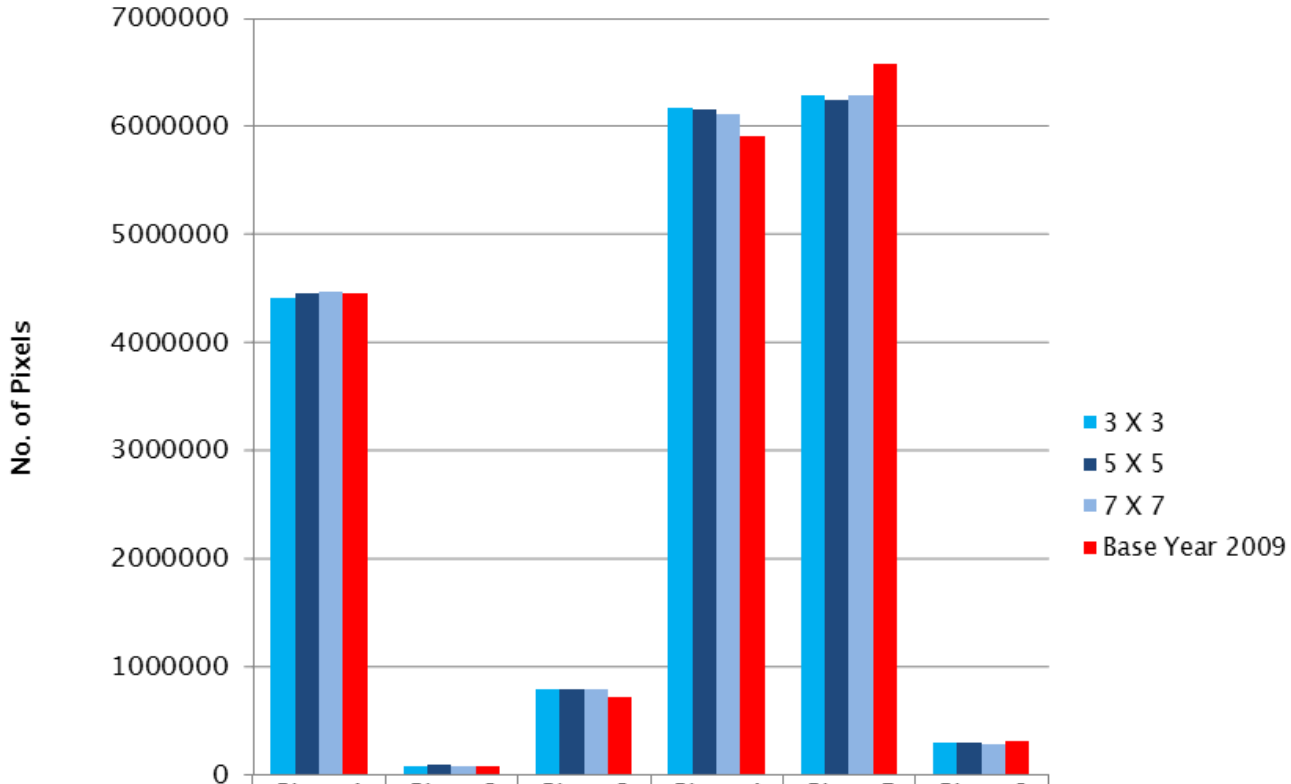


| | Class 1 | Class 2 | Class 3 | Class 4 | Class 5 | Class 6 |
|---|---|---|---|---|---|---|
| 3 X 3 | 4413383 | 78753 | 791784 | 6162320 | 6282715 | 291045 |
| 5 X 5 | 4457884 | 87140 | 791539 | 6158956 | 6234003 | 290478 |
| 7 X 7 | 4462533 | 78749 | 792192 | 6112968 | 6286533 | 287025 |
| Base Year 2009 | 4447033 | 80269 | 716817 | 5897578 | 6573068 | 305235 |

Figure 8.7 The result of forecasting LULC in 2013 based on probability of change to others classes (class 1 – residential, class 2 – commercial, class 3 – industrial, class 4 – bright surface, class 5 – vegetation, class 6 – water) within 3 by 3, 5 by 5 and 7 by 7 cell CA-windows.

Figure 8.7 shows a comparison of the three CA-windows applied to the base LULC map of 2009. It provides summaries of analytical results for the first four year projections to 2013 showing variation in the rate of change when changing the size of CA-window. From the three alternatives, the central cell's neighbourhood 5 by 5 CA-window gradually increased the pixel value (the analysis results can be accepted) for each class (RCI) from the base year to the 2013 of the forecast. This is due to fact that the CA-window of 5 by 5 cells which is also a model of neighbourhood influence will tend to predict growth to cells which are nearby to existing urban cells. However, there is no evidence here that it is the best. The

choice of window makes a small difference to the outcome and so the important outcome is that the CA model is fairly robust to the choice of window size. To say that one is better than the other would require validation data, which is generally impossible to acquire for forecasts and in the present case (2013) was beyond the scope of this thesis. Moreover, the forecasts continue for the years 2017 and 2021 for which validation is not currently possible.

Figure 8.8 shows the simulation results for 2013, 2017 and 2021 based on the model of four years' change in LULC between 2005 and 2009. Expansion of the RCI class is based on two assumptions: (i) through the in-filling of pixels (areas) within the current distribution of existing bright surface pixels, and (ii) through expansion and growth, based on a CA 5 by 5 cells neighbourhood, from existing areas. Both assumptions produce a characteristic new outline for a future model of urban growth and change simulation. The simulation shows that forecasting based on the CA with a 5 by 5 cell neighbourhood assumes that if a built land (RCI) class is found within the neighbourhood of a bright surface pixel, then the central cell has a non-zero probability of being classified as the built land class. The transition probability value for the central cell of the neighbourhood is:

$$p\left(x_{o_t}=Built\ Land \mid x_{o_{t-1}}=BS \ \ and\ x_j=Built\ Land\right)=probability\ value_{class}.$$

The number of cells that changed from bright surface to built land (RCI) was based on the transition probability values of 0.0245 (0.0131 (R) or 0.0115 (I)). Some of these changes in land use as indicated in the land use maps appear as a mismatch in reality. However, after the adjusted transitions of bright surface and vegetation to RCI to forest over a period of 4 years, the result seems reasonable (Table 8.5). Based on the simulation results (Figure 8.8 and Table 8.5), change simulations of bright surface are increased from 32.73% in 2009 to 34.18 in 2013, 35.51% in 2017 and to 36.71% in 2021 (less than 2% increases in each period). This could be caused by a smaller percentage in vegetation area due to allowable development in the bright surface (bare land) class. RCI land use increased between 2013 to 2021 with proportionate values in the study area. The majority of the increases in the area of RCI land use were in the growth areas around existing large areas of those classes.

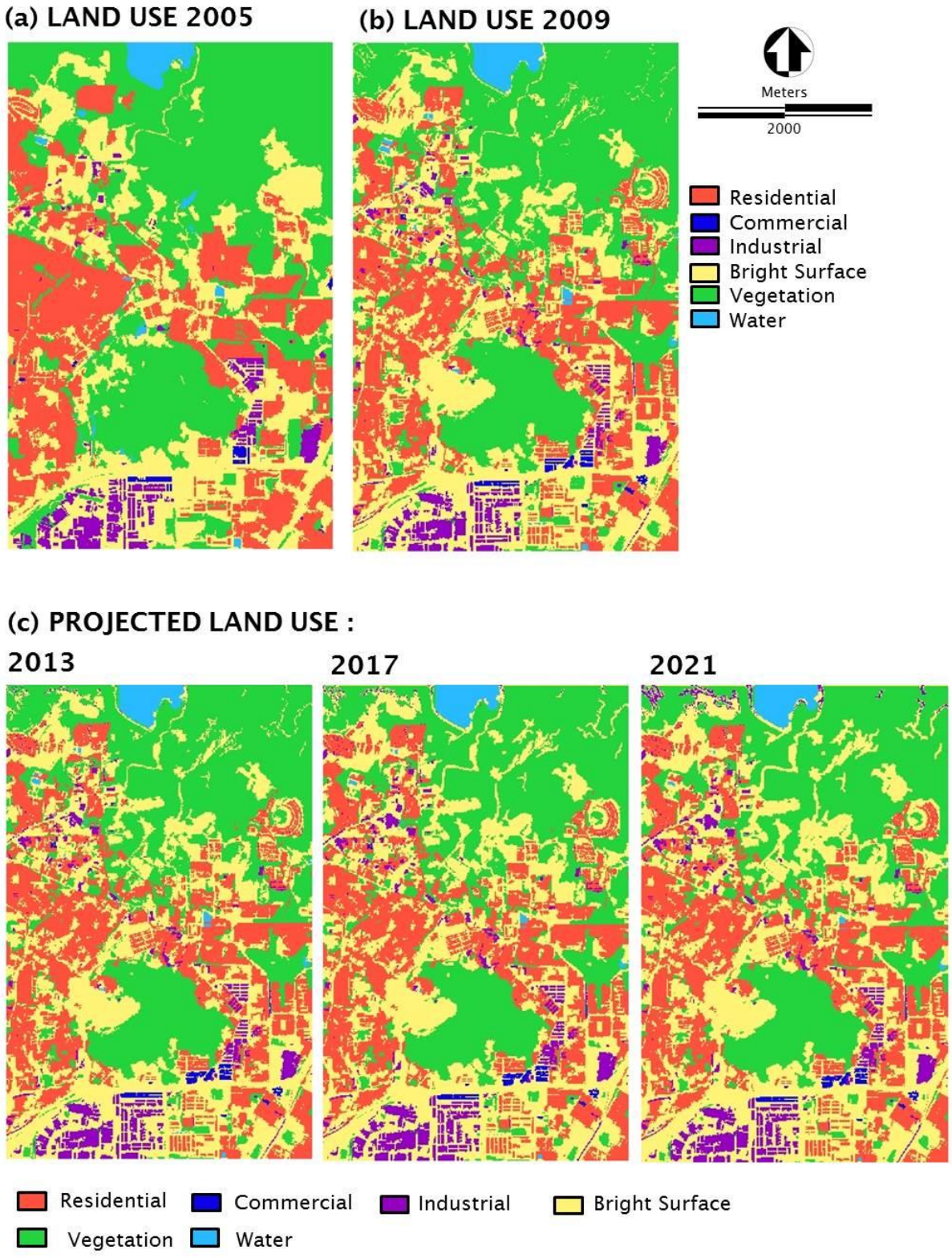


Figure 8.8 LULC forecasted as a result of CA simulation: (a) LULC map of 2005, (b) LULC map of 2009, (c) Forecasting LULC in 2013 to 2021 based on the probability of change.

The simulated LULC in 2013, 2017 and 2021 was compared quantitatively with the reference LULC map of 2005 and 2009, and the number of cells in every class that changed, either increased or decreased, was counted. Comparison results are shown in Figure 8.9 with detailed statistical values displayed in Table 8.5.

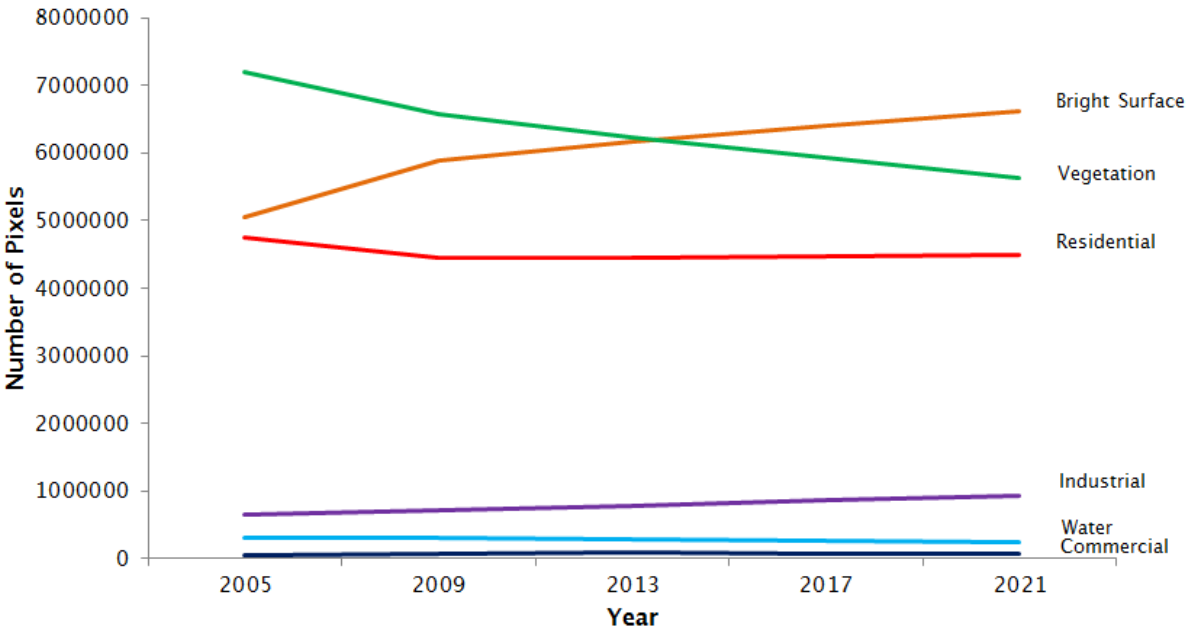


Figure 8.9 Comparison of simulation results for 2013, 2017 and 2021 with actual spatial pattern changes of LULC types in 2005 and 2009.

The overall results in Table 8.5 show a predominant increase in built-up areas (RCI) and bright surface from 2013 to 2021 and a commensurate decrease in area of vegetation. Interestingly, the bright surfaces class, which in many cases might reflect an intermediate stage of development between vegetation and built land, increases in area through time. The study area is a high potential for development, and the bright surface area or cleared land is demanded for the development.

Table 8.5 Object-based LULC forecasted based on the CA model until year 2021.

| LULC | 2005 | | 2009 | | 2013 | | 2017 | | 2021 | |
|---|---|---|---|---|---|---|---|---|---|---|
| | No. of Pixels | % of total area | No. of Pixels | % of total area | No. of Pixels | % of total area | No. of Pixels | % of total area | No. of Pixels | % of total area |
| Residential | 4759995 | 26.42 | 4447033 | 24.68 | 4457884 | 24.74 | 4470983 | 24.81 | 4562011 | 25.53 |
| Commercial | 61533 | 0.34 | 80269 | 0.45 | 87140 | 0.48 | 85595 | 0.48 | 85595 | 0.50 |
| Industrial | 644995 | 3.58 | 716817 | 3.98 | 791539 | 4.39 | 864216 | 4.80 | 937696 | 5.20 |
| Bright Surface | 5052880 | 28.04 | 5897578 | 32.73 | 6158956 | 34.18 | 6399652 | 35.51 | 6614664 | 36.70 |
| Vegetation | 7193448 | 39.92 | 6573068 | 36.48 | 6234003 | 34.59 | 5928597 | 32.90 | 556653 | 30.90 |
| Water | 307149 | 1.70 | 305235 | 1.69 | 290478 | 1.61 | 270957 | 1.50 | 253481 | 1.40 |
| **Total** | **18020000** | **100.00** | **18020000** | **100.00** | **18020000** | **100.00** | **18020000** | **100.00** | **18020000** | **100.00** |

### 8.4.4 Validation and Forecast Comparison

- **Comparing between OB LULC 2009 (OB 2009) with Projected CA 2009 (PCA2009)**

This comparison therefore acts as a validation based on observed data in 2009 of the CA forecast of LULC in 2009 which itself is based on LULC data from 2005.

**i) OB LULC 2009 (OB 2009)**

The OB 2009 data were discussed in Chapter 5 in which the analysis indicated a classification accuracy of 78.0% for object-based classification. The purpose of these data is to create a forecasting model in anticipation of changes in land use in the years following.

**ii) Projected CA 2009 (PCA2009)**

The simulation iteration based on four years' forecasting started from the base year in 2005 with an accuracy of 79.3% for object-based classification. Within each time step, each LULC map was considered in turn as belonging to one of the main categories: residential, commercial, industrial, bright surface, vegetation and water. These values changed within the model time-period based on neighbourhood cell pixels. The transition rules used a 5 by 5 CA-window neighbourhood to forecast LULC type in the future based on the states of the cells in the filter. The number of iterations chosen determined the number of time steps used in the simulation.

Table 8.6 Comparison of 2009 Land Use Plan and 2009 forecast

| LULC | OB LULC 2009 (OB 2009) | | Projected CA 2009 (PCA2009) | | Difference Proportion |
|---|---|---|---|---|---|
| | area (Ha) | % | area (Ha) | % | (%) |
| Residential | 444.47 | 24.67 | 476.47 | 26.44 | +1.77% |
| Commercial | 8.03 | 0.45 | 7.53 | 0.42 | -0.03% |
| Industrial | 71.70 | 3.98 | 72.03 | 4.00 | -0.02% |
| Bright Surface | 589.76 | 32.73 | 531.33 | 29.49 | +3.24% |
| Vegetation | 657.30 | 36.48 | 684.15 | 37.97 | +1.49% |
| Water | 30.52 | 1.69 | 30.46 | 1.69 | - |
| **Total** | 1802 | 100.00 | 1802 | 100.00 | |

Table 8.6 shows that the difference between the forecasted proportions (CA2009) and the planned proportions (LULC2009) in each LULC class are as follows; residential is +1.77%, commercial is -0.03%, industrial is -0.02%, bright surface is +3.24%%, vegetation is +1.49% and water is no change. Thus, small percentage differences in comparison to the observed data are shown, although the result of PCA2009 is based on data from 2005. Both results are shown in Figure 8.10.

Figure 8.11 and Table 8.7 represent the image differences between OB2009 and PCA2009. The overall accuracy of comparing both datasets is 73.29% indicating a strong agreement, considering all classes.

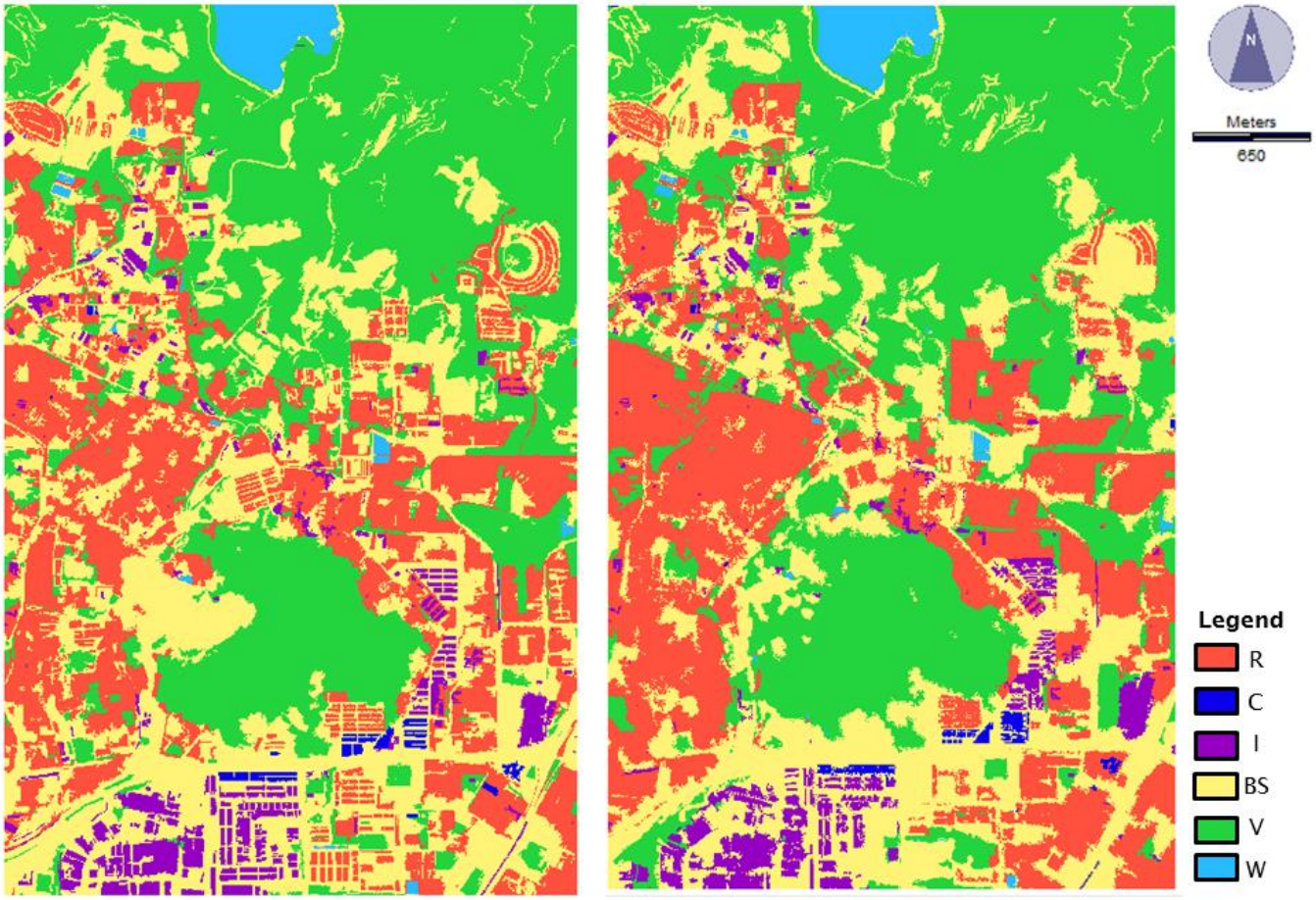


Figure 8.10 Comparison between OB LULC 2009 (OB 2009) with Projected CA 2009 (PCA2009).

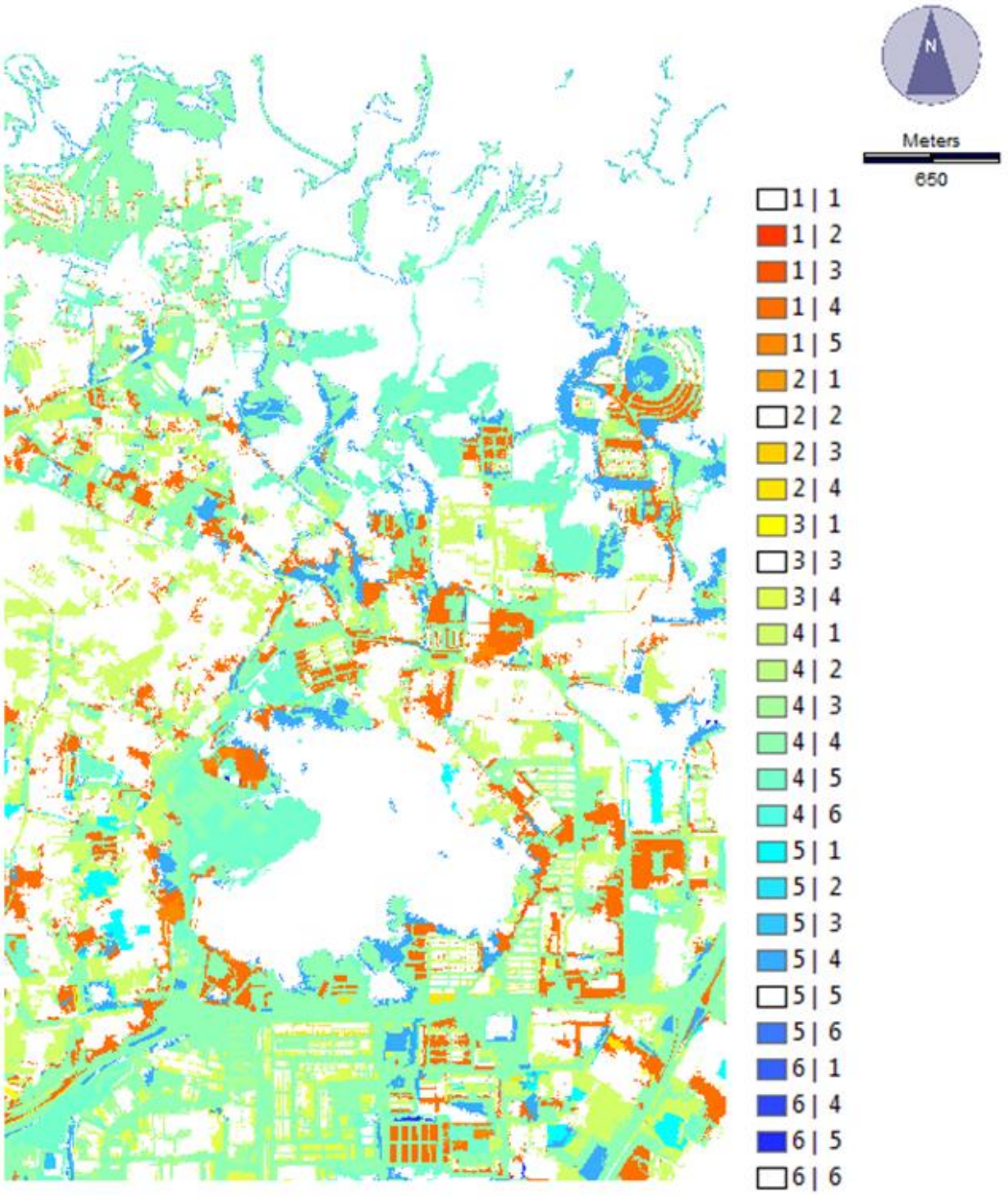


Note: Class (1) Residential, (2) Commercial, (3) Industrial, (4) Bright Surface, (5) Vegetation, (6) Water.

Figure 8.11 Difference image between OB LULC 2009 (OB2009) and Projected CA 2009 (PCA2009).

Table 8.7 Cross-tabulation of OB LULC 2009 (OB2009) land use (columns) against Projected CA 2009 (PCA2009) land use (rows) by number of pixels.

| | | OB2009 land use | | | | | | | |
|---|---|---|---|---|---|---|---|---|---|
| | | **(1) Residential** | **(2) Commercial** | **(3) Industrial** | **(4) Bright Surface (BS)** | **(5) Vegetation** | **(6) Water** | **PCA2009 Total** | **User's Accuracy (%)** |
| Projected CA 2009 land use | **(1)Residential** | 3301566 | 367 | 3029 | 1336277 | 123191 | 365 | 4764795 | **69.29** |
| | **(2)Commercial** | 6 | 55727 | 0 | 19539 | 49 | 0 | 75321 | **73.99** |
| | **(3)Industrial** | 3137 | 60 | 507974 | 203067 | 6091 | 0 | 720329 | **70.52** |
| | **(4)BS** | 1030494 | 24115 | 205814 | 3324997 | 723535 | 4393 | 5313348 | **62.58** |
| | **(5)Vegetation** | 111830 | 0 | 0 | 1008964 | 5718216 | 2516 | 6841526 | **83.58** |
| | **(6)Water** | 0 | 0 | 0 | 4734 | 1986 | 297961 | 304681 | **97.79** |
| | **OB2009 Total** | 4447033 | 80269 | 716817 | 5897578 | 6573068 | 305235 | 18020000 | |
| **Producer's Accuracy (%)** | | **74.24** | **69.43** | **70.87** | **56.38** | **89.99** | **97.62** | | |
| **Overall Accuracy = 73.29%** | | | | | | | | | |

- **Comparing between LULC 2013 (formal Land Use Plan 2013) with Projected CA 2013 (PCA2013)**

### i) LULC 2013 (Formal Land Use Plan 2013)

The LULC in the study area was divided into 13 categories which were aggregated to six classes for the purposes of this research. As a reminder, the six categories are residential, commercial, industrial, bright surface, vegetation and water. In this case, the area of bright surfaces in the Plan is expected to be larger than in the LULC maps of this thesis because the Plan includes areas of infrastructure and utilities, and also buildings of institutions and public amenities. The raster data were georeferenced with the same map projection of the Universal Transverse Mercator (Hemisphere: N, Zone Number: 47 with datum WGS 84).

### ii) Projected CA 2013 (PCA2013)

The CA simulation based on four years' forecasting started from the base year in 2009. The transition rules used a 5 by 5 CA-window neighbourhood to forecast LULC type in the future based on the states of the cells in the filter. These values changed within the modelling period based on the neighbourhood cell pixels. The number of iterations chosen established the number of time steps used in the simulation. The resulting map allocated all pixels to one of the main LULC categories: residential, commercial, industrial, bright surface, vegetation and water.

Table 8.8 Comparison of 2013 Land Use Plan and 2013 forecast

| LULC | LULC 2013 (Current Land Use) | | Projected CA 2013 (PCA2013) | | Difference Proportion |
|---|---|---|---|---|---|
| | area (Ha) | % | area (Ha) | % | (%) |
| Residential | 415.08 | 23.03 | 445.79 | 24.74 | +1.71% |
| Commercial | 34.59 | 1.92 | 8.71 | 0.48 | -1.44% |
| Industrial | 141.43 | 7.85 | 79.15 | 4.39 | -3.46% |
| Bright Surface | 530.34 | 29.43 | 615.9 | 34.18 | +4.75% |
| Vegetation | 644.13 | 35.75 | 623.4 | 34.59 | -1.16% |
| Water | 36.42 | 2.02 | 29.05 | 1.61 | -0.41% |
| **Total** | 1802 | 100 | 1802 | 100 | |

Table 8.8 shows that the difference between the forecasted proportions (CA2013) and the planned proportions (LULC2013) in each LULC class are as follows; residential is +1.71%, commercial is -1.44%, industrial is -3.46%, bright surface is +4.75%%, vegetation is -1.16% and water is -0.41%.

Industrial area needs to be treated with caution because it is under-predicted compared to the current land use (2013). Bright surface class is over-predicted by 4.75% (relating to misclassification in the OB classification process applied to data in 2009 leading to OB2009). Both results are shown in Figure 8.12.

Figure 8.13 and Table 8.9 represent the image differences between LULC2013 and PCA2013. The overall accuracy of comparing both datasets is 52.07% indicating only a fair agreement after considering all classes. This is because there are clearly there are pixel-level errors in both datasets which it was not possible here to correct. However, the changes in each are more comparable illustrating the significant activities on the ground and the plan approved by planning agencies.

.

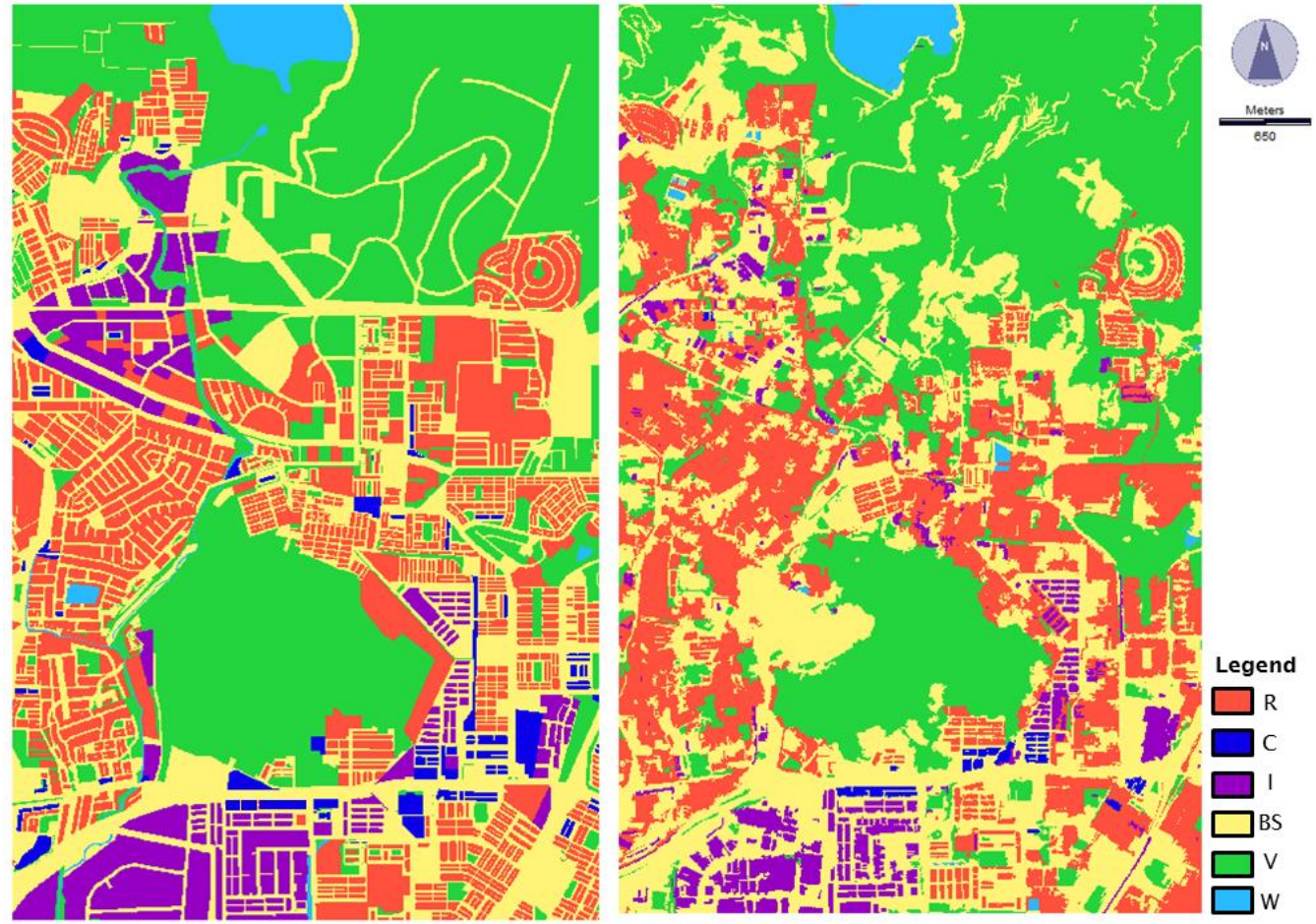


Figure 8.12 Comparing between LULC 2013 (formal land use plan 2013) with Projected CA 2013 (PCA2013).

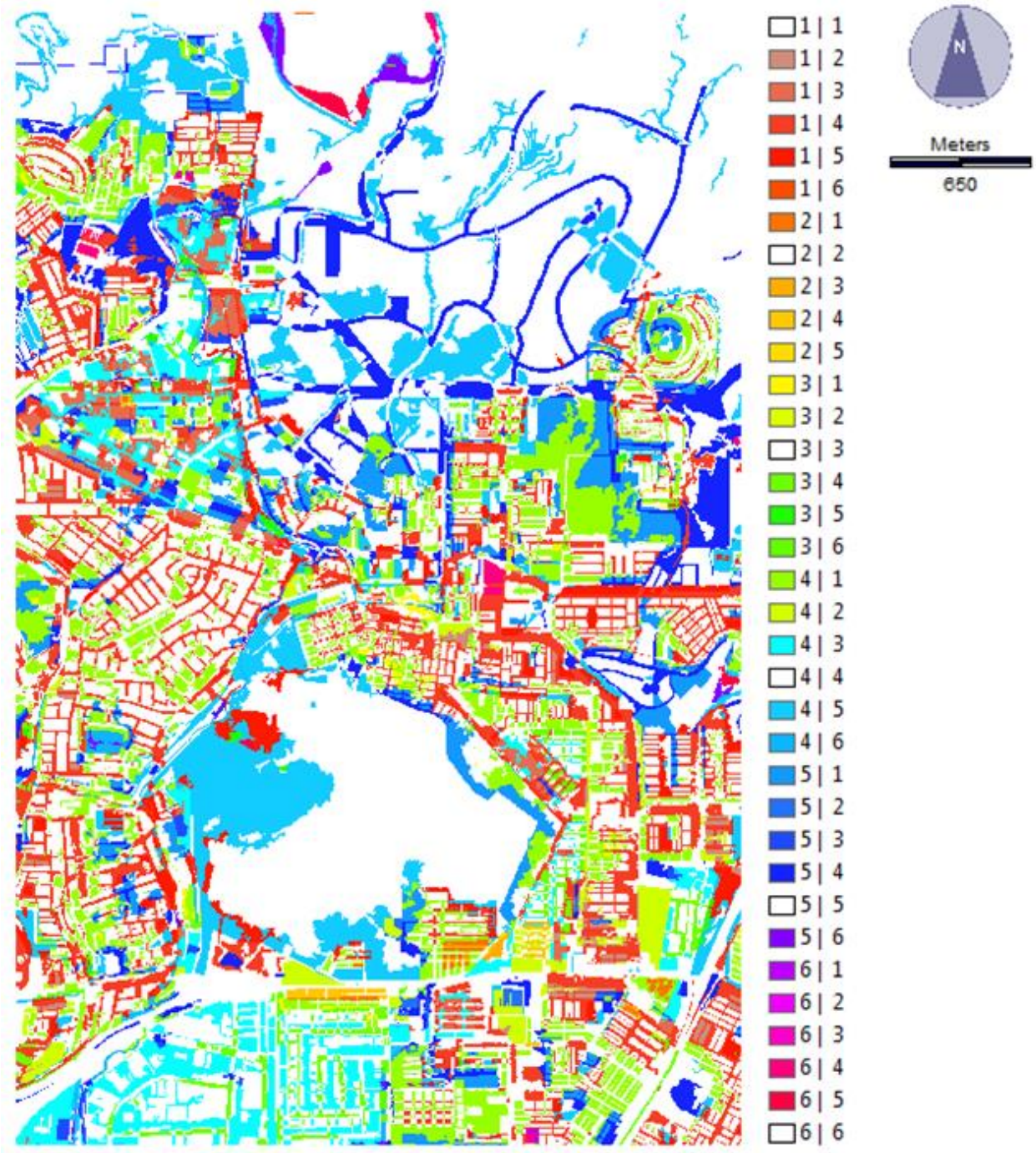


Note: Class (1) Residential, (2) Commercial, (3) Industrial, (4) Bright Surface, (5) Vegetation, (6) Water.

Figure 8.13 Difference image between the formal land use plan in 2013 (LULC2013) and Projected CA 2013 (PCA2013).

Table 8.9 Cross-tabulation of Projected CA 2013 (PCA2013) land use (columns) against LULC 2013 (formal land use plan 2013) land use (rows) by number of pixels.

| | | Projected CA 2013 land use | | | | | | | |
|---|---|---|---|---|---|---|---|---|---|
| | | **(1)** | **(2)** | **(3)** | **(4)** | **(5)** | **(6)** | | **User's** |
| | | **Residential** | **Commercial** | **Industrial** | **Bright Surface (BS)** | **Vegetation** | **Water** | **LULC2013 Total** | **Accuracy (%)** |
| LULC 2013 | **(1)Residential** | 1990634 | 25296 | 59973 | 1453158 | 618492 | 3284 | 4150837 | **47.96** |
| | **(2)Commercial** | 90818 | 5550 | 12196 | 212213 | 25013 | 140 | 345930 | **1.60** |
| | **(3)Industrial** | 209855 | 8064 | 426807 | 682817 | 85964 | 823 | 1414330 | **30.18** |
| | **(4)BS** | 1739028 | 39062 | 248668 | 2242262 | 1005209 | 29171 | 5303400 | **42.28** |
| | **(5)Vegetation** | 416693 | 781 | 35891 | 1463181 | 4494120 | 30618 | 6441284 | **69.77** |
| | **(6)Water** | 15505 | 0 | 8654 | 59335 | 57738 | 222987 | 364219 | **61.22** |
| | **PCA2013 Total** | 4462533 | 78753 | 792189 | 6112966 | 6286536 | 287023 | 18020000 | |
| **Producer's Accuracy (%)** | | **44.61** | **7.05** | **53.88** | **36.68** | **71.49** | **77.69** | | |
| **Overall Accuracy = 52.07%** | | | | | | | | | |

- **Comparing the Proposed 2020 Land Use (P2020) and Projected CA 2021 (PCA2021)**

**i) Proposed 2020 Land use (P2020) by Selayang City Council Local Plan**

It is simply not possible to validate a future forecast of land use, except in the sense of a hindcast which involves forecasting a previous time from an even earlier time such that comparison with reality becomes possible. However, it is of interest here to compare the forecasted LULC change maps against the formal Land Use Plan of the Selayang City Council for 2020 (P2020). This is made possible because the thesis author is an employee of the Council Planning Department and, thus, was able to gain access to the Plan, presenting an unusual opportunity for such a comparison. The function of the land use plan for 2020 for the study area is in navigating and controlling development, as well as to identify areas that have been zoned for future development that are committed. These needs are translated into a spatial form or a land use activity and reflected in land use plans, policies and development actions. Land use planning, therefore, derives from the need to satisfy these needs on the ground, in a rational manner and within a technical framework.

Original data are in the form of a vector cadastral GIS land use map (polygon coverage) which was converted to a raster format with a pixel cell size of 1 m. The land-use in the study area is divided into 13 categories which were aggregated to the six classes of this thesis for the purposes of this research. As a reminder, the six categories are residential, commercial, industrial, bright surface, vegetation and water. In this case, the area of bright surfaces is expected to be larger than in the LULC maps of this thesis because the Plan includes areas of infrastructure and utilities, and also buildings of institutions and public amenities. The raster data were georeferenced with the same map projection of the Universal Transverse Mercator (Hemisphere: N, Zone Number: 47 with datum WGS 84).

**ii) Projected CA 2021 (PCA2021)**

The simulation iteration based on four years' forecasting started from the base year in 2009. Within each time step, each LULC map was considered in turn as belonging to one of the main categories: residential, commercial, industrial,

bright surface, vegetation and water used a 5 by 5 CA-window neighbourhood to forecast LULC type in the future based on the states of its cells in the filter.

Table 8.10 Comparison of 2020 Plan and 2021 forecast

| LULC | Proposed 2020 (Local Plan Land Use) | | Projected 2021 (CA) | | Difference Proportion |
|---|---|---|---|---|---|
| | area (Ha) | % | area (Ha) | % | (%) |
| Residential | 366.201 | 20.32 | 456.20 | 25.30 | +4.98% |
| Commercial | 33.37 | 1.85 | 8.56 | 0.50 | -1.35% |
| Industrial | 149.30 | 8.29 | 93.77 | 5.20 | -3.09% |
| Bright Surface | 671.36 | 37.26 | 661.47 | 36.70 | -0.56% |
| Vegetation | 542.43 | 30.10 | 556.67 | 30.90 | +0.80% |
| Water | 39.35 | 2.18 | 25.34 | 1.40 | -0.78% |
| **Total** | **1802.00** | **100.00** | **1802.00** | **100.00** | |

The result of the CA model (PCA2021) was compared against the 2020 Selayang City Council Local Plan (P2020) as shown in Figure 8.14. It should be remembered that there is a one year difference between the forecast and the Plan, but this is expected to have a relatively minor effect relative to the changes observed from 2009 to 2020/2021.

Table 8.10 shows that the difference between the forecasted proportions and the planned proportions in each LULC class are as follows; residential is +4.98%, commercial is -1.35%, industrial is -3.09%, bright surface is -0.56%, vegetation is +0.80% and water is -0.78%. In object-based classification, the IKONOS imagery in 2005 shows village buildings and small objects segmented together, falling into the same category and classified as bright surface. The residential class including the planned and unplanned housing area and bright surfaces. These both produced misclassification even though a large supervised sample was developed for each type of land use class. This problem can arise when the residential areas are mixed with bright surfaces and roofs which are not clearly identified and the classification result is then based on neighbouring pixels or surrounding land use. Residential area was over-predicted by 4.98% (because the existing residential proportion is 26.42% in

2005 and 24.68% in year 2009, representing potentially over-prediction of the residential area for the reasons given above relating to misclassification in the OB classification process.

Through the CA process, the growth cells are applied sequentially, one cell at a time, and the entire neighbouring area is updated after annual iterations to form the basis for growth in the four-year period. In addition, the increase in the residential proportion projected in year 2021 is likely to occur as a function of the percentage of land available for development.

The CA projection also reduced the industrial area which is lower by -3.09% compared to the Plan for 2020. It should be remembered that neither dataset is being used here as the truth. Rather, it is of interest to compare them since one represents a projection forwards in time of historical patterns (and a model for doing so) and the other represents an organisational attempt to plan. From the real data P2020 in Figure 8.14 (upper-west side), it can be seen that the growth in the industrial area is outside the designated growth areas (development areas) and it is close to water features (dam-clear water). However, in the OB classification-based forecast (PCA2021) the industrial class is not detected in that specific area. The purpose of included the Plan for 2009 or similar, and analyse the changes in the Plan alongside the changes in the CA forecast. That is changes from 2009 to 2020/21 in both the Plan and the CA. This is because there are clearly differences between the two which are cannot correct for. But the changes in each may be more comparable. Image comparison is still valid in this case to show the significant activities on the ground and the plan approved by planning agencies.

The following Table 8.11 and Figure 8.15 represent the image differences between P2020 and CA2021. The overall accuracy is 52.04% indicating a fair agreement after considering all classes. This is because there are clearly differences between the two which are cannot correct for. But the changes in each may be more comparable to show the significant activities on the ground and the plan approved by planning agencies.

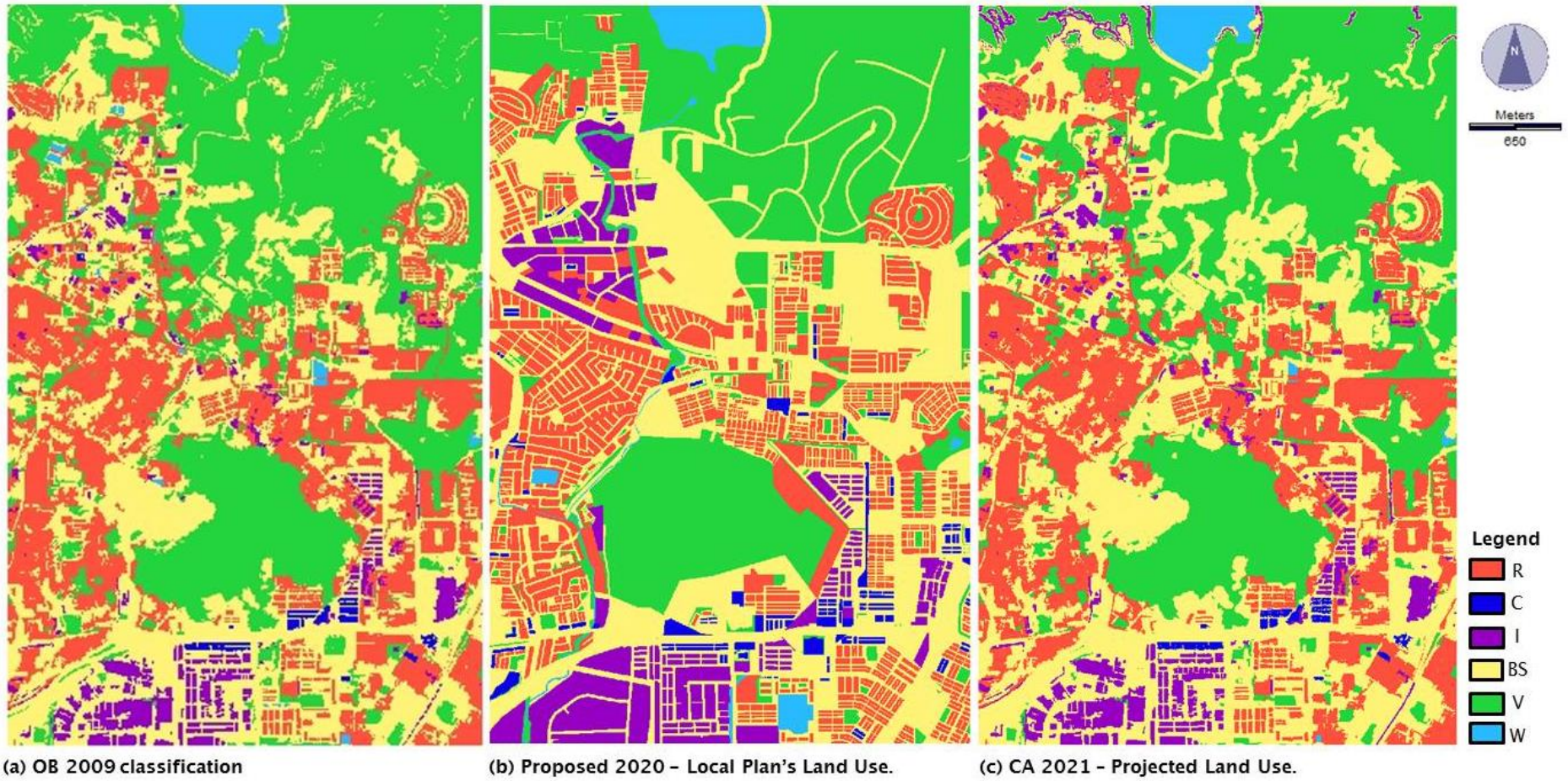


Figure 8.14 Comparing results between (a) Plan 2009 (OB classification), (b)Proposed 2020 land use, and (c) Projected CA 2021 land use.

Table 8.11 Cross-tabulation of Proposed 2020 (P2020) land use (columns) against Projected CA 2021 (PCA2021) land use (rows) by number of pixels.

| | | Proposed 2020 land use | | | | | | | |
|---|---|---|---|---|---|---|---|---|---|
| | | **(1)** | **(2)** | **(3)** | **(4)** | **(5)** | **(6)** | | **User's** |
| | | **Residential** | **Commercial** | **Industrial** | **Bright Surface (BS)** | **Vegetation** | **Water** | **PCA2021 Total** | **Accuracy (%)** |
| Projected CA 2021 land use | **(1)Residential** | 2016654 | 102489 | 228583 | 1896848 | 280533 | 36904 | 4562011 | 44.21 |
| | **(2)Commercial** | 5000 | 31112 | 9815 | 39623 | 45 | 0 | 85595 | 36.35 |
| | **(3)Industrial** | 70296 | 14569 | 449765 | 276218 | 109211 | 17637 | 937696 | 47.96 |
| | **(4)BS** | 1175451 | 168856 | 751496 | 3052639 | 1368330 | 97892 | 6614664 | 46.15 |
| | **(5)Vegetation** | 387141 | 16667 | 53284 | 1434342 | 3630329 | 44790 | 5566553 | 65.22 |
| | **(6)Water** | 7470 | 0 | 13 | 13929 | 35823 | 196246 | 253481 | 77.42 |
| | **P2020 Total** | 3662012 | 333693 | 1492956 | 6713599 | 5424271 | 393469 | 18020000 | |
| **Producer's Accuracy (%)** | | 55.07 | 9.32 | 30.13 | 45.47 | 66.93 | 49.88 | | |
| **Overall Accuracy = 52.04%** | | | | | | | | | |

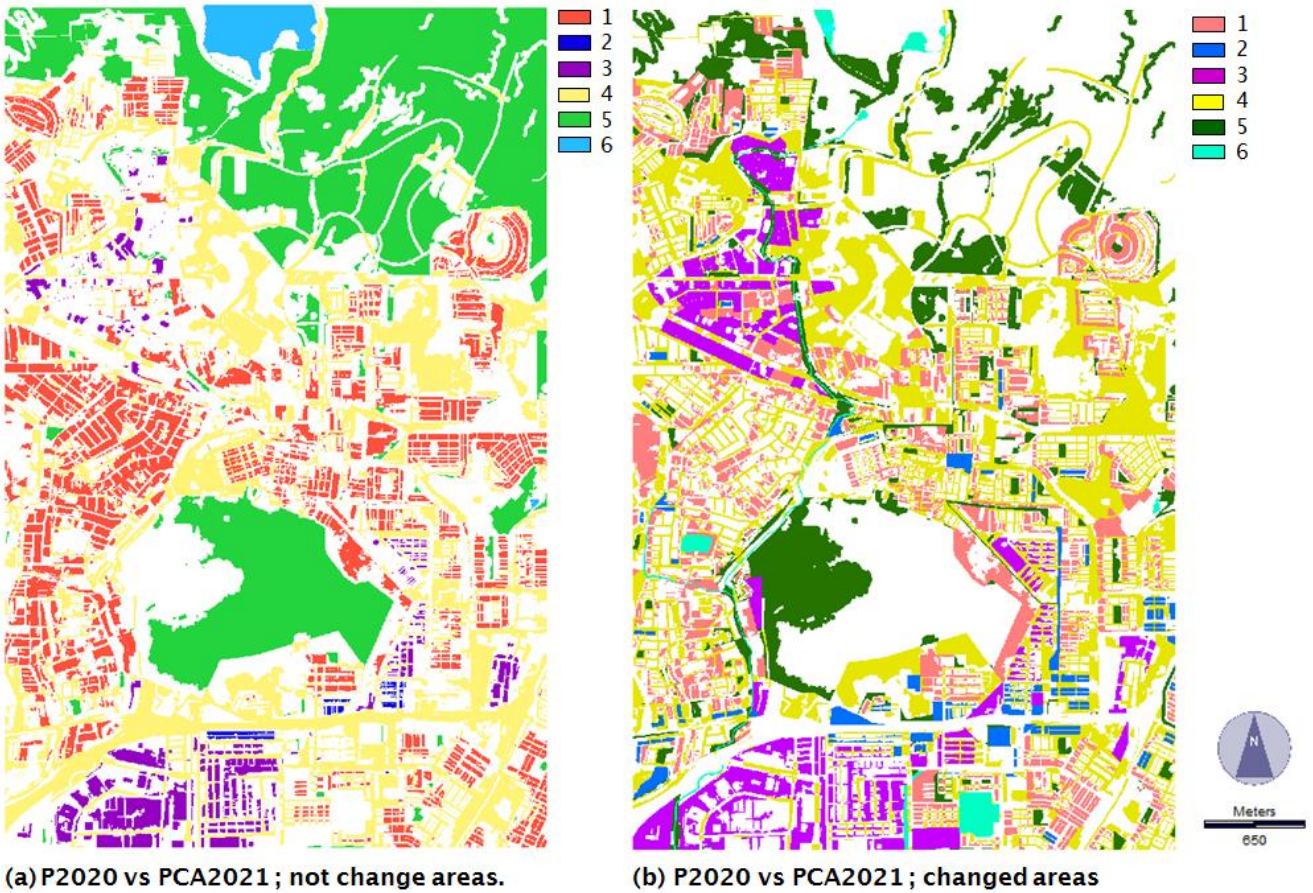


(a) P2020 vs PCA2021 ; not change areas. (b) P2020 vs PCA2021 ; changed areas

**(1) Residential (2) Commercial (3) Industrial (4) Bright Surface (5) Vegetation (6) Water**

Figure 8.15 Image differencing between Proposed 2020 (P2020) land use and Projected CA 2021 (PCA2021) land use; (a) not change areas, (b) changed areas.

- **Comparing between OB LULC 2009 (OB 2009) with Projected CA 2021 (PCA2021) and Proposed 2020 Land Use (P2020)**

It was of interest to compare the P2020 Plan with both the PCA2021 with the OB 2009 land use map to test whether the forecast is closer than the historical LULC distribution.

### i) Difference OB 2009 vs PCA2021

Initially, the 2009 LULC map was compared to the forecast in 2021 which was based on applying the CA-Markov model to the 2009 data. This represents an attempt to determine the effect of the model. The result of the CA-Markov analysis for 2021 showed that the classes of land use changed at rates determined in part from the transition probabilities for the 2005-2009 4-year period. From the result, the land class growth was as follows, namely, residential is 0.62%, commercial is 0.05%, industrial is 1.22%, bright surface is 3.97%, Vegetation is -5.58% and water is -0.29%. The result of this comparison is shown in Table 8.12.

Figure 8.16 represent the image differences between OB 2009 and PCA2021. The overall accuracy is 90.16%, indicating a large correlation between the maps. The figure also shows changes (2009 & 2021) in the area of land use as a function of the CA forecast model. The grey colour indicates areas that are stable, representing six classes of LULC combined. Meanwhile, the other colours show change areas when the Markov-CA model is applied.

### ii) Difference OB 2009 vs P2020

A comparative analysis was conducted between OB 2009 and P2020 to examine the differences between the Plan in 2020 and the historical LULC distribution. The goal here was to test whether the CA-Markov model helps to bring the LULC distribution closer to the Plan distribution in 2020. If this is true, it would potentially represent some evidence that the model is working usefully. The LULC in 2009 was compared with the lots of polygon cadastral planned land use in 2020 (represented as raster data) (Figure 8.17). Table 8.12 (b) shows the difference in LULC proportions between the six classes. The results of this comparison showed that the residential class was 4.36% greater in the OB 2009 map, as discussed above. The interpretation above (for the CA

forecast) was that the discrepancy is the result of misclassification of residential land in 2005 and 2009, as a function of the OBIA approach. This finding is borne out in the present comparison. The vegetation class proportions exceed by +6.38% the proportions in the Plan for 2020. In the forecast for 2021, the discrepancy is only +0.8% by comparison. For the vegetation class the reduction in area is logical because it may represent new areas to be developed, and this development causes the vegetation land use class to be reduced. This, therefore, represents potential evidence that the CA-Markov model is working usefully, bringing the vegetation proportion in line with the 2020 Plan. Similar arguments apply to the bright surfaces class for which the discrepancy in proportion is -4.53% here, but only -0.56% in the forecast. For both the vegetation and bright surfaces classes, the CA-Markov forecast (which uses 2009 data as its starting point) of the proportional areas is much closer to the 2020 Plan than in the 2009 LULC map. For the other classes, except water, the forecasted proportions are; commercial is +1.40%, industrial -4.31%, and water -0.49%. The overall accuracy is 52.45, indicating a fair agreement between different datasets (Table 8.14).

Table 8.12 The difference proportion values between OB 2009 with PCA2021 and P2020

**a. OB 2009 vs. PCA2021**

| LULC | OB LULC 2009 | | Projected 2021 (PCA2021) | | Difference Proportion |
|---|---|---|---|---|---|
| | area (Ha) | % | area (Ha) | % | (%) |
| Residential | 444.70 | 24.68 | 456.2 | 25.3 | +0.62% |
| Commercial | 8.04 | 0.45 | 8.56 | 0.5 | +0.05% |
| Industrial | 71.68 | 3.98 | 93.77 | 5.2 | +1.22% |
| Bright Surface | 589.77 | 32.73 | 661.47 | 36.7 | +3.97% |
| Vegetation | 657.31 | 36.48 | 556.67 | 30.9 | -5.58% |
| Water | 30.50 | 1.69 | 25.34 | 1.4 | -0.29% |
| **Total** | **1802.00** | **100.00** | **1802.00** | **100.00** | |

**b. OB 2009 vs. P2020**

| LULC | OB LULC 2009 | | Proposed 2020 (P2020) | | Difference Proportion |
|---|---|---|---|---|---|
| | area (Ha) | % | area (Ha) | % | (%) |
| Residential | 444.70 | 24.68 | 366.201 | 20.32 | +4.36% |
| Commercial | 8.04 | 0.45 | 33.37 | 1.85 | -1.40% |
| Industrial | 71.68 | 3.98 | 149.3 | 8.29 | -4.31% |
| Bright Surface | 589.77 | 32.73 | 671.36 | 37.26 | -4.53% |
| Vegetation | 657.31 | 36.48 | 542.43 | 30.10 | +6.38% |
| Water | 30.50 | 1.69 | 39.35 | 2.18 | -0.49% |
| **Total** | **1802.00** | **100.00** | **1802.00** | **100.00** | |

The most important result in this Table 8.8 shows that vegetation and bright surfaces are much higher and indicated are both areas changed in the future plans. However, when comparing P2020 and PCA2021 (see Table 8.6) both vegetation and bright surface are much closer in the forecasted result than they are in the 2009 map.

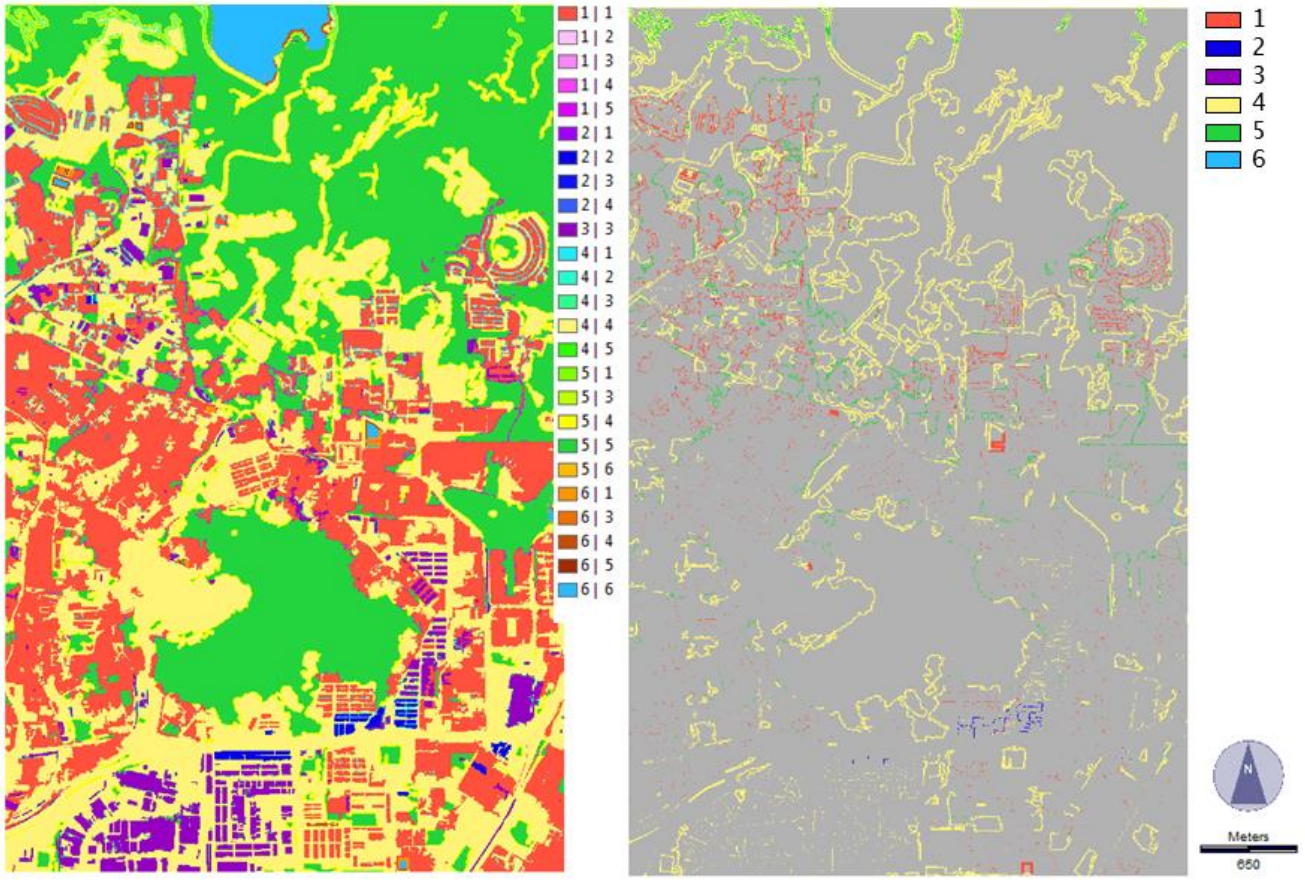


(a) OB LULC 2009 vs PCA2021

(b) The result of growth areas by CA 5 x 5 cells – transition probabilities (six classes of land use) PCA2021

Figure 8.16 Comparison of OB LULC 2009 and PCA2021.

Table 8.13 Cross-tabulation of OB LULC 2009 (OB 2009) (columns) against Projected CA 2021 (PCA2021) land use (rows) by number of pixels.

| | | Proposed 2020 land use | | | | | | | |
|---|---|---|---|---|---|---|---|---|---|
| | | **(1)** | **(2)** | **(3)** | **(4)** | **(5)** | **(6)** | | **User's** |
| | | **Residential** | **Commercial** | **Industrial** | **Bright Surface (BS)** | **Vegetation** | **Water** | **PCA2021 Total** | **Accuracy (%)** |
| OB LULC 2009 | **(1)Residential** | 4292552 | 518 | 0 | 242384 | 2059 | 24498 | 4562011 | 94.09 |
| | **(2)Commercial** | 118 | 76941 | 0 | 8536 | 0 | 0 | 85595 | 89.89 |
| | **(3)Industrial** | 2001 | 1400 | 716817 | 158177 | 57514 | 1787 | 937696 | 76.44 |
| | **(4)BS** | 9111 | 1410 | 0 | 5488151 | 1087299 | 28693 | 6614664 | 82.97 |
| | **(5)Vegetation** | 143251 | 0 | 0 | 330 | 5422964 | 8 | 5566553 | 97.42 |
| | **(6)Water** | 0 | 0 | 0 | 0 | 3232 | 250249 | 253481 | 98.72 |
| | **OB2009 Total** | 4447033 | 80269 | 716817 | 5897578 | 6573068 | 305235 | 18020000 | |
| **Producer's Accuracy (%)** | | **96.53** | **95.85** | **100.00** | **93.06** | **82.50** | **81.99** | | |
| **Overall Accuracy = 90.16%** | | | | | | | | | |

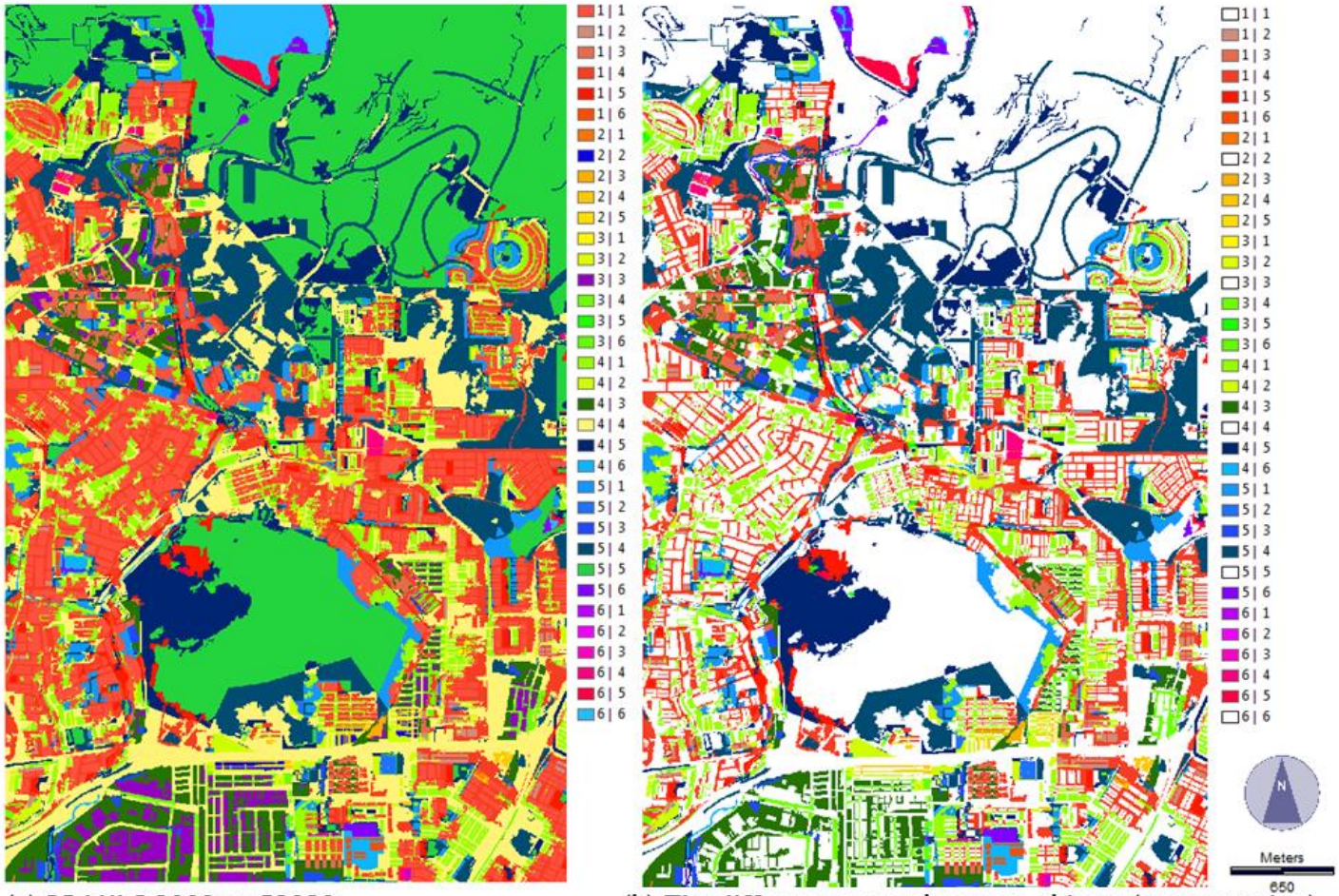


(a) OB LULC 2009 vs P2020

(b) The difference areas between objects (segmentation) and lots (polygon)

Figure 8.17 Comparison of OB LULC 2009 and P2020.

Table 8.14 Cross-tabulation of OB LULC 2009 (OB 2009) (columns) against Proposed 2020 (P2020) land use (rows) by number of pixels.

| | | Proposed 2020 land use | | | | | | | |
|---|---|---|---|---|---|---|---|---|---|
| | | **(1)** | **(2)** | **(3)** | **(4)** | **(5)** | **(6)** | | **User's** |
| | | **Residential** | **Commercial** | **Industrial** | **Bright Surface (BS)** | **Vegetation** | **Water** | **P2020 Total** | **Accuracy (%)** |
| OB LULC 2009 | **(1)Residential** | 1965802 | 4371 | 43610 | 1172018 | 465027 | 11184 | 36662012 | 43.09 |
| | **(2)Commercial** | 100353 | 27595 | 12520 | 166861 | 26009 | 355 | 333693 | 8.27 |
| | **(3)Industrial** | 206132 | 10142 | 405412 | 771107 | 98970 | 1193 | 1492956 | 27.15 |
| | **(4)BS** | 1862479 | 38142 | 225567 | 2735503 | 1809200 | 42708 | 6713599 | 40.75 |
| | **(5)Vegetation** | 281750 | 19 | 22668 | 969355 | 4109004 | 41475 | 5424271 | 75.75 |
| | **(6)Water** | 30517 | 0 | 7040 | 82734 | 64858 | 208320 | 393469 | 52.94 |
| | **OB2009 Total** | 4447033 | 80269 | 716817 | 5897578 | 6573068 | 305235 | 18020000 | |
| **Producer's Accuracy (%)** | | **44.20** | **34.38** | **56.56** | **46.38** | **62.51** | **68.25** | | |
| **Overall Accuracy = 52.45%** | | | | | | | | | |

## 8.5 Discussion

The fine spatial resolution of the LULC data produced for this research allows for more detailed descriptions of LULC transitions over time. The basic goal of this chapter was to answer the two most important research questions. The CA method was used to forecast future LULC distributions based on observed changes in RCI LULC from the previous result in Chapter 5. The CA analysis in this chapter, was able to show the amount of change through probability transition estimated with a four-year gap and to provide a forecast for other years (2009, 2013, 2017 and 2021). The analysis done here was based on a single run of the CA-Markov model. However, it is important to point out that it would be possible to explore the uncertainty in the forecasts through multiple runs of the CA or transition probability forecast. It is important that the probabilities are exploratory by example change from vegetation to bare ground (bright surface) with probability 0.06 if at least two neighbours are bare ground.

In general, the CA-Markov method was used to highlight the potential transition of LULC in pixels based on the probability of change. Arsanjani et al. (2013) stated that the approach is capable of forecasting the most probable sites for development, estimating the likely amount of change as well as allocating the estimated quantity within the study area. Levinson et al. (2012) highlighted some aspects of the Markov chain model that deserve critical attention, and some directions of extension that could improve the model's output. In other words, they use the Markov Chain analysis in combination with other methods to generate results that suit their own objectives.

In this case, the CA model does not stand alone based on traditional transition probability values to produce a projection map. Most researchers highlighted that it needs to be combined with other procedures such as the multi-criteria analysis for the transition value (Shafizadeh Moghadam & Helbich 2013). The method works well to produce results based on the transition probability of change value. The result of the CA for 2013 was based on two contributions; (i) the probability of change in LULC with high accuracy produced by fine spatial resolution data of 2005 and 2009, and (ii) the central cell state neighbourhood hypotheses by a simple logical expression. Both inputs are sufficient to produce a basic simulation using a CA to forecast changed area within the

defined period. As a result, it can forecast change within the projection map, as seen in Figure 8.8. The CA results showed clear urban expansion related to the bright surface class and demonstrated that urban growth areas are strongly linked to forecasted change values. The increase in LULC in 2013 is within the forecasted values of the (then) planning of new infrastructure aimed at supporting population increases.

This chapter used the OB classification for LULC based on image change detection from infrequent data of fine spatial resolution. The method CA-Markov model is an efficient way of using transition probabilities to forecast changes, meaning that it is not necessary to build all of the rules from the bottom up for the purposes of further dynamic research of CA. RCI and others classes (vegetation, bright surface and water) are combinations of LULC properly classified through the OB method producing highly accurate urban mapping. The analysis also provided a detailed description of how each class might change within the four-year period in fine resolution pixel transitions. The transition result provides an overview of descriptive values of changes in LULC during the monitoring period to show the changes that might occur. The result of land-use changes at pixel or cell level enabled an image-based forecast to be generated according to the probabilities of changes that were estimated. This information may be useful when used in conjunction with the calibration model with Landsat ETM+ data to diagnose future LULC change.

Input from the probability of change value of RCI provides information on the suitability of land for future development, and acts as a basic guideline for the policy maker. This LULC guideline for optimal LULC and directing development can be expected in the study area. The estimated probability values and the central cell neighbourhoods of different sizes showed that, by varying the size of the neighbourhood configuration, significant impact on the behaviour of the cellular automata model could be identified (Liu 2009). However, when applying this model to simulate the process of urban development, it assumed the RCI LULC from the bright surface class to be the new changed area. What has not been studied in this model is the impact of cell scale (i.e., pixel size) (using the established algorithm value (Gaussian) of model CA-windows 3 by 3, 5 by 5 and 7 by 7) and the interactions between cell scale and the neighbourhood size on the model's outcomes.

The result of CA in this analysis was generated from the IKONOS satellite sensor imagery using fine spatial resolution data. There was no additional input (except suitability map and overlay with constraint map), but it depended on an element of spatial contiguity as well as knowledge of the likely spatial distribution of transitions of the Markov chain analysis (equation 8.1) and CA-windows algorithm. A problem in the examination of LULC changes using satellite sensor images is that transition matrices with constant observation intervals cannot always be obtained. Thus, Takada et al. (2010) developed a computer program to calculate a yearly transition matrix from an original transition matrix that had an arbitrary observation period. This can be used for comparison of yearly transition matrices among different observation periods when temporal change of exogenous driving factors occurs, and for the analysis of spatial heterogeneity in yearly transition matrices. Some researchers agreed that the main limitation of the Markov Cellular Automata model is that it assumes the factors of change in the past still remain the same in the future (Yagoub & Al Bizreh 2014). In this research, the adjusted probability matrix reduced the change amongst the RCI classes (class 1 to class 3) to zero and enforced them to stay as 100% not changed within the first transition to explore the effect of this on the forecast. The CA-Markov model allows a reasonable way of identifying the changed value condition in a future forecast, so supporting the LULC planning policy and the monitoring of development by applying appropriate suitability maps and using a classified image with high accuracies of projection.

The comparison on observed data in 2009 of the CA forecast of LULC in 2009 which itself is based on LULC data from 2005 acts as a validation with the level of accuracy 73.29%. This purpose to create a forecasting model in anticipation of changes in land use in the years following. The comparison analysis between the proposed 2020 land use (P2020) and projected CA 2021 land use (PCA2021) showed the gap between cadastral data and OB classification by lots and objects. The graphic (Figure 8.15) is a quick way to see how a pair of maps agree and disagree about two fundamental questions concerning quantity and location simultaneously. The pairs of maps agree in terms of the quantity of cells in each category and the location of cells in each category. Yang et al. (2012) highlighted the difficulty of comparing a simulation result by visual comparison and the need to make quantitative comparisons. The different spatial level and form of plan and raster data require interpretation skills and

the ability to build up and manage the database within an information support system. Of relevance here is the notion of matching the resolution of imagery to the scale of spatial variation in a scene, perhaps represented by objects, for a particular application (Aplin & Atkinson 2001). Both datasets have advantages and disadvantages but have a good interpretation in the field of town planning, particularly land use planning. Cadastral data even if interpreted as "proposed land use," is rigid in nature because all development is determined by specific lots (ownership of land). Lots are sometimes not updated properly (i.e. committed development) and it is possible that the current land use data are missing due to the absence of lots (not up-to-date or error). Moreover, cadastral data cannot reflect the real situation on the ground such as the occurrence of ground work involving land that is flattened and deforestation (e.g., Figure 8.18). This should be checked by data from satellite sensor imagery that can be produced with high quality of land use classification, although not lot-based, for example; using OB classification through pixel segmentation by building polygons.

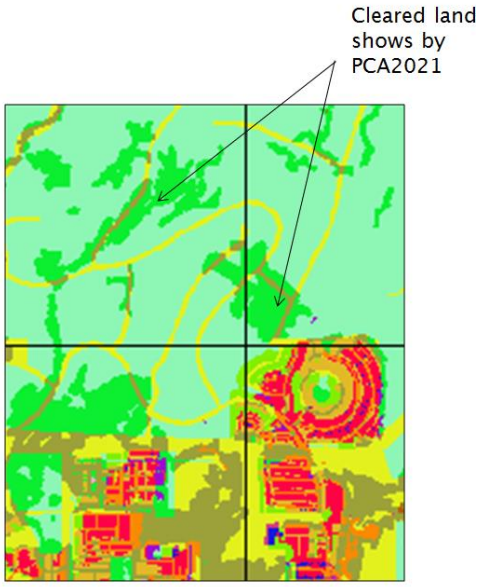


Figure 8.18 Land which has been levelled, not shown in the 2020 Plan.

Classification from satellite sensor images is at least able to show something that is 'real' on the ground. As an example, in the PCA2021 forecast, the area of agriculture / forest was invaded or flattened for a particular purpose. This cannot be found in the cadastral data P2020. In addition, the OB land use classification includes classes based on the “building line”. The buildings as in

objects can be used as the determinants of human activity in land use classes, respectively. The cadastral map is insufficient to determine the correct location because of the out of date measuring technologies and also the complexity of the archive. The combination of cadastral data (P2020) and OB classification-forecast (PCA2021) is a realistic approach and much needed in practice for the purpose of interpretation of planning rules so that a more accurate development can be established and planning policies can be updated. This consideration should be transformed into a digital map with legal validity conditional upon correction of errors. It also could be used to update or inform the P2020 map.

Although the result in this study is not meant to represent actual change values in the future, the results may be appropriate to be used as useful guidelines for any development planning policies regarding the implications for compatible and incompatible land uses. Land use, like forest fragmentation caused by changes in human land use activities, is of primary concern for sustainability. Land available for future requirements constitutes three types: undeveloped land, under-developed land and old disused areas, and land which has been given approval for development. Undeveloped land does not have any established use or permanent structures and can be developed immediately or in the near future. Existing land uses in these stable areas (bright surface) shall be maintained and incompatible land uses eliminated. The intrinsic characteristics of stable areas in terms of their geophysical and built environment will be analysed, and opportunities exploited to enhance their existing character and identity. To maintain a stable and sustainable area, a strategy shall be implemented which builds on the existing strengths of stable developed areas and improves their overall environment. This strategy will be one of minimal intervention sufficient to consolidate the fabric of these areas in order to improve anomalies or shortcomings.

This research suggests that future land use planning and development activities should consider the influence of observed and future forecasted change values from past data. Furthermore, any development in sensitive areas such as forest reserve areas which are deemed important for water infiltration should be restricted and monitored thoroughly.

## 8.6 Conclusion

The analysis in this chapter has demonstrated an efficient method to simulate dynamic LULC change simulation based on a highly accurate OB classification from fine spatial resolution data. It represents an important instrument for protecting and enhancing human-made and natural areas with positive roles to play in guiding appropriate development to the right place that is generally acceptable to communities. The change detection analysis of 2005 and 2009 played an important role in driving the LULC change forecast in each LULC class, including in built up and natural settings. Moreover, it was possible to forecast change in RCI to 2013, 2017 and 2021. It is important that simulation models of LULC change, particularly CA models where land management decisions are made at the pixel level, are capable of forecasting LULC between the main features of RCI. Results confirmed initial estimates of expected changes in the extent of RCI and bright surface as built land areas for the future. The differences between the forecast in 2021 and the planning in 2020 are likely to indicate where the original LULC classifications in 2005 and 2009 were in error (e.g., Residential class) or where planning policy has changed from the historical period (2005-to-2009) to the future (2020). This model can be extensively interrogated to generate several alternative solutions to urban planning problems.

# 9. Discussion

## 9.1 Thesis overview

This research was defined by the problems that exist in town planning practice in adopting land use classification techniques, calibration, monitoring of changes in land use and forecasting using remote sensing methods. The effectiveness of urban remote sensing methods have been demonstrated by many researchers (Mitsova et al. 2011; Olofsson et al. 2013; Rashed 2008; Small 2001; Yu & Ng 2007; Zhao 2011; Bhaskaran et al. 2010; Blaschke 2010).

In Malaysia, land use development is spatially complex especially in built-up areas that comprise residential, commercial and industrial (RCI) land use areas. A comprehensive development plan is needed to control the uses of land and to provide the basic framework for development of new areas. The conceptual framework of the National Land Use Information Centre (NLUIC) in Malaysia involves compilation of spatial data on land use planning for district, state and national levels in a GIS-based format as part of a statutory plan. No strong methodology has been developed for using remote sensing for monitoring rather than GIS.

Remote sensing research provides several major benefits for urban studies. It can be used to relate different human and natural variables in developing an understanding of indirect and direct drivers of urban change. It also offers information on the potential, feedbacks of such changes on the drivers in the urban environment. Regarding the availability of remote sensing data, medium-resolution remote sensing data have been used to examine large-dimensional urban phenomena or processes since the early 1970s when Landsat -1 was successfully launched. Free access to the Landsat archive from mid-2008 has enabled town planners or urban researchers to retrospectively view the Earth's surface, and time-series of remotely sensed data can be used to develop a historical perspective of urban attributes or changing processes. The launch of IKONOS, delivering very fine spatial resolution images, allowed detailed work concerning the urban environment. The combining of satellite sensor imagery such as frequent Landsat ETM+ 30m resolution series data and infrequent data of IKONOS 1m (pan-sharpened) from 2005 to 2009 provided

the initial concept of urban monitoring. Holland & Aplin (2013) also used the same data for monitoring, though using a different classification technique, a particular plant in degrading agricultural or ecologically sensitive land.

The significance of this research focused on the process of preparing a land use classification and developing maps of land use change. A complex classification was required to characterise the urban landscape and to be consistent with FDTCP Peninsular Malaysia practices. It also aimed to provide clearer monitoring of land use change using systematic and automated methods. The results of classification and monitoring can be combined to allow work at any scale or level of forecasting of land use change generated by the CA model. All these methods are very useful in town planning practice to projecting the existing land use change forward into the future, and this means effectively projecting current land use planning policy into the future.

There were two innovative concepts involved in this research. Firstly land use OB classification of RCI from IKONOS fine spatial resolution (infrequent), and brightness and greenness at multiple time-points (frequent data) was used for urban monitoring from Landsat ETM+ and it zoomed in to the small 18 zone training sites. That gave clear information on the spectral reflectance on greenness (forestation and deforestation) and brightness (built up land) in feature space distribution (x, y) thus identifying how and when the change occurred.

Secondly, an automated monitoring method was designed to detect the changes based on maximum difference values by developing the programming script in IDL software, in order to know the direction of change and magnitude in CVA. The automated process can provide a prediction of the type of land use change between classes, and the years of change. A model for monitoring land use change will help decision-makers to formulate future land use planning. There is great potential for the development of remote sensing methods that integrate and exploit both multispectral and multi-temporal information (Mello et al. 2013).

The classification clearly showed that the use of infrequent fine satellite images were very helpful for mapping land use and land cover, especially the

RCI map (residential, commercial and industrial) and it consistently fitted the monitoring model of change. The approach used in the study was very effective in fulfilling the objectives and was implemented. The study explored use of a pixel-based classification using coarse spatial resolution satellite sensor data and an object-based classification using fine resolution satellite sensor data. Both classification techniques required very good accuracy and information about the spatial and spectral signatures of the change that occurred in the study area between 2005-2009, in order to perform post-classification change detection.

The methods used in the process of strengthening the monitoring of change included Calibration and Multivariate Alteration Detection by Canty & Nielsen (2008) and the Tasselled Cap transformation method. These are valuable tools for capture and assessment of brightness and greenness for multispectral satellite coarse spatial images, using the differences of values to detect the changed area, especially where deforestation has led to new development, as highlighted by Crist & Cicone (1984). This calibration method was tested, although atmospheric correction should be taken into consideration in pre-processing for applications where a common radiometric scale is assumed among the multi-temporal remote sensing data (Song et al. 2001). The results contributed to the generation of a programming script towards automated monitoring of change within the four-year period. This dynamic monitoring was continued by investigating and analysing the direction and magnitude of change by using the Change Vector Analysis result as described in detail in Chapter 6.

Post-classification object-based change detection has been found to be a suitable method in this research. The method was applied to quantitative change detection, either giving expected change results or pseudo-expected results of land use change by referring to the lookup table. The quantified change using the difference classification results of the IKONOS data revealed the land use changes that occurred between 2005 and 2009 with high accuracy. This information was combined with the Landsat ETM+ time-series from 2005 to 2009. The technique of using object-based classification and post-classification gave a more reliable method to fit the model for forecasting (transition method) within four-year periods. Both data sets were used to

produce a cellular automata (CA) model of land-use change in four-year projected (2013, 2017, 2021), and that model was used to evaluate the likely outcomes under different planning scenarios.

## 9.2 Discussion of Findings

The aim of the analysis was to explore the effectiveness of land use and land cover classification for mapping, monitoring of change and predicting the future change in the study area for comparison with land use planning. These three aspects all involved the assessment of class accuracy, the reliability of the scale used and its capability of being applied at the state level.

The significance of the findings and contributions of this research are in the process of preparing a complex land use classification (RCI) and analysis of change therein, the novel use of Landsat data to infer the date of LULC change and the comparison of the CA forecast with Planning Department data for the same period. All these methods are potentially useful in the practice of town planning in Malaysia.

**RCI class accuracy**

Throughout this research, accuracy assessment has been performed on a per-pixel basis and object basis. First, the per-pixel accuracy involved four LULC classes i.e. building, brightness surface, vegetation and water, using a standard measure (root mean square error (RMSE)) of accuracy assessment in SMMA. The overall accuracy assessment result on per-pixel analysis is calculated from the differences between the original DN pixels (reflectance), and the modelled SMMA. Overall, the model has been judged to be accurate where the RMSE has a low value (e.g. > 0.1), and the fraction (proportion) was not lower than 0 or larger than 1. The most important result from this stage of calculating the fraction value or proportional value for each class was representing the proportion of land use and land cover. The proportion of Landsat ETM+ data between the years 2005 and 2009 was still in the prediction range (F) based on object-based classification.

However, the class accuracy for water is not an accurate value. This was because a small dark surface area (actually bright surface pixels) was recognised as a greater source of error and the pure pixel detected it as being the same as the water reflectance value. At the same time, it is not a big impact on the overall classification result because the real water feature is easy to identify in the study area.

Second, the object-based accuracy classification was evaluated for two sets of IKONOS data, 2005 and 2009; an error matrix was generated from the Definiens software (eCognition) for the six classes - residential, commercial, industrial (same as building class in per-pixel classification), vegetation, bright surface and water. Based on the defined sample, high-resolution data were enough to identify the land use of building as represented by residential, commercial and industrial (RCI) land use. The classifications have high accuracies of 79.3% and 78.0% from the IKONOS data 2005 and 2009. In all object-based classifications using eCognition, the user relies on the accuracy assessment in this way. However, since the accuracy assessment here is based on the known samples (which were considered accurate as they were taken from the reference data), accuracy is conditional upon the knowledge of an analyst who has taken the samples. Nevertheless, misclassification is still an issue although the overall result (79.3% and 78.0% level of accuracies) acceptable between residential classes, including the planned and unplanned housing area and brightness surface. These both produced misclassification while a supervised sample had already been developed for each type of land use class. This problem occurred because both categories occur in the same area, especially when the residential areas are mixed with bright surfaces and roofs which are not clearly identified and the generalised result is based on the neighbouring pixel or surrounding land use. The residential class also include some village areas where the size of house building is relatively small as streets or green areas. This issue was overcome by using a supervised OB classification procedure and subsequent manual on-screen editing.

All six classes still require further analysis for mapping land use (RCI) in a way that is consistent with the current practice of the Federal Department of Town and Country Planning (FDTCP) peninsular Malaysia.

**Reliability of scale used and transferability to the state level**

The methods used in this study can be implemented at the state level to district level (detail classification). The training areas allowed accurate classification of the whole study area (district level), and so plans at this level could be aggregated to develop state level plans.

The methods appropriate in the field of town planning in Malaysia. These necessarily involve the preparation of land-use plans as a foundation for planning to support the National Physical Plan in Malaysia. The method used is very reliable and objectivity can be achieved. However, there are several things that need to be taken into consideration when this method is applied on a much larger scale between calibration and radiometric correction in the first phase of pre-processing. It is impossible to obtain cloud-free or haze-free data. So the method of atmospheric correction must be a necessary stage in ensuring the time-series data reliability when dealing with pixel-based classification. This involved the collection of pure pixels or end-members of the exact reflectance value for the surface to represent LULC in larger areas with 30 m spatial resolution. The Landsat TM image can be accessed freely from the US Geological Survey, Earth Resources Observation and Science Center (EROS). In addition, to obtain high spatial resolution data such as IKONOS data for a relative larger area will involve an enormous cost. Spatial and temporal variability need to be taken into consideration whereby phenomena are monitored over time using multi-temporal imagery (Aplin 2006).

However, the suggestion here is the IKONOS imagery should be concentrated on certain built up or urban areas and the rest of area should be covered by Landsat imagery or similar. This will reduce the cost of IKONOS data as it will be used only and more appropriately for the built-up area. Outside the built-up area an analysis can be made from Landsat TM image data 30m resolution or any coarse resolution data. In an object-based classification using the IKONOS data, the most important information to run the analysis is knowledge-based and the reference data for the particular area. In this case, site familiarisation as an important tool when running the analysis using the remote-sensing data. The other option is information that will explain the

reference data (training data) such as a cadastral land use plan. This information will give an input to the object-based classification before the overall object-based classification results.

### Implications for town planning, management and the decision maker

The most important part of this study was the development of an effective method for monitoring land use and land cover change between the combination of different sensors, scales and time scales for OB classification, automated monitoring process and future prediction. All these methods can be combined into a town planning technique to sustain the monitoring of change and to manage urban change. Figure 9.1 illustrates the whole process of the research outcome. The study revealed the usefulness of various remote-sensing data and analysis techniques in the context of land use land cover change detection in urban studies, in the complex landscape between human and natural features.

Rapid urban development and increasing land-use changes due to increasing population and economic growth are big issues, especially for urban management and town planners. In meeting the demand of ever-changing urban land uses, the methods here can be applied, which are also the main tools in developing plans. These land use and land cover changes can be substantial but are difficult to grasp when they occur incrementally. From the monitoring method, data from satellites have dramatically illustrated the rates at which these human-induced changes are occurring nationwide and time-series mapping shows when change occurred. This information is very useful to develop the database and provides a strong visual portrayal of recognised growth patterns, and dramatically conveys how progress of certain areas or cities results in profound changes in the landscape.

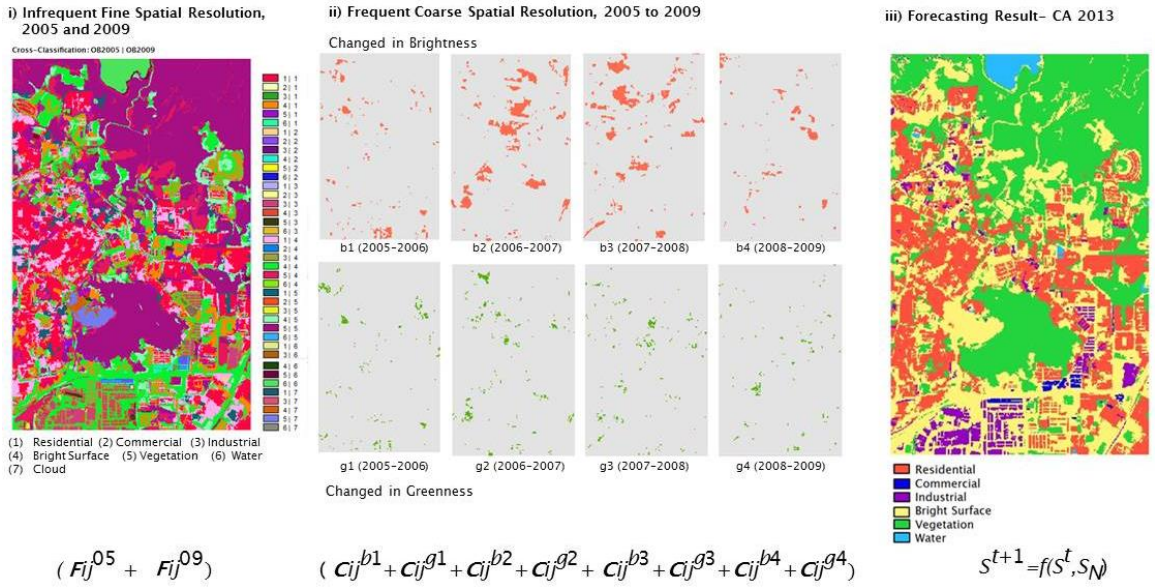


Figure 9.1 The research outcome from the combination of fine and coarse spatial resolution satellite sensor imagery regarding analyses of (i) change detection, (ii) monitoring of change and (iii) forecasting.

There are several possibilities that could be considered in the monitoring of, and forecasting of land use strategies in town planning or urban management:

i. The greatest demand for land will be for urban expansion but the potential land available for urban development is relatively small. It is possible to integrate forecasts regarding land suitability for development e.g. terrain, network access and infrastructure.
ii. Through detecting multiple changes of land use, it can be shown that it can provide an 'alarm' function to alert the monitoring purpose when changes have occurred. Ground verification is still needed to test and validate change and to compare this with the automated results.
iii. The spatial distribution from Figure 9.2 will become an initial model to quantify the land use change over time from vegetation (forest) to built-up area.

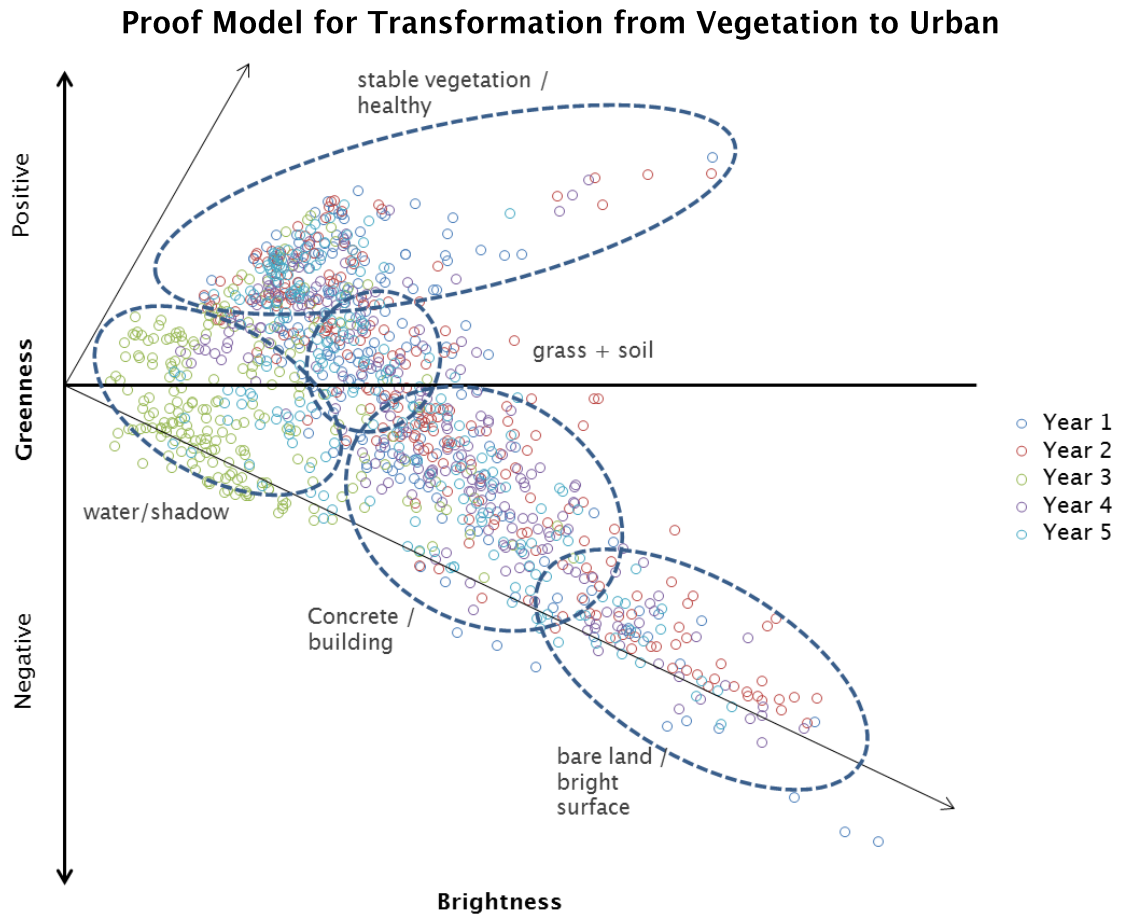


Figure 9.2 Overall empirical models of Feature Space by vector distribution transformation from vegetation to urban class.

Figure 9.2 is based on a manual interpretation-direct recognition from empirical analysis of the 18 point zone areas in Chapter 7. The model depends on the interpreter's experience, skill and judgement to interpret the image from the land use classification in order to identify the type of change. This manual identification technique is part of the interpretation of land use change in town planning field. However, it will be more helpful if the method can be developed as fully automatic through identification of the pattern vector distribution in feature space. It will help the decision-maker make a correct judgement from the model design.

CA-MARKOV model is an efficient way of using transition probabilities to forecast changes, meaning that it is not necessary to build all of the rules from the bottom up in Chapter 8. The result of CA for 2013 generated two contributions; (i) the probability value of change in LULC with high accuracy produced by fine spatial resolution data of 2005 and 2009, and (ii) forecasting

amounts to projecting the existing land use change forward into the future, and this means effectively projecting current land use planning policy into the future. Differences between the forecast and the planning are likely to indicate where planning *policy* has changed. The result of land-use changes in pixels or cells from the change analysis (objective 1) (i.e., the set of transition probabilities) enabled a simulated forecast to be generated using a CA model. While several parameters of the CA model were explored, of greatest interest was the comparison of the forecast with a formal Plan for LULC in 2020.

## 9.3 Limitations of the research

The first limitation of the research was dealing with the series of multi-date data captured in a tropical country such as Malaysia. The thick cloud cover from archive satellite remote sensing images was a great challenge, whether from coarse or fine spatial resolution data. Besides the cloud cover issue, the frequently captured data by the U.S. Geological Survey (USGS), Earth Resources Observation and Science Center (EROS) are SLC-off (Scan Line Corrector) for all the images. This compensates for the forward motion of Landsat 7 but this failed to start from 2003 onwards. However, the data still can be used through the correct technique to fill in the gaps.

Secondly, dealing with the calibration of multiple images (five images or more), the atmospheric correction needed to be conducted before starting the monitoring analysis. It included the LULC pixels to ensure that the reflectance values were represented correctly by the removal of haze, aerosol, and cloud. The method can be done using software with the right technique of atmospheric correction and calibration. This involved a lot of time consuming work and was a self-learning process to complete the calibration for more than five images especially in mixed features (e.g. urban areas).

Thirdly, there is still a long way before a fully automated RCI classification can be generated. This is because the existing process and software require a sample-based or knowledge-based supervised image classification. This means that human vision recognition is still required to guide the software to classifying the objects features of RCI.

Fourthly, as mentioned before, the 'alarm' functions of monitoring urban change needs to be done automatically. In this study, the programming script was already developed, based on max-min images pixel differences as the basis for the automated urban monitoring using coarse spatial resolution. There may be some limitation because detailed spatial variability in certain land use classes is not taken into consideration. In this case, the integration from fine spatial resolution data still depends on identifying the type of land use involved in the change.

Fifthly, Regarding the SLC-off issue of the five Landsat ETM+ images the selection of pure pixels is to reveal the Pseudo-invariant features （PIFs) selected by IR-MAD. By doing this on the IKONOS image can observe the types of surface that were stable over 2005-2009, and it provides confirmation of the visual interpretation in Chapter 7. The targets are more variable in the normalised data than in the raw DN. The high coefficient of variation (CV) values for the dense vegetation is probably due to the red reflectance being so low, around 1%, which is very low. Dense forest is usually no lower than 2% reflectance in the NIR. There may also be some surprises. Maybe some surfaces that thought would be stable, actually changed, and vice versa. Landsat data lack the spatial resolution to create maps of change but they can give an insight into the processes occurring because ETM+ measures energy fluxes associated with land cover change - e.g. vegetation growth. If we want to model future land cover we need to predict both spatial pattern and process. Hence we need Object-Based and spectral change vectors.

Lastly, the result of CA in this analysis was totally generated from the IKONOS satellite sensor imagery using fine spatial resolution data. There was no additional input to enhance the suitability map like the planning scenario (i.e. if the land near to main road or infrastructure normally increased the land demand for the development). Another problem, the examination of land-use changes using satellite sensor images is that transition matrices with constant observation intervals cannot always be obtained, and it depended on an element of spatial contiguity as well as knowledge of the likely spatial distribution of transitions of the Markov chain analysis. The different spatial level and form of plan (cadastral) and raster (OB classification) data require of

interpretation skills and ability to build up and manage the database with information system support for the large scale area. This research suggests that future land use planning and development activities should consider the influence of observed and future like change values from the past data. The forecasting land use change analysis was derived from several observations of the past land use change, for example, through infrequent land use map. In addition, due to limited information on spatial land use change in the future for the study area, this study projected land use change for the future through previous observations of land use change and the possibility of what might happen in the future.

# 10. Conclusion

The analysis reported in this thesis was structured into three main chapters on classification, monitoring and forecasting and this provided some understanding of how the urban area studied in Malaysia has grown over a period of time. This was enabled using fine resolution maps of land use class (focusing on the residential, commercial and industrial, RCI, classes), multiple date data, and probabilities of change obtained from pixel-based change analysis and by accounting for the influence of cell neighbourhoods. The research results reported here depend on the accuracy of classification and subsequently the accuracies of the probability values generated as a result.

The thesis has also reviewed suitable methods and models that have been applied to characterise past-present scenarios such as to forecast future urban growth using multi-source satellite sensor imagery. All these approaches are important in land use planning to ensure that the land use (with a focus on built-up area) is closely monitored and development and growth areas are sustainability controlled.

The major contributions of the research start with OB classification of RCI from remote sensing data. The OB classification was shown to be a suitable method for classifying land use accurately, particularly when the focus is on RCI classes. In particular, such classification is known to be challenging and this research quantified what is possible by rigorously assessing the accuracy of classification. This research strongly suggested that land use mapping must be undertaken using fine spatial resolution multispectral data using the object-based classification method. The research produced a reliable land use map with three years reference data provided for validation (2007, 2010 and 2013). There is still a need for further exploration of the parameters, spectral reflectance, and increase in accuracy through site familiarisation.

The process of land use classification provided the starting point for the subsequent updating process as a means of year-by-year monitoring of land use development. The maps produced year-by-year indicated the land use changes and produced a detailed change analysis of urban development such that the research can contribute to planning policies directly. More importantly, for the first time, multi-source remotely sensed imagery (IKONOS and Landsat)

were combined to identify the date of change. This was enabled through a transformation of the Landsat data into Tasselled Cap space, and subsequent interrogation of the Landsat time-series which “filled in the gaps” between the temporally separated IKONOS RCI maps.

In addition, the research continued with the forecasting of future growth of land use (RCI), as important urban entities, to simulate the pattern of urban expansion based on data calibration. A key contribution here was to expand a pixel-level transition probability approach to include, in a formal manner, the contribution of neighbouring cells. All these contributions are of direct interest to town planners who will be able to use the new data to support better decision-making.

This research fine spatial and temporal resolution monitoring of land use through remote sensing using the techniques described above can reveal the complexity of spatial and temporal landscape pattern, providing some new and interesting perspectives on urban morphology. Land use policies in Malaysia have played a vital role in shaping the landscape. The hierarchy of the land use planning system is driven to play a more important role in forming this new urban pattern and this can be revealed using the analysis above. Thus, this research demonstrated that dynamic analysis of remote sensing data is needed in the town planning field, especially when land use change monitoring at the macro level (national and state).

In light of this research, some recommendations can be made for practitioners (planners):

i. The OB classification method applied to fine spatial resolution satellite sensor imagery is strongly suggested to be used for preparation of land use maps.
ii. RCI can be explored through the rule set tool as a standard parameter in OB classification. This has not been shown before.
iii. Using multi-date remote sensing satellite data requires calibration with very accurate co-registration.
iv. Landsat data lack the spatial resolution to create maps of change but they can give an insight into the *date of change* because ETM measures energy fluxes associated with land cover changes.

v. Forecasting based on probability values, can be improved by considering multi-criteria factors of urban expansion and urban growth, specifically the effect of cell neighbours on likely changes.
vi. Future research should be focused on urban morphology, especially for historic cities or capital cities from the 'future-past model' by combining multi-source satellite sensor imagery.

Remote sensing technology provides new opportunities for a wide range of urban applications. The process demonstrates that multi-temporal remote sensing data and techniques allow extensive monitoring of spatial effects in urban areas over a comparatively long time period providing reproducible and consistent mapping results. This allows supporting effective land management and policy-based decision-making that require spatial knowledge, comparative datasets for understanding the model, and prediction of land conversion in cities.

Remote sensing data were used as part of developing an over-arching approach for town planning (land use mapping, monitoring and forecasting). The study has achieved all the research objectives listed in Chapter 1 of the thesis. It has identified that the process of urban remote sensing can be used for the purpose of land use delineation, monitoring changes in land use area, identifying the date of change, and forecast future land use states from the classification of multi-date and multi-source remote sensing data.

Urban remote sensing research currently faces very interesting challenges for the future. Some recommendations based on the analysis undertaken here are:

- Monitoring of incompatible land use (e.g. squatter's area in city) within the planned areas should be pursued. This may involve the quantification of uncertainties (i.e., population by race, level of income, ageing society and age group) and a qualitative approach for certain variables (i.e. family background) to control the land use in a sustainable manner.
- Projecting land use in the future; a land use dynamic model may be deemed suitable for use. This will integrate spatial and temporal data from fine spatial resolution satellite sensor imagery. The change rate

between land use classes follows the reality from the current planning policy rate or government policy and the evidence of ground change.

- Time-series studies can be carried out to explore the linkage of economic trends to the development of urban areas (including change of urban size). In addition, future time-series studies should explore other extreme land uses (between RCI) which may influence urbanisation of an area.
- This research provided a first exploration and demonstration of some important concepts, for the first time, with a ready interpretation in the town planning context. Future research should expand these ideas adopting rigorous methods for their implementation (e.g. explore parameter space, issues of spatial and temporal scale, and increase accuracy).

# Appendices

## Appendix 1 : Multi-date calibration method of Landsat ETM+ by Canty (2010)

The linear combination of the intensities for all bands in the first image is represented by the random vector $G_1$, thus creating a scalar image characterised by the random variable:

$$\boldsymbol{U} = a^{\mathrm{T}} G_1 \tag{1}$$

The vector of coefficients, $a$, is as yet unspecified. The same is done for the second image, represented by $G_2$, forming the linear combination;

$$\boldsymbol{V} = b^{\mathrm{T}} G_2 \tag{2}$$

The result is a scalar difference image, $\boldsymbol{U}-\boldsymbol{V}$. The change information is now contained in a single image. Nielsen et al. (1998) suggested that vector $G_1$ and $G_2$ are presented in standard canonical correlation analysis (CCA) as described by Hotelling (1936). This has similarities with correlation, but is a more natural framework in which to look for change. The correlation of CCA, between the random variables $\boldsymbol{U}$ and $\boldsymbol{V}$, is given by :

$$\rho = \frac{\mathrm{cov}\,(\boldsymbol{U},\boldsymbol{V})}{\sqrt{\mathrm{var}\,(\boldsymbol{U})}\sqrt{\mathrm{var}\,(\boldsymbol{V})}} \tag{3}$$

Arbitrary multiples of $\boldsymbol{U}$ and $\boldsymbol{V}$ would clearly have the same correlation, so a constraint must be chosen. A convenient one is

$$\mathrm{var}(\boldsymbol{U})=\mathrm{var}(\boldsymbol{V})=1 \quad (4)$$

Note that, under this constraint, the variance of the difference image is

$$\mathrm{var}(\boldsymbol{U}\text{-}\boldsymbol{V})=\mathrm{var}(\boldsymbol{U})+\mathrm{var}(\boldsymbol{V})-2\mathrm{cov}(\boldsymbol{U},\boldsymbol{V}) = 2(1-\mathrm{p}) \quad (5)$$

Therefore, vectors *a* and *b* which maximize the correlation in equation 5.3 under the constraints of equation 5.4 will, in fact, minimise the variance of the difference image.

An alternative scheme is to examine the MAD variates directly. The random variable *Z* represents the sum of the squares of the standardised MAD variates,

$$Z=\sum_{i=1}^{N}\left(\frac{M_i}{\sigma M_i}\right)^2 \quad (6)$$

where $\sigma \mathrm{M_i}$ is the variance in its pixel intensities. Then, since the no-change observations are expected to be normally distributed and uncorrelated, the random variable *Z* should be Chi-square distributed with *N* degrees of freedom. For each iteration, the observations can, thus, be given weights determined by the Chi-square distribution, namely:

$$\Pr(\text{no change})=1-P\,x^2;N^{(Z)} \quad (7)$$

Pr(no change) is the probability that a sample *z* drawn from the Chi-square distribution could be larger. A small *z* implies a correspondingly large probability. Iteration of the MAD transformation continues until some stopping criterion is met, such as a lack of significant change in the canonical correlations *pi*, *i* = 1…*N*.

## Appendix 2 : Pseudo-invariant features (PIFs) target

Regarding the SLC-off issue of the five Landsat ETM images the selection of pure pixels is to reveal the PIFs selected by IR-MAD. By doing this on the IKONOS image can observe the types of surface that were stable over 2005-2009, and it provides confirmation of the visual interpretation in Chapter 7. There may also be some surprises. Maybe some surfaces that were expected to would be stable, actually changed, and vice versa.

This was done as follows:

Step 1 create density slice of the ChiSq band 0-15 (values chosen by trial & error, but this could be done based on the ChiSq distribution).

Step 2 is output the range to a class image.

Step 3 use post classification to Sieve the pixels. Set ‘Group Min Threshold’ to 36 and ‘Number of Neighbours’ to 4. These values are chosen to roughly correspond to 6x6 pixels, i.e. 30m x 30m area.

The green pixels show possible PIFs. Most of them are in vegetation, but note that the large grey roof building in the zoom window was also classified, as were areas in the highway and some roads.

Step 4 is doing a similar thing for the pixels at the 'top end' of the ChiSq distribution, i.e. those that have changed. If able do these on the IKONOS image meaning will be able to choose examples of a number of land cover transitions of interest, for example:

Vegetated > Residential
Vegetated > Bare
Bare > Vegetated
Bare > Commercial/Industrial

Step 5 is to make ROIs of some of these transitions, then transfer them to the Landsat images. In that way will know the geographical area is correct – each of them contained a land cover change at some time during 2005–2009.

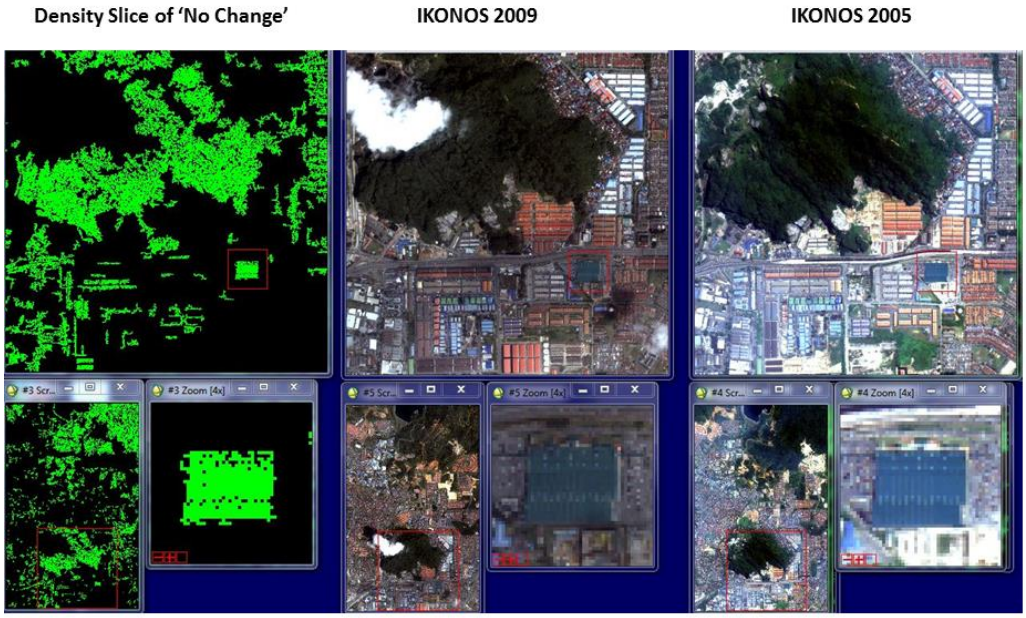


Figure A2.10.1 The sample of 'Big Grey Roof' as PIFs target from IKONOS data 2005 and 2009.

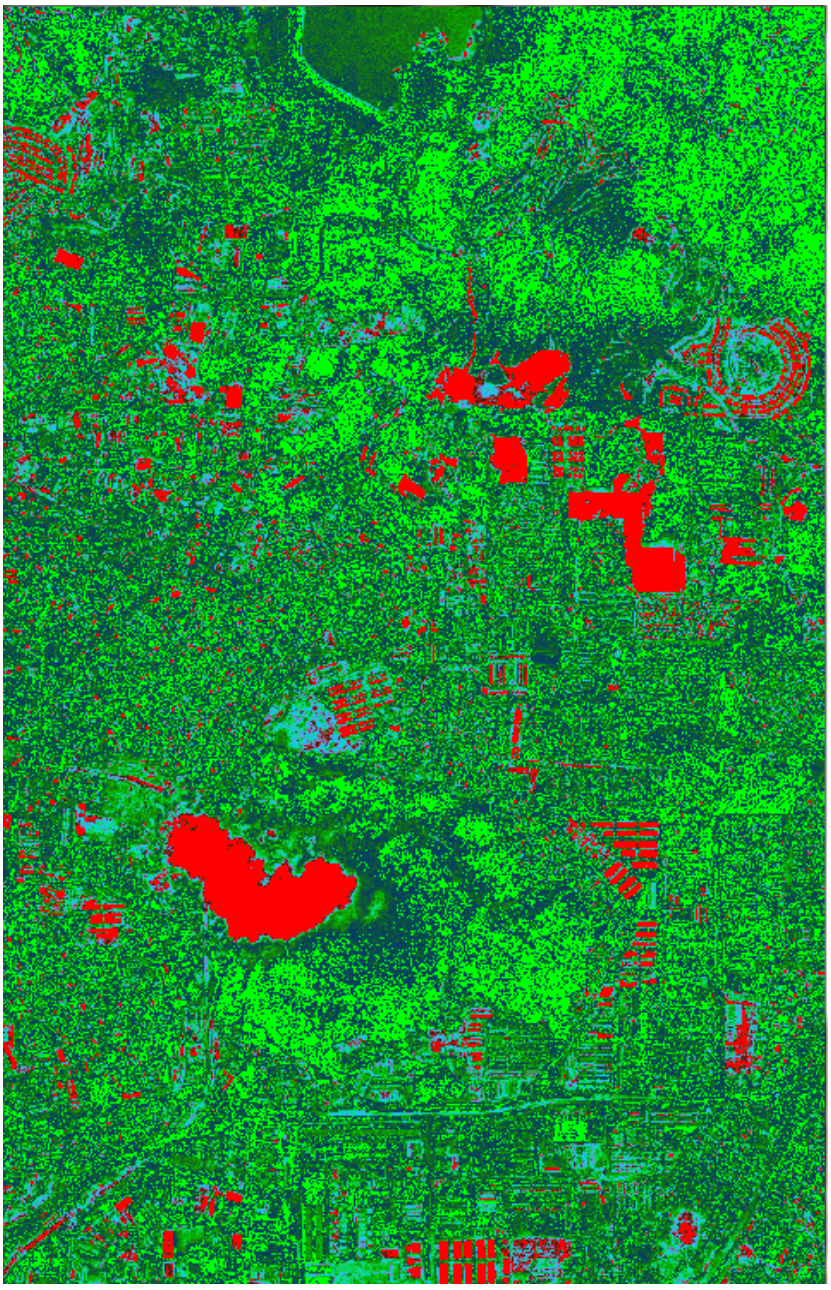

Figure A2.10.2 Use the Chi Square (ChiSq) band from IR-MAD result between IKONOS 2005/2009 to identify areas of change (red) and no change (green).

Figure A2.2 is to reveal the PIFs selected by IR-MAD. By doing this on the IKONOS image that can see the types of surface that were stable over 2005-2009, and it provides confirmation of the visual interpretation.

## Result of Pseudo-invariant features (PIFs) target

The first thing to note is that the grey roof and dense vegetation clusters are much tighter than those based on the DN values, so the normalisation has worked. The bare ground is not as good, but that is a small spatially variable target, which is not ideal. However, the coefficient of variation (CV) has increased for all three surfaces, which is a surprise.

This analysis provides a good starting point for Chapter 7, the aim of which is to understand the spectral expression of changes in land use. In this part are chosen three 'pseudo-invariant' targets (dense vegetation, roof and bare soil), and will show how the process of atmospheric correction and normalisation worked to standardise these 'pure' surfaces (Figure A2.4 to Figure A2.6 use the boxplots). Of course, the real world is not 'pure', but they will lead into the main part of the chapter, which as to understand the greenness-brightness FS is a useful way to visualise change in a rapidly developing urban area.

Bare ground PIFs look quite variable but look at the absolute values - the differences in reflectance between years are actually very small and meaning the normalisation to reflectance worked well for these 'pure' surfaces.

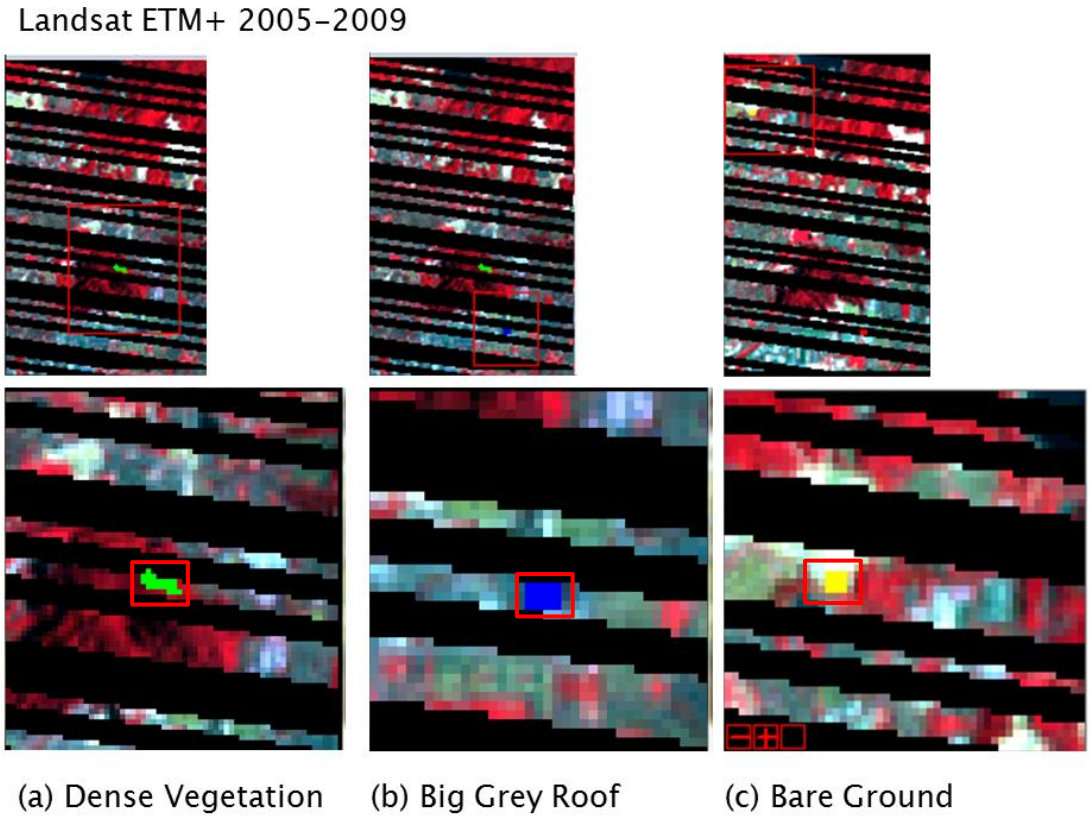


Figure A2.10.3 Samples of Pure Pixel – Dense Vegetation, Big Grey Roof and Bare Ground

Table A2.10.1 Samples of Pure Pixel – Dense Vegetation

| Year | B1 | B2 | B3 | B4 | B5 | B6 |
|---|---|---|---|---|---|---|
| 2005 | 0 | 3 | 1 | 17 | 12 | 4 |
| 2005 | 0 | 3 | 1 | 18 | 13 | 5 |
| 2005 | 1 | 3 | 2 | 19 | 13 | 5 |
| 2005 | 0 | 3 | 2 | 18 | 14 | 5 |
| 2005 | 1 | 3 | 1 | 16 | 12 | 4 |
| 2005 | 0 | 2 | 1 | 16 | 12 | 5 |
| 2005 | 0 | 3 | 1 | 17 | 12 | 4 |
| 2005 | 0 | 4 | 1 | 19 | 14 | 6 |
| 2005 | 0 | 4 | 2 | 20 | 14 | 5 |
| 2005 | 0 | 3 | 1 | 20 | 15 | 6 |
| 2005 | 1 | 3 | 2 | 20 | 14 | 5 |
| 2005 | 1 | 3 | 1 | 17 | 13 | 5 |
| 2005 | 0 | 3 | 1 | 16 | 11 | 4 |
| 2005 | 0 | 3 | 1 | 16 | 12 | 4 |
| 2005 | 1 | 2 | 1 | 16 | 11 | 4 |
| 2005 | 0 | 3 | 1 | 19 | 13 | 5 |
| 2005 | 1 | 4 | 1 | 20 | 15 | 5 |
| 2005 | 0 | 2 | 2 | 16 | 12 | 5 |
| 2005 | 1 | 3 | 1 | 18 | 13 | 5 |
| 2005 | 1 | 3 | 2 | 17 | 13 | 4 |
| 2005 | 1 | 4 | 2 | 18 | 14 | 6 |
| 2005 | 1 | 2 | 1 | 13 | 10 | 4 |
| 2005 | 0 | 3 | 1 | 17 | 12 | 4 |
| 2005 | 1 | 3 | 2 | 19 | 14 | 5 |
| 2005 | 0 | 2 | 1 | 13 | 10 | 4 |
| 2005 | 1 | 3 | 1 | 16 | 11 | 4 |
| 2005 | 0 | 3 | 1 | 16 | 12 | 5 |
| 2005 | 1 | 3 | 2 | 16 | 13 | 5 |
| 2005 | 0 | 3 | 1 | 15 | 11 | 4 |
| 2005 | 0 | 1 | 1 | 9 | 8 | 3 |
| 2005 | 1 | 2 | 1 | 12 | 9 | 4 |
| 2005 | 0 | 3 | 2 | 15 | 12 | 5 |
| 2005 | 0 | 3 | 2 | 16 | 12 | 5 |
| 2005 | 0 | 2 | 1 | 15 | 12 | 5 |
| 2006 | 0.7992 | 2.8752 | 1.442 | 14.752 | 11.753 | 4.5414 |
| 2006 | 0.7992 | 3.4296 | 1.6681 | 18.667 | 13.488 | 5.3129 |
| 2006 | 0.7992 | 3.7067 | 1.442 | 19.646 | 13.488 | 5.3129 |
| 2006 | 0.7992 | 3.4296 | 1.216 | 15.078 | 12.001 | 4.7986 |
| 2006 | 0.7992 | 2.8752 | 0.9899 | 13.773 | 11.753 | 4.7986 |
| 2006 | 0.7992 | 3.4296 | 1.216 | 14.752 | 11.009 | 4.7986 |
| 2006 | 1.0768 | 3.1524 | 1.216 | 15.078 | 12.001 | 4.7986 |
| 2006 | 1.3544 | 3.7067 | 1.6681 | 18.014 | 14.479 | 5.5701 |

| | | | | | | |
|---|---|---|---|---|---|---|
| 2006 | 1.9095 | 3.9839 | 1.216 | 19.646 | 14.975 | 6.0844 |
| 2006 | 1.0768 | 3.7067 | 1.6681 | 19.32 | 15.223 | 5.8273 |
| 2006 | 1.3544 | 3.4296 | 1.442 | 19.972 | 14.479 | 5.5701 |
| 2006 | 0.7992 | 2.8752 | 0.9899 | 13.12 | 10.266 | 4.2842 |
| 2006 | 0.7992 | 2.8752 | 1.216 | 13.12 | 11.009 | 4.027 |
| 2006 | 1.0768 | 2.8752 | 1.442 | 13.447 | 11.257 | 4.5414 |
| 2006 | 1.0768 | 2.8752 | 0.9899 | 12.468 | 10.266 | 4.027 |
| 2006 | 1.6319 | 3.1524 | 1.216 | 16.383 | 12.744 | 5.0557 |
| 2006 | 1.3544 | 3.1524 | 1.442 | 17.362 | 12.744 | 5.3129 |
| 2006 | 0.5217 | 2.8752 | 0.9899 | 15.404 | 10.761 | 4.7986 |
| 2006 | 1.0768 | 3.1524 | 0.9899 | 16.383 | 12.249 | 4.7986 |
| 2006 | 1.0768 | 3.4296 | 1.442 | 15.404 | 13.24 | 5.5701 |
| 2006 | 1.3544 | 3.1524 | 1.442 | 15.404 | 12.992 | 5.5701 |
| 2006 | 1.0768 | 2.598 | 0.9899 | 11.489 | 9.5222 | 4.027 |
| 2006 | 0.7992 | 3.4296 | 1.216 | 13.773 | 12.001 | 5.0557 |
| 2006 | 0.7992 | 2.598 | 1.216 | 15.404 | 12.001 | 4.7986 |
| 2006 | 0.7992 | 2.598 | 0.9899 | 13.12 | 9.5222 | 4.2842 |
| 2006 | 1.0768 | 3.1524 | 0.9899 | 13.773 | 12.001 | 5.0557 |
| 2006 | 1.3544 | 2.598 | 1.216 | 12.468 | 10.514 | 4.2842 |
| 2006 | 1.0768 | 2.8752 | 1.442 | 14.752 | 12.496 | 4.5414 |
| 2006 | 0.7992 | 2.598 | 0.7639 | 11.815 | 10.018 | 4.5414 |
| 2006 | 0.5217 | 1.7664 | 0.7639 | 9.205 | 6.3002 | 2.7411 |
| 2006 | 1.0768 | 1.7664 | 0.7639 | 8.8788 | 6.548 | 2.7411 |
| 2006 | 0.7992 | 3.1524 | 2.3463 | 12.794 | 11.753 | 5.3129 |
| 2006 | 0.7992 | 2.598 | 1.442 | 11.489 | 9.5222 | 4.5414 |
| 2006 | 1.6319 | 3.1524 | 0.9899 | 12.794 | 11.257 | 4.5414 |
| 2007 | 1.4289 | 3.1126 | 1.8614 | 15.378 | 10.6 | 3.802 |
| 2007 | 1.4289 | 3.7063 | 1.6252 | 17.681 | 13.66 | 4.8621 |
| 2007 | 1.4289 | 3.4095 | 1.6252 | 18.833 | 13.66 | 5.1271 |
| 2007 | 0.7906 | 3.1126 | 1.6252 | 14.994 | 11.365 | 4.3321 |
| 2007 | 0.7906 | 3.1126 | 1.1529 | 13.458 | 11.11 | 4.0671 |
| 2007 | 1.1098 | 2.8157 | 1.6252 | 13.074 | 11.365 | 4.5971 |
| 2007 | 0.7906 | 2.8157 | 2.0976 | 15.378 | 12.13 | 4.3321 |
| 2007 | 1.4289 | 3.7063 | 1.6252 | 18.449 | 14.17 | 4.5971 |
| 2007 | 1.7481 | 3.7063 | 1.8614 | 19.601 | 14.425 | 5.1271 |
| 2007 | 1.4289 | 3.1126 | 1.8614 | 19.985 | 14.425 | 5.1271 |
| 2007 | 0.7906 | 3.4095 | 0.9167 | 19.985 | 14.425 | 4.8621 |
| 2007 | 0.7906 | 2.5188 | 1.1529 | 11.154 | 10.09 | 4.0671 |
| 2007 | 0.4714 | 2.8157 | 1.8614 | 12.69 | 10.6 | 4.0671 |
| 2007 | 1.4289 | 2.222 | 1.1529 | 12.306 | 10.09 | 3.802 |
| 2007 | 0.4714 | 2.8157 | 1.8614 | 12.306 | 10.345 | 3.802 |
| 2007 | 1.1098 | 3.4095 | 2.0976 | 15.378 | 12.895 | 5.1271 |
| 2007 | 1.1098 | 2.8157 | 0.9167 | 15.378 | 12.13 | 4.5971 |
| 2007 | 0.4714 | 2.8157 | 0.9167 | 13.842 | 10.09 | 3.537 |
| 2007 | 1.4289 | 3.4095 | 0.9167 | 16.529 | 12.64 | 4.3321 |

| | | | | | | |
|---|---|---|---|---|---|---|
| 2007 | 0.7906 | 3.4095 | 2.0976 | 15.378 | 12.385 | 4.8621 |
| 2007 | 1.1098 | 2.5188 | 0.9167 | 14.226 | 12.385 | 4.5971 |
| 2007 | 1.1098 | 2.222 | 1.1529 | 10.386 | 9.3247 | 3.537 |
| 2007 | 0.7906 | 2.8157 | 1.1529 | 14.61 | 11.62 | 4.5971 |
| 2007 | 0.4714 | 2.8157 | 0.9167 | 13.842 | 10.855 | 3.802 |
| 2007 | 1.4289 | 2.5188 | 0.9167 | 13.458 | 9.8348 | 3.802 |
| 2007 | 0.7906 | 3.1126 | 1.6252 | 14.994 | 11.62 | 4.0671 |
| 2007 | 1.1098 | 2.5188 | 1.1529 | 11.538 | 9.5798 | 4.0671 |
| 2007 | 0.4714 | 3.1126 | 1.6252 | 13.458 | 11.365 | 4.3321 |
| 2007 | 0.7906 | 2.222 | 0.6805 | 10.386 | 9.0697 | 3.802 |
| 2007 | 0.4714 | 1.9251 | 0.9167 | 7.6985 | 6.2643 | 2.2119 |
| 2007 | 0.7906 | 2.222 | 0.2082 | 8.4664 | 7.2845 | 3.272 |
| 2007 | 1.7481 | 3.1126 | 1.6252 | 13.458 | 11.62 | 4.5971 |
| 2007 | 0.4714 | 2.5188 | 0.4444 | 10.386 | 9.0697 | 3.802 |
| 2007 | 0.1523 | 3.1126 | 1.6252 | 12.306 | 10.855 | 3.802 |
| 2008 | 2.123 | 3.7935 | 1.8644 | 17.101 | 12.729 | 5.0056 |
| 2008 | 2.123 | 5.041 | 2.7087 | 19.441 | 15.076 | 6.0104 |
| 2008 | 1.8795 | 4.542 | 2.9198 | 21.113 | 14.137 | 6.0104 |
| 2008 | 2.123 | 3.544 | 2.4976 | 15.429 | 12.964 | 5.0056 |
| 2008 | 2.123 | 3.544 | 1.8644 | 15.429 | 11.791 | 5.0056 |
| 2008 | 1.636 | 3.544 | 1.8644 | 15.094 | 12.025 | 4.7544 |
| 2008 | 1.636 | 3.7935 | 1.6533 | 16.432 | 11.321 | 4.7544 |
| 2008 | 1.8795 | 3.7935 | 2.9198 | 19.107 | 13.668 | 5.7592 |
| 2008 | 1.8795 | 4.542 | 2.4976 | 20.11 | 14.372 | 5.7592 |
| 2008 | 2.123 | 3.7935 | 2.4976 | 19.441 | 14.372 | 5.7592 |
| 2008 | 1.636 | 4.043 | 2.4976 | 20.11 | 13.668 | 6.0104 |
| 2008 | 1.8795 | 3.2945 | 2.0754 | 13.423 | 11.321 | 4.5032 |
| 2008 | 1.8795 | 3.544 | 1.8644 | 14.426 | 10.148 | 4.5032 |
| 2008 | 1.8795 | 3.544 | 2.4976 | 14.426 | 12.025 | 4.7544 |
| 2008 | 2.3666 | 3.045 | 1.8644 | 13.757 | 11.087 | 4.5032 |
| 2008 | 1.8795 | 3.7935 | 2.7087 | 17.435 | 12.26 | 5.508 |
| 2008 | 1.636 | 3.7935 | 2.4976 | 16.766 | 13.433 | 4.7544 |
| 2008 | 2.123 | 3.2945 | 1.8644 | 15.763 | 10.383 | 4.7544 |
| 2008 | 1.3925 | 4.043 | 2.4976 | 17.101 | 12.495 | 5.0056 |
| 2008 | 1.8795 | 4.043 | 2.9198 | 17.435 | 13.668 | 5.0056 |
| 2008 | 1.636 | 3.7935 | 2.0754 | 16.432 | 12.729 | 6.0104 |
| 2008 | 1.3925 | 2.7955 | 2.0754 | 12.085 | 9.6786 | 4.0008 |
| 2008 | 2.3666 | 3.544 | 2.9198 | 16.097 | 12.025 | 5.7592 |
| 2008 | 1.636 | 3.544 | 2.0754 | 15.094 | 12.729 | 4.7544 |
| 2008 | 1.636 | 3.045 | 2.0754 | 13.423 | 9.6786 | 4.252 |
| 2008 | 2.123 | 3.544 | 2.4976 | 13.757 | 11.321 | 5.508 |
| 2008 | 1.8795 | 3.045 | 1.6533 | 11.751 | 10.852 | 4.0008 |
| 2008 | 1.636 | 3.544 | 2.4976 | 15.094 | 12.495 | 4.5032 |
| 2008 | 1.8795 | 2.546 | 1.8644 | 10.748 | 9.444 | 4.252 |
| 2008 | 1.636 | 2.546 | 1.2311 | 8.4071 | 6.8626 | 2.4937 |

| | | | | | | |
|---|---|---|---|---|---|---|
| 2008 | 1.3925 | 2.7955 | 1.4422 | 9.0758 | 7.332 | 3.4985 |
| 2008 | 2.3666 | 3.2945 | 2.7087 | 15.094 | 11.791 | 6.2616 |
| 2008 | 1.636 | 2.7955 | 1.6533 | 11.416 | 9.2093 | 4.5032 |
| 2008 | 1.636 | 3.544 | 2.0754 | 13.088 | 11.321 | 4.252 |
| 2009 | 2.2399 | 4.9507 | 2.8334 | 18.247 | 14.427 | 5.0375 |
| 2009 | 2.4889 | 5.408 | 3.2151 | 19.866 | 14.22 | 6.0158 |
| 2009 | 2.2399 | 5.408 | 3.2151 | 19.597 | 13.805 | 5.7712 |
| 2009 | 2.2399 | 4.722 | 3.4059 | 19.057 | 14.22 | 6.505 |
| 2009 | 1.9909 | 4.2646 | 2.4517 | 15.278 | 11.939 | 4.7929 |
| 2009 | 2.2399 | 4.4933 | 2.8334 | 16.627 | 12.976 | 5.5266 |
| 2009 | 2.4889 | 4.9507 | 3.2151 | 18.787 | 14.427 | 5.7712 |
| 2009 | 2.4889 | 5.408 | 3.4059 | 21.216 | 15.671 | 6.0158 |
| 2009 | 2.4889 | 5.408 | 3.7876 | 20.406 | 15.256 | 5.7712 |
| 2009 | 1.9909 | 5.408 | 3.0242 | 20.136 | 15.671 | 7.7279 |
| 2009 | 2.7379 | 4.9507 | 3.4059 | 20.406 | 15.878 | 5.7712 |
| 2009 | 2.4889 | 4.2646 | 3.4059 | 17.437 | 13.39 | 5.5266 |
| 2009 | 2.2399 | 4.9507 | 3.2151 | 16.627 | 12.354 | 5.5266 |
| 2009 | 1.9909 | 4.4933 | 2.8334 | 15.548 | 11.939 | 5.0375 |
| 2009 | 2.4889 | 4.722 | 3.0242 | 16.627 | 12.976 | 5.0375 |
| 2009 | 2.4889 | 5.6367 | 3.4059 | 20.136 | 16.293 | 6.0158 |
| 2009 | 2.4889 | 4.722 | 3.4059 | 19.597 | 15.049 | 6.7496 |
| 2009 | 2.2399 | 4.9507 | 3.4059 | 17.167 | 13.598 | 5.7712 |
| 2009 | 2.2399 | 5.6367 | 3.4059 | 20.406 | 15.671 | 6.0158 |
| 2009 | 2.2399 | 5.6367 | 3.2151 | 18.787 | 13.598 | 6.0158 |
| 2009 | 2.4889 | 4.4933 | 3.0242 | 16.897 | 13.598 | 5.7712 |
| 2009 | 2.2399 | 4.2646 | 2.8334 | 14.198 | 10.281 | 4.5483 |
| 2009 | 2.7379 | 4.722 | 3.2151 | 17.977 | 13.805 | 5.0375 |
| 2009 | 2.7379 | 4.9507 | 3.2151 | 18.787 | 15.049 | 6.0158 |
| 2009 | 1.7419 | 4.0359 | 3.0242 | 15.008 | 11.525 | 4.7929 |
| 2009 | 2.2399 | 4.722 | 3.2151 | 16.897 | 13.39 | 4.7929 |
| 2009 | 2.2399 | 4.4933 | 3.2151 | 16.087 | 12.769 | 5.5266 |
| 2009 | 2.2399 | 4.9507 | 3.2151 | 17.437 | 13.39 | 6.0158 |
| 2009 | 2.2399 | 4.4933 | 2.8334 | 14.468 | 12.976 | 4.7929 |
| 2009 | 1.9909 | 3.3498 | 2.4517 | 11.229 | 8.6223 | 3.5699 |
| 2009 | 2.4889 | 4.4933 | 3.0242 | 14.468 | 11.525 | 5.0375 |
| 2009 | 2.2399 | 4.9507 | 3.4059 | 16.897 | 13.598 | 5.7712 |
| 2009 | 2.7379 | 5.408 | 3.2151 | 16.087 | 13.805 | 5.5266 |
| 2009 | 2.4889 | 4.4933 | 3.0242 | 16.627 | 13.598 | 5.7712 |

Table A2.10.2 Samples of Pure Pixel – Bare Ground

| Year | B1 | B2 | B3 | B4 | B5 | B6 |
|---|---|---|---|---|---|---|
| 2005 | 15 | 23 | 32 | 23 | 38 | 30 |
| 2005 | 10 | 17 | 25 | 24 | 35 | 25 |
| 2005 | 19 | 27 | 36 | 25 | 38 | 30 |
| 2005 | 10 | 17 | 26 | 22 | 36 | 26 |
| 2005 | 14 | 21 | 29 | 23 | 40 | 30 |
| 2005 | 16 | 24 | 32 | 24 | 42 | 33 |
| 2005 | 11 | 18 | 29 | 24 | 36 | 25 |
| 2005 | 10 | 17 | 26 | 23 | 35 | 24 |
| 2005 | 9 | 15 | 23 | 22 | 32 | 21 |
| 2006 | 9.4038 | 15.9031 2 | 0.4308 | 22.256 | 31.5804 | 23.0581 |
| 2006 | 6.9057 | 12.8540 1 | 6.1357 | 24.2136 | 28.8541 | 17.9146 |
| 2006 | 15.7879 | 22.0012 2 | 9.247 | 21.9297 | 34.0589 | 27.9445 |
| 2006 | 9.1262 | 14.2399 1 | 9.3005 | 23.2348 | 29.8455 | 19.7148 |
| 2006 | 9.4038 | 15.3487 2 | 2.0132 | 23.8874 | 30.8369 | 21.5151 |
| 2006 | 12.7346 | 19.2293 2 | 6.7604 | 23.5611 | 32.5718 | 24.344 |
| 2006 | 8.016 | 13.4084 1 | 9.3005 | 22.5823 | 34.0589 | 23.3153 |
| 2006 | 6.073 | 11.4680 1 | 4.5533 | 22.5823 | 29.102 | 18.9433 |
| 2006 | 6.9057 | 11.4680 1 | 6.1357 | 21.9297 | 33.811 | 22.801 |
| 2007 | 12.919 | 20.6283 2 | 9.2575 | 24.9764 | 35.8481 | 27.1238 |
| 2007 | 6.2165 | 11.4251 1 | 4.3786 | 26.5122 | 29.7273 | 17.8481 |
| 2007 | 17.0682 | 24.4877 3 | 2.5639 | 22.6727 | 32.0226 | 26.0637 |
| 2007 | 6.5356 | 12.3158 1 | 5.5595 | 24.2085 | 28.1971 | 19.4382 |
| 2007 | 12.5998 | 20.0346 2 | 8.7852 | 23.8245 | 31.0025 | 22.6185 |
| 2007 | 16.749 | 23.8940 3 | 2.5639 | 25.7443 | 34.828 | 27.6538 |
| 2007 | 10.0465 | 16.7689 2 | 2.8808 | 24.2085 | 34.573 | 25.5337 |
| 2007 | 4.9398 | 9.9407 1 | 1.3083 | 23.4406 | 26.6669 | 15.1979 |
| 2007 | 11.9615 | 18.8470 2 | 4.534 | 26.1282 | 39.4186 | 28.7139 |
| 2008 | 11.8642 | 19.2625 3 | 1.6266 | 21.7816 | 36.6653 | 26.8598 |
| 2008 | 11.1336 | 19.0130 2 | 5.9274 | 22.4503 | 35.7266 | 26.3574 |
| 2008 | 13.5688 | 21.2585 2 | 9.938 | 21.1129 | 31.5026 | 25.3526 |
| 2008 | 8.2112 | 13.5240 1 | 7.2732 | 20.4442 | 28.9213 | 18.8215 |
| 2008 | 10.89 | 16.7675 2 | 5.2942 | 19.4411 | 26.1053 | 20.8311 |
| 2008 | 13.0818 | 18.7635 2 | 4.872 | 19.4411 | 27.2786 | 20.8311 |
| 2008 | 9.1854 | 15.5200 2 | 1.4948 | 21.1129 | 28.6866 | 19.8263 |
| 2008 | 5.2889 | 9.7815 1 | 1.574 | 21.1129 | 23.9933 | 13.7975 |
| 2008 | 9.1854 | 15.2705 2 | 0.6504 | 21.7816 | 31.972 | 21.5846 |
| 2009 | 10.9548 | 16.3852 | 24.0173 | 19.5965 | 28.7313 | 22.1586 |
| 2009 | 8.4648 | 12.9548 | 17.3377 | 19.5965 | 26.8655 | 17.7561 |
| 2009 | 13.1958 | 19.8155 | 26.6892 | 17.9769 | 29.1459 | 22.8924 |
| 2009 | 6.2238 | 10.4392 | 12.7574 | 18.7867 | 23.7559 | 15.0656 |
| 2009 | 9.9588 | 15.6991 | 21.3455 | 19.0566 | 26.4509 | 19.9574 |
| 2009 | 12.4488 | 17.2999 | 24.0173 | 17.9769 | 28.524 | 21.9141 |
| 2009 | 7.9668 | 12.04 | 15.8109 | 19.3266 | 26.4509 | 18.0006 |

| | | | | | | |
|---|---|---|---|---|---|---|
| 2009 | 3.9828 | 7.6949 | 8.1771 | 19.5965 | 21.8901 | 12.6197 |
| 2009 | 7.9668 | 12.04 | 15.2384 | 18.7867 | 29.9751 | 20.6911 |

Table A2.10.3 Samples of Pure Pixel – Big Grey Roof

| Year | B1 | B2 | B3 | B4 | B5 | B6 |
|---|---|---|---|---|---|---|
| 2005 | 9 | 9 | 7 | 10 | 47 | 48 |
| 2005 | 8 | 9 | 7 | 10 | 47 | 47 |
| 2005 | 9 | 10 | 9 | 9 | 34 | 35 |
| 2005 | 9 | 9 | 7 | 10 | 48 | 51 |
| 2005 | 9 | 9 | 7 | 10 | 48 | 51 |
| 2005 | 9 | 10 | 7 | 10 | 49 | 52 |
| 2005 | 9 | 10 | 7 | 10 | 50 | 54 |
| 2005 | 9 | 9 | 8 | 8 | 35 | 36 |
| 2005 | 9 | 11 | 9 | 11 | 46 | 50 |
| 2005 | 11 | 11 | 9 | 11 | 46 | 49 |
| 2005 | 9 | 10 | 9 | 10 | 37 | 41 |
| 2005 | 11 | 12 | 10 | 11 | 48 | 50 |
| 2006 | 9.1262 | 9.5277 | 7.0934 | 9.5313 | 51.4081 | 53.6622 |
| 2006 | 8.5711 | 9.5277 | 7.0934 | 9.5313 | 52.3995 | 52.8907 |
| 2006 | 9.1262 | 10.0821 | 9.128 | 8.5525 | 33.5632 | 34.3739 |
| 2006 | 8.8487 | 9.2505 | 6.8674 | 9.5313 | 55.8693 | 50.3189 |
| 2006 | 8.8487 | 9.2505 | 7.3195 | 10.1839 | 47.4426 | 50.3189 |
| 2006 | 9.1262 | 10.0821 | 7.3195 | 9.5313 | 48.9296 | 51.3476 |
| 2006 | 9.4038 | 10.6365 | 7.3195 | 9.5313 | 50.1689 | 53.1479 |
| 2006 | 8.8487 | 9.5277 | 7.7716 | 8.2262 | 35.2981 | 35.6598 |
| 2006 | 9.4038 | 11.468 | 9.5801 | 10.5101 | 46.2033 | 49.5474 |
| 2006 | 10.7916 | 11.468 | 9.354 | 10.8364 | 45.7076 | 48.2615 |
| 2006 | 9.6814 | 10.6365 | 8.6758 | 9.8576 | 37.033 | 40.8034 |
| 2006 | 11.3468 | 12.5768 | 10.0322 | 10.8364 | 47.4426 | 49.2902 |
| 2007 | 10.0465 | 10.5345 | 7.5296 | 10.7701 | 48.0897 | 48.0604 |
| 2007 | 10.0465 | 10.5345 | 7.2934 | 11.154 | 49.6199 | 50.1805 |
| 2007 | 9.4082 | 10.5345 | 7.0572 | 10.3861 | 41.2038 | 40.9048 |
| 2007 | 10.0465 | 10.5345 | 6.821 | 11.154 | 48.5997 | 49.6505 |
| 2007 | 10.3657 | 11.1283 | 7.2934 | 11.154 | 49.1098 | 49.9155 |
| 2007 | 10.3657 | 10.8314 | 7.5296 | 10.7701 | 50.385 | 51.2406 |
| 2007 | 10.3657 | 11.1283 | 8.2381 | 11.154 | 50.895 | 52.5657 |
| 2007 | 9.7273 | 10.8314 | 7.5296 | 10.3861 | 40.4387 | 38.5196 |
| 2007 | 10.6848 | 11.722 | 9.1828 | 12.6899 | 47.3246 | 50.9756 |
| 2007 | 10.6848 | 11.722 | 9.6551 | 12.6899 | 47.0695 | 50.4455 |
| 2007 | 10.0465 | 10.8314 | 9.1828 | 11.154 | 42.2239 | 42.76 |
| 2007 | 11.004 | 12.6126 | 10.5998 | 12.6899 | 45.7944 | 48.3254 |

| | | | | | | |
|---|---|---|---|---|---|---|
| 2008 | 10.6465 | 11.2785 | 8.1968 | 11.4164 | 48.868 | 48.9651 |
| 2008 | 10.1595 | 11.029 | 8.1968 | 11.4164 | 51.2147 | 52.2307 |
| 2008 | 9.6724 | 10.7795 | 8.1968 | 10.4133 | 40.8893 | 42.6852 |
| 2008 | 9.9159 | 11.029 | 7.7746 | 11.4164 | 49.1027 | 50.2211 |
| 2008 | 10.89 | 11.7775 | 8.6189 | 11.4164 | 49.1027 | 50.9747 |
| 2008 | 11.1336 | 11.7775 | 8.6189 | 11.7507 | 51.4493 | 49.4675 |
| 2008 | 10.6465 | 11.2785 | 8.4078 | 12.0851 | 53.796 | 54.9939 |
| 2008 | 10.1595 | 11.7775 | 8.4078 | 10.7476 | 41.3586 | 39.922 |
| 2008 | 10.403 | 11.029 | 9.6743 | 13.0882 | 48.3987 | 50.9747 |
| 2008 | 10.1595 | 11.7775 | 9.4632 | 13.4225 | 47.9293 | 49.7187 |
| 2008 | 9.9159 | 11.2785 | 9.0411 | 12.0851 | 43.236 | 41.4292 |
| 2008 | 11.1336 | 11.7775 | 9.8854 | 13.0882 | 47.9293 | 49.7187 |
| 2009 | 11.7018 | 13.1835 | 10.6581 | 12.5784 | 48.633 | 49.5526 |
| 2009 | 11.4528 | 13.4122 | 9.513 | 12.3085 | 50.706 | 52.9768 |
| 2009 | 11.7018 | 12.7261 | 9.513 | 11.2287 | 41.7918 | 44.4162 |
| 2009 | 11.4528 | 12.9548 | 9.1313 | 12.0385 | 49.0476 | 50.0417 |
| 2009 | 11.9508 | 13.4122 | 10.4672 | 12.5784 | 47.5964 | 50.0417 |
| 2009 | 12.4488 | 13.4122 | 10.8489 | 12.5784 | 48.4256 | 50.0417 |
| 2009 | 11.4528 | 13.6409 | 10.6581 | 12.3085 | 49.8768 | 51.5093 |
| 2009 | 11.2038 | 12.9548 | 10.4672 | 11.4987 | 42.2064 | 42.9487 |
| 2009 | 11.7018 | 13.4122 | 11.4215 | 12.8483 | 41.3771 | 41.9703 |
| 2009 | 11.9508 | 13.6409 | 11.6123 | 12.8483 | 41.9991 | 41.9703 |
| 2009 | 10.9548 | 12.4974 | 10.6581 | 12.3085 | 36.8163 | 35.1218 |
| 2009 | 11.9508 | 14.5556 | 13.5208 | 12.8483 | 44.0722 | 44.4162 |

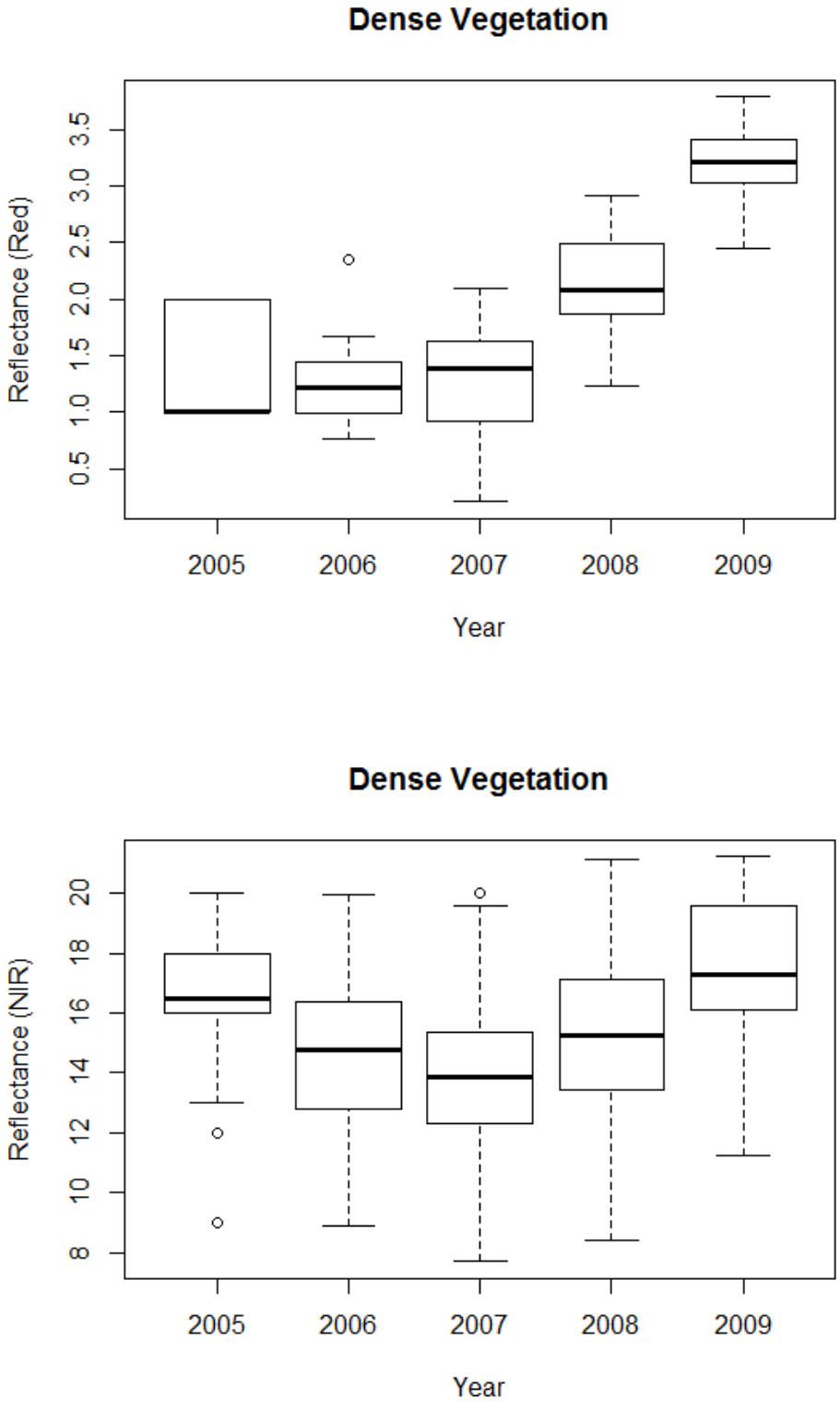


Figure A2.10.4 Pure Pixel of Dense Vegetation with red and NIR reflectance.

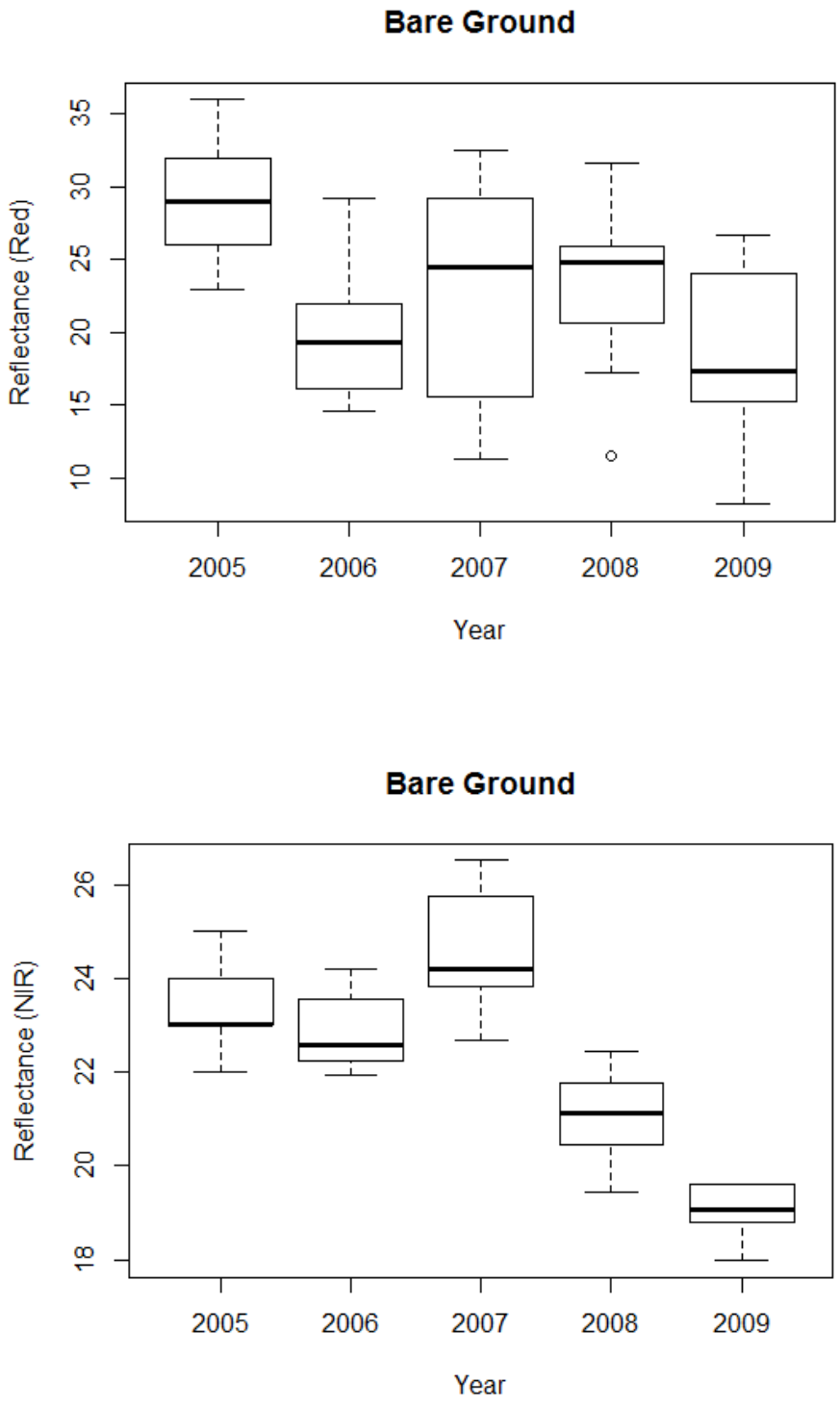


Figure A2.10.5 Pure Pixel of Bare Ground with red and NIR reflectance.

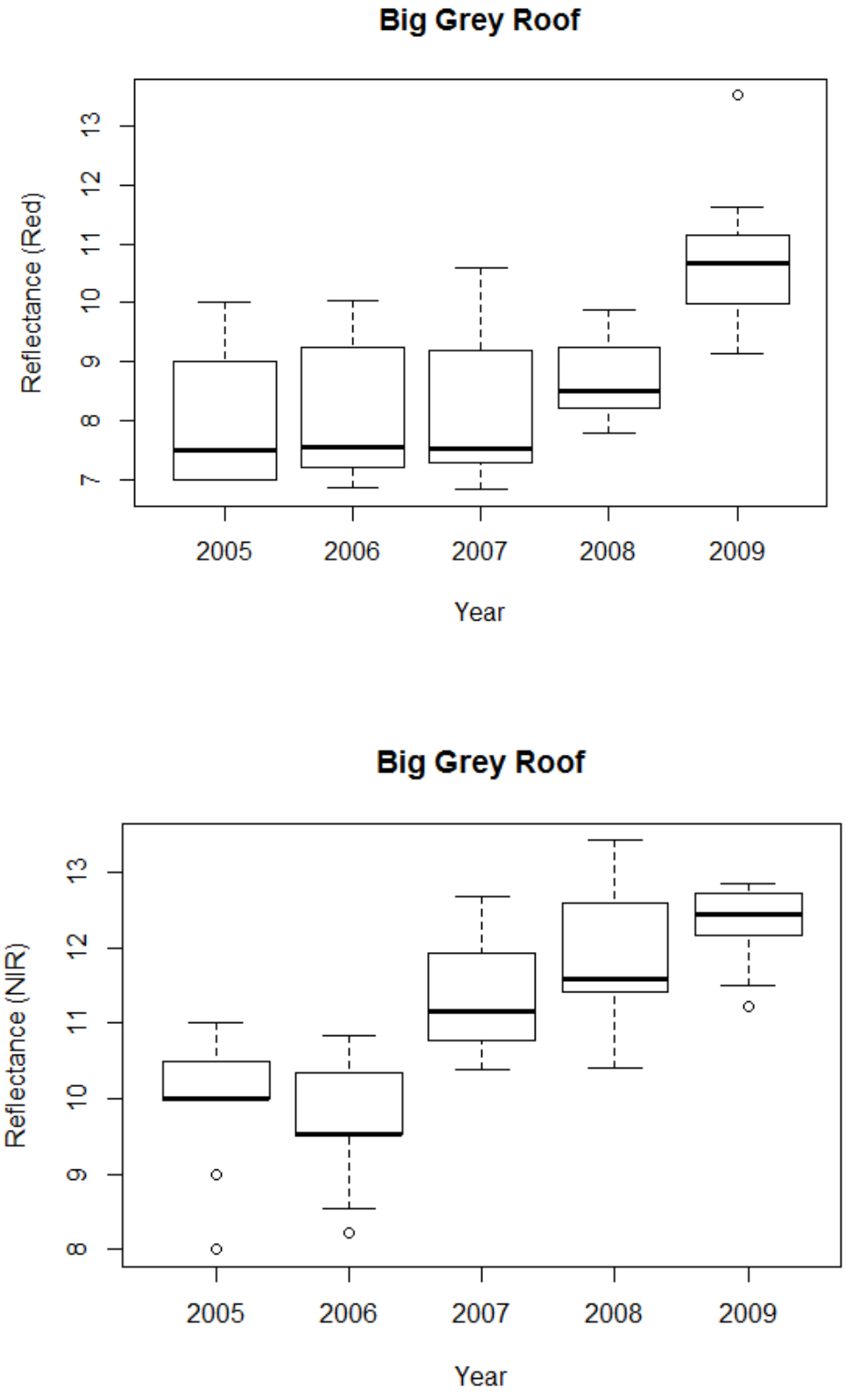


Figure A2.10.6 Pure Pixel of Bare Ground with red and NIR reflectance.

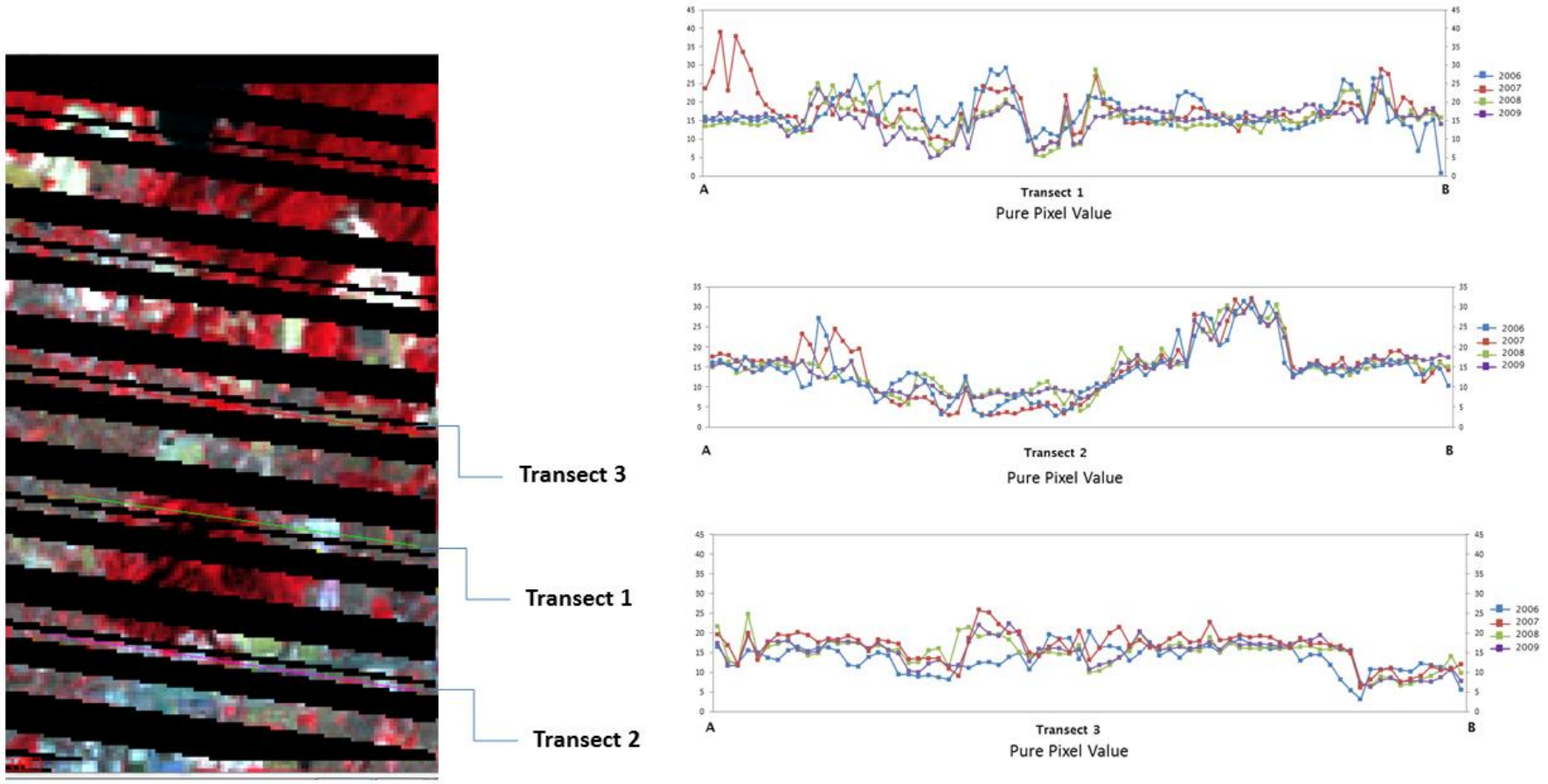


Figure A2.10.7 Transect for 3 areas of Landsat ETM+2006 to 2009.

# Appendix 3 : Geometric corrections

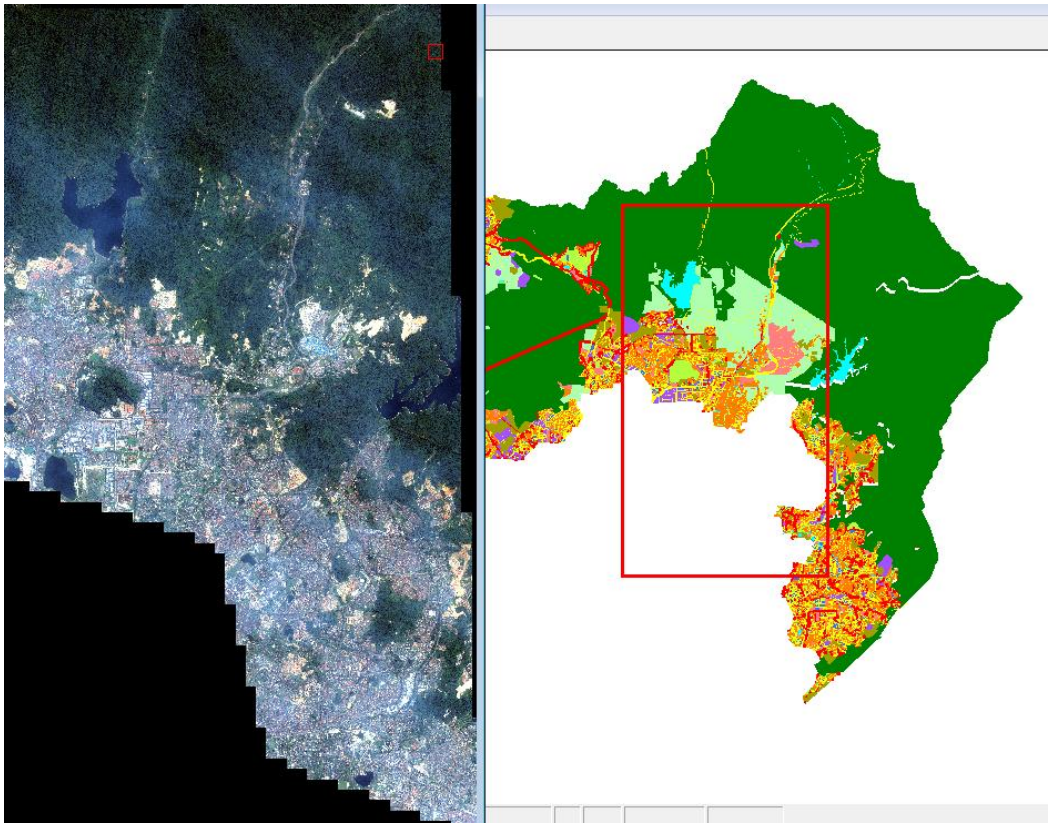

Figure A3.10.8 Study Area at Gombak District, Selangor, Peninsular Malaysia.

**1) IKONOS 2005**
Source Image ID: 2009030403412690000010907616
Product Image ID: 003
Sensor: IKONOS-2
Acquired Nominal GSD
  Pan Cross Scan: 0.86 meters
  Pan Along Scan: 0.88 meters
Scan Azimuth: 0.00 degrees
Scan Direction: Forward
Panchromatic TDI Mode: 13
Nominal Collection Azimuth: 32.6771 degrees
Nominal Collection Elevation: 73.01476 degrees
Sun Angle Azimuth: 46.9962 degrees
Sun Angle Elevation: 60.90609 degrees
Acquisition Date/Time: 2009-03-04 03:41 GMT
Percent Cloud Cover: 3
Product Line: Geo
Processing Level: Standard Geometrically Corrected
Image Type: PAN/MSI
Interpolation Method: Cubic Convolution
Multispectral Algorithm: Projective
Stereo: Mono
Mosaic: No
Map Projection: Universal Transverse Mercator
  UTM Specific Parameters
    Hemisphere: N
    Zone Number: 47
Datum: WGS84

Product Order Pixel Size: 1.0000000000 meters
Product Order Map Units:  meters
MTFC Applied: Yes
DRA Applied: No
Media: DVD
Product Media Format: DVD
File Format: GeoTIFF
  TIFF Tiled: No
  Compressed: No
  Bits per Pixel per Band: 11 bits per pixel
Multispectral Files: RGB

**2) IKONOS 2009**
Source Image ID: 2009030403412690000010907616
Product Image ID: 003
Sensor: IKONOS-2
Acquired Nominal GSD
  Pan Cross Scan: 0.8670490980 meters
  Pan Along Scan: 0.8406801820 meters
  MS Cross Scan: 3.4681963921 meters
  MS Along Scan: 3.3627207279 meters
Scan Azimuth: 179.9978056880 degrees
Scan Direction: Reverse
Panchromatic TDI Mode: 13
Nominal Collection Azimuth: 89.3600 degrees
Nominal Collection Elevation: 75.83155 degrees
Sun Angle Azimuth: 109.9884 degrees
Sun Angle Elevation: 62.33025 degrees
Acquisition Date/Time: 2009-03-04 03:41 GMT
Percent Cloud Cover: 4

Product Line: Geo
Processing Level: Standard Geometrically Corrected
Image Type: PAN/MSI
Interpolation Method: Cubic Convolution
Multispectral Algorithm: Projective
Stereo: Mono
Mosaic: No
Map Projection: Universal Transverse Mercator
  UTM Specific Parameters
    Hemisphere: N
    Zone Number: 47
Datum: WGS84
Product Order Pixel Size: 1.0000000000 meters
Product Order Map Units:  meters
MTFC Applied: Yes
DRA Applied: No
Media: DVD
Product Media Format: DVD
File Format: GeoTIFF
  TIFF Tiled: No
  Compressed: No
  Bits per Pixel per Band: 11 bits per pixel
Multispectral Files: BGRN


Figure A3.10.9 Image to Image registration of IKONOS 2005 and IKONOS 2009

Table A3.1 GCPs Image to Image Registration for IKONOS 2005 and 2009

| Points | Base X | Base Y | Wrap X | Wrap Y | Predict X | Predict Y | Error X | Error Y | RMS Error |
|---|---|---|---|---|---|---|---|---|---|
| 1 | 44.50 | 2367.00 | 555.75 | 3236.50 | 555.82 | 3236.68 | 0.07 | 0.18 | 0.19 |
| 2 | 2809.00 | 1678.50 | 3311.00 | 2527.25 | 3311.05 | 2527.30 | 0.05 | 0.05 | 0.07 |
| 3 | 2661.50 | 3807.50 | 3171.25 | 4677.50 | 3171.57 | 4677.32 | 0.32 | -0.18 | 0.36 |
| 4 | 2666.00 | 3811.50 | 3187.00 | 4637.00 | 3120.61 | 4653.12 | 0.28 | -0.14 | 0.32 |
| 5 | 2583.75 | 3763.25 | 3094.00 | 4632.25 | 3093.63 | 4632.56 | -0.37 | 0.31 | 0.48 |
| 6 | 2623.75 | 3686.50 | 3133.75 | 4555.25 | 3133.38 | 4555.16 | -0.37 | -0.09 | 0.38 |
| 7 | 1256.25 | 4993.25 | 1766.50 | 5864.50 | 1766.59 | 5864.71 | 0.09 | 0.21 | 0.23 |
| 8 | 112.00 | 3417.75 | 621.66 | 4285.18 | 621.56 | 4284.88 | -0.10 | -0.30 | 0.32 |
| 9 | 2362.25 | 4813.00 | 2875.12 | 5690.42 | 2875.12 | 5690.42 | -0.00 | -0.00 | 0.00 |
| 10 | 2360.75 | 4965.50 | 2874.06 | 5844.12 | 2874.06 | 5844.12 | -0.00 | 0.00 | 0.00 |
| 11 | 105.00 | 4448.25 | 612.99 | 5313.18 | 612.99 | 5313.18 | -0.00 | 0.00 | 0.00 |
| 12 | 220.00 | 4480.25 | 728.14 | 5345.62 | 728.14 | 5345.62 | 0.00 | -0.00 | 0.00 |
| 13 | 280.50 | 744.50 | 793.17 | 1615.17 | 793.17 | 1615.17 | 0.00 | -0.00 | 0.00 |
| 14 | 1182.50 | 2498.50 | 1691.16 | 3362.76 | 1691.16 | 3362.76 | -0.00 | 0.00 | 0.00 |
| 15 | 1267.00 | 2464.00 | 1775.45 | 3327.78 | 1775.45 | 3327.78 | -0.00 | -0.00 | 0.00 |
| 16 | 885.50 | 2099.75 | 1394.79 | 2964.80 | 1394.79 | 2964.80 | 0.00 | 0.00 | 0.00 |
| 17 | 967.25 | 1980.00 | 1476.28 | 2844.33 | 1476.28 | 2844.33 | 0.00 | 0.00 | 0.00 |
| 18 | 816.75 | 2308.00 | 1326.22 | 3173.70 | 1326.22 | 3173.70 | -0.00 | 0.00 | 0.00 |
| 19 | 1713.50 | 4547.50 | 2224.37 | 5419.76 | 2224.37 | 5419.76 | 0.00 | 0.00 | 0.00 |
| 20 | 1938.50 | 4552.50 | 2449.81 | 5425.85 | 2449.81 | 5425.85 | -0.00 | -0.00 | 0.01 |

Number of selected points = 20
Total RMS Error = 0.204391

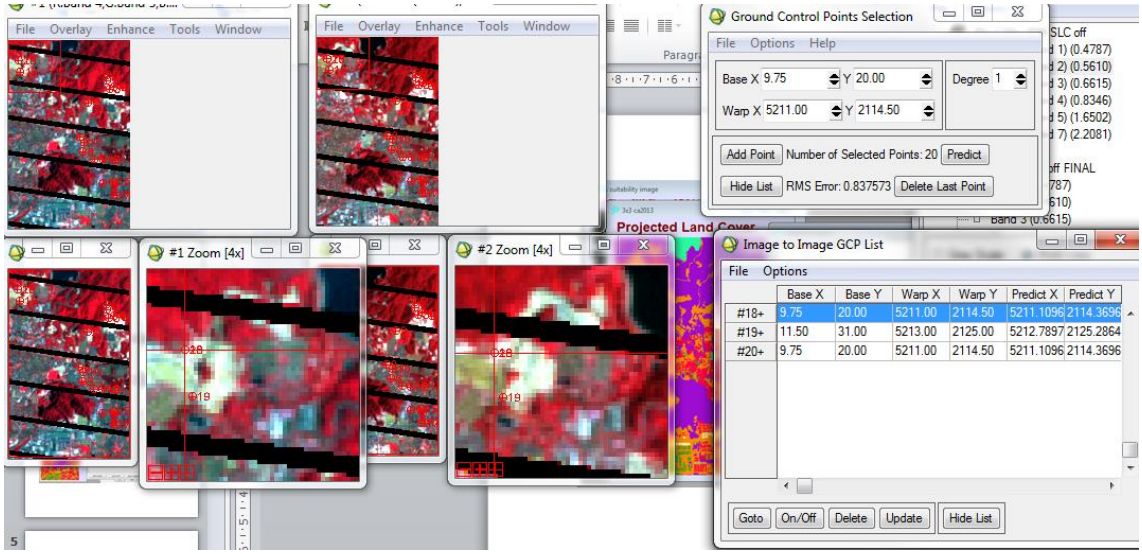


Figure A3.10.10 Image to Image registration of Landsat ETM+ 2005 and 2006.

Table A3.2 GCPs Image to Image Registration for Landsat ETM+ 2005 and 2006.

| Points | Base X | Base Y | Wrap X | Wrap Y | Predict X | Predict Y | Error X | Error Y | RMS Error |
|---|---|---|---|---|---|---|---|---|---|
| 1 | 100.00 | 45.00 | 5301.63 | 2137.08 | 5301.14 | 2138.26 | -0.49 | 1.18 | 1.28 |
| 2 | 75.25 | 60.00 | 5276.00 | 2154.25 | 5276.36 | 2153.58 | 0.36 | -0.67 | 0.76 |
| 3 | 95.75 | 47.00 | 5297.25 | 2139.50 | 5296.89 | 2140.32 | -0.36 | 0.82 | 0.90 |
| 4 | 100.00 | 45.00 | 5301.63 | 2137.08 | 5301.14 | 2138.26 | -0.49 | 1.18 | 1.28 |
| 5 | 93.75 | 33.75 | 5294.75 | 2127.50 | 5294.92 | 2127.02 | 0.17 | -0.48 | 0.51 |
| 6 | 110.50 | 45.50 | 5310.25 | 2140.50 | 5311.63 | 2138.66 | 1.38 | -1.84 | 2.31 |
| 7 | 93.00 | 39.00 | 5294.75 | 2132.50 | 5294.16 | 2132.30 | -0.59 | -0.20 | 0.62 |
| 8 | 70.50 | 106.25 | 5271.75 | 2200.00 | 5271.45 | 2199.99 | -0.30 | -0.01 | 0.30 |
| 9 | 67.75 | 92.50 | 5267.75 | 2187.00 | 5268.74 | 2186.22 | 0.99 | -0.78 | 1.26 |
| 10 | 71.75 | 97.75 | 5273 | 2190.75 | 5272.73 | 2191.47 | -0.27 | 0.72 | 0.76 |
| 11 | 81.25 | 113.5 | 5282.5 | 2207 | 5282.2 | 2207.25 | -0.3 | 0.25 | 0.39 |
| 12 | 89.5 | 113.25 | 5290.5 | 2207.25 | 5290.47 | 2206.98 | -0.03 | -0.27 | 0.27 |
| 13 | 101.5 | 114.25 | 5303 | 2207.75 | 5302.49 | 2207.97 | -0.51 | 0.22 | 0.56 |
| 14 | 89.5 | 136.25 | 5290.5 | 2230 | 5290.4 | 2230.1 | -0.1 | 0.1 | 0.14 |
| 15 | 99 | 134.5 | 5299.5 | 2228.5 | 5299.94 | 2228.36 | 0.44 | -0.14 | 0.46 |
| 16 | 103 | 147.5 | 5303.75 | 2241.25 | 5303.92 | 2241.45 | 0.17 | 0.2 | 0.27 |
| 17 | 99.25 | 147 | 5300.25 | 2241.25 | 5300.16 | 2240.94 | -0.09 | -0.31 | 0.32 |
| 18 | 9.75 | 20 | 5211 | 2114.5 | 5211.11 | 2114.37 | 0.11 | -0.13 | 0.17 |
| 19 | 11.5 | 31 | 5213 | 2125 | 5212.79 | 2125.29 | -0.21 | 0.29 | 0.36 |
| 20 | 89.5 | 33.75 | 5290.5 | 2140.50 | 5282.2 | 2199.99 | 0.17 | -0.48 | 0.17 |

Number of selected points = 20
Total RMS Error = 0.837573

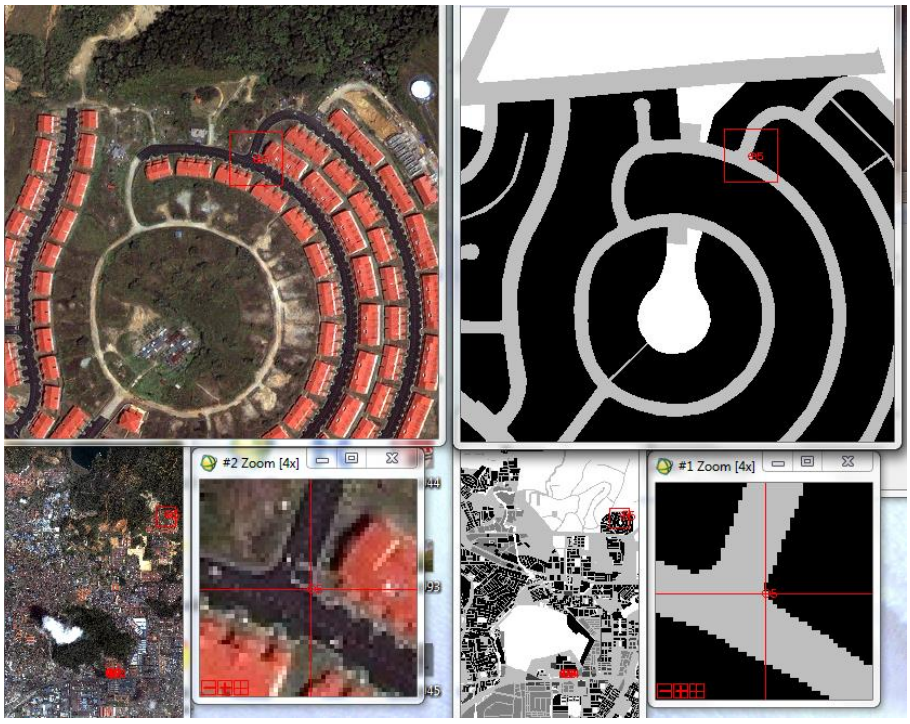


Figure A3.10.11 Image to Image registration of IKONOS 2009 and P2020.

# Appendix 4: Chapter 6 – Calibration and Standardisation

## b) Calibration and standardisation of the 2005 and 2007 images

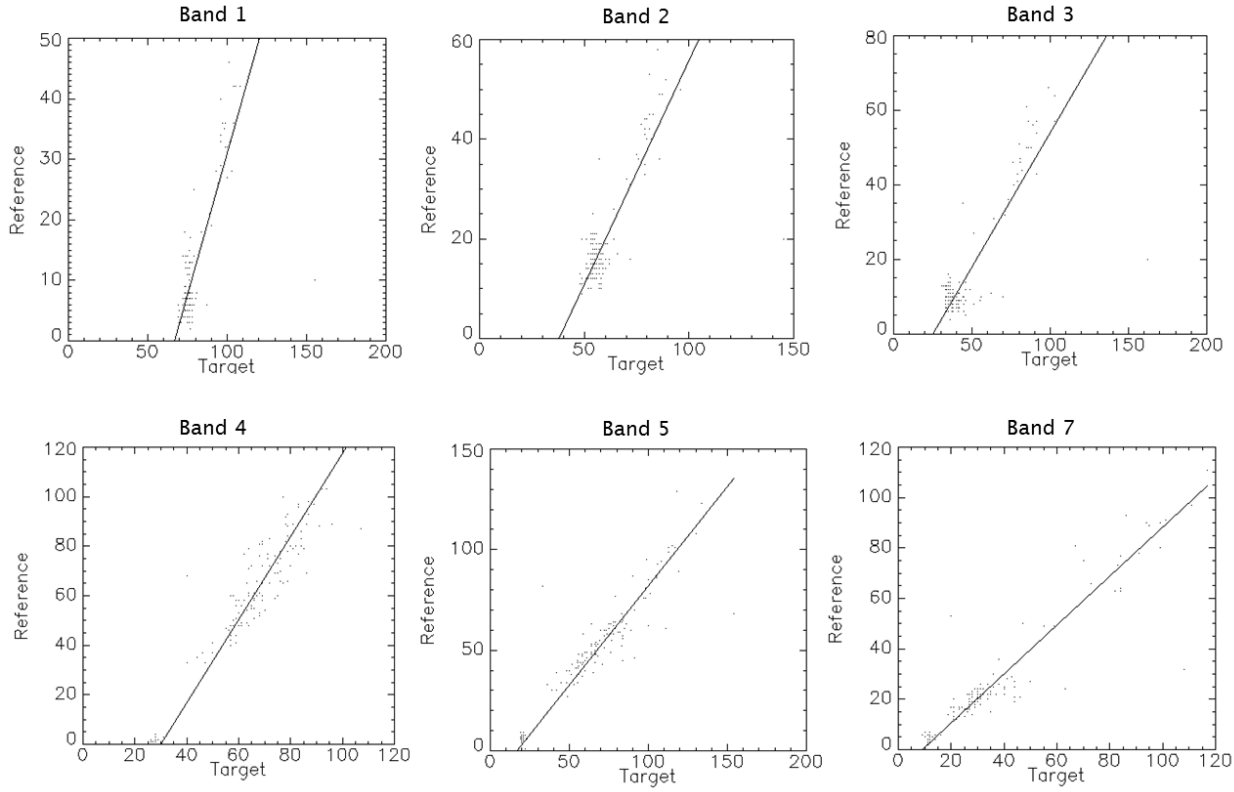


Figure A4.10.12 Regressions of the Landsat ETM+ 2005 reference scene on the Landsat ETM+2007 target (uncalibrated) scene.

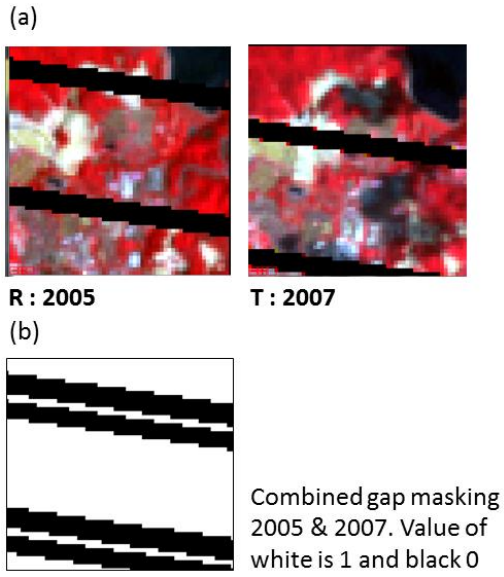


Figure A4.10.13 (a) Shows images 2005 and 2007 of the targets picked out as invariant, (b) combined gap masking.

Table A4.10.4 Orthogonal regression coefficients and statistics for radiometric normalisation of the images of Landsat ETM+2005 and Landsat ETM+2007.

| Band | Intercept | Sigma | Slope | Sigma | Correlation (r) | RMSE |
|---|---|---|---|---|---|---|
| 1 (0.4787) | -62.2991 | 5.4458 | 0.9303 | 0.0684 | 0.7489 | 5.4717 |
| 2 (0.5610) | -34.3616 | 4.0569 | 0.8978 | 0.0671 | 0.7438 | 6.1327 |
| 3 (0.6615) | -18.3319 | 2.0025 | 0.7226 | 0.0400 | 0.8323 | 7.1440 |
| 4 (0.8346) | -50.6691 | 3.6135 | 1.6776 | 0.0568 | 0.9260 | 6.3905 |
| 5 (1.6502) | -16.8259 | 2.5182 | 0.9897 | 0.0364 | 0.9145 | 8.5951 |
| 7 (2.2081) | -9.1870 | 1.3385 | 0.9732 | 0.0311 | 0.9333 | 6.4146 |

Table A4.10.5 Comparison of means and variances for Landsat ETM+2005 and Landsat ETM+2007, with *t*-test and *F*-test for 147 training and 74 test pixels.

| | Band 1 | Band 2 | Band 3 | Band 4 | Band 5 | Band 7 |
|---|---|---|---|---|---|---|
| Target mean | 78.5811 | 58.9730 | 46.3378 | 61.0270 | 61.9595 | 34.1757 |
| Reference mean | 10.4189 | 18.1081 | 14.6622 | 49.6622 | 43.7838 | 24.1486 |
| Normalised mean | 10.8055 | 18.5853 | 15.1502 | 51.7125 | 44.4933 | 24.0724 |
| t-Statistic | -0.5996 | -0.5793 | -0.5471 | -1.2072 | -0.4796 | 0.0818 |
| *P*-value | 0.5506 | 0.5642 | 0.5860 | 0.2312 | 0.6330 | 0.9350 |
| Target variance | 83.616638 | 119.97187 | 369.541809 | 406.602112 | 800.614685 | 494.475494 |
| Reference mean | 94.849487 | 125.82378 | 260.993835 | 1047.843140 | 866.089600 | 557.498230 |
| Normalised mean | 72.367973 | 96.70612 | 192.937561 | 1144.374634 | 784.155945 | 468.315186 |
| *F*-Statistic | 1.310656 | 1.301094 | 1.352737 | 1.092124 | 1.104486 | 1.190434 |
| *P*-value | 0.250144 | 0.263155 | 0.199190 | 0.707571 | 0.672284 | 0.458286 |

## c) Calibration and standardisation of the 2005 and 2008 images

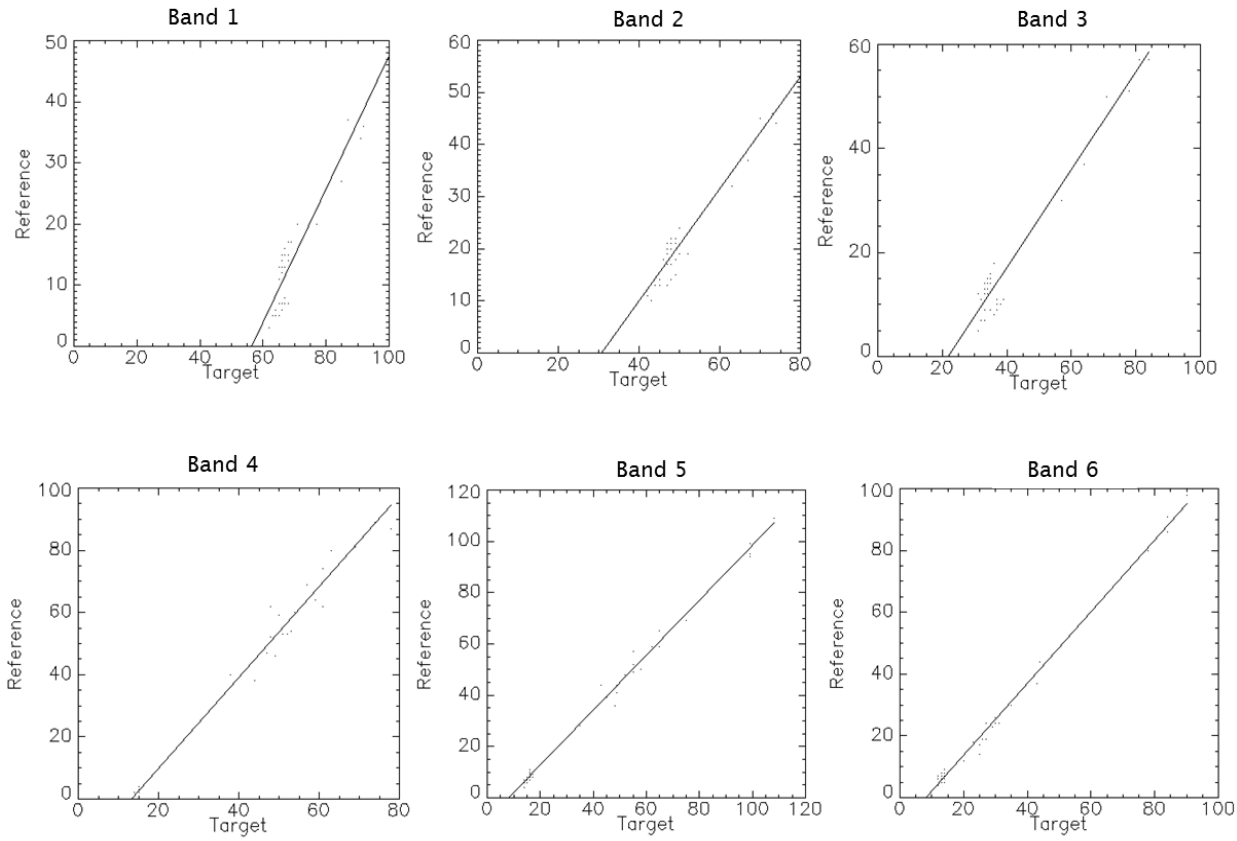


Figure A4.10.14 Regressions of the Landsat ETM+ 2005 reference scene on the Landsat ETM+2008 target (uncalibrated) scene.

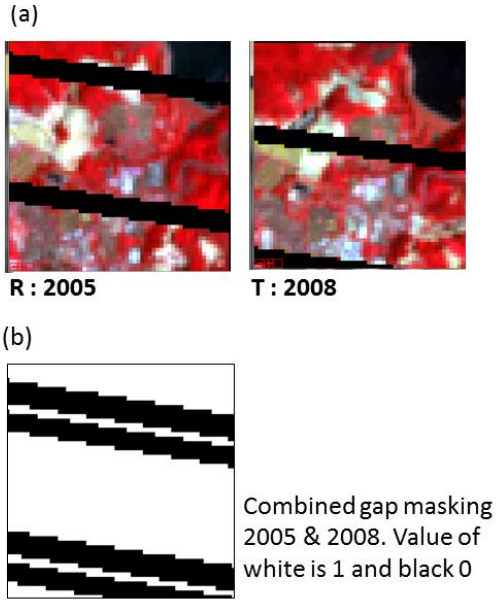


Figure A4.10.15 (a) Shows images 2005 and 2008 of the targets picked out as invariant, (b) combined gap masking.

Table A4.10.6 Orthogonal regression coefficients and statistics for radiometric normalisation of the images of Landsat ETM+2005 and Landsat ETM+2008.

| Band | Intercept | Sigma | Slope | Sigma | Correlation (r) | RMSE |
|---|---|---|---|---|---|---|
| 1 (0.4787) | -61.8780 | 4.8216 | 1.0951 | 0.0685 | 0.9363 | 2.4013 |
| 2 (0.5610) | -33.3803 | 2.5633 | 1.0803 | 0.0493 | 0.9646 | 1.8424 |
| 3 (0.6615) | -20.9770 | 1.6580 | 0.9462 | 0.0386 | 0.9714 | 2.4785 |
| 4 (0.8346) | -19.7161 | 1.2022 | 1.4646 | 0.0291 | 0.9930 | 2.2024 |
| 5 (1.6502) | -8.8761 | 0.7225 | 1.0737 | 0.0147 | 0.9966 | 1.7822 |
| 7 (2.2081) | -9.7724 | 0.5394 | 1.1660 | 0.0156 | 0.9968 | 1.3543 |

Table A4.10.7 Comparison of means and variances for Landsat ETM+2005 and Landsat ETM+2008, with *t*-test and *F*-test for 38 training and 19 test pixels.

| | Band 1 | Band 2 | Band 3 | Band 4 | Band 5 | Band 7 |
|---|---|---|---|---|---|---|
| Target mean | 68.1053 | 50.1579 | 38.5263 | 40.9474 | 41.7895 | 24.9474 |
| Reference mean | 12.1579 | 20.0526 | 14.4737 | 39.2105 | 35.8421 | 19.2105 |
| Normalised mean | 12.7008 | 20.8060 | 15.4760 | 40.2545 | 35.9934 | 19.3171 |
| t-Statistic | -0.6495 | -1.0789 | -1.3151 | -1.0056 | -0.2012 | -0.2027 |
| *P*-value | 0.5242 | 0.2949 | 0.2050 | 0.3279 | 0.8428 | 0.8416 |
| Target variance | 39.543858 | 50.584797 | 121.152046 | 762.052673 | 799.397644 | 254.497070 |
| Reference mean | 59.140354 | 58.719199 | 107.818695 | 1503.842041 | 943.251648 | 350.064331 |
| Normalised mean | 47.418629 | 59.036343 | 108.463715 | 1634.592773 | 921.575439 | 346.023560 |
| *F*-Statistic | 1.247197 | 1.005399 | 1.005982 | 1.086944 | 1.023521 | 1.011678 |
| *P*-value | 0.644315 | 0.991012 | 0.990044 | 0.861557 | 0.961209 | 0.980622 |

### d) Calibration and standardisation of the 2005 and 2009 image

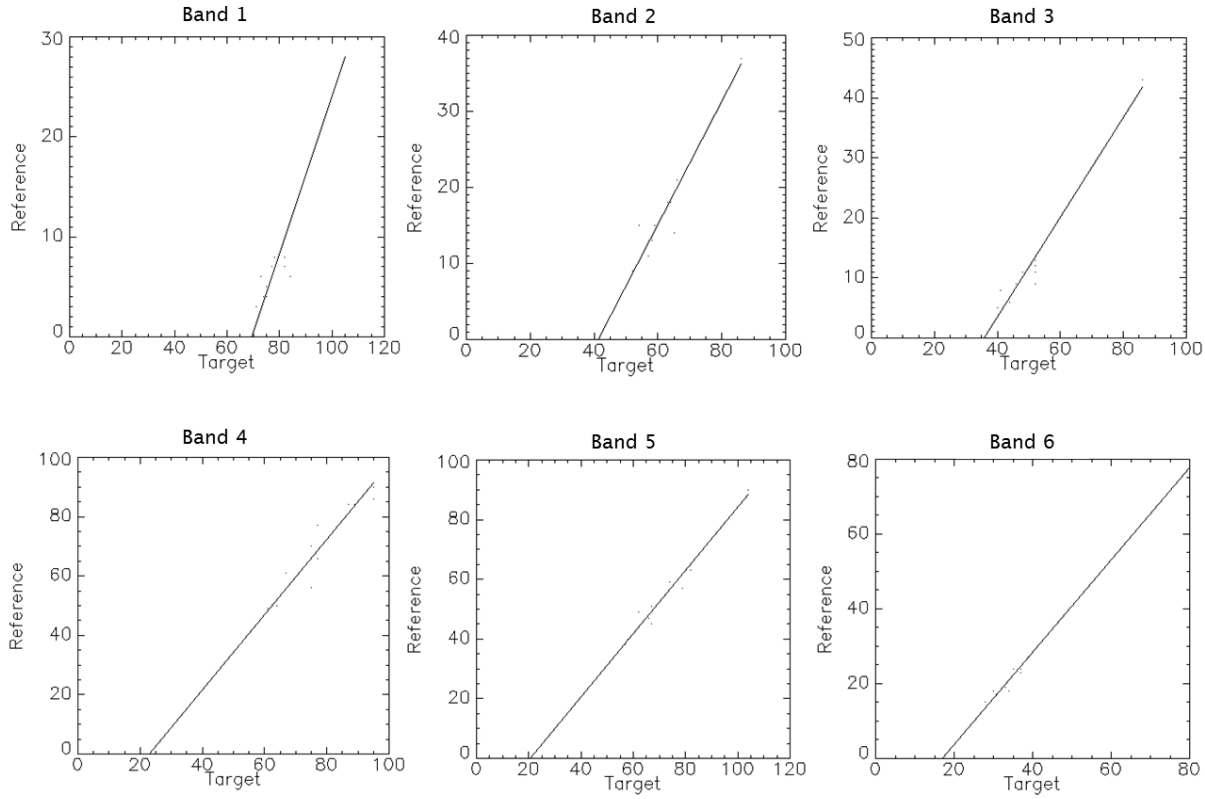


Figure A4.10.16 Regressions of the Landsat ETM+ 2005 reference scene on the Landsat ETM+2009 target (uncalibrated) scene.

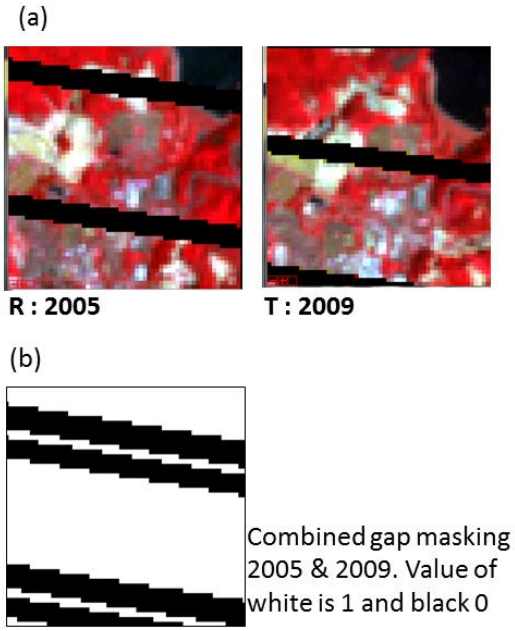


Figure A4.10.17 (a) Shows images 2005 and 2008 of the targets picked out as invariant, (b) combined gap masking.

Table A4.10.8 Orthogonal regression coefficients and statistics for radiometric normalisation of the images of Landsat ETM+2005 and Landsat ETM+2009.

| Band | Intercept | Sigma | Slope | Sigma | Correlation (r) | RMSE |
|---|---|---|---|---|---|---|
| 1 (0.4787) | -54.8190 | 7.4272 | 0.7888 | 0.0927 | 0.9435 | 2.1717 |
| 2 (0.5610) | -33.6089 | 5.6106 | 0.8124 | 0.0893 | 0.9499 | 2.0139 |
| 3 (0.6615) | -30.1540 | 3.1108 | 0.8355 | 0.0593 | 0.9781 | 1.8456 |
| 4 (0.8346) | -29.8799 | 12.1363 | 1.2780 | 0.1533 | 0.9413 | 3.5146 |
| 5 (1.6502) | -22.5744 | 5.3600 | 1.0682 | 0.0727 | 0.9798 | 2.2122 |
| 7 (2.2081) | -21.1840 | 1.4035 | 1.2369 | 0.0346 | 0.9965 | 1.0281 |

Table A4.10.9 Comparison of means and variances for Landsat ETM+2005 and Landsat ETM+2009, with *t*-test and *F*-test for 11 training and 6 test pixels.

| | Band 1 | Band 2 | Band 3 | Band 4 | Band 5 | Band 7 |
|---|---|---|---|---|---|---|
| Target mean | 80.0000 | 60.6667 | 50.6667 | 70.3333 | 65.5000 | 36.8333 |
| Reference mean | 9.6667 | 17.3333 | 13.5000 | 61.1667 | 48.1667 | 25.1667 |
| Normalised mean | 8.2868 | 15.6781 | 12.1761 | 60.0096 | 47.3897 | 24.3751 |
| t-Statistic | 1.2062 | 0.8518 | 1.0842 | 0.3777 | 0.2989 | 0.6497 |
| *P*-value | 0.2817 | 0.4332 | 0.3278 | 0.7212 | 0.7770 | 0.5445 |
| Target variance | 86.800003 | 77.066666 | 184.666656 | 122.666672 | 119.900002 | 163.766647 |
| Reference mean | 76.266655 | 99.066673 | 161.100006 | 420.166656 | 245.766693 | 274.966675 |
| Normalised mean | 54.010559 | 50.866562 | 128.896698 | 200.365036 | 136.80018 | 250.550171 |
| *F*-Statistic | 1.412069 | 1.947580 | 1.249838 | 2.097006 | 1.796540 | 1.097452 |
| *P*-value | 0.714193 | 0.482002 | 0.812641 | 0.435669 | 0.535830 | 0.921209 |

# Appendix 5: Chapter 7 – Empirical Result of CVA-Feature Space Results for 18 point target zone change reflectance and thematic change of Landsat ETM+ 2005 to 2009.

**Empirical result A**

**CVA-Feature Space results for 18 point target zone change reflectance and thematic change of Landsat ETM+ 2005 to 2009.**

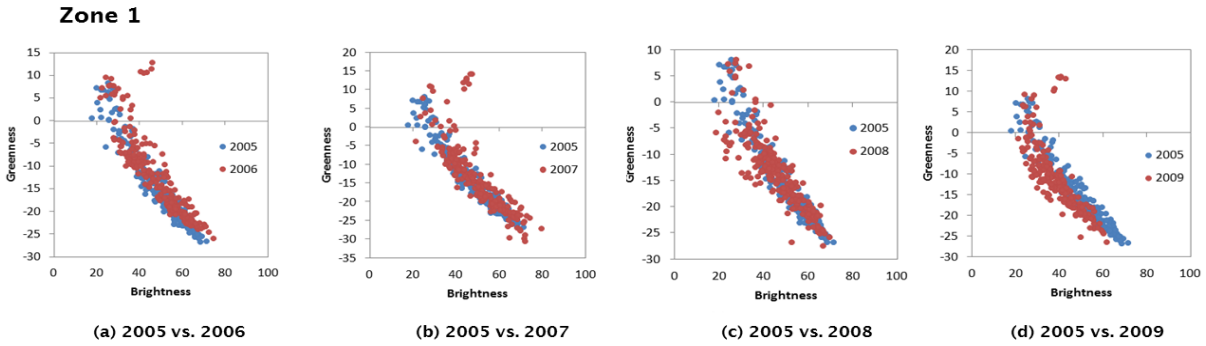


Figure A5.10.18 The direction and magnitude of change within yearly time series in feature space, zone 1.

From the correlation distribution result, the starting year of change for Zone 1 is 2008 with 20% change from the bright surface to building.

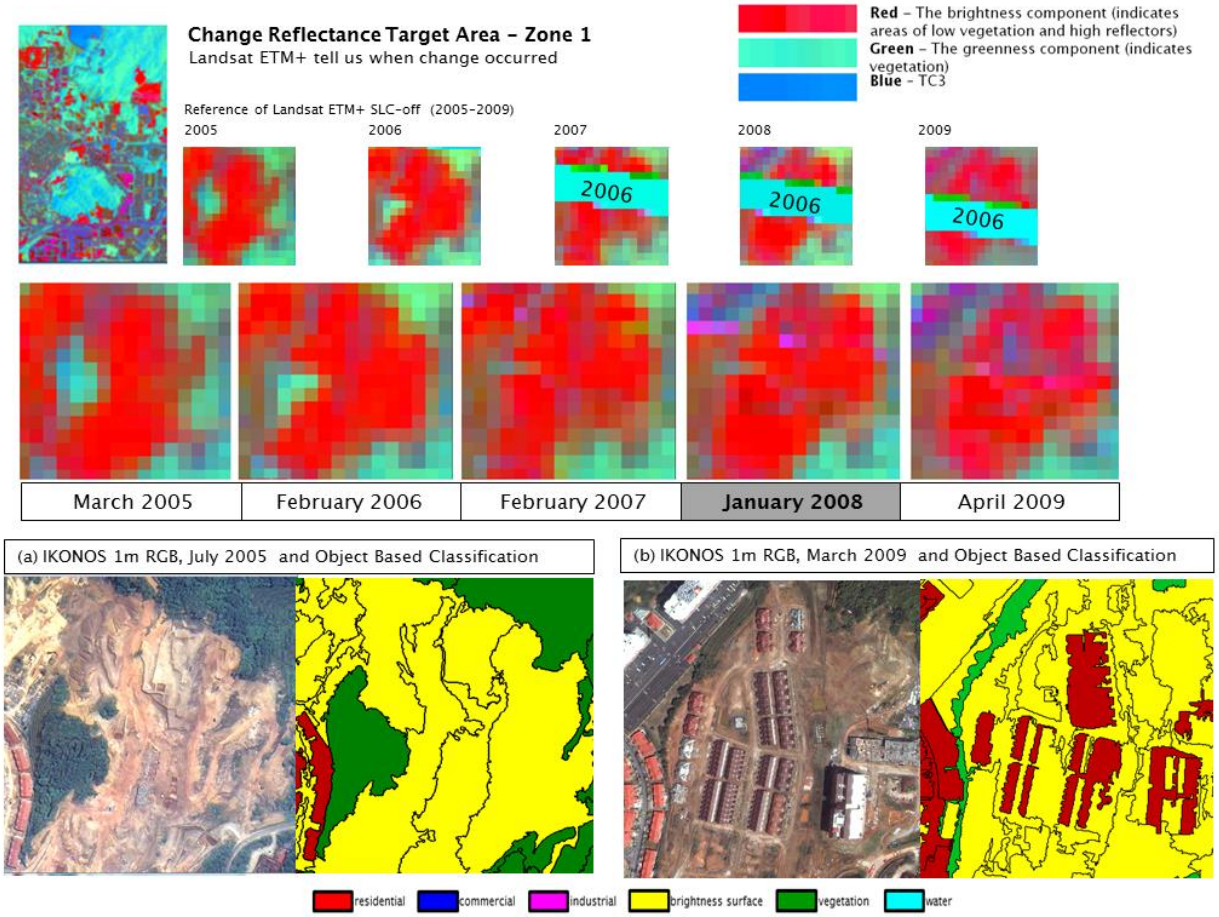


Figure A5.10.19 The transition of change between greenness and brightness from Landsat ETM+ 2005 to 2009 for zone 1 denotes when change occurred. The IKONOS data defined the type of change.

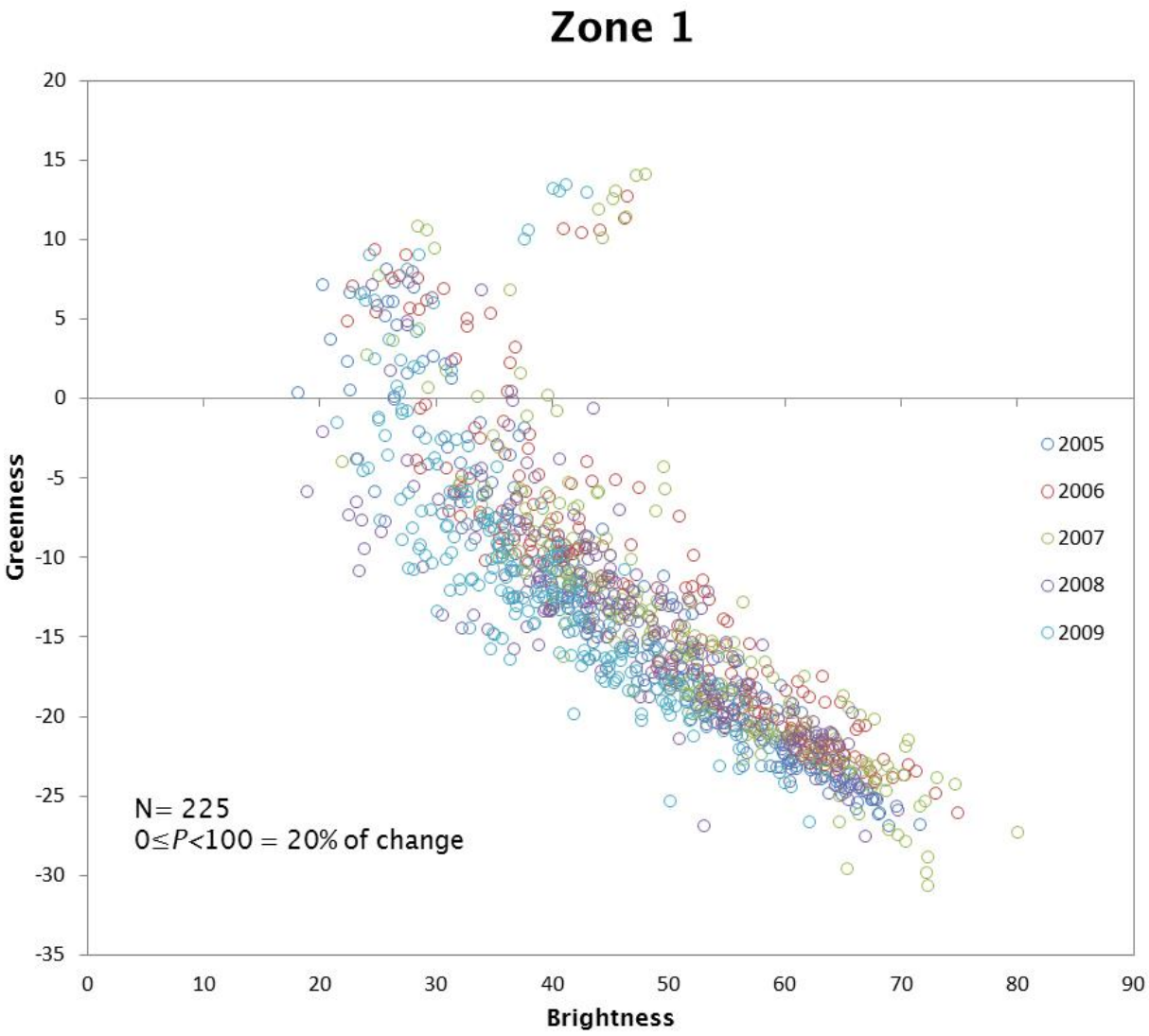


Figure A5.10.20 The feature space transition of change vector between greenness and brightness from Landsat ETM+ 2005 to 2009, zone 1.

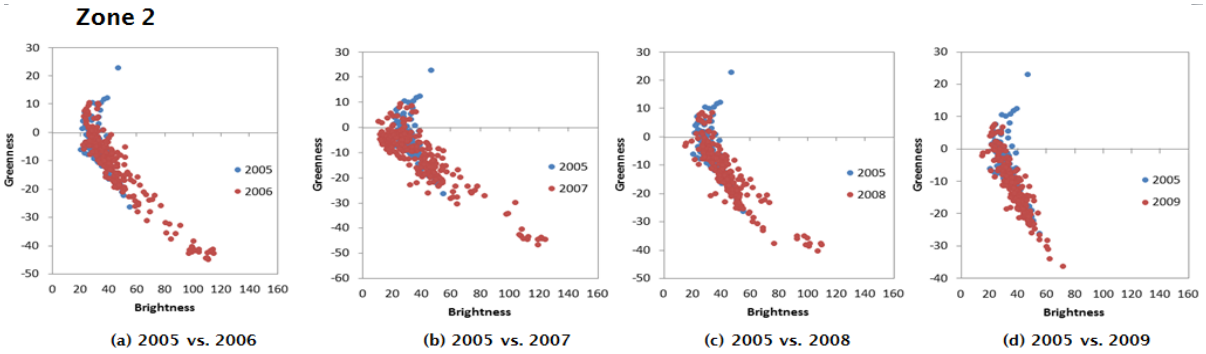


Figure A5.10.21 The direction and magnitude of change within yearly time series in feature space, zone 2.

From the correlation distribution result, the starting year of change for Zone 2 is 2006 with 50% change from the bright surface to building.

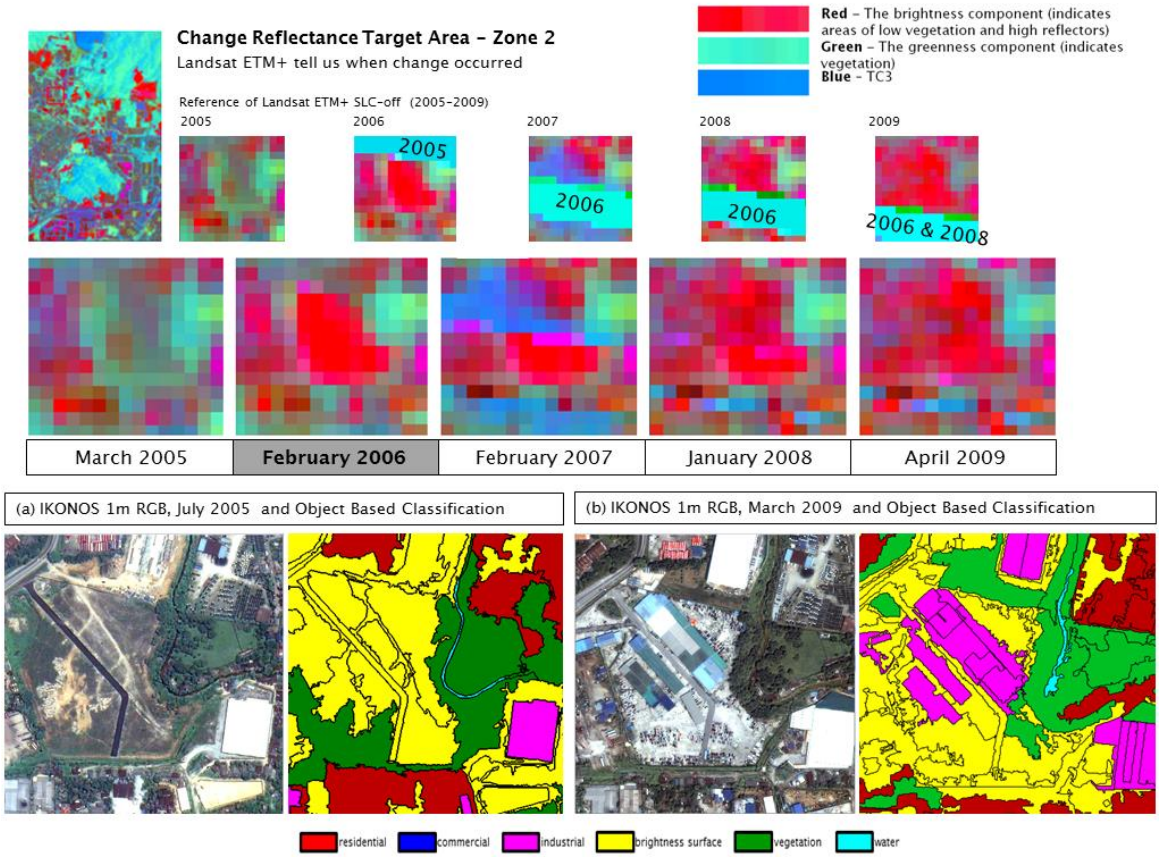


Figure A5.10.22 The transition of change between greenness and brightness from Landsat ETM+ 2005 to 2009 for zone 2 denotes when change occurred. The IKONOS data defined the type of change.

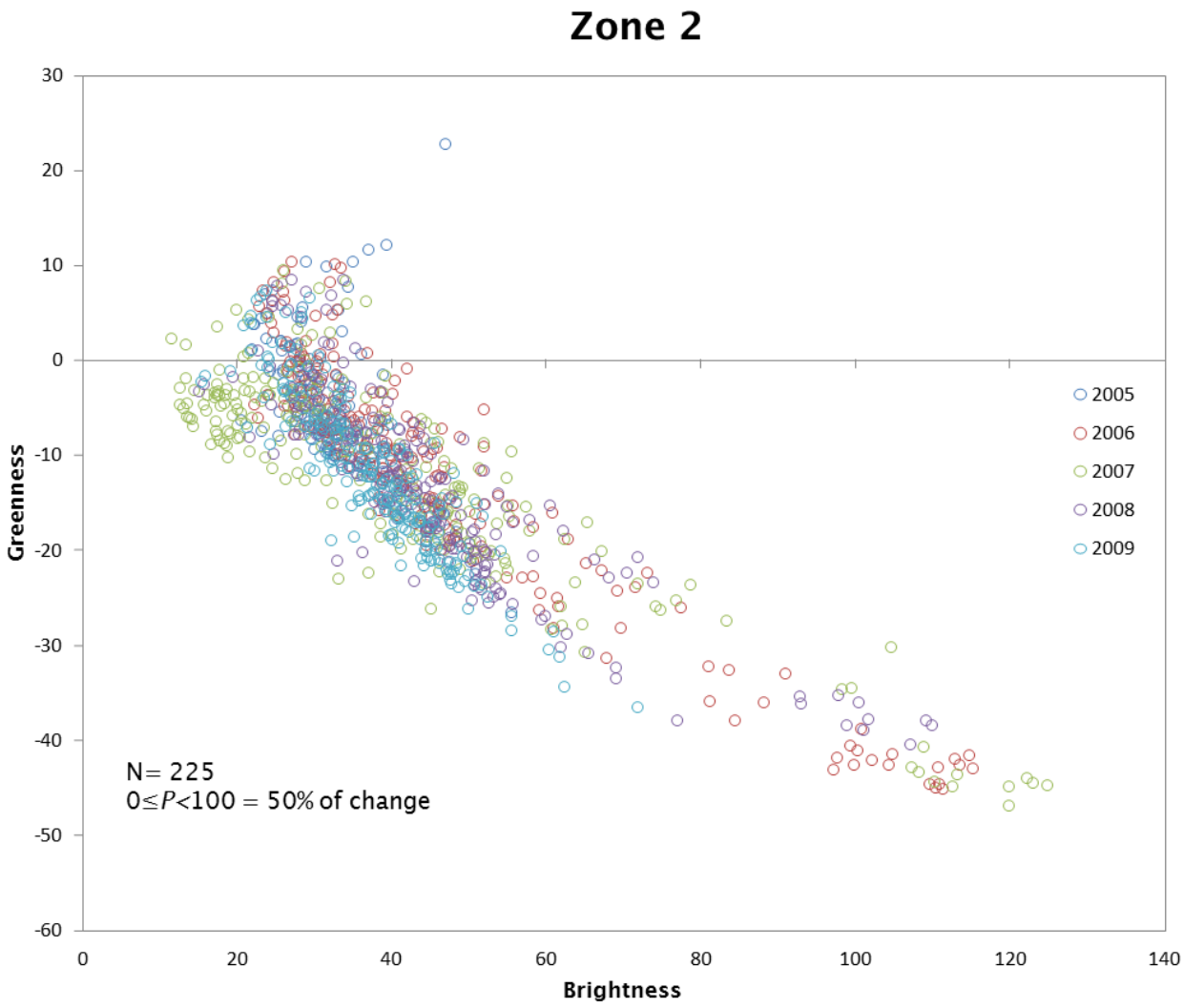


Figure A5.10.23 The feature space transition of change vector between greenness and brightness from Landsat ETM+ 2005 to 2009, zone 2.

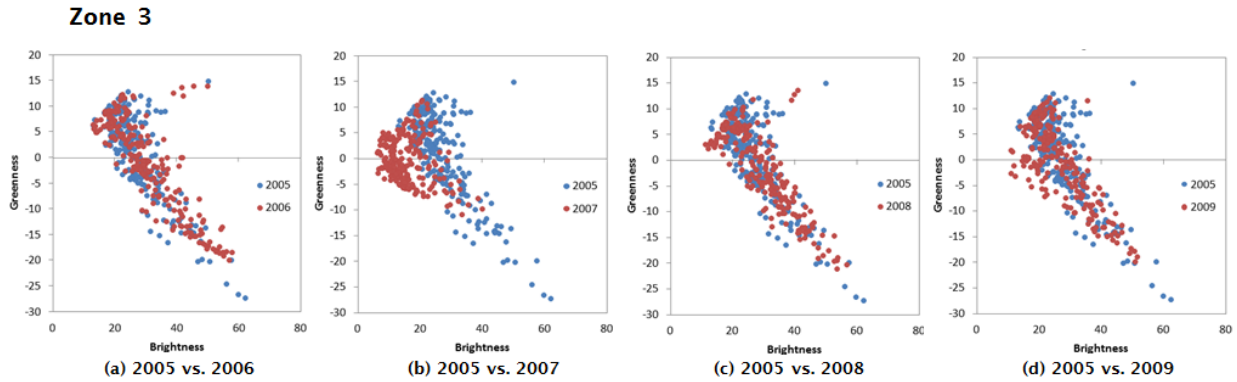


Figure A5.10.24 The direction and magnitude of change within yearly time series in feature space, zone 3

From the correlation distribution result, the starting year of change for Zone 3 is 2006 with 50% change from the vegetation to bright surface.

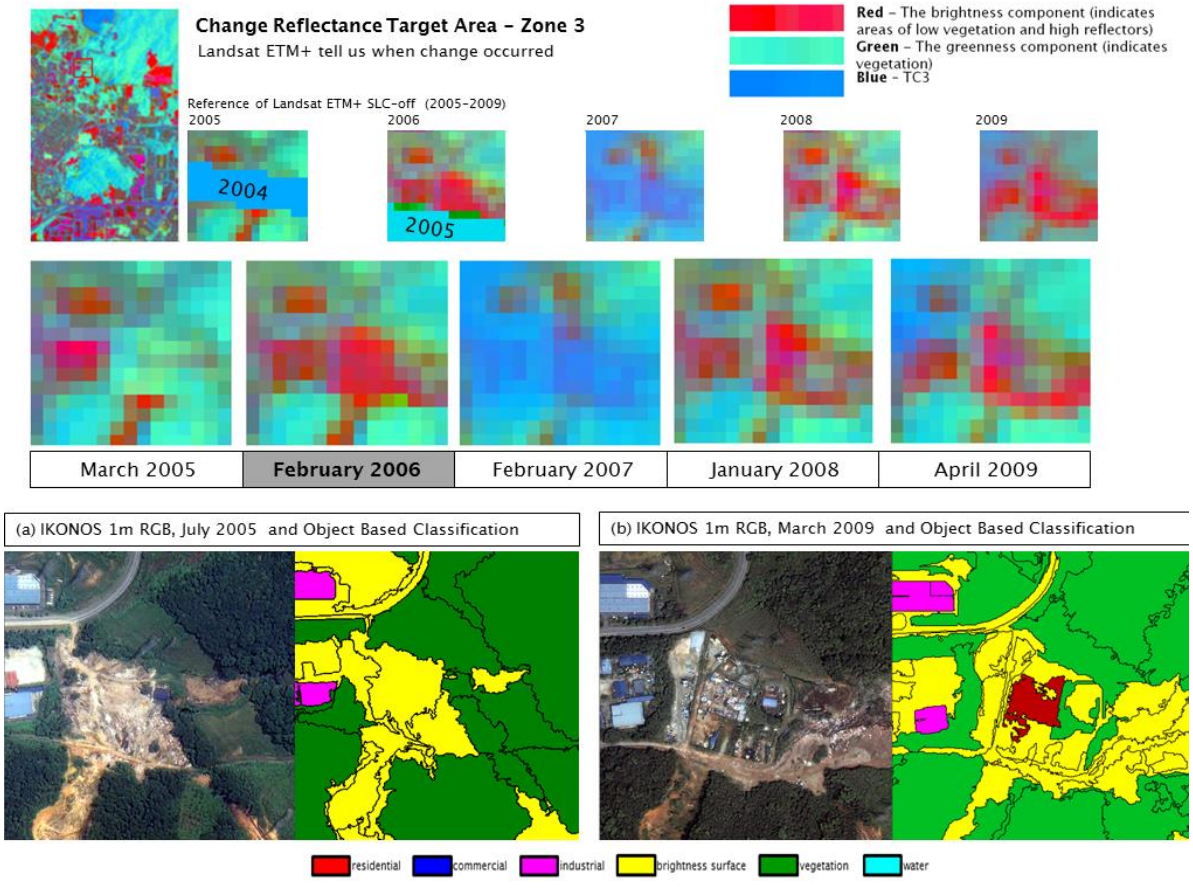


Figure A5.10.25 The transition of change between greenness and brightness from Landsat ETM+ 2005 to 2009 for zone 3 denotes when change occurred. The IKONOS data defined the type of change.

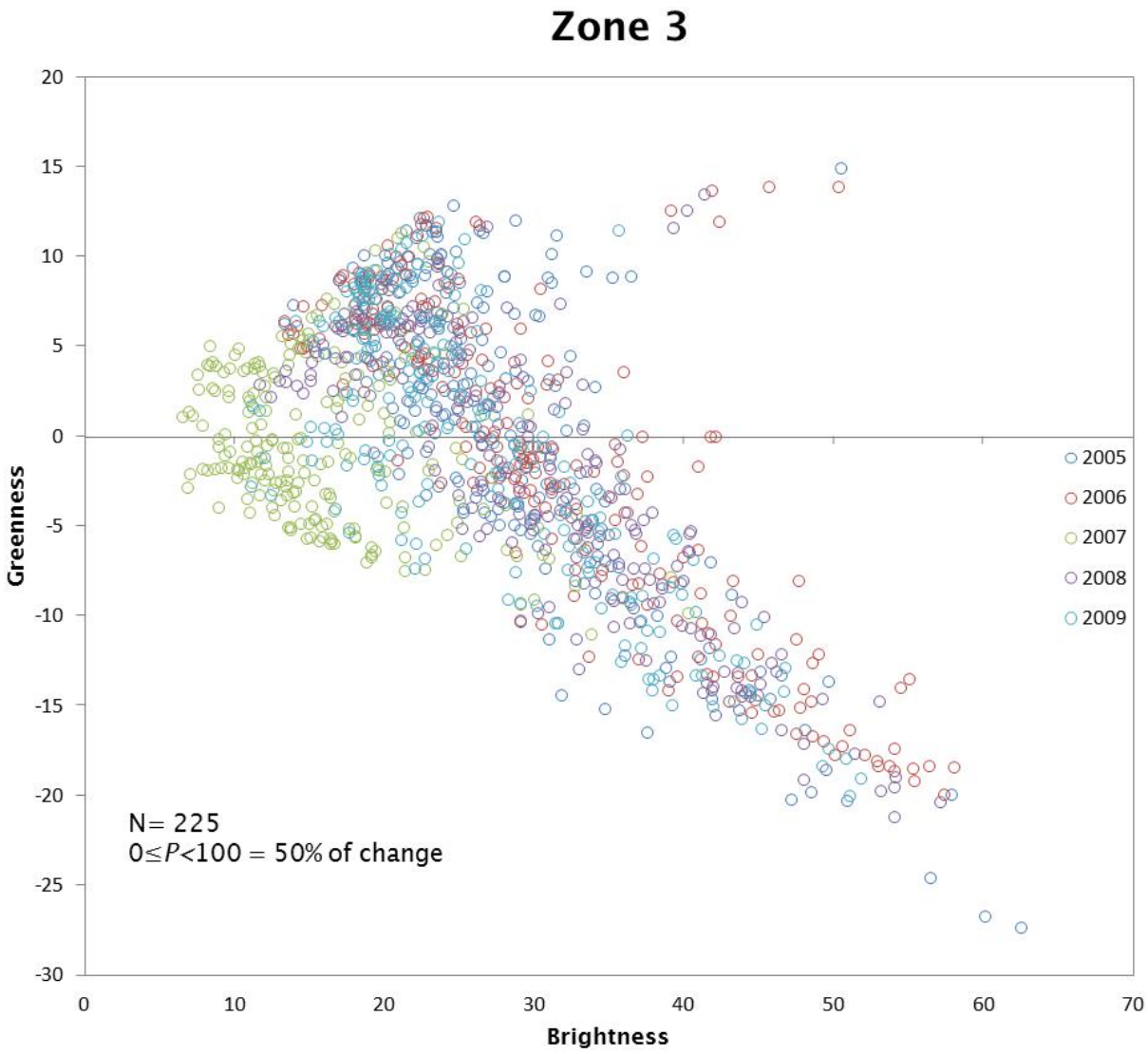


Figure A5.10.26 The feature space transition of change vector between greenness and brightness from Landsat ETM+ 2005 to 2009, zone 3.

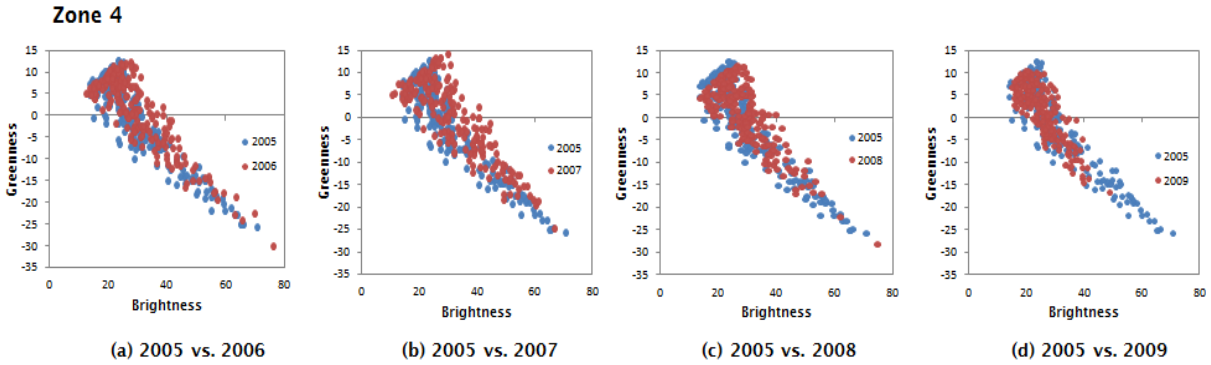


Figure A5.10.27 The direction and magnitude of change within yearly time series in feature space, zone 4.

From the correlation distribution result, the starting year of change for Zone 4 is 2006 with 20% change from bright surface to vegetation.

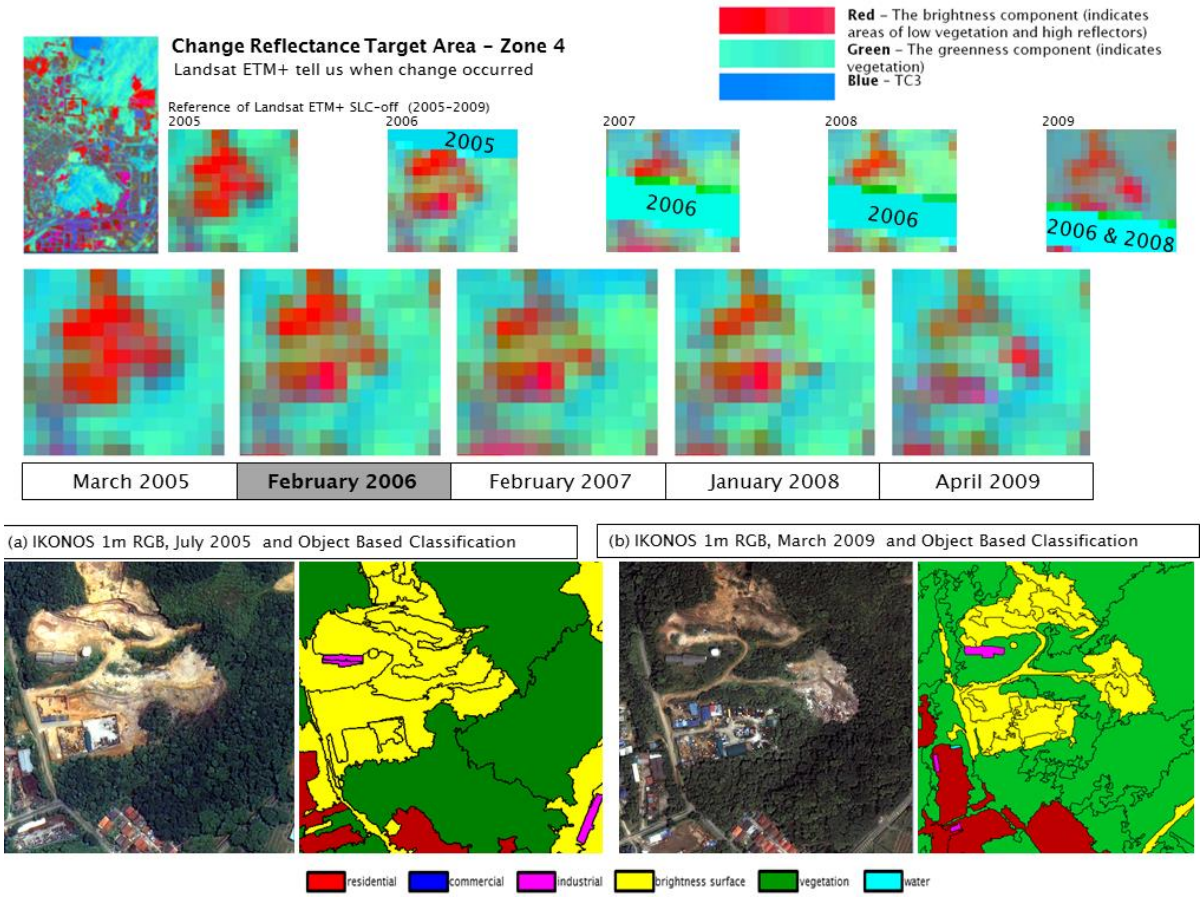


Figure A5.10.28 The transition of change between greenness and brightness from Landsat ETM+ 2005 to 2009 for zone 4 denotes when change occurred. The IKONOS data defined the type of change.

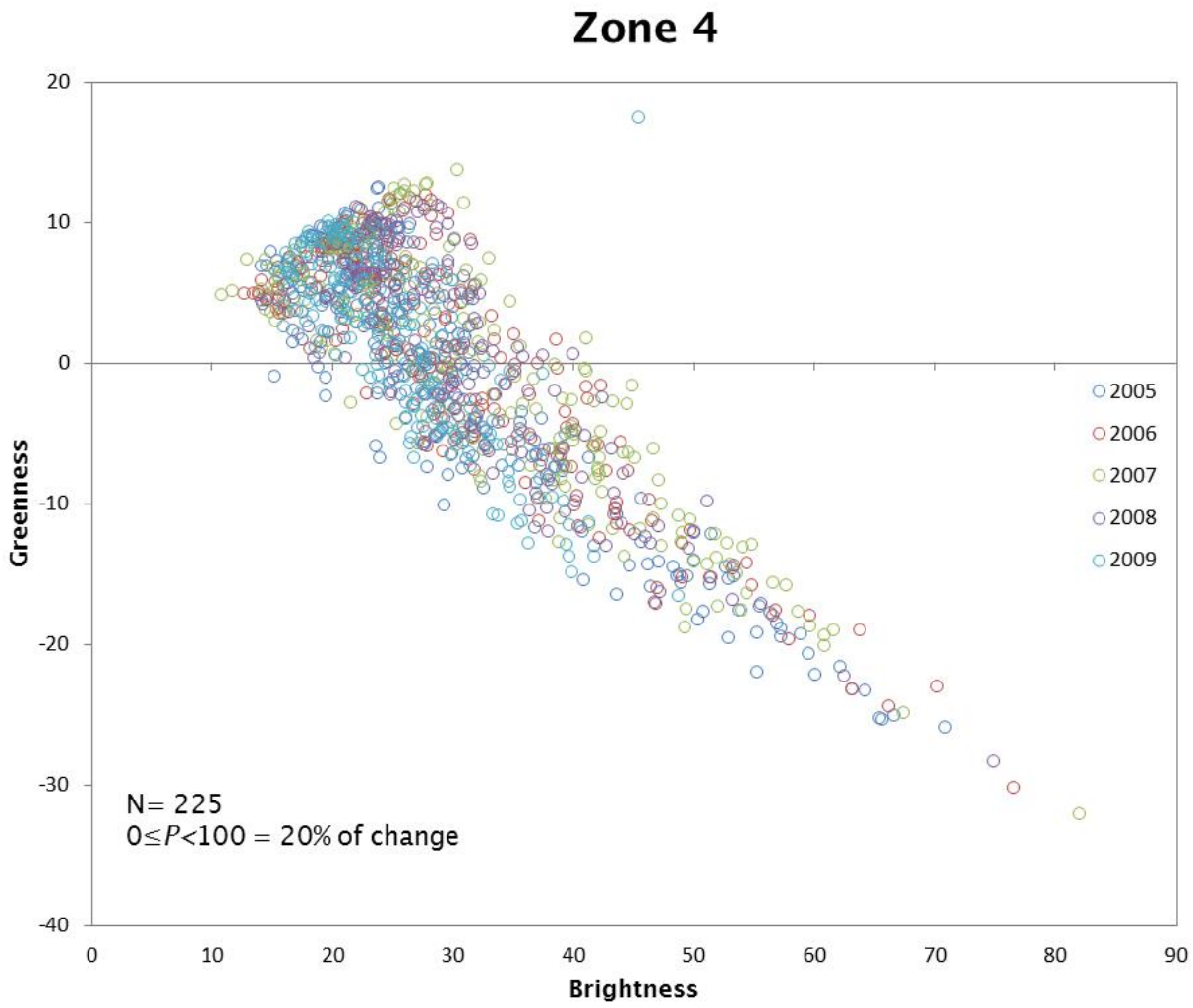


Figure A5.10.29 The feature space transition of change vector between greenness and brightness from Landsat ETM+ 2005 to 2009, zone 4.

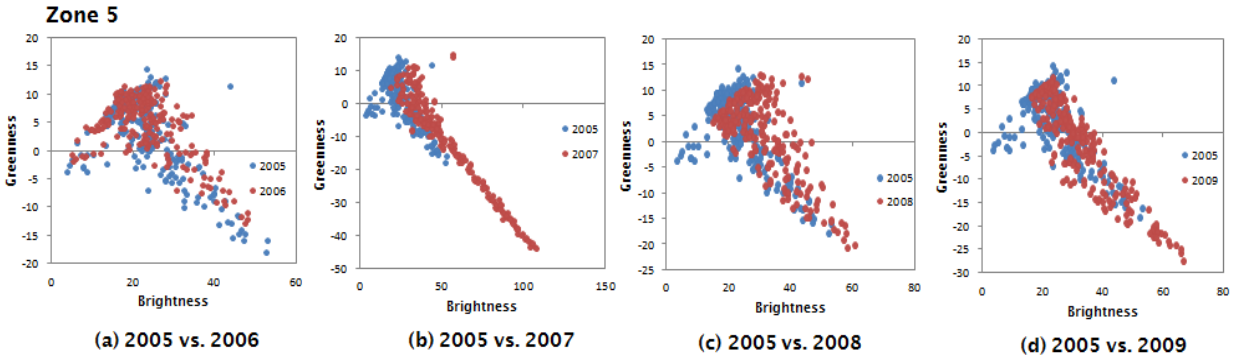


Figure A5.10.30 The direction and magnitude of change within yearly time series in feature space, zone 5.

From the correlation distribution result, the starting year of change for Zone 5 is 2007 with 90% change from water to bright surface.

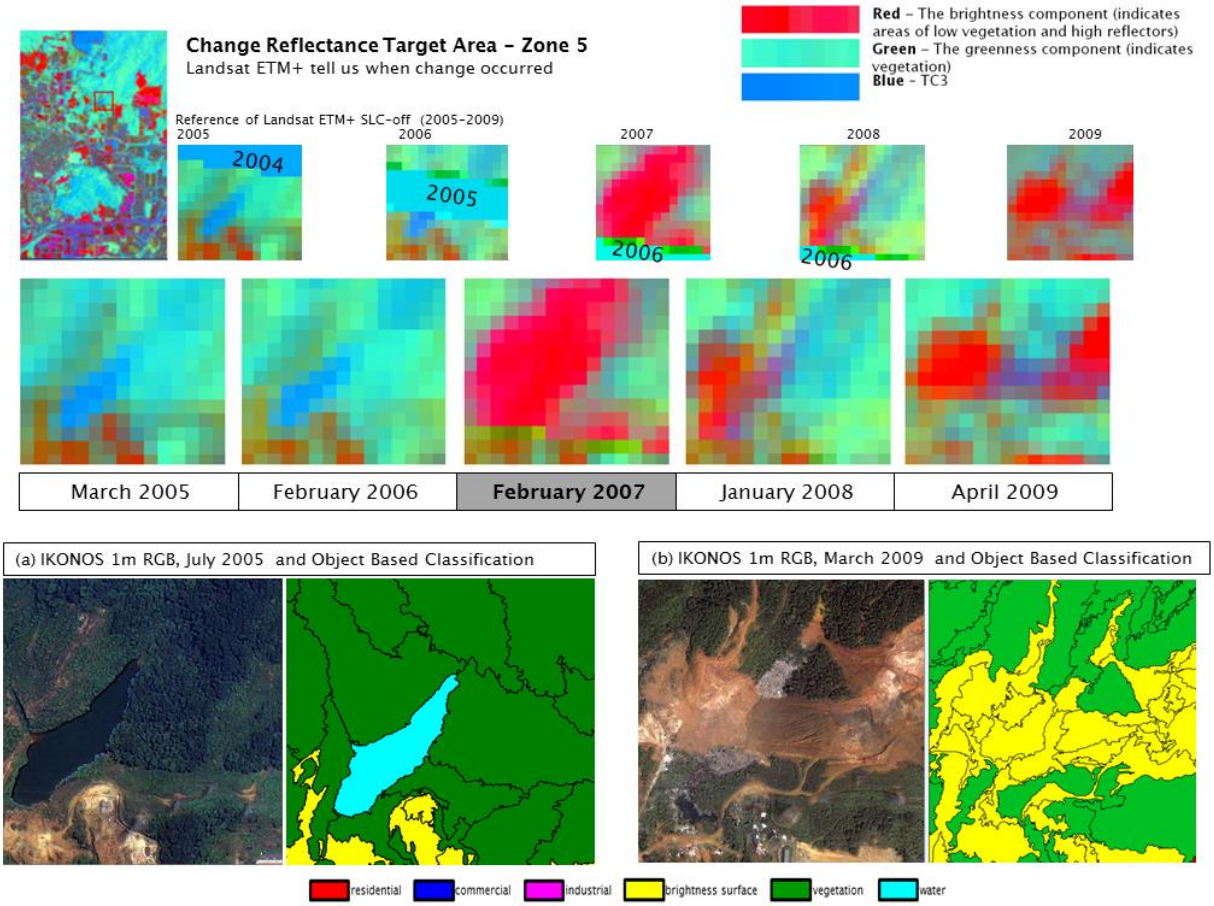


Figure A5.10.31 The transition of change between greenness and brightness from Landsat ETM+ 2005 to 2009 for zone 5 denotes when change occurred. The IKONOS data defined the type of change.

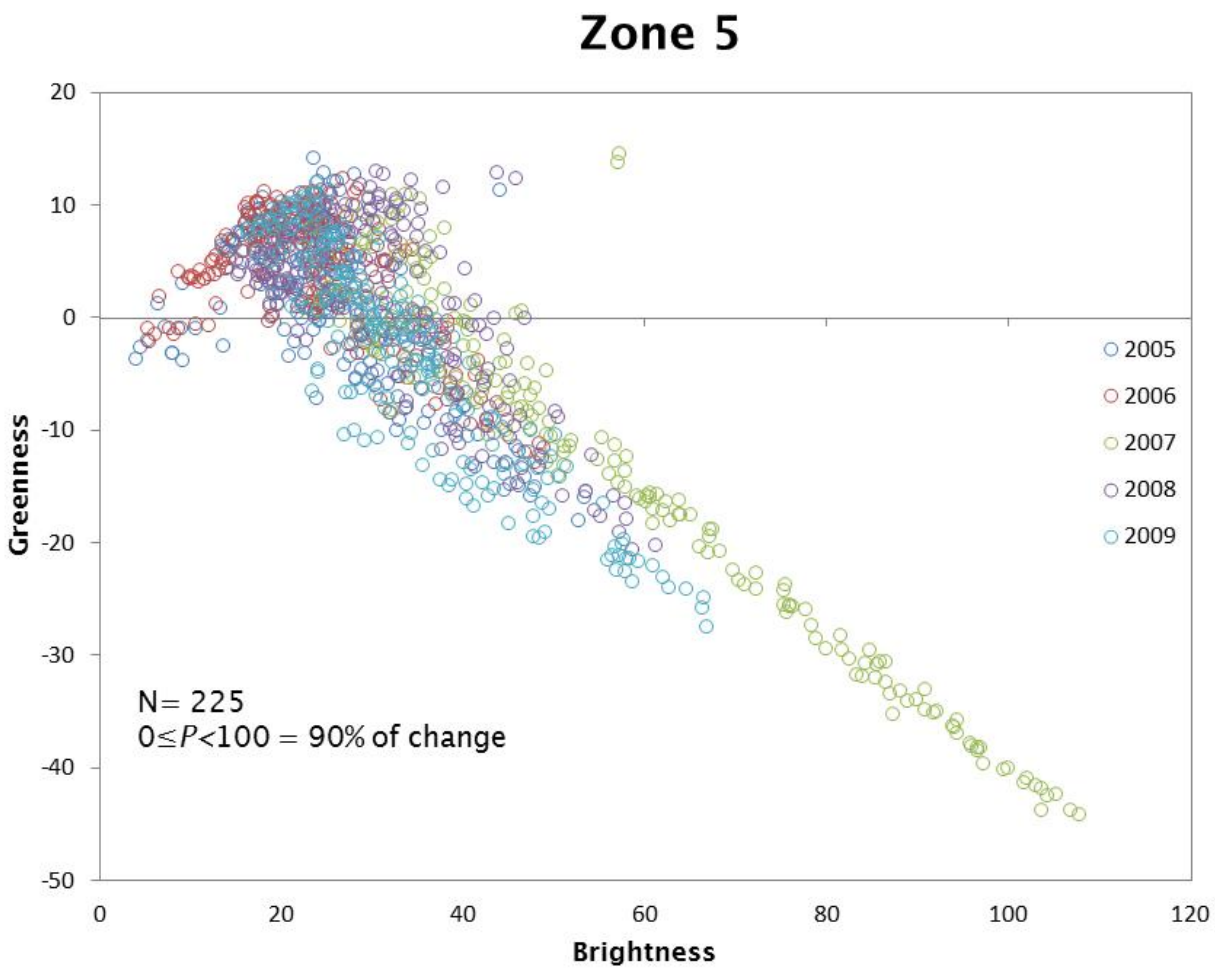


Figure A5.10.32 The feature space transition of change vector between greenness and brightness from Landsat ETM+ 2005 to 2009, zone 5.

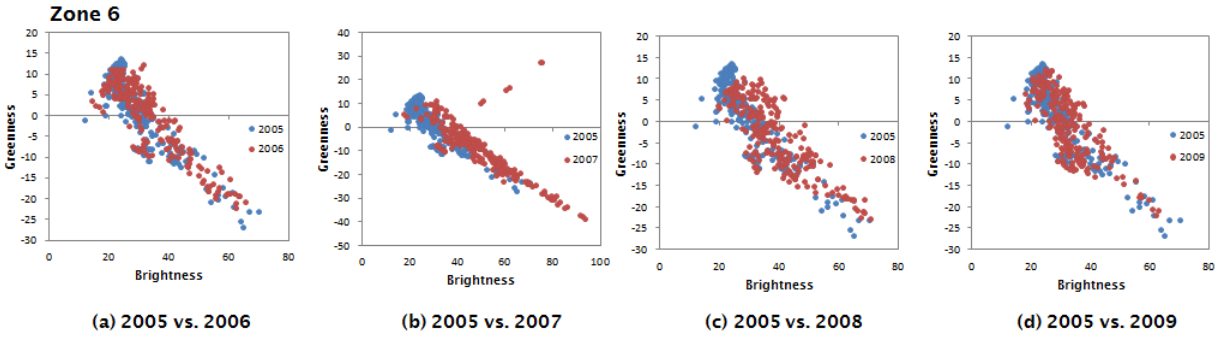


Figure A5.10.33 The direction and magnitude of change within yearly time series in feature space, zone 6.

From the correlation distribution result, the starting year of change for Zone 6 is 2007 with 90% change from bright surface to building.

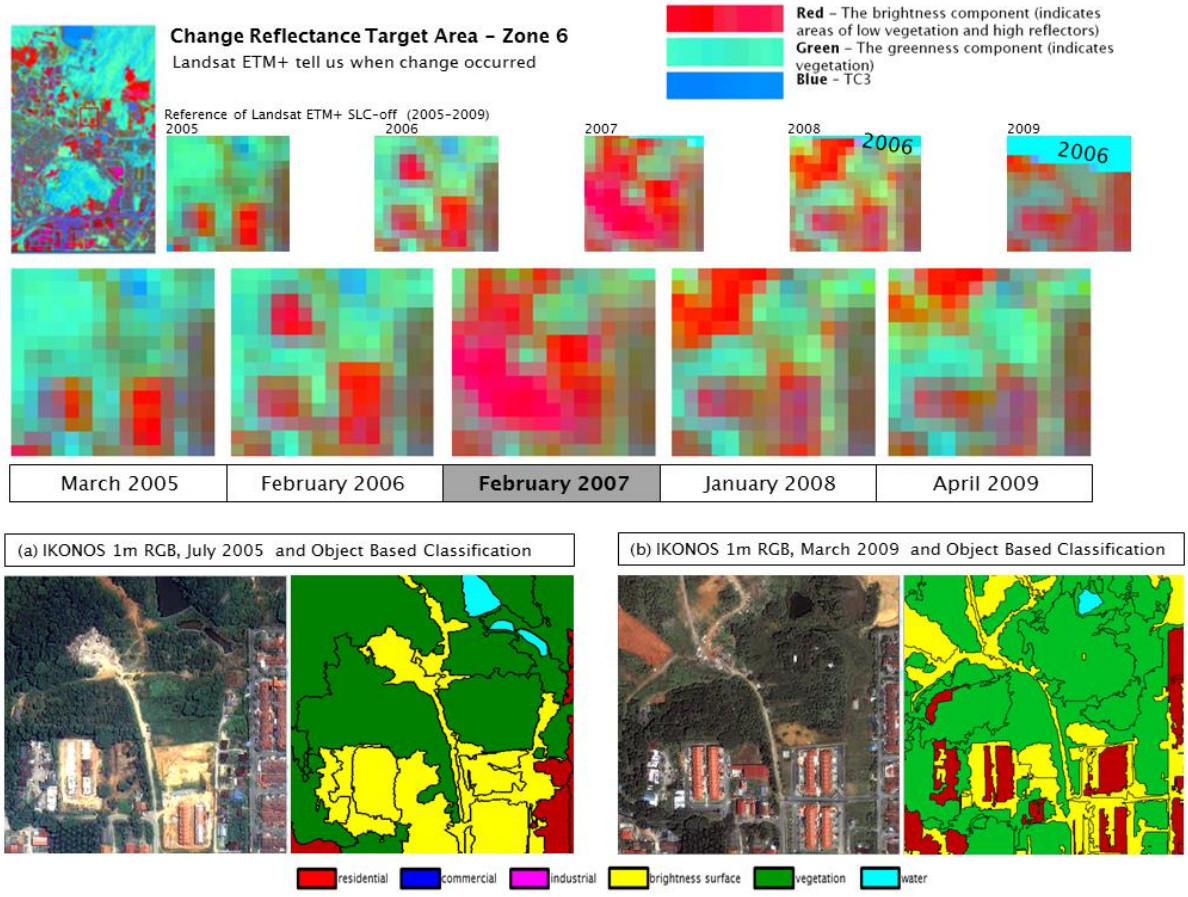


Figure A5.10.34 The transition of change between greenness and brightness from Landsat ETM+ 2005 to 2009 for zone 6 denotes when change occurred. The IKONOS data defined the type of change.

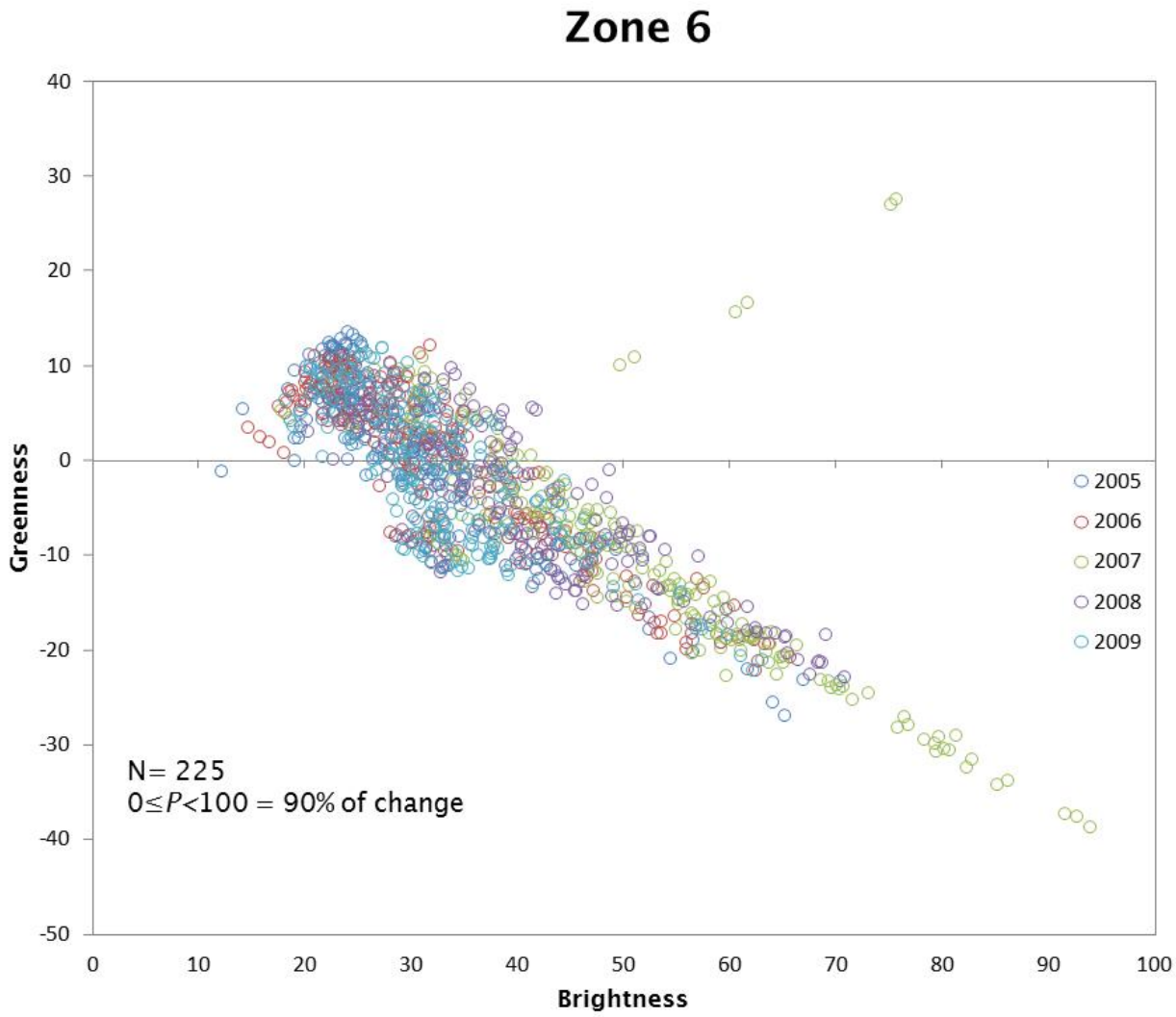


Figure A5.10.35 The feature space transition of change vector between greenness and brightness from Landsat ETM+ 2005 to 2009, zone 6.

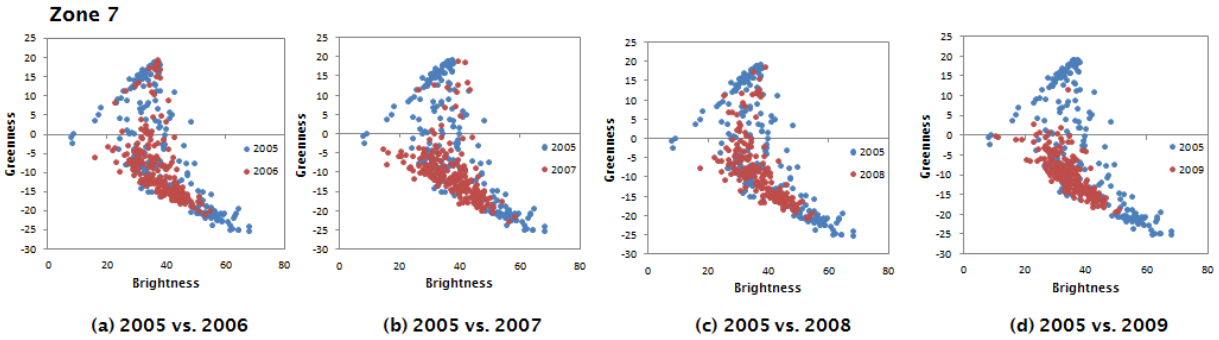


Figure A5.10.36 The direction and magnitude of change within yearly time series in feature space, zone 7.

From the correlation distribution result, the starting year of change for Zone 7 is 2007 with 50% change from bright surface to building.

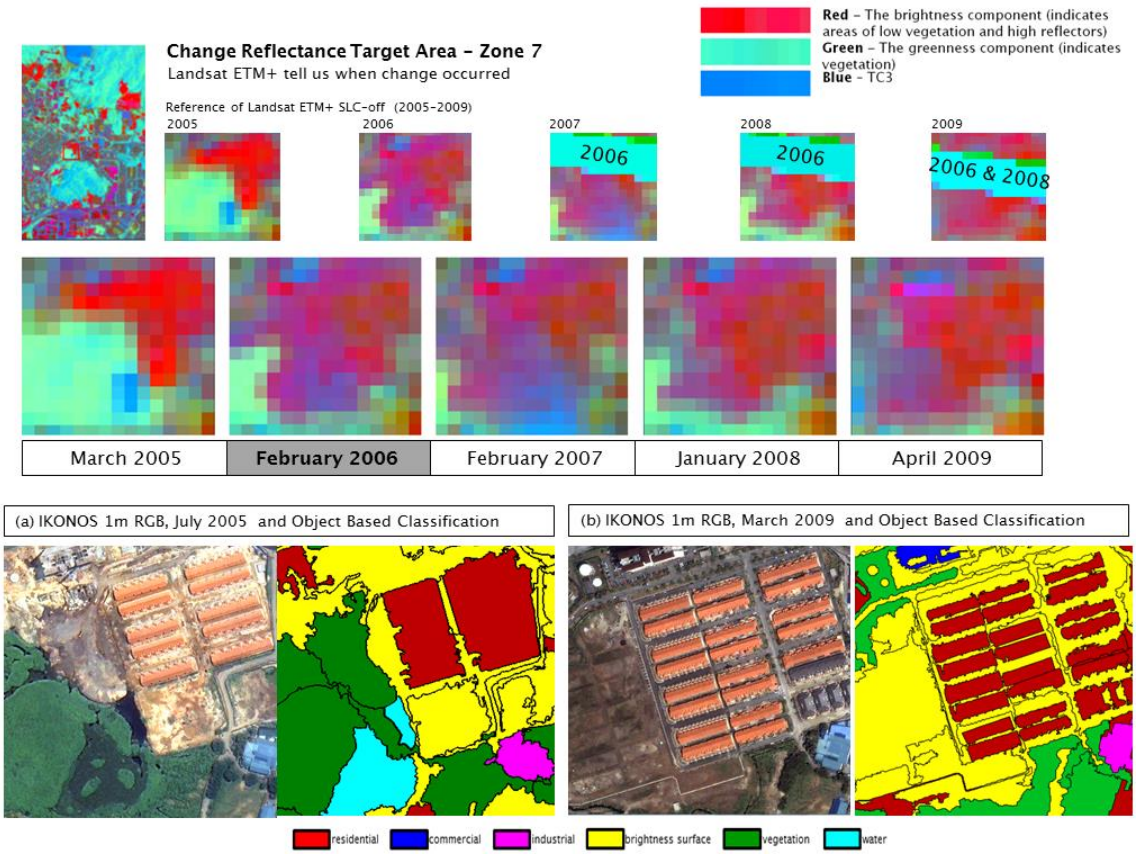


Figure A5.10.37 The transition of change between greenness and brightness from Landsat ETM+ 2005 to 2009 for zone 7 denotes when change occurred. The IKONOS data defined the type of change.

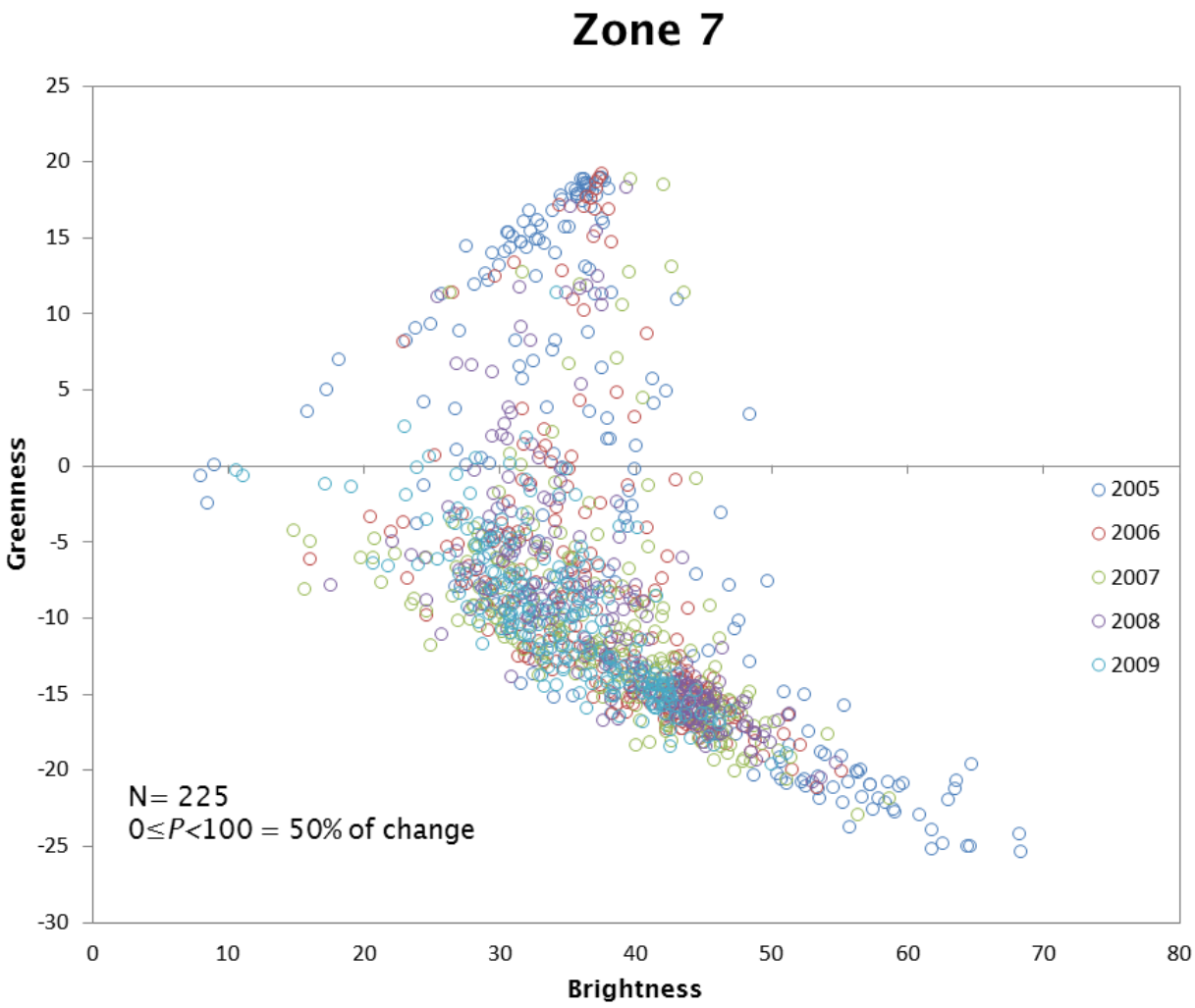


Figure A5.10.38 The features space transition of change vector between greenness and brightness from Landsat ETM+ 2005 to 2009, zone 7.

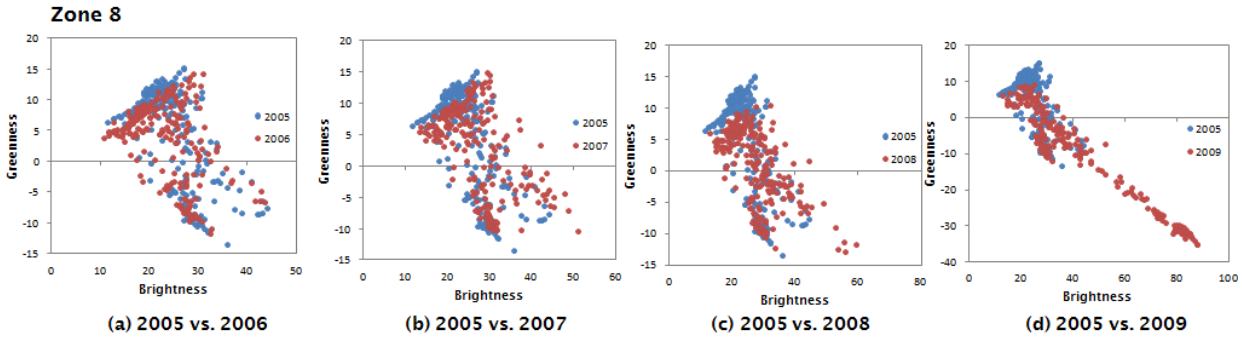


Figure A5.10.39 The direction and magnitude of change within yearly time series in feature space, zone 8.

From the correlation distribution result, the starting year of change for Zone 8 is 2009 with 50% change from vegetation to bright surface.

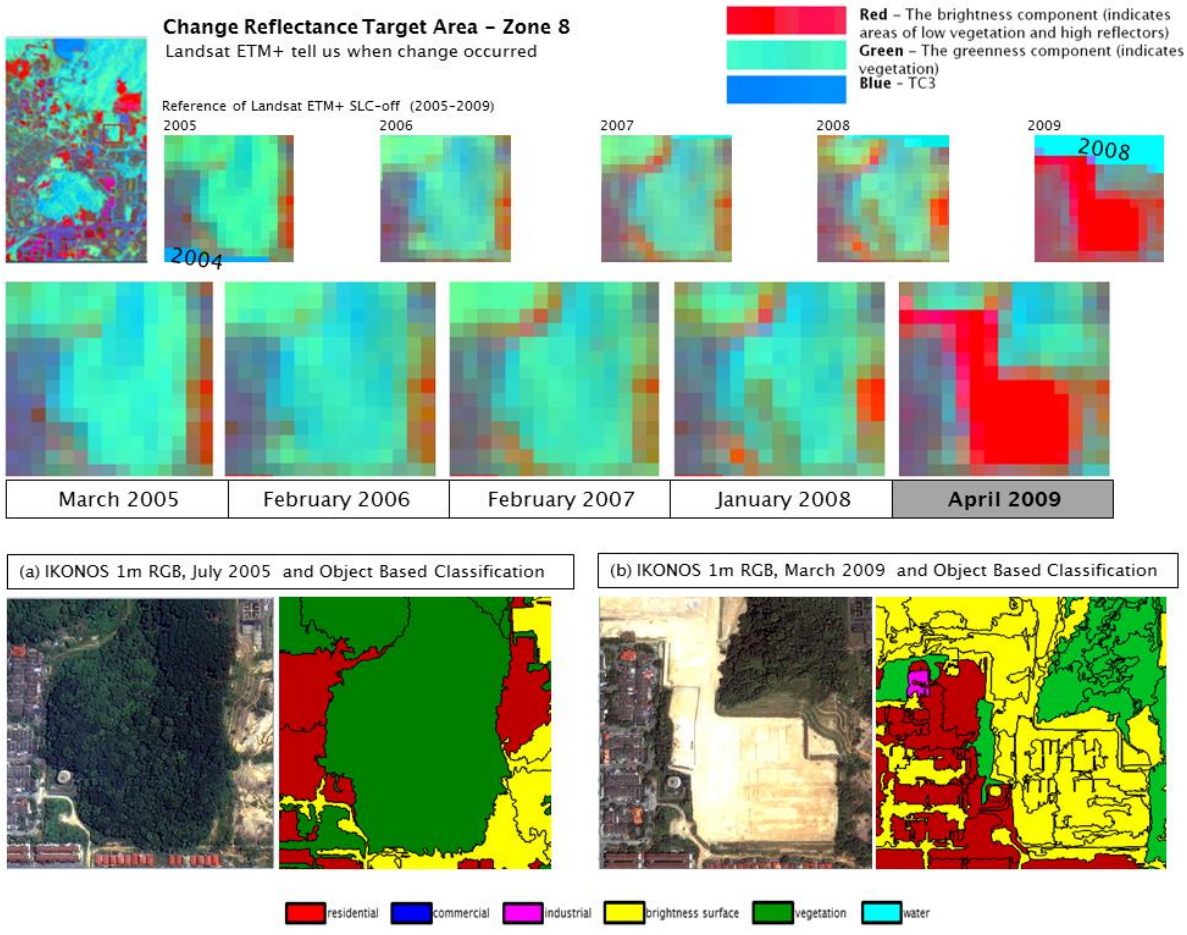


Figure A5.10.40 The transition of change between greenness and brightness from Landsat ETM+ 2005 to 2009 for zone 8 denotes when change occurred. The IKONOS data defined the type of change.

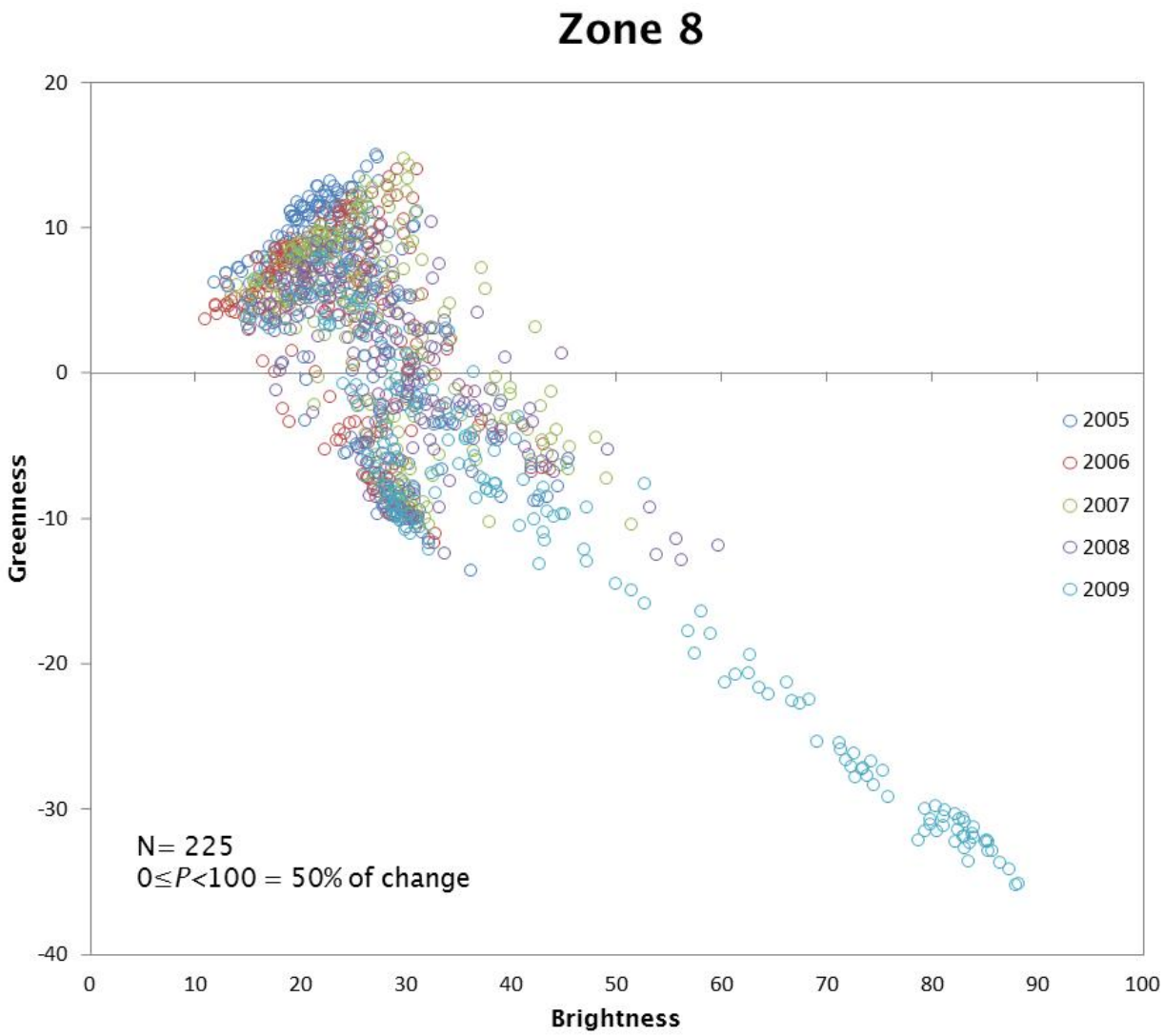


Figure A5.10.41 The feature space transition of change vector between greenness and brightness from Landsat ETM+ 2005 to 2009, zone 8.

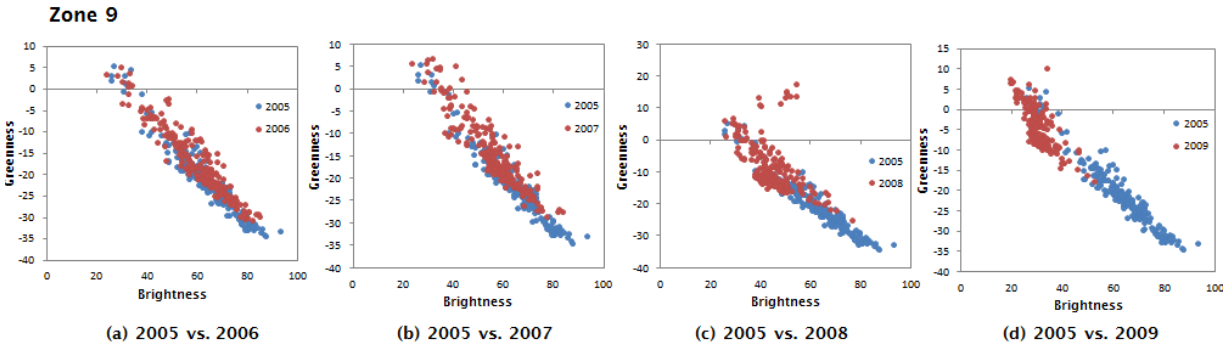


Figure A5.10.42 The direction and magnitude of change within yearly time series in feature space, zone 9.

From the correlation distribution result, the starting year of change for Zone 9 is 2007 with 50% change from bright surface to building.

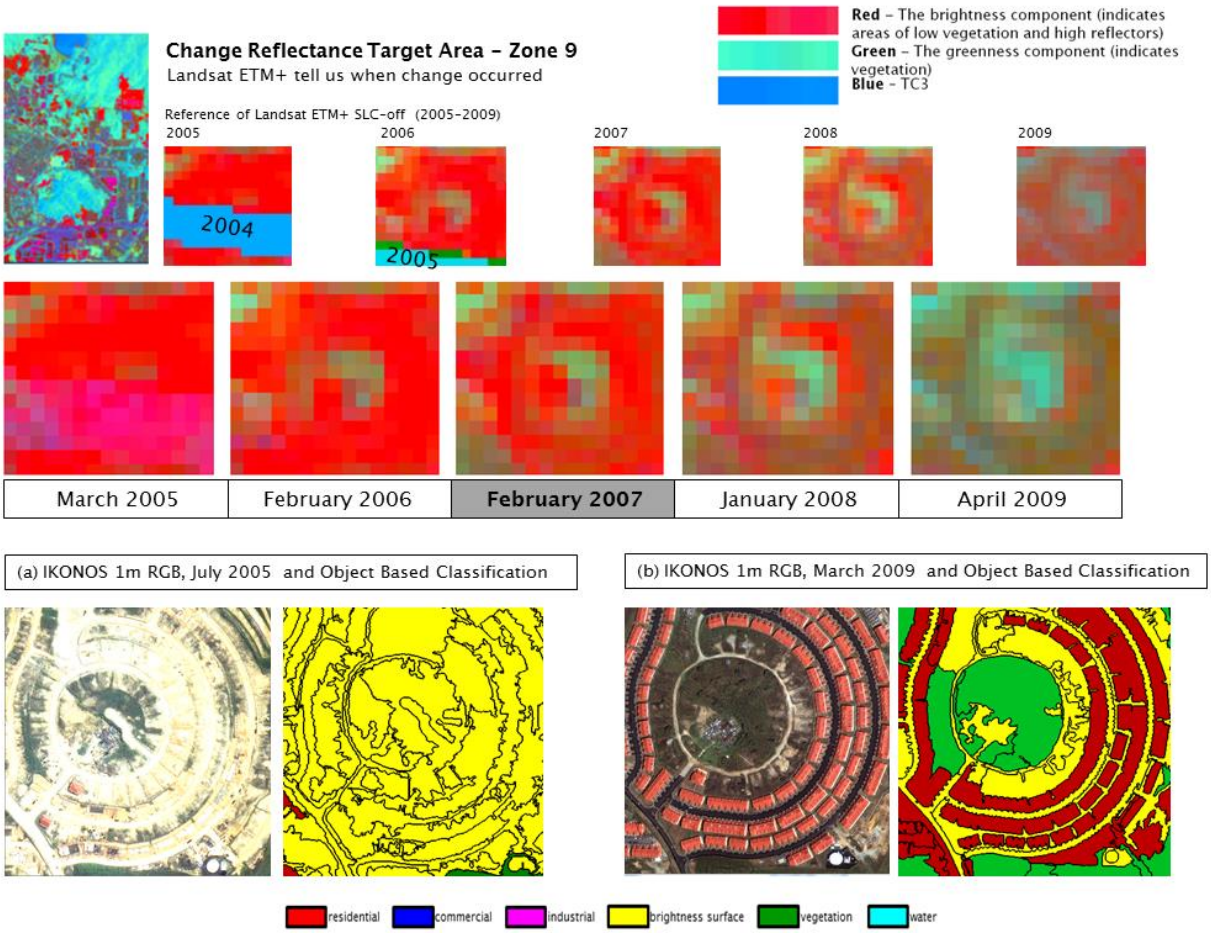


Figure A5.10.43 The transition of change between greenness and brightness from Landsat ETM+ 2005 to 2009 for zone 9 denotes when change occurred.The IKONOS data defined the type of change.

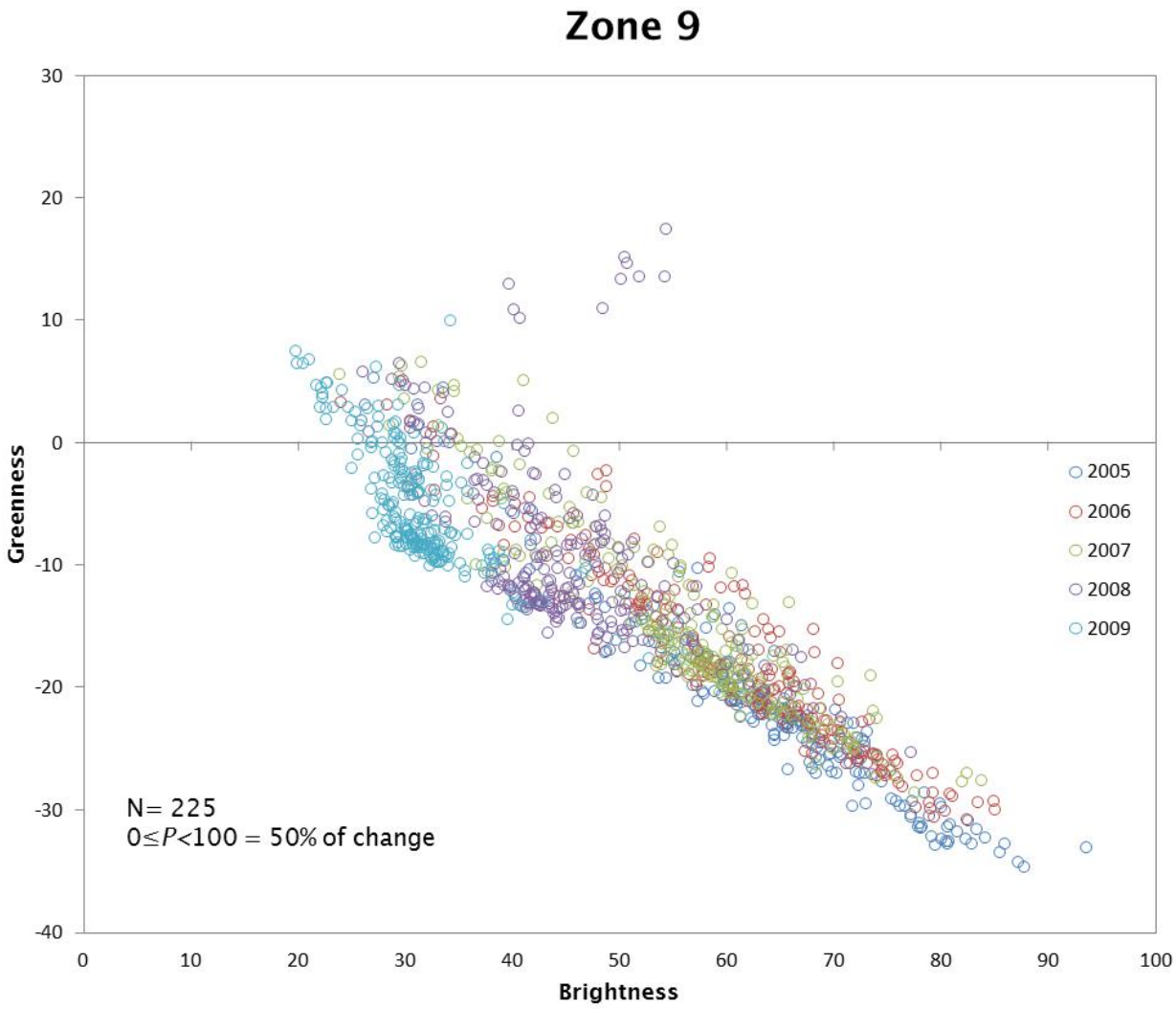


Figure A5.10.44 The feature space transition of change vector between greenness and brightness from Landsat ETM+ 2005 to 2009, zone 9.

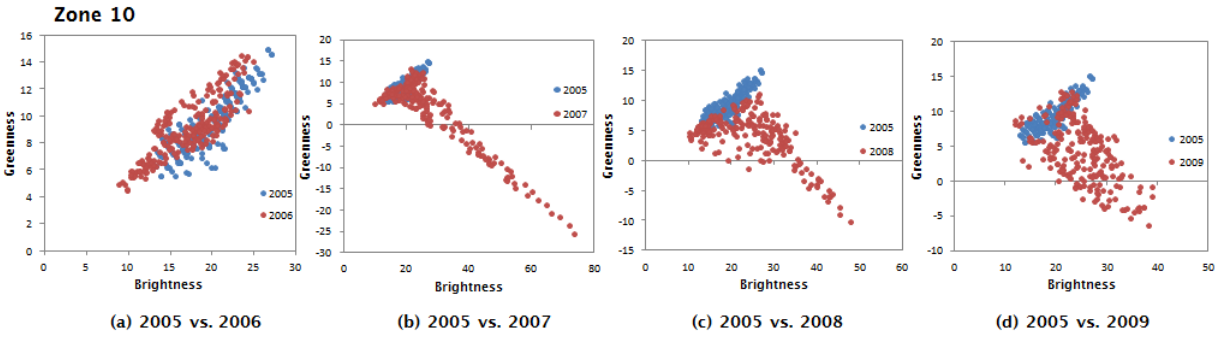


Figure A5.10.45 The direction and magnitude of change within yearly time series in feature space, zone 10.

From the correlation distribution result, the starting year of change for Zone 10 is 2007 with 20% change from vegetation to bright surface.

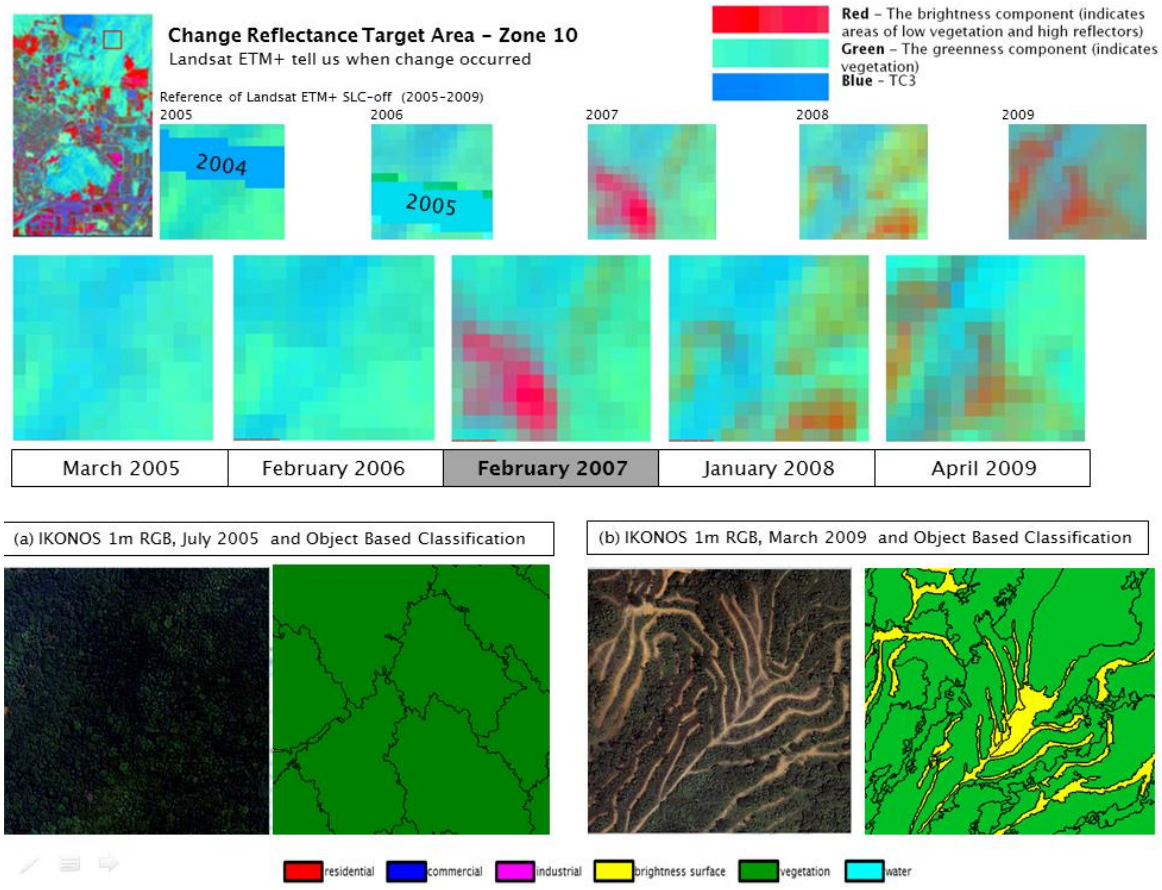


Figure A5.10.46 The transition of change between greenness and brightness from Landsat ETM+ 2005 to 2009 for zone 10 denotes when change occurred. The IKONOS data defined the type of change.

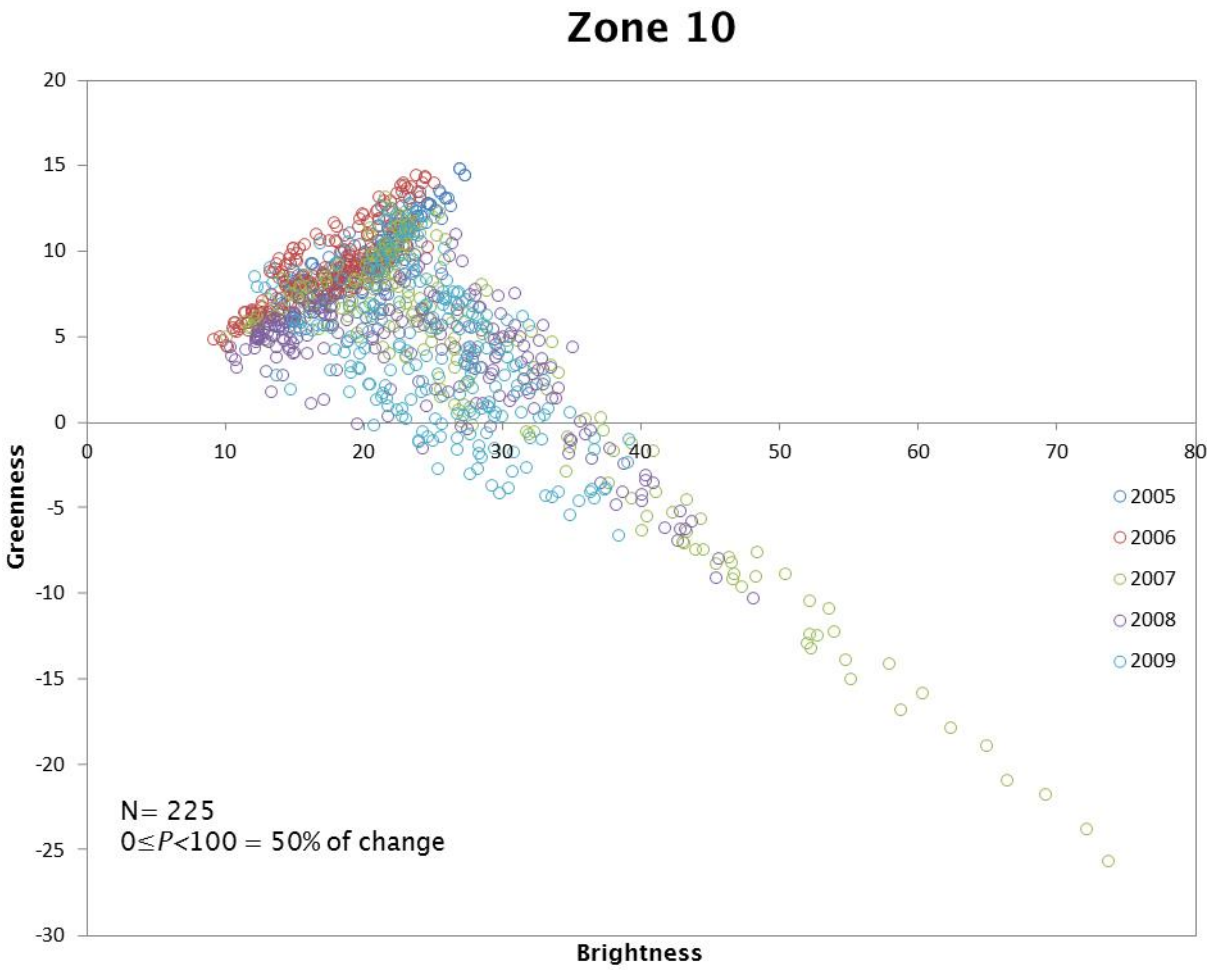


Figure A5.10.47 The feature space transition of change vector between greenness and brightness from Landsat ETM+ 2005 to 2009, zone 10.

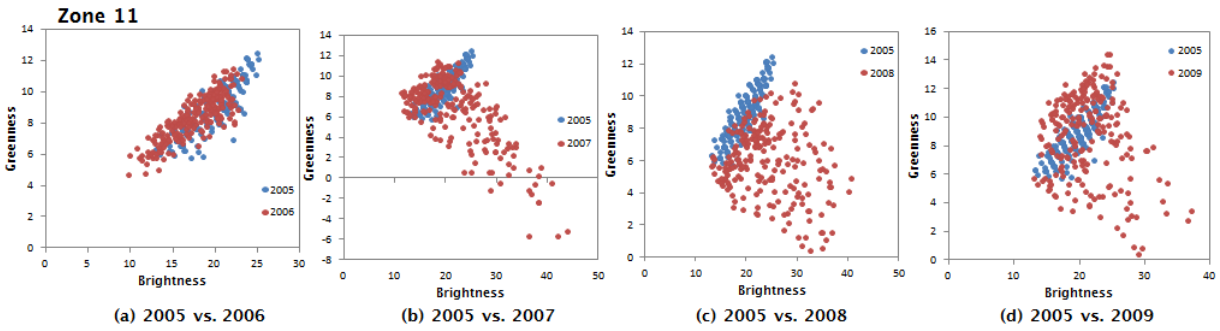


Figure A5.10.48 The direction and magnitude of change within yearly time series in feature space, zone 11.

From the correlation distribution result, the starting year of change for Zone 11 is 2007 with 20% change from vegetation to bright surface.

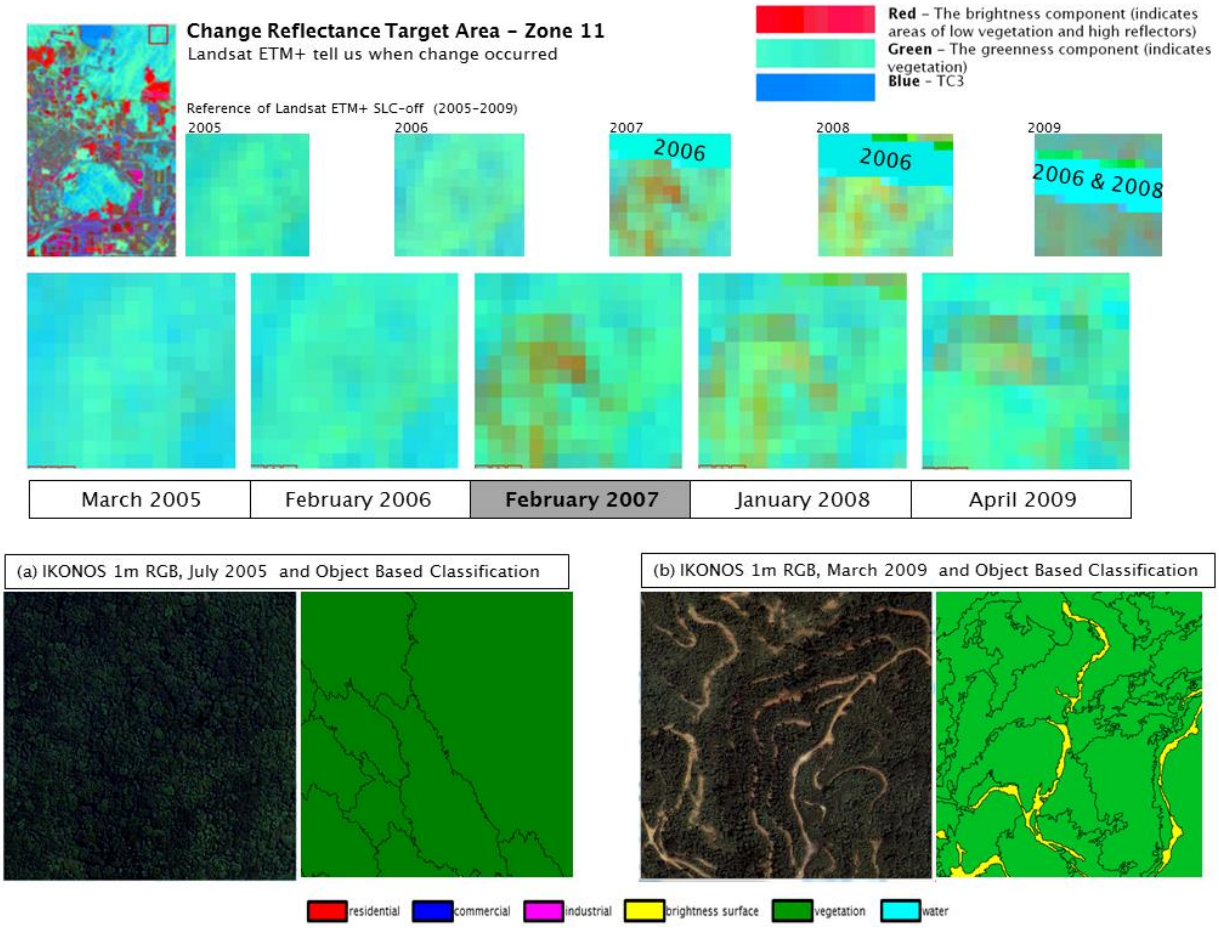


Figure A5.10.49 The transition of change between greenness and brightness from Landsat ETM+ 2005 to 2009 for zone 11 denotes when change occurred.The IKONOS data defined the type of change.

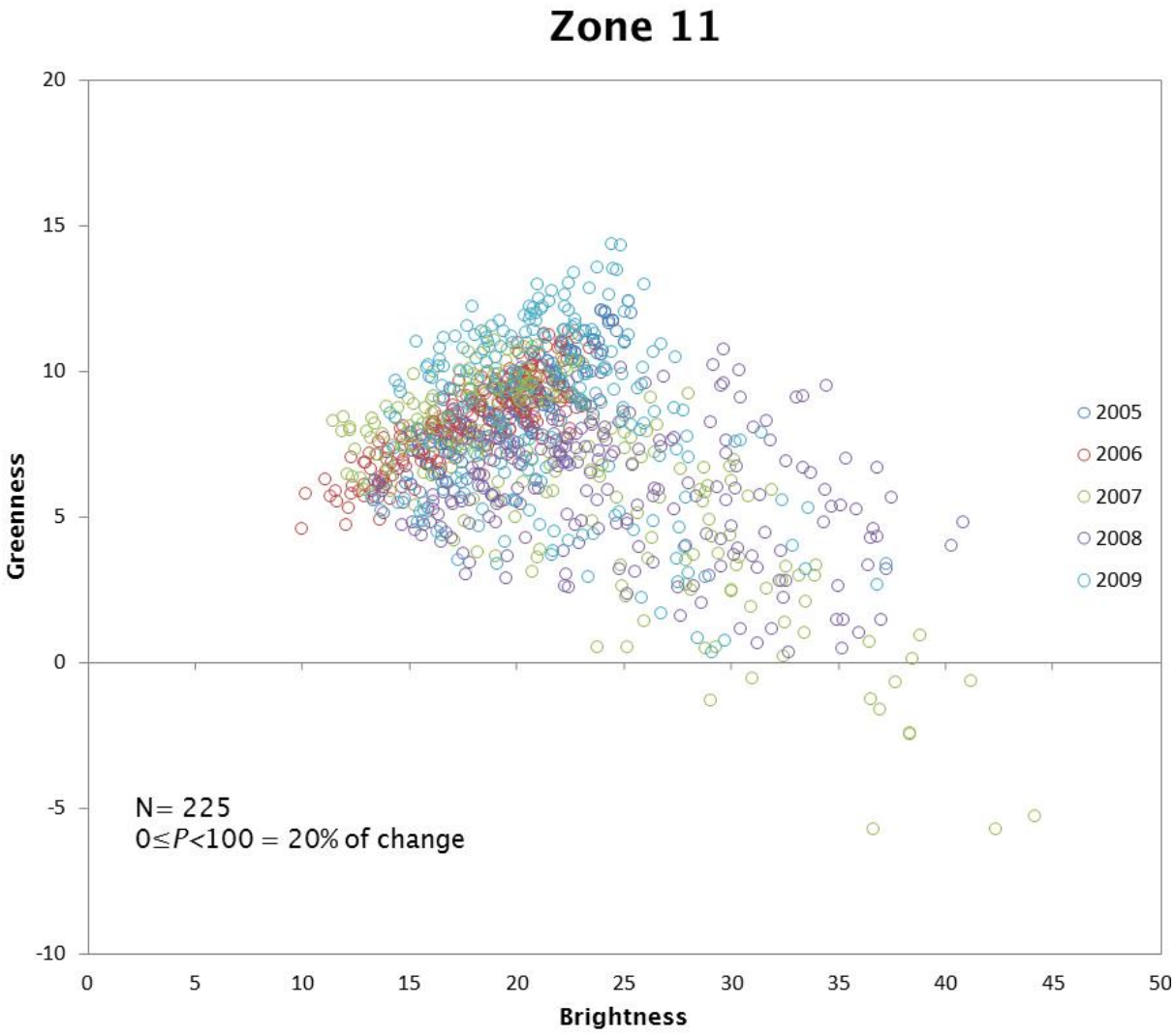


Figure A5.10.50 The feature space transition of change vector between greenness and brightness from Landsat ETM+ 2005 to 2009, zone 11.

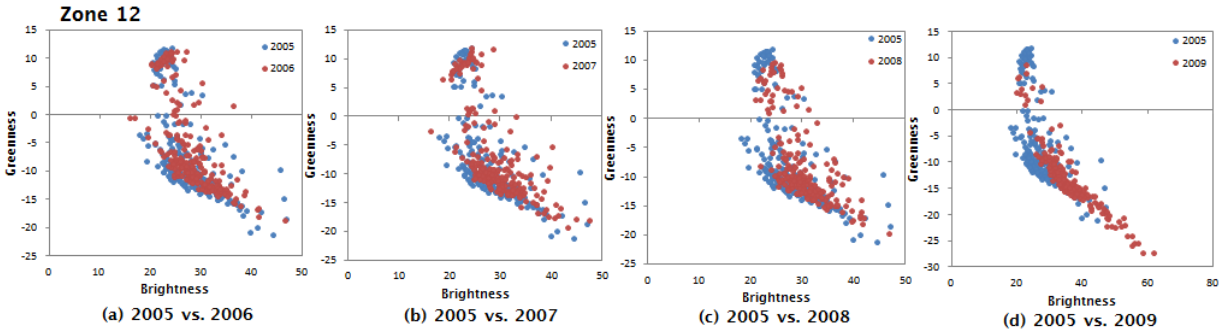


Figure A5.10.51 The direction and magnitude of change within yearly time series in feature space, zone 12.

From the correlation distribution result, the starting year of change for Zone 12 is 2009 with 50% change from vegetation to building.

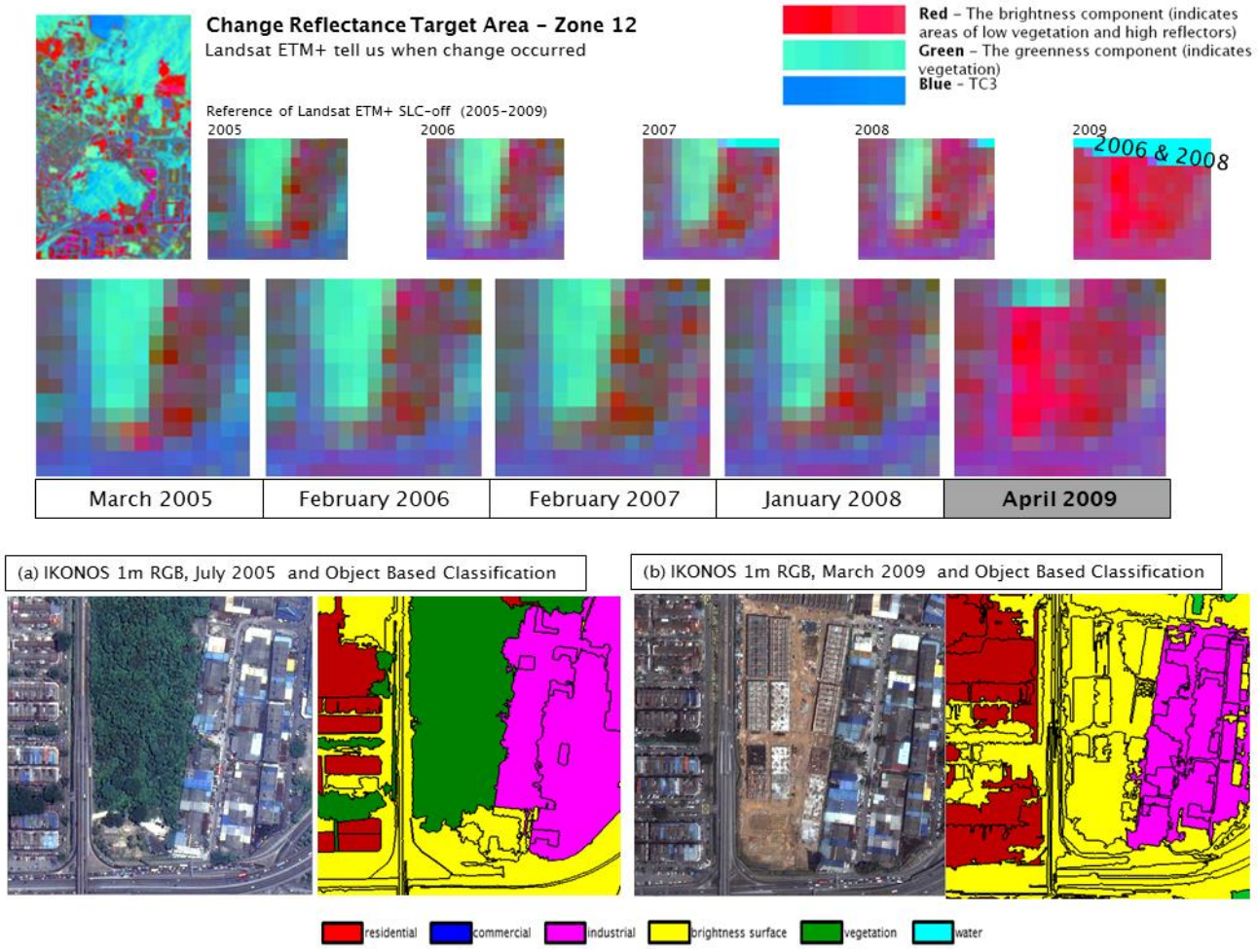


Figure A5.10.52 The transition of change between greenness and brightness from Landsat ETM+ 2005 to 2009 for zone denotes when change occurred The IKONOS data defined the type of change.

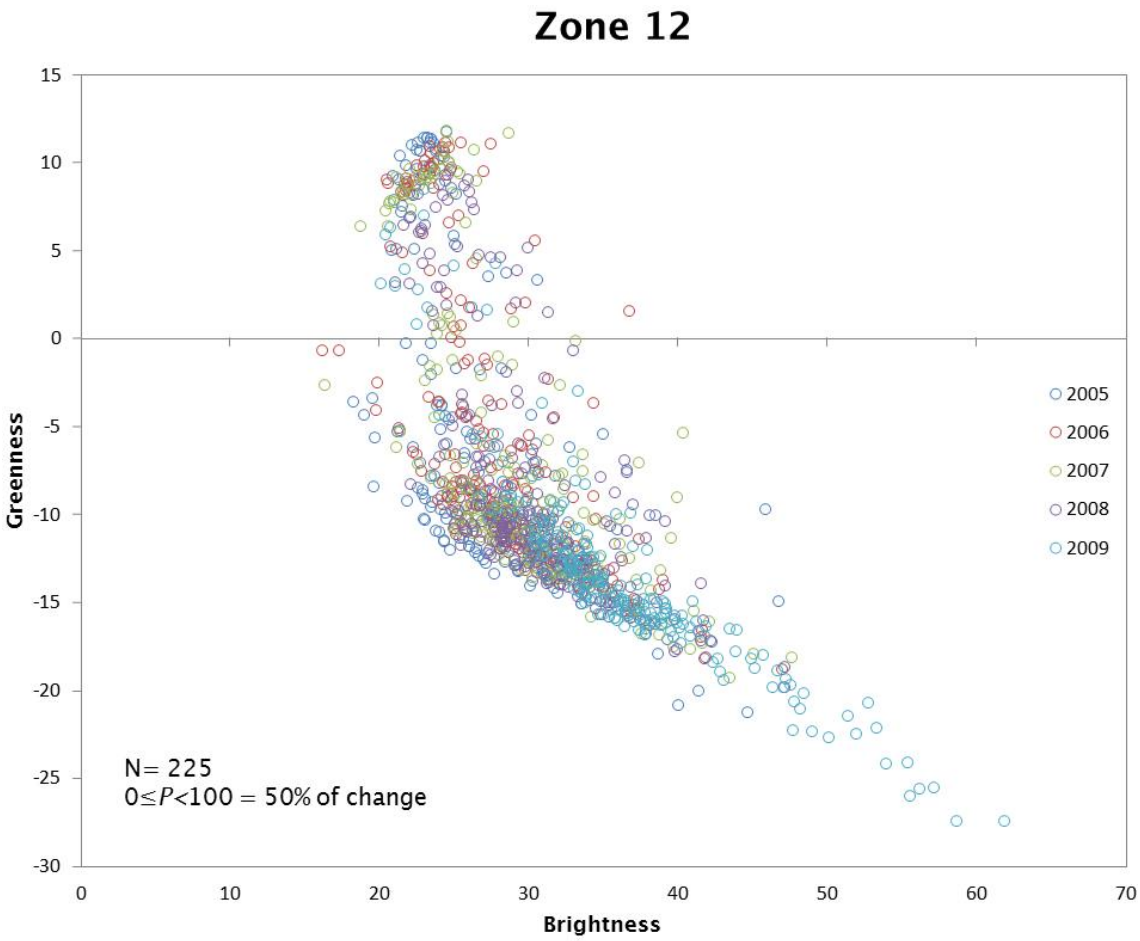


Figure A5.10.53 The feature space transition of change vector between greenness and brightness from Landsat ETM+ 2005 to 2009, zone 12.

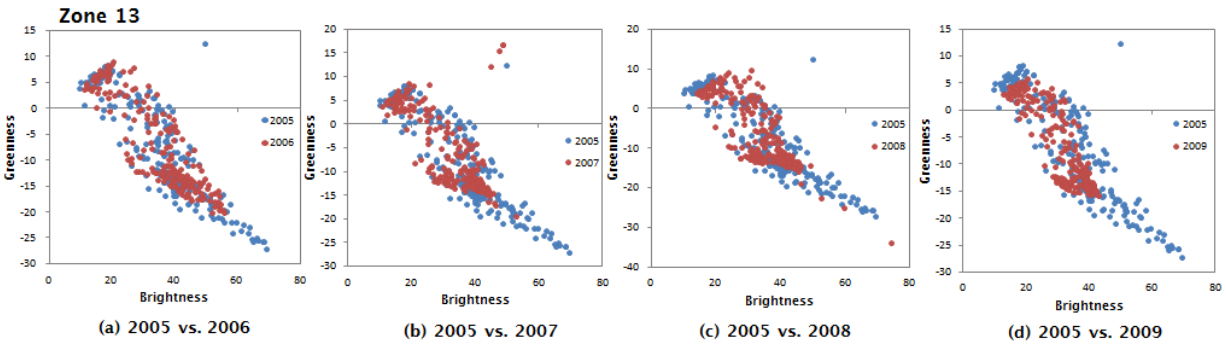


Figure A5.10.54 The direction and magnitude of change within yearly time series in feature space, zone 13.

From the correlation distribution result, the starting year of change for Zone 13 is 2007 with 50% change from bright surface to building.

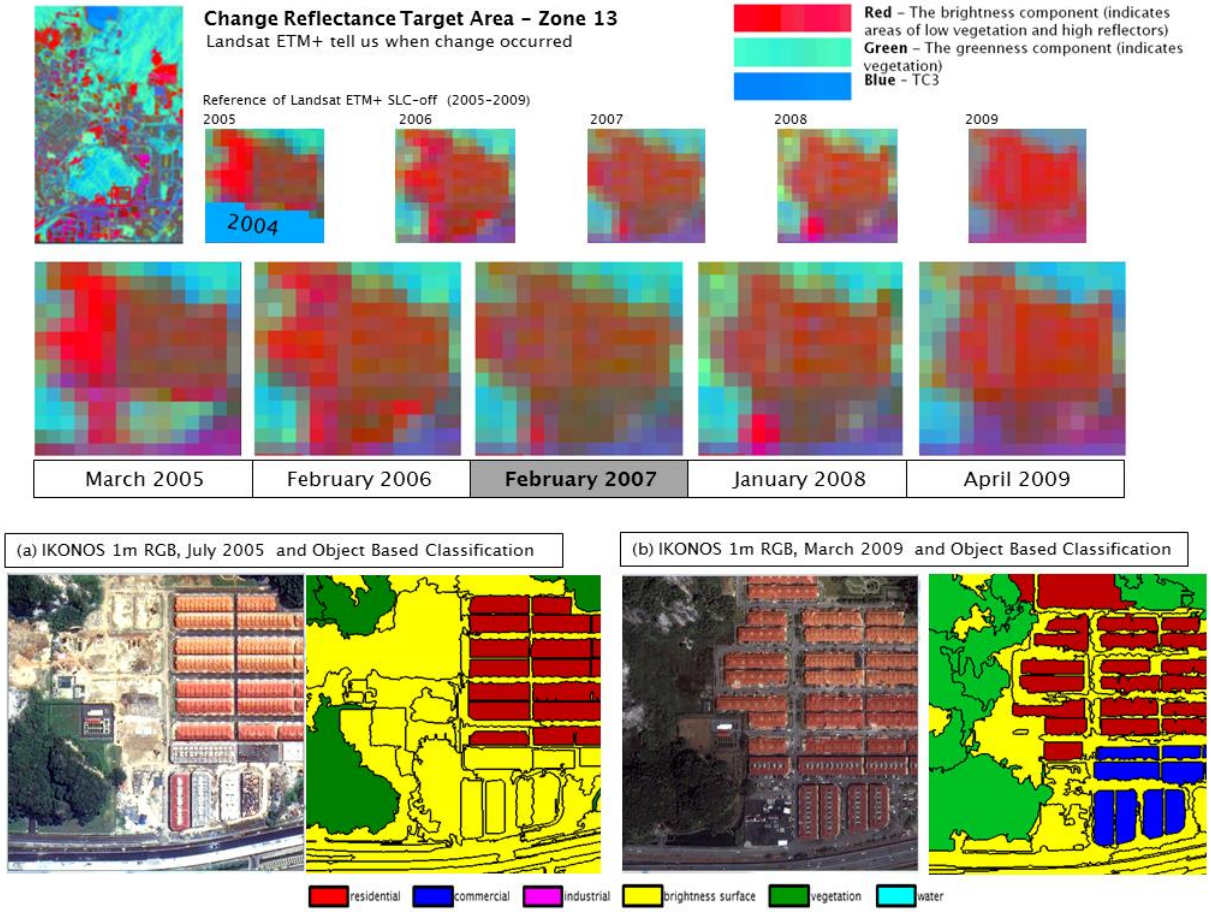


Figure A5.10.55 The transition of change between greenness and brightness from Landsat ETM+ 2005 to 2009 for zone 13 denotes when change occurred. The IKONOS data defined the type of change.

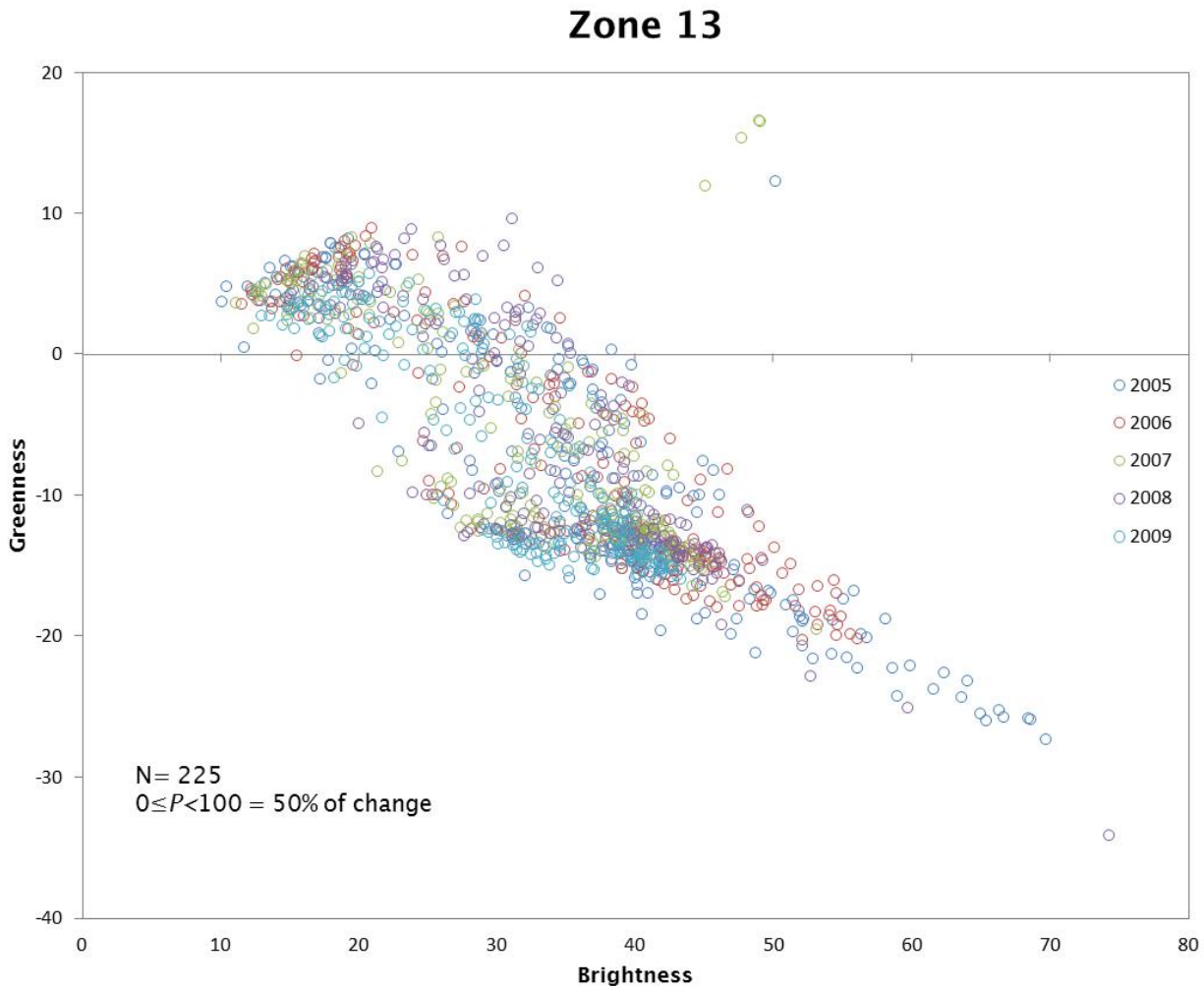


Figure A5.10.56 The feature space transition of change vector between greenness and brightness from Landsat ETM+ 2005 to 2009, zone 13.

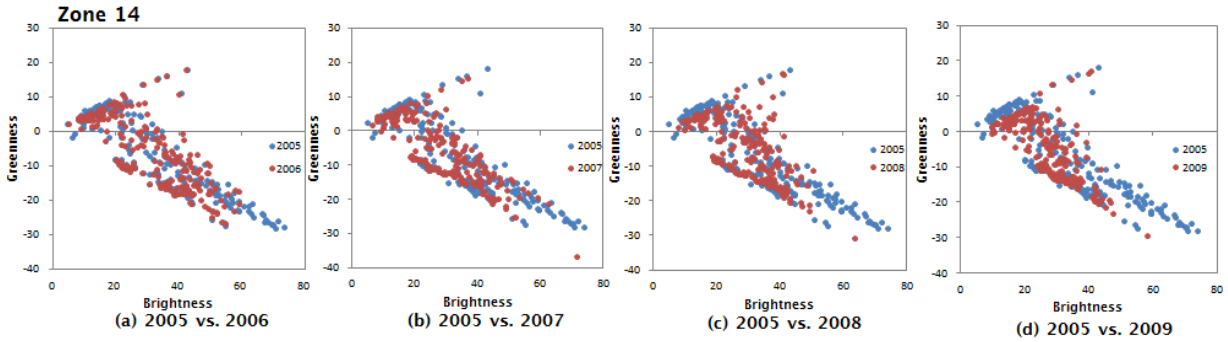


Figure A5.10.57 The direction and magnitude of change within yearly time series in feature space, zone 14.

From the correlation distribution result, the starting year of change for Zone 14 is 2007 with 50% change from bright surface to building.

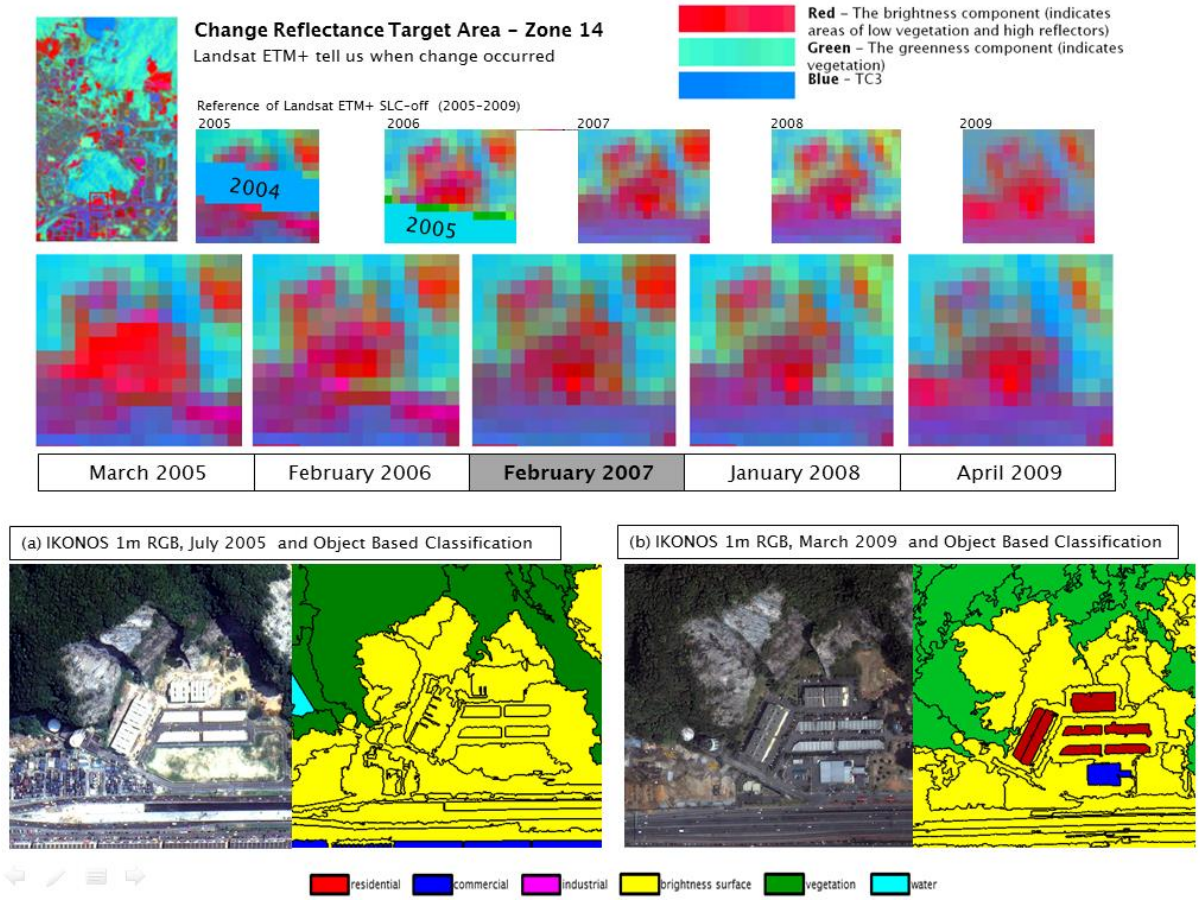


Figure A5.10.58 The transition of change between greenness and brightness from Landsat ETM+ 2005 to 2009 for zone 14 denotes when change occurred. The IKONOS data defined the type of change.

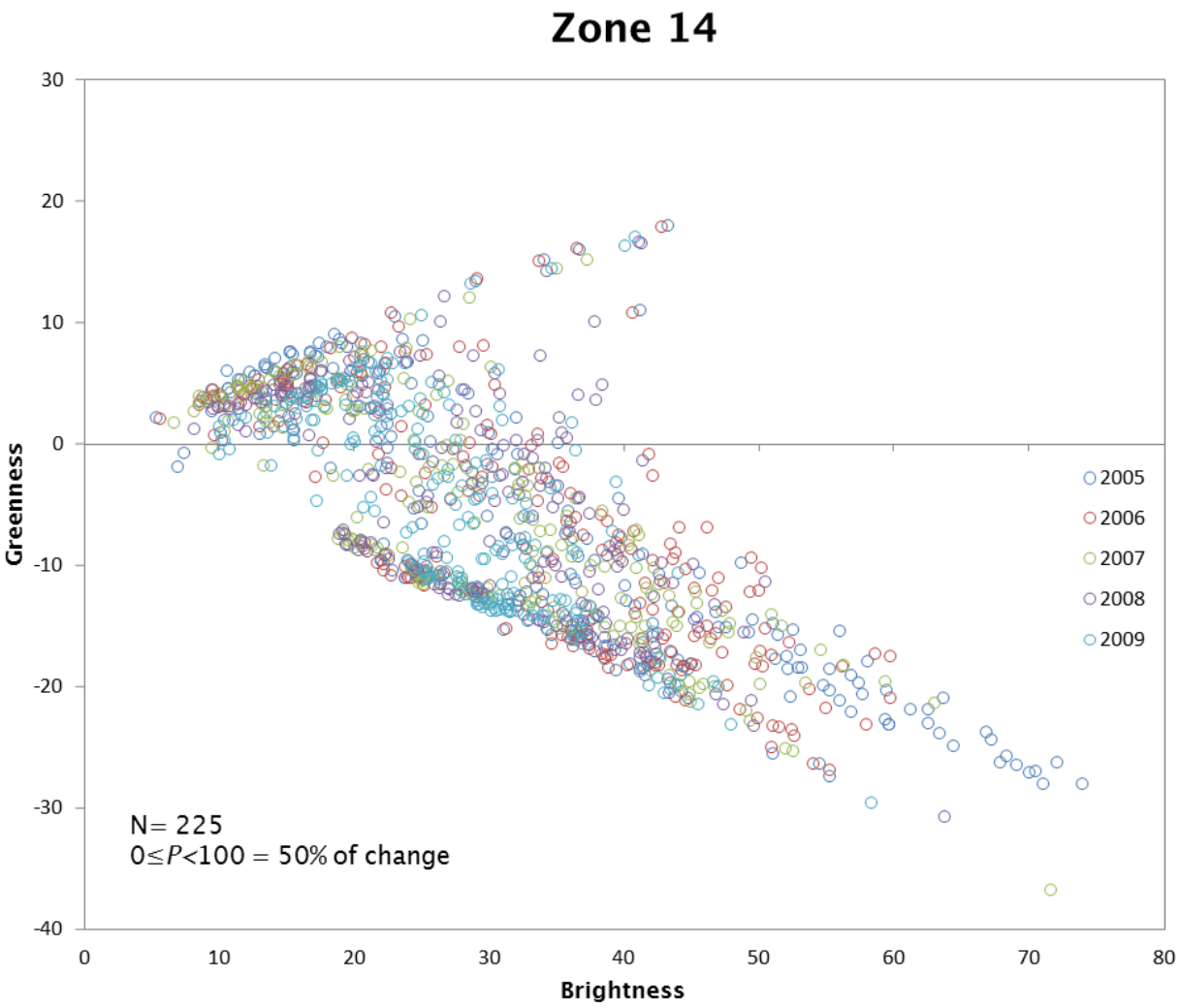


Figure A5.10.59 The feature space transition of change vector between greenness and brightness from Landsat ETM+ 2005 to 2009, zone 14.

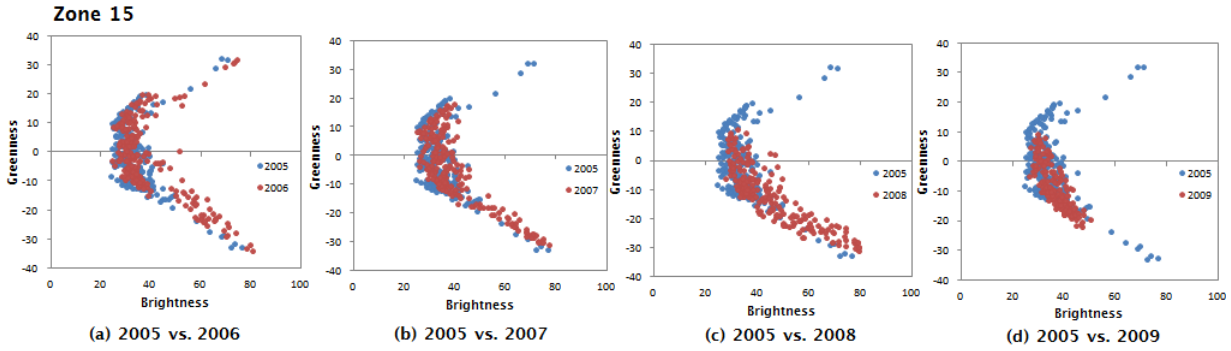


Figure A5.10.60 The direction and magnitude of change within yearly time series in feature space, zone 15.

From the correlation distribution result, the starting year of change for Zone 15 is 2008 with 90% change from vegetation to bright surface and building.

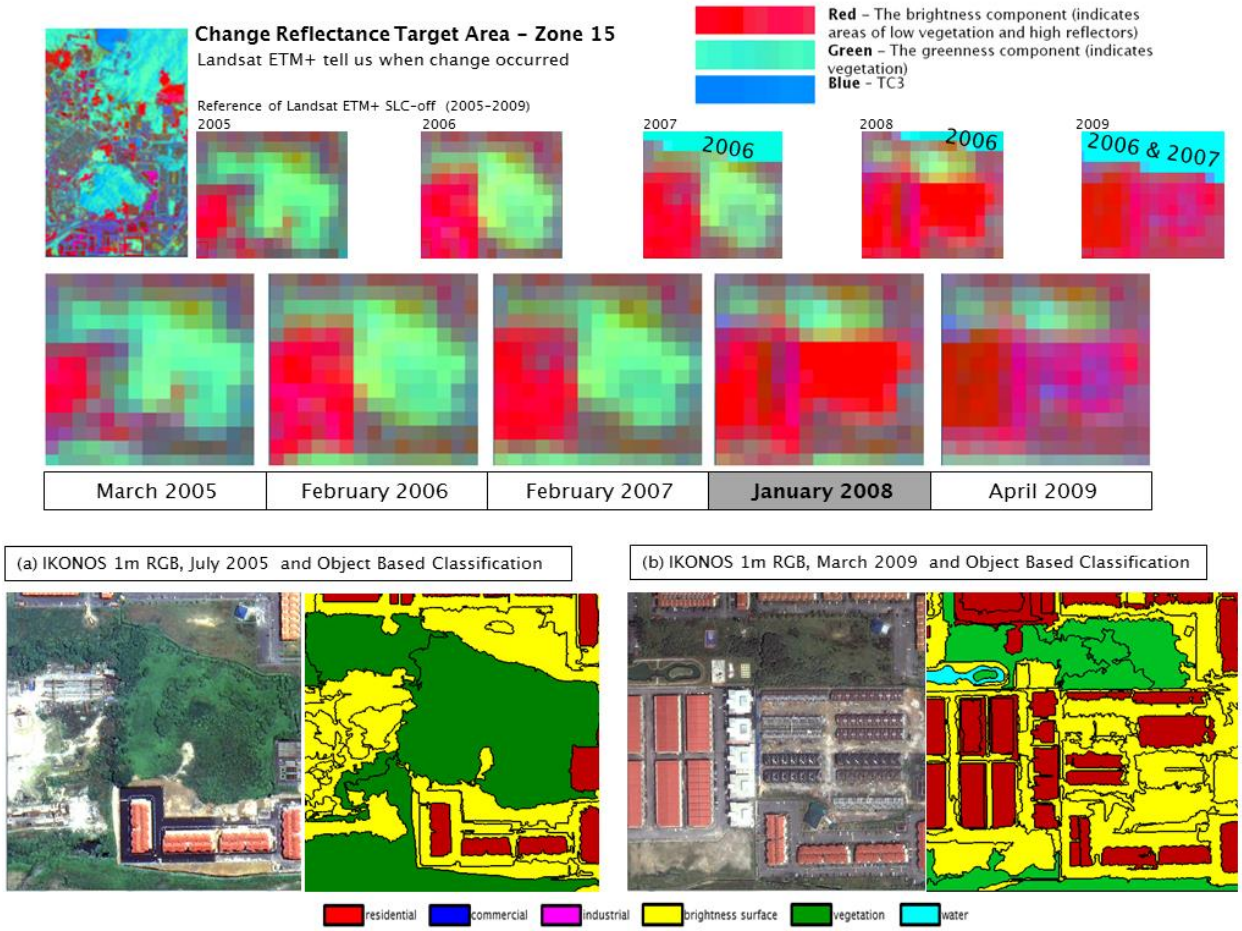


Figure A5.10.61 The transition of change between greenness and brightness from Landsat ETM+ 2005 to 2009 for zone 15 denotes when change occurred. The IKONOS data defined the type of change.

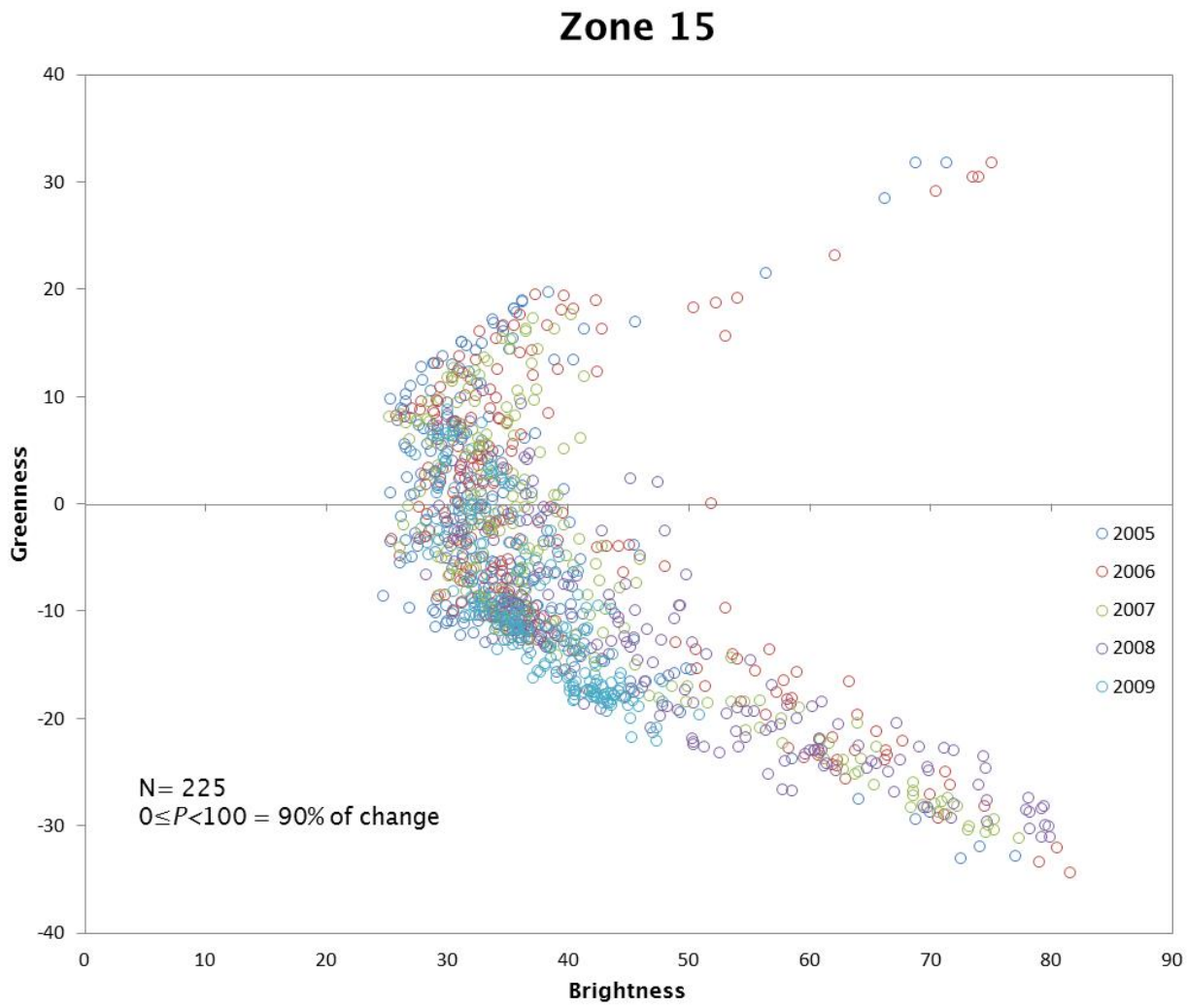


Figure A5.10.62 The feature space transition of change vector between greenness and brightness from Landsat ETM+ 2005 to 2009, zone 15.

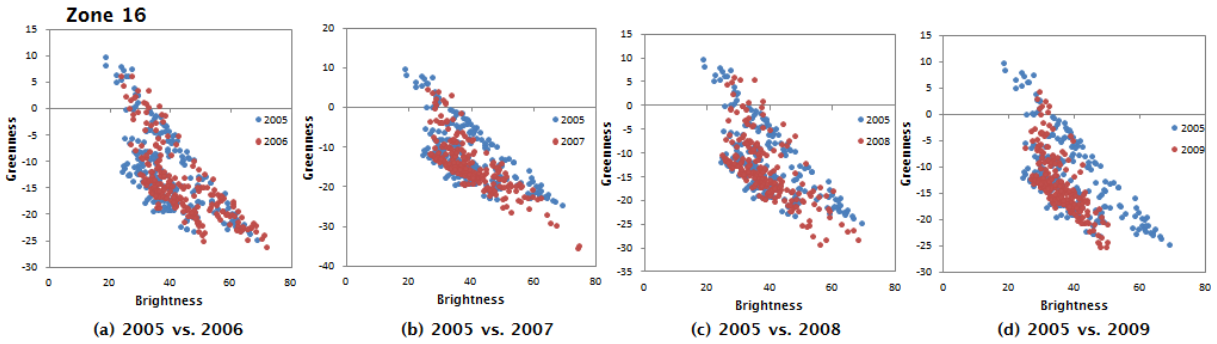


Figure A5.10.63 The direction and magnitude of change within yearly time series in feature space, zone 16.

From the correlation distribution result, the starting year of change for Zone 16 is 2007 with 50% change from bright surface to building.

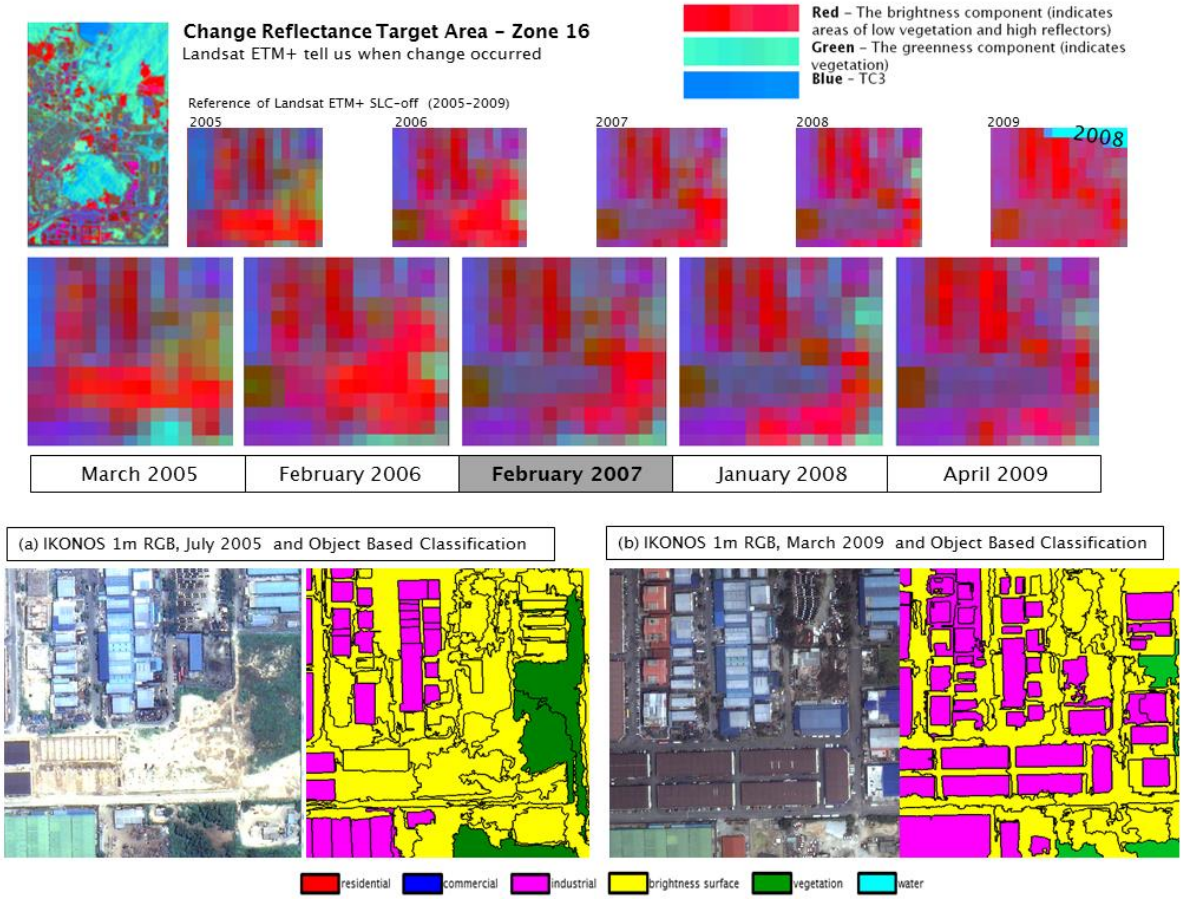


Figure A5.10.64 The transition of change between greenness and brightness from Landsat ETM+ 2005 to 2009 for zone 16 denotes when change occurred. The IKONOS data defined the type of change.

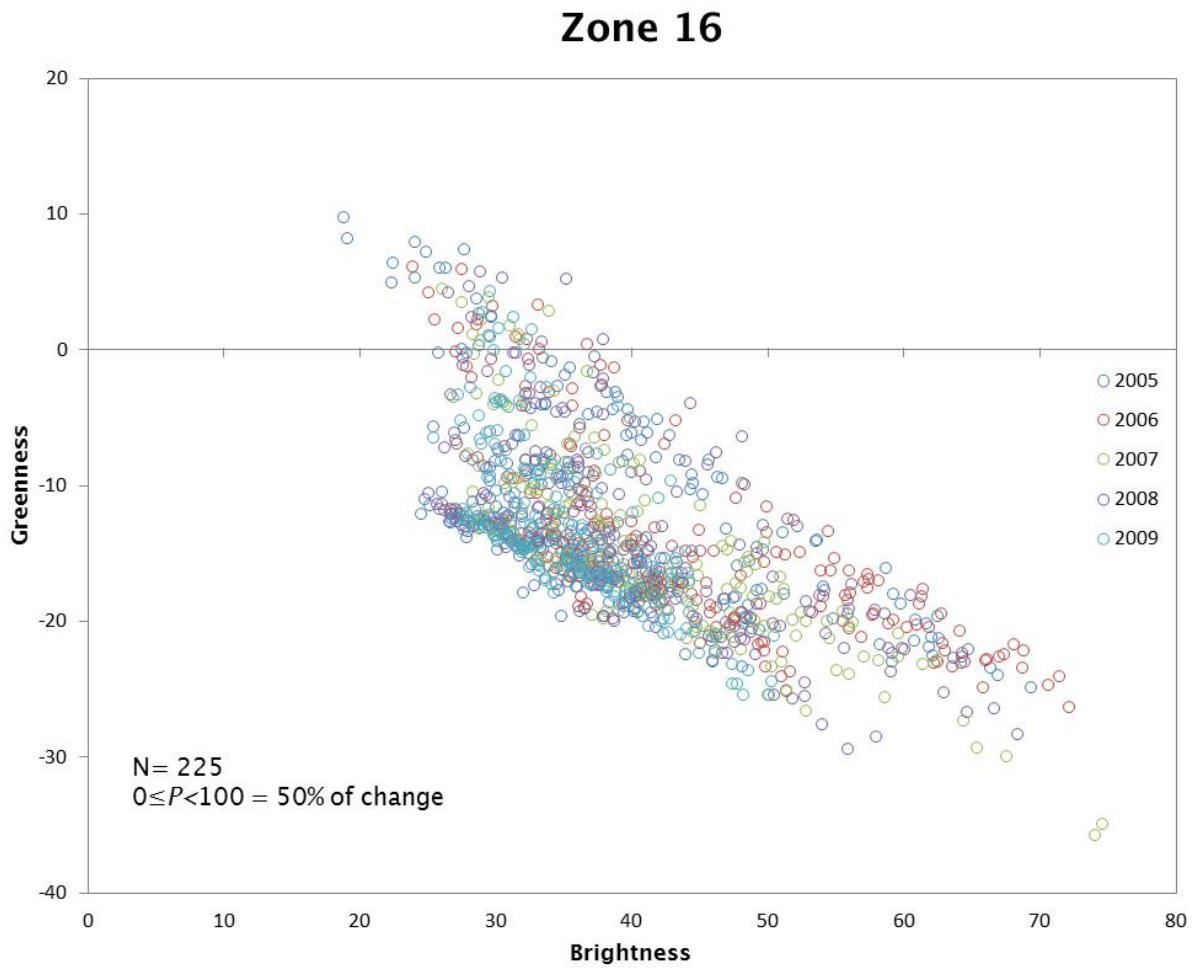


Figure A5.10.65 The feature space transition of change vector between greenness and brightness from Landsat ETM+ 2005 to 2009, zone 16.

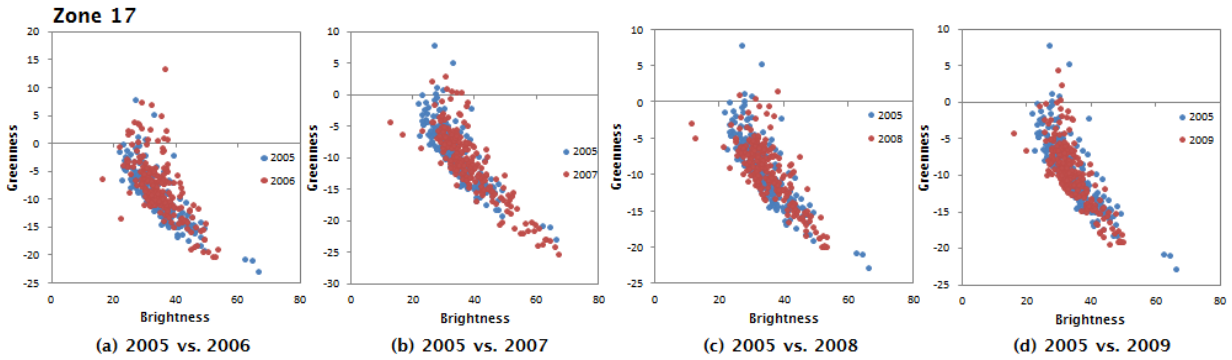


Figure A5.10.66 The direction and magnitude of change within yearly time series in feature space, zone 17.

From the correlation distribution result, the starting year of change for Zone 17 is 2008 with 50% change from bright surface to building.

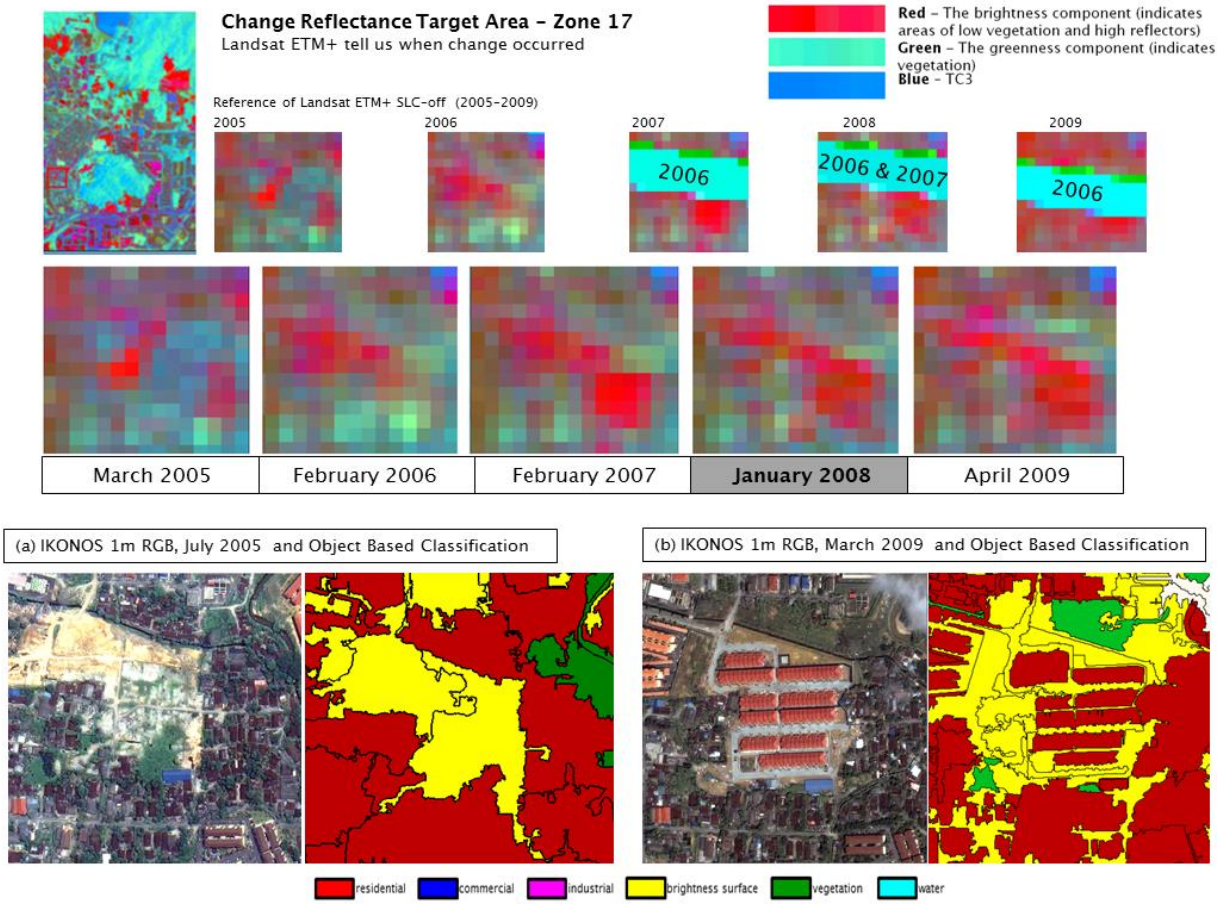


Figure A5.10.67 The transition of change between greenness and brightness from Landsat ETM+ 2005 to 2009 for zone 17 denotes when change occurred. The IKONOS data defined the type of change.

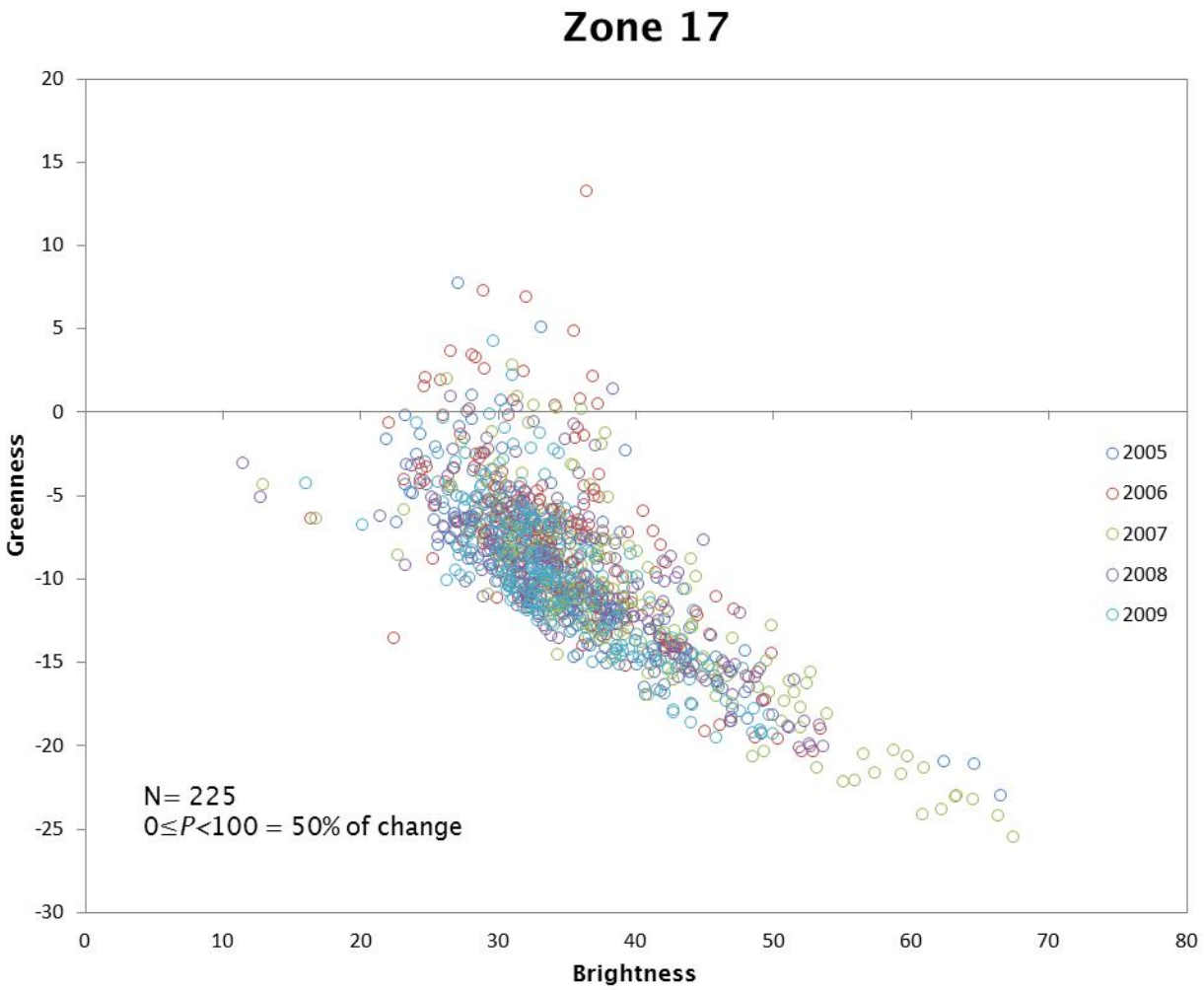


Figure A5.10.68 The feature space transition of change vector between greenness and brightness from Landsat ETM+ 2005 to 2009, zone 17.

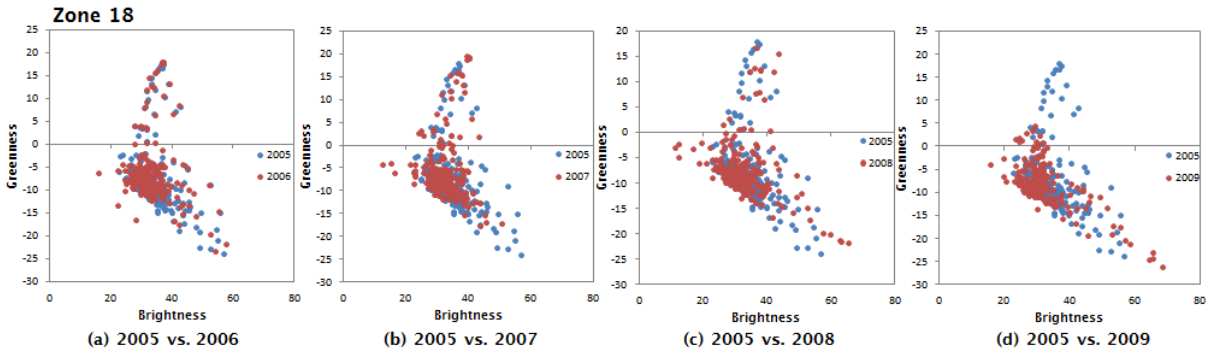


Figure A5.10.69 The direction and magnitude of change within yearly time series in feature space, zone 18.

From the correlation distribution result, the starting year of change for Zone 18 is 2008 with 20% change from vegetation to bright surface.

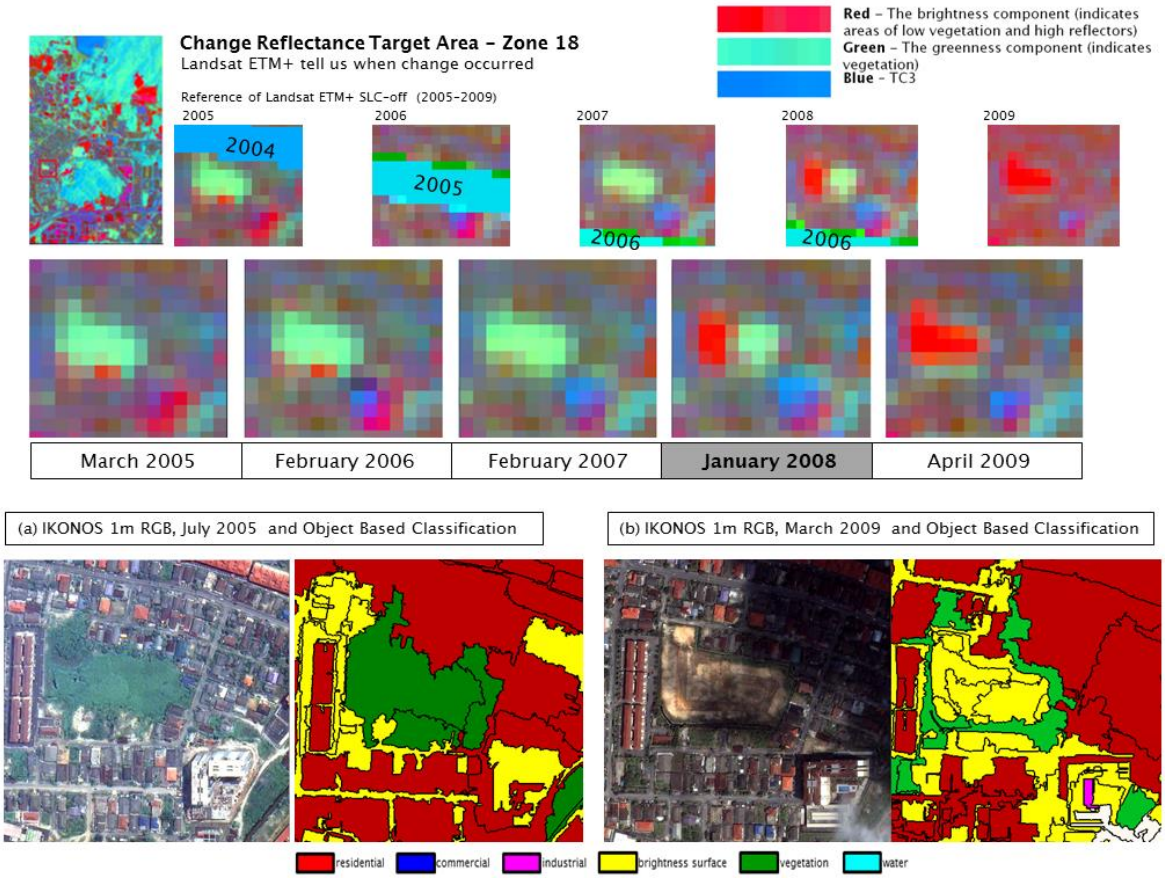


Figure A5.10.70 The transition of change between greenness and brightness from Landsat ETM+ 2005 to 2009 for zone 18 denotes when change occurred. The IKONOS data defined the type of change.

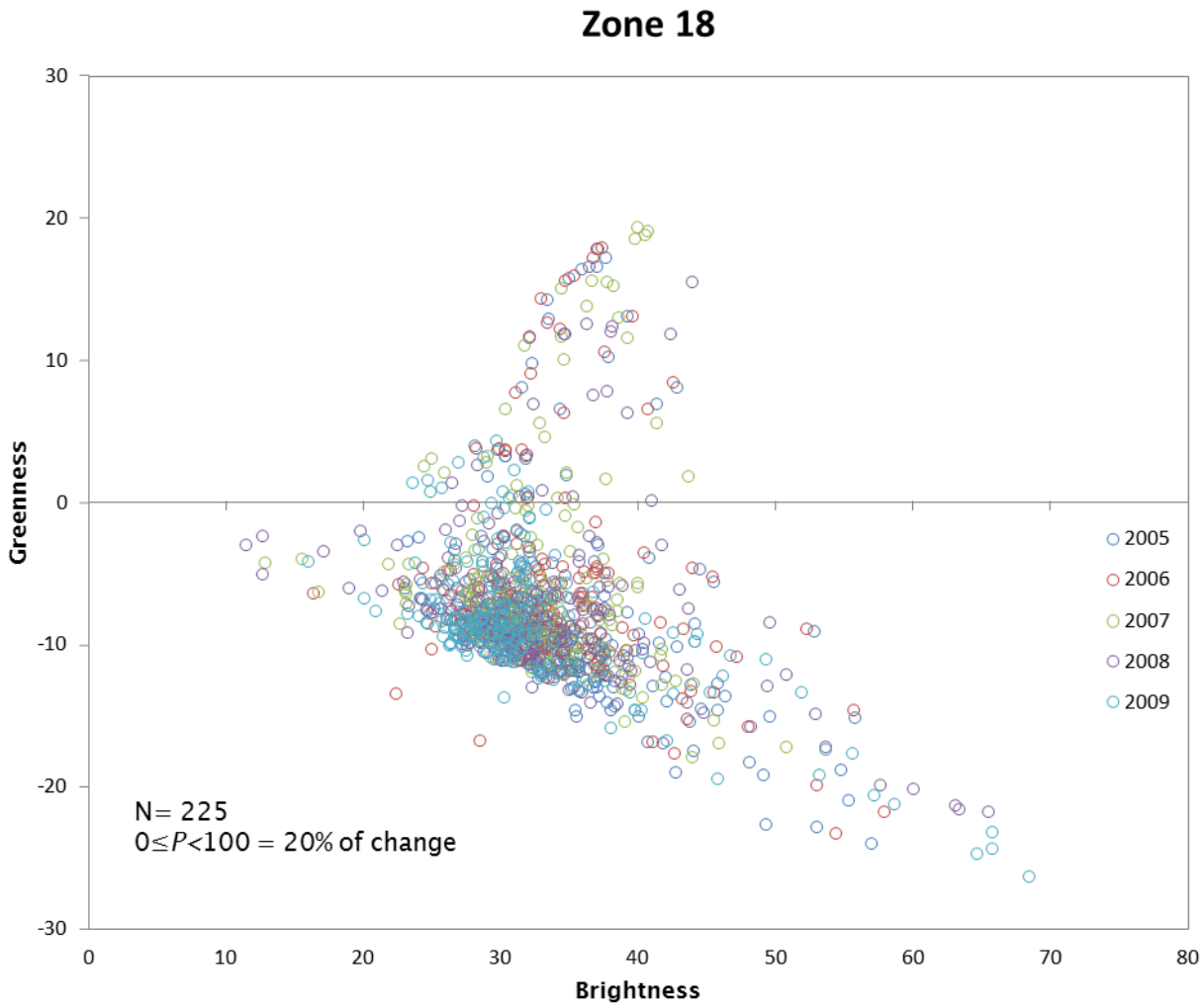


Figure A5.10.71 The feature space transition of change vector between greenness and brightness from Landsat ETM+ 2005 to 2009, zone 18.

# Appendix 6: Chapter 7 – Empirical Result of Validation of No Change (NC) vector of TC result between greenness and brightness for 18 point target zone samples for no change occurring between 2005-2009.

**Empirical result B**

**Validation of No Change (NC) vector of TC result between greenness and brightness for 18 point target zone samples for no change occurring between 2005-2009.**

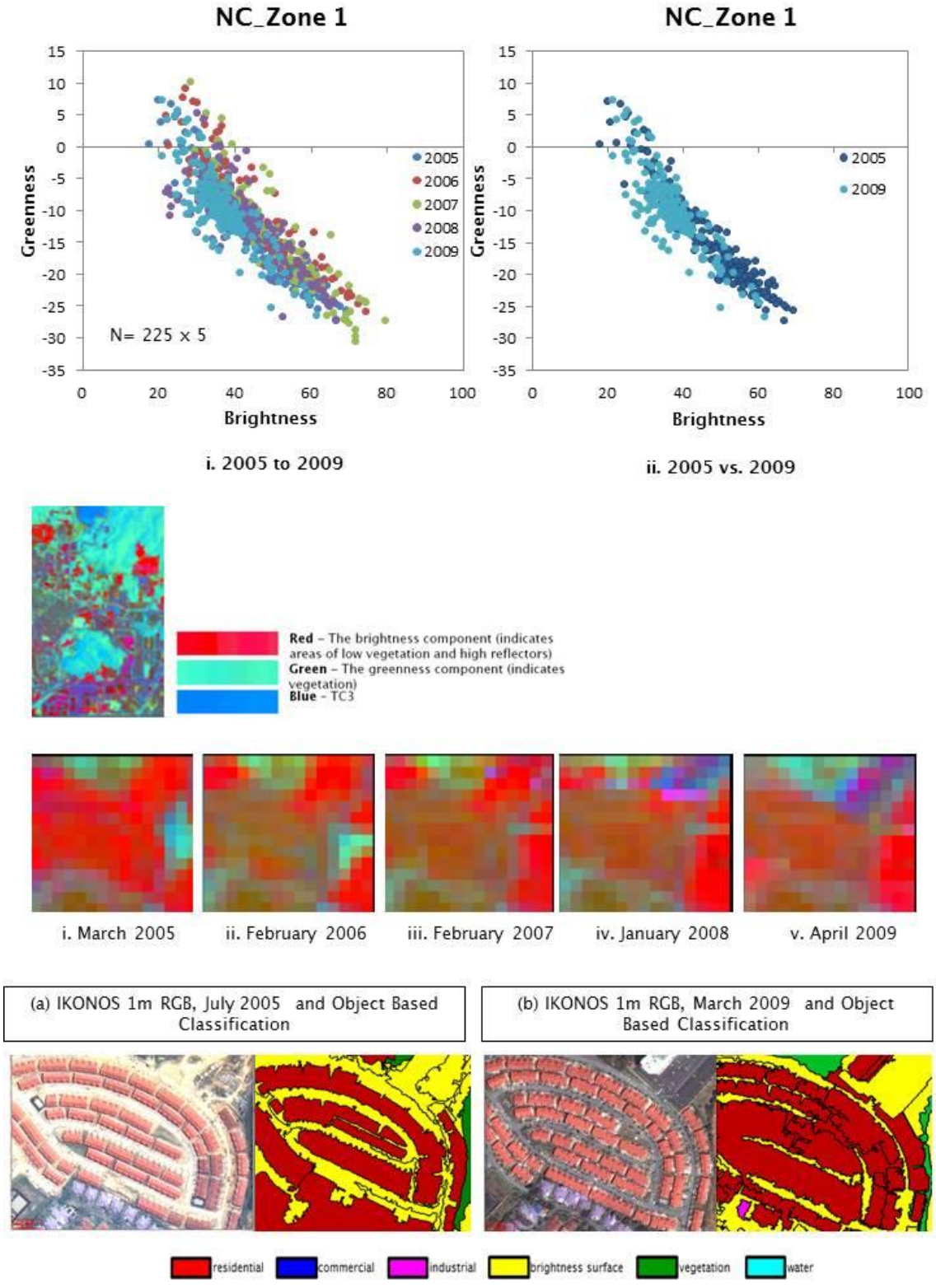


Figure A6.10.72 Validation from the feature space of no change (NC) shown by the TC result between greenness and brightness from Zone 1, Landsat ETM+ 2005 to 2009.

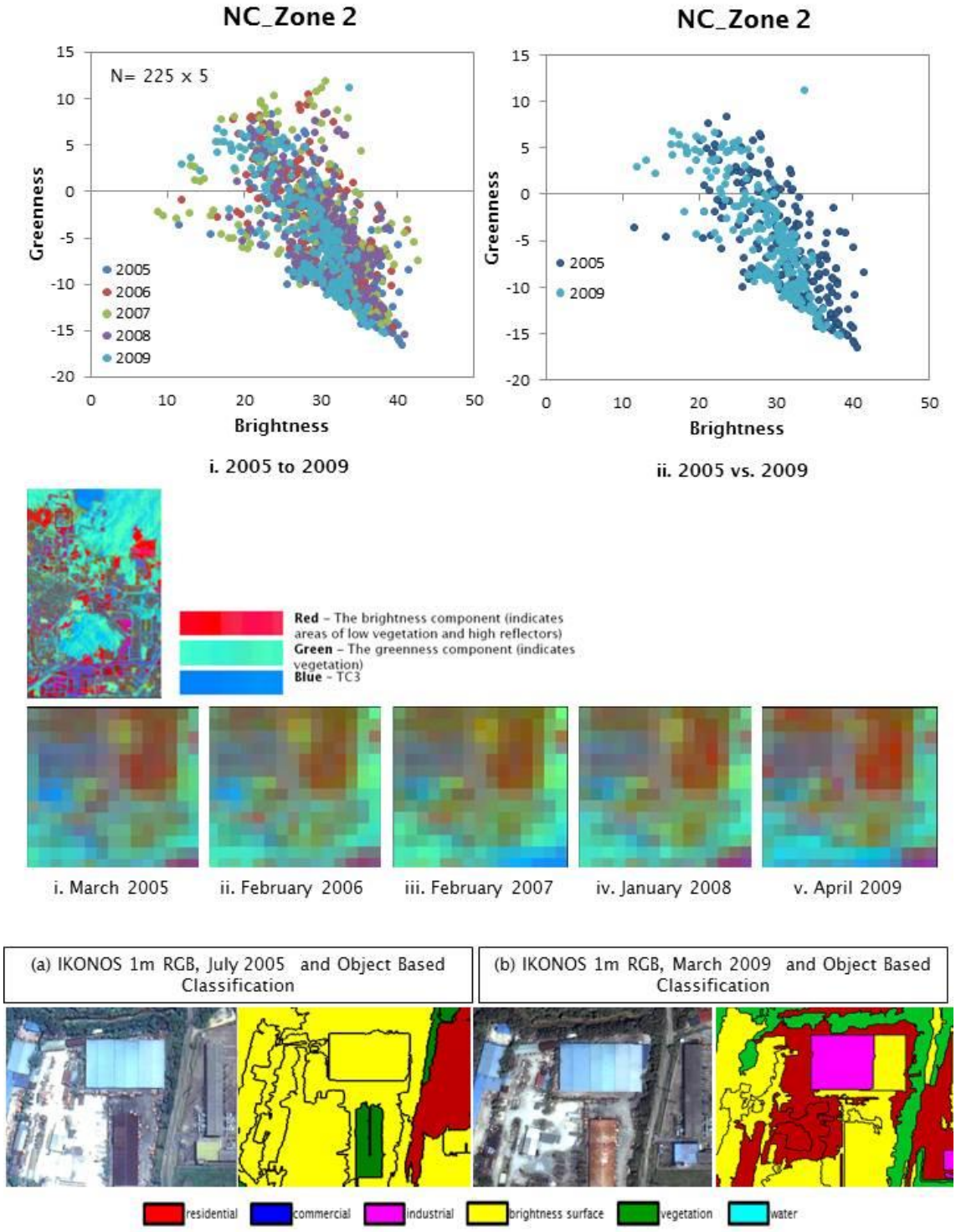


Figure A6.10.73 Validation from the feature space of no change (NC) shown by the TC result between greenness and brightness from Zone 2, Landsat ETM+ 2005 to 2009.

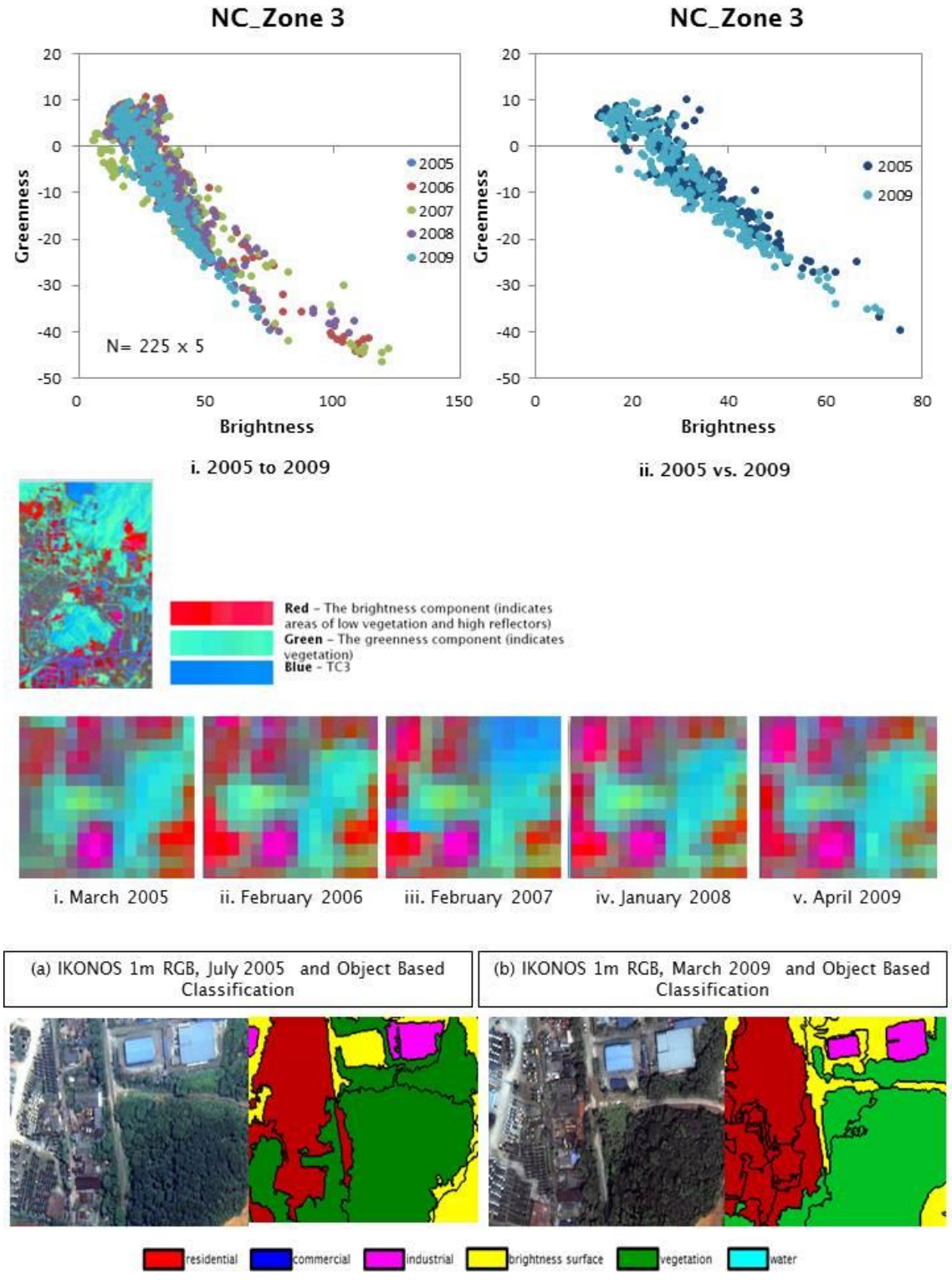


Figure A6.10.74 Validation from the feature space of no change (NC) shown by the TC result between greenness and brightness from Zone 3, Landsat ETM+ 2005 to 2009.

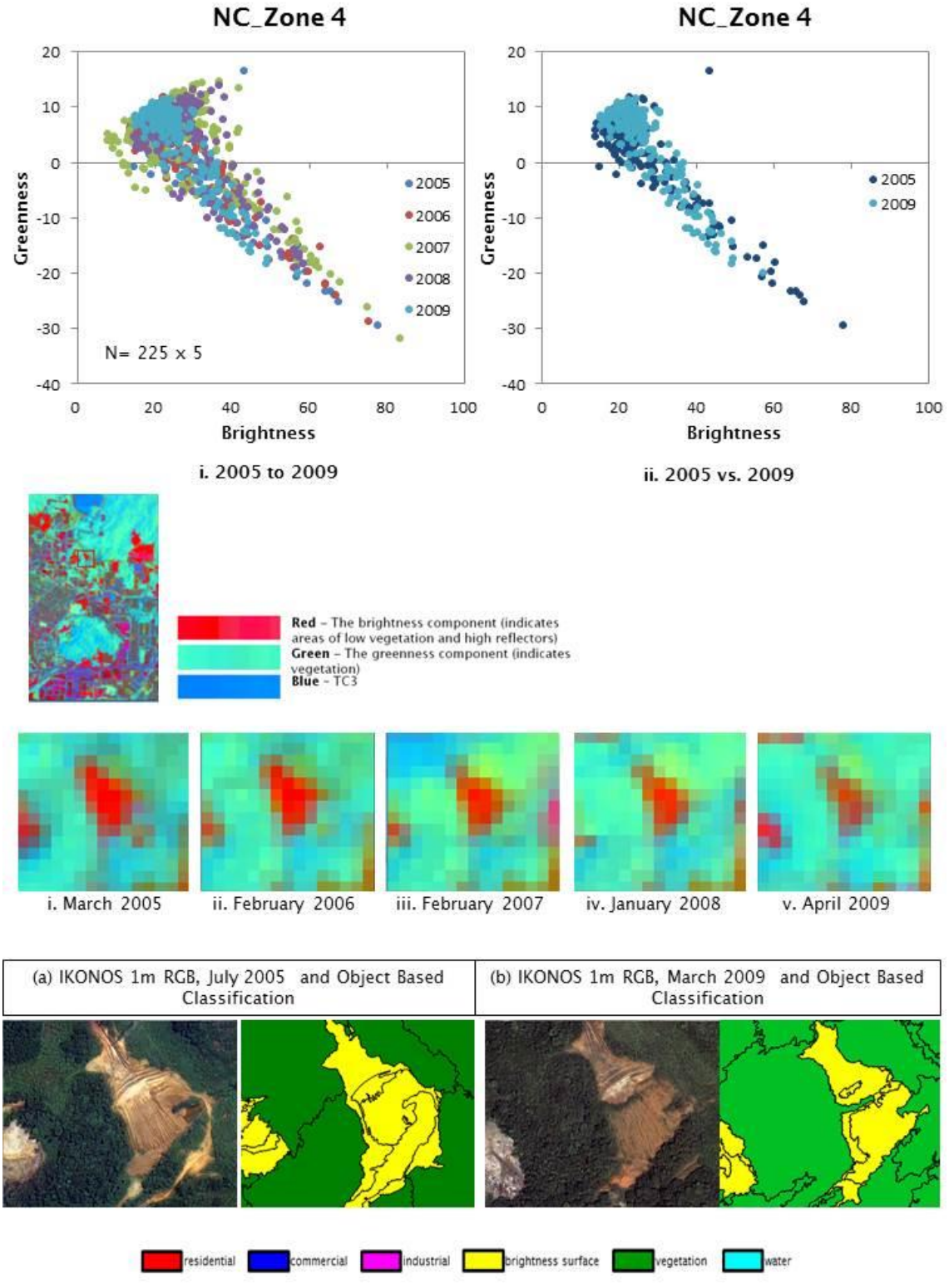


Figure A6.10.75 Validation from the feature space of no change (NC) shown by the TC result between greenness and brightness from Zone 4, Landsat ETM+ 2005 to 2009.

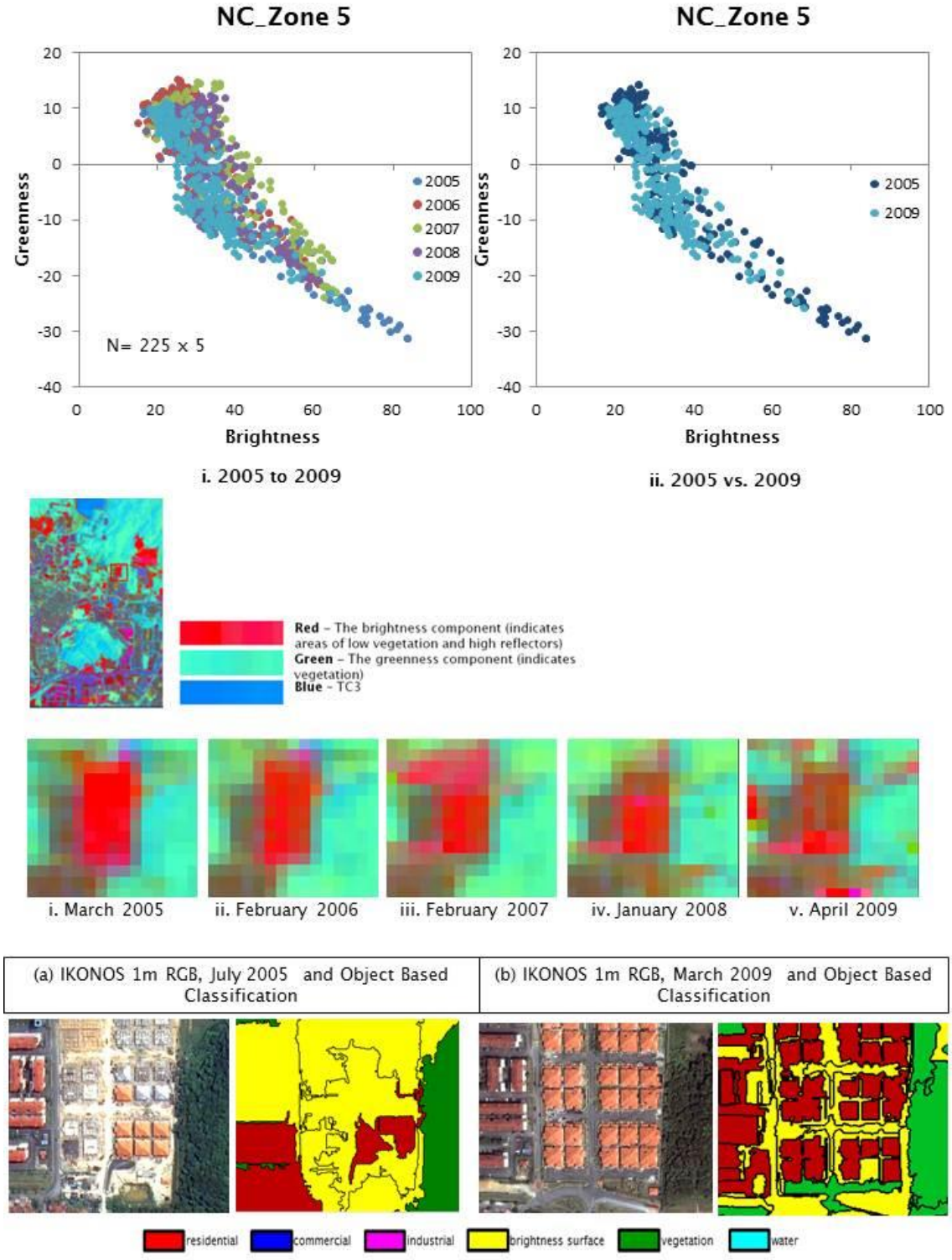


Figure A6.10.76 Validation from the feature space of no change (NC) shown by the TC result between greenness and brightness from Zone 5, Landsat ETM+ 2005 to 2009.

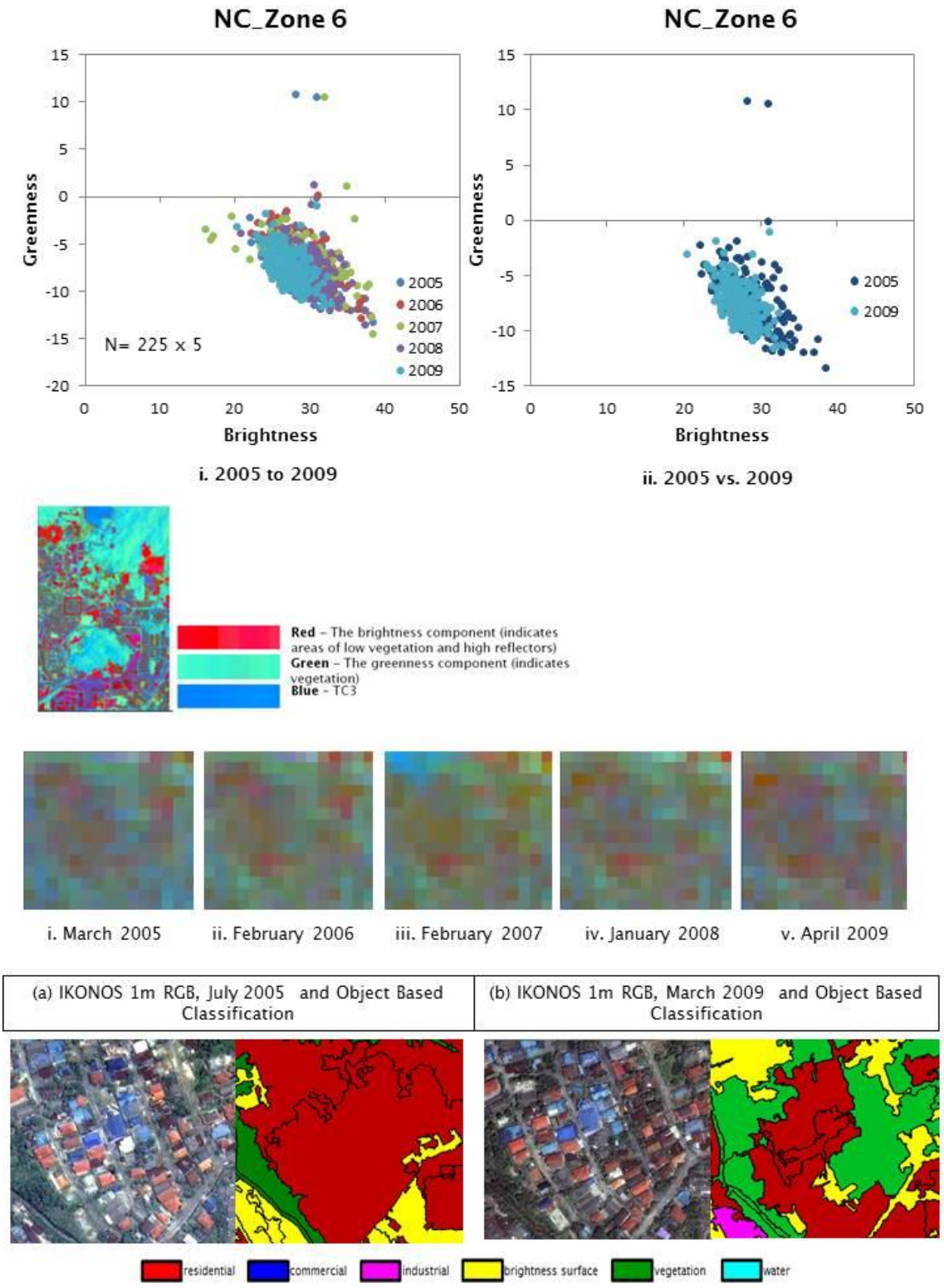


Figure A6.10.77 Validation from the feature space of no change (NC) shown by the TC result between greenness and brightness from Zone 6, Landsat ETM+ 2005 to 2009.

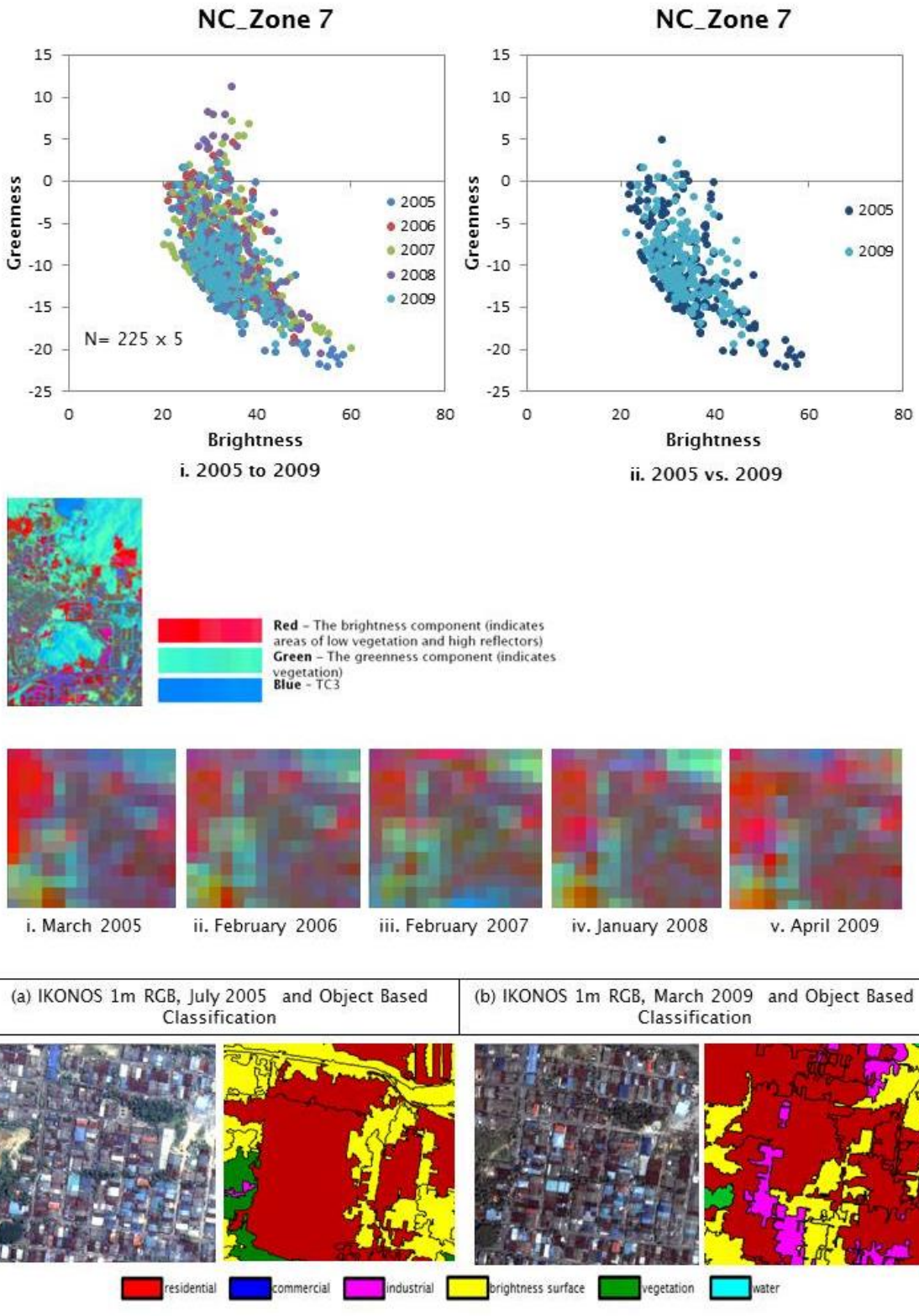


Figure A6.10.78 Validation from the feature space of no change (NC) shown by the TC result between greenness and brightness from Zone 7, Landsat ETM+ 2005 to 2009.

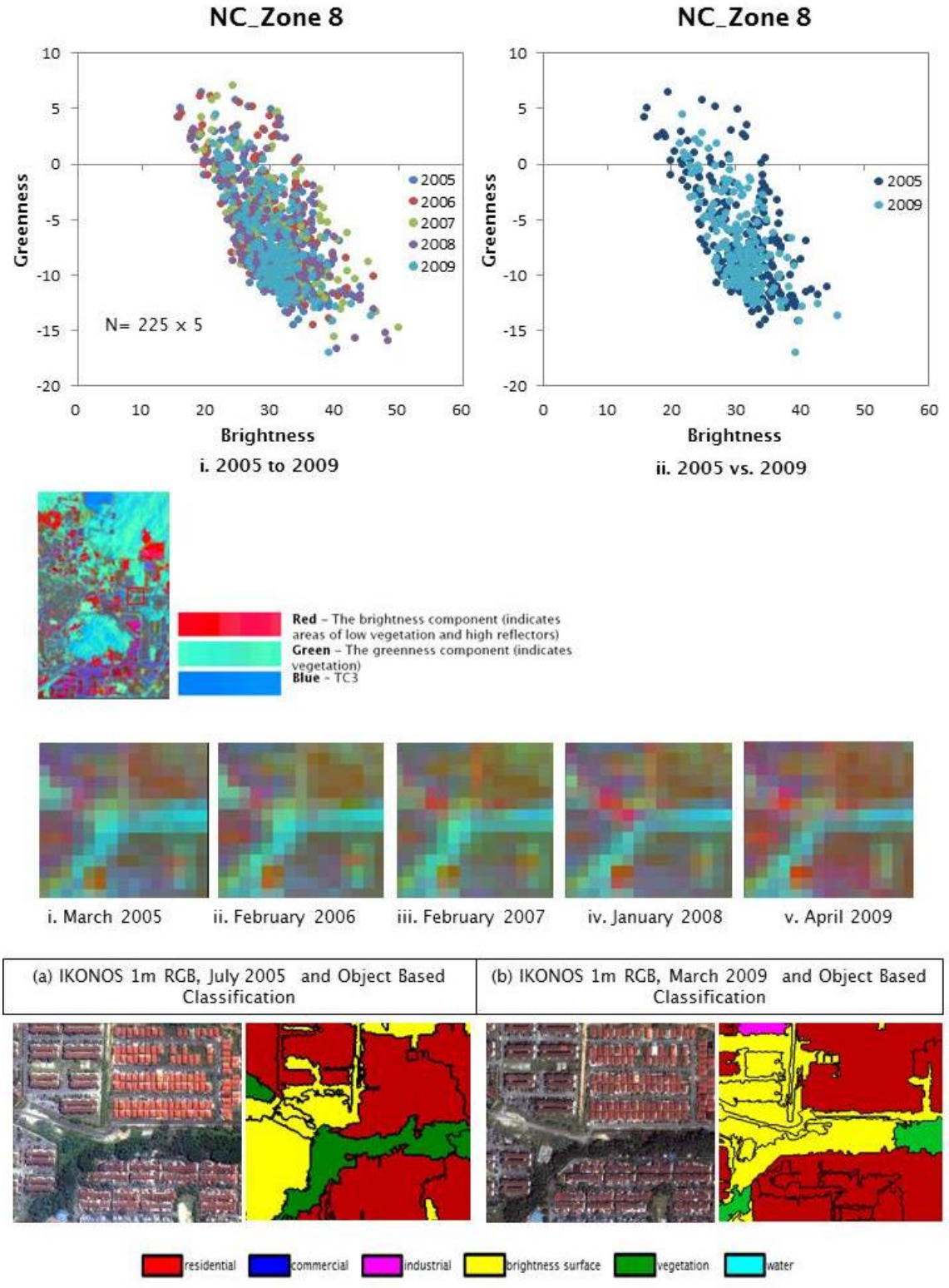


Figure A6.10.79 Validation from the feature space of no change (NC) shown by the TC result between greenness and brightness from Zone 8, Landsat ETM+ 2005 to 2009.

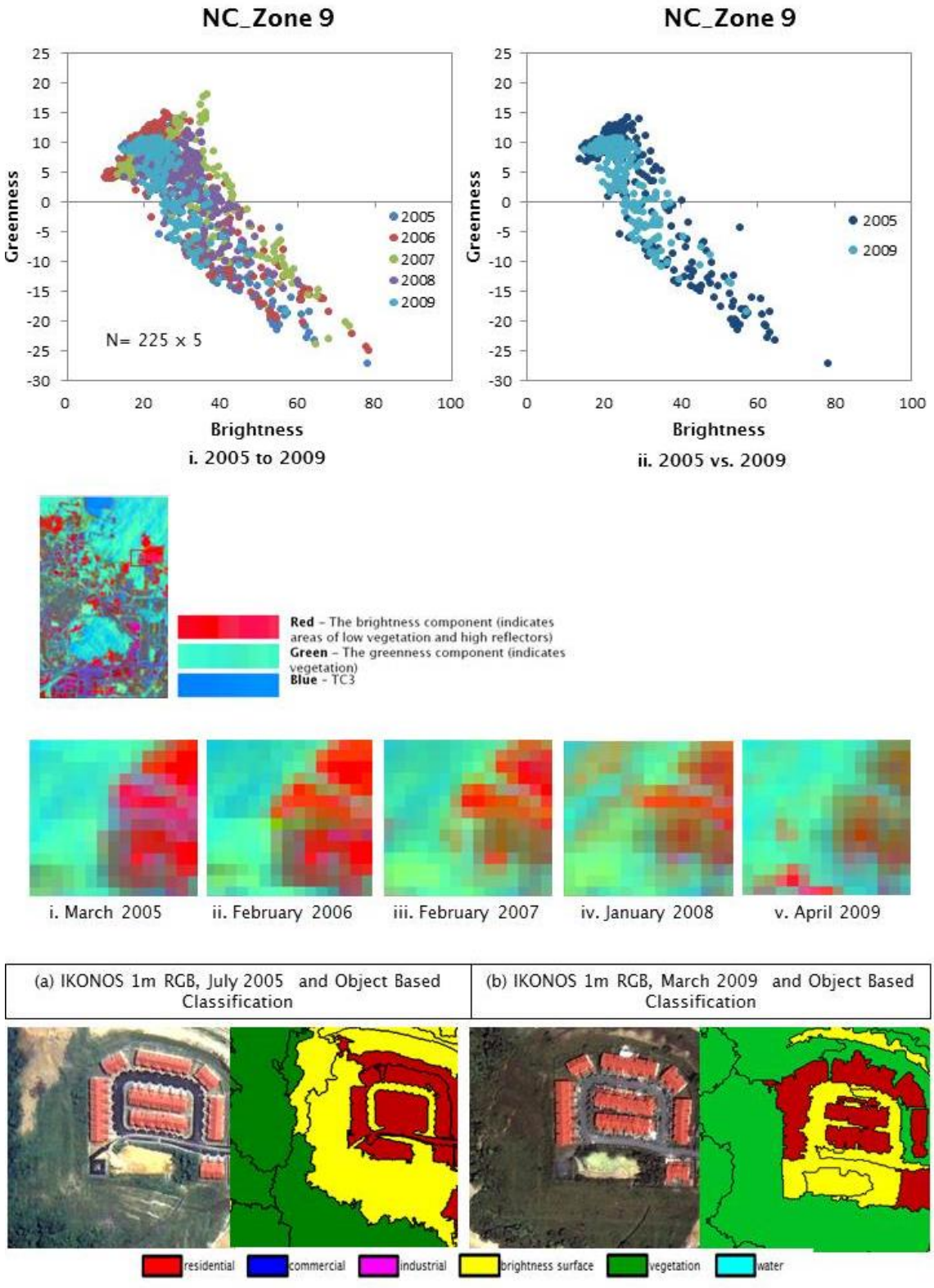


Figure A6.10.80 Validation from the feature space of no change (NC) shown by the TC result between greenness and brightness from Zone 9, Landsat ETM+ 2005 to 2009.

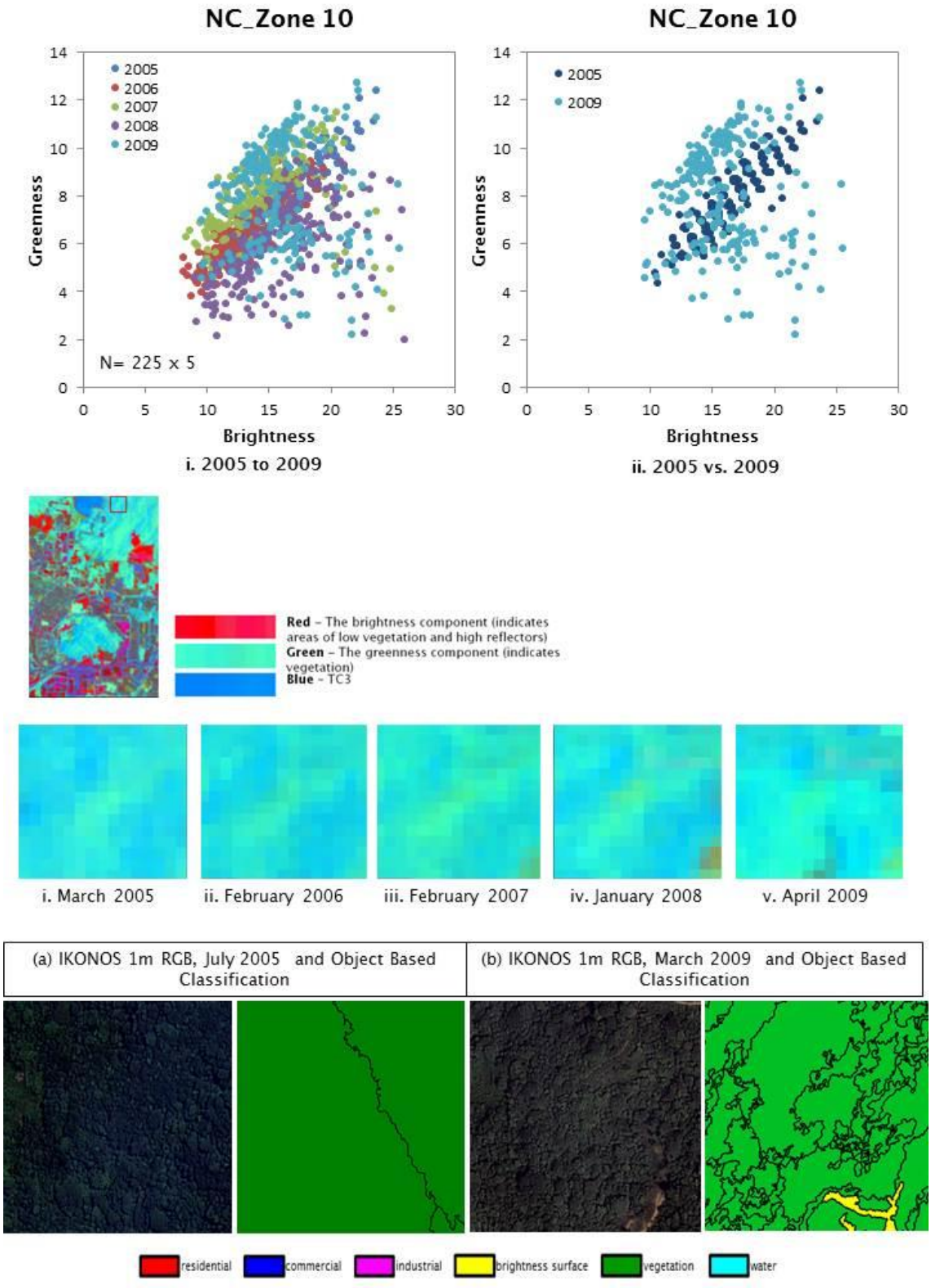


Figure A6.10.81 Validation from the feature space of no change (NC) shown by the TC result between greenness and brightness from Zone 10, Landsat ETM+ 2005 to 2009.

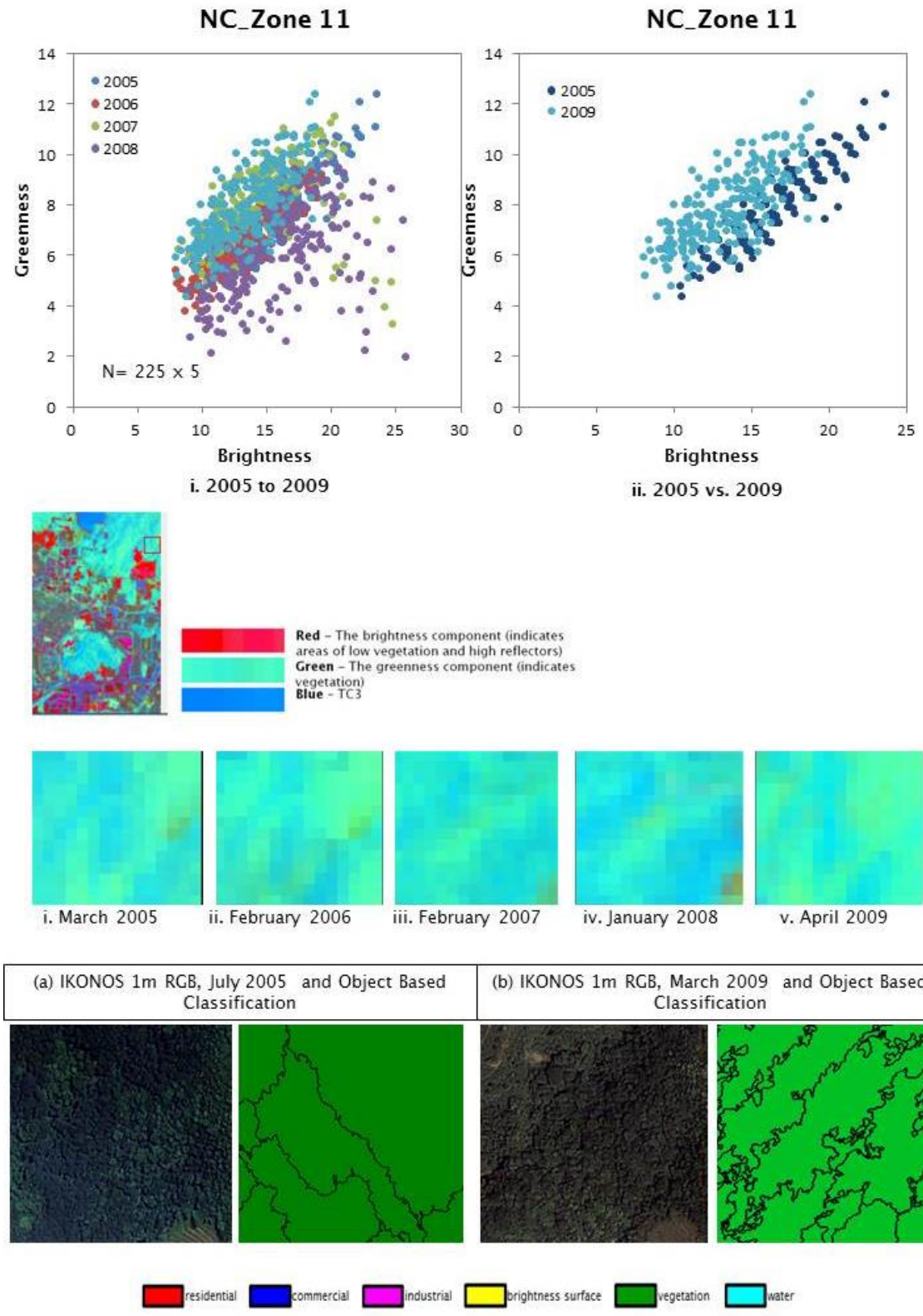


Figure A6.10.82 Validation from the feature space of no change (NC) shown by the TC result between greenness and brightness from Zone 11, Landsat ETM+ 2005 to 2009.

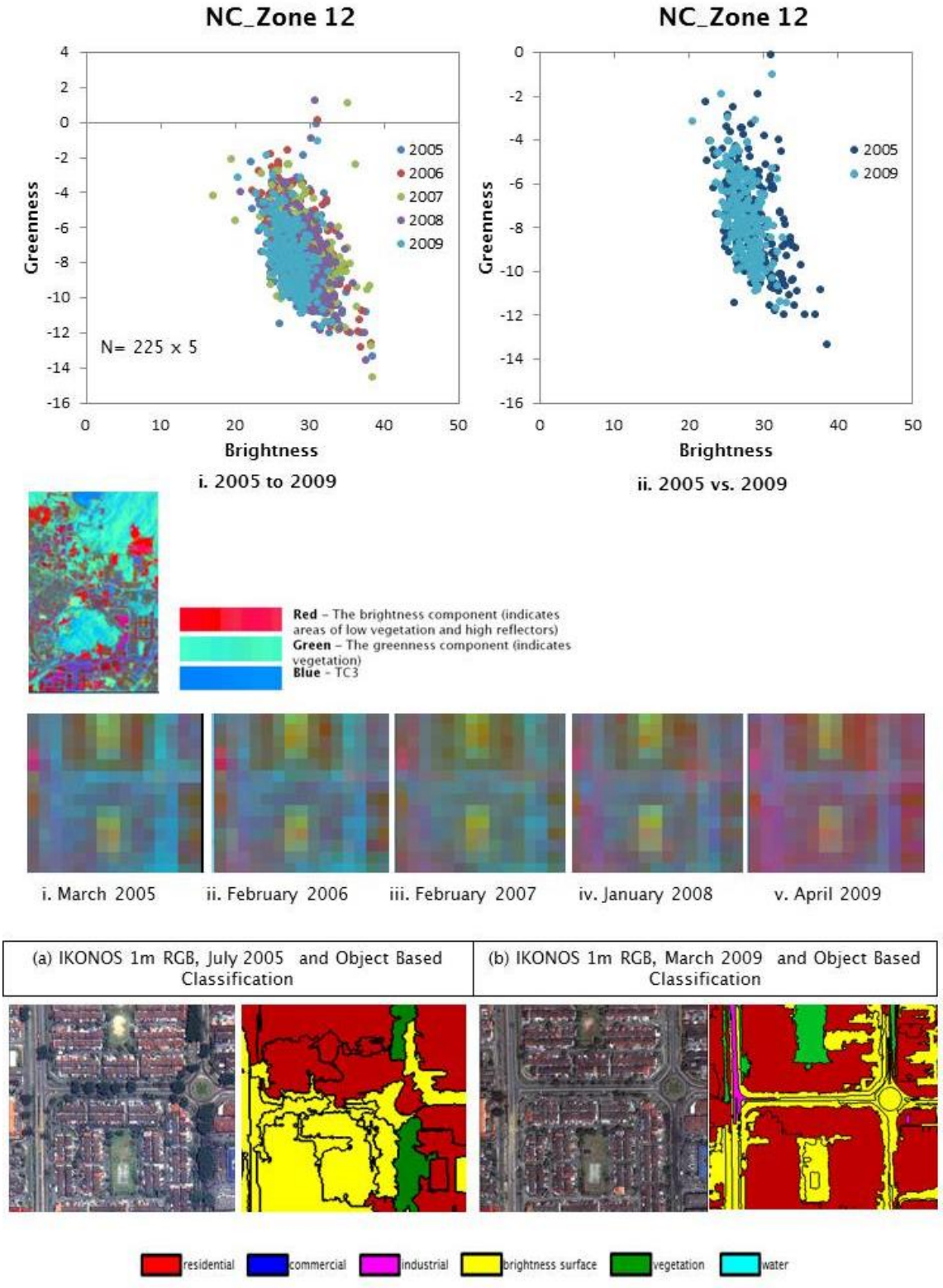


Figure A6.10.83 Validation from the feature space of no change (NC) shown by the TC result between greenness and brightness from Zone 12, Landsat ETM+ 2005 to 2009.

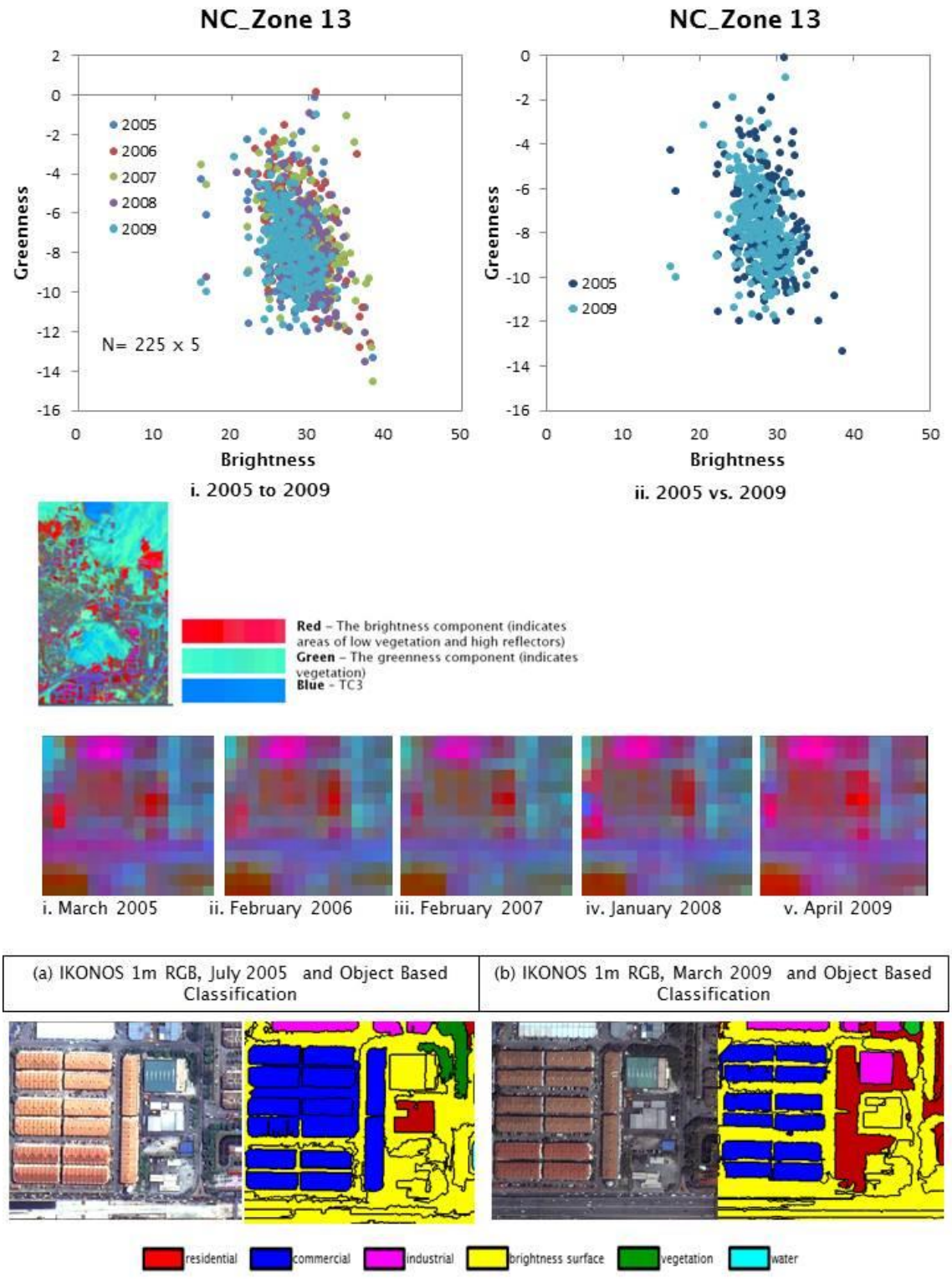


Figure A6.10.84 Validation from the feature space of no change (NC) shown by the TC result between greenness and brightness from Zone 13, Landsat ETM+ 2005 to 2009.

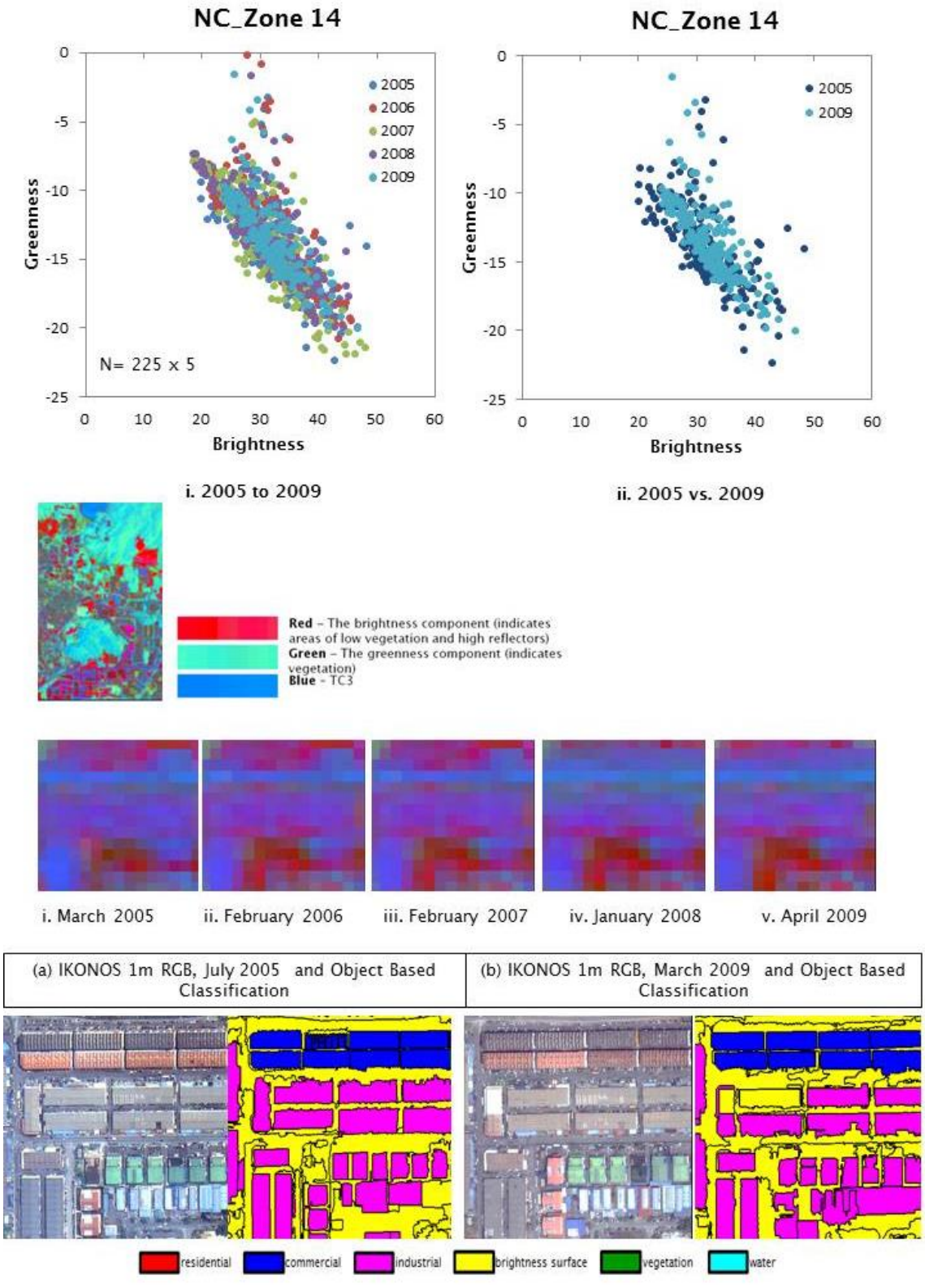


Figure A6.10.85 Validation from the feature space of no change (NC) shown by the TC result between greenness and brightness from Zone 14, Landsat ETM+ 2005 to 2009.

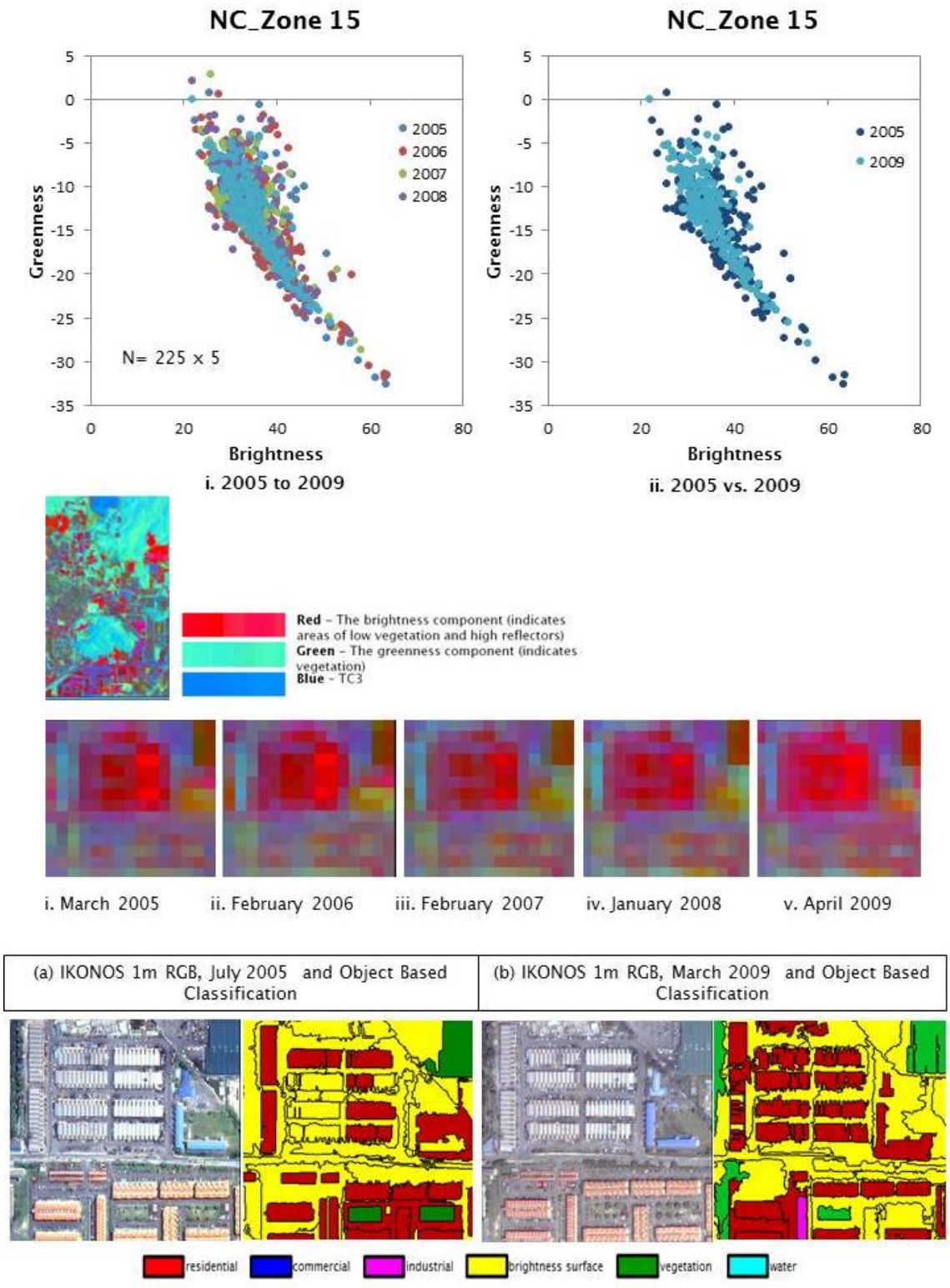


Figure A6.10.86 Validation from the feature space of no change (NC) shown by the TC result between greenness and brightness from Zone 15, Landsat ETM+ 2005 to 2009.

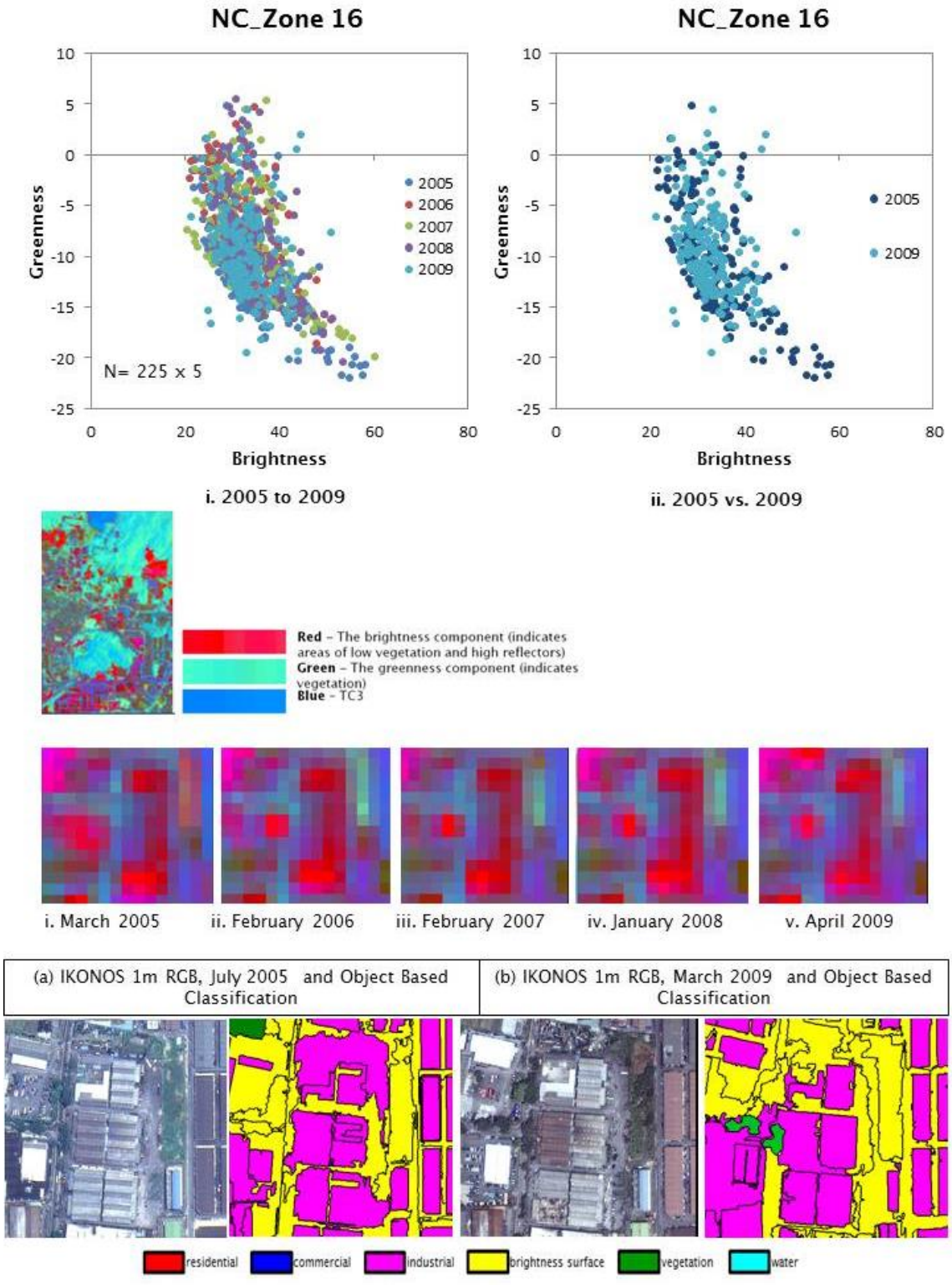


Figure A6.10.87 Validation from the feature space of no change (NC) shown by the TC result between greenness and brightness from Zone 16, Landsat ETM+ 2005 to 2009.

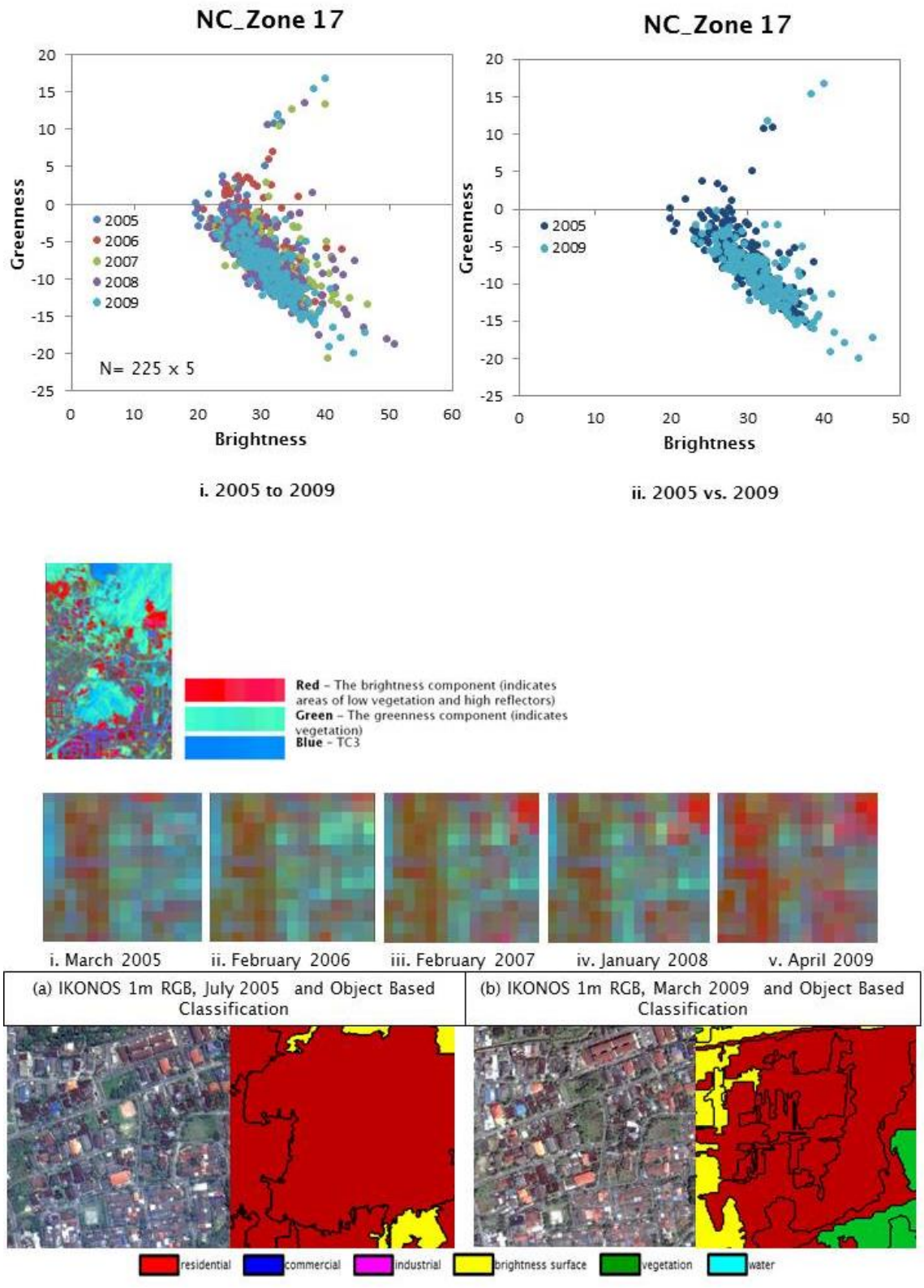


Figure A6.10.88 Validation from the feature space of no change (NC) shown by the TC result between greenness and brightness from Zone 17, Landsat ETM+ 2005 to 2009.

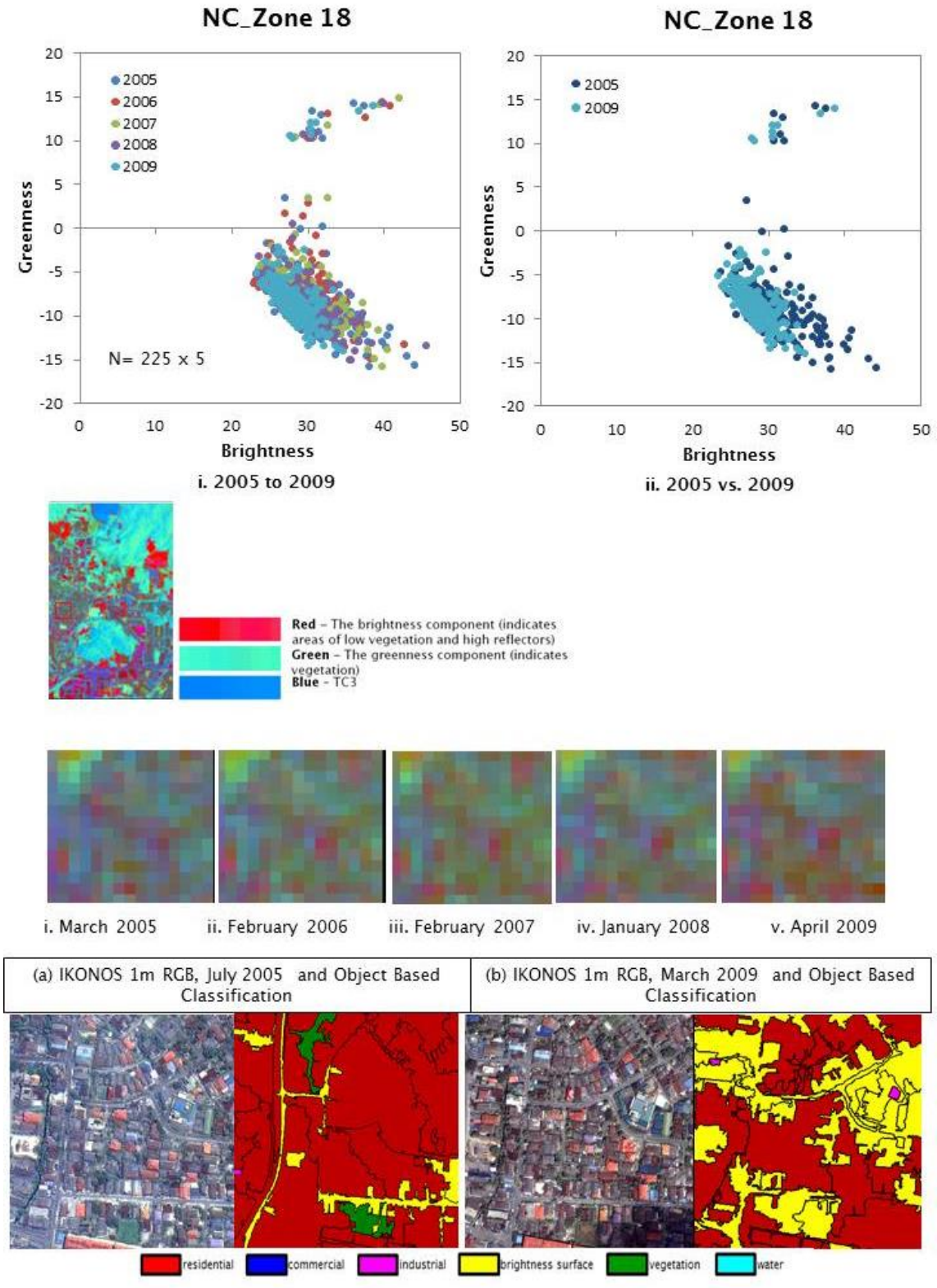


Figure A6.10.89 Validation from the feature space of no change (NC) shown by the TC result between greenness and brightness from Zone 18, Landsat ETM+ 2005 to 2009.

# List of References

Al-Ahmadi, K., Heppenstall, A., Hogg, J. & See,L., 2009. A Fuzzy Cellular Automata Urban Growth Model (FCAUGM) for the City of Riyadh, Saudi Arabia. Part 1: Model Structure and Validation. *Applied Spatial Analysis and Policy*, 2(1), pp.65–83.

Al-Ahmadi, K., Heppenstall, A., Hogg, J. & See,L., 2009. A Fuzzy Cellular Automata Urban Growth Model (FCAUGM) for the City of Riyadh, Saudi Arabia. Part 2: Scenario Testing. *Applied Spatial Analysis and Policy*, 2(2), pp.85–105.

Al-Ahmadi, K., See, L., Heppenstall, A. & Hogg, J., 2009. Calibration of a fuzzy cellular automata model of urban dynamics in Saudi Arabia. *Ecological Complexity*, 6(2), pp.80–101.

Alberti, M., Weeks, R. & Coe, S., 2004. Urban Land-Cover Change Analysis in Central Puget Sound. *Photogrammetric Engineering & Remote Sensing*, 70(9), pp.1043–1052.

Alkheder, S. & Shan, J., 1997. Cellular Automata Urban Growth Simulation and Evaluation - A Case Study of Indianapolis. *Engineering.purdue.edu* , pp.1–19.

Almeida, D., Batty, M., Miguel, A., Monteiro, V. & Ca, G., 2003. Stochastic cellular automata modeling of urban land use dynamic: empirical development and estimation. *Urban Systems*, 27, pp.481–509.

Amarsaikhan, D., Blotevogel, H.H., Ganzorig, M. & Moon, T. H., 2009. Applications of remote sensing and geographic information systems for urban land-cover change studies in Mongolia. *Geocarto International*, 24(4), pp.257–271.

Anderson, .J.R., Hardy, E.E., Roach, J.T., Witmer, R.E., 1976. A Land Use And Land Cover Classification System For Use With Remote Sensor Data. *Geological Survey Professional Paper 964 : A revision of the land use classification system as presented in U.S. Geological Survey Circular 671*

Aplin, P., 2006. On scales and dynamics in observing the environment. *International Journal of Remote Sensing*, 27(11), pp.2123–2140.

Aplin, P. & Atkinson, P.M., 2001. Sub-pixel land cover mapping for per-field classification. *International Journal of Remote Sensing*, 22(14), pp.2853–2858.

Aplin, P., Atkinson, P.M. & Curran, P.J., 1999. Fine Spatial Resolution Simulated Satellite Sensor Imagery for Land Cover Mapping in the United Kingdom. *Remote Sensing of Environment*, 68(3), pp.206–216.

Araya, Y.H. & Cabral, P., 2010. Analysis and Modeling of Urban Land Cover Change in Setúbal and Sesimbra, Portugal. *Remote Sensing*, 2(6), pp.1549–1563.

Asner, G.P. & Heidebrecht, K.B., 2002. Spectral unmixing of vegetation, soil and dry carbon cover in arid regions: Comparing multispectral and hyperspectral observations. *International Journal of Remote Sensing*, 23(19), pp.3939–3958.

Aspinall, R.J. & Hill, M.J., 1997. Land Cover Change: A Method For Assessing The Reliability of Land Cover Change Measured From Remotely-Sensed Data. *IEEE International*, Volume:1, pp.269–271.

Atkinson, P.M., Cutler, M.E.J. & Lewis, H., 1997. Mapping sub-pixel proportional land cover with AVHRR imagery. *International Journal of Remote Sensing*, 18:4, pp.917–935.

Baatz, M. & Schäpe, A., 2000. Multiresolution Segmentation: an optimization approach for high quality multi-scale image segmentation J. Strobl, ed. *Journal of Photogrammetry and Remote Sensing*, 58(3–4), pp.12–23.

Baisantry, M., Negi, D.S. & Manocha, O.P., 2012. Change vector Analysis using Enhanced PCA and Inverse. *Defence Science Journal*, 62(4), pp.236–242.

Bakr, N., Weindorf, D.C., Bahnassy, M.H., Marei, S.M. & El-Badawi, M.M., 2010. Monitoring land cover changes in a newly reclaimed area of Egypt using multi-temporal Landsat data. *Applied Geography*, 30(4), pp.592–605.

Ban, Y., Hu, H. & Rangel, I.M., 2010. Fusion of Quickbird MS and RADARSAT SAR data for urban land-cover mapping: object-based and knowledge-based approach. *International Journal of Remote Sensing*, 31(6), pp.1391–1410.

Batty, M., 1997. Cellular Automata and Urban Form: A Primer. *Journal of the American Planning Association*, 63(2), pp.266–274.

Batty, M., 2005. *Cities and Complexity: Understanding Cities With Cellular Automata, Agent-Based Models, and Fractals.*, Massachusetts Institute of Technology.

Bauer, T. & Steinnocher, K., 2001. Per parcel land use classification in urban areas applying a rule-based technique. *Image (Rochester, N.Y.)*, 6, pp.24–27.

Bayarsaikhan, U., Boldgiv, B., Kim, K. R., Park, K. A. & Lee, D., 2009. Change detection and classification of land cover at Hustai National Park in Mongolia. *International Journal of Applied Earth Observation and Geoinformation*, 11(4), pp.273–280.

Bellens, R., Gautama, S., Martinez-Fonte, L., Philips, W., Chan, J. C. W. & Canters, F., 2008. Improved Classification of VHR Images of Urban Areas Using Directional Morphological Profiles. *IEEE Transactions on Geoscience and Remote Sensing*, 46(10), pp.2803–2813.

Berberoglu, S., 2000. The integration of spectral and textural information using neural networks for land cover mapping in the Mediterranean. *Computers & Geosciences*, 26(4), pp.385–396.

Bhaskaran, S., Paramananda, S. & Ramnarayan, M., 2010. Per-pixel and object-oriented classification methods for mapping urban features using Ikonos satellite data. *Applied Geography*, 30(4), pp.650–665.

Bhatta, B., Saraswati, S. & Bandyopadhyay, D., 2010. Urban sprawl measurement from remote sensing data. *Applied Geography*, 30(4), pp.731–740.

Blaschke, T., 2010. Object based image analysis for remote sensing. *ISPRS Journal of Photogrammetry and Remote Sensing*, 65(1), pp.2–16.

Blaschke, T., Lang, S., Lorup, E., Strobl, J. & Zeil, P ., 2000. Object-Oriented Image Processing in an Integrated GIS / Remote Sensing Environment and Perspectives for Environmental Applications. *Environment Information for Planning, Politics and The Public*, 2, pp.555–570.

Blaschke, T., Burnett, C. & Pekkarinen, A., 2006. Image Segmentation Methods for Object-based Analysis and Classifi cation (Chapter 12). In *Remote Sensing Image Analysis: Including the Spatial Domain*. pp. 211–236.

Boucher, a & Kyriakidis, P., 2006. Super-resolution land cover mapping with indicator geostatistics. *Remote Sensing of Environment*, 104(3), pp.264–282.

Bourne, L.S., 1971. Physical Adjustment Processes and Land Use Succession: A Conceptual Review and Central City Example. *Economic Geography*, 47(1), pp.1–15.

Bouziani, M., Goita, K. & He, D.-C., 2010. Rule-Based Classification of a Very High Resolution Image in an Urban Environment Using Multispectral Segmentation Guided by Cartographic Data. *IEEE Transactions on Geoscience and Remote Sensing*, 48(8), pp.3198–3211.

Bruton, M.J., 2007. *Malaysia, The Planning of Nation*. PERSADA. Kuala Lumpur.

Bruzzone, L., 2000. Unsupervised Change Detection. *IEEE Transactions On Geoscience And Remote Sensing,*, 38(3), pp.1171–1182.

Campbell, J.B., 2006. *Introduction to Remote Sensing, Fourth Edition* fourth., The Guilforth Press; 4th edition.

Canty, M.J., 2010. *Image Analysis, Classification, and Change Detection in Remote Sensing With Algorithms for ENVI/ICL* Second Edi., CRC Press, Taylor & Francais Group.

Canty, M.J. & Nielsen, A. a., 2008. Automatic radiometric normalization of multitemporal satellite imagery with the iteratively re-weighted MAD transformation. *Remote Sensing of Environment*, 112(3), pp.1025–1036.

Caselles, V. & Garcia, M.J., 1989. An alternative simple approach to estimate atmospheric correction in multitemporal studies. *International Journal of Remote Sensing*, 10(6), pp.1127–1134.

Chavez, P.S., 1996. Image-Based Atmospheric Corrections - Revisited and Improved. *Photogrammetric Engineering & Remote Sensing*, 62(9), pp.1025-1036.

Chen, X., Yu, S.-X. & Zhang, Y.-P., 2013. Evaluation of Spatiotemporal Dynamics of Simulated Land Use/Cover in China Using a Probabilistic Cellular Automata-Markov Model. *Pedosphere*, 23(2), pp.243-255.

Chen, Z. & Wang, J., 2010. Land use and land cover change detection using satellite remote sensing techniques in the mountainous Three Gorges Area, China. *International Journal of Remote Sensing*, 31(6), pp.1519-1542.

Choi, K.-Y. & Milton, E.., 1999. A Multispectral Transform for the Suppression of Clouds Shadows. *The Fourth International Airborne Remote Sensing Conference and Exhibition, 21st Canadian Symposium on Remote Sensing. ERIM International Inc., Ottawa, Canada*, pp.762-769.

Chopard, B. & Droz, M., 1998. *Cellular Automata Modeling of Physical Systems*, Cambridge University Press.

Clarke, K.C. & Gaydos, L.J., 2010. Loose-coupling a cellular automaton model and GIS: long-term urban growth prediction for San Francisco and Washington/Baltimore. *International journal of geographical information science: IJGIS*, 12(7), pp.699-714.

Corcoran, P., Winstanley, A. & Mooney, P., 2010. Segmentation performance evaluation for object-based remotely sensed image analysis. *International Journal of Remote Sensing*, 31(3), pp.617-645.

Crippen, R., 1990. Calculating the vegetation index faster. *Remote Sensing of Environment*, 34(1), pp.71-73.

Crist, E.P. & Cicone, R.C., 1984. A Physically-Based Transformation of Thematic Mapper Data-The TM Tasseled Cap. *IEEE Transactions on Geoscience and Remote Sensing*, GE-22(3), pp.256-263.

Definiens AG, 2009. *Definiens eCognition Developer 8-User Guide* Document V : Definiens AG. Germany.

Deng, J., Wang, K., Li, J. & Deng, Y., 2009. Urban Land Use Change Detection Using Multisensor Satellite Images1. *Pedosphere*, 19(1), pp.96-103.

Deng, J.S., Wang, K., Deng, Y.H. & Qi, G.J., 2008. PCA-based land-use change detection and analysis using multitemporal and multisensor satellite data. *International Journal of Remote Sensing*, 29(16), pp.4823-4838.

Drăguţ, L. & Blaschke, T., 2006. Automated classification of landform elements using object-based image analysis. *Geomorphology*, 81(3-4), pp.330-344.

Du, Y., Wen, W., Cao, F. & Ji. M., 2010. A case-based reasoning approach for land use change prediction. *Expert Systems with Applications*, 37(8), pp.5745-5750.

Eastman, J. R., 2003. *IDRISI Kilimanjaro: Guide to GIS and Image Processing*. Worcester, MA: Clark Labs, Clark University.

Elhadi, E.M. & Zomrawi, N., 2010. Change Detection Analysis By Using Ikonos And Quick Bird Imageries. *Journal of American Science*, 6(2), pp.171–175.

Elmore, A.J., Mustard, J.F., Manning, S. & Lobell, D. B., 2000. Quantifying Vegetation Change in Semiarid Environments: Precision and Accuracy of Spectral Mixture Analysis and the Normalized Difference Vegetation Index. *Remote Sensing of Environment*, 102(January), pp.87–102.

Evans, B., 1993. Why we no longer need a town planning profession. *Planning Practice and Research*, 8(1), pp.9–15.

Federal Department Town and Country Planning Peninsular Malaysia, 2013. *Manual of Geospatial Data Management*, Kuala Lumpur.

Federal Department of Town and Country Planning Peninsular Malaysia (JPBD SM), 2007. *Land Use Classification and Meta Data Format for Development Plans (version 8).*, Kuala Lumpur.

Federal Department of Town and Country Planning Peninsular Malaysia (JPBD SM), 2005. *National Physical Plan (NPP)*, Kuala Lumpur.

Federal Department of Town and Country Planning Peninsular Malaysia (JPBD SM), 2006. *National Urban Policy*, Kuala Lumpur.

Federal Department of Town and Country Planning Peninsular Malaysia (JPBD SM), 2010. *Selayang City Council (MPS) Local Plan 2020*, Selangor.

Federal Department of Town and Country Planning Peninsular Malaysia (JPBD SM), 2002. *State Selangor Structure Plan (RSN) of Selangor , Report of Survey*, Selangor.

Foody, G.M., 2002. Status of land cover classification accuracy assessment. *Remote Sensing of Environment*, 80(1), pp.185–201.

Foody, G.M. & Mathur, A., 2004. A relative evaluation of multiclass image classification by support vector machines. *IEEE Transactions on Geoscience and Remote Sensing*, 42(6), pp.1335–1343.

Franklin, S.E. & Wulder, M. A., 2002. Remote sensing methods in medium spatial resolution satellite data land cover classification of large areas. *Progress in Physical Geography*, 26(2), pp.173–205.

Fraser, R., Olthof, I., Carriere, M., Deschamps, A. & Pouliot, D., 2011. A method for trend-based change analysis in Arctic tundra using the 25-year Landsat archive. *Polar Record*, 48(01), pp.83–93.

Frauman, E. & Wolff, E., 2005. Segmentation Of Very High Spatial Resolution Satellite Images In Urban Areas For Segments-Based Classification. *Proceedings for 3rd International Symposium Remote Sensing and Data Fusion Over Urban Areas.* Tempe, Arizona.

Fugate, D., Tarnavsky, E. & Stow, D., 2010. A Survey of the Evolution of Remote Sensing Imaging Systems and Urban Remote Sensing Applications T. Rashed & C. Jürgens, eds. *Remote Sensing and Digital Image Processing*, 10, pp.119–139.

Fung, P.W., Grebbin, G. & Attikiouzel, Y., 1990. Contextual classification and segmentation of textured images. *International Conference on Acoustics, Speech, and Signal Processing*, pp.2329–2332.

Gamanya, R., Demaeyer, P. & Dedapper, M., 2009. Object-oriented change detection for the city of Harare, Zimbabwe. *Expert Systems with Applications*, 36(1), pp.571–588.

Geneletti, D. & Gorte, B.G.H., 2003. A method for object-oriented land cover classification combining Landsat TM data and aerial photographs. *International Journal of Remote Sensing*, 24(6), pp.1273–1286.

Gluch, R.M. & Ridd, M.K., 2010. The V-I-S Model: Quantifying the Urban Environment. In T. Rashed & C. Jürgens, eds. *Remote Sensing of Urban and Suburban Areas, Remote Sensing and Digital Image Processing.* Remote Sensing and Digital Image Processing. Dordrecht: Springer Netherlands, pp. 85–116.

Gómez, C., White, J.C. & Wulder, M. A., 2011. Characterizing the state and processes of change in a dynamic forest environment using hierarchical spatio-temporal segmentation. *Remote Sensing of Environment*, 115(7), pp.1665–1679.

Goodwin, N.R., Collett, L. J., Denham, R. J., Flood, N. & Tindall, D., 2013. Cloud and cloud shadow screening across Queensland, Australia: An automated method for Landsat TM/ETM+ time series. *Remote Sensing of Environment*, 134, pp.50–65.

Gray, J. & Song, C., 2013. Consistent classification of image time series with automatic adaptive signature generalization. *Remote Sensing of Environment*, 134, pp.333–341.

Guan, D., Li, H. F., Inohae, T., Su, W., Nagaie, T. & Hokao, K., 2011. Modeling urban land use change by the integration of cellular automaton and Markov model. *Ecological Modelling*, 222(20–22), pp.3761–3772.

Guttenberg, A.Z., 1959. Journal of the American Institute of Planners. *Journal Of The American Institute Of Planners*, 25:3(October 2011), pp.143–150.

H.Yamamoto, K. & P.Finn, M., 2012. Approximating Tasseled Cap Values to Evaluate Brightness, Greenness, and Wetness for the Advanced Land Imager (ALI). *Scientific Investigation Report 2012-5057*, (U.S.Geological Survey, Reston, Virginia:2012).

Hall, O., 2003. A Multiscale Object-Specific Approach to Digital Change Detection. *International Journal of Applied Earth Observation and Geoinformation*, 4(4), pp.311–327.

Hay, G., 2003. A comparison of three image-object methods for the multiscale analysis of landscape structure. *ISPRS Journal of Photogrammetry and Remote Sensing*, 57(5–6), pp.327–345.

Hay, G.J., Marceau, D.J. & Dub, P., 2001. A multiscale framework for landscape analysis: Object-specific analysis and upscaling. *Landscape Ecology*, (1995), pp.471–490.

Healey, P., 1996. The communicative turn in planning theory and its implications for spatial strategy formation. *Environment and Planning B□: Planning and Design.*, 23, pp.217–234.

Heo, J. & Thomas, W.F., 2000. A Standardized Radiometric Normalization Method for Change Detection Using Remotely Sensed Imagery. *Photogrammetric Engineering & Remote Sensing*, 66(2), pp.173–181.

Herold, M., Liu, X. & Clarke, K.C., 2003. Spatial Metrics and Image Texture for Mapping Urban Land Use. *Photogrammetric Engineering & Remote Sensing*, 69(9), pp.991–1001.

Herold, M. & Roberts, D.A., 2010. The Spectral Dimension in Urban Remote Sensing. In T. Rashed & C. Jurgens, eds. *Remote Sensing of Urban and Suburban Areas, Remote Sensing and Digital Image Processing*. pp. 47–65.

Hester, D.B., Nelson, S.A.C., Cakir, H. I., Khorram, S. & Cheshire, H., 2010. High-resolution land cover change detection based on fuzzy uncertainty analysis and change reasoning. *International Journal of Remote Sensing*, 31(2), pp.455–475.

Holland, J. & Aplin, P., 2013. Super-resolution image analysis as a means of monitoring bracken (Pteridium aquilinum) distributions. *ISPRS Journal of Photogrammetry and Remote Sensing*, 75, pp.48–63.

Huang, Z., Jia, X. & Ge, L., 2010. Sampling approaches for one-pass land-use/land-cover change mapping. *International Journal of Remote Sensing*, 31(6), pp.1543–1554.

Im, J. & Jensen, J., 2005. A change detection model based on neighborhood correlation image analysis and decision tree classification. *Remote Sensing of Environment*, 99(3), pp.326–340.

Jacquin, a, Misakova, L. & Gay, M., 2008. A hybrid object-based classification approach for mapping urban sprawl in periurban environment. *Landscape and Urban Planning*, 84(2), pp.152–165.

Jantz, C. A., Goetz, S. J., Donato, D. & Claggett, P., 2010. Designing and implementing a regional urban modeling system using the SLEUTH cellular urban model. *Computers, Environment and Urban Systems*, 34(1), pp.1–16.

Jensen, J.R., 2000. *Remote Sensing of the Environment: An Earth Resource Perspective*, Prentice Hall.

Ji, C.Y., 2000. Land-Use Classification of Remotely Sensed Data Using Kohonen Self-Organizing Feature Map Neural Networks. *Photogrammetric Engineering & Remote Sensing*, 66(12), pp.1451–1460.

Johnson, B.A., Tateishi, R. & Hoan, N.T., 2013. A hybrid pansharpening approach and multiscale object-based image analysis for mapping diseased pine and oak trees. *International Journal of Remote Sensing*, 34(20), pp.6969–6982.

Johnson, R.D. & Kasischke, E.S., 1998. Change vector analysis: A technique for the multispectral monitoring of land cover and condition. *International Journal of Remote Sensing*, 19(3), pp.411–426.

Jokar Arsanjani, J., Helbich, M., Kainz, W. & Darvishi Boloorani, A., 2013. Integration of logistic regression, Markov chain and cellular automata models to simulate urban expansion. *International Journal of Applied Earth Observation and Geoinformation*, 21, pp.265–275.

Kahya, O., Bayram, B. & Reis, S., 2010. Land cover classification with an expert system approach using Landsat ETM imagery: a case study of Trabzon. *Environmental monitoring and assessment*, 160(1–4), pp.431–8.

Kardoulas, N.G., Bird, A.C. & Lawan, A.I., 1996. Geometric Correction of SPOT and Landsat Imagery: A Comparison of M a p and GPS-Derived Control Points. *Photogrammetric Engineering & Remote Sensing*, 62(10), pp.1173–1177.

Kaufman, Y.J., Wald, A.E., Remer, L. A. & Flynn, L., 1997. The MODIS 2.1-μm channel-correlation with visible reflectance for use in remote sensing of aerosol. *IEEE Transactions on Geoscience and Remote Sensing*, 35(5), pp.1286–1298.

Kauth, R.. & Thomas, G.., 1976. The Tasselled Cap -- A Graphic Description of the Spectral-Temporal Development of Agricultural Crops as Seen by LANDSAT. *Symposium on Machine Processing of Remotely Sensed Data, June 29 - July 1, 1976*.

L., W., Sousa, W.P. & P., G., 2004. Integration of object-based and pixel-based classification for mapping mangroves with IKONOS imagery. *International Journal of Remote Sensing*, 25(24), pp.5655–5668.

Levinson, D., El-geneidy, A. & Wasfi, R., 2012. A Markov Chain Model of Land Use Change in the Twin Cities , 1958–2005. *Proceeding of the 10th International Symposium on Spatial Accuracy Assessment in Natural Resources and Environmental Sciences,* pp.345–350.

Li, H., Gu, H., Han, Y. & Yang, J., 2010. Object-oriented classification of high-resolution remote sensing imagery based on an improved colour structure code and a support vector machine. *International Journal of Remote Sensing*, 31(6), pp.1453–1470.

Liu, X. & Jr, R.G.L., 2002. Urban change detection based on an artificial neural network. *International Journal of Remote Sensing*, 23(12), pp.2513–2518.

Liu, Y., 2009. *Modelling Urban Development with Geographical Information System and Cellular Automata*, CRC Press, Taylor & Francais Group.

Liu, Y. & Phinn, S.R., 2003. Modelling urban development with cellular automata incorporating fuzzy-set approaches. *Computers, Environment and Urban Systems*, 27(6), pp.637–658.

Lloyd, C.D., Berberoglu, S., Curran, P. J. & Atkinson, P. M., 2004. A comparison of texture measures for the per-field classification of Mediterranean land cover. *International Journal of Remote Sensing*, 25(19), pp.3943–3965.

Lopez, E., Bocco, G., Mendoza, M. & Duhau, E., 2001. Predicting land-cover and land-use change in the urban fringe A case in Morelia city , Mexico. *Landscape and Urban Planning*, 55, pp.271–285.

Lu, D., Li, G., Moran, E., Batistella, M. & Freitas, C.C., 2011. Mapping impervious surfaces with the integrated use of Landsat Thematic Mapper and radar data: A case study in an urban–rural landscape in the Brazilian Amazon. *ISPRS Journal of Photogrammetry and Remote Sensing*, 66(6), pp.798–808.

Lu, D. & Weng, Q., 2007. A survey of image classification methods and techniques for improving classification performance. *International Journal of Remote Sensing*, 28(5), pp.823–870.

Lu, D. & Weng, Q., 2006. Use of impervious surface in urban land-use classification. *Remote Sensing of Environment*, 102(1–2), pp.146–160.

Lunetta, R., 2004. Impacts of imagery temporal frequency on land-cover change detection monitoring. *Remote Sensing of Environment*, 89(4), pp.444–454.

Malila, W.A., 1980. Change Vector Analysis□: An Approach for Detecting Forest Changes with Landsat. *Symposium on Machine Processing of Remotely Sensed Data and Soil Information Syspems and Remote Sensing and Soil Survey, June 3-6, 1980*, pp.326–335.

Martin, L. & Howarth, P., 1989. Change-detection accuracy assessment using SPOT multispectral imagery of the rural-urban fringe☆. *Remote Sensing of Environment*, 30(1), pp.55–66.

Mas, J.-F., 1999. Monitoring land-cover changes: A comparison of change detection techniques. *International Journal of Remote Sensing*, 20(1), pp.139–152.

Mather, P. & Brandt, T., 2004. *Classification Methods for Remotely Sensed Data* Second., CRC Press.

Mather, P.& Koch, M., 2004. *Computer Processing of Remotely-Sensed Image: An Introduction* 3 edition., John Wiley & Sons.

Mello, M.P. et al., 2013. STARS: A New Method for Multitemporal Remote Sensing. *IEEE Transactions on Geoscience and Remote Sensing*, 51(4), pp.1897–1913.

Mitsova, D., Shuster, W. & Wang, X., 2011. A cellular automata model of land cover change to integrate urban growth with open space conservation. *Landscape and Urban Planning*, 99(2), pp.141–153.

Mohd, I., Ahmad, F. & Wan Abd Aziz, W.N., 2009. Exploiting town planning factors in land development: Case study of urban housing in Kuala Lumpur, Malaysia. *Journal of Facilities Management*, 7(4), pp.307–318.

Morandé, F., Petermann, A. & Vargas, M., 2008. Determinants of Urban Vacant Land. *The Journal of Real Estate Finance and Economics*, 40(2), pp.188–202.

Nguyen, M.Q., Atkinson, P.M. & Lewis, H.G., 2006. Superresolution mapping using a hopfield neural network with fused images. *IEEE Transactions on Geoscience and Remote Sensing*, 44(3), pp.736–749.

Nielsen, A.A., 2007. The regularized iteratively reweighted MAD method for change detection in multi- and hyperspectral data. *IEEE transactions on image processing: a publication of the IEEE Signal Processing Society*, 16(2), pp.463–78.

Nutini, F., Boschetti, M., Brivio, P.A., Bocchi, S. & Antoninetti, M., 2013. Land-use and land-cover change detection in a semi-arid area of Niger using multi-temporal analysis of Landsat images. *International Journal of Remote Sensing*, 34(13), pp.4769–4790.

Olofsson, P., Foody, G. M., Stehman, S. V. & Woodcock, C. E., 2013. Making better use of accuracy data in land change studies: Estimating accuracy and area and quantifying uncertainty using stratified estimation. *Remote Sensing of Environment*, 129, pp.122–131.

Owen, S., Mackenzie, A., Bunce, R., Stewart, H., Donovan, R., Stark, G. & Hewitt, D., 2006. Urban land classification and its uncertainties using principal component and cluster analyses: A case study for the UK West Midlands. *Landscape and Urban Planning*, 78(4), pp.311–321.

Petit, C.C. & Lambin, E.F., 2001. Integration of multi-source remote sensing data for land cover change detection. *International Journal of Geographical Information Science*, 15(8), pp.785–803.

Pijanowski, B., Brown, D., Shellito, B. & Manik, G., 2002. Using neural networks and GIS to forecast land use changes: a Land Transformation Model. *Computers, Environment and Urban Systems*, 26(6), pp.553–575.

Raja, R.A.A., Anand, V., Kumar, A.S., Maithani, S. & Kumar, V.A., 2012. Wavelet Based Post Classification Change Detection Technique for Urban Growth Monitoring. *Journal of the Indian Society of Remote Sensing*, 41(1), pp.35–43.

Rashed, T., Weeks, J.R., Roberts, D., Rogan, J. & Powell, R., 2003. Measuring the Physical Composition of Urban Morphology Using Multiple Endmember Spectral Mixture Models. *Photogrammetric Engineering & Remote Sensing*, 69(9), pp.1011–1020.

Rashed, T., 2008. Remote sensing of within-class change in urban neighborhood structures. *Computers, Environment and Urban Systems*, 32(5), pp.343–354.

Razali, S.M., Marin, A., Nuruddin, A.A., Shafri, H.Z.M. & Hamid, H.A., 2014. Capability of integrated MODIS imagery and ALOS for oil palm, rubber and forest areas mapping in tropical forest regions. *Sensors (Basel, Switzerland)*, 14(5), pp.8259–82.

Richter, R. & Schläpfer, D., 2011. *Atmospheric/Topographic Correction for Satellite Imagery. In: DLR Report DLR-IB 565-02/11*, Wessling, Germany.

Ridd, M.K., 1995. Exploring a V-I-S (vegetation-impervious surface-soil) model for urban ecosystem analysis through remote sensing: comparative anatomy for cities. *International Journal of Remote Sensing*, 16(12), pp.2165–2185.

Rizvi, I. A., Mohan, B.K. & Bhatia, P.R., 2010. Automatic object extraction using object based image classification technique from high resolution remotely sensed images. *Proceedings of the International Conference and Workshop on Emerging Trends in Technology - ICWET '10*, (Icwet), p.623.

Rogan, J. & Chen, D., 2004. Remote sensing technology for mapping and monitoring land-cover and land-use change. *Progress in Planning*, 61(4), pp.301–325.

Rossi, R.E., Dungan, J.L. & Beck, L.R., 1994. Kriging in the Shadows□: Geostatistical Interpolation for Remote Sensing. *Remote Sensing of Environment*, 49, pp.32–40.

Samat, N., 2007. Integrating Gis And Cellular Automata Spatial Model In Evaluating Urban Growth: Prospects And Challenges. *Jurnal Alam Bina*, 9(1).

Schöpfer, E., Lang, S. & Strobl, J., 2010. Segmentation and object-Based Imaged Analysis. In T. Rashed & C. Jürgens, eds. *Remote Sensing of Urban and Suburban Areas, Remote Sensing and Digital Image Processing*. Remote Sensing and Digital Image Processing. Dordrecht: Springer Netherlands, pp. 181–192.

Schwert, B., Rogan, J., Giner, N.M., Ogneva-Himmelberger, Y., Blanchard, S. D.& Woodcock, C., 2013. A comparison of support vector machines and manual change detection for land-cover map updating in Massachusetts, USA. *Remote Sensing Letters*, 4(9), pp.882–890.

Selamat, M.H., Selamat, A., Othman, M. S., Mohd Shamsuddin, N. H. & Mohd Zulkepli, N. I., 2012. A review on Geographical Information System ( GIS ) in Town Planning: Malaysia Experience. *Geoinformatica: An International Journal (GIIJ)*, (2), pp.27–38.

Settle, J.J. & Drake, N. A., 1993. Linear mixing and the estimation of ground cover proportions. *International Journal of Remote Sensing*, 14(6), pp.1159–1177.

Shackelford, A.K. & Davis, C.H., 2003. A Hierarchical Fuzzy Classification Approach for High-Resolution Multispectral Data Over Urban Areas. *IEEE Transactions on Geoscience and Remote Sensing*, 41(9), pp.1920–1932.

Shafizadeh Moghadam, H. & Helbich, M., 2013. Spatiotemporal urbanization processes in the megacity of Mumbai, India: A Markov chains-cellular automata urban growth model. *Applied Geography*, 40, pp.140–149.

Silva, T.S. & Tagliani, P.R. A., 2012. Environmental planning in the medium littoral of the Rio Grande do Sul coastal plain – Southern Brazil: Elements for coastal management. *Ocean & Coastal Management*, 59, pp.20–30.

Sims, F.M. & Mesev, V., 2007. Use of Ancillary Data in Object Based Classification of High Resolution Satellite Data. *2007 Urban Remote Sensing Joint Event*, pp.1–10.

Singh, A., 1989. Review Article Digital change detection techniques using remotely-sensed data. *International Journal of Remote Sensing*, 10(6), pp.989–1003.

Small, C., 2001. Estimation of urban vegetation abundance by spectral mixture analysis. *International Journal of Remote Sensing*, 22(7), pp.1305–1334.

Small, C. & Lu, J.W.T., 2006. Estimation and vicarious validation of urban vegetation abundance by spectral mixture analysis. *Remote Sensing of Environment*, 100(4), pp.441–456.

Smith, G.M. & Milton, E.J., 1999. The use of the empirical line method to calibrate remotely sensed data to reflectance. *International Journal of Remote Sensing*, 20(13), pp.2653–2662.

Smits, P.C. & Annoni, a., 2000. Toward specification-driven change detection. *IEEE Transactions on Geoscience and Remote Sensing*, 38(3), pp.1484–1488.

Somers, B., Asner, G. P., Tits, L. & Coppin, P., 2011. Endmember variability in Spectral Mixture Analysis: A review. *Remote Sensing of Environment*, 115(7), pp.1603–1616.

Song, C., Woodcock, C.E., Seto, K. C., Lenney, M. P. & Macomber, S. A., 2001. Classification and Change Detection Using Landsat TM Data When and How to Correct Atmospheric Effects? *Remote Sensing of Environment*, 75(2), pp.230–244.

Stow, D., Lopez, A., Lippitt, C., Hinston, S. & Weeks, J., 2007. Object-based classification of residential land use within Accra, Ghana based on QuickBird satellite data. *International journal of remote sensing*, 28(22), pp.5167–5173.

Strahler, A.H., Woodcock, C.E. & Smith, J. a., 1986. On the nature of models in remote sensing. *Remote Sensing of Environment*, 20(2), pp.121–139.

Takada, T., Miyamoto, A. & Hasegawa, S.F., 2010. Derivation of a yearly transition probability matrix for land-use dynamics and its applications. *Landscape Ecology*, 25(4), pp.561–572.

Taubenböck, H., Esch, T. & Roth, A., 2006. An Urban Classification Approach Based On An Object – Oriented Analysis Of High Resolution Satellite Imagery For A Spatial Structuring Within Urban Areas. In *1st EARSeL Workshop of the SIG Urban Remote Sensing*. pp. 1–8.

Tehrany, M.S., Pradhan, B. & Jebur, M.N., 2013. Remote Sensing Data Reveals Eco-Environmental Changes in Urban Areas of Klang Valley, Malaysia: Contribution from Object Based Analysis.

Thomas, N., Hendrix, C. & Congalton, R.G., 2003. A Comparison of Urban Mapping Methods Using High-Resolution Digital Imagery. *Photogrammetric Engineering & Remote Sensing*, 69(9), pp.963–972.

Tompkins, S., Mustard, J.F. & Forsyth, D.W., 1997. Optimization of Endmembers for Spectral Mixture Analysis. *Remote Sensing of Environment*, 59(3), pp.472–489.

Tuia, D., Pacifici, F., Kanevski, M. & Emery, W. J., 2009. Classification of Very High Spatial Resolution Imagery Using Mathematical Morphology and Support Vector Machines. *IEEE Transactions on Geoscience and Remote Sensing*, 47(11), pp.3866–3879.

Vitousek, P.M., 1994. Beyond Global Warming: Ecology and Global Change. *Ecological Society of America Article DOI: 10.2307/1941591*, 75(7), pp.1861–1876.

Wacker, A.G. & Landgrebe, D.A., 1972. Minimum Distance Classification in Remote Sensing The Laboratory for Applications of Remote Sensing. *LARS Technical Report.* Paper 25. Purdue Libraries.

Wahab, A.A., 2011. The Monitoring of Landuse Development using Quantum GIS. *Federal Department Town & Country Planning*. Kuala Lumpur.

Wahab, A.A., 2011. The Potential Uses Of Qgis-Grass In Town And Country Planning. *Federal Department Town & Country Planning*. Kuala Lumpur.

Walter, V., 2004. Object-based classification of remote sensing data for change detection. *ISPRS Journal of Photogrammetry and Remote Sensing*, 58(3–4), pp.225–238.

Watanachaturaporn, P., Arora, M.K. & Varshney, P.K., 2008. Multisource Classification Using Support Vector Machines: An Empirical Comparison with Decision Tree and Neural Network Classifiers. *Photogrammetric Engineering & Remote Sensing*, 74(2), pp.239–246.

Weeks, E.S., Ausseil, A. G. E., Shepherd, J. D. & Dymond, J. R., 2013. Remote sensing methods to detect land-use/cover changes in New Zealand's "indigenous" grasslands. *New Zealand Geographer*, 69(1), pp.1–13.

White, R. & Engelen, G., 1993. Cellular automata and fractal urban form: a cellular modelling approach to the evolution of urban land-use patterns. *Environment and Planning A*, 25(8), pp.1175–1199.

White, R. & Engelen, G., 1997. Cellular automata as the basis of integrated dynamic regional modelling. *Environment and Planning : Planning and Design.*, 24(page 15), pp.235–246.

White, R., Uljee, I. & Engelen, G., 2012. Integrated modelling of population, employment and land-use change with a multiple activity-based variable grid cellular automaton. *International Journal of Geographical Information Science*, (February 2012), pp.1–30.

Willhauck, G., 2000. Comparison of object oriented classification techniques and standard image analysis for the use of change detection between SPOT multispectral satellite images and aerial photos . *International Archives of Photogrammetry and Remote Sensing.*, XXXIII(Part B3), pp.214–221.

Wilson, R.T., 2013. Py6S: A Python interface to the 6S radiative transfer model. *Computers & Geosciences*, 51, pp.166–171.

Woodcock, C.E. & Strahler, A.H., 1987. The factor of scale in remote sensing. *Remote Sensing of Environment*, 21(3), pp.311–332.

World Bank, 2014. *World Development Indicators 2014*, The World Bank.

Wu, D., Liu, J., Wang, S. & Wang, R., 2009. Simulating urban expansion by coupling a stochastic cellular automata model and socioeconomic indicators. *Stochastic Environmental Research and Risk Assessment*, 24(2), pp.235–245.

Wu, F. & Martin, D., 2002. Urban expansion simulation of Southeast England using population surface modelling and cellular automata. *Environment and Planning A*, 34(10), pp.1855–1876.

Yagoub, M.M. & Al Bizreh, A.A., 2014. Prediction of Land Cover Change Using Markov and Cellular Automata Models: Case of Al-Ain, UAE, 1992–2030. *Journal of the Indian Society of Remote Sensing*, 42(3), pp.665–671.

Yang, L., Xian, G., Klaver, J. M. & Deal, B., 2003. Urban Land-Cover Change Detection through Sub-Pixel Imperviousness Mapping Using Remotely Sensed Data. *Photogrammetric Engineering & Remote Sensing*, 69(9), pp.1003–1010.

Yang, X., Zheng, X.-Q. & Lv, L.-N., 2012. A spatiotemporal model of land use change based on ant colony optimization, Markov chain and cellular automata. *Ecological Modelling*, 233, pp.11–19.

Yu, X.J. & Ng, C.N., 2007. Spatial and temporal dynamics of urban sprawl along two urban–rural transects: A case study of Guangzhou, China. *Landscape and Urban Planning*, 79(1), pp.96–109.

Zhang, P. & Atkinson, P.M., 2008. Modelling the effect of urbanization on the transmission of an infectious disease. *Mathematical Biosciences*, 211(1), pp.166–85.

Zhao, G., 2011. The effect of land use categories resolution on geography cellular automata model. *IEEE Geoscience and Remote Sensing Letters*, (126), pp.5614–5617.

Zhou, W. & Troy, a., 2008. An object-oriented approach for analysing and characterizing urban landscape at the parcel level. *International Journal of Remote Sensing*, 29(11), pp.3119–3135.

Zurita-Milla, R., Kaiser, G., Clevers, J., Schneider, W. & Schaepman, M.E., 2009. Downscaling time series of MERIS full resolution data to monitor vegetation seasonal dynamics. *Remote Sensing of Environment*, 113(9), pp.1874–1885.

Zurita-Milla, R., 2008. *Mapping and monitoring heterogeneous landscape: spatial , spectral and temporal unmixing of MERIS data*. PhD Thesis. Netherlands.

Zurita-Milla, R., Kaiser,G., Schneider, W. & Schaepman, M.E., 2007. Spatial Unmixing Of Meris Data For Monitoring Vegetation Dynamics. *In Proceedings of the Envisat Symposium, 23-27 April 2007, Montreux, Switzerland*.

Zurita-Milla, R., Clevers, J. & Schaepman, M.E., 2008. Unmixing-Based Landsat TM and MERIS FR Data Fusion. *IEEE Geoscience and Remote Sensing Letters*, 5(3), pp.453–457.